frontiers | Research Topics

Insights in genetics of common and rare diseases 2022

Edited by
Jordi Pérez-Tur and Erica E. Davis

Published in
Frontiers in Genetics
Frontiers in Pediatrics

ISSN 1664-8714
ISBN 978-2-8325-4928-5
DOI 10.3389/978-2-8325-4928-5

About Frontiers

Frontiers is more than just an open access publisher of scholarly articles: it is a pioneering approach to the world of academia, radically improving the way scholarly research is managed. The grand vision of Frontiers is a world where all people have an equal opportunity to seek, share and generate knowledge. Frontiers provides immediate and permanent online open access to all its publications, but this alone is not enough to realize our grand goals.

Frontiers journal series

The Frontiers journal series is a multi-tier and interdisciplinary set of open-access, online journals, promising a paradigm shift from the current review, selection and dissemination processes in academic publishing. All Frontiers journals are driven by researchers for researchers; therefore, they constitute a service to the scholarly community. At the same time, the *Frontiers journal series* operates on a revolutionary invention, the tiered publishing system, initially addressing specific communities of scholars, and gradually climbing up to broader public understanding, thus serving the interests of the lay society, too.

Dedication to quality

Each Frontiers article is a landmark of the highest quality, thanks to genuinely collaborative interactions between authors and review editors, who include some of the world's best academicians. Research must be certified by peers before entering a stream of knowledge that may eventually reach the public - and shape society; therefore, Frontiers only applies the most rigorous and unbiased reviews. Frontiers revolutionizes research publishing by freely delivering the most outstanding research, evaluated with no bias from both the academic and social point of view. By applying the most advanced information technologies, Frontiers is catapulting scholarly publishing into a new generation.

What are Frontiers Research Topics?

Frontiers Research Topics are very popular trademarks of the *Frontiers journals series*: they are collections of at least ten articles, all centered on a particular subject. With their unique mix of varied contributions from Original Research to Review Articles, Frontiers Research Topics unify the most influential researchers, the latest key findings and historical advances in a hot research area.

Find out more on how to host your own Frontiers Research Topic or contribute to one as an author by contacting the Frontiers editorial office: frontiersin.org/about/contact

Insights in genetics of common and rare diseases: 2022

Topic editors

Jordi Pérez-Tur — Institute of Biomedicine of Valencia, Spanish National Research Council (CSIC), Spain

Erica E. Davis — Stanley Manne Children's Research Institute, Ann & Robert H. Lurie Children's Hospital of Chicago, United States

Citation

Pérez-Tur, J., Davis, E. E., eds. (2024). *Insights in genetics of common and rare diseases: 2022*. Lausanne: Frontiers Media SA. doi: 10.3389/978-2-8325-4928-5

Table of contents

frontiers | Frontiers in Genetics

TYPE Perspective
PUBLISHED 06 September 2022
DOI 10.3389/fgene.2022.1000744

OPEN ACCESS

EDITED BY
Jordi Pérez-Tur,
Institute of Biomedicine of Valencia (CSIC), Spain

REVIEWED BY
Izzet Yavuz,
Dicle University, Turkey

*CORRESPONDENCE
Holm Schneider,
holm.schneider@uk-erlangen.de

SPECIALTY SECTION
This article was submitted to Genetics of Common and Rare Diseases, a section of the journal Frontiers in Genetics

RECEIVED 22 July 2022
ACCEPTED 04 August 2022
PUBLISHED 06 September 2022

CITATION
Schneider H (2022), Ectodermal dysplasias: New perspectives on the treatment of so far immedicable genetic disorders.
Front. Genet. 13:1000744.
doi: 10.3389/fgene.2022.1000744

Ectodermal dysplasias: New perspectives on the treatment of so far immedicable genetic disorders

Holm Schneider*

Center for Ectodermal Dysplasias and Department of Pediatrics, University Hospital Erlangen, Friedrich-Alexander University Erlangen-Nürnberg, Erlangen, Germany

The past decade has witnessed an expansion of molecular approaches facilitating the differential diagnosis of ectodermal dysplasias, a group of genetic diseases characterized by the lack or malformation of hair, teeth, nails, and certain eccrine glands. Moreover, advances in translational research have increased the therapeutic opportunities for such rare diseases, and new dental, surgical, and ophthalmic treatment options are likely to offer relief to many individuals affected by ectodermal dysplasias. In X-linked hypohidrotic ectodermal dysplasia (XLHED), the genetic deficiency of the signaling molecule ectodysplasin A1 (EDA1) may even be overcome before birth by administration of a recombinant replacement protein. This has been shown at least for the key problem of male subjects with XLHED, the nearly complete absence of sweat glands and perspiration which can lead to life-threatening hyperthermia. Prenatal treatment of six boys by injection of an EDA1 replacement protein into the amniotic fluid consistently induced the development of functional sweat glands. Normal ability to sweat has so far persisted for >5 years in the two oldest boys treated *in utero*. Thus, timely replacement of a missing protein appears to be a promising therapeutic strategy for the most frequent ectodermal dysplasia and possibly additional congenital disorders.

KEYWORDS

ectodermal dysplasia, molecular therapy, ectodysplasin A, neonatal Fc receptor, stem cell, prosthodontic rehabilitation, tissue-engineering

Introduction

The genetic basis of the prenatal development of vertebrates has been studied extensively for almost five decades, leading to a more comprehensive understanding of the interplay between the many genes involved and the developmental windows in which their expression is required. In the field of medicine, this knowledge may have both diagnostic and therapeutic implications.

The ectoderm, one of three germ layers in the early embryo, gives rise to the central and peripheral nervous system, the neural crest cells, the tooth placodes, and the epidermis with its appendages. Impaired ectodermal development, thus, can result in

a variety of congenital disorders, including 189 conditions initially classified as ectodermal dysplasias (Freire-Maia, 1971; Pagnan and Visinoni, 2014). Three molecular pathways, namely ectodysplasin A, Wnt/β-catenin and tumor protein 63 (p63) signaling, have been found to play major roles in the budding and morphogenesis of ectodermal derivatives (Mikkola and Thesleff, 2003; Mikkola, 2007; Harris et al., 2008; Cui et al., 2014). Almost all genes known to regulate the position, shape, or number of teeth or hairs have important functions in the mediation of cell communication, which is generally considered the most important mechanism driving embryonic development (Thesleff, 2003). Integration of genomics has been instrumental in explaining complex sequential interactions between epithelium and mesenchyme that direct ectodermal differentiation. This brought about a new classification system for ectodermal dysplasias (Wright et al., 2019; Peschel et al., submitted) based on the molecular pathways rather than just the anatomical structures affected. Grouping rare diseases according to shared characteristics of pathogenesis is expected to facilitate differential diagnosis as well as genetic counselling and becomes even more important with molecular therapies on the horizon.

Several research groups have used animal models to establish successful approaches to treating disorders of ectodermal development (e.g., Gaide and Schneider, 2003; Hermes et al., 2014; Watanabe et al., 2015; Jia et al., 2017a; Jia et al., 2017b). Although the pharmaceutical industry has remained reluctant to invest in such strategies, one of them, namely the prenatal replacement of missing EDA1 in children with the most prevalent ectodermal dysplasia, the X-linked hypohidrotic form (XLHED), is currently being evaluated in a worldwide clinical study (ClinicalTrials.gov identifier: NCT04980638). This trial constitutes the first attempt to investigate a pharmacotherapy of genetic disease in patients *in utero*. If successful, knowledge transfer to the treatment of other congenital disorders will be facilitated. For ectodermal dysplasias caused by variants of the gene *TP63* (encoding the transcription factor p63), the typical skin and corneal lesions may be amenable to cell therapy using genetically corrected autologous stem cells. Last but not least, small molecule drugs are being increasingly used to improve the outcome of prosthodontic treatment, the longevity of dental implants, results of the surgical repair of orofacial clefts, or ocular surface regeneration. Similar small molecule therapies might also be developed for the treatment of other manifestations of ectodermal dysplasias.

Molecular therapy before birth

In hypohidrotic forms of ectodermal dysplasia, such as XLHED, the congenital absence of most if not all sweat glands (Schneider et al., 2011) causes the main clinical problem. Why is that? While exercising, for example, muscles produce heat. In response, heat sensors in the hypothalamus send a signal to the sweat glands that induces perspiration. The sweat subsequently evaporates from the skin, and this evaporation cools the body. Sweating is essential for our thermoregulation particularly during outdoor activities on sunny days, in cases of a febrile virus infections, or in hot environments. Young infants exposed to heat are at highest risk of developing a heat-related illness. If you place a newborn who cannot sweat in an incubator, his head will soon become red and warm to the touch, the respiratory rate will go up dramatically, but his body temperature will rise despite panting. Within a few hours a life-threatening situation may develop (Blüschke et al., 2010). An older child at risk of overheating will intuitively search for water, shade, or cold surfaces to cool himself down, but such opportunities may not be as readily available as needed. Being unable to sweat is life-threatening—from the hour of birth! Apart from hypo- or anhidrosis there are other cardinal symptoms of XLHED, such as missing or misshapen teeth which do not erupt on time. Oligodontia and heat intolerance are usually more severe in boys with XLHED than in affected girls because male patients have a single copy of the X chromosome that carries the disease-causing mutation, while in females the two X chromosomes most often differ in genetic content and the variant is usually expressed in only about half the cells. The absence of multiple teeth, however, allows non-invasive prenatal diagnosis as early as 5 months before birth by tooth bud counting during a routine fetal ultrasound scan (Wünsche et al., 2015; Hammersen et al., 2019).

Clinical trials of postnatal protein replacement

Individuals with XLHED lack functional EDA1, a heterotrimeric transmembrane protein of the TNF family, the signaling part of which is released by the protease furin leading to its circulation with the blood stream. For more than 15 years an international research consortium has been investigating a recombinant replacement protein that resembles natural EDA1. In this molecule named Fc-EDA, the receptor binding domains are linked by Fc fragments of immunoglobulins. It binds to the natural EDA1 receptor (EDAR) and activates the signaling cascade inducing the formation of sweat glands, hair, and teeth. Fc-EDA has been evaluated in clinical trials: first in a Phase I study in adults with XLHED who received five doses of the drug intravenously (ClinicalTrials.gov identifier: NCT01564225). Two dose cohorts were investigated, in which no relevant side effects, except for the formation of anti-drug antibodies, were observed. Then we conducted a Phase 2 dose-escalation study in infants with XLHED who were treated within 28 days after birth (ClinicalTrials.gov identifier: NCT01775462), and we assessed safety, pharmacokinetics, and efficacy of Fc-EDA. Unfortunately, almost no sweat ducts could be detected by confocal laser-

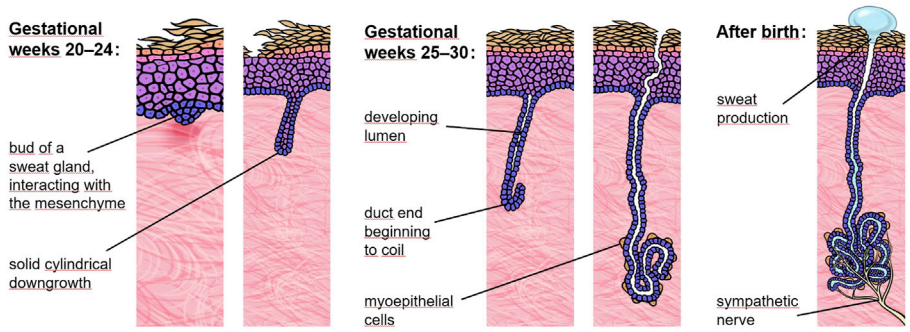

FIGURE 1
Eccrine sweat gland development. In the human fetus, eccrine sweat glands begin to form in palmoplantar skin and a bit later (around gestational week 20) across the rest of the body. At 30 weeks of gestation most sweat glands have already completed the critical portion of development but still lack sympathetic innervation.

scanning microscopy after postnatal dosing and the subjects were unable to perspirate (Körber et al., 2020). Hence, the most important aim had not been achieved. We reasoned that, if there was any chance of success, we would need to administer the drug within the natural time window of sweat gland formation.

Treatment with Fc-EDA *in utero*

In humans, eccrine sweat gland development starts around gestational week 20 with the formation of a placode in the epidermis. This placode soon undergoes solid cylindrical downgrowth into the mesenchyme (Figure 1). Once long enough, a lumen develops, the duct end begins to coil and becomes surrounded by myoepithelial cells. All these events take place in gestational weeks 20–30 (Ersch and Stallmach, 1999). Sympathetic innervation of the gland, however, is only completed postnatally. Thus, in order to rescue sweat gland formation, delivery of Fc-EDA at the end of the second trimester of pregnancy appeared to be the most rational approach. That brings us back to an essential component of our replacement protein, the Fc fragments, which allow a new drug-delivery method using the neonatal Fc receptor (FcRn). In mammals, including human babies, FcRn is situated in gut epithelia and mediates the uptake of maternal antibodies from breast milk. It binds the Fc portion of such antibodies and transports them across the intestinal epithelium into the baby's blood (Martins et al., 2016). FcRn-mediated transcytosis is already operational in the fetus in the third trimester of pregnancy when a fetus regularly swallows amniotic fluid. In *Tabby* mice, a naturally occurring animal model of XLHED, prenatal administration of Fc-EDA into the amniotic cavity of affected embryos was shown to prevent the disease completely (Hermes et al., 2014). This treatment only corrected the development of hair, teeth, and sweat glands in the presence of intact FcRn, proving that the therapeutic route of the drug is systemic rather than through a direct effect on the skin and oral epithelia (Schneider et al., 2018). In dogs with XLHED, minimally invasive delivery of Fc-EDA into the amniotic fluid also rescued the formation of skin appendages and teeth (Margolis et al., 2019).

During this time we were approached by a pregnant woman with a family history of XLHED who was concerned that the twins she was carrying would be affected. Her older son had the disease and showed a complete absence of sweat glands and perspiration. Prenatal tooth germ counting led to the diagnosis of XLHED in both male twins. We investigated the functional impact of the *EDA* variant identified in the family, c.911A>G (p.Y304C), which was demonstrated to result in an insoluble EDA1 protein with complete loss of function and, thus, represents a null mutation. The parents requested compassionate use of Fc-EDA to treat the affected dichorionic twins *in utero*. This request was considered by our team and finally approved by the ethics committee of our university hospital. Using ultrasound guidance, we administered two doses of the drug into each amniotic cavity at gestational weeks 26 and 31. Postnatally, an intriguing finding was the rise in the number of tooth germs. After treatment *in utero* we detected 10 and 8 tooth buds, respectively, whereas prenatal sonography and MRI had revealed no more than two tooth germs in either twin (Schneider et al., 2018). The untreated older brother had three teeth and one additional tooth bud in total. Even more impressive was the normal sweat-duct density on the soles of the feet, while we did not observe any sweat ducts in the untreated older brother. The twins' ability to perspire, quantified by measuring pilocarpine-induced sweat production, also proved to be normal. To date pilocarpine-

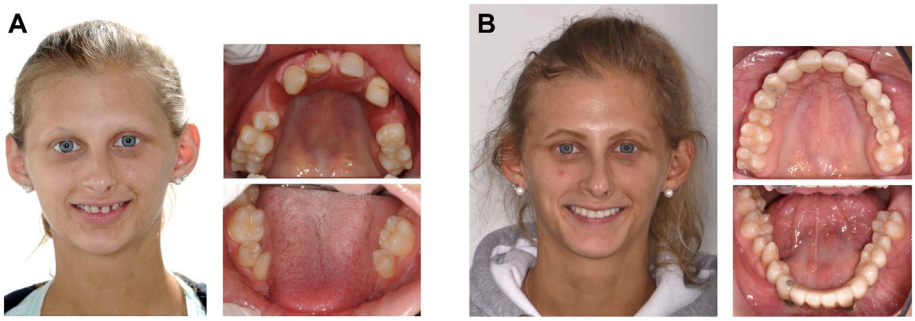

FIGURE 2
Oral rehabilitation in a woman with ectodermal dysplasia missing 14 permanent teeth. **(A)**, affected female adolescent before multidisciplinary dental treatment. **(B)**, results of prostodontic rehabilitation. (Photos: Prof. Dr. Stephan Eitner, Department of Prosthodontics, and Dr. Dr. Ines Willershausen, Department of Orthodontics and Orofacial Orthopedics, University Hospital Erlangen).

induced sweating has remained at roughly the same level. No hyperthermic episodes or XLHED-related hospitalizations have occurred. And there are good reasons to assume that once sweat glands are normally formed they will work permanently.

Half a year later we treated another affected boy who received, however, only one dose of Fc-EDA *in utero*. This boy developed slightly fewer sweat glands and produced less sweat than the treated twins, suggesting an advantage of repeated dosing (Schneider et al., 2018). Although the replacement protein was detectable in cord blood samples, confirming an efficient uptake from amniotic fluid into the fetal blood, Fc-EDA serum concentrations in the pregnant women always remained below the detection limit, indicating minimal if any maternal drug exposure. Anti-drug antibodies that had been found after intravenous administration in adult males and non-pregnant females did not appear to be elicited in the mother when Fc-EDA was delivered intra-amniotically (Körber et al., 2020). Transillumination of the treated infants' eyelids revealed a larger amount of Meibomian glands than usually present in subjects with XLHED (Schneider et al., 2018). In all three treated boys, we observed increased, basically normal saliva production. Thus, the prenatal therapy does not only rescue sweat gland development but also seems to have an impact on the function of other eccrine glands. Three more affected boys received Fc-EDA on a named-patient basis repeatedly between gestational weeks 25 and 31 and are now able to perspire as efficiently as the infants we had treated before.

The efficacy and safety of Fc-EDA (now also called ER004) as a prenatal pharmacotherapy for male subjects with XLHED is currently being investigated in a multicenter clinical trial, benefitting from the PRIME scheme of the European Medicines Agency and fast-track designation by the FDA. Up to 20 patients will be treated *in utero* with three injections of Fc-EDA, the first one at the beginning of gestational week 26. At the age of 6 months, the pilocarpine-induced sweat volume and other efficacy endpoints will be compared to data of untreated affected relatives.

Generation of replacement tissues for therapies after birth

Ectodermal dysplasias resulting from a dysfunctional p63 protein, in particular ankyloblepharon-ectodermal dysplasia-cleft lip/palate (AEC) syndrome and ectrodactyly-ectodermal dysplasia-cleft lip/palate (EEC) syndrome, are characterized by typical tissue defects. Most of the children with AEC syndrome suffer from painful skin erosions that can lead to infection, scarring, and hair loss (Siegfried et al., 2005; Maillard et al., 2019). In patients with EEC syndrome, recurrent corneal lesions are frequently observed, culminating in loss of vision (Felipe et al., 2012). The primary cause of the slow corneal healing process appears to be a malfunction and later disappearance of limbal stem cells (Di Iorio et al., 2012). Orofacial clefts that are typical manifestations of both AEC and EEC syndrome require surgical treatment of soft tissue and bone defects. Patients with many types of ectodermal dysplasia, irrespective of the molecular pathway impaired, are afflicted with a lack of teeth. Preservation of oral function includes dental implant therapy, often associated with bone augmentation prior to implant placement.

Regenerative therapies for skin and corneal lesions

In patients with AEC syndrome, treatment of chronic skin lesions based on the expansion and grafting of genetically corrected autologous keratinocytes might be feasible and has been discussed (Koch and Koster, 2021). This may involve the generation of patient-specific induced pluripotent stem cells,

correction of the disease-causing *TP63* mutation with genome editing techniques, subsequent differentiation of corrected stem cells into keratinocytes, and production of keratinocyte sheets to be transplanted onto the chronic wound, a technically very challenging and time-consuming approach. Alternatively, such keratinocyte sheets could also be produced from patient-derived epidermal stem stells, as shown recently by the successful regeneration of almost an entire, fully functional epidermis on a child with severe junctional epidermolysis bullosa (Hirsch et al., 2017; Kueckelhaus et al., 2021). In this respect, the CRISPR/Cas genome editing system may hold a lot of promise. Novel engineered CRISPR-associated endonucleases allow for much higher specificity and fewer off-target effects than previous systems, which has improved gene editing for autosomal dominant diseases that cannot be tackled by alternative allele-specific gene therapy (Caruso et al., 2022).

Similar strategies might be used to treat non-healing corneal abrasions in patients with EEC or AEC syndrome. Human limbal stem cells, which are crucial for corneal epithelial regeneration and for the maintenance of a physical barrier between the clear, avascular cornea and the vascularized conjunctiva, can be cultured *in vitro* for transplantation (Rama et al., 2010). Autologous, *ex vivo* expanded epithelial cells containing limbal stem cells were approved some years ago as an advanced-therapy medicinal product to treat severe limbal stem cell deficiency (Pellegrini et al., 2018). Regeneration of the cornea with this method has led to the recovery of vision in numerous patients and is one of the first examples of a successful stem cell therapy (Pellegrini et al., 2018; De Luca et al., 2019). Considering the healthy marriage of gene and stem cell therapy in other fields (Nogrady, 2019), I see sense in merging the two also for the treatment of p63-associated syndromes.

In addition, the small molecule drug PRIMA-1^{MET}, a p53 reactivator which has been tested in clinical trials for the treatment of malignant neoplastic disease, was recently shown to rescue epidermal differentiation and to improve wound healing in patients with AEC syndrome when applied topically to affected regions of the skin (Aberdam et al., 2020). Its mechanism of action, however, has remained unclear.

New dental treatment options

Dental care of individuals with ectodermal dysplasias is challenging, but may profit tremendously from novel biomaterials and oral rehabilitation strategies. Treatment during childhood ranges from tooth shape corrections using composite build-ups to removable partial or complete dental prostheses and orthodontic appliances. Presurgical infant orthopedics and maxillofacial surgery are required for cleft palate repair (in case of p63-associated syndromes). If many secondary teeth are absent, orthodontic space closure as well as teeth distribution to improve prosthetic restoration will be helpful. This is often accompanied by maxillofacial surgery preparing the jawbone for dental implants. Alternatively, autogenous tooth transplantation may be considered.

Present-day prosthodontic rehabilitation concepts frequently include the replacement of at least some missing teeth by endosseous implants. As a result of hypo- or even anodontia, however, the bony ridge of the jaw that normally holds the teeth in place fails to develop properly. Therefore, bone grafting is a common prerequisite for implant surgery in patients with ectodermal dysplasias (Chrcanovic, 2018). Guided alveolar ridge augmentation involves the transplantation of bone from another site of the body, donor bone, or synthetic bone substitute that is covered with a semi-permeable membrane. Natural osteogenesis then leads to a new bony base for the implant (Chrcanovic, 2018). Stability and long-term survival of dental implants depend on their osseointegration. Various small molecules with osteoinductive activity have been investigated that induce for example bone morphogenetic protein-2 signaling or the Wnt pathway. Such small molecule drugs can be administered together with biomaterials and direct the differentiation of target cells, improve survival of the newly formed tissue in the body, or stimulate endogenous stem cells to enhance tissue repair (Lu and Atala, 2014).

Today the outcome of multidisciplinary dental care is usually satisfactory and sometimes astonishing (Figure 2). This has contributed to increased self-esteem of children, adolescents, and adults with ectodermal dysplasias.

Conclusion

Therapeutic perspectives for individuals affected by ectodermal dysplasias have become exciting. Drug targeting *via* the neonatal Fc receptor may cure a so far immedicable genetic deficiency: the life-threatening inability to sweat associated with XLHED. Such treatment is efficient *in utero*, but without significant therapeutic effects if performed after birth. A pivotal clinical trial of fetal therapy that could lead to an approval of the new drug is now recruiting patients. In this study, Fc-EDA will be administered to XLHED-affected male fetuses, trying to confirm the clinical improvements we have seen in the first six boys treated *in utero*. Last but not least, the same drug delivery route might be usable for the treatment of other disorders of early development. Translational research is also paving the way to more effective regenerative therapies for skin and corneal lesions using patient-derived epidermal or limbal stem stells. Furthermore, dental treatment options based on novel biomaterials, replacement of missing jawbone, and prosthodontic rehabilitation exist that will help improve oral function in almost all individuals with ectodermal dysplasias.

Data availability statement

Access to the original data of clinical trials is restricted to protect confidential or proprietary information. The data that support the findings reported here are available from the author upon reasonable request. Requests to access these datasets should be directed to Holm Schneider, holm.schneider@uk-erlangen.de.

Ethics statement

The studies involving human participants were reviewed and approved by Ethics Commission, University of Erlangen-Nürnberg, or Clinical Ethics Committee, University Hospital Erlangen. Written informed consent to participate in this study was provided by the participants' legal guardian/next of kin. Written informed consent was obtained from the individual(s) for the publication of any potentially identifiable images or data included in this article.

Author contributions

HS wrote the manuscript.

Funding

This work has been funded by the German Federal Ministry of Education and Research (grant 01KG2008 to HS) and by the EspeRare Foundation (Switzerland).

Acknowledgments

I would like to express my deep gratitude to all my colleagues at the Center for Ectodermal Dysplasias Erlangen (CEDER), to the many collaborators involved in this work, to our public funders (Deutsche Forschungsgemeinschaft, Care-for-Rare Foundation, German Federal Ministry of Education and Research, German-Swiss-Austrian ectodermal dysplasia patient organization, National Foundation for Ectodermal Dysplasias, Forberg Foundation, EspeRare Foundation) as well as to our industry partners (Edimer Pharmaceuticals, Inc., Pierre Fabre Medicament), and particularly to the patients and their families who have supported every step of our research.

Conflict of interest

HS is inventor on a patent related to the prenatal treatment of XLHED. He signed, however, a Remuneration Waiver Agreement with the Free State of Bavaria to relinquish any personal financial gain from this invention.

Publisher's note

References

Aberdam, E., Roux, L. N., Secretan, P. H., Boralevi, F., Schlatter, J., Morice-Picard, F., et al. (2020). Improvement of epidermal covering on AEC patients with severe skin erosions by PRIMA-1(MET)/APR-246. *Cell. Death Dis.* 11, 30. doi:10.1038/s41419-020-2223-8

Blüschke, G., Nüsken, K. D., and Schneider, H. (2010). Prevalence and prevention of severe complications of hypohidrotic ectodermal dysplasia in infancy. *Early Hum. Dev.* 86, 397–399. doi:10.1016/j.earlhumdev.2010.04.008

Caruso, S. M., Quinn, P. M. J., Lopes da Costa, B., and Tsang, S. H. (2022). CRISPR/Cas therapeutic strategies for autosomal dominant disorders. *J. Clin. Invest.* 132, e158287. doi:10.1172/JCI158287

Chrcanovic, B. (2018). Dental implants in patients with ectodermal dysplasia: A systematic review. *J. Craniomaxillofac. Surg.* 46, 1211–1217. doi:10.1016/j.jcms.2018.05.038

Cui, C. Y., Yin, M., Sima, J., Childress, V., Michel, M., Piao, Y., et al. (2014). Involvement of Wnt, Eda and Shh at defined stages of sweat gland development. *Development* 141, 3752–3760. doi:10.1242/dev.109231

De Luca, M., Aiuti, A., Cossu, G., Parmar, M., Pellegrini, G., and Robey, P. G. (2019). Advances in stem cell research and therapeutic development. *Nat. Cell. Biol.* 21, 801–811. doi:10.1038/s41556-019-0344-z

Di Iorio, E., Kaye, S. B., Ponzin, D., Barbaro, V., Ferrari, S., Bohm, E., et al. (2012). Limbal stem cell deficiency and ocular phenotype in ectrodactyly-ectodermal dysplasia-clefting syndrome caused by p63 mutations. *Ophthalmology* 119, 74–83. doi:10.1016/j.ophtha.2011.06.044

Ersch, J., and Stallmach, T. (1999). Assessing gestational age from histology of fetal skin: An autopsy study of 379 fetuses. *Obstet. Gynecol.* 94, 753–757. doi:10.1016/s0029-7844(99)00379-8

Felipe, A. F., Abazari, A., Hammersmith, K. M., Rapuano, C. J., Nagra, P. K., and Peiro, B. M. (2012). Corneal changes in ectrodactyly-ectodermal dysplasia-cleft lip and palate syndrome: Case series and literature review. *Int. Ophthalmol.* 32, 475–480. doi:10.1007/s10792-012-9585-6

Freire-Maia, N. (1971). Ectodermal dysplasias. *Hum. Hered.* 21, 309–312. doi:10.1159/000152419

Gaide, O., and Schneider, P. (2003). Permanent correction of an inherited ectodermal dysplasia with recombinant EDA. *Nat. Med.* 9, 614–618. doi:10.1038/nm861

Hammersen, J., Wohlfart, S., Goecke, T., Köninger, A., Stepan, H., Gallinat, R., et al. (2019). Reliability of prenatal detection of X-linked hypohidrotic ectodermal dysplasia by tooth germ sonography. *Prenat. Diagn.* 39, 796–805. doi:10.1002/pd.5384

Harris, M. P., Rohner, N., Schwarz, H., Perathoner, S., Konstantinidis, P., and Nüsslein-Volhard, C. (2008). Zebrafish eda and edar mutants reveal conserved and ancestral roles of ectodysplasin signaling in vertebrates. *PLoS Genet.* 4, e1000206. doi:10.1371/journal.pgen.1000206

Hermes, K., Schneider, P., Krieg, P., Dang, A., Huttner, K., and Schneider, H. (2014). Prenatal therapy in developmental disorders: Drug targeting via intra-amniotic injection to treat X-linked hypohidrotic ectodermal dysplasia. *J. Invest. Dermatol.* 134, 2985–2987. doi:10.1038/jid.2014.264

Hirsch, T., Rothoeft, T., Teig, N., Bauer, J. W., Pellegrini, G., De Rosa, L., et al. (2017). Regeneration of the entire human epidermis using transgenic stem cells. *Nature* 551, 327–332. doi:10.1038/nature24487

Jia, S., Zhou, J., Fanelli, C., Wee, Y., Bonds, J., Schneider, P., et al. (2017a). Small-molecule Wnt agonists correct cleft palates in *Pax9* mutant mice *in utero*. *Development* 144, 3819–3828. doi:10.1242/dev.157750

Jia, S., Zhou, J., Wee, Y., Schneider, P., and D'Souza, R. N. (2017b). Anti-EDAR agonist antibody therapy resolves palate defects in Pax9-/- mice. *J. Dent. Res.* 96, 1282–1289. doi:10.1177/0022034517726073

Koch, P. J., and Koster, M. (2021). Rare genetic disorders: Novel treatment strategies and insights into human biology. *Front. Genet.* 12, 714764. doi:10.3389/fgene.2021.714764

Körber, I., Klein, O., Morhart, P., Faschingbauer, F., Grange, D., Clarke, A., et al. (2020). Safety and immunogenicity of Fc-EDA, a recombinant ectodysplasin A1 replacement protein, in human subjects. *Br. J. Clin. Pharmacol.* 86, 2063–2069. doi:10.1111/bcp.14301

Kueckelhaus, M., Rothoeft, T., De Rosa, L., Yeni, B., Ohmann, T., Maier, C., et al. (2021). Transgenic epidermal cultures for junctional epidermolysis bullosa – 5-year outcomes. *N. Engl. J. Med.* 385, 2264–2270. doi:10.1056/NEJMoa2108544

Lu, B., and Atala, A. (2014). Small molecules and small molecule drugs in regenerative medicine. *Drug Discov. Today* 19, 801–808. doi:10.1016/j.drudis.2013.11.011

Maillard, A., Alby, C., Gabison, E., Doan, S., Caux, F., Bodemer, C., et al. (2019). P63-related disorders: Dermatological characteristics in 22 patients. *Exp. Dermatol.* 28, 1190–1195. doi:10.1111/exd.14045

Margolis, C. A., Schneider, P., Huttner, K., Kirby, N., Houser, T. P., Wildman, L., et al. (2019). Prenatal treatment of X-linked hypohidrotic ectodermal dysplasia using recombinant ectodysplasin in a canine model. *J. Pharmacol. Exp. Ther.* 370, 806–813. doi:10.1124/jpet.118.256040

Martins, J. P., Kennedy, P. J., Santos, H. A., Barrias, C., and Sarmento, B. (2016). A comprehensive review of the neonatal Fc receptor and its application in drug delivery. *Pharmacol. Ther.* 161, 22–39. doi:10.1016/j.pharmthera.2016.03.007

Mikkola, M. (2007). p63 in skin appendage development. *Cell. Cycle* 6, 285–290. doi:10.4161/cc.6.3.3798

Mikkola, M., and Thesleff, I. (2003). Ectodysplasin signaling in development. *Cytokine Growth Factor Rev.* 14, 211–224. doi:10.1016/s1359-6101(03)00020-0

Nogrady, B. (2019). Stem-cell and genetic therapies make a healthy marriage. *Nature* 569, S23–S25. doi:10.1038/d41586-019-01442-w

Pagnan, N. A. B., and Visinoni, Á. F. (2014). Update on ectodermal dysplasias clinical classification. *Am. J. Med. Genet. A* 164, 2415–2423. doi:10.1002/ajmg.a.36616

Pellegrini, G., Ardigo, D., Milazzo, G., Iotti, G., Guatelli, P., Pelosi, D., et al. (2018). Navigating market authorization: The path holoclar took to become the first stem cell product approved in the European union. *Stem Cells Transl. Med.* 7, 146–154. doi:10.1002/sctm.17-0003

Peschel, N., Wright, J. T., Koster, M. I., Clarke, A. J., Fete, M., Hadj-Rabia, S., et al. (submitted). Molecular pathway-based classification of ectodermal dysplasias: first five-yearly update. *Genes.* submitted.

Rama, P., Matuska, S., Paganoni, G., Spinelli, A., De Luca, M., and Pellegrini, G. (2010). Limbal stem-cell therapy and long-term corneal regeneration. *N. Engl. J. Med.* 363, 147–155. doi:10.1056/NEJMoa0905955

Schneider, H., Faschingbauer, F., Schuepbach-Mallepell, S., Korber, I., Wohlfart, S., Dick, A., et al. (2018). Prenatal correction of X-linked hypohidrotic ectodermal dysplasia. *N. Engl. J. Med.* 378, 1604–1610. doi:10.1056/NEJMoa1714322

Schneider, H., Hammersen, J., Preisler-Adams, S., Huttner, K., Rascher, W., and Bohring, A. (2011). Sweating ability and genotype in individuals with X-linked hypohidrotic ectodermal dysplasia. *J. Med. Genet.* 48, 426–432. doi:10.1136/jmg.2010.084012

Siegfried, E., Bree, A., Fete, M., and Sybert, V. P. (2005). Skin erosions and wound healing in ankyloblepharon-ectodermal defect-cleft lip and/or palate. *Arch. Dermatol.* 141, 1591–1594. doi:10.1001/archderm.141.12.1591

Thesleff, I. (2003). Developmental biology and building a tooth. *Quintessence Int.* 34, 613–620.

Watanabe, M., Kim, A. G., and Flake, A. W. (2015). Tissue engineering strategies for fetal myelomeningocele repair in animal models. *Fetal diagn. Ther.* 37, 197–205. doi:10.1159/000362931

Wright, J. T., Fete, M., Schneider, H., Zinser, M., Koster, M. I., Clarke, A. J., et al. (2019). Ectodermal dysplasias: Classification and organization by phenotype, genotype and molecular pathway. *Am. J. Med. Genet. A* 179, 442–447. doi:10.1002/ajmg.a.61045

Wünsche, S., Jüngert, J., Faschingbauer, F., Mommsen, H., Goecke, T., Schwanitz, K., et al. (2015). Noninvasive prenatal diagnosis of hypohidrotic ectodermal dysplasia by tooth germ sonography. *Ultraschall Med.* 36, 381–385. doi:10.1055/s-0034-1384933

frontiers | Frontiers in Genetics

TYPE Review
PUBLISHED 07 October 2022
DOI 10.3389/fgene.2022.987867

OPEN ACCESS

EDITED BY
Jordi Pérez-Tur,
Institute of Biomedicine of Valencia (CSIC), Spain

REVIEWED BY
Michael G. Fehlings,
Toronto Western Hospital, Canada
Caterina Licini,
Università Politecnica delle Marche, Italy

*CORRESPONDENCE
Jácome Bruges-Armas,
brugesarmas@gmail.com

†These authors have contributed equally to this work

SPECIALTY SECTION
This article was submitted to Genetics of Common and Rare Diseases, a section of the journal Frontiers in Genetics

RECEIVED 06 July 2022
ACCEPTED 16 September 2022
PUBLISHED 07 October 2022

CITATION
Couto AR, Parreira B, Power DM, Pinheiro L, Madruga Dias J, Novofastovski I, Eshed I, Sarzi-Puttini P, Pappone N, Atzeni F, Verlaan J-J, Kuperus J, Bieber A, Ambrosino P, Kiefer D, Khan MA, Mader R, Baraliakos X and Bruges-Armas J (2022), Evidence for a genetic contribution to the ossification of spinal ligaments in Ossification of Posterior Longitudinal Ligament and Diffuse idiopathic skeletal hyperostosis: A narrative review. *Front. Genet.* 13:987867. doi: 10.3389/fgene.2022.987867

Evidence for a genetic contribution to the ossification of spinal ligaments in Ossification of Posterior Longitudinal Ligament and Diffuse idiopathic skeletal hyperostosis: A narrative review

Ana Rita Couto[1,2†], Bruna Parreira[1,2†], Deborah M. Power[3], Luís Pinheiro[4], João Madruga Dias[5,6], Irina Novofastovski[7], Iris Eshed[8], Piercarlo Sarzi-Puttini[9], Nicola Pappone[10], Fabiola Atzeni[11], Jorrit-Jan Verlaan[12], Jonneke Kuperus[13], Amir Bieber[7], Pasquale Ambrosino[14], David Kiefer[15], Muhammad Asim Khan[16], Reuven Mader[7,17,18], Xenofon Baraliakos[18] and Jácome Bruges-Armas[1,2*]

[1]Hospital de Santo Espirito da Ilha Terceira EPER, SEEBMO, Angra do Heroísmo, Portugal, [2]CHRC Campus Nova Medical School, Lisboa, Portugal, [3]University of Algarve, Center of Marine Science (CCMAR), Faro, Portugal, [4]Hospital de Santo Espirito da Ilha Terceira EPER, Orthopedics Service, Angra do Heroísmo, Portugal, [5]Centro Hospitalar Do Medio Tejo EPE Unidade de Torres Novas, Rheumatology Department, Santarém, Portugal, [6]CHRC Campus Nova Medical School, EpiDoc Research Unit, CEDOC, Lisboa, Portugal, [7]Emek Medical Center, Rheumatology Unit, Afula, Israel, [8]Sheba Medical Center, Tel Aviv, Israel, [9]Luigi Sacco University Hospital, Rheumatology Unit, Milano, Italy, [10]Istituti Clinici Scientifici Maugeri IRCCS, Neuromotor Rehabilitation Unit of Telese Terme Institute, Pavia, Italy, [11]Universita Degli Studi di Messina, Rheumatology Unit, Clinical and Experimental Medicine, Messina, Italy, [12]University Medical Centre, Department of Orthopedics, Utrecht, Netherlands, [13]Universitair Medisch Centrum Utrecht, Utrecht, Netherlands, [14]Istituti Clinici Scientifici Maugeri IRCCS, Cardiac Rehabilitation Unit of Telese Terme Institute, Pavia, Italy, [15]Ruhr-Universitat Bochum, Rheumazentrum Ruhrgebiet, Bochum, Germany, [16]Case Western Reserve University, Cleveland, OH, United States, [17]Rappaport Faculty of Medicine, Technion, Haifa, Israel, [18]Ruhr University Bochum, Rheumazentrum Ruhrgebiet, Herne, Germany

Diffuse Idiopathic Skeletal Hyperostosis (DISH) and Ossification of the Posterior Longitudinal Ligament (OPLL) are common disorders characterized by the ossification of spinal ligaments. The cause for this ossification is currently unknown but a genetic contribution has been hypothesized. Over the last decade, many studies on the genetics of ectopic calcification disorders have been performed, mainly on OPLL. Most of these studies were based on linkage analysis and case control association studies. Animal models have provided some clues but so far, the involvement of the identified genes has not been confirmed in human cases. In the last few years, many common variants in several genes have been associated with OPLL. However, these associations have not been at definitive levels of significance and evidence of functional significance is generally modest. The current evidence suggests a multifactorial aetiopathogenesis for DISH and OPLL with a subset of cases showing a stronger genetic component.

KEYWORDS

ossification, genetics, ectopic calcification, diffuse idiopathic skeletal hyperostosis, ossification of posterior longitudinal ligament

1 Introduction

The spine is a columnar structure composed of bony vertebrae interconnected by intervertebral discs and supported by ligaments, such as the anterior and posterior longitudinal ligaments, ligament nuchae and ligamentum flavum. The spinal canal, enclosed within the foramen of the vertebrae, contains the spinal cord. In the intervertebral spaces, the canal is protected by the ligament flavum posteriorly and the posterior longitudinal ligament anteriorly. Spinal stenosis consists in the reduction of the area of the spinal canal, leading to motor neuron deficits and related neurological symptoms, depending on the location of the stenosis (Bai et al., 2022). In the elderly population, the most common cause of spinal cord impairment is the degenerative cervical myelopathy (DCM). DCM can be secondary to osteoarthritic degeneration or to ligamentous ossifications such as the Ossification of the Posterior Longitudinal Ligament (OPLL) or the ossification of the Ligament Flavum (OLF) (Nouri et al., 2015). OPLL, frequently in association with DISH, can result in various degrees of neurological complications that can range from a slowly progressive painless myelopathy to a rapid progression of a neurological deficit even after minor injury (Takayuki et al., 2021; Prabhu et al., 2022). The physical and socioeconomic burden of disability associated with DCM is expected to grow evenly, due to the ageing population (Badhiwala et al., 2020). It is thus crucial to improve the diagnosis and assessment of disorders involved in DCM for early detection and swift intervention.

This review will focus on genetic studies of the ossification of the anterior and posterior longitudinal ligaments, the Diffuse Idiopathic Skeletal Hyperostosis (DISH) [MIM: 106400] and the Ossification of the Posterior Longitudinal Ligament (OPLL) [MIM: 602475], respectively. A short outline of DISH, OPLL and OLF can be seen in Table 1. These conditions may co-occur in some patients suggesting possible common etiopathogenic factors (Nouri et al., 2015; Takayuki et al., 2021). The objective was to collect and present evidences that supports a genetic foundation, based on the following observations: 1) familial aggregation reports, 2) animal models, 3) associated genetic variants and 4) genetics of associated disorders.

2 Familial aggregation reports

2.1 DISH

Reports of familial DISH are scarce. Beardwell, A. in 1969 (Beardwell, 1969), describes a family with Ankylosing Vertebral Hyperostosis (AVH), by the third decade, with many family members also presenting tylosis (punctuate hyperkeratosis). As demonstrated by the author, the X-ray of the affected family members showed ossification of paraspinal distribution, mainly in the lower thoracic region and also some osteophytosis and marginal sclerosis of the sacroiliac joints.

TABLE 1 Brief characterization, main symptoms and epidemiology of DISH, OPLL and OLF.

Disorder	Characterized by	Main symptom	Epidemiology
DISH	Calcification and ossification of the anterior longitudinal ligament affecting, in particular, the right side of the spine with preservation of the intervertebral disc space. Peripheral joints, such as elbow, shoulder, hip, knee and heel are commonly affected (Okazaki et al., 1976; Gorman et al., 2005; Bruges-Armas et al., 2006; Couto et al., 2017; Parreira et al., 2020)	Dysphagia (Beardwell, 1969). Axial pain, elbow, knee and metacarpophalangeal pain, swelling and deformity (Okazaki et al., 1976)	Elderly males are mostly affected. DISH prevalence is 17.6% using x-ray and ranges from 17.4% to 27,2% using computed tomography [33, (Ikuma et al., 2022)
OPLL	Ectopic hyperostosis and calcification of the posterior longitudinal ligament at the cervical, thoracic and lumbar spine (Fornaciari et al., 2009)	Myelopathy and/or radiculopathy (Fornaciari and Giuffra, 2013)	More common in males of asian populations, with a prevalence of 2–4% in japan as compared with 0.01–2% in non-Asian populations (Matsunaga et al., 2006)
OLF	Calcification of the ligamentum flavum (LF) not extending to the closed spinal bony arch (Yamagami et al., 2000). Calcium pyrophosphate dehydrate (CPPD) and hidroxyapatite are thought to be main players in this calcification (Ellman et al., 1978; Brown et al., 1991)	Thoracic myelopathy and spinal stenosis (Miyasaka et al., 1982)	Higher prevalence in males of Asian populations, especially the Japanese, with the incidence of 12% in thoracic OLF (Caswell et al., 1987)

Another report of familial DISH, described 2 families; one had 4 siblings showing AVH by the fourth decade and two other family members had probably AVH. The second family was dentified after hip surgery of two sisters aged 71 and 82 years. The proband had five daughters, two of them affected by AVH and other two with a mild phenotype, classified as possible AVH (Abiteboul et al., 1985). An unusual DISH-like phenotype was described in a family with severe cervical disease lacking the extensive dorsal involvement (Gorman et al., 2005).

In Azores region, twelve families were identified presenting early onset (third decade) of DISH and/or Chondrocalcinosis (CC). The affected members had a pyrophosphate arthropathy showing exuberant axial and peripheral enthesopathic calcifications, meaning calcification of the connective tissues in the attachments of tendons or ligaments to the bones, in joints other than the spine (Bruges-Armas et al., 2006). Genetic studies in these families suggest that the phenotype DISH/CC is polygenic and influenced by the interaction of several, small-effect gene variants and possibly by unidentified environmental factors (Couto et al., 2017; Parreira et al., 2020). Similar cases, of patients with CPPD and/or CC and DISH, were mentioned in other studies (Okazaki et al., 1976), also showing familial aggregation (van der Korst et al., 1974; Bruges-Armas et al., 2006).

A postmortem examination of a skeleton allowed the diagnosis of DISH and ankylosing spondylitis in the same patient (Jordana et al., 2009). An extensive radiographic survey on several members of the Medici family (15th–17th century), demonstrated that DISH, rheumatoid arthritis and uric acid gout affected several family members (Fornaciari et al., 2009; Fornaciari and Giuffra, 2013). A study of 13 royal Egyptian mummies detected ossifications at the anterior aspects of the spines in five male mummies but only four fulfilled the criteria for DISH (Saleem and Hawass, 2014).

2.2 OPLL

The cause of OPLL is unclear but people of Asian heritage, have a higher likelihood of developing this condition (Choi et al., 2011). Familial aggregation of cervical OPLL was first demonstrated in a study assessing 347 families (Terayama, 1989); the relative risk of first degree relatives came to have OPLL was five times greater than expected in the general population. Another study shows a prevalence of 27% with a relative risk seven times that of the general population (Tanikawa et al., 1986). Other OPLL familial cases included the report of familial thoracic OPLL in Caucasian siblings (Tanabe et al., 2002) (Terayama, 1989).

The mode of inheritance for OPLL is still poorly defined due to the absence of large families, late onset of the disorder, environmental effects and sex differences (Koga et al., 1998). However, segregation studies shows that OPLL have both autosomal dominant (Tanikawa et al., 1986) and autosomal recessive (Hamanishi et al., 1995) patterns of inheritance. As discussed later, ectopic ossification resembling OPLL, as seen in the tiptoe walking mouse (ttw) or also called tiptoe walking of Yoshimura (twy), is inherited as an autosomal recessive disease with complete penetrance (Ikegawa et al., 2007).

3 Animal models for Ossification of Spinal Ligaments

The study of mouse strain models and the progress of strategies to find genetic mutations, affecting the mineralization pattern, have permitted the discovery of many genes and proteins to be evaluated.

3.1 DISH

Natural cases—unknown gene

Some natural cases of DISH have been observed in dogs (Kranenburg et al., 2010; Kranenburg et al., 2014; Togni et al., 2014; Bossens et al., 2016) and, as in humans, the disease is more common in older male animals and is more frequent in the boxer breed (Kranenburg et al., 2010). The high occurrence of DISH in one dog breed and the low or absence occurrence in the other breeds is suggestive of a genetic mechanism (Ostrander et al., 2000). In 2016 Bossens et al. (2016), reported the presence of DISH, in a nine year old female cat. According to the authors the phenotype was very similar to canine DISH displayed contiguous ossification ventral and lateral to the vertebra prolonging from thoracic area to the lumbosacral junction. As far as we know, there are no reports of OPLL in dogs or other types of companion animals

Gene involved in humans—*ENT1*

ENT1 (6p21.1) in humans is known as solute carrier family 29 member 1 (***SLC29A1***). The gene encodes one of the four equilibrative nucleoside transporters which transfers hydrophilic nucleosides across the plasma membrane (Bicket et al., 2016). The protein is ubiquitously expressed and is involved in purine metabolism being responsible for transporting the majority of adenosine. It is known that adenosine signaling regulate bone formation (Carroll et al., 2012). Currently no human phenotype or disease has been directly linked with this gene

ENT1$^{-/-}$ *mice*

Mice lacking *ENT1* (*ENT1*$^{-/-}$) exhibit progressive ectopic calcification of the paraspinal tissues in the cervical and thoracic area homologous to human DISH. In intervertebral discs, these mice also present a significant downregulation of *Enpp1*, *Ank* and *Alpl* genes (Warraich et al., 2013). Another study, showed that *ENT1*–/– mice presented low bone density in the midshaft of the femur and in the lower half of the spinal column. Additionally, the authors confirmed that ***ENT1***$^{-/-}$ mice presented osteoid formations in the thoracic and cervical portions of the spinal column (Hinton et al., 2014)

3.2 OPLL

Gene involved—*ENPP1*
In humans, *ENPP1* (6q23.2) encodes one of the seven members of the ectonucleotide pyrophosphate phosphodiesterase family (Buckley et al., 1990). ENPP1 is a membrane glycoprotein responsible to hydrolysing extracellular nucleotide triphosphates (ATP) to generate pyrophosphate, thereby working as a physiological inhibitor of calcification (Stefan et al., 2005) (Kato et al., 2012). The protein is expressed in various tissues, including bone and cartilage (Caswell et al., 1987; Caswell and Russell, 1988). Some human diseases are linked to this gene. It is known that mutations in *ENPP1* gene are the cause of Generalized arterial Calcification of Infancy (GACI) (Rutsch et al., 2003), Hypophosphatemic rickets (Levy-Litan et al., 2010), Cole disease (Eytan et al., 2013) and Pseudoxanthoma elasticum, since in some GACI cases, mutations in *ENPP1* also caused a characteristic pseudoxanthoma skin lesions and angioid streaks of the retina (Nitschke and Rutsch, 2012)
Twy walking Yoshimura mouse
The spinal hyperostotic mouse twy develop spontaneous ossification of the spinal ligaments very similar to human OPLL. The ossification also occurs in joint capsules, chondral tissues, tendon entheses and peripheral ligaments (Yamazaki et al., 1991) (Okawa et al., 1998). The twy phenotype is caused by a nonsense mutation in *NPPS* also called *ENPP1* gene, resulting in a minor expression and consequently less protein activity (Okawa et al., 1998). According to Hajjawi et al. (2014), *ENPP1*$^{-/-}$ knock-out mice also shown a lower bone density and calcification of joints, vertebrae and soft tissues including trachea, ear pinna and whisker follicles.This mouse model has also been used for studies on the contribution of Fas-mediated cell death and inflammation to the pathobiology of cervical spondylotic myelopathy (Yu et al., 2011)
Gene involved - *LEP/LEPR*
In humans, *LEP* (7q32.1) encodes a protein responsible to regulate energy homeostasis. The protein is related to bone metabolism since is a potent inhibitor of bone *in vivo* (Elefteriou et al., 2004). In female mice, the protein promotes the transdifferentiation of vascular smooth muscle cells to osteoblasts by increasing RANKL expression (Liu et al., 2014) In humans, mutations in *LEP* gene cause morbid obesity (Montague et al., 1997)
ZFR rat
The Zucker fatty rat (ZFR) was originally used to study obesity, hyperinsulinemia, hypercholesterolemia and hyperlipidemia. This murine model also displays ossification of the spinal ligaments, histopathologically similar to human OPLL (Okano et al., 1997). The ZFR phenotype is caused by a mutation in the leptin receptor gene (*LEPR*) (Phillips et al., 1996)

4 Genetic variants associated with OSL in humans

4.1 Genetic studies of DISH

Some of the earliest genetic studies were performed on genes belonging to Major Histocompatibility complex, specifically Human Leucocyte Antigens (HLA) (Brewerton et al., 1973; Schlosstein et al., 1973), but this association was never confirmed.

In a small study, polymorphisms of the Collagen Type I Iα1 (COL1A1), and Vitamin D Receptor (VDR) were investigated, but the authors concluded that these genes do not seem to be related to DISH etiology (Havelka et al., 2002). One more study, investigated polymorphisms of the collagen 6A1 gene (*COL6A1*) in Czech and Japanese DISH patients and the polymorphism, in intron 32, was associated with the disorder in Japanese patients but failed the association test with DISH Czech patients (Table 2). However, the authors suggested that *COL6A1* could be related to ectopic bone formation in spinal ligaments (Tsukahara et al., 2005). Due to the possible common aetiopathogenesis of OPLL and DISH, a genotyping study (intron 6; −4) on the *COL11A2* gene was performed, and no significant difference was observed between both cohorts (Havelka et al., 2001). Jun et al (Jun and Kim, 2012) described that two polymorphisms in the *FGF2* gene were associated with DISH (Table 2). Another study identified a genetic variant in the *PPP2R2D* gene significantly associated with a phenotype characterized by DISH and CC. It was proposed that *PPP2R2D* may contribute to the development of this disorder (Parreira et al., 2020). Although these variants are significantly associated with DISH, the direct evidence for pathogenicity is lacking.

4.2 Genetic studies in OPLL

Many genetic studies of OPLL have been performed and it is now well established that genetic factors are implicated in its etiology (Terayama, 1989) (Table 3). In the same way as DISH, the initial genetic studies of OPLL were performed on HLA and the possible association is much discussed in the literature (Sakou et al., 1991; Yamaguchi, 1991; Matsunaga et al., 1999). Very close to the HLA region on the chromosome 6 is *COL11A2* and common variants of this gene have been associated with OPLL (Koga et al., 1998; Maeda et al., 2001a). The

TABLE 2 Genes and genetic variants associated with DISH. The protein physiological function is also mentioned. Gene function was obtained from GeneCards database.

Gene	Chr	Gene function	Type of study	SNVs	Molecular mechanism	Ref
COL6A1	21	Collagen VI is a main structural component of microfibrils. Mutations in this gene may result in Bethlem Myopathy	Case control association study in Japanese individuals (97 DISH patients and 298 controls)	rs2236486 (p = 0.0022)	Frequent polymorphism (MAF 0.39) Unclear association	Tsukahara et al. (2005)
FGF2	4	FGF2 protein has been involved in diverse biological processes, such as limb and nervous system development, tumour growing and wound healing	Case control association study (154 OPLL patients -3 patients with DISH)	rs1476217 (p = 0.003) rs3747676 (p = 0.002)	3 prime UTR variant (MAF 0.48) 3 prime UTR variant (MAF 0.35)Unclear association	Jun and Kim, (2012)
PPP2R2D	10	PPP2R2D protein is a crucial serine/threonine protein phosphatase that controls basal cellular activities by dephosphorylating substrates. Its is known that phosphatases influence the transforming growth factor beta (TGF-beta) superfamily signalling, which regulates numerous cellular responses	Whole exome sequencing (4 patients) and case control study (n = 65)	rs34473884 (p = 0.028)	Missense variant (MAF 0.18) Unclear association	Parreira et al. (2020)

polymorphism in intron 6 (-4A) seems to confer protection to OPLL furthermore, it was proven that this polymorphism of *COL11A2* affects the splicing of exon 6 in cells obtained from spinal ligaments from OPLL patients (Maeda et al., 2001b).

According to Nakamura et al. (1999) the deletion of T, 11 nucleotides upstream of the splice acceptor site of intron 20 (IVS20-11delT) of *ENPP1* is associated with OPLL. However, He et al. (2013) described that the polymorphism TT genotype of C973T and IVS15-14T as well as the wild type IVS20 (lack of deletion) were related with disease severity. Another study found a polymorphism (IVS15-14T-- > C) in *ENPP1* gene associated with OPLL susceptibility and severity (Koshizuka et al., 2002). Interestingly, in one study the authors found that the ENPP1 variant (IVS20-11delT) and the SNP (A861G) in the leptin receptor gene (LEPR) were more frequent in OPLL patients affected in the thoracic spine compared to patients whose OPLL was restricted to cervical spine. The authors suggested that the two variants (IVS20-11delT and A861G) are associated with more extensive OPLL, but not with frequency of its occurrence (Tahara et al., 2005).

The *COL6A1* gene is intensely associated to OPLL and polymorphisms in this gene are considered useful markers of OPLL (Tanaka et al., 2003; Kong et al., 2007; Wang et al., 2018a). However this association is not always confirmed in all the studies performed (Furushima et al., 2002; Liu et al., 2010). Polymorphisms in *COL6A1* gene were associated with DISH in the Japanese population (Tsukahara et al., 2005) suggesting that *COL6A1* may contribute in pathological ectopic ossification.

Positive associations of *BMP2,* an important regulator of bone metabolism, with OPLL were found with the SNPs rs3178250 (Wang et al., 2008), rs2273073 (Chen et al., 2008; Yan et al., 2013) and rs1949007 (Chen et al., 2008) (Table 3). Yan et al. (2013), confirmed that the SNP rs227373 in the *BMP2* gene is associated with the higher level of Smad4 protein expression and with activity of alkaline phosphatase. On the other hand, according to Kim et al. (2014a) the SNPs rs2273073 and rs1949007, in Korean patients, are not associated with OPLL. Other study (Liu et al., 2010), performed in Chinese Han population, also failed to show association between *BMP2* gene and OPLL. A genome-wide linkage study performed with 214 OPLL affected sib-pairs identified a chromosome region (20p12), linked with OPLL (Karasugi et al., 2013). This region contains 25 genes, of which two are good candidates: Jagged 1 (*JAG1*), which is involved in endochondral bone formation (Nobta et al., 2005) and *BMP2*. Furthermore, deleterious coding variants of *BMP2* in peripheral blood samples was recently demonstrated (Chen et al., 2016). Three other polymorphisms (rs996544, rs965291 and rs1116867) were screened in Han Chinese subjects and the authors found that rs1116867 and rs965291 were related with the manifestation and extend of OPLL (Yan et al., 2010).

Other bone morphogenetic protein genes have been associated with OPLL; two SNPs in *BMP-9* were found to be associated with OPLL: rs75024165 and rs34379100 (Ikuma et al., 2022). *BMP-4* SNPs rs17563 (Mader et al., 2013; Cudrici et al., 2021), rs76335800 and a specific haplotype, TGGGCTT (Mader et al., 2013), were identified as risk factors for developing OPLL in the Chinese population. Furushima et al. (Ramos et al., 2015) also confirmed the association of *BMP-4* with OPLL, in a large scale screening study, in which only *BMP-4* reached criteria of suggestive evidence of linkage. In a recent study, BMP-4 has even been proposed as a new therapeutic option for treating bone diseases due to its role on a RUNX2/CHRDLI/BMP4 pathway. Several SNPs in gene

TABLE 3 Genes and genetic variants associated with OPLL predisposition. The protein physiological function is also mentioned. Protein function was obtained from GeneCards database.

Gene	Chr	Physiological function	Study type	SNP ID - significantly associated	Association explained?	References
IL-1β	2	Stimulates thymocyte proliferation by promoting the IL-2 release, B-cell maturation and proliferation and fibroblast growth factor activity	Case-control association study with 120 OPLL (43 Female) patients and 306 controls (140 Female) (unrelated Japanese)	*IL1B AbaI* variant (gender specific—female) (p = 0.001)	Intronic polymorphism	Ogata et al. (2002)
			Assessed 5 candidate gene polymorphisms		Unclear association	
AHSG	3	Promotes endocytosis, possesses opsonic properties and influences the mineral phase of bone. AHSG protein have affinity for barium ions and calcium	Large Scale Case-control study in Japanese individuals. 711 OPLL patients and 896 controls	rs2077119 (p = 0.0011)	SNP in Promoter region	Horikoshi et al. (2006)
			Assessed 35 candidate genes; 109 SNPs		MAF 0.36 Unclear association	
ACE	17	Angiotensin converting enzyme-2 is important in the renin-angiotensin system	Case control association study in Korean individuals. 95 OPLL patients and 274 controls	rs4646994 (genotype DD p < 0.001; D allele p = 0.009)	SNP in intronic region	Kim et al. (2014b)
			Assessed I/D polymorphism in *ACE*		Unclear association	
BMP2	20	Induces bone and cartilage formation; member of TGFβ superfamily	Case control study with 192 OPLL patients and 304 controls	rs3178250 (p = 0.003 gender specific—males)	3 prime UTR variant	Wang et al. (2008)
			Assessed 2 SNPs in Exon 3 of BMP2		MAF 0.27 Unclear association	
			Case control study with 57 OPLL patients and 135 controls	rs2273073 (p <0.001) susceptibility to OPLL	Missense variant	Chen et al. (2008)
			Assessed 2 SNPs in exon 2 of *BMP2* gene	rs1049007 (p=<0.001) severity of OPLL	MAF 0.03 Synonymous variant MAF 0.25 Unclear association	
			Case control study with 420 OPLL patients and 506 controls	rs2273073 (p < 0.001)	Missense mutation (MAF 0.03)	Yan et al. (2013)
			Assessed all coding sequencing of *BMP2* gene	rs235768 (p = 0.005)	Missense—Deleterious (MAF 0.23) This study provides evidence that the mutation (rs2273073) is associated with level of Smad4 protein expression and activity of ALP.	
BMP4	14	BMP4 protein promotes bone and cartilage formation	Nonparametric linkage study with 126 affected sib-pairs	Only *BMP4* gene reached criteria of suggestive evidence of linkage (NPL = 2.23; p = 0.035)	Molecular variants not identified	Furushima et al. (2002)
			Used microsatellite markers in 88 candidate genes		Unclear association	
			Case control association study in Chinese individuals. 179 OPLL patients and 298 controls	rs17563 (genotype: p = 0.039; Allele: p = 0.014)	Missense variant	Meng et al. (2010)
			Assessed 2 polymorphisms in *BMP4* gene		MAF 0.33Unclear Association	
			Association study in Chinese individuals. 450 OPLL patients and 550 matched controls	rs17563	Missense variant	Ren et al. (2012a)
				rs76335800	MAF 0.33 (benign)	
					3 prime UTR variant MAF 0.30 (Benign)	
			Complete genomic *BMP4* coding		Unclear association	

(Continued on following page)

TABLE 3 (*Continued*) Genes and genetic variants associated with OPLL predisposition. The protein physiological function is also mentioned. Protein function was obtained from GeneCards database.

Gene	Chr	Physiological function	Study type	SNP ID - significantly associated	Association explained?	References
BMP9	10	BMP9 has been called as a osteogenic, and chondrogenic factor and it could be involved in bone formation	Association study in Chinese individuals. 450 OPLL patients and 550 matched controls Complete genomic *BMP9* coding	rs75024165 ($p < 0.001$)	Missense variant	Ren et al. (2012b)
				rs34379100 ($p < 0.001$)	MAF <0.01 (Benign)	
					3 prime UTR variant MAF 0.17 (3′ Region) Unclear association	
COL11A2	6	COL11A2 protein may promote ectopic bone formation by enhancing endochondral ossification. In addition COL11A2 also play a role in fibrillogenesis	Genetic linkage, association and haplotype analysis study in 53 Japanese families containing 91 OPLL affected sib pairs	Promoter (−182) ($p = 0.02$)	Linkage, association and haplotype analysis suggestive of a genetic locus for OPLL susceptibility in chromosome 6p, within or near COL11A2	Koga et al. (1998)
				rs1799907 ($p = 0.0004$)		
				rs1799910 ($p = 0.02$)		
				rs1799911 ($p = 0.03$)		
				Haplotypes		
			Association study (Haplotype association) in 161 OPLL patients and 163 controls	rs1799907 ($p = 0.0003$)	This study provides evidence of the functional impact of rs1799907 as a splice site mutation (MAF 0.32) which confers protection against ossification	Maeda et al. (2001a)
				Haplotype with 4 SNPs, male association		
COL17A1	10	COL17A1 is involved in the integrity of the hemidesmosome and the attachment of basal keratinocytes to the underlying basement membrane	WES and association studies in Chinese individuals. 28 unrelated OPLL patients and 100 healthy controls	rs805698 ($p = 0.00023$)	Missense variant (MAF 0.18) Tolerated effect	Wei et al. (2014)
				rs4918079 ($p = 0.003$)	Synonymous variant (MAF 0.33) Unclear association	
COL6A1	21	COL6A1 is a cell binding protein involved in the increase of bone mass	Genomewide linkage study followed by fine mapping and haplotype analysis of 142 affected sib pairs. 280 OPLL patients and 210 controls	intron 32 (−29) ($p = 0.000003$)	Identified COL6A1 as strongly associated with OPLL but did not find any functional impact of the identified polymorphisms	(Tanaka et al., 2003; Kong et al., 2007)
				rs2236485 ($p = 0.0002$) (MAF 0.13)		
				rs2236486 ($p = 0.00005$) (MAF 0.39)		
				rs2236487 ($p = 0.00006$) (MAF 0.37)		
			Case control association study with 90 OPLL patients and 155 controls	Promoter (−572) ($p = 0.000215$)	Promoter variant	Kong et al. (2007)
				Intron 32 (−29) rs2236486 ($p = 0.00483$)	Frequent Intronic variant - MAF 0.39 Unclear association	
			Association study with 100 OPLL patients and 100 controls (Han Chinese). Assessed 3 SNPs, previous identified by whole genome sequencing, in 30 OPLL patients (Wang et al., 2018b)	rs201153092 ($p = 0.000114$)	Missense, MAF<0.01	Wang et al. (2018a)
				rs13051496 ($p = 0.01116$)	Missense, MAF 0.11	
ENPP1	6	ENPP1 play a key role in bone mineralization and soft tissue calcification by controling pyrophosphate levels	ttw mouse studies	Gly568stop	Mouse Model for OPLL with nonsense mutation originating a truncated protein with loss of enzymatic activity	Okawa et al. (1998)
			Association study using 323 OPLL patients and 332 controls	IVS20-11delT ($p = 0.0029$)	Frequent polymorphism	Nakamura et al. (1999)
			Assessed all coding sequencing of ENPP1 gene		Unknow pathological mechanism of association with disease	
			Case-control association study with 180 OPLL patients and 265 controls	IVS15-14T-- > C ($p < 0.0001$)	Highly Significate in Young female and severe OPLL patients. Unknown	Koshizuka et al. (2002)

(Continued on following page)

TABLE 3 (*Continued*) Genes and genetic variants associated with OPLL predisposition. The protein physiological function is also mentioned. Protein function was obtained from GeneCards database.

Gene	Chr	Physiological function	Study type	SNP ID - significantly associated	Association explained?	References
					pathological mechanism of association with disease	
			Association study with 95 OPLL Chinese patients and 90 controls. Assessed 4 SNPs in ENPP1	C973T ($p < 0.001$) IVS15-14T-C ($p = 0.026$)	Unclear association	He et al. (2013)
ESR1	6	ESR1 protein play a role in bone tissues and is essential for sexual development and reproductive function	Case-control association study with 120 OPLL patients (43Female) and 306 controls (140Female)—unrelated Japanese	ER (XbaI) female gender specific	Intronic polymorphism	Ogata et al. (2002)
			Assessed 5 genes; 5 SNPs	($p = 0.007$)	Unclear association	
			Large Scale Case-control study of 711 Japanese OPLL patients and 896 controls	rs9340799 ($p = 0.017$), no correction	Frequent Intronic polymorphism	Horikoshi et al. (2006)
			Assessed 35 candidate genes; 109 SNPs	rs2228480 ($p = 0.034$, no correction	Unclear association	
HLA	6	HLA is closely related in the presentation of foreign antigens to the immune system	Family based association study in 33 families of patients with OPLL.		Unclear Association	Sakou et al. (1991)
			Family based association study in 24 families of patients with OPLL.		Unclear Association	Matsunaga et al. (1999)
IL-15RA	10	Increase cell proliferation and expression of an apoptosis inhibitor	A case control study in Chinese individuals. 235 OPLL patients and 250 controls	rs2228059	Tolerated missense variant MAF 0.45 Unclear association	Guo et al. (2014)
			Association study in Korean individuals. 166 OPLL patients and 230 controls	rs2228059	Tolerated missense variant MAF 0.45 Unclear association	Kim et al. (2011)
IL-17RC	3	IL-17RC is involved in regulation of bone metabolism by accelerating osteoblast differentiation	Association study in Han Chinese individuals. 100 OPLL patients and 100 controls	rs199772854 ($p = 0.006515$) rs76999397 ($p = 0.003234$) rs189013166 ($p = 0.01827$)	Missense variant MAF<0.01 Synonymous variant MAF 0.03 Synonymous variant MAF 0.02	Wang et al. (2018a)
			Assessed 3 SNPs, previously identified by whole genome sequencing, in 30 OPLL patients (Wang et al., 2018b)			
RUNX2	6	RUNX2 play a role in osteoblastic differentiation and skeletal morphogenesis	Case control study (Sequenom system) in Chinese individuals. 82 OPLL patients and 118 controls	rs1321075 ($p = 0.043$)	Intron Variant	Liu et al. (2010)
			Assessed 19 SNPs in 4 candidate genes	rs12333172 ($p = 0.034$)	MAF 0.18 Intronic variant MAF 0.13 Unclear association	
			Association study with 80 OPLL patients and 80 controls	rs1321075	Intron variant, MAF 0.18 Intron variant, MAF 0.13 Intron variant, MAF 0.47	Chang et al. (2017)
			Assessed 3 SNPs	rs12333172 rs1406846		
RXRB	6	RXRB protein is a member of retinoid receptor family, involved in regulation of a wide variety of biological processes	Association study and haplotype analysis in Japanese individuals. 134 OPLL patients and 158 controls	3′UTR (+140) ($p = 0.0028$) 3′UTR (+561) ($p = 0.034$)	Unclear association	Numasawa et al. (1999)

(Continued on following page)

TABLE 3 (*Continued*) Genes and genetic variants associated with OPLL predisposition. The protein physiological function is also mentioned. Protein function was obtained from GeneCards database.

Gene	Chr	Physiological function	Study type	SNP ID - significantly associated	Association explained?	References
		including development, differentiation, and cellular metabolism				
TGFB1	19	TGFB1 mediates bone development and metabolism	A case control with 46 OPLL patients and 273 controls	rs1982073 (p =)	Frequent Polymorphism MAF 0.45 Unclear association	Kamiya et al. (2001)
TGFB3	14	Involved in embryogenesis and cell differentiation	Large Scale Case-control study in Japanese individuals. 711 OPLL patients and 896 controls	rs2268624 (p = 0.00040/p = 0.044 after Bonferoni Correction)	Intronic polymorphisms with high MAFs	Horikoshi et al. (2006)
			Assessed 35 candidate genes; 109 SNPs	rs2284792 (p = 0.037) no correction	Unclear association	
VDR	12	Plays a central role in calcium homeostasis	Case-control study with 63 OPLL patients and 126 controls	VDR FF genotype	Unclear association	Kobashi et al. (2008)
RSPH9	6	Plays a role in membranous ossification	Genome Wide association study in Japanese individuals. 1130 OPLL patients and 7135 controls followed by an association study (for replication) in 548 OPLL Japanese patients and 6469 controls	rs927485 ($p = 9.4 \times 10^{-9}$)	Trough Gene expression analysis in and around OPLL associated loci authors suggest that *RSPH9* and *STK38L* genes might be linked in OPLL aetiology through the membranous ossification process. Furthermore, *HAO1*, *RSPO2* and *CCDC91* genes might be involved through the endochondral ossification process	(Nakajima et al., 2014; Nakajima et al., 2016)
STK38L	12	Plays a role in the membranous ossification process		rs11045000 ($p = 2.95 \times 10^{-11}$)		
RSPO2	8	Implicated in the endochondral ossification process		rs374810 ($p = 1.88 \times 10^{-13}$)		
CCDC91	12			rs13279799 ($p = 1.28 \times 10^{-10}$)		
HAO1	20	Implicated in the endochondral ossification process		rs1979679 ($p = 4.34 \times 10^{-12}$)		
				rs2423294 ($p = 1.10 \times 10^{-13}$)		
FGFR1	8	Plays an essential role in the regulation of embryonic development, cell proliferation, differentiation and migration	Association study with 157 OPLL patients and 222 controls	rs13317 (p = 0.02)	3 prime UTR variant	Jun and Kim, (2012)
			Assessed 9 SNPs in 3 genes		MAF 0.23 Unclear Association	
BID	22	Has a role in apoptosis signaling	Association study with 157 Korean OPLL patients and 209 controls	rs8190315 (p = 0.0052)	Tolerated Missense Variant MAF 0.05 Synonymous variant	Chon et al. (2014)
			Assessed 2 coding SNPs in BID	rs2072392 (p = 0.0052)	MAF 0.05 Unclear association	
TGFBR2	3	TGFBR2 protein is a regulator of transcription of several genes related to cell proliferation	Association study with 21 OPLL patients and 42 controls	rs11466512 (p = 0.007) rs56105708 (p = 0.024)	Splice region variant MAF 0.27 Rare Benign Missense Variant MAF <0.01 Unclear Association	Jekarl et al. (2013)
VKORC1	16	Involved in vitamin K metabolism	Association study with 98 Korean OPLL patients and 200 controls	rs9923231 (p = 0.004) (female)	Uppstream gene variant MAF 0.36 Unclear Association	Chin et al. (2013)
IFNG	12	IFNG is a protein that activates the macrophages	Association study with 135 OPLL patients and 222 controls	rs2430561 rs3138557	Intronic Variant MAF 0.28 Tandem repeat Unclear association	Kim et al. (2012)
BMPR-IA	10	Bone morphogenetic protein receptor responsible for the initiation of osteogenic differentiation	Association study with 356 OPLL patients and 617 controls. (Han Chinese)	rs11528010 (4A < C) (p < 0.001)	Missense variant MAF 0.50 5′UTR MAF 0.35	Wang et al. (2018c)

(Continued on following page)

TABLE 3 (*Continued*) Genes and genetic variants associated with OPLL predisposition. The protein physiological function is also mentioned. Protein function was obtained from GeneCards database.

Gene	Chr	Physiological function	Study type	SNP ID - significantly associated	Association explained?	References
			Assessed all exon regions of *BMPR-IA* gene	rs34755052 (-349C > T) ($p < 0.001$)		
MiR-199	19	Involved in regulation of inflammation and chondrogenic differentiation	Association study in Korean individuals. 207 OPLL patients and 200 controls	rs3746444 ($p = 0.039$)	Non-coding transcript exon variant	Lim et al. (2016)
			Assessed 4 genes/SNPs		MAF 0.18	

Abbreviations: *IL-1β*: Interleukin 1 Beta, *AHSG*: Alpha 2-Heremans-Schmid glycoprotein, *ACE*: Angiotensin I Converting Enzyme, *BMP2*: Bone Morphogenetic Protein 2, *BMP4*: Bone Morphogenetic Protein 4, *BMP9*: Bone Morphogenetic Protein 9, *COL11A2*: Collagen Type XI, Alpha 2, *COL17A1*: Collagen Type XVII, Alpha 1, *COL6A1*: Collagen Type VI, Alpha 1, *ENPP1*: Ectonucleotide pyrophosphatase/phosphodiesterase 1, *ESR1*: Estrogen Receptor 1, *HLA*: Human Leukocyte antigen, *IL-15RA*: Interleukin 15 Receptor Alpha, *IL-17RC*: Interleukin-17, receptor C, *RUNX2*: Run-Related Transcription Factor 2, *RXRB*: Retinoid X Receptor Beta, *TGFβ1*: Transforming Growth factor Beta 1, *TGFβ3*: Transforming Growth factor Beta 3, *VDR*: Vitamin D Receptor, *RSPH9*: radial spoke head 9 homolog, *STK38L*: serine/threonine kinase 38 like, *RSPO2*: R-spontin 2, *CCDC91*: Coiled-coil domain containing 91, *HOA1*: Hydroxyacid oxidase 1, *FGFR1*: Fibroblast Growth Factor Receptor 1, *BID*: BH3 Interacting Domain Death Agonist, *TGFBR2*: Transforming Growth Factor Beta Receptor II, *VKORC1*: Vitamin K epoxide reductase complex subunit 1, *IFNG*: Interferon Gamma, *BMPR-IA*: Bone morphogenetic protein receptor type IA. NA: Not applicable. * This polymorphisms was found in all OPLL, patients and according to the authors is a novel nucleotide variation.

RUNX2 have also been associated with OPLL (Liu et al., 2010; Chang et al., 2017).

Another important gene with contradictory results is *TGFβ1*, that according to Kamiya et al. (2001), is genetically associated to OPLL (869T > C; rs1982073). However, Han et al. (2013) showed that the SNP previously associated with OPLL (rs1982073) and the SNP located in the promoter region (rs1800469) are not associated with OPLL in

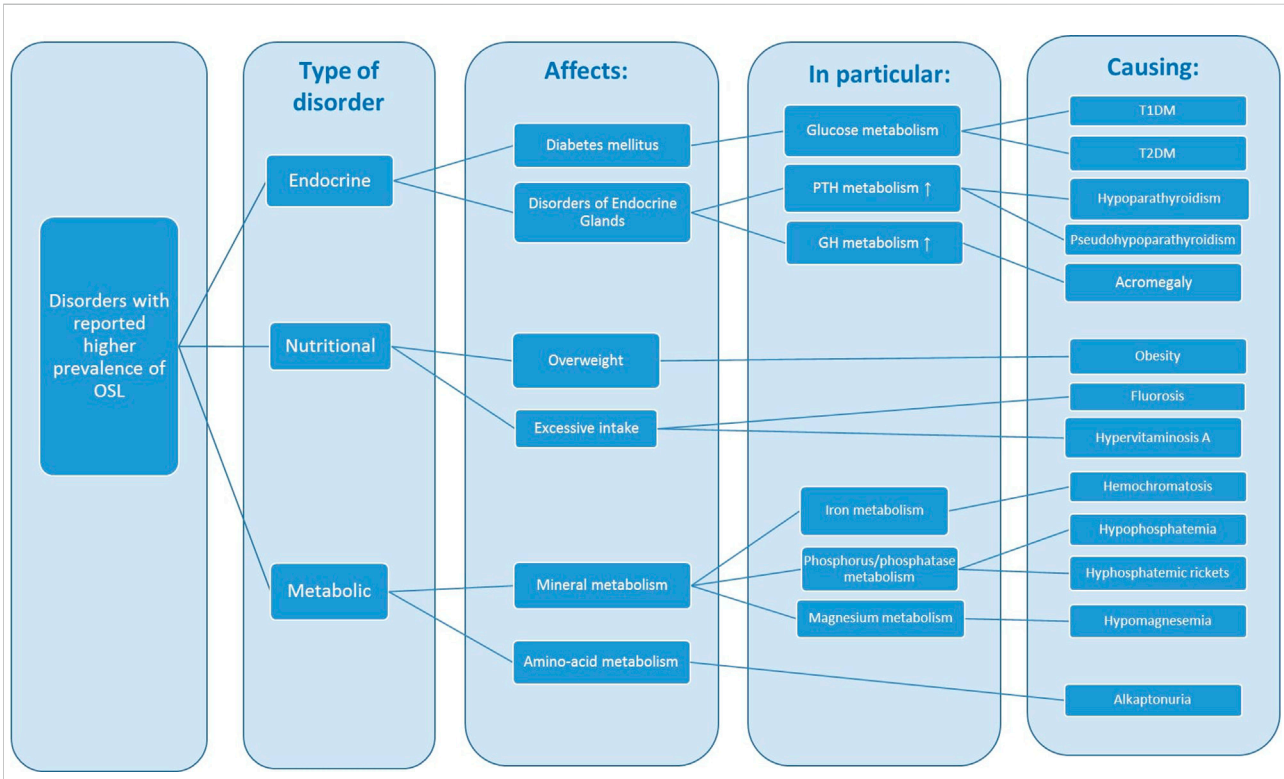

FIGURE 1
Disorders associated with a higher prevalence of OSL. GH: growth hormone, PTH: parathormone, IGF-A: insulin growth factor 1, HGA: homogentisic acid.

TABLE 4 Monogenic disorders previously associated with OSL. Lack of inheritance means that it is still unconfirmed.

Disorder	Inheritance	OMIM	Gene/Locus involved
Hypophosphatemic rickets/osteomalacia	AD	193100	*FGF23*
	AR	241520	*DMP1*
	AR	613312	*ENPP1*
	AR	241530	*SLC34A3*
	XLD	307800	*PHEX*
	XLR	300554	*CLCN5*
Hypophosphatasia	AR	241500	*ALPL*
	AR	241510	
	AR, AD	146300	
Pseudohypoparathyroidism	AD	103580	*GNAS1*
Hypoparathyroidism	AD	146200	*GCM2*
	AD/AR	146200	*PTH*
Alkaptonuria	AR	203500	*HGD*
Acromegaly	Somatic/AD	102200	*AIP*
		102200	*GNAS1*
	X linked	300943	*GPR101*
	AD	610755	*CDKN1B*
	AD	131100	*MEN1*
	Somatic	174800	*GNAS*
	AD	160980	*PRKAR1A*
Familial Hypocalciuric Hypercalcemia	AD	145980	*CASR*
	AD	145981	*GNA11*
	AD	600740	*AP2S1*

AbbreviationsAD -Autosomal Dominant, AR- Autosomal Recessive, XLD, and XLR - X-linked Dominant and Recessive.

Korean populations. Interestingly, in the chondrocytes of adjacent cartilaginous areas and in the ossified matrix of OPLL the TGF-β1 gene is overexpressed. The same authors tested the association between rs1982073 and the radiological appearance of OPLL, and they verified that SNP rs1982073 is associated to the specific area of the ossified lesion, and not to the onset of OPLL. The "C" allele could be a risk factor for patients with OPLL in cervical, thoracic, and/or lumbar spine (Kawaguchi et al., 2003).

In relation to ossification of the ligamentum flavum several genes and loci have been associated with thoracic Ossification of Ligamentum Flavum (OLF) (Kong et al., 2007; Liu et al., 2010; Qu et al., 2017; Qu et al., 2021).

5 Associated disorders

The presence of OSL has been described in association with numerous diseases of diverse etiologies. The type of disorders, the main pathways affected and the consequences, including the main anomalies identified in laboratory analysis, are outlined in Figure 1.

The OSL associated disorders can be of endocrine, nutritional or metabolic nature. The main endocrine associated disorders—diabetes mellitus, acromegaly and hypoparathyroidism—are characterized by disturbances in the metabolism of glucose, growth hormone (GH), and parathyroid hormone (PTH), leading to hypocalcemia, hyperphosphatemia, hyperglycemia and hyperinsulinemia. These endocrine anomalies are often linked to obesity, which can also have a strong genetic basis. The excessive intake of fluoride and vitamin A leads to OSL resembling DISH. Disturbances in mineral metabolism namely phosphorus phosphatase and calcium can also originate disorders that have been reported in association with OSL: familial hypocalciuric hypercalcemia, hypophosphatemic rickets and hypophosphatasia.

5.1 Monogenic disorders

Table 4 lists a subset of DISH and OPLL cases originated by monogenic disorders. With the exception of alkaptonuria, characterized by the levels of Homogentisic acid, all of the other disorders are directly involved in calcium and phosphate homeostasis. As expected, genes related in hypophosphatemic rickets and hypophosphatasia are directly involved in phosphate homeostasis. However, the reports of OSL are not related to all

TABLE 5 Complex disorders previously associated with OSL. AD stands for Autosomal Dominant, AR for Autosomal Recessive. Lack of inheritance means that it is not confirmed.

Disorder	Type	Inheritance	OMIM	Gene/Locus involved
Non-insulin-dependent Type 2 Diabetes mellitus	Monogenic - MODY	AD	606391	Genetically Heterogeneous—associated with mutations in 13 genes
	Polygenic		125853	Many susceptibility locus identified, including in *ENPP1*
Abdominal Obesity - Metabolic Syndrome	Monogenic	AR	615812	*DYRK1B*
			200100	*MTP*
	Polygenic		605552	*AOMS1*
				AOMS2
Obesity	Monogenic	AR	614962	*LEP*
		AR	614963	*LEPR*
		AR	600955	*PCSK1*
		AR	609734	*POMC*
	Polygenic		601665	Genetically heterogeneous but including *ENPP1* as susceptibility gene

types of hypophosphatasia disorders. Saito et al. (2011), reported a case of OPLL with hypophosphatemic rickets/osteomalacia caused by a splice donor site mutation in the *ENPP1* gene. Cases of hypoparathyroidism associated with changes similar to DISH are also reported in the literature (Lambert and Becker, 1989; Unverdi et al., 2009; John and Suthar, 2016). The genes *GNAS*, *GCM2* and *PTH*, closely related to hypoparathryroidism, play a role in both calcium and phosphorus metabolism. According to what we know, there is only one case described of a patient with DISH and familial hypocalciuric hypercalcemia (FHH). The patient, a 45-year-old diabetic woman, have hypercalcemia secondary to FHH and developed dysphagia because of external esophageal compression from DISH. According to the authors, the relationship between FHH and DISH remains unproven (Rivas and Lado-Abeal, 2013). Acromegaly is a rare condition of high elevated somatic growth and distorted proportions arising from hypersecretion of growth hormone (GH) and insulin-like growth factor 1 (IGF-1) due to adenomas and pathogenic pituitary secretion (Ben-Shlomo and Melmed, 2008). According to Altomonte et al. (1992), GH levels may act as bone promoting factors in DISH.

5.2 "Risk-factor" complex disorders

The etiology of "risk-factor" OSL disorders is complex, and determined by the interaction of inherited and environmental factors, such as age, smoking, alcohol consumption, diet and physical inactivity. These factors, as already know, effect type 2 diabetes mellitus (T2D) and obesity, two of the known risk factor for developing DISH. Even though heterogeneous, there are some monogenic forms of these OSL disorders; see Table 5 for more details. Diabetes mellitus is considered to be a heterogeneous group of disorders having as a main characteristic persistent hyperglycemia (Pillai and Littlejohn, 2014). Obesity is considered a complex and a multifactorial disease, however there are monogenic cases reported that are related to mutations in genes of the leptin/melanocortin system involved in food intake regulation (Huvenne et al., 2016). It is interesting to see that genetic variants in *LEPR* gene, as occurs in the ZFR murine model, can cause obesity, hypercholesterolemia, hyperinsulinemia, hyperlipidemia and also ossification of spinal ligaments, similar to human OPLL (Okano et al., 1997). Furthermore, there are studies reporting increased levels of serum leptin in female patients with OPLL (Ikeda et al., 2011) (Feng et al., 2018) as well as in DISH patients (Tenti et al., 2017). The osteogenic effects of leptin/leptin receptor (LepR) in conjunction with mechanical stress, on the ossification of the posterior ligament, through its interaction with osteogenic markers such as osteopontin, osteocalcin and *RUNX2*, were also recently shown (Chen et al., 2018). It is also pertinent to mention that *ENPP1* is a predisposition gene for both obesity and type 2 diabetes. The importance of leptin/*LEPR* in disorders such as DISH, with an important metabolic association, remain to be revealed.

5.3 Other rheumatic disorders coexisting with Ossification of Spinal Ligaments

The co-existence of DISH with other rheumatic disorders was first reported in 1950 by Forestier and Rotes Querol (Forrestier, 1950). Subsequent studies indicate, in some cases that up to 50% of DISH patients also have OPLL proposing that they share common etiopathogenic factors. Simultaneous OPLL and OLF are also very common in the literature (Li et al., 2012; Onishi et al., 2016). In addition, the co-existence of the three OSL disorders—DISH; OPLL and OLF has also been described in the literature (Guo et al., 2011). The association of DISH with psoriatic arthritis in the literature (Ben-Shlomo and Melmed, 2008) is common but studies

TABLE 6 Rheumatic disorders previously seen coexisting with OSL. AD stands for Autosomal Dominant, AR for Autosomal Recessive. Lack of inheritance means that it is not confirmed.

Disorder	Inheritance	OMIM	Gene/Locus involved	Mechanism
ACDC	AR	211800	NT5E	Pyrophosphate metabolism
Ankylosing Spondylitis	Multifactorial	106300	*HLA-B*	MHC Peptide presentation
	AD	183840	*SPDA2 locus*	
		613238	*SPDA3 locus*	
Chondrocalcinosis	AD	118600	*ANKH*	Pyrophosphate metabolism
	AD	600668	*CCAL1 locus*	
	AR	602643	*TNFRSB1*	

concluded that is a side effect of retinoids treatment (Bologna et al., 1991). Other rheumatic diseases co-existing with DISH include: hyperostosis frontalis interna (Arlet et al., 1978; Mazières et al., 1978; Ciocci et al., 1985; Fukunishi et al., 1987; Fukunishi and Hosokawa, 1988), CPPD and/or CC (Resnick et al., 1978a; Bruges-Armas et al., 2006), gout (Resnick et al., 1978a; Littlejohn and Hall, 1982; Constantz, 1983; Fornaciari et al., 2009), rheumatoid arthritis (Resnick et al., 1978a; Resnick et al., 1978b; Forster et al., 1981; Mata et al., 1995), osteoarthritis (Resnick et al., 1978a), Heberden and Bouchard nodes (Schlapbach et al., 1992) and Paget's disease (Mazières et al., 1978; Morales et al., 1993).

DISH and Ankylosing Spondylitis (AS) generally have a distinct radiographic appearance but sometimes, possibly in the early disease stages, they are difficult to distinguish radiologically (Williamson and Reginato, 1984; Olivieri et al., 1987; Olivieri et al., 1989; Rillo et al., 1989; Troise Rioda and Ferraccioli, 1990; Olivieri, 1991; Passiu et al., 1991; Maertens et al., 1992; Tishler and Yaron, 1992; Jattiot et al., 1995; Moreno et al., 1996; Kozanoglu et al., 2002; Jordana et al., 2009; Wooten, 2009; Macia-Villa et al., 2016; Kuperus et al., 2018). OPLL has also been observed in patients with AS but this coexistence is probably coincidental (Kim et al., 2007). Chondrocalcinosis, is characterized by the deposition of calcium containing crystals in synovial membranes, articular cartilage and, sometimes it can also affect periarticular soft tissues. Curiously, in some patients, the deposition of calcium crystals—hydroxyapatite or CPPD—can also occur in the spinal ligaments (Resnick and Pineda, 1984; Muthukumar et al., 2000) but this is usually difficult to differentiate from ossification (Ehara et al., 1998). *ANKH* is the only monogenic cause identified for CC (Table 6); a recent study described a gain-of-function mutation in the gene *TNFRSF11B*, which resulted in early-onset osteoarthritis and CC (Ramos et al., 2015). A recently described hereditary autosomal recessive ectopic mineralization syndrome in patients with arterial Calcification due to deficiency of CD73 (ACDC), was the result of a loss of function mutations in the 5′-nucleoside Ecto (*NT5E*) gene. These patients had erosive peripheral arthropathy and axial enthesopathic calcifications, resembling DISH although with decreased disc space height and the presence of large intervertebral disk calcifications (Cudrici et al., 2021). The similarities to both DISH and AS of the outcome of spine imaging of ACDC patients are noteworthy.

6 Discussion

6.1 Familial aggregation reports

The existence of a small number of family reports, with early-onset and exuberant phenotypes, in which the genetic cause was not identified and most of the times was not even investigated, raises the possibility that there are some cases of monogenic DISH and OPLL. There are possibly three main types of OSL: A sporadic form, a type that is secondary to associated metabolic disorders and a hereditary type. It is now clear that most OSL cases do not follow a simple, single gene Mendelian inheritance pattern, but instead are multifactorial disorders developing in individuals with a genetic predisposition from a variety of genetic variants in different genes.

6.2 Animal models

The existence of spontaneous and manipulated animal models for both DISH and OPLL could facilitate the identification of causal human genetic factors. It seems probable that the human phenotype of OPLL and DISH are likely to be caused by mutations in genes that underlie the animal models for these disorders. As far as we know, there are no reports of *SLC29A1* (ENT1 mice model for DISH) human gene mutations in association with DISH. The association of *ENPP1* with OPLL susceptibility (31, 47–49) is still unsubstantiated (50). Interestingly, in one study the authors found that the combination of variants in *ENPP1* and *LEPR* genes was associated with the location and extension of OPLL (51). An interesting report about hypophosphatemic rickets in an OPLL patient due to a homozygous mutation in the *ENPP1* gene (53), substantiates the likely importance of this gene in the etiopathogenic mechanism of OSL.

The case of the *ank* mouse has been quite different. In humans, analysis in the *ANKH* gene has identified several mutations that segregate with CC phenotype but only in a very limited subset of

pedigrees. The co-coexistence of spinal ossification with CC is well supported in the literature (10, 12, 13), indicating a strong genetic link between these disorders. The genetic confirmation between spinal ossification and CC comes from two animal models—twy and *ankh* mice—the mouse models for OPLL and CC, develop spinal ossification and hydroxyapatite arthropathy. Both genes, *ENPP1* and *ANKH*, regulate PPi levels thus having an essential role in bone mineralization and soft tissue calcification. The association of *ENPP1* variants with Chondrocalcinosis, is considered a minor determinant of the disease (58, 59).

6.3 Genetic variants association

Three different genetic variants in *COL6A1* have been associated with both DISH and OPLL. Results from these studies are inconsistent due to the type of variant associated, the lack of explanation of the pathogenic mechanism and the low numbers of individuals studied. Further progress in investigation of DISH requires a concerted approach, similar to the ones used to target the genetic basis of OPLL. In the latter case linkage studies, candidate gene association studies and even genome wide association studies were performed and revealed that OPLL is genetically heterogenous. Despite all the studies, and the large number of genes that have been associated with OSL, most of the associations are still inconsistent because genetic variants were localized in non-coding regions. Several genes involved many potential low risk effects in OSL inheritance, so there is insufficient power and analysis for their detection.

6.4 Genetics of associated disorders

The higher prevalence of OSL in patients with endocrine, nutritional and metabolic disorders made us wonder if the known genetic cause for these associated disorders could help to clarify the putative genetic pathways involved in the etiology of OSL. The ectopic calcification occurring is most probably predisposed by the balance between the expression of specific genes that act directly or indirectly on the phosphorus to calcium ratio. The crucial role of angiogenesis in DISH etiology has also been suggested, as it might be the common pathogenic background of some conditions included in metabolic syndrome. Nonetheless, there are several case reports of patients with monogenic metabolic disorders with the occurrence of DISH and OPLL.

7 Conclusion

A validated set of classification criteria for diseases characterized by ectopic mineralization of spinal tissues is of utmost importance for genetic studies so homogeneous phenotype groups can be established for investigation. This is particularly important in DISH because this disease is characterized by the ossification of the anterior spinal ligaments and generalized symmetrical enthesopathic calcifications, which may well be among the first manifestations of the disease or the main evidence of the disease in a subset of patients. At this time, DISH disease is requiring a validated set of criteria to robustly describe and establish homogeneous cohorts of patients. A more comprehensive designation of DISH, including patients with early phase disease, are clearly indispensable for genetic studies (Mader et al., 2013). On the other hand, great advances have been made in understanding the presentation of different types of OPLL.

Taken together the collected evidence suggests OSL has a heterogeneous genetic basis. The rapid advance in methods for genetic studies has brought new and interesting insights into ectopic calcification, and is providing confirmation about the importance of genes for the regulation of Pi/PPi levels, which control mineralization. Future genome-scale approaches will contribute to pinpoint susceptibility genes. However, to provide sufficient analytical power, the number of patients needs to be enlarged and the clinical/radiological disease classification, especially in DISH patients, needs substantial improvement. International collaborations are essential to increase sample size and overcome analytical challenges caused by the genetic heterogeneity of these complex diseases of calcification.

Author contributions

BP and AC wrote the manuscript; all the authors provided critical revision and contributed to the final version of the manuscript.

Conflict of interest

The authors declare that the research was conducted in the absence of any commercial or financial relationships that could be construed as a potential conflict of interest.

Publisher's note

References

Abiteboul, M., Mazières, B., and Ménard, H. (1985). [2 new familial cases of ankylosing vertebral hyperostosis]. *Rev. Rhum. Mal. Osteoartic.* 52, 645–647.

Altomonte, L., Zoli, A., Mirone, L., Marchese, G., Scolieri, P., Barini, A., et al. (1992). Growth hormone secretion in diffuse idiopathic skeletal hyperostosis. *Ann. Ital. Med. Int.* 7 (1), 30–33.

Arlet, P., Le Tallec, Y., Mazieres, B., Arlet, J., Timbal, X., and Boulard, C. (1978). Association between ankylosing vertebral hyperostosis and frontalis interna hyperostosis. *Nouv. Presse Med.* 7 (33), 2968.

Badhiwala, J. H., Ahuja, C. S., Akbar, M. A., Witiw, C. D., Nassiri, F., Furlan, J. C., et al. (2020). Degenerative cervical myelopathy - update and future directions. *Nat. Rev. Neurol.* 16 (2), 108–124. doi:10.1038/s41582-019-0303-0

Bai, Q., Wang, Y., Zhai, J., Wu, J., Zhang, Y., and Zhao, Y. (2022). Current understanding of tandem spinal stenosis: Epidemiology, diagnosis, and surgical strategy. *EFORT Open Rev.* 7 (8), 587–598. doi:10.1530/EOR-22-0016

Beardwell, A. (1969). Familial ankylosing vertebral hyperostosis with tylosis. *Ann. Rheum. Dis.* 28, 518–523. doi:10.1136/ard.28.5.518

Ben-Shlomo, A., and Melmed, S. (2008). *Endocrinol. Metab. Clin. North Am.* 37 (1), 101–122. doi:10.1016/j.ecl.2007.10.002

Bicket, A., Mehrabi, P., Naydenova, Z., Wong, V., Donaldson, L., Stagljar, I., et al. (2016). Novel regulation of equlibrative nucleoside transporter 1 (ENT1) by receptor-stimulated Ca2+-dependent calmodulin binding. *Am. J. Physiol. Cell Physiol.* 310 (10), C808–C820. doi:10.1152/ajpcell.00243.2015

Bologna, C., Poirier, J. L., Herisson, C., and Simon, L. (1991). Hip and spinal ossification enthesopathies induced by etretinate therapy in peripheral psoriatic arthritis. *Rev. Rhum. Mal. Osteoartic.* 58 (9), 595–599.

Bossens, K., Bhatti, S., Van Soens, I., Gielen, I., and Van Ham, L. (2016). Diffuse idiopathic skeletal hyperostosis of the spine in a nine-year-old cat. *J. Small Anim. Pract.* 57 (1), 33–35. doi:10.1111/jsap.12371

Brewerton, D. A., Hart, F. D., Nicholls, A., Caffrey, M., James, D. C., and Sturrock, R. D. (1973). Ankylosing spondylitis and HL-A 27. *Lancet* 1, 904–907. doi:10.1016/s0140-6736(73)91360-3

Brown, T. R., Quinn, S. F., and D'Agostino, A. N. (1991). Deposition of calcium pyrophosphate dihydrate crystals in the ligamentum flavum: Evaluation with MR imaging and CT. *Radiology* 178 (3), 871–873. doi:10.1148/radiology.178.3.1994435

Bruges-Armas, J., Couto, A. R., Timms, A., Santos, M. R., Bettencourt, B. F., Peixoto, M. J., et al. (2006). Ectopic calcification among families in the Azores: Clinical and radiologic manifestations in families with diffuse idiopathic skeletal hyperostosis and chondrocalcinosis. *Arthritis Rheum.* 54 (4), 1340–1349. doi:10.1002/art.21727

Buckley, M. F., Loveland, K. A., McKinstry, W. J., Garson, O. M., and Goding, J. W. (1990). Plasma cell membrane glycoprotein PC-1. cDNA cloning of the human molecule, amino acid sequence, and chromosomal location. *J. Biol. Chem.* 265 (29), 17506–17511. doi:10.1016/s0021-9258(18)38193-6

Carroll, S. H., Wigner, N. A., Kulkarni, N., Johnston-Cox, H., Gerstenfeld, L. C., and Ravid, K. (2012). A2B adenosine receptor promotes mesenchymal stem cell differentiation to osteoblasts and bone formation *in vivo*. *J. Biol. Chem.* 287 (19), 15718–15727. doi:10.1074/jbc.M112.344994

Caswell, A. M., Ali, S. Y., and Russell, R. G. (1987). Nucleoside triphosphate pyrophosphatase of rabbit matrix vesicles, a mechanism for the generation of inorganic pyrophosphate in epiphyseal cartilage. *Biochim. Biophys. Acta* 924 (2), 276–283. doi:10.1016/0304-4165(87)90023-7

Caswell, A. M., and Russell, R. G. (1988). Evidence that ecto-nucleoside-triphosphate pyrophosphatase serves in the generation of extracellular inorganic pyrophosphate in human bone and articular cartilage. *Biochim. Biophys. Acta* 966 (3), 310–317. doi:10.1016/0304-4165(88)90080-3

Chang, F., Li, L., Gao, G., Ding, S., Yang, J., Zhang, T., et al. (2017). Role of Runx2 polymorphisms in risk and prognosis of ossification of posterior longitudinal ligament. *J. Clin. Lab. Anal.* 31 (4), e22068. doi:10.1002/jcla.22068

Chen, S., Zhu, H., Wang, G., Xie, Z., Wang, J., and Chen, J. (2018). Combined use of leptin and mechanical stress has osteogenic effects on ossification of the posterior longitudinal ligament. *Eur. Spine J.* 27 (8), 1757–1766. doi:10.1007/s00586-018-5663-4

Chen, X., Guo, J., Cai, T., Zhang, F., Pan, S., Zhang, L., et al. (2016). Targeted next-generation sequencing reveals multiple deleterious variants in OPLL-associated genes. *Sci. Rep.* 6, 26962. doi:10.1038/srep26962

Chen, Z., Meng, H., Xing, G., Yuan, H., Zhao, F., Liu, R., et al. (2008). Age-related differences in pulmonary and cardiovascular responses to SiO2 nanoparticle inhalation: Nanotoxicity has susceptible population. *Environ. Sci. Technol.* 42 (23), 8985–8992. doi:10.1021/es800975u

Chin, D. K., Han, I. B., Ropper, A. E., Jeon, Y. J., Kim, D. H., Kim, Y. S., et al. (2013). Association of VKORC1-1639g>A polymorphism with susceptibility to ossification of the posterior longitudinal ligament of the spine: A Korean study. *Acta Neurochir.* 155 (10), 1937–1942. doi:10.1007/s00701-013-1747-4

Choi, B. W., Song, K. J., and Chang, H. (2011). Ossification of the posterior longitudinal ligament: A review of literature. *Asian Spine J.* 5 (4), 267–276. doi:10.4184/asj.2011.5.4.267

Chon, J., Hong, J. H., Kim, J., Han, Y. J., Lee, B. W., Kim, S. C., et al. (2014). Association between BH3 interacting domain death agonist (BID) gene polymorphism and ossification of the posterior longitudinal ligament in Korean population. *Mol. Biol. Rep.* 41 (2), 895–899. doi:10.1007/s11033-013-2933-4

Ciocci, A., Buratti, L., and Maurelli, G. (1985). Vertebral hyperostosis and hyperostosis frontalis interna. *Rev. Rhum. Mal. Osteoartic.* 52 (4), 227–230.

Constantz, R., and B, R. (1983). Case report 237: Gout associated with diffuse idiopathic skeletal hyperostosis (DISH). *Skelet. Radiol.* 10 (2), 117–120. doi:10.1007/BF00360796

Couto, A. R., Parreira, B., Thomson, R., Soares, M., Power, D. M., Stankovich, J., et al. (2017). Combined approach for finding susceptibility genes in DISH/chondrocalcinosis families: Whole-genome-wide linkage and IBS/IBD studies. *Hum. Genome Var.* 4, 17041. doi:10.1038/hgv.2017.41

Cudrici, C. D., Newman, K. A., Ferrante, E. A., Huffstutler, R., Carney, K., Betancourt, B., et al. (2021). Multifocal calcific periarthritis with distinctive clinical and radiological features in patients with CD73 deficiency. *Rheumatology* 61, 163–173. doi:10.1093/rheumatology/keab270

Ehara, S., Shimamura, T., NakamuRa, R., and YamazaKi, K. (1998). Paravertebral ligamentous ossification: DISH, OPLL and OLF. *Eur. J. Radiol.* 27 (3), 196–205. doi:10.1016/s0720-048x(97)00164-2

Elefteriou, F., Takeda, S., Ebihara, K., Magre, J., PataNoN.Kim, C. A., et al. (2004). Serum leptin level is a regulator of bone mass. *Proc. Natl. Acad. Sci. U. S. A.* 101 (9), 3258–3263. doi:10.1073/pnas.0308744101

Ellman, M. H., Vazquez, T., Ferguson, L., and MaNdelN. (1978). Calcium pyrophosphate deposition in ligamentum flavum. *Arthritis Rheum.* 21 (5), 611–613. doi:10.1002/art.1780210512

Eytan, O., Morice-Picard, F., Sarig, O., Ezzedine, K., Isakov, O., Li, Q., et al. (2013). Cole disease results from mutations in ENPP1. *Am. J. Hum. Genet.* 93 (4), 752–757. doi:10.1016/j.ajhg.2013.08.007

Feng, B., Cao, S., Zhai, J., Ren, Y., Hu, J., Tian, Y., et al. (2018). Roles and mechanisms of leptin in osteogenic stimulation in cervical ossification of the posterior longitudinal ligament. *J. Orthop. Surg. Res.* 13 (1), 165. doi:10.1186/s13018-018-0864-4

Fornaciari, G., Giuffra, V., Giusiani, S., Fornaciari, A., Villari, N., and Vitiello, A. (2009). The 'gout' of the Medici, grand dukes of florence: A palaeopathological study. *Rheumatol. Oxf.* 48 (4), 375–377. doi:10.1093/rheumatology/ken493

Fornaciari, G., and Giuffra, V. (2013). The "gout of the Medici": Making the modern diagnosis using paleopathology. *Gene* 528 (1), 46–50. doi:10.1016/j.gene.2013.04.056

Forrestier, J., and R.-Q, J. (1950). Senile ankylosing hyperostosis of the spine. *Ann. Rheum. Dis.* 9, 321–330. doi:10.1136/ard.9.4.321

Forster, T. J., Leek, J. C., and Robbins, D. L. (1981). Peripheral hyperostosis in rheumatoid arthritis in the absence of axial involvement. *J. Rheumatol.* 8 (4), 653–657.

Fukunishi, I., Hayabara, T., and Hosokawa, K. (1987). A case of diffuse idiopathic skeletal hyperostosis (DISH) with hyperostosis frontalis interna. *Rinsho Shinkeigaku* 27 (8), 1013–1016.

Fukunishi, I., and Hosokawa, K. (1988). Schizophrenic psychosis with a tendency of systemic ossification. *Jpn. J. Psychiatry Neurol.* 42 (2), 217–222. doi:10.1111/j.1440-1819.1988.tb01973.x

Furushima, K., Shimo-Onoda, K., Maeda, S., Nobukuni, T., Ikari, K., Koga, H., et al. (2002). Large-scale screening for candidate genes of ossification of the posterior longitudinal ligament of the spine. *J. Bone Min. Res.* 17 (1), 128–137. doi:10.1359/jbmr.2002.17.1.128

Gorman, C., Jawad, A. S. M., and Chikanza, I. (2005). A family with diffuse idiopathic skeletal hyperostosis. *Ann. Rheum. Dis.* 64, 1794–1795. doi:10.1136/ard.2004.033852

Guo, Q., Lv, S. Z., Wu, S. W., Tian, X., and Li, Z. Y. (2014). Association between single nucleotide polymorphism of IL15RA gene with susceptibility to ossification of the posterior longitudinal ligament of the spine. *J. Orthop. Surg. Res.* 9, 103. doi:10.1186/s13018-014-0103-6

Guo, Q., Ni, B., Yang, J., Zhu, Z., and Yang, J. (2011). Simultaneous ossification of the posterior longitudinal ligament and ossification of the ligamentum flavum causing upper thoracic myelopathy in DISH: Case report and literature review. *Eur. Spine J.* 20 (2), S195–S201. doi:10.1007/s00586-010-1538-z

Hajjawi, M. O., MacRae, V. E., Huesa, C., Boyde, A., Millan, J. L., Arnett, T. R., et al. (2014). Mineralisation of collagen rich soft tissues and osteocyte lacunae in Enpp1(-/-) mice. *Bone* 69, 139–147. doi:10.1016/j.bone.2014.09.016

Hamanishi, C., Tan, A., Yamane, T., ToMiharaM.FuKuda, K., and Tanaka, S. (1995). Ossification of the posterior longitudinal ligament. Autosomal recessive trait. *Spine (Phila Pa 1976)* 20 (2), 205–207. doi:10.1097/00007632-199501150-00014

Han, I. B., Ropper, A. E., Jeon, Y. J., Park, H. S., Shin, D. A., Teng, Y. D., et al. (2013). Association of transforming growth factor-beta 1 gene polymorphism with genetic susceptibility to ossification of the posterior longitudinal ligament in Korean patients. *Genet. Mol. Res.* 12 (4), 4807–4816. doi:10.4238/2013.February.28.26

Havelka, S., Uitterlinden, A. G., Fang, Y., Arp, P. P., Pavelkova, A., VeselaM., et al. (2002). Collagen type I(alpha 1) and vitamin D receptor polymorphisms in diffuse idiopathic skeletal hyperostosis. *Clin. Rheumatol.* 21 (4), 347–348. doi:10.1007/s100670200093

Havelka, S., VeselaM.Pavelkova, A., Ruzickova, S., Koga, H., Maeda, S., et al. (2001). Are DISH and OPLL genetically related? *Ann. Rheum. Dis.* 60 (9), 902–903.

He, Z., Zhu, H., Ding, L., Xiao, H., Chen, D., and XueF. (2013). Association of NPP1 polymorphism with postoperative progression of ossification of the posterior longitudinal ligament in Chinese patients. *Genet. Mol. Res.* 12 (4), 4648–4655. doi:10.4238/2013.October.18.3

Hinton, D. J., McGee-Lawrence, M. E., Lee, M. R., Kwong, H. K., Westendorf, J. J., and Choi, D. S. (2014). Aberrant bone density in aging mice lacking the adenosine transporter ENT1. *PLoS One* 9 (2), e88818. doi:10.1371/journal.pone.0088818

Horikoshi, T., Maeda, K., Kawaguchi, Y., Chiba, K., Mori, K., Koshizuka, Y., et al. (2006). A large-scale genetic association study of ossification of the posterior longitudinal ligament of the spine. *Hum. Genet.* 119 (6), 611–616. doi:10.1007/s00439-006-0170-9

Huvenne, H., Dubern, B., Clement, K., and Poitou, C. (2016). Rare genetic forms of obesity: Clinical approach and current treatments in 2016. *Obes. Facts* 9 (3), 158–173. doi:10.1159/000445061

Ikeda, Y., Nakajima, A., Aiba, A., Koda, M., Okawa, A., Takahashi, K., et al. (2011). Association between serum leptin and bone metabolic markers, and the development of heterotopic ossification of the spinal ligament in female patients with ossification of the posterior longitudinal ligament. *Eur. Spine J.* 20 (9), 1450–1458. doi:10.1007/s00586-011-1688-7

Ikegawa, S. (2007). in Tiptoe walking (ttw) mouse *in* OPLL: Ossification of the posterior longitundinal ligament. Editors K. Yonenobu, K. Nakamura, and Y. Toyama (Hicom, Japan: Springer), 71–76.

Ikuma, H., Hirose, T., Nakamura, D., Yamashita, K., Ueda, M., Sasaki, K., et al. (2022). The prevalence and characteristics of diffuse idiopathic skeletal hyperostosis (DISH): A cross-sectional study of 1519 Japanese individuals. *Diagn. (Basel)* 12 (5), 1088. doi:10.3390/diagnostics12051088

Jattiot, F., Goupille, P., and Valat, J. P. (1995). Coexistence of diffuse idiopathic skeletal hyperostosis and ankylosing spondylitis in two patients. *Clin. Exp. Rheumatol.* 13 (3), 405–406.

Jekarl, D. W., Paek, C. M., An, Y. J., Kim, Y. J., Kim, M., Kim, Y., et al. (2013). TGFBR2 gene polymorphism is associated with ossification of the posterior longitudinal ligament. *J. Clin. Neurosci.* 20 (3), 453–456. doi:10.1016/j.jocn.2012.05.031

John, D. R., and Suthar, P. P. (2016). Radiological features of long-standing hypoparathyroidism. *Pol. J. Radiol.* 81, 42–45. doi:10.12659/PJR.896104

Jordana, X., Galtes, I., Couto, A. R., Gales, L., Damas, M., Lima, M., et al. (2009). The coexistence of ankylosing spondylitis and diffuse idiopathic skeletal hyperostosis--a postmortem diagnosis. *Clin. Rheumatol.* 28 (3), 353–356. doi:10.1007/s10067-008-1068-9

Jun, J. K., and Kim, S. M. (2012). Association study of fibroblast growth factor 2 and fibroblast growth factor receptors gene polymorphism in Korean ossification of the posterior longitudinal ligament patients. *J. Korean Neurosurg. Soc.* 52 (1), 7–13. doi:10.3340/jkns.2012.52.1.7

Kamiya, M., HarAdA, A., MizunoM.Iwata, H., and Yamada, Y. (2001). Association between a polymorphism of the transforming growth factor-beta1 gene and genetic susceptibility to ossification of the posterior longitudinal ligament in Japanese patients. *Spine 1976* 26 (11), 1264–1266. doi:10.1097/00007632-200106010-00017

Karasugi, T., Nakajima, M., Ikari, K., Tsuji, T., Matsumoto, M., and Chiba, K. (2013). A genome-wide sib-pair linkage analysis of ossification of the posterior longitudinal ligament of the spine. *J. Bone Min. Metab.* 31 (2), 136–143. doi:10.1007/s00774-012-0404-y

Kato, K., Nishimasu, H., Okudaira, S., Mihara, E., Ishitani, R., Takagi, J., et al. (2012). Crystal structure of Enpp1, an extracellular glycoprotein involved in bone mineralization and insulin signaling. *Proc. Natl. Acad. Sci. U. S. A.* 109 (42), 16876–16881. doi:10.1073/pnas.1208017109

Kawaguchi, Y., Furushima, K., Sugimori, K., Inoue, I., and Kimura, T. (2003). Association between polymorphism of the transforming growth factor-beta1 gene with the radiologic characteristic and ossification of the posterior longitudinal ligament. *Spine 1976* 28 (13), 1424–1426. doi:10.1097/01.BRS.0000068245.27017.9F

Kim, D. H., Jeong, Y. S., Chon, J., Yoo, S. D., Kim, H. S., Kang, S. W., et al. (2011). Association between interleukin 15 receptor, alpha (IL15RA) polymorphism and Korean patients with ossification of the posterior longitudinal ligament. *Cytokine* 55 (3), 343–346. doi:10.1016/j.cyto.2011.05.016

Kim, D. H., Yun, D. H., Kim, H. S., Min, S. K., Yoo, S. D., Lee, K. H., et al. (2014). The insertion/deletion polymorphism of Angiotensin I converting Enzyme gene is associated with ossification of the posterior longitudinal ligament in the Korean population. *Ann. Rehabil. Med.* 38 (1), 1–5. doi:10.5535/arm.2014.38.1.1

Kim, K. H., Kuh, S. U., Park, J. Y., Lee, S. J., Park, H. S., Chin, D. K., et al. (2014). Association between BMP-2 and COL6A1 gene polymorphisms with susceptibility to ossification of the posterior longitudinal ligament of the cervical spine in Korean patients and family members. *Genet. Mol. Res.* 13 (1), 2240–2247. doi:10.4238/2014.March.31.4

Kim, K. T., Kim, D. H., Chung, J. Y., Lee, S., Joo, J., Nah, S. S., et al. (2012). Association of interferon gamma polymorphism with ossification of the posterior longitudinal ligament in the Korean population. *Immunol. Invest.* 41 (8), 876–887. doi:10.3109/08820139.2012.714437

Kim, T. J., Jun, J. B., Joo, K. B., and Uhm, W. S. (2007). Prevalence of ossification of posterior longitudinal ligament in patients with ankylosing spondylitis. *J. Rheumatol.* 34 (12), 2460–2462.

Kobashi, G., Ohta, K., Washio, M., Okamoto, K., Sasaki, S., Yokoyama, T., et al. (2008). FokI variant of vitamin D receptor gene and factors related to atherosclerosis associated with ossification of the posterior longitudinal ligament of the spine: A multi-hospital case-control study. *Spine 1976* 33 (16), E553–E558. doi:10.1097/BRS.0b013e31817e9de2

Koga, H., Sakou, T., TakEtomi, E., Hayashi, K., Numasawa, T., Harata, S., et al. (1998). Genetic mapping of ossification of the posterior longitudinal ligament of the spine. *Am. J. Hum. Genet.* 62 (6), 1460–1467. doi:10.1086/301868

Kong, Q., Ma, X., Li, F., Guo, Z., Qi, Q., Li, W., et al. (2007). COL6A1 polymorphisms associated with ossification of the ligamentum flavum and ossification of the posterior longitudinal ligament. *Spine 1976* 32 (25), 2834–2838. doi:10.1097/BRS.0b013e31815b761c

Koshizuka, Y., Kawaguchi, H., Ogata, N., Ikeda, T., Mabuchi, A., Seichi, A., et al. (2002). Nucleotide pyrophosphatase gene polymorphism associated with ossification of the posterior longitudinal ligament of the spine. *J. Bone Min. Res.* 17 (1), 138–144. doi:10.1359/jbmr.2002.17.1.138

Kozanoglu, E., Guzel, R., Guler-UysalF.and Goncu, K. (2002). Coexistence of diffuse idiopathic skeletal hyperostosis and ankylosing spondylitis: A case report. *Clin. Rheumatol.* 21 (3), 258–260. doi:10.1007/pl00011224

Kranenburg, H. C., Westerveld, L. A., Verlaan, J. J., Oner, F. C., Dhert, W. J. A., Voorhout, G., et al. (2010). The dog as an animal model for DISH? *Eur. Spine J.* 19 (8), 1325–1329. doi:10.1007/s00586-010-1280-6

Kranenburg, H. J., Hazewinkel, H. A., and Meij, B. P. (2014). Naturally occurring spinal hyperostosis in dogs as a model for human spinal disorders. *ILAR J.* 55 (1), 150–163. doi:10.1093/ilar/ilu012

Kuperus, J. S., Waalwijk, J. F., Regan, E. A., van der Horst-Bruinsma, I. E., Oner, F. C., de Jong, P. A., et al. (2018). Simultaneous occurrence of ankylosing spondylitis and diffuse idiopathic skeletal hyperostosis: A systematic review. *Rheumatol. Oxf.* 57 (12), 2120–2128. doi:10.1093/rheumatology/key211

Lambert, R. G., and Becker, E. J. (1989). Diffuse skeletal hyperostosis in idiopathic hypoparathyroidism. *Clin. Radiol.* 40 (2), 212–215. doi:10.1016/s0009-9260(89)80101-1

Levy-Litan, V., Hershkovitz, E., Avizov, L., Leventhal, N., Bercovich, D., Chalifa-Caspi, V., et al. (2010). Autosomal-recessive hypophosphatemic rickets is associated with an inactivation mutation in the ENPP1 gene. *Am. J. Hum. Genet.* 86 (2), 273–278. doi:10.1016/j.ajhg.2010.01.010

Li, M., Meng, H., Du, J., Tao, H., Luo, Z., and Wang, Z. (2012). Management of thoracic myelopathy caused by ossification of the posterior longitudinal ligament combined with ossification of the ligamentum flavum-a retrospective study. *Spine J.* 12 (12), 1093–1102. doi:10.1016/j.spinee.2012.10.022

Lim, J. J., Shin, D. A., Jeon, Y. J., Kumar, H., Sohn, S., Min, H. S., et al. (2016). Association of miR-146a, miR-149, miR-196a2, and miR-499 polymorphisms with ossification of the posterior longitudinal ligament of the cervical spine. *PLoS One* 11 (7), e0159756. doi:10.1371/journal.pone.0159756

Littlejohn, G. O., and Hall, S. (1982). Diffuse idiopathic skeletal hyperostosis and new bone formation in male gouty subjects. A radiologic study. *Rheumatol. Int.* 2 (2), 83–86. doi:10.1007/BF00541250

Liu, G. Y., Liang, Q. H., Cui, R. R., Liu, Y., Wu, S. S., Shan, P. F., et al. (2014). Leptin promotes the osteoblastic differentiation of vascular smooth muscle cells from female mice by increasing RANKL expression. *Endocrinology* 155 (2), 558–567. doi:10.1210/en.2013-1298

Liu, Y., Zhao, Y., Chen, Y., Shi, G., and Yuan, W. (2010). RUNX2 polymorphisms associated with OPLL and OLF in the Han population. *Clin. Orthop. Relat. Res.* 468 (12), 3333–3341. doi:10.1007/s11999-010-1511-5

Macia-Villa, C. C., Sifuentes-Giraldo, W. A., and Medina-Luezas, J. (2016). Simultaneous occurrence of ankylosing spondylitis and diffuse idiopathic skeletal hyperostosis (Forestier-Rotes-Querol disease). *Reumatol. Clin.* 57, 2120–2128. doi:10.1093/rheumatology/key211

Mader, R., Verlaan, J. J., and Buskila, D. (2013). Diffuse idiopathic skeletal hyperostosis: Clinical features and pathogenic mechanisms. *Nat. Rev. Rheumatol.* 9 (12), 741–750. doi:10.1038/nrrheum.2013.165

Maeda, S., Ishidou, Y., Koga, H., TakEtomi, E., Ikari, K., Komiya, S., et al. (2001). Functional impact of human collagen alpha2(XI) gene polymorphism in pathogenesis of ossification of the posterior longitudinal ligament of the spine. *J. Bone Min. Res.* 16 (5), 948–957. doi:10.1359/jbmr.2001.16.5.948

Maeda, S., Koga, H., MatSunaga, S., Numasawa, T., Ikari, K., Furushima, K., et al. (2001). Gender-specific haplotype association of collagen alpha2 (XI) gene in ossification of the posterior longitudinal ligament of the spine. *J. Hum. Genet.* 46 (1), 1–4. doi:10.1007/s100380170117

Maertens, M., Mielants, H., Verstraete, K., and Veys, E. M. (1992). Simultaneous occurrence of diffuse idiopathic skeletal hyperostosis and ankylosing spondylitis in the same patient. *J. Rheumatol.* 19 (12), 1978–1983.

Mata, S., WolFeF.Joseph, L., and Esdaile, J. M. (1995). Absence of an association of rheumatoid arthritis and diffuse idiopathic skeletal hyperostosis: A case-control study. *J. Rheumatol.* 22 (11), 2062–2064.

Matsunaga, S., and Sakou, T. (2006). in *Opll: Disease entity, incidence, literature search, and prognosis*. Editors K. Y. OPLL, K. Nakamura, and Y. Toyama (Tokyo: Springer).

Matsunaga, S., YaMaguchiM.Hayashi, K., and Sakou, T. (1999). Genetic analysis of ossification of the posterior longitudinal ligament. *Spine (Phila Pa 1976)* 24 (10), 937–938. doi:10.1097/00007632-199905150-00002

Mazières, B., Jung-Rozenfarb, M., and Arlet, J. (1978). Paget's disease, ankylosing vertebral hyperostosis and hyperostosis frontalis interna. *Sem. Hop.* 54 (13-16), 521–525.

Meng, X. L., Wang, H., Yang, H., Hai, Y., Tian, B. p., and Lin, X. (2010). T allele at site 6007 of bone morphogenetic protein-4 gene increases genetic susceptibility to ossification of the posterior longitudinal ligament in male Chinese Han population. *Chin. Med. J.* 123 (18), 2537–2542.

Miyasaka, K., Kaneda, K., Ito, T., Takei, H., Sugimoto, S., and TsuruM. (1982). Ossification of spinal ligaments causing thoracic radiculomyelopathy. *Radiology* 143 (2), 463–468. doi:10.1148/radiology.143.2.7071348

Montague, C. T., Farooqi, I. S., Whitehead, J. P., Soos, M. A., Rau, H., Wareham, N. J., et al. (1997). Congenital leptin deficiency is associated with severe early-onset obesity in humans. *Nature* 387 (6636), 903–908. doi:10.1038/43185

Morales, A. A., Valdazo, P., Corres, J., Talbot, J. R., PerezF.and Baylink, D. J. (1993). Coexistence of Paget's bone disease and diffuse idiopathic skeletal hyperostosis in males. *Clin. Exp. Rheumatol.* 11 (4), 361–365.

Moreno, A. C., Gonzalez, M. L., DuffinM.Lopez-Longo, F. J., Carreno, L., and Forrester, D. M. (1996). Simultaneous occurrence of diffuse idiopathic skeletal hyperostosis and ankylosing spondylitis. *Rev. Rhum. Engl. Ed.* 63 (4), 292–295.

Muthukumar, N., Karuppaswamy, U., and Sankarasubbu, B. (2000). Calcium pyrophosphate dihydrate deposition disease causing thoracic cord compression: Case report. *Neurosurgery* 46 (1), 222–225. doi:10.1097/00006123-200001000-00047

Nakajima, M., Kou, I., Ohashi, H., and Ikegawa, S. (2016). Identification and functional characterization of RSPO2 as a susceptibility gene for ossification of the posterior longitudinal ligament of the spine. *Am. J. Hum. Genet.* 99 (1), 202–207. doi:10.1016/j.ajhg.2016.05.018

Nakajima, M., Takahashi, A., Tsuji, T., Karasugi, T., Baba, H., Uchida, K., et al. (2014). A genome-wide association study identifies susceptibility loci for ossification of the posterior longitudinal ligament of the spine. *Nat. Genet.* 46 (9), 1012–1016. doi:10.1038/ng.3045

Nakamura, I., Ikegawa, S., OkAwA, A., Okuda, S., Koshizuka, Y., KawagucHi, H., et al. (1999). Association of the human NPPS gene with ossification of the posterior longitudinal ligament of the spine (OPLL). *Hum. Genet.* 104 (6), 492–497. doi:10.1007/s004390050993

Nitschke, Y., and Rutsch, F. (2012). Generalized arterial calcification of infancy and pseudoxanthoma elasticum: Two sides of the same coin. *Front. Genet.* 3, 302. doi:10.3389/fgene.2012.00302

Nobta, M., Tsukazaki, T., Shibata, Y., Xin, C., Moriishi, T., Sakano, S., et al. (2005). Critical regulation of bone morphogenetic protein-induced osteoblastic differentiation by Delta1/Jagged1-activated Notch1 signaling. *J. Biol. Chem.* 280 (16), 15842–15848. doi:10.1074/jbc.M412891200

Nouri, A., Tetreault, L., Singh, A., Karadimas, S. K., and Fehlings, M. G. (2015). Degenerative cervical myelopathy: Epidemiology, genetics, and pathogenesis. *Spine (Phila Pa 1976)* 40 (12), E675–E693. doi:10.1097/BRS.0000000000000913

Numasawa, T., Koga, H., Ueyama, K., Maeda, S., Sakou, T., Harata, S., et al. (1999). Human retinoic X receptor beta: Complete genomic sequence and mutation search for ossification of posterior longitudinal ligament of the spine. *J. Bone Min. Res.* 14 (4), 500–508. doi:10.1359/jbmr.1999.14.4.500

Ogata, N., Koshizuka, Y., Miura, T., Iwasaki, M., Hosoi, T., Shiraki, M., et al. (2002). Association of bone metabolism regulatory factor gene polymorphisms with susceptibility to ossification of the posterior longitudinal ligament of the spine and its severity. *Spine 1976* 27 (16), 1765–1771. doi:10.1097/00007632-200208150-00015

Okano, T., Ishidou, Y., KatoM.Imamura, T., Yonemori, K., OriguchiN., et al. (1997). Orthotopic ossification of the spinal ligaments of zucker fatty rats: A possible animal model for ossification of the human posterior longitudinal ligament. *J. Orthop. Res.* 15 (6), 820–829. doi:10.1002/jor.1100150606

Okawa, A., Goto, S., Moriya, H., Nakamura, Y., and Ikegawa, S. (1998). Mutation in Npps in a mouse model of ossification of the posterior longitudinal ligament of the spine. *Nat. Genet.* 19 (3), 271–273. doi:10.1038/956

Okazaki, T., SaiTo, T., MiTomo, T., and Siota, Y. (1976). Pseudogout: Clinical observations and chemical analyses of deposits. *Arthritis Rheum.* 19 (3), 293–305. doi:10.1002/1529-0131(197605/06)19:3+<293:aid-art1780190704>3.0.co;2-r

Olivieri, I. (1991). Coexisting diffuse idiopathic skeletal hyperostosis and ankylosing spondylitis. *Clin. Rheumatol.* 10 (1), 95. doi:10.1007/BF02208043

Olivieri, I., Trippi, D., Gherardi, S., and Pasero, G. (1987). Coexistence of ankylosing spondylitis and diffuse idiopathic skeletal hyperostosis: Another report. *J. Rheumatol.* 14 (5), 1058–1060.

Olivieri, I., Vitali, C., GemiGnani, G., and Pasero, G. (1989). Concomitant ankylosing spondylitis and DISH. *J. Rheumatol.* 16 (8), 1170–1172.

Onishi, E., Sano, H., and Matsushita, M. (2016). Surgical treatment for thoracic myelopathy due to simultaneous ossification of the posterior longitudinal ligament and ligamentum flavum at the same level. *Clin. Spine Surg.* 29, E389–E395. doi:10.1097/BSD.0000000000000059

Ostrander, E. A., Galibert, F., and Patterson, D. F. (2000). Canine genetics comes of age. *Trends Genet.* 16 (3), 117–124. doi:10.1016/s0168-9525(99)01958-7

Parreira, B., Couto, A. R., Rocha, F., Sousa, M., Faustino, V., Power, D. M., et al. (2020). Whole exome sequencing of patients with diffuse idiopathic skeletal hyperostosis and calcium pyrophosphate crystal chondrocalcinosis. *Acta Reumatol. Port.* 45 (2), 116–126.

Passiu, G., Sebastiani, G. D., and Tuveri, M. A. (1991). Diffuse idiopathic skeletal hyperostosis of the cervical spine in a patient with ankylosing spondylitis. Description of a personal case. *Ann. Ital. Med. Int.* 6 (1), 61–64.

Phillips, M. S., Liu, Q., Hammond, H. A., Dugan, V., Hey, P. J., Caskey, C. J., et al. (1996). Leptin receptor missense mutation in the fatty Zucker rat. *Nat. Genet.* 13 (1), 18–19. doi:10.1038/ng0596-18

Pillai, S., and Littlejohn, G. (2014). Metabolic factors in diffuse idiopathic skeletal hyperostosis - a review of clinical data. *Open Rheumatol. J.* 8, 116–128. doi:10.2174/1874312901408010116

Prabhu, R. M., Rathod, T. N., Mohanty, S. S., Hadole, B. S., Marathe, N. A., and Rai, A. K. (2022). A case of cervical OPLL and DISH mimicking stroke. *Surg. Neurol. Int.* 13, 158. doi:10.25259/SNI_247_2022

Qu, X., Chen, Z., Fan, D., Xiang, S., Sun, C., Zeng, Y., et al. (2017). Two novel BMP-2 variants identified in patients with thoracic ossification of the ligamentum flavum. *Eur. J. Hum. Genet.* 25 (5), 565–571. doi:10.1038/ejhg.2017.2

Qu, X., Hou, X., Chen, Z., Chen, G., Fan, T., and Yang, X. (2021). Association analysis and functional study of COL6A1 single nucleotide polymorphisms in thoracic ossification of the ligamentum flavum in the Chinese Han population. *Eur. Spine J.* 30 (10), 2782–2790. doi:10.1007/s00586-021-06932-y

Ramos, Y. F., Bos, S. D., van der Breggen, R., Kloppenburg, M., Ye, K., Lameijer, E. W. E. M. W., et al. (2015). A gain of function mutation in TNFRSF11B encoding osteoprotegerin causes osteoarthritis with chondrocalcinosis. *Ann. Rheum. Dis.* 74 (9), 1756–1762. doi:10.1136/annrheumdis-2013-205149

Ren, Y., Feng, J., Liu, Z. z., Wan, H., Li, J. h., and Lin, X. (2012). A new haplotype in BMP4 implicated in ossification of the posterior longitudinal ligament (OPLL) in a Chinese population. *J. Orthop. Res.* 30 (5), 748–756. doi:10.1002/jor.21586

Ren, Y., Liu, Z. z., Feng, J., Wan, H., Li, J. h., Wang, H., et al. (2012). Association of a BMP9 haplotype with ossification of the posterior longitudinal ligament (OPLL) in a Chinese population. *PLoS One* 7 (7), e40587. doi:10.1371/journal.pone.0040587

Resnick, D., Curd, J., Shapiro, R. F., and Wiesner, K. B. (1978). Radiographic abnormalities of rheumatoid arthritis in patients with diffuse idiopathic skeletal hyperostosis. *Arthritis Rheum.* 21 (1), 1–5. doi:10.1002/art.1780210101

Resnick, D., and Pineda, C. (1984). Vertebral involvement in calcium pyrophosphate dihydrate crystal deposition disease. Radiographic-pathological correlation. *Radiology* 153 (1), 55–60. doi:10.1148/radiology.153.1.6089266

Resnick, D., Shapiro, R. F., Wiesner, K. B., Niwayama, G., Utsinger, P. D., and Shaul, S. R. (1978). Diffuse idiopathic skeletal hyperostosis (DISH) [ankylosing hyperostosis of Forestier and Rotes-Querol]. *Semin. Arthritis Rheum.* 7 (3), 153–187. doi:10.1016/0049-0172(78)90036-7

Rillo, O. L., Scheines, E. J., Moreno, C., Barreira, J. C., Porrini, A. A., and Maldonado Cocco, J. A. (1989). Coexistence of diffuse idiopathic skeletal hyperostosis and ankylosing spondylitis. *Clin. Rheumatol.* 8 (4), 499–503. doi:10.1007/BF02032103

Rivas, A. M., and Lado-Abeal, J. (2013). Diffuse idiopathic skeletal hyperostosis and familial hypocalciuric hypercalcemia: A unique association in a young female. *Am. J. Med. Sci.* 346 (3), 247–249. doi:10.1097/MAJ.0b013e31828b663b

Rutsch, F., Ruf, N., Vaingankar, S., Toliat, M. R., Suk, A., Hohne, W., et al. (2003). Mutations in ENPP1 are associated with 'idiopathic' infantile arterial calcification. *Nat. Genet.* 34 (4), 379–381. doi:10.1038/ng1221

Saito, T., Shimizu, Y., Hori, M., Taguchi, M., Igarashi, T., Fukumoto, S., et al. (2011). A patient with hypophosphatemic rickets and ossification of posterior longitudinal ligament caused by a novel homozygous mutation in ENPP1 gene. *Bone* 49 (4), 913–916. doi:10.1016/j.bone.2011.06.029

Sakou, T., TakEtomi, E., MatSunaga, S., YaMaguchiM.Sonoda, S., and YaShiki, S. (1991). Genetic study of ossification of the posterior longitudinal ligament in the cervical spine with human leukocyte antigen haplotype. *Spine (Phila Pa 1976)* 16 (11), 1249–1252. doi:10.1097/00007632-199111000-00001

Saleem, S. N., and Hawass, Z. (2014). Ankylosing spondylitis or diffuse idiopathic skeletal hyperostosis in royal Egyptian mummies of 18th -20th dynasties? CT and archaeology studies. *Arthritis Rheumatol.* 66 (12), 3311–3316. doi:10.1002/art.38864

Schlapbach, P., Beyeler, C., Gerber, N. J., van der Linden, S., Burgi, U., Fuchs, W. A., et al. (1992). The prevalence of palpable finger joint nodules in diffuse idiopathic skeletal hyperostosis (DISH). A controlled study. *Br. J. Rheumatol.* 31 (8), 531–534. doi:10.1093/rheumatology/31.8.531

Schlosstein, L., Terasaki, P. I., Bluestone, R., and Pearson, C. M. (1973). High association of an HL-A antigen, W27, with ankylosing spondylitis. *N. Engl. J. Med.* 288 (14), 704–706. doi:10.1056/NEJM197304052881403

Stefan, C., Jansen, S., and Bollen, M. (2005). NPP-Type ectophosphodiesterases: Unity in diversity. *Trends biochem. Sci.* 30 (10), 542–550. doi:10.1016/j.tibs.2005.08.005

Tahara, M., Aiba, A., Yamazaki, M., Ikeda, Y., Goto, S., Moriya, H., et al. (2005). The extent of ossification of posterior longitudinal ligament of the spine associated with nucleotide pyrophosphatase gene and leptin receptor gene polymorphisms. *Spine (Phila Pa 1976)* 30 (8), 877–880. doi:10.1097/01.brs.0000160686.18321.ad

Takayuki, M., Takashi, H., Toshitaka, Y., Hiroyuki, I., Yu, M., Satoru, E., et al. (2021). Association between diffuse idiopathic skeletal hyperostosis and thoracic kyphosis in patients with cervical myelopathy: A retrospective observational study. *BMC Musculoskelet. Disord.* 22 (1), 964. doi:10.1186/s12891-021-04851-z

Tanabe, J., Sarin, H., and Kindt, G. (2002). Familial ossification of the posterior longitudinal ligament (OPLL) in the thoracic spine: Case report. *Surg. Neurol.* 58 (6), 403–405. doi:10.1016/s0090-3019(02)00927-8

Tanaka, T., Ikari, K., Furushima, K., Okada, A., Tanaka, H., Furukawa, K. I., et al. (2003). Genomewide linkage and linkage disequilibrium analyses identify COL6A1, on chromosome 21, as the locus for ossification of the posterior longitudinal ligament of the spine. *Am. J. Hum. Genet.* 73 (4), 812–822. doi:10.1086/378593

Tanikawa, E., Furuya, K., and Nakajima, H. (1986). Genetic study on ossification of posterior longitudinal ligament. *Bull. Tokyo Med. Dent. Univ.* 33 (3), 117–128.

Tenti, S., Palmitesta, P., GiordaNoN.GaleazziM.and FiorAvAnti, A. (2017). Increased serum leptin and visfatin levels in patients with diffuse idiopathic skeletal hyperostosis: A comparative study. *Scand. J. Rheumatol.* 46 (2), 156–158. doi:10.1080/03009742.2016.1188981

Terayama, K. (1989). Genetic studies on ossification of the posterior longitudinal ligament of the spine. *Spine (Phila Pa 1976)* 14 (11), 1184–1191. doi:10.1097/00007632-198911000-00009

Tishler, M., and Yaron, M. (1992). Two cases of diffuse idiopathic skeletal hyperostosis and ankylosing spondylitis. *Br. J. Rheumatol.* 31 (8), 569–571. doi:10.1093/rheumatology/31.8.569-b

Togni, A., Morgan, J. P., and SteFFenF. (2014). Radiographic and MRI characteristics of lumbar disseminated idiopathic spinal hyperostosis and spondylosis deformans in dogs. *J. Small Anim. Pract.* 55 (7), 343–349. doi:10.1111/jsap.12218

Troise Rioda, W., and Ferraccioli, G. F. (1990). DISH and ankylosing spondylitis. Case report and review of the literature. *Clin. Exp. Rheumatol.* 8 (6), 591–593.

Tsukahara, S., Miyazawa, N., Akagawa, H., Forejtova, S., Pavelka, K., Tanaka, T., et al. (2005). COL6A1, the candidate gene for ossification of the posterior longitudinal ligament, is associated with diffuse idiopathic skeletal hyperostosis in Japanese. *Spine* 30 (20), 2321–2324. doi:10.1097/01.brs.0000182318.47343.6d

Unverdi, S., Ozturk, M. A., Inal, S., Selek, H., Goker, B., Haznedaroglu, C., et al. (2009). Idiopathic hypoparathyroidism mimicking diffuse idiopathic skeletal hyperostosis. *J. Clin. Rheumatol.* 15 (7), 361–362. doi:10.1097/RHU.0b013e3181bb9865

van der Korst, J. K., Geerards, J., and Driessens, F. C. (1974). A hereditary type of idiopathic articular chondrocalcinosis. Survey of a pedigree. *Am. J. Med.* 56 (3), 307–314. doi:10.1016/0002-9343(74)90612-3

Wang, H., Jin, W., and Li, H. (2018). Genetic polymorphisms in bone morphogenetic protein receptor type IA gene predisposes individuals to ossification of the posterior longitudinal ligament of the cervical spine via the smad signaling pathway. *BMC Musculoskelet. Disord.* 19 (1), 61. doi:10.1186/s12891-018-1966-1

Wang, H., Yang, Z. h., Liu, D. m., Wang, L., Meng, X. l., and Tian, B. p. (2008). Association between two polymorphisms of the bone morpho-genetic protein-2 gene with genetic susceptibility to ossification of the posterior longitudinal ligament of the cervical spine and its severity. *Chin. Med. J.* 121 (18), 1806–1810. doi:10.1097/00029330-200809020-00010

Wang, P., Liu, X., Zhu, B., Ma, Y., Yong, L., Teng, Z., et al. (2018). Association of IL17RC and COL6A1 genetic polymorphisms with susceptibility to ossification of the thoracic posterior longitudinal ligament in Chinese patients. *J. Orthop. Surg. Res.* 13 (1), 109. doi:10.1186/s13018-018-0817-y

Wang, P., Liu, X., Zhu, B., Ma, Y., Yong, L., Teng, Z., et al. (2018). Identification of susceptibility loci for thoracic ossification of the posterior longitudinal ligament by whole-genome sequencing. *Mol. Med. Rep.* 17 (2), 2557–2564. doi:10.3892/mmr.2017.8171

Warraich, S., Bone, D. B. J., Quinonez, D., Ii, H., Choi, D. S., Holdsworth, D. W., et al. (2013). Loss of equilibrative nucleoside transporter 1 in mice leads to progressive ectopic mineralization of spinal tissues resembling diffuse idiopathic skeletal hyperostosis in humans. *J. Bone Min. Res.* 28 (5), 1135–1149. doi:10.1002/jbmr.1826

Wei, W., He, H. L., Chen, C. Y., Zhao, Y., Jiang, H. L., Liu, W. T., et al. (2014). Whole exome sequencing implicates PTCH1 and COL17A1 genes in ossification of the posterior longitudinal ligament of the cervical spine in Chinese patients. *Genet. Mol. Res.* 13 (1), 1794–1804. doi:10.4238/2014.March.17.7

Williamson, P. K., and Reginato, A. J. (1984). Diffuse idiopathic skeletal hyperostosis of the cervical spine in a patient with ankylosing spondylitis. *Arthritis Rheum.* 27 (5), 570–573. doi:10.1002/art.1780270514

Wooten, M. (2009). The coexistence of ankylosing spondylitis and diffuse idiopathic skeletal hyperostosis. *Clin. Rheumatol.* 28 (5), 619. doi:10.1007/s10067-009-1111-5

Yamagami, T., Kawano, N., and Nakano, H. (2000). Calcification of the cervical ligamentum flavum--case report. *Neurol. Med. Chir.* 40 (4), 234–238. doi:10.2176/nmc.40.234

Yamaguchi, M. (1991). Genetic study on OPLL in the cervical spine with HLA haplotype. *Nihon Seikeigeka Gakkai Zasshi* 65 (8), 527–535.

Yamazaki, M., Moriya, H., Goto, S., Saitoh, Y., Arai, K., and Nagai, Y. (1991). Increased type XI collagen expression in the spinal hyperostotic mouse (TWY/TWY). *Calcif. Tissue Int.* 48, 182–189. doi:10.1007/bf02570553

Yan, L., Chang, Z., Liu, Y., Li, Y. B., He, B. R., and Hao, D. J. (2013). *A single nucleotide polymorphism in the human bone morphogenetic protein-2 gene (109T > G) affects the Smad signaling pathway and the predisposition to ossification of the posterior longitudinal ligament of the spine. Chin. Med. J.* 126 (6), 1112–1118.

Yan, L., Zhao, W. g., Li, J. j., Yang, H., Wang, H., and Lin, X. (2010). Linkage of three polymorphisms on chromosome 20p12 to ossification of the posterior longitudinal ligament of spine and its severity in Han Chinese patients. *Chin. Med. J.* 123 (17), 2341–2346.

Yu, W. R., Liu, T., Kiehl, T. R., and Fehlings, M. G. (2011). Human neuropathological and animal model evidence supporting a role for Fas-mediated apoptosis and inflammation in cervical spondylotic myelopathy. *Brain* 134 (5), 1277–1292. doi:10.1093/brain/awr054

frontiers | Frontiers in Genetics

TYPE Perspective
PUBLISHED 25 January 2023
DOI 10.3389/fgene.2023.1129207

OPEN ACCESS

EDITED BY
Jordi Pérez-Tur,
Institute of Biomedicine of Valencia (CSIC), Spain

REVIEWED BY
Athar Ansari,
Wayne State University, United States

*CORRESPONDENCE
Matteo Vecellio,
matteo.vecellio@ndorms.ox.ac.uk

SPECIALTY SECTION
This article was submitted to Genetics of Common and Rare Diseases, a section of the journal Frontiers in Genetics

RECEIVED 21 December 2022
ACCEPTED 16 January 2023
PUBLISHED 25 January 2023

CITATION
Davidson C, Wordsworth BP, Cohen CJ, Knight JC and Vecellio M (2023), Chromosome conformation capture approaches to investigate 3D genome architecture in Ankylosing Spondylitis. *Front. Genet.* 14:1129207. doi: 10.3389/fgene.2023.1129207

Chromosome conformation capture approaches to investigate 3D genome architecture in Ankylosing Spondylitis

Connor Davidson[1,2], B. Paul Wordsworth[2], Carla J. Cohen[2,3], Julian C. Knight[1] and Matteo Vecellio[2,4]*

[1]Wellcome Centre of Human Genetics, University of Oxford, Oxford, United Kingdom, [2]Nuffield Department of Orthopaedics, Rheumatology and Musculoskeletal Sciences, Botnar Research Centre, University of Oxford, Oxford, United Kingdom, [3]MRC WIMM Centre for Computational Biology, MRC Weatherall Institute for Molecular Medicine, University of Oxford, Oxford, United Kingdom, [4]Centro Ricerche Fondazione Italiana Ricerca Sull'Artrite (FIRA), Fondazione Pisana x la Scienza ONLUS, San Giuliano Terme, Italy

Ankylosing Spondylitis (AS) is a chronic inflammatory arthritis of the spine exhibiting a strong genetic background. The mechanistic and functional understanding of the AS-associated genomic loci, identified with Genome Wide Association Studies (GWAS), remains challenging. Chromosome conformation capture (3C) and derivatives are recent techniques which are of great help in elucidating the spatial genome organization and of enormous support in uncover a mechanistic explanation for disease-associated genetic variants. The perturbation of three-dimensional (3D) genome hierarchy may lead to a plethora of human diseases, including rheumatological disorders. Here we illustrate the latest approaches and related findings on the field of genome organization, highlighting how the instability of 3D genome conformation may be among the causes of rheumatological disease phenotypes. We suggest a new perspective on the inclusive potential of a 3C approach to inform GWAS results in rheumatic diseases. 3D genome organization may ultimately lead to a more precise and comprehensive functional interpretation of AS association, which is the starting point for emerging and more specific therapies.

KEYWORDS

genomics, three dimensional genome, ankylosing spondylitis, chromosome conformation capture (3C), topologically associated domain (TAD), rheumatic and musculoskeletal disease

Introduction

The combination of environmental and genetic factors may lead to the development of complex diseases (Hunter, 2005). Ankylosing Spondylitis (AS) is a common form of arthritis primarily affecting the spine, characterised by inflammation at the entheses (Bridgewood et al., 2019) and sacroiliac joints (Brewerton et al., 1973). AS is a highly heritable disease with more than 100 genomic loci found implicated in increasing the risk (International Genetics of Ankylosing Spondylitis Consortium et al., 2013; Ellinghaus et al., 2016). Genome wide association studies (GWAS) have been very successful in polygenic disease as they identified thousands of common genetic variants or single nucleotide polymorphisms (SNPs), which can have a phenotypical individual effect (Huo et al., 2019; Crouch and Bodmer, 2020). The identification of a causal variant from GWAS data may help our understanding of complex traits biology, suggesting new target genes and methods of controlling them. Unfortunately, disease-associated loci often contain multiple genes

making the scenario extremely challenging; genetic variants in proximal vicinity tend to be inherited together, in a phenomenon called linkage disequilibrium (LD), making difficult to identify the causal variant underpinning the association (Cano-Gamez and Trynka, 2020). In recent years, large-scale epigenomic projects have mapped hundreds of thousands of potential regulatory sites in the human genome, but only a small proportion of these elements are proximal to transcription start sites (Bagchi and Iyer, 2016). In AS, we and others were able to successfully identify the causal functional SNPs at the Interleukin 23 Receptor (*IL23R*), endoplasmic reticulum aminopeptidase 1 (*ERAP1*) and RUNX Family Transcription Factor 3 (*RUNX3*) genomic loci elucidating their transcriptional regulation (Keidel et al., 2013; Roberts et al., 2016; Vecellio et al., 2016; Vecellio et al., 2018; Vecellio et al., 2021).

The three-dimensional (3D) organization of the genome is essential in facilitating fundamental processes which occur in the cell nucleus including, transcriptional regulation, DNA damage and replication (McCord et al., 2020). Over the last 20 years, chromosome conformation capture (3C) techniques have been widely used to identify and estimate the frequency of interaction of multiple genomic loci in the genome (Dekker et al., 2002; Phillips-Cremins et al., 2013; Hansen et al., 2018; Haws et al., 2022). In 3C methodology, restriction enzyme digestion followed by re-ligation of cross-linked chromatin in the nucleus of a cell, allows to detect the spatial vicinity between DNA sequences (de Wit and de Laat, 2012). 3C experiments have revealed that chromosomes are folded in complex structures emerging at different scales. These structures can be impacted by disease-associated SNPs, as reported extensively (Gorkin et al., 2019; Anania and Lupianez, 2020; Tsuchiya et al., 2021). Recent studies in polygenic disorders (Girdhar et al., 2022) show that using 3D genome architecture investigation has the utility to clarify the role of disease associated SNPs and to link them to specific genes to understand the phenotype and account for biological function (Khunsriraksakul et al., 2022; Zhao et al., 2022).

Original 3C methods are low-throughput and not able to define if multiple regions interact simultaneously or mutually exclusively. For this reason, several technologies deriving from the standard 3C have been developed, including Hi-C (high-throughput chromosome conformation capture) which allows the analysis of spatial genome organization and chromosome folding through sequencing (Dekker et al., 2002; van Steensel and Dekker, 2010; Dekker et al., 2013).

Here, we explore a selection of 3C methods (i.e. Hi-C, Tiling Capture-C) which might facilitate the understanding of 3D organization and chromosomal interactions and their impact in rheumatic diseases pathophysiology. We emphasise the importance of 3C approaches to inform GWAS interpretation, and their possible future application in precision medicine in prioritizing potential drug targets in polygenic rheumatic disorders including AS.

The 3D genome and the nuclear architecture

Chromosomes fold into compartments, often indicated as A and B, which refer to genomic loci with similar transcriptional activity that physically segregate in 3D space. In addition, contact domains, consist in any visible domains corresponding to elevated chromatin interactions regions. Topologically associated domains (TADs) are the hallmarks of genomic organization (see Figure 1) and are defined as local organizational domains taught to be formed primarily by loop extrusion where boundaries are most conserved during cell differentiation (<1 MB scale) (Gorkin et al., 2019; Goel and Hansen, 2021). TAD dysregulation is linked to various diseases, including neurological disorders and tumorigenesis (Medrano-Fernandez and Barco, 2016; Yang et al., 2019). As demonstrated by Lupianez et al. using CRISPR/Cas9 genome editing and 3C methods, the disruption of TADs might lead to a rewiring of long-range regulatory architectures and result in a pathogenic phenotype. Specifically, the authors focused on rare limb malformations and identified several rearrangements in the *epha4/pax3* (EPH Receptor A4/Paired Box 3) locus in mice causing disruption of the TAD, chromatin structural changes and the aberrant expression of developmental genes (Lupianez et al., 2015; Lupianez et al., 2016). In addition, Luppino and others have demonstrated the loss of cohesin leads to reduced chromatin mixing thus affecting the topology and transcriptional bursting frequencies of boundary-proximal genes (Luppino et al., 2020).

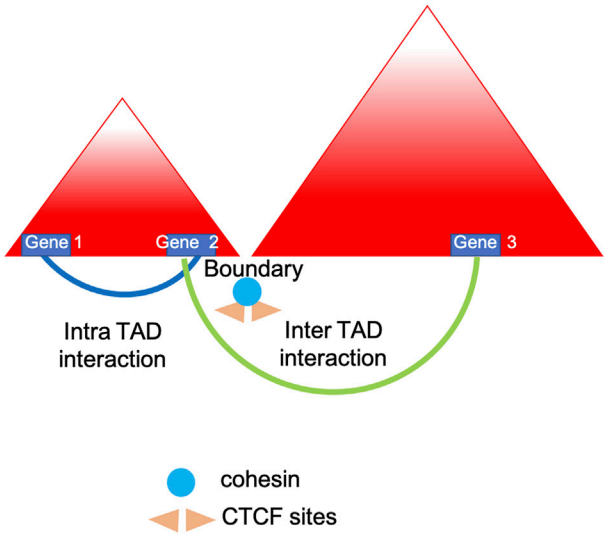

FIGURE 1
TADs insulation. Simplified model showing how topologically associated domains (TADs) are insulated by borders which are leaky enough to influence and regulate nearby genes expression (Luppino et al., 2020).

Loop boundaries are enriched in CCCTC-binding factor (CTCF) and cohesin, two architectural necessary proteins involved in long-range genome looping. It has been postulated that these two proteins form domains by a loop extrusion process. First proposed in 2015 following mathematical simulations and polymer modelling, the loop extrusion model (see Figure 2) suggests that a chromatin loop of increasing size is extruded by the cohesin complex until it is stalled by a pair of convergently oriented CTCF-bound sites (de Wit et al., 2015; Sanborn et al., 2015). The cohesin complex extrudes a loop uni- or bi-directionally until it faces an occupied CTCF binding site and then the loop is stabilized (Fudenberg et al., 2017). Several studies have explored the interplay between compartmentalization and chromatin looping, showing that the depletion of CTCF has no effect on compartments (Nora et al., 2017), while cohesin (and/

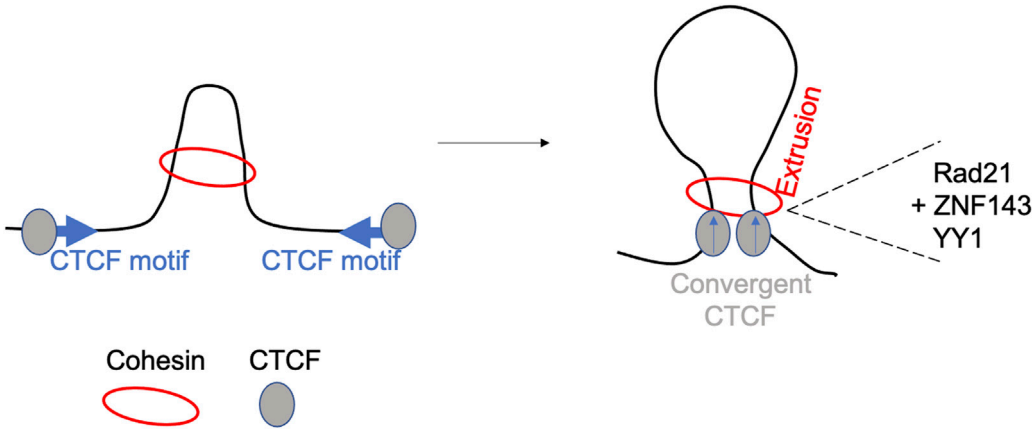

FIGURE 2
The loop-extrusion model. The model shows the generation of long-range cis-interactions, following extrusion by cohesin, CTCF cognate sites binding and involvement of other accessory proteins including YY1, RAD21 and ZNF143 (Hansen et al., 2018).

or RAD21) removal brings to the loss of domains and TADs making compartmentalization more prominent (Haarhuis et al., 2017; Wutz et al., 2017). In addition to CTCF and cohesin, boundaries frequently colocalize with active transcription start sites along with additional genomic factors such as YY1, RAD21 and ZNF143 which exhibit enrichment at strong boundaries (Hsieh et al., 2015; Bonev et al., 2017). Boundaries which are depleted of CTCF and YY1 are defined as weak boundaries. In addition, chromatin immunoprecipitation (ChIP)-seq experiments have revealed enrichment for ASH2L (ASH2 like, histone lysine methyltransferase complex subunit), H3K4Me3, SP1 (specificity protein 1) among other factors enriched at these boundaries. The role of RNA polymerase II has been investigated by Hsieh and others (Hsieh et al., 2015) demonstrating that active transcription mediated genome folding has a crucial role in the maintenance of the enhancer-promoter and promoter-promoter domains. Following the inhibition of RNA polymerase II, the intensity of those domains is significantly reduced without affecting higher-order chromatin organization (Hsieh et al., 2020). Stable enhancer-promoter interactions have been observed during the formation of *Drosophila* embryos, suggesting these interactions are important in developmental stages, cell fate decision and limb formation (Ghavi-Helm et al., 2014; Ji et al., 2016). Abnormalities in enhancer-promoter interactions, such as mutation in encoding proteins genes or enhancer-binding proteins lead to disease like Cornelia de Lange syndrome, often referred as enhanceropathy (Olley et al., 2018). The process of transcription termination at the 3' of a gene requires the recruitment of specific factors, which cross-talk with the initiation and enhancement machinery required for the start of transcription. 3C approach has been crucial in demonstrating the formation of gene loops showing interaction between transcription factors associated with promoter and those linked with transcription termination (Al-Husini et al., 2020).

The generation of comprehensive and high-resolution 3D genome maps may facilitate the discovery of small alterations (Chakraborty and Ay, 2019) which can lead a cascade of aberrant molecular events and drive disease phenotype.

3C-derived technologies to map the 3D genome

Recent advances in specific methods to investigate the 3D genome architecture include development of high-throughput chromosome conformation capture (Hi-C), Hi-ChIP and Tiled Capture (Mumbach et al., 2016; Galan et al., 2020; Oudelaar, 2022). All three methods capture genomic regions linked *via* 3D interactions, that are detected by Next-Generation Sequencing (NGS).

Hi-C was introduced in 2009, using biotinylation to enrich for proximity ligated contacts and thus modifying the library amplification process. Specifically, HiC takes advantage of using universal adapters and primers for high throughput sequencing. The unbiased "all *versus* all" approach clearly has a real advantage in defining all the genomic interactions genome wide (Lieberman-Aiden et al., 2009). It has been demonstrated that during differentiation, transcriptional changes occur when there is alteration in the strength of long-range interactions and the development of cell-type specific enhancer-promoter contacts (Bonev et al., 2017). Further, these interactions occur primarily in the same TAD and are strongly correlated with gene expression demonstrating how TADs constrain enhancer activity (Symmons et al., 2014).

Recently, Micro-C was developed from Hi-C, moving to a capture-fine (~1 kb) to a nucleosome level of resolution (~200bp) (Krietenstein et al., 2020). Formaldehyde and disuccinimidyl glutarate are used for fixation and cross-linking steps, while chromatin is digested with micrococcal nuclease (MNase), instead of restriction enzymes, to reach nucleosome-level resolution. Restriction enzymes sites are not equally distributed and not all the DNA is readily accessible as it is affected by nucleosomal accessibility (Szerlong and Hansen, 2011); using micrococcal nuclease digestion takes advantage of local DNA accessibility and facilitates the retention of intact nucleosomes (Voong et al., 2017). Micro-C has revealed two different classes of CTCF loops: those dependent on RNA-binding region (RBR) and those which are not (Hansen et al., 2019).

Hi-ChIP has been developed to delineate promoter-enhancer interactions by leveraging principles of *in situ* Hi-C (Mumbach

TABLE 1 A summary of the different techniques routinely used to analyse the conformation of the genome.

Technique	3C	4C	Hi-C	Micro-C	Hi-ChIP	ChIA-PET	Tiled-C
Chromatin looping	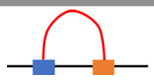			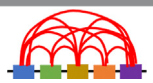	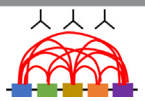	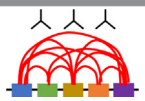	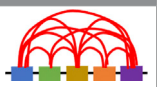
Type	One to one	One to all	All to all	All to all	All to all	All to all	All to all Some to all
Main steps	- Restriction enzyme digestion	- Restriction enzyme digestion	- Restriction enzyme digestion	-Double cross linking	- Restriction enzyme digestion	- Restriction enzyme digestion	- Restriction enzyme or MNase digestion
	- PCR	- microarray	- sonication	- MNase digestion	- sonication	- sonication	- biotinylated capture oligonucleotides enrichment
			- sequencing	- sequencing	- chromatin IP	- chromatin IP	- sequencing
Resolution	standard experiments generate 10–50 kb resolution (locus specific)	from 200–400 bp to 3–4 kb depending on the frequency of four or six base cutter restriction enzymes sites	from 400 bp to 4 kb depending on the frequency of four or six base cutter restriction enzymes sites	~200bp	From 1kb to 50 kb	from 100 bp to 1 kb	from 20bp to 2 kb (locus specific)
References	Dekker et al. (2002)	Meddens et al. (2016)	Lieberman-Aiden et al. (2009)	Szerlong and Hansen, (2011); Voong et al., 2017; Krietenstein et al., 2020	Mumbach et al. (2016)	Fullwood et al. (2010)	Oudelaar et al. (2020)

et al., 2016), combining long-range contacts investigation with enrichment of specific histone proteins (i.e H3K27Ac) associated with active regions of the genome. Recently, Chandra and others performed Hi-ChIP to provide evidence of non-coding genetic variants having effect on gene expression (i.e. cis-eQTL) and cell-specific gene regulation in five immune cell types (Chandra et al., 2021). Another method coupling ChIP with 3C is ChIA-PET, a chromatin interaction analysis by paired-end tag sequencing (Fullwood et al., 2009). With this approach is possible to detect all chromatin interactions mediated by a specific protein of interest, immunoprecipitated using specific antibodies (Li et al., 2002; Fullwood et al., 2010). In 2013, ChIA-PET was used to described for the first time the genome-wide chromatin interactions of cohesin (DeMare et al., 2013).

Tiling Capture C was designed to identify at high resolution level the interaction between promoter and enhancer within TADs. This method uses a panel of specific capture oligonucleotides tiled across all contiguous restriction fragments within specified genomic regions, typically around 1Mb (Downes et al., 2022), to obtain enrichment for specific interactions and subsequent targeted sequencing. High-resolution maps with low-cells input makes Tiled-C at forefront of the 3C methods. Oudelaar et al. developed the Tiled-C approach to characterize the chromatin architecture of mouse erythroid cells during *in vivo* differentiation, focusing on the α-globin locus (Oudelaar et al., 2020). Recently, the same group has generated the most detailed genomic local interaction map at base-pair resolution (20bp), using a micrococcal nuclease (MN) based 3C approach. MN is an enzyme digesting the genome largely independent of DNA sequence: the authors benefit of MN to demonstrate the effects of the depletion of two crucial elements, cohesin and CTCF, on chromatin architecture (Hua et al., 2021; Aljahani et al., 2022). A summary of the different chromatin conformation techniques here presented is showed in Table 1.

The investigation of 3D genome topology has dramatically evolved over the past decade: technological advances have boost the field to an unprecedented level (Bouwman et al., 2022). Ongoing efforts are made in providing more accurate data analysis for a better understanding and interpretation of the functional consequence of these changes.

Investigating the 3D genome in rheumatic diseases and AS

The 3D genome organization has been investigated in autoimmune and rheumatic disease, but more is yet to come. In 2012, 3C was used to identify physical interaction between the chromosome region 16p13, often associated with increased risk for a plethora of autoimmune diseases, including multiple sclerosis (Zuvich et al., 2011), primary biliary cirrhosis (Mells et al., 2011) and systemic lupus erythematosus (SLE) (Gateva et al., 2009), with *DEXI* (dexamethasone-induced protein), a gene with previous unknown function, revealed as a strong candidate for autoimmune disease (Davison et al., 2012).

Meddens and others performed circular chromosome conformation capture (4C)-seq to analyse chromatin interactions in inflammatory bowel disease (IBD) susceptibility loci and DNA regulatory elements providing novel relevant

candidate genes (Meddens et al., 2016). In a recent work by Carini and others, the authors explored the genomic architecture of whole blood obtained from rheumatoid arthritis (RA) patients investigating a possible chromosome conformation signature (including *IFNAR1*, *IL-21R*, *IL-23*, *IL-17A* and *CXCL13*), before and after the administration of methotrexate (MTX) treatment. This was important to identify the non-responders to disease modified anti-rheumatic drugs such as MTX and, whether there was an association between the chromatin signature and RA-specific expression quantitative trait loci (eQTL) (Carini et al., 2018). Integrating data from Hi-C with gene expression profiling and disease activity scores has been successful in a recent work on SLE, where the authors established the genomic interaction landscape identifying specific SLE-associated loops (Zhao et al., 2022).

Nearly 90% of disease-associated SNPs are located in non-coding regions (Ricano-Ponce and Wijmenga, 2013). The role of specific GWAS hits can be elucidated *via* 3D genome analysis, thus clarifying which genes are influenced by which particular SNP through a spatial connection (Li et al., 2020). Our group has recently demonstrated the presence of a chromatin loop between the AS-associated SNP *rs4648889* and the distal promoter of the *RUNX3* gene, confirming together with other functional experiments previously reported the primacy of this genetic variant in the association with *RUNX3* in AS (Cohen et al., 2021). The complexity of the *RUNX3* locus is also confirmed by Capture-C experiments showing multiple interactions among different SNPs and the *RUNX3* promoter (personal communication).

In 2015 the Orozco group investigated chromatin interactions between disease-associated genetic variants and their functional targets in B and T cells in four autoimmune disease, including RA, type 1 diabetes, psoriatic arthritis, and juvenile idiopathic arthritis. They performed Capture Hi-C and demonstrated that only few looping interactions were common to both cell lines and disease-associated SNPs interact with candidate genes relevant to the disease and located megabases away (Martin et al., 2015).

It is important to dissect the role of chromatin contacts at diverse genomic loci: the usage of 3D genome structure to perform gene prioritization will be very informative to define new drug targets and evaluate if a therapy is working or a more effective therapy is needed.

As previously demonstrated, genetic variations can influence 3D chromatin conformation, together with accessibility and gene expression (Gorkin et al., 2019). Long-distance eQTLs potentially regulate gene expression and spatial gene regulatory interactions are supposed to be the drivers of the heritability of complex traits. Our completed genome-wide study of chromatin interactions and the regulatory effects of AS-associated genetic variants is unprecedented in the field and it will be very informative in identifying genes and cells to prioritize as therapeutic targets (Brown et al., unpublished data). On the same line, promoter capture Hi-C and RNA-sequencing approaches were recently used to link associated variants of systemic sclerosis (a connective tissue immune-mediated disease) with their target genes, especially in CD4+T cells and $CD14^+$ monocytes obtained from 10 patients and five matched healthy controls. The authors identified new potential targets genes and 15 other potential drug targets for repurposing of drugs already in use in other immune-mediated diseases (Gonzalez-Serna et al., 2022).

In RA, a comprehensive genomic map has been recently generated to link risk-associated genetic variants with functional chromatin interactions, active regulatory DNA elements and differential gene expression in fibroblast-like synoviocytes, providing the proof of concept for a causal role of these cells in RA susceptibility (Ge et al., 2021).

The examples provided in this section show once again the importance of a multimodal approach for the identification of cell types and molecular states critically associated with rheumatic diseases. The generation of a comprehensive and high-resolution 3D genome map may yield insights in disease-associated TAD appearance and chromosome loop strengths.

Discussion

Although chromosome conformation capture is a relatively new field of investigation, understanding 3D genome folding and its influence on gene expression has rapidly grown beside the innovation of 3C methods. The relevance of looping formation and genomic organization together with the identification of architectural proteins associated with boundaries might shed light on the functional and mechanistic implications in different diseases, as demonstrated in these seminal works focused on neurological disorders and cancer (Bharadwaj et al., 2014; Weischenfeldt et al., 2017; Zhu et al., 2020). Further, disease-associated genetic variants may disrupt higher-order genomic organization, due to elimination of annotated boundaries (Ibn-Salem et al., 2014). Normal and disease-associated TAD structure data may yield valuable and perhaps diagnostically important information on gene regulation and disease aetiology. Several diseases could be linked to an aberrant chromatin loop dynamic (Mehrjouy et al., 2018). This suggests an increased interest in studying genome looping and how this may affect gene expression and function in diseases (Krumm and Duan, 2019).

3C approaches might be useful in addressing an unmet clinical need of predicting those patients who will not respond to specific treatments and thus facilitating earlier access to more effective therapies and a better quality of life. The integration of 3C methodologies with functional data (i.e. eQTL) may pinpoint individual loci into a gene regulatory network which is critical to our understanding of complex diseases. Single-cell genomic assays might be a promising tool for the quantification of molecular traits (i.e. transcriptomics, chromatin accessibility, transcription factors occupancy and time-course trajectories of cells) at single cell level (Buenrostro et al., 2015; Zheng et al., 2017; Cuomo et al., 2020; Del Priore et al., 2021). Recently it has been elegantly demonstrated that genetic variants associated with differential binding of PU.1, a master transcription factor regulating myeloid development and having a substantial effect on neutrophils function (McKercher et al., 1996; Siwaponanan et al., 2017), are predominantly cell type specific, associated with specific chromatin state, and regulate enhancer-promoter interactions and downstream gene expression, exhibiting association with IBD susceptibility (Watt et al., 2021). Additionally, PU.1 has been found involved in regulating the interaction loop at *DDX60L* (Probable ATP-dependent RNA helicase DDX60-like) promoter thus inducing overexpression of this gene in $CD4^+$ T Cells from SLE patients (Zhao et al., 2022).

The dynamic interplay between genomic sequence, 3D chromatin structure and a specific pathological process such AS, is crucial in defining a powerful strategy to discover novel genetic regions potential for diagnostic or therapeutic purposes. Nevertheless, it is important to bear in mind that a combination of more genetic variants (i.e. haplotypes) may have a higher risk on the probability of developing a particular disorder, while individually may have a mild influence.

Concluding remarks

The last decade has been a remarkable time for genetic research in AS, from genetic association studies to genetics-driven novel clinical trials (Baeten et al., 2013; van der Heijde et al., 2019; Izana Bioscience, 2021). The identification of few hundreds genomic loci make the overall analysis challenging, considering most of them are enriched not only in immune cell-specific enhancers, but also in osteoclasts or stromal cells, having a crucial involvement in the pathogenesis of AS. Contemplating the results of GWAS suggests that a traditional *in vitro* approach to uncover the mechanistic contribution of disease-associated SNPs is not sufficient anymore. Times for integration of genetic fine mapping of AS loci with DNA architecture and 3D chromatin interactions, DNA accessibility, single-cell gene expression and gene editing are mature as they occur in related disorders (Al-Mossawi and Coates, 2018; Penkava et al., 2020; Yager et al., 2021), and it appears only a matter of time before they are fully applied in AS.

Data availability statement

The original contributions presented in the study are included in the article/supplementary material, further inquiries can be directed to the corresponding author.

Author contributions

Writing – original draft, CD and MV; Writing – Review and Editing, CD, BPW, CJC, JCK and MV, and all authors reviewed and approved the final version.

Conflict of interest

The authors declare that the research was conducted in the absence of any commercial or financial relationships that could be construed as a potential conflict of interest.

Publisher's note

All claims expressed in this article are solely those of the authors and do not necessarily represent those of their affiliated organizations, or those of the publisher, the editors and the reviewers. Any product that may be evaluated in this article, or claim that may be made by its manufacturer, is not guaranteed or endorsed by the publisher.

References

Al-Husini, N., Medler, S., and Ansari, A. (2020). Crosstalk of promoter and terminator during RNA polymerase II transcription cycle. *Biochim. Biophys. Acta Gene Regul. Mech.* 1863 (12), 194657. doi:10.1016/j.bbagrm.2020.194657

Al-Mossawi, H., and Coates, L. C. (2018). Personalized medicine - a new reality in psoriatic arthritis? *Nat. Rev. Rheumatol.* 14 (8), 449–451. doi:10.1038/s41584-018-0043-3

Aljahani, A., Hua, P., Karpinska, M. A., Quililan, K., Davies, J. O. J., and Oudelaar, A. M. (2022). Analysis of sub-kilobase chromatin topology reveals nano-scale regulatory interactions with variable dependence on cohesin and CTCF. *Nat. Commun.* 13 (1), 2139. doi:10.1038/s41467-022-29696-5

Anania, C., and Lupianez, D. G. (2020). Order and disorder: Abnormal 3D chromatin organization in human disease. *Brief. Funct. Genomics* 19 (2), 128–138. doi:10.1093/bfgp/elz028

Baeten, D., Baraliakos, X., Braun, J., Sieper, J., Emery, P., van der Heijde, D., et al. (2013). Anti-interleukin-17A monoclonal antibody secukinumab in treatment of ankylosing spondylitis: A randomised, double-blind, placebo-controlled trial. *Lancet* 382 (9906), 1705–1713. doi:10.1016/S0140-6736(13)61134-4

Bagchi, D. N., and Iyer, V. R. (2016). The determinants of directionality in transcriptional initiation. *Trends Genet.* 32 (6), 322–333. doi:10.1016/j.tig.2016.03.005

Bharadwaj, R., Peter, C. J., Jiang, Y., Roussos, P., Vogel-Ciernia, A., Shen, E. Y., et al. (2014). Conserved higher-order chromatin regulates NMDA receptor gene expression and cognition. *Neuron* 84 (5), 997–1008. doi:10.1016/j.neuron.2014.10.032

Bonev, B., Mendelson Cohen, N., Szabo, Q., Fritsch, L., Papadopoulos, G. L., Lubling, Y., et al. (2017). Multiscale 3D genome rewiring during mouse neural development. *Cell.* 171 (3), 557–572. doi:10.1016/j.cell.2017.09.043

Bouwman, B. A. M., Crosetto, N., and Bienko, M. (2022). The era of 3D and spatial genomics. *Trends Genet.* 38 (10), 1062–1075. doi:10.1016/j.tig.2022.05.010

Brewerton, D. A., Hart, F. D., Nicholls, A., Caffrey, M., James, D. C., and Sturrock, R. D. (1973). Ankylosing spondylitis and HL-A 27. *Lancet* 1 (7809), 904–907. doi:10.1016/s0140-6736(73)91360-3

Bridgewood, C., Watad, A., Russell, T., Palmer, T. M., Marzo-Ortega, H., Khan, A., et al. (2019). Identification of myeloid cells in the human enthesis as the main source of local IL-23 production. *Ann. Rheum. Dis.* 78 (7), 929–933. doi:10.1136/annrheumdis-2018-214944

Buenrostro, J. D., Wu, B., Chang, H. Y., and Greenleaf, W. J. (2015). ATAC-seq: A method for assaying chromatin accessibility genome-wide. *Curr. Protoc. Mol. Biol.* 109 (21), 1–21. doi:10.1002/0471142727.mb2129s109

Cano-Gamez, E., and Trynka, G. (2020). From GWAS to function: Using functional genomics to identify the mechanisms underlying complex diseases. *Front. Genet.* 11, 424. doi:10.3389/fgene.2020.00424

Carini, C., Hunter, E., Ramadass, A. S., Green, J., Akoulitchev, A., et al.Scottish Early Rheumatoid Arthritis Inception cohort Investigators (2018). Chromosome conformation signatures define predictive markers of inadequate response to methotrexate in early rheumatoid arthritis. *J. Transl. Med.* 16 (1), 18. doi:10.1186/s12967-018-1387-9

Chakraborty, A., and Ay, F. (2019). The role of 3D genome organization in disease: From compartments to single nucleotides. *Semin. Cell. Dev. Biol.* 90, 104–113. doi:10.1016/j.semcdb.2018.07.005

Chandra, V., Bhattacharyya, S., Schmiedel, B. J., Madrigal, A., Gonzalez-Colin, C., Fotsing, S., et al. (2021). Promoter-interacting expression quantitative trait loci are enriched for functional genetic variants. *Nat. Genet.* 53 (1), 110–119. doi:10.1038/s41588-020-00745-3

Cohen, C. J., Davidson, C., Selmi, C., Bowness, P., and Knight, J. C. (2021). Wordsworth BP and Vecellio disruption of c-MYC binding and chromosomal looping involving genetic variants associated with ankylosing spondylitis upstream of the RUNX3 promoter. *Front. Genet.* 12, 741867. doi:10.3389/fgene.2021.741867

Crouch, D. J. M., and Bodmer, W. F. (2020). Polygenic inheritance, GWAS, polygenic risk scores, and the search for functional variants. *Proc. Natl. Acad. Sci. U. S. A.* 117 (32), 18924–18933. doi:10.1073/pnas.2005634117

Cuomo, A. S. E., Seaton, D. D., McCarthy, D. J., Martinez, I., Bonder, M. J., Garcia-Bernardo, J., et al. (2020). Single-cell RNA-sequencing of differentiating iPS cells reveals dynamic genetic effects on gene expression. *Nat. Commun.* 11 (1), 810. doi:10.1038/s41467-020-14457-z

Davison, L. J., Wallace, C., Cooper, J. D., Cope, N. F., Wilson, N. K., Smyth, D. J., et al. (2012). Long-range DNA looping and gene expression analyses identify DEXI as an autoimmune disease candidate gene. *Hum. Mol. Genet.* 21 (2), 322–333. doi:10.1093/hmg/ddr468

de Wit, E., and de Laat, W. (2012). A decade of 3C technologies: Insights into nuclear organization. *Genes. Dev.* 26 (1), 11–24. doi:10.1101/gad.179804.111

de Wit, E., Vos, E. S., Holwerda, S. J., Valdes-Quezada, C., Verstegen, M. J., Teunissen, H., et al. (2015). CTCF binding polarity determines chromatin looping. *Mol. Cell.* 60 (4), 676–684. doi:10.1016/j.molcel.2015.09.023

Dekker, J., Marti-Renom, M. A., and Mirny, L. A. (2013). Exploring the three-dimensional organization of genomes: Interpreting chromatin interaction data. *Nat. Rev. Genet.* 14 (6), 390–403. doi:10.1038/nrg3454

Dekker, J., Rippe, K., Dekker, M., and Kleckner, N. (2002). Capturing chromosome conformation. *Science* 295 (5558), 1306–1311. doi:10.1126/science.1067799

Del Priore, I., Ma, S., Strecker, J., Jacks, T., LaFave, L. M., and Buenrostro, J. D. (2021). Protocol for single-cell ATAC sequencing using combinatorial indexing in mouse lung adenocarcinoma. *Star. Protoc.* 2 (2), 100583. doi:10.1016/j.xpro.2021.100583

DeMare, L. E., Leng, J., Cotney, J., Reilly, S. K., Yin, J., Sarro, R., et al. (2013). The genomic landscape of cohesin-associated chromatin interactions. *Genome Res.* 23 (8), 1224–1234. doi:10.1101/gr.156570.113

Downes, D. J., Smith, A. L., Karpinska, M. A., Velychko, T., Rue-Albrecht, K., Sims, D., et al. (2022). Capture-C: A modular and flexible approach for high-resolution chromosome conformation capture. *Nat. Protoc.* 17 (2), 445–475. doi:10.1038/s41596-021-00651-w

Ellinghaus, D., Jostins, L., Spain, S. L., Cortes, A., Bethune, J., Han, B., et al. (2016). Analysis of five chronic inflammatory diseases identifies 27 new associations and highlights disease-specific patterns at shared loci. *Nat. Genet.* 48 (5), 510–518. doi:10.1038/ng.3528

Fudenberg, G., Abdennur, N., Imakaev, M., Goloborodko, A., and Mirny, L. A. (2017). Emerging evidence of chromosome folding by loop extrusion. *Cold Spring Harb. Symp. Quant. Biol.* 82, 45–55. doi:10.1101/sqb.2017.82.034710

Fullwood, M. J., Han, Y., Wei, C. L., Ruan, X., and Ruan, Y. (2010). Chromatin interaction analysis using paired-end tag sequencing. *Curr. Protoc. Mol. Biol.* 89 (21), 15.1–21.15. doi:10.1002/0471142727.mb2115s89

Fullwood, M. J., Liu, M. H., Pan, Y. F., Liu, J., Xu, H., Mohamed, Y. B., et al. (2009). An oestrogen-receptor-alpha-bound human chromatin interactome. *Nature* 462 (7269), 58–64. doi:10.1038/nature08497

Galan, S., Machnik, N., Kruse, K., Diaz, N., Marti-Renom, M. A., and Vaquerizas, J. M. (2020). CHESS enables quantitative comparison of chromatin contact data and automatic feature extraction. *Nat. Genet.* 52 (11), 1247–1255. doi:10.1038/s41588-020-00712-y

Gateva, V., Sandling, J. K., Hom, G., Taylor, K. E., Chung, S. A., Sun, X., et al. (2009). A large-scale replication study identifies TNIP1, PRDM1, JAZF1, UHRF1BP1 and IL10 as risk loci for systemic lupus erythematosus. *Nat. Genet.* 41 (11), 1228–1233. doi:10.1038/ng.468

Ge, X., Frank-Bertoncelj, M., Klein, K., McGovern, A., Kuret, T., Houtman, M., et al. (2021). Functional genomics atlas of synovial fibroblasts defining rheumatoid arthritis heritability. *Genome Biol.* 22 (1), 247. doi:10.1186/s13059-021-02460-6

Ghavi-Helm, Y., Klein, F. A., Pakozdi, T., Ciglar, L., Noordermeer, D., Huber, W., et al. (2014). Enhancer loops appear stable during development and are associated with paused polymerase. *Nature* 512 (7512), 96–100. doi:10.1038/nature13417

Girdhar, K., Hoffman, G. E., Bendl, J., Rahman, S., Dong, P., Liao, W., et al. (2022). Chromatin domain alterations linked to 3D genome organization in a large cohort of schizophrenia and bipolar disorder brains. *Nat. Neurosci.* 25 (4), 474–483. doi:10.1038/s41593-022-01032-6

Goel, V. Y., and Hansen, A. S. (2021). The macro and micro of chromosome conformation capture. *Wiley Interdiscip. Rev. Dev. Biol.* 10 (6), e395. doi:10.1002/wdev.395

Gonzalez-Serna, D., Shi, C., Kerick, M., Hankinson, J., Ding, J., McGovern, A., et al. (2022). Functional genomics in primary T cells and monocytes identifies mechanisms by which genetic susceptibility loci influence systemic sclerosis risk. *Arthritis Rheumatol.* doi:10.1002/art.42396

Gorkin, D. U., Qiu, Y., Hu, M., Fletez-Brant, K., Liu, T., Schmitt, A. D., et al. (2019). Common DNA sequence variation influences 3-dimensional conformation of the human genome. *Genome Biol.* 20 (1), 255. doi:10.1186/s13059-019-1855-4

Haarhuis, J. H. I., van der Weide, R. H., Blomen, V. A., Yanez-Cuna, J. O., Amendola, M., van Ruiten, M. S., et al. (2017). The cohesin release factor WAPL restricts chromatin loop extension. *Cell.* 169 (4), 693–707. doi:10.1016/j.cell.2017.04.013

Hansen, A. S., Cattoglio, C., Darzacq, X., and Tjian, R. (2018). Recent evidence that TADs and chromatin loops are dynamic structures. *Nucleus* 9 (1), 20–32. doi:10.1080/19491034.2017.1389365

Hansen, A. S., Hsieh, T. S., Cattoglio, C., Pustova, I., Saldana-Meyer, R., Reinberg, D., et al. (2019). Distinct classes of chromatin loops revealed by deletion of an RNA-binding region in CTCF. *Mol. Cell.* 76 (3), 395–411. doi:10.1016/j.molcel.2019.07.039

Haws, S. A., Simandi, Z., Barnett, R. J., and Phillips-Cremins, J. E. (2022). 3D genome, on repeat: Higher-order folding principles of the heterochromatinized repetitive genome. *Cell.* 185 (15), 2690–2707. doi:10.1016/j.cell.2022.06.052

Hsieh, T. H., Weiner, A., Lajoie, B., Dekker, J., Friedman, N., and Rando, O. J. (2015). Mapping nucleosome resolution chromosome folding in yeast by micro-C. *Cell.* 162 (1), 108–119. doi:10.1016/j.cell.2015.05.048

Hsieh, T. S., Cattoglio, C., Slobodyanyuk, E., Hansen, A. S., Rando, O. J., Tjian, R., et al. (2020). Resolving the 3D landscape of transcription-linked mammalian chromatin folding. *Mol. Cell.* 78 (3), 539–553. doi:10.1016/j.molcel.2020.03.002

Hua, P., Badat, M., Hanssen, L. L. P., Hentges, L. D., Crump, N., Downes, D. J., et al. (2021). Defining genome architecture at base-pair resolution. *Nature* 595 (7865), 125–129. doi:10.1038/s41586-021-03639-4

Hunter, D. J. (2005). Gene-environment interactions in human diseases. *Nat. Rev. Genet.* 6 (4), 287–298. doi:10.1038/nrg1578

Huo, Y., Li, S., Liu, J., Li, X., and Luo, X. J. (2019). Functional genomics reveal gene regulatory mechanisms underlying schizophrenia risk. *Nat. Commun.* 10 (1), 670. doi:10.1038/s41467-019-08666-4

Ibn-Salem, J., Kohler, S., Love, M. I., Chung, H. R., Huang, N., Hurles, M. E., et al. (2014). Deletions of chromosomal regulatory boundaries are associated with congenital disease. *Genome Biol.* 15 (9), 423. doi:10.1186/s13059-014-0423-1

International Genetics of Ankylosing Spondylitis ConsortiumCortes, A., Hadler, J., Pointon, J. P., Robinson, P. C., Karaderi, T., et al. (2013). Identification of multiple risk variants for ankylosing spondylitis through high-density genotyping of immune-related loci. *Nat. Genet.* 45 (7), 730–738. doi:10.1038/ng.2667

Izana Bioscience, L. (2021). *Efficacy and safety of namilumab for moderate-to-severe axial spondyloarthritis (NAMASTE)*. Available at: https://ClinicalTrialsgov/show/NCT03622658.

Ji, X., Dadon, D. B., Powell, B. E., Fan, Z. P., Borges-Rivera, D., Shachar, S., et al. (2016). 3D chromosome regulatory landscape of human pluripotent cells. *Cell. Stem Cell.* 18 (2), 262–275. doi:10.1016/j.stem.2015.11.007

Keidel, S., Chen, L., Pointon, J., and Wordsworth, P. (2013). ERAP1 and ankylosing spondylitis. *Curr. Opin. Immunol.* 25 (1), 97–102. doi:10.1016/j.coi.2012.11.002

Khunsriraksakul, C., McGuire, D., Sauteraud, R., Chen, F., Yang, L., Wang, L., et al. (2022). Integrating 3D genomic and epigenomic data to enhance target gene discovery and drug repurposing in transcriptome-wide association studies. *Nat. Commun.* 13 (1), 3258. doi:10.1038/s41467-022-30956-7

Krietenstein, N., Abraham, S., Venev, S. V., Abdennur, N., Gibcus, J., Hsieh, T. S., et al. (2020). Ultrastructural details of mammalian chromosome architecture. *Mol. Cell.* 78 (3), 554–565. doi:10.1016/j.molcel.2020.03.003

Krumm, A., and Duan, Z. (2019). Understanding the 3D genome: Emerging impacts on human disease. *Semin. Cell. Dev. Biol.* 90, 62–77. doi:10.1016/j.semcdb.2018.07.004

Li, Q. L., Ito, K., Sakakura, C., Fukamachi, H., Inoue, K., Chi, X. Z., et al. (2002). Causal relationship between the loss of RUNX3 expression and gastric cancer. *Cell.* 109 (1), 113–124. doi:10.1016/s0092-8674(02)00690-6

Li, Y., Tao, T., Du, L., and Zhu, X. (2020). Three-dimensional genome: Developmental technologies and applications in precision medicine. *J. Hum. Genet.* 65 (6), 497–511. doi:10.1038/s10038-020-0737-7

Lieberman-Aiden, E., van Berkum, N. L., Williams, L., Imakaev, M., Ragoczy, T., Telling, A., et al. (2009). Comprehensive mapping of long-range interactions reveals folding principles of the human genome. *Science* 326 (5950), 289–293. doi:10.1126/science.1181369

Lupianez, D. G., Kraft, K., Heinrich, V., Krawitz, P., Brancati, F., Klopocki, E., et al. (2015). Disruptions of topological chromatin domains cause pathogenic rewiring of gene-enhancer interactions. *Cell.* 161 (5), 1012–1025. doi:10.1016/j.cell.2015.04.004

Lupianez, D. G., Spielmann, M., and Mundlos, S. (2016). Breaking TADs: How alterations of chromatin domains result in disease. *Trends Genet.* 32 (4), 225–237. doi:10.1016/j.tig.2016.01.003

Luppino, J. M., Park, D. S., Nguyen, S. C., Lan, Y., Xu, Z., Yunker, R., et al. (2020). Cohesin promotes stochastic domain intermingling to ensure proper regulation of boundary-proximal genes. *Nat. Genet.* 52 (8), 840–848. doi:10.1038/s41588-020-0647-9

Martin, P., McGovern, A., Orozco, G., Duffus, K., Yarwood, A., Schoenfelder, S., et al. (2015). Capture Hi-C reveals novel candidate genes and complex long-range interactions with related autoimmune risk loci. *Nat. Commun.* 6, 10069. doi:10.1038/ncomms10069

McCord, R. P., Kaplan, N., and Giorgetti, L. (2020). Chromosome conformation capture and beyond: Toward an integrative view of chromosome structure and function. *Mol. Cell.* 77 (4), 688–708. doi:10.1016/j.molcel.2019.12.021

McKercher, S. R., Torbett, B. E., Anderson, K. L., Henkel, G. W., Vestal, D. J., Baribault, H., et al. (1996). Targeted disruption of the PU.1 gene results in multiple hematopoietic abnormalities. *EMBO J.* 15 (20), 5647–5658. doi:10.1002/j.1460-2075.1996.tb00949.x

Meddens, C. A., Harakalova, M., van den Dungen, N. A., Foroughi Asl, H., Hijma, H. J., Cuppen, E. P., et al. (2016). Systematic analysis of chromatin interactions at disease associated loci links novel candidate genes to inflammatory bowel disease. *Genome Biol.* 17 (1), 247. doi:10.1186/s13059-016-1100-3

Medrano-Fernandez, A., and Barco, A. (2016). Nuclear organization and 3D chromatin architecture in cognition and neuropsychiatric disorders. *Mol. Brain* 9 (1), 83. doi:10.1186/s13041-016-0263-x

Mehrjouy, M. M., Fonseca, A. C. S., Ehmke, N., Paskulin, G., Novelli, A., Benedicenti, F., et al. (2018). Regulatory variants of FOXG1 in the context of its topological domain organisation. *Eur. J. Hum. Genet.* 26 (2), 186–196. doi:10.1038/s41431-017-0011-4

Mells, G. F., Floyd, J. A., Morley, K. I., Cordell, H. J., Franklin, C. S., Shin, S. Y., et al. (2011). Genome-wide association study identifies 12 new susceptibility loci for primary biliary cirrhosis. *Nat. Genet.* 43 (4), 329–332. doi:10.1038/ng.789

Mumbach, M. R., Rubin, A. J., Flynn, R. A., Dai, C., Khavari, P. A., Greenleaf, W. J., et al. (2016). HiChIP: Efficient and sensitive analysis of protein-directed genome architecture. *Nat. Methods* 13 (11), 919–922. doi:10.1038/nmeth.3999

Nora, E. P., Goloborodko, A., Valton, A. L., Gibcus, J. H., Uebersohn, A., Abdennur, N., et al. (2017). Targeted degradation of CTCF decouples local insulation of chromosome domains from genomic compartmentalization. *Cell.* 169 (5), 930–944. doi:10.1016/j.cell.2017.05.004

Olley, G., Ansari, M., Bengani, H., Grimes, G. R., Rhodes, J., von Kriegsheim, A., et al. (2018). BRD4 interacts with NIPBL and BRD4 is mutated in a Cornelia de Lange-like syndrome. *Nat. Genet.* 50 (3), 329–332. doi:10.1038/s41588-018-0042-y

Oudelaar, A. M., Beagrie, R. A., Gosden, M., de Ornellas, S., Georgiades, E., Kerry, J., et al. (2020). Dynamics of the 4D genome during *in vivo* lineage specification and differentiation. *Nat. Commun.* 11 (1), 2722. doi:10.1038/s41467-020-16598-7

Oudelaar, A. M. (2022). Deciphering the regulatory logic of a chromatin domain boundary. *Nat. Genet.* 54 (7), 914–915. doi:10.1038/s41588-022-01086-z

Penkava, F., Velasco-Herrera, M. D. C., Young, M. D., Yager, N., Nwosu, L. N., Pratt, A. G., et al. (2020). Single-cell sequencing reveals clonal expansions of pro-inflammatory synovial CD8 T cells expressing tissue-homing receptors in psoriatic arthritis. *Nat. Commun.* 11 (1), 4767. doi:10.1038/s41467-020-18513-6

Phillips-Cremins, J. E., Sauria, M. E., Sanyal, A., Gerasimova, T. I., Lajoie, B. R., Bell, J. S., et al. (2013). Architectural protein subclasses shape 3D organization of genomes during lineage commitment. *Cell.* 153 (6), 1281–1295. doi:10.1016/j.cell.2013.04.053

Ricano-Ponce, I., and Wijmenga, C. (2013). Mapping of immune-mediated disease genes. *Annu. Rev. Genomics Hum. Genet.* 14, 325–353. doi:10.1146/annurev-genom-091212-153450

Roberts, A. R., Vecellio, M., Chen, L., Ridley, A., Cortes, A., Knight, J. C., et al. (2016). An ankylosing spondylitis-associated genetic variant in the IL23R-IL12RB2 intergenic region modulates enhancer activity and is associated with increased Th1-cell differentiation. *Ann. Rheum. Dis.* 75 (12), 2150–2156. doi:10.1136/annrheumdis-2015-208640

Sanborn, A. L., Rao, S. S., Huang, S. C., Durand, N. C., Huntley, M. H., Jewett, A. I., et al. (2015). Chromatin extrusion explains key features of loop and domain formation in wild-type and engineered genomes. *Proc. Natl. Acad. Sci. U. S. A.* 112 (47), E6456–E6465. doi:10.1073/pnas.1518552112

Siwaponanan, P., Siegers, J. Y., Ghazali, R., Ng, T., McColl, B., Ng, G. Z., et al. (2017). Reduced PU.1 expression underlies aberrant neutrophil maturation and function in beta-thalassemia mice and patients. *Blood* 129 (23), 3087–3099. doi:10.1182/blood-2016-07-730135

Symmons, O., Uslu, V. V., Tsujimura, T., Ruf, S., Nassari, S., Schwarzer, W., et al. (2014). Functional and topological characteristics of mammalian regulatory domains. *Genome Res.* 24 (3), 390–400. doi:10.1101/gr.163519.113

Szerlong, H. J., and Hansen, J. C. (2011). Nucleosome distribution and linker DNA: Connecting nuclear function to dynamic chromatin structure. *Biochem. Cell. Biol.* 89 (1), 24–34. doi:10.1139/O10-139

Tsuchiya, H., Ota, M., Sumitomo, S., Ishigaki, K., Suzuki, A., Sakata, T., et al. (2021). Parsing multiomics landscape of activated synovial fibroblasts highlights drug targets linked to genetic risk of rheumatoid arthritis. *Ann. Rheum. Dis.* 80 (4), 440–450. doi:10.1136/annrheumdis-2020-218189

van der Heijde, D., Song, I. H., Pangan, A. L., Deodhar, A., van den Bosch, F., Maksymowych, W. P., et al. (2019). Efficacy and safety of upadacitinib in patients with active ankylosing spondylitis (SELECT-AXIS 1): A multicentre, randomised, double-blind, placebo-controlled, phase 2/3 trial. *Lancet* 394 (10214), 2108–2117. doi:10.1016/S0140-6736(19)32534-6

van Steensel, B., and Dekker, J. (2010). Genomics tools for unraveling chromosome architecture. *Nat. Biotechnol.* 28 (10), 1089–1095. doi:10.1038/nbt.1680

Vecellio, M., Chen, L., Cohen, C. J., Cortes, A., Li, Y., Bonham, S., et al. (2021). Functional genomic analysis of a RUNX3 polymorphism associated with ankylosing spondylitis. *Arthritis Rheumatol.* 73 (6), 980–990. doi:10.1002/art.41628

Vecellio, M., Cortes, A., Roberts, A. R., Ellis, J., Cohen, C. J., Knight, J. C., et al. (2018). Evidence for a second ankylosing spondylitis-associated RUNX3 regulatory polymorphism. *RMD Open* 4 (1), e000628. doi:10.1136/rmdopen-2017-000628

Vecellio, M., Roberts, A. R., Cohen, C. J., Cortes, A., Knight, J. C., Bowness, P., et al. (2016). The genetic association of RUNX3 with ankylosing spondylitis can be explained by allele-specific effects on IRF4 recruitment that alter gene expression. *Ann. Rheum. Dis.* 75 (8), 1534–1540. doi:10.1136/annrheumdis-2015-207490

Voong, L. N., Xi, L., Wang, J. P., and Wang, X. (2017). Genome-wide mapping of the nucleosome landscape by micrococcal nuclease and chemical mapping. *Trends Genet.* 33 (8), 495–507. doi:10.1016/j.tig.2017.05.007

Watt, S., Vasquez, L., Walter, K., Mann, A. L., Kundu, K., Chen, L., et al. (2021). Genetic perturbation of PU.1 binding and chromatin looping at neutrophil enhancers associates with autoimmune disease. *Nat. Commun.* 12 (1), 2298. doi:10.1038/s41467-021-22548-8

Weischenfeldt, J., Dubash, T., Drainas, A. P., Mardin, B. R., Chen, Y., Stutz, A. M., et al. (2017). Pan-cancer analysis of somatic copy-number alterations implicates IRS4 and IGF2 in enhancer hijacking. *Nat. Genet.* 49 (1), 65–74. doi:10.1038/ng.3722

Wutz, G., Varnai, C., Nagasaka, K., Cisneros, D. A., Stocsits, R. R., Tang, W., et al. (2017). Topologically associating domains and chromatin loops depend on cohesin and are regulated by CTCF, WAPL, and PDS5 proteins. *EMBO J.* 36 (24), 3573–3599. doi:10.15252/embj.201798004

Yager, N., Cole, S., Lledo Lara, A., Maroof, A., Penkava, F., Knight, J. C., et al. (2021). *Ex vivo* mass cytometry analysis reveals a profound myeloid proinflammatory signature in psoriatic arthritis synovial fluid. *Ann. Rheum. Dis.* 80 (12), 1559–1567. doi:10.1136/annrheumdis-2021-220280

Yang, M., Vesterlund, M., Siavelis, I., Moura-Castro, L. H., Castor, A., Fioretos, T., et al. (2019). Proteogenomics and Hi-C reveal transcriptional dysregulation in high hyperdiploid childhood acute lymphoblastic leukemia. *Nat. Commun.* 10 (1), 1519. doi:10.1038/s41467-019-09469-3

Zhao, M., Feng, D., Hu, L., Liu, L., Wu, J., Hu, Z., et al. (2022). 3D genome alterations in T cells associated with disease activity of systemic lupus erythematosus. *Ann. Rheumatic Dis.* 2022, 2022-222653. annrheumdis-2022-222653. doi:10.1136/ard-2022-222653

Zheng, G. X., Terry, J. M., Belgrader, P., Ryvkin, P., Bent, Z. W., Wilson, R., et al. (2017). Massively parallel digital transcriptional profiling of single cells. *Nat. Commun.* 8, 14049. doi:10.1038/ncomms14049

Zhu, H., Uuskula-Reimand, L., Isaev, K., Wadi, L., Alizada, A., Shuai, S., et al. (2020). Candidate cancer driver mutations in distal regulatory elements and long-range chromatin interaction networks. *Mol. Cell.* 77 (6), 1307–1321. doi:10.1016/j.molcel.2019.12.027

Zuvich, R. L., Bush, W. S., McCauley, J. L., Beecham, A. H., De Jager, P. L., et al.International Multiple Sclerosis Genetics Consortium (2011). Interrogating the complex role of chromosome 16p13.13 in multiple sclerosis susceptibility: Independent genetic signals in the CIITA-CLEC16A-SOCS1 gene complex. *Hum. Mol. Genet.* 20 (17), 3517–3524. doi:10.1093/hmg/ddr250

frontiers | Frontiers in Pediatrics

TYPE Original Research
PUBLISHED 14 March 2023
DOI 10.3389/fped.2023.1157630

OPEN ACCESS

EDITED BY
Jordi Pérez-Tur,
Institute of Biomedicine of Valencia, Spain

REVIEWED BY
Samira Kalayinia,
Shaheed Rajaei Cardiovascular Medical and Research Center, Iran
Himanshu Goel,
Hunter Genetics, HNEkidshealth, Australia

*CORRESPONDENCE
Erika T. Allred
✉ etallred@health.ucsd.edu

SPECIALTY SECTION
This article was submitted to Genetics of Common and Rare Diseases, a section of the journal Frontiers in Pediatrics

RECEIVED 02 February 2023
ACCEPTED 24 February 2023
PUBLISHED 14 March 2023

CITATION
Allred ET, Perens EA, Coufal NG, Sanford Kobayashi E, Kingsmore SF and Dimmock DP (2023) Genomic sequencing has a high diagnostic yield in children with congenital anomalies of the heart and urinary system. Front. Pediatr. 11:1157630. doi: 10.3389/fped.2023.1157630

Genomic sequencing has a high diagnostic yield in children with congenital anomalies of the heart and urinary system

Erika T. Allred[1,2]*, Elliot A. Perens[1], Nicole G. Coufal[1,2], Erica Sanford Kobayashi[2,3], Stephen F. Kingsmore[2] and David P. Dimmock[2]

[1]Department of Pediatrics, University of California, San Diego, CA, United States, [2]Rady Children's Institute for Genomic Medicine, San Diego, CA, United States, [3]Department of Pediatrics, Children's Hospital of Orange County, Orange, CA, United States

Background: Congenital heart defects (CHD) and congenital anomalies of the kidney and urinary tract (CAKUT) account for significant morbidity and mortality in childhood. Dozens of monogenic causes of anomalies in each organ system have been identified. However, even though 30% of CHD patients also have a CAKUT and both organs arise from the lateral mesoderm, there is sparse overlap of the genes implicated in the congenital anomalies for these organ systems. We sought to determine whether patients with both CAKUT and CHD have a monogenic etiology, with the long-term goal of guiding future diagnostic work up and improving outcomes.

Methods: Retrospective review of electronic medical records (EMR), identifying patients admitted to Rady Children's Hospital between January 2015 and July 2020 with both CAKUT and CHD who underwent either whole exome sequencing (WES) or whole genome sequencing (WGS). Data collected included demographics, presenting phenotype, genetic results, and mother's pregnancy history. WGS data was reanalyzed with a specific focus on the CAKUT and CHD phenotype. Genetic results were reviewed to identify causative, candidate, and novel genes for the CAKUT and CHD phenotype. Associated additional structural malformations were identified and categorized.

Results: Thirty-two patients were identified. Eight patients had causative variants for the CAKUT/CHD phenotype, three patients had candidate variants, and three patients had potential novel variants. Five patients had variants in genes not associated with the CAKUT/CHD phenotype, and 13 patients had no variant identified. Of these, eight patients were identified as having possible alternative causes for their CHD/CAKUT phenotype. Eighty-eight percent of all CAKUT/CHD patients had at least one additional organ system with a structural malformation.

Conclusions: Overall, our study demonstrated a high rate of monogenic etiologies in hospitalized patients with both CHD and CAKUT, with a diagnostic rate of 44%. Thus, physicians should have a high suspicion for genetic disease in this population. Together, these data provide valuable information on how to approach acutely ill patients with CAKUT and CHD, including guiding diagnostic work up for associated phenotypes, as well as novel insights into the genetics of CAKUT and CHD overlap syndromes in hospitalized children.

KEYWORDS

genomics, congenital anomalies, kidneys, heart, sequencing, hospital

Introduction

Congenital birth defects frequently have an underlying molecular etiology. For example, there are over 40 genes each that are associated with congenital anomalies of the kidney and urinary tract (CAKUT) and congenital heart defects (CHD) (1, 2). Causative molecular variants that span these two systems are less well characterized, and we sought to better define these.

CAKUT represent a heterogeneous group of disorders ranging from mild urinary tract dilation to bilateral renal agenesis (1). Kidney malformations are one of the most common congenital anomalies, representing 20%–30% of all prenatally detected anomalies (3, 4). CAKUT are known to carry significant morbidity in the pediatric population, accounting for 45% of chronic kidney disease (CKD) and about 30% of end stage kidney disease (ESKD) (5). Over 40 single-gene defects have been implicated in CAKUT, with a Mendelian molecular etiology detected in up to 26% of all cases (1, 6). It is estimated that hundreds of additional monogenic defects have yet to be discovered in CAKUT, with identification complicated by incomplete penetrance and variable expressivity, along with suspected contributions from epigenetic and environmental factors (6, 7).

Additional causes of CAKUT include many well-known genetic syndromes which present with extra-renal manifestations, such as Fraser syndrome, CHARGE syndrome, and DiGeorge (8). Interestingly, each of these syndromes include CHD in their phenotypes. CHD is the primary cause of congenital anomalies in children, representing almost one third of all congenital anomalies, and is the most common cause of death before the age of one year (9, 10). CHD also has a strong genetic basis, with over 40 monogenic gene defects identified (2).

Several studies have highlighted a strong clinical correlation between non-syndromic CHD and CAKUT, with 20%–30% of all patients with CHD also found to have CAKUT (8). These findings suggest a genetic overlap between the etiology of both anomalies, which has been supported by several mouse models demonstrating a single gene to be responsible for both CHD and CAKUT (7). The monogenic overlap between CHD and CAKUT has yet to be fully evaluated in human studies, with only sporadic case reports describing single gene causes of both (11, 12). In addition, the current known monogenic causes of CAKUT do not overlap with those of CHD, despite the well-known clinical overlap and similar embryologic origin of cardiac and kidney development (13, 14). However, there are no human studies specifically evaluating the genetics of individuals with both CAKUT and CHD, and thus the contribution of monogenic defects to this population is still unknown.

There is a significant clinical need to further identify and characterize the genetic underpinnings and presenting phenotypes of patients with both CAKUT and CHD due to the well-known interdependent relationship of the two organ systems. Cardiorenal syndrome encompasses a spectrum of disorders in which dysfunction of one organ system induces dysfunction in the other (15). This syndrome is a significant cause of morbidity and mortality in hospitalized patients, with both the Studies of Left Ventricular Dysfunction (SOLVD) Prevention Trial and Candesartan in Heart Failure: Assessment of Reduction in Mortality and Morbidity (CHARM) study noting almost a doubling in the mortality rate of heart failure patients if they experienced a decline in kidney function (16, 17). This impact is magnified and more likely to occur in patients who already possess a congenital anomaly in either organ system.

Due to the pervasiveness and significant disease burden of CAKUT and CHD in the pediatric population, we performed a descriptive and analytic cross-sectional evaluation of the prevalence of patients with both CAKUT and CHD. We analyzed patients at a single-center tertiary hospital who had diagnostic whole exome sequencing (WES) and/or whole genome sequencing (WGS). Using this information, we sought to further elucidate the phenotypic spectrum and candidate genetic underpinnings of patients affected by both CAKUT and CHD. We anticipate that this information will improve patient outcomes by increasing providers' diagnostic and prognostic capabilities, with future aspirations to include implementation of prophylactic measures and the reduction of unnecessary interventions.

Methods

Study design

We performed a retrospective chart review of electronic medical records (EMR) of all patients who had received diagnostic WES and/or WGS and had ICD10 diagnosis codes of Q20–28 (congenital malformations of cardiac chambers and connections) or Q60–69 (included congenital malformations of the urinary system) that were cared for at Rady Children's Hospital between January 2015 and July 2020. Available individual patient imaging studies were then evaluated to identify patients with both CAKUT and CHD. Imaging studies reviewed included any or all of the following: kidney and bladder ultrasounds (RUS), vesicoureteral cystograms (VCUG), dimercaptosuccinic acid (DMSA) scans, mercaptoacetyltriglycine (MAG3) scans, computed tomography (CT) scans of the abdomen, magnetic resonance imaging (MRI) of the abdomen, CT scans of the heart, MRIs of the heart, and echocardiograms (ECHO). Patients were excluded if their imaging failed to show *both* CAKUT and CHD, if the EMR represented the parent of a child under investigation, if cardiac imaging revealed only a patent foramen ovale (PFO) or patent ductus arteriosus (PDA) that resolved by 12 months of age without surgical intervention, or if kidney imaging was only notable for hydronephrosis that resolved within the first year of life without intervention. Data collected included: demographic data (e.g., sex, race/ethnicity, date of birth), diagnoses, patient age at time of WGS/WES sequencing, additional imaging, presenting phenotype, maternal pregnancy history, human phenotype ontology (HPO) terms, and all genome wide sequencing (GWS) results.

This study is limited due to its analysis of a single center with a small population. In addition, results were interpreted with the

recognition that genetic testing was confined to WGS and WES only. These limitations will be explored further in the discussion section of this paper.

Diagnostic WGS and WES analysis and interpretation

Clinical WES and WGS were performed in laboratories accredited by the College of American Pathologists and certified through the Clinical Laboratory Improvement Amendments. The analysis and interpretation protocol were adapted from the NSIGHT2 study (18).

WGS results were reinterpreted for this study using Opal Clinical (Fabric Genomics). Genes associated with CAKUT and CHD were identified using the Phenolyzer algorithm (19). Opal then re-annotated variants using the resultant gene panel for the Variant Annotation, Analysis & Search Tool (VAAST) variant prioritizer Phevor algorithm, re-ranking with the specific Human Phenotype Ontology (HPO) terms, "abnormal heart morphology" and "abnormal renal morphology". Automatically generated, ranked results were manually re-interpreted through iterative Opal searches and filters.

Results

We identified 323 cases with the defined ICD10 diagnosis codes corresponding to congenital malformations of cardiac chambers and connections or the urinary system and diagnostic WGS or WES results (**Figure 1**). Of those cases, 105 were excluded after being identified as isolated CHD, 24 were excluded for isolated CAKUT, 11 were parental charts of children under investigation, and 105 had neither CAKUT nor CHD as defined in the current study. Twenty-three percent of all cases with CHD were also found to have CAKUT. In total, we identified 32 cases with CAKUT and CHD who had received diagnostic WGS or WES. Demographic information is detailed in **Table 1**. Fourteen cases underwent WES and 18 cases underwent WGS. Due to the limited number of overall cases, WGS and WES results were interpreted as one cohort. We identified eight cases with pathogenic or likely pathogenic variants in genes known to cause CAKUT and CHD. Three cases had four variants of uncertain significance (VUS) suspected to be disease causing in genes known to cause CAKUT and CHD. Three cases had four variants (2 classified as pathogenic, 2 VUS) in genes not previously associated with CAKUT and CHD. Five cases had eight reported variants (some cases had more than one variant) in genes not previously associated with CAKUT and CHD and not suspected to be the cause of the CAKUT/CHD phenotype due to a lack of supporting literature. Thirteen cases had no variants identified *via* focused reinterpretation of WGS or WES for genes and disorders associated with CAKUT or CHD. Of the 18 cases without genetic results related to their CAKUT/CHD phenotype, four were infants of diabetic mothers (IDM), three patients were found to have VACTERL association, and one case had both a diabetic mother and VACTERL association. Therefore, eight out of the 18 cases without a causative molecular diagnosis (44%) were suspected of having an identifiable, putative etiology for their CAKUT/CHD phenotype.

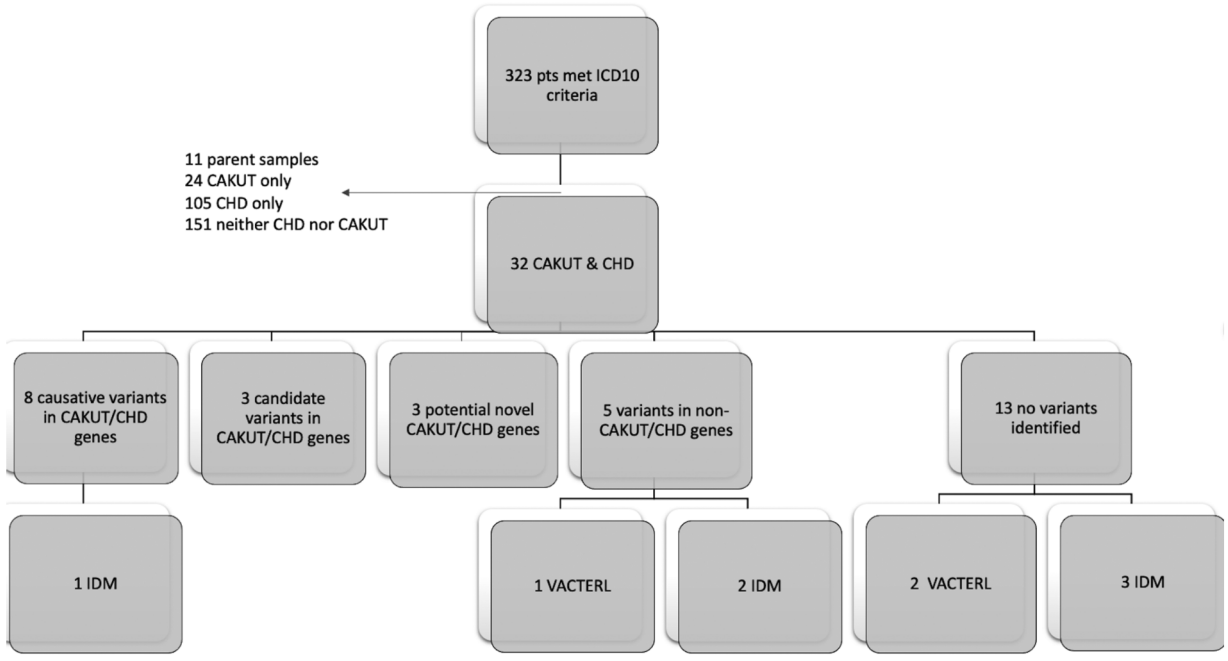

FIGURE 1
Flow diagram of patient inclusion and results: Infant of diabetic mother (IDM), Congenital heart defect (CHD), Congenital anomaly of kidney and urinary tract system (CAKUT).

10.3389/fped.2023.1157630

TABLE 1 Study population characteristics.

	Total (*N*, %)	CAKUT/CHD-Related Molecular Diagnosis
Total number of patients	32	14 (44)
Males	18 (56)	5 (28)
Females	14 (44)	9 (64)
Genomes	18 (56)	8 (39)
Exomes	14 (44)	6 (43)
Median age at time of testing, years	3	3
Race*:		
Asian OR Pacific Islander OR Hawaiian	5 (15)	2 (40)
Asian AND Black	1 (3)	1 (100)
Black/African American	1 (3)	1 (100)
Black/African American AND White	1 (3)	1 (100)
Hispanic/Latinx	3 (9)	2 (67)
Other	1 (3)	0 (0)
White	20 (62)	7 (35)

*Race was self-reported.

All causative, candidate, and novel variants were found in genes associated with genetic syndromes, with the exception of *PLD1*, which is associated with CHD alone (Developmental cardiac valvular defect, MIM 212093). Please see Table 2 for a detailed evaluation of all identified variants.

Novel, putative CAKUT/CHD gene associations were substantiated by evidence demonstrating presence of the protein product in both organ systems or research supporting physiologic or structural abnormalities in one organ system but not the other (Table 3). For example, *VPS4A* has been associated with cerebellar hypoplasia, cataracts, impaired intellectual development, congenital microcephaly, dystonia, dyserythropoietic anemia, and growth retardation (CIMDAG syndrome, MIM 619273) and with recurrent urinary tract infections, which frequently indicates an underlying structural anomaly (e.g., vesicoureteral reflux or obstruction) (19). However, there were no reports of CHD associated with this disorder.

In total, GWS identified a suspected genetic etiology in 44% of cases with CAKUT/CHD phenotypes, with another 13% identified as having a likely environmental etiology, and an additional 13% with VACTERL syndrome. In total, 70% of cases were determined to have a suspected etiology for their presentation.

The most common CAKUT phenotype identified was hydronephrosis, seen in 22/32 (69%) of all cases. The most common CHD phenotype identified was septal defects, identified in 22/32 (69%) of all cases. Additional phenotypic information can be found in Table 4.

We also identified additional structural anomalies in other organ systems in 28 out of the 32 cases (88%). Additional organ systems were classified based on ICD10 codes and included: respiratory, eye/ear/face/neck, cleft lip and palate, nervous system, musculoskeletal (msk), digestive, genital, and other circulatory. The most common additional organ systems affected were the nervous system (53% of cases) and musculoskeletal systems (44% of cases). Structural brain anomalies were the most common anomalies identified in the nervous system. Pectus anomalies and scoliosis were the most common anomalies identified in the musculoskeletal system. Additional organ system involvement is detailed in Table 5.

Patients with only CAKUT and CHD and no other organ system involvement included the following case ID numbers: 3005, 3010, 1009, and 3013. Two of these cases did not have an identifiable etiology for their CAKUT and CHD phenotype. ID 1009 was found to have trisomy 21 and ID 3,013 had two suspected disease-causing variants in the PLD1 gene, the only gene in this group without an associated syndromic phenotype.

Discussion

Rare genes identified

In this study of a small, but ancestrally diverse cohort of 32 cases diagnosed with both CAKUT and CHD, we identified molecular etiologies in 14 cases (44%). This yield is higher than that observed for patients with either CAKUT or CHD alone, suggesting that a genetic etiology should be highly suspected and evaluated for in patients with both CAKUT and CHD. We identified 12 distinct monogenic disorders, representing 86% of all genetic diagnoses (Table 2). This yield is significantly higher than either CHD or CAKUT alone, for which most identified genetic causes are due to copy number variants (CNVs) or chromosomal abnormalities (13, 14). Recently, however, a paper published by Sweeney et al. in 2021 reports point mutations as the most common genetic etiology for a small cohort of CHD cases with WGS (20). It is feasible that the differences in genetic defects identified in our study and Sweeney et al. vs. historical literature are due to the technologic limits of genetic testing prior to the advent of WES and WGS. With increasing use of more comprehensive diagnostic technology, it is likely our identification of common genetic defects will continue to expand. These results suggest that monogenic causes of both CAKUT and CHD are much more common than previously expected and may differ in genetic etiology from CHD and CAKUT alone. In addition, these results suggest that genetic testing by GWS should be considered more frequently in the diagnostic evaluation of children with CHD, CAKUT, or both of unknown etiology.

Our study identified 15 monogenic causes of both CAKUT and CHD that would not have been identified by standard gene panels for CHD or CAKUT alone. Of the four common gene panels used for etiologic assessment of CAKUT, only 1–2 of our 14 patients (7%–14%) would have received a diagnosis, depending on the panel used. Genes identified in our patient population and included on CAKUT gene panels were *GREB1l* and *LRP4*. CHD gene panels were more likely to identify a molecular etiology, with most expanded panels (>50 genes) expected to yield a diagnosis in 2–5 of our 14 patients (14%–36%), depending on the panel used. CHD-associated genes identified in our patient population and included in gene panels included: *ACTA2, CHD7,*

TABLE 2 Identified variants *via* WGS/WES.

Gene	MIM Gene ID#	MIM Phenotype ID#	Chromosome: genomic coordinates	Size	Variant	Zygosity (Inheritance)	Classification
Causative Variants							
Patient 1007							
CHD7	608,892	214,800	8:61,654,796		c.807del *p*.Ala270ProfsTer35	Heterozygous (not maternal)	Pathogenic
Patient 1008							
KAT6B	605,880	606,170	10:76,788,744		c.4162C > T *p*.Gln1388Ter	Heterozygous (*de novo*)	Likely pathogenic
35 Genes		614,671		847KB	Chr16:29,453,701-30,300,900, dup (16p11.2)	Heterozygous (paternal)	Pathogenic
Patient 1010							
FGF10	602,115	149,730		171KB	Chr5:44,247,363-44,418,819, del(5p12)	Deletion (paternal)	Pathogenic
Patient 1011							
GREB1l	*617,782*	617,805	18:19,076,462		c.3194C > T, *p*.Thr1065ile	Heterozygous (maternal)	Likely pathogenic
Patient 1002							
ADNP	611,386	615,873			c.2157C > G, *p*.Tyr719Ter	Heterozygous (De Novo)	Pathogenic
Patient 1003							
NSD1	606,681	117,550			c.4039delA, *p*.Arg1347GlyfsX25	Heterozygous (De Novo)	Pathogenic
Patient 1005							
EFTUD2	603,892	610,536			c.1861-2A > C, IVS18-2A > C	Heterozgyous (De Novo)	Pathogenic
Patient 1009							
280 Genes		190,685		48,130KB	Chr21:1-48,129,895, dup (21p13q22.3)	Duplication (De Novo)	Pathogenic
Candidate Variants							
Patient 2007							
ACTA2	102,620	611,788	10:90,701,120		c.482 T > G *p*.Val161Ala	Heterozygous (maternal)	VUS
Patient 2001							
ATP6AP2	300,556	300,423			C.212G > A, *p*.Arg71His	Heterozygous (De Novo)	VUS
Patient 3013							
PLD1	602,382	212,093			c.55G > A, *p*.Ala19Thr	Heterozygous (maternal)	VUS
PLD1	602,382	212,093			c.1504C > T, *p*.Arg502Trp	Heterozgyous (paternal)	VUS
Novel Variants							
Patient 2006							
LRP4	604,270	212,780	11:46,895,119		c.4255A > G *p*.Met1419Val	Heterozygous (paternal)	VUS
LRP4	604,270	212,780	11:46,900,844		c.2837C > G *p*.Pro946Arg	Heterozygous (maternal)	VUS
Patient 1004							
PCDH15	605,514	601,067			c.733C > T, *p*.Arg245Ter	Heterozygous (maternal)	Pathogenic
Patient 1006							
VPS4A	609,982	619,273			c.298G > A, *p*.Glu100Lys	Heterozygous (*de novo*)	Likely Pathogenic
Non-CAKUT/CHD Variants							
Patient 2005							
KRT25	616,646	616,760	17:38,911,310		c.214C > T *p*.Arg72Trp	Hemizygous (maternal)	VUS
KRT25	616,646	616,760		6KB	Chr17:38,909,549-38,915,466, del (17q21.2)	Heterozygous (paternal)	VUS
Patient 1001							
FLG	135,940				c.3892delT, *P*.Ser1298LeufsX148	Heterozygous (maternal)	Pathogenic
PKD2	173,910				c.2291A > T, *p*.Gln764Leu	Heterozygous (maternal)	VUS
Patient 2002							
GCK	138,079				C.137G > T, *p*.Arg46Met	Heterozygous (maternal)	VUS
POLG2	604,983				c.341G > A, *p*.Trp114Ter	Heterozygous (paternal)	VUS
Patient 2004							
OBSL1	610,991	612,921			c.5108G > A, *p*.gly1703Glu	Heterozygous (paternal)	VUS
OBSL1	610,991	612,921			c.1255C > T, *p*.Arg419Cys	Heterozygous (maternal)	VUS
Patient 2003							
MT-TK	590,060				m.8340G > A	Heteroplasmy 2% (maternal)	Pathogenic
MT-TS2	590,085				m.12223A > G	Homplasmic	VUS

TABLE 3 Potential novel CAKUT/CHD genes.

Gene	Variants	Syndrome	Prior Literature
PCDH15	c.733C > T *p*.Arg245Ter	Usher Syndrome	PCDH15 -CD2 expression has been found in heart, kidney, thymus, spleen, testis, retina and cochlea.
VPS4A	c.298G > A *p*.Glu100Lys	CIMDAG Syndrome	Found in individuals with frequent UTIs. No reported CHD.
LRP4	1. c.4255A > G *p*.Met1419Val 2. c.2837C > G *p*.Pro946Arg	Cenani-Lenz Syndactyly Syndrome	Causes renal agenesis. No reported CHD

TABLE 4 CAKUT and CHD phenotype*.

	N	%
CAKUT Phenotype:		
Hydronephrosis	22	69
Vesicoureteral reflux	5	16
Renal Agenesis	3	9
Hypo/Dysplasia	3	9
Ectopy	1	3
CHD Phenotype:		
Sepal Defects	22	69
Valvular Anomalies	9	28
Dilated Heart Chambers	5	16
Coarctation of Aorta	4	13
Tetralogy of Fallot	2	6
Hypoplastic Left Heart	1	3
Transposition of Great Arteries	1	3

*Patients may have more than 1 phenotype in each category.

EFTUD2, NSD1 and *PLD1*. Overall, these findings demonstrate substantial genetic heterogeneity in this population, and importantly they suggest a lack of significant overlap with genes commonly identified in isolated cases of CHD or CAKUT. Our results also suggest that these patients are likely to be underdiagnosed by gene panels, often the first genetic test utilized. We suggest that the etiologic evaluation of children with both CAKUT and CHD should be with diagnostic GWS and not by gene panel sequencing. The diagnostic superiority of GWS over gene panels is likely as a result of unrecognized phenotype expansion.

Novel CAKUT and CHD genes

We identified three putative novel gene associations with CAKUT and CHD herein (*LRP4, PCDH15, VPS4A*). These genes contained a suspected disease-causing variant in an affected child, but the gene had not been previously associated with CAKUT and CHD. In one such case, variants in the *PCDH15* gene have been associated with Usher syndrome (MIM 601067), which presents with hearing and vision loss, and matched the clinical phenotype for this patient (21). The protein product of *PCDH15* is also expressed in other organ systems, including the heart and kidney (21). Thus, it was feasible that deleterious variation in this gene could be associated with both CAKUT and CHD phenotypes, as observed in this case. The variant identified in our patient was predicted to cause loss of function of the protein product through truncation or nonsense-mediated mRNA decay. Additional studies will be required to confirm that this is a recurrent phenotype expansion.

The other two genes identified have been implicated in kidney anomalies but have no prior reports of association with CHD (22, 23). The *LRP4* gene has been associated with renal agenesis (23). Of the two variants identified in our patient, in silico prediction tools supported a deleterious effect of one variant on the protein structure/function due to the alteration of a highly conserved amino acid, and discordant results for the other variant. The *VPS4* gene is associated with recurrent kidney infections, generally suggesting an underlying kidney anomaly (22). In addition, the GeneDx in silico analysis supported a deleterious effect of the VPS4A missense variant on protein structure/function. Additional phenotype expansion case reports or *in vivo* studies will be required for causal gene association with CHD and CAKUT.

Environmental factors

Several environmental teratogens have also been associated with CAKUT and CHD anomalies including certain drugs, chemicals, and fetal exposure to hyperglycemia (24). Fetal structural defects are three to four-fold higher in infants born to diabetic mothers. These anomalies can affect a number of organ systems including: neurologic, gastrointestinal, kidney, and heart (25). Our study identified six cases with mothers who had diabetes requiring insulin therapy during pregnancy. Of note, five of these cases (83%) did not have an identifiable genetic etiology for their presentation. These findings suggest that genetic testing may have a low yield in patients with a likely environmental etiology for CAKUT and CHD.

Our study also identified three cases with VACTERL association and no known genetic etiology. The etiopathogenesis of VACTERL association is still unknown, but theories include possible teratogenic exposures, a malformation cascade, combination of environmental and epigenetic factors, or disturbances in developmental processes essential to all affected organ systems (24, 26). Overall, of the 18 cases in our study without a genetic diagnosis, seven cases (39%) had a suspected environmental etiology for their presentation. Our study suggests that the majority of patients with CAKUT and CHD will have an identifiable etiology for their anomalies, and thus a thorough history should evaluate for exposure to environmental teratogens, physical exam and imagining should evaluate for VACTERL association, and genetic evaluation should include WES or WGS.

Expanding the phenotype of patients with CAKUT and CHD

Previously CAKUT and CHD have both been found as solitary anomalies or co-existing with other organ system malformations (3, 4, 7, 8, 27–31). Overall, 40%–60% of patients with a CAKUT

10.3389/fped.2023.1157630

TABLE 5 Additional organ systems with structural congenital anomalies.

Pt ID	Gene	Respiratory	Eye, ear, face, neck	Cleft lip & palate	Nervous System	MSK	Digestive	Genital	Other Circulatory
1007	*CHD7*	X	X						
1005	*EFTUD2*		X	X	X	X			
1008	*KAT6B*		X		X	X	X		
1002	*ADNP*	X			X	X			
1010	*FGF10*	X							
1003	*NSD1*					X			
1011	*GREB1L*				X				
2007	*ACTA2*	X							
2001	*ATP6AP2*				X	X		X	
1004	*PCHD15*	X	X		X	X			
1006	*VPS4A*				X				
2006	*LRP4*				X				
3011			X		X	X			
3012					X	X	X		
2003					X	X			
3004					X		X	X	
2002	*GCK POLG2*					X			
3014					X			X	
2005	*KRT25*				X				
2004	*OSLB1*				X	X			
1001	*FLG*					X		X	
3006		X							X
3001					X	X			X
3002						X		X	
3003					X				
3008					X				
3015				X			X		
3007								X	
		6/32 (19%)	5/32 (16%)	2/32 (6%)	17/32 (53%)	14/32 (44%)	4/32 (13%)	6/32 (19%)	2/32 (6%)

or CHD have an additional extra-renal or extra-cardiac abnormality (7, 8, 27–30). CHD and CAKUT are known to co-occur in 25%–30% of affected individuals, more than any other concurrent organ system anomalies (7, 8, 31). During study subject ascertainment, 23% of hospitalized CHD cases were found to also have an identifiable CAKUT, in accord with published literature (7, 8, 31). Electronic medical record review also identified additional organ system anomalies in 28 cases (88%) with CAKUT and CHD (**Table 5**). The most commonly identified extra-renal/cardiac malformations were those in the nervous system (53% of all cases), with mainly brain malformations, and musculoskeletal system (44% of all cases), with primarily scoliosis and pectus anomalies identified. While underpowered for statistical analysis, certain organ system associations appeared to co-occur more commonly in those with genetic diagnoses or those without. For example, respiratory and eye/ear/face/neck anomalies were more likely to occur in those patients with a genetic etiology than those without, with nine out of 11 malformations (82%) identified in those with an underlying genetic diagnosis. In contrast, cleft lip/palate, musculoskeletal, and nervous system anomalies occurred at about an equal rate in cases with and without a genetic diagnosis. Digestive, other circulatory, and genital anomalies occurred more frequently in cases without a molecular diagnosis, with 10 out of 12 malformations (83%) identified in those without a genetic etiology. If substantiated in larger cohorts, these findings may guide prioritization for diagnostic GWS.

Overall, we found significantly more extra-renal/cardiac malformations in our patients with both CAKUT and CHD than has been reported with either CAKUT or CHD alone (7, 8, 31). These findings may be related to the high rate of genetic syndromes identified in this study, with 13 of our 14 genetic diagnoses (93%) herein related to a previously identified syndrome. However, additional structural malformations were identified just as commonly in those with environmental causes and no identifiable etiology for their presentation. Patients with CHD or CAKUT and additional organ system anomalies have higher morbidity and mortality, and thus our data may be biased, since hospital admission was among the selection criteria (27, 29). Despite this possible skewing, these results still provide valuable information on what additional diagnostic work up should be considered, and suggest that hospitalized pediatric patients with both CAKUT and CHD should be evaluated for additional organ system malformations, most specifically in the musculoskeletal and nervous systems.

Limitations

Our study has several limitations that need to be addressed. Primarily, this is a small study at a single tertiary center, which

limited our ability to adequately power this analysis and provide any statistical evaluations. Secondly, we evaluated only hospitalized patients with CAKUT and CHD. This filter was set specifically to evaluate the sickest of this population, in order to better direct acute care and management. However, in limiting our population in this fashion, our findings may not be generalizable to patients who have not been hospitalized.

In addition,, we only evaluated those patients with exome and genome sequencing, missing those in which a genetic diagnosis is made *via* microarray, karyotype, or gene panels only. Without this information, we do not know if the patients diagnosed through these testing strategies would present with a different phenotype than our current patient population. It is also unclear if some of the more commonly known CAKUT/CHD genes were screened out with these testing methodologies, thus negating the need for more thorough genetic testing strategies. As reanalysis was only applied to those with WGS, it is also possible that additional genetic diagnoses were missed in those patients who only had WES.

Furthermore, we recognize the limitations of WES in comparison with WGS. Due to the nature of WES, this type of sequencing may have missed small CNVs, mitochondrial variants, intronic variation, repeat expansion, mobile insertion elements and coverage of PCR-free genomes (32). Bertoli-Avella et al. found a 14% increase in diagnostic yield of WGS over WES in a cohort of over 300 patients (32). Taking these findings into account, it's possible we may have missed up to 2 molecular diagnoses in our WES cohort, that may have been identified had WGS been available.

Our study did not identify any repeat implicated genes in our population. These findings likely signify a lack of saturation due to our small patient cohort.

Future directions

Although our study evaluated a small subset of patients at a single center, it is the first of its kind to specifically evaluate the genotype and phenotype of this patient population. This study provides a launching point to encourage additional studies interrogating all genetic testing in this patient population and to expand the evaluation to patients in both the inpatient and outpatient setting across multiple centers. Additional evaluation should also focus on those patients with CAKUT and CHD and no other affected organ system, as these may have a different and more enriched diagnostic yield.

Data availability statement

The data analyzed in this study is subject to the following licenses/restrictions: All data associated with this study are present in the paper. While no DNA sequence was generated as a part of this published work, all novel DNA sequence variants have been uploaded to ClinVar under our institutional identifier, Organization ID: 506081. Requests to access these datasets should be directed to etallred@health.ucsd.edu.

Ethics statement

The studies involving human participants were reviewed and approved by UCSD IRB. Written informed consent from the participants' legal guardian/next of kin was not required to participate in this study in accordance with the national legislation and the institutional requirements.

Author contributions

ETA, EAP, NGC, ESK, and DPD contributed to the conception and design of the study. SFK, DPD, and ETA organized the database. ETA performed data collection and wrote the first manuscript. All authors contributed to the article and approved the submitted version.

Funding

This work was supported by the Nephrology T32 NIH Grant, #5T32DK104717–05

Conflict of interest

DPD is employed by Creyon Bio, Inc; reports previous consulting fees from Audentes and BioMarin; serves on a scientific advisory board for Taysha Gene Therapies; is an advisor to Pioneering Medicine VII, Inc; and is an inventor on United States patent 8718950B2 assigned to The HudsonAlpha Institute for Biotechnology.

The remaining authors declare that the research was conducted in the absence of any commercial or financial relationships that could be construed as a potential conflict of interest.

Publisher's note

References

1. Capone VP, Morello W, Taroni F, Montini G. Genetics of congenital anomalies of the kidney and urinary tract: the current state of play. *Int J Mol Sci*. (2017) 18(4):796. doi: 10.3390/ijms18040796

2. Prendiville T, Jay PY, Pu WT. Insights into the genetic structure of congenital heart disease from human and murine studies on monogenic disorders. *Cold Spring Harb Perspect Med*. (2014) 4(10):a013946. doi: 10.1101/cshperspect.a013946

3. Elder JS. Antenatal hydronephrosis. Fetal and neonatal management. *Pediatr Clin North Am*. (1997) 44(5):1299–321. doi: 10.1016/S0031-3955(05)70558-7

4. Grisoni ER, Gauderer MW, Wolfson RN, Izant RJ. Antenatal ultrasonography: the experience in a high risk perinatal center. *J Pediatr Surg*. (1986) 21(4):358–61. doi: 10.1016/S0022-3468(86)80204-4

5. Smith JM, Stablein DM, Munoz R, Hebert D, McDonald RA. Contributions of the transplant registry: the 2006 annual report of the north American pediatric renal trials and collaborative studies (NAPRTCS). *Pediatr Transplant*. (2007) 11(4):366–73. doi: 10.1111/j.1399-3046.2007.00704.x

6. Van der Ven AT, Vivante A, Hildebrandt F. Novel insights into the pathogenesis of monogenic congenital anomalies of the kidney and urinary tract. *J Am Soc Nephrol*. (2018) 29(1):36–50. doi: 10.1681/ASN.2017050561

7. San Agustin JT, Klena N, Granath K, Panigrahy A, Stewart E, Devine W, et al. Genetic link between renal birth defects and congenital heart disease. *Nat Commun*. (2016) 7:11103. doi: 10.1038/ncomms11103

8. Gabriel GC, Pazour GJ, Lo CW. Congenital heart defects and ciliopathies associated with renal phenotypes. *Front Pediatr*. (2018) 6:175. doi: 10.3389/fped.2018.00175

9. Khairy P, Ionescu-Ittu R, Mackie AS, Abrahamowicz M, Pilote L, Marelli AJ. Changing mortality in congenital heart disease. *J Am Coll Cardiol*. (2010) 56 (14):1149–57. doi: 10.1016/j.jacc.2010.03.085

10. Dolk H, Loane M, Garne E. Group ESoCAEW. Congenital heart defects in Europe: prevalence and perinatal mortality, 2000 to 2005. *Circulation*. (2011) 123 (8):841–9. doi: 10.1161/CIRCULATIONAHA.110.958405

11. De Tomasi L, David P, Humbert C, Silbermann F, Arrondel C, Tores F, et al. Mutations in GREB1l cause bilateral kidney agenesis in humans and mice. *Am J Hum Genet*. (2017) 101(5):803–14. doi: 10.1016/j.ajhg.2017.09.026

12. Sanna-Cherchi S, Khan K, Westland R, Krithivasan P, Fievet L, Rasouly HM, et al. Exome-wide association study identifies GREB1l mutations in congenital kidney malformations. *Am J Hum Genet*. (2017) 101(6):1034. doi: 10.1016/j.ajhg.2017.11.003

13. Nees SN, Chung WK. Genetic basis of human congenital heart disease. *Cold Spring Harb Perspect Biol*. (2020) 12(9):a036749. doi: 10.1101/cshperspect.a036749

14. Sanna-Cherchi S, Westland R, Ghiggeri GM, Gharavi AG. Genetic basis of human congenital anomalies of the kidney and urinary tract. *J Clin Invest*. (2018) 128(1):4–15. doi: 10.1172/JCI95300

15. Rangaswami J, Bhalla V, Blair JEA, Chang TI, Costa S, Lentine KL, et al. Cardiorenal syndrome: classification, pathophysiology, diagnosis, and treatment strategies: a scientific statement from the American heart association. *Circulation*. (2019) 139(16):e840–e78. doi: 10.1161/CIR.0000000000000664

16. Dries DL, Exner DV, Domanski MJ, Greenberg B, Stevenson LW. The prognostic implications of renal insufficiency in asymptomatic and symptomatic patients with left ventricular systolic dysfunction. *J Am Coll Cardiol*. (2000) 35 (3):681–9. doi: 10.1016/S0735-1097(99)00608-7

17. Hillege HL, Nitsch D, Pfeffer MA, Swedberg K, McMurray JJ, Yusuf S, et al. Renal function as a predictor of outcome in a broad spectrum of patients with heart failure. *Circulation*. (2006) 113(5):671–8. doi: 10.1161/CIRCULATIONAHA.105.580506

18. Kingsmore SF, Cakici JA, Clark MM, Gaughran M, Feddock M, Batalov S, et al. A randomized, controlled trial of the analytic and diagnostic performance of singleton and trio, rapid genome and exome sequencing in ill infants. *Am J Hum Genet*. (2019) 105(4):719–33. doi: 10.1016/j.ajhg.2019.08.009

19. Yang H, Robinson PN, Wang K. Phenolyzer: phenotype-based prioritization of candidate genes for human diseases. *Nat Methods*. (2015) 12(9):841–3. doi: 10.1038/nmeth.3484

20. Sweeney NM, Nahas SA, Chowdhury S, Batalov S, Clark M, Caylor S, et al. Rapid whole genome sequencing impacts care and resource utilization in infants with congenital heart disease. *NPJ Genom Med*. (2021) 6(1):29. doi: 10.1038/s41525-021-00192-x

21. Alagramam KN, Yuan H, Kuehn MH, Murcia CL, Wayne S, Srisailpathy CR, et al. Mutations in the novel protocadherin PCDH15 cause usher syndrome type 1F. *Hum Mol Genet*. (2001) 10(16):1709–18. doi: 10.1093/hmg/10.16.1709

22. Seu KG, Trump LR, Emberesh S, Lorsbach RB, Johnson C, Meznarich J, et al. VPS4A Mutations in humans cause syndromic congenital dyserythropoietic Anemia due to cytokinesis and trafficking defects. *Am J Hum Genet*. (2020) 107(6):1149–56. doi: 10.1016/j.ajhg.2020.10.013

23. Li Y, Pawlik B, Elcioglu N, Aglan M, Kayserili H, Yigit G, et al. LRP4 Mutations alter wnt/beta-catenin signaling and cause limb and kidney malformations in cenani-lenz syndrome. *Am J Hum Genet*. (2010) 86(5):696–706. doi: 10.1016/j.ajhg.2010.03.004

24. Stevenson RE, Hunter AG. Considering the embryopathogenesis of VACTERL association. *Mol Syndromol*. (2013) 4(1–2):7–15. doi: 10.1159/000346192

25. Mills JL. Malformations in infants of diabetic mothers. *Teratology*. (1982) 25:385–94. Birth Defects Res A Clin Mol Teratol. 2010;88(10):769-78. doi: 10.1002/tera.1420250316

26. Reutter H, Hilger AC, Hildebrandt F, Ludwig M. Underlying genetic factors of the VATER/VACTERL association with special emphasis on the "renal" phenotype. *Pediatr Nephrol*. (2016) 31(11):2025–33. doi: 10.1007/s00467-016-3335-3

27. Leow EH, Lee JH, Hornik CP, Ng YH, Hays T, Clark RH, et al. Congenital anomalies of the kidney and urinary tract (CAKUT) in critically ill infants: a multicenter cohort study. *Pediatr Nephrol*. (2022) 38(1):161–72. doi: 10.1007/s00467-022-05542-0

28. Murugapoopathy V, Gupta IR. A primer on congenital anomalies of the kidneys and urinary tracts (CAKUT). *Clin J Am Soc Nephrol*. (2020) 15(5):723–31. doi: 10.2215/CJN.12581019

29. Bensemlali M, Bajolle F, Ladouceur M, Fermont L, Lévy M, Le Bidois J, et al. Associated genetic syndromes and extracardiac malformations strongly influence outcomes of fetuses with congenital heart diseases. *Arch Cardiovasc Dis*. (2016) 109 (5):330–6. doi: 10.1016/j.acvd.2016.01.006

30. Miller A, Riehle-Colarusso T, Alverson CJ, Frías JL, Correa A. Congenital heart defects and major structural noncardiac anomalies, Atlanta, Georgia, 1968 to 2005. *J Pediatr*. (2011) 159(1):70–8.e2. doi: 10.1016/j.jpeds.2010.12.051

31. Sagar VVSS, Acharya S, Gomase S, Singh RK, Shukla S, Kumar S, et al. Ventricular septal defect (VSD) as an extra renal manifestation in congenital anomalies of kidney and urinary tract (CAKUT) syndrome: a rare case report. *Med Sci*. (2022) 26(41):e2003. doi: 10.54905/disssi/v26i119/ms41e2003

32. Bertoli-Avella AM, Beetz C, Ameziane N, Eugenia Rocha M, Guatibonza P, Calvo M, et al. Successful application of genome sequencing in a diagnostic setting: 1007 index cases from a clinically heterogeneous cohort. *Eur J Hum Genet*. (2021) 29(1):141–53. doi: 10.1038/s41431-020-00713-9

frontiers | Frontiers in Pediatrics

TYPE Original Research
PUBLISHED 17 March 2023
DOI 10.3389/fped.2023.1141665

OPEN ACCESS

EDITED BY
Jordi Pérez-Tur,
Institute of Biomedicine of Valencia, Spain

REVIEWED BY
Birsen Karaman,
Istanbul University, Türkiye
Aldesia Provenzano,
University of Florence, Italy

*CORRESPONDENCE
Aihua Yin
yinaihua0131@163.com

†These authors have contributed equally to this work.

SPECIALTY SECTION
This article was submitted to Genetics of Common and Rare Diseases, a section of the journal Frontiers in Pediatrics

RECEIVED 10 January 2023
ACCEPTED 01 March 2023
PUBLISHED 17 March 2023

CITATION
Wang Y, Liu C, Hu R, Geng J, Lu J, Zhao X, Xiong Y, Wu J and Yin A (2023) Prenatal phenotype features and genetic etiology of the Williams-Beuren syndrome and literature review.
Front. Pediatr. 11:1141665.
doi: 10.3389/fped.2023.1141665

Prenatal phenotype features and genetic etiology of the Williams-Beuren syndrome and literature review

Yunan Wang[1,2†], Chang Liu[1,2†], Rong Hu[1,2], Juan Geng[3], Jian Lu[1,2], Xianzhe Zhao[3], Ying Xiong[1,2], Jing Wu[1,2] and Aihua Yin[1,2*]

[1]Medical Genetic Center, Guangdong Women and Children Hospital, Guangzhou, China, [2]Maternal and Children Metabolic-Genetic Key Laboratory, Guangdong Women and Children Hospital, Guangzhou, China, [3]Ultrasonic Diagnosis Deparment, Guangdong Women and Children Hospital, Guangzhou, China

Objective: To share our experience on prenatal diagnosis of Williams-Beuren syndrome(WBS) and to improve the awareness, diagnosis, and intrauterine monitoring of the fetuses of this disease.
Methods: The study retrospectively evaluated 14 cases of WBS diagnosed prenatally by single nucleotide polymorphism array (SNP-array). Clinical data from these cases were systematically reviewed, including maternal demographics, indications for invasive prenatal diagnosis, ultrasound findings, SNP-array results, trio-medical exome sequencing (Trio-MES) results, QF-PCR results, pregnancy outcomes and follow-ups.
Results: A total of 14 fetuses were diagnosed with WBS and their prenatal phenotypes were assessed retrospectively. In our case series, the most common ultrasound features were intrauterine growth retardation (IUGR), congenital cardiovascular defects, abnormal fetal placental doppler indices, thickened nuchal translucency(NT) and polyhydramnios. Other less common ultrasound features include fetal hydrops, hydroderma, bilateral pleural effusion, subependymal cysts, etc. Parental chromosome analysis was performed in seven pairs of parents, and all the deletions on chromosome 7q11.23 were *de novo*.
Conclusion: Prenatal ultrasound features of WBS cases are highly variable, with IUGR, cardiovascular abnormalities and abnormal fetal placental doppler indices, being the most common intrauterine phenotypes. Our case series expand the intrauterine phenotypes of WBS, including cardiovascular abnormalities right aortic arch(RAA) combined with persistent right umbilical vein(PRUV) and elevated the ratio of end-systolic peak flow velocity to end-diastonic peak flow velocity(S/D). In the meantime, with the decrease in the cost of the next-generation sequencing, the method may become widely used in prenatal diagnosis in the near future.

KEYWORDS

williams-Beuren syndrome (WBS), prenatal diagnosis, sonographic features, SNP-array, intrauterine phenotypes

Introduction

Williams–Beuren syndrome (WBS) is a relatively rare microdeletion disease caused by mispairing of low-copy DNA repetitive elements during meiosis. Most patients with WBS have similar deletion sizes resulting in the loss of one copy of 25–27 genes on chromosome 7q11.23 (1), and the typical deletion of the syndrome is 1.4–1.5 Mb. This

disorder affects multisystem, and the cardinal features include cardiovascular disease (especially supravalvar aortic stenosis), a specific facial features and a distinctive cognitive and behavioral disability and hyper sociability. But limited information has been collected on the intrauterine phenotype features of WBS. Until now, only about 29 prenatal cases of WBS have been reported (2–11). The prenatal diagnosis of WBS is difficult due to the atypical features of prenatal ultrasound. However, due to the uncertain prognosis of WBS, the detection rate should be improved for timely intrauterine intervention.

In our case series, fourteen fetuses with WBS identified by single nucleotide polymorphism array (SNP-array) are described. We provide clinical features, intrauterine phenotypes and molecular cytogenetic results of the 14 cases, and we compare them with published data to outline distinguishing and shared features. To our knowledge, this study is the most extensive prenatal study of the detailed molecular analysis of WBS cases using chromosomal microarray analysis (CMA) techniques.

Material and methods

Subject

We reviewed 14 consecutive fetuses of WBS diagnosed at our Center from January 2016 to September 2021. Clinical data from these cases were systematically reviewed, including maternal demographics, indications for invasive prenatal diagnosis, ultrasound findings, SNP-array results, trio-medical exome sequencing (Trio-MES) results, QF-PCR results, pregnancy outcomes and follow-up data. Each case underwent a routine ultrasound scan at primary hospitals, and referred to our center for reassessment. Their initial indications for invasive prenatal diagnosis include anomalies on ultrasonography (Case 1–12), high risks for large deletion of chromosome 7 (case 13) and high risks for WBS (case 14) by expanded noninvasive prenatal testing (NIPT). After ultrasound reassessment and genetic counseling, all pregnant women received invasive prenatal diagnosis, and the types of prenatal diagnosis were chosen according to their gestational ages (**Table 1**). Maternal age ranges from 23 to 33 years, with an average of 28.7 years. The gestational age at prenatal diagnosis ranges from 13 to 32 weeks, with an average of 25.6 weeks. Follow-up data were collected on height, weight, facial features, physical activity, and mental responses of newborns. This study has been approved by the Institutional Review Board/ Medical Ethics Committee of Guangdong Women and Children Hospital (IRB reference number: 201801073). Written informed consent was obtained from each participating family.

Cytogenetic and molecular analyses

G-banding (320–400 bands) was performed on metaphase chromosomes of amniotic fluid cells/ umbilical cord blood lymphocytes/ villus cells using standard procedures (12). Genomic DNA was extracted from fetal uncultured amniotic fluids /umbilical cord blood lymphocytes/ villus cells and their parents' peripheral blood using the Lab-Aid 820 automation system (Zee San Biotech Company, Fujian, China).

SNP-array analysis was performed on a commercial CytoScan 750 K Array (Affymetrix, Santa Clara, CA) containing 750,436 25–85mer oligonucleotide probes, including 550,000 non-polymorphic probes and 200,436 SNP probes (13). The labeling and hybridization of the genomic DNA was performed following the manufacturer's protocol. Results were analyzed by Affymetrix Chromosome Analysis Suite software.

Medical exome sequencing

Genomic DNA was extracted using a Qiagen DNA blood mini kit (Qiagen GmbH, Hilden, Germany). Library preparation and target enrichment were performed using a SureSelectXT Clinical Research Exome kit (Agilent Technologies, Santa Clara, CA) according to the manufacturer's specifications. Then, Trio-MES was performed using 2×150 bp in the paired end mode of the NextSeq 500 platform (Illumina, San Diego, CA) to obtain an average coverage of above 110×, with 97.6% of target bases covered at least 10× (14). Sequence quality analysis and filtering of mapped target sequences were performed with the "varbank" exome and genome analysis pipeline v.2.1 as described previously. Analysis of genetic results was based on the genomic variation database (http://dgv.tcag.ca/dgv/app/home), DECIPHER database (https://decipher.sanger.ac.uk/), and OMIM database (http://www.ncbi.nlm.nih.gov/omim). Found variants were further verified by Sanger sequencing.

Results

Intrauterine phenotypes

Fourteen fetuses were diagnosed with WBS. Their prenatal phenotype features were reviewed retrospectively. Clinical characteristics and genetic results are shown in **Table 1**. In our case series, the most common ultrasound features were as follows: intrauterine growth retardation (IUGR) (9/14, 64.3%), congenital cardiovascular defects (6/14, 42.9%), abnormal fetal placental doppler indices (7/14, 50%), thickened NT (2/14, 14.3%) and polyhydramnios (2/14, 14.3%). The most common cardiovascular abnormalities in our study encompass vascular ring (3/6, 50%), ventricular septal defect (VSD) (1/6, 16.7%), persistent left superior vena cava (PLSVC)(1/6, 16.7%), enlarged right atrium (1/6, 16.7%), abnormal connection between the portal vein (PV) sinus and the right atrium (RA) (1/6, 16.7%), elevated blood flow rate of the aortic valve (1/6, 16.7%), abnormal extending of descending aortic arch (extends to the left obviously) (1/6, 16.7%). **Figure 1** shows some typical ultrasound features of cardiovascular abnormalities in these cases. Abnormal fetal placental doppler indices in our study include elevated ratio of end-systolic peak flow velocity to end-diastonic peak flow

TABLE 1 Genetic results of all reported fetuses with Williams–Beuren syndrome (WBS).

	NO.	Maternal age	Gestational age at diagnosis	expanded NIPT	Prenatal Diagnosis	Genetic tests	Fetal karyotype	CMA result		Inheritance	Outcome of pregnancy
								CNVs type	Size (Mb)		
Present cases	*case 1*	*26*	*31*	*/*	*PUBS*	*SNP array,G-banding,QF-PCR*	*46,XX*	*arr[GRCh37] 7q11.23 (72557179_74628840)x1*	*2.1*	*/*	*TOP*
	case 2	*29*	*23*	*/*	*Amniocentesis*	*SNP array,G-banding,QF-PCR*	*46,XX*	*arr[GRCh37] 7q11.23 (72624166_74209678)x1*	*1.59*	*/*	*TOP*
	case 3	*31*	*31*	*low risk*	*PUBS*	*SNP array,G-banding,QF-PCR*	*46,XY*	*arr[GRCh37] 7q11.23 (72701098_74136633)x1*	*1.4*	*de novo*	*TOP*
	case 4	*29*	*29*	*low risk*	*Amniocentesis*	*SNP array,G-banding,QF-PCR*	*46,XX*	*arr[GRCh37] 7q11.23 (72669480_74154209)x1*	*1.5*	*de novo*	*TOP*
	case 5	*23*	*32*	*low risk*	*Amniocentesis*	*SNP array,G-banding,Trio-MES, QF-PCR*	*46,XY*	*arr[GRCh37] 7q11.23 (72692113_74154209)x1*	*1.5*	*de novo*	*Delivery by CS and died a week later*
	case 6	*29*	*24*	*low risk*	*PUBS*	*SNP array,G-banding,QF-PCR*	*46,XY,inv(9) (p11q13)*	*arr[GRCh37] 7q11.23 (72723370_74136633)x1*	*1.4*	*/*	*TOP*
	case 7	*30*	*32*	*/*	*Amniocentesis*	*SNP array,G-banding,QF-PCR*	*46,XY*	*arr[GRCh37] 7q11.23 (72677084_74154209)x1*	*1.5*	*/*	*Delivery by CS at 35w3d*
	case 8	*26*	*13*	*/*	*CVS*	*SNP array,G-banding,Trio-MES, QF-PCR*	*46,XX*	*arr[GRCh37] 7q11.22q21.11 (72081552_77582265)x1*	*5.5*	*de novo*	*TOP*
	case 9	*27*	*25*	*/*	*Amniocentesis*	*SNP array,G-banding,QF-PCR*	*47,XXX*	*arr[GRCh37] (X)×3 7q11.23 (72664089_74154209)x1*	*1.5*	*/*	*TOP*
	case 10	*27*	*29*	*low risk*	*PUBS*	*SNP array,G-banding,Trio-MES, QF-PCR*	*46,XY*	*arr[GRCh37] 7q11.23 (72633240_74154209)x1*	*1.5*	*de novo*	*TOP*
	case 11	*31*	*24*	*/*	*Amniocentesis*	*SNP array,G-banding,Trio-MES, QF-PCR*	*46,XY*	*arr[GRCh37] 7q11.23 (72723371_74146927)x1*	*1.4*	*de novo*	*TOP*
	case 12	*30*	*22*	*high risk for large deletion of chromosome 7*	*Amniocentesis*	*SNP array,G-banding,QF-PCR*	*46,XY,del(7) (q11.2q21)*	*arr[GRCh37] 7q11.21q21.11 (64256482_85672186)x1*	*21.4*	*/*	*TOP*
	case 13	*31*	*20*	*high risk for WBS*	*Amniocentesis*	*SNP array, G-banding,QF-PCR*	*46,XY*	*arr[GRCh37] 7q11.23 (72718124_74154209)x1*	*1.4*	*de novo*	*TOP*
	case 14	*33*	*24*	*/*	*Amniocentesis*	*SNP array, G-banding,QF-PCR*	*46,XY,inv(9) (p12q13)*	*arr[GRCh37] 7q11.23 (72636884_74v146927)x1 11q12.1 (56812656_59398190)x3 (VOUS)*	*1.5*	*/*	*TOP*
Dadelszen et al., 2000	case 15	25	30	/	/	FISH,G-banding	46,XX, t(6;7) (q27;q11.23)	/	/	/	Died shortly after delivery
Kontos et al., 2008	case 16	34	23	/	Amniocentesis	MLPA,FISH	46,XX	/	/	/	TOP
Krzeminska et al., 2009	case 17	31	20	/	/	FISH	/	/	/	/	TOP
	case 18	22	25	/	/	Prenatal BoBs, FISH	46,XX	/	/	*de novo*	TOP

(*continued*)

10.3389/fped.2023.1141665

TABLE 1 Continued

	NO.	Maternal age	Gestational age at diagnosis	expanded NIPT	Prenatal Diagnosis	Genetic tests	Fetal karyotype	CMA result		Inheritance	Outcome of pregnancy
								CNVs type	Size (Mb)		
Popowski, Vialard, Leroy, Bault, & Molina, 2011											
Marcato et al., 2014	case 19	36	20+2	/		Prenatal BoBs, FISH,array CGH	46,XX	/	/	*de novo*	TOP
	case 20	31	32	/		G-banding, Prenatal BoBs, FISH,array CGH	46,XX	/	/	*de novo*	TOP
	case 21	30	13	/		G-banding,FISH, array CGH	46,XY	/	/	*de novo*	TOP
Kobalka, Mrak, Gunning, 2017	case 22	28	34	/		Not mentioned	/	/	/	/	Stillborn
Srinivasan, Howley, Cuneo,& Chatfield, 2018	case 23	/	34	/		FISH	/	/	/	/	Delivery by CS
MZ Yuan et al. 2019	case 24	35	23	low risk	Amniocentesis	SNP array,G-banding,QF-PCR	46,XY	arr[GRCh37] 7q11.23 (72745047_74138460)x1	1.39	*de novo*	TOP
	case 25	27	22	low risk	Amniocentesis	SNP array,G-banding,QF-PCR	46,XX	arr[GRCh37] 7q11.23 (72732834_74136633)x1	1.4	*de novo*	Delivery by CS
	case 26	37	20	low risk	Amniocentesis	SNP array,G-banding,QF-PCR	46,XY	arr[GRCh37] 7q11.23 (72725759_74154209)x1	1.43	*de novo*	TOP
	case 27	34	23	low risk	Amniocentesis	SNP array,G-banding,QF-PCR	46,XX	arr[GRCh37] q11.23 (72624166_74207565)x1	1.58	*de novo*	TOP
	case 28	33	24+4	low risk	Amniocentesis	SNP array,G-banding,QF-PCR	46,XX	arr[GRCh37] 7q11.23 (72765457_74175640)x1	1.588	*de novo*	DCDA, selective fetocide
	case 29	32	32+2	low risk	Amniocentesis	SNP array,G-banding,QF-PCR	46,XY	arr[GRCh37] 7q11.23 (72621722_74209949)x1	1.504	*de novo*	TOP
	case 30	28	24	low risk	Amniocentesis	SNP array,G-banding,QF-PCR	46,XY	arr[GRCh37] q11.23 (72650120_74154527)x1	1.41	*de novo*	TOP
YH Dang et al. 2019	case 31	16	20	/	Amniocentesis	Prenatal BoBs,SNP array	47, XXY	arr[GRCh37] 7q11.23 (72718123_74154209)x1	1.4	/	TOP
	case 32	31	22	/	Amniocentesis	Prenatal BoBs,SNP array	/	arr[GRCh37] 7q11.23 (72765457_74257046)x1	1.49	*de novo*	TOP
	case 33	24	22	/	Amniocentesis	Prenatal BoBs,SNP array	/	arr[GRCh37] 7q11.23 (72655376_74154209)x1	1.5	*de novo*	TOP
	case 34	31	33+3	/	Amniocentesis	Prenatal BoBs,SNP array	/	arr[GRCh37] 7q11.23 (72713282_74154209)x1	1.44	*de novo*	TOP
	case 35	37	24	/		Prenatal BoBs,SNP array	/	arr[GRCh37] 7q11.23 (72723370_74146927)x1	1.4	*de novo*	TOP
Ruibin Huang et al. 2022	case 36	31	23	/		SNP array,QF-PCR	/	arr[GRCh37] 7q11.23 (72723370_74154209)x1	1.43	/	TOP
		27	33	/			/		1.53	/	TOP

(*continued*)

10.3389/fped.2023.1141665

10.3389/fped.2023.1141665

TABLE 1 Continued

NO.	Maternal age	Gestational age at diagnosis	expanded NIPT	Prenatal Diagnosis	Genetic tests	Fetal karyotype	CMA result		Inheritance	Outcome of pregnancy
							CNVs type	Size (Mb)		
case 37					SNP array,QF-PCR		arr[GRCh37] 7q11.23 (72624203_74154497)x1			
case 38	29	30	/		SNP array,QF-PCR	/	arr[GRCh37] 7q11.23 (72718277_74143060)x1	1.42	/	Lost to follow-up
case 39	34	22	/		SNP array,QF-PCR	/	arr[GRCh37] 7q11.23 (72718277_74142190)x1	1.42	/	TOP
case 40	38	33	/		SNP array,QF-PCR	/	arr[GRCh37] 7q11.23 (72718278_74143030)x1	1.42	/	TOP
case 41	33	31	/		SNP array,QF-PCR	/	arr[GRCh37] 7q11.23 (72557180_74628840)x1	2.07	/	TOP
case 42	23	27	/		SNP array,QF-PCR	/	arr[GRCh37] 7q11.23 (72701099_74136633)x1	1.44	/	TOP
case 43	32	24	/		SNP array,QF-PCR	/	arr[GRCh37] 7q11.23 (72723371_74141494)x1	1.42	/	TOP

PUBS, Percutaneous cord blood sampling; CVS, Chorionic Villus Sampling; TOP, termination of pregnancy; CS, cesarean section; DCDA dichorionic diamniotic; VOUS,variants of uncertain significant.
Case 16–23 all accept molecular analysis, including prenatal BoBs analysis or FISH etc., the CNV type were not available, so the molecular results of case 16–23 were not represented in the table.

velocity of umbilical artery (S/D) (5/7, 71.4%), absence of diastolic of middle cerebral artery (MCA) (1/7, 14.3%) and absence of diastolic of umbilical artery (UA) (1/7, 14.3%). Other less common ultrasound features include persistent right umbilical vein (PRUV) (1/14, 7.1%), fetal hydrops (1/14, 7.1%), hydroderma (1/14, 7.1%), left pleural effusion(1/14, 7.1%), bilateral subependymal cysts(1/14, 7.1%), thickened nuchal fold (NF) (1/14, 7.1%), absence of venous duct (1/14, 7.1%), duodenal atresia (DA) (1/14, 7.1%), low-lying conus medullaris (1/14, 7.1%), and abnormal posture of hands (1/14, 7.1%) (**Table 2**). **Figure 2** shows some less common ultrasound features in our study.

Cytogenetic and molecular analyses

All 14 fetuses underwent G-banded karyotype analysis, two abnormal karyotypes were found: 47, XXX (Case 9), 46, XY,del (7)(q11.2q21) (Case 12) (**Figure 3**). Besides of these, SNP-array analysis found deletions encompassing the WBS critical region (WBSCR) in all 14 fetuses. They had different sizes and loci of chromosome microdeletion, eleven cases had common deletion sizes, ranging from 1.4 to 1.5 Mb. Case 1 had a 2.1 Mb deletion at 7q11.22-q21.11, involved 40 protein-coding genes. Case 8 had a 5.5 Mb deletions at 7q11.22-q21.11, involved 71 protein-coding genes. Case 12 had a 21.4 Mb deletion at 7q11.21-q21.11, involving 93 protein-coding genes. The deletions of the 14 cases are shown in **Figure 4**.

Case 3, 5, 8, 10 and 11 received Trio-MES additionally, but no more pathogenic variant was found. Another two pairs of parents (Case 4 and 13) accepted CMA analysis. These results indicated that all deletions on chromosome 7q11.23 in the seven cases (Case 3, 4, 5, 8, 10, 11 and13) were *de novo*.

Follow ups

After detailed genetic counseling, twelve families (Case 1–4, 6, 8–14) decided to terminate the pregnancies. All aborted fetuses had typical WBS facial features, including low nasal bridge, palpebral edema, long philtrum, wide mouth, big ears, small chin, and retrognathia.

Case 5 was delivered at 33^{+3} gestational age by cesarean section (CS) for fetal distress, and his birth weight was 1.32 kg. The newborn had distinctive facial features, including wide forehead, periorbital fullness, epicanthal folds, flat nasal bridge, a short upturned nose, long philtrum, and wide mouth. The newborn was transferred to the Neonatal Intensive Care Unit (NICU) for very low birth weight and respiratory distress, and died a week later for severe respiratory distress syndrome. Case 7 was delivered at 35^{+3} gestational age by CS for fetal distress, and his birth weight was 1.7 kg. The APGAR scores were 9, 10, and 10 at 1, 5, and 10 min, respectively. His appearances are consistent with representative facial phenotypes including straight and neat eyebrows, high wide nose, and broad forehead. He was transferred to the NICU for very low birth weight and

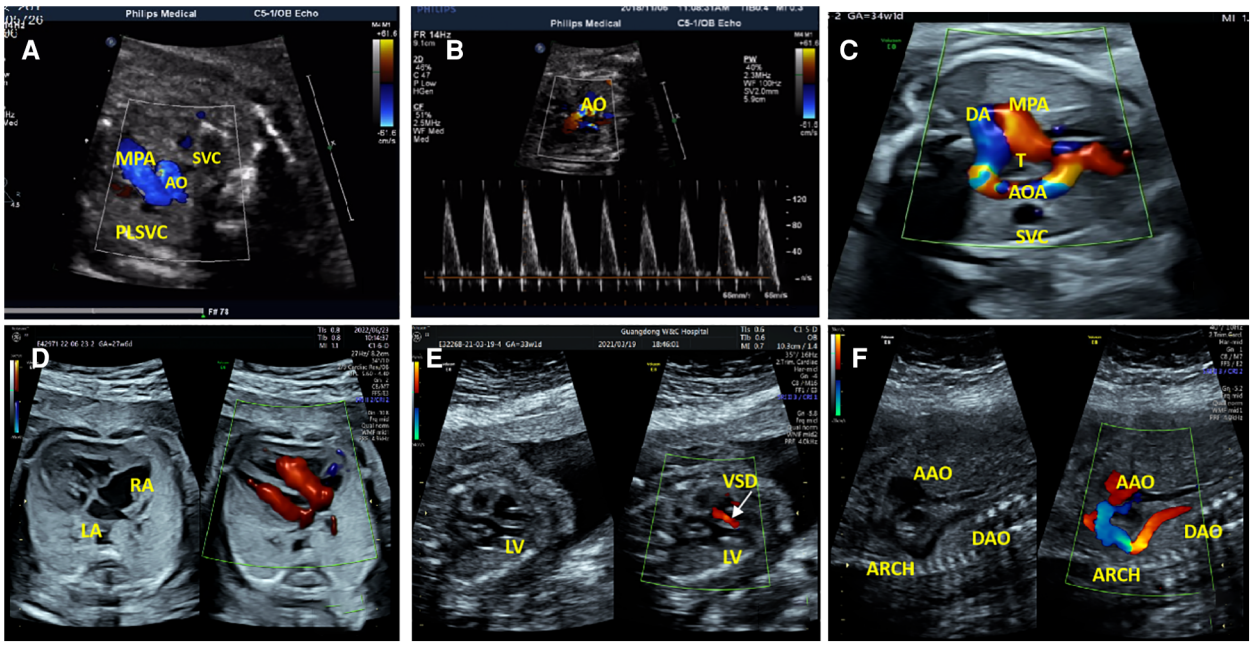

FIGURE 1
The most common cardiovascular abnormalities in our study. (A) The ultrasound examination of case 1 showed a small additional vessel found at the main pulmonary artery (MPA) left in the three-vessel view. SVC, Superior Vena Cava; AO, Aorta; PLSVC, Persistent Left Superior Vena Cava. (B)The color Doppler ultrasonic images of case 1 in the left ventricular outflow tract view showed elevated blood flow rate of the aortic valve. (C)The ultrasonic examination of case 7 showed that the aortic arch was on the right side of the trachea (T), the MPA was on the left side of the T, and they constituted U-shaped ring of blood vessels at the three-vessel view. AOA, Aortic Arch; DA, Ductus Arteriosus. (D) Two-dimensional and color Doppler ultrasonic images of case 9 showed enlargement of the right atrium (RA) in the four-chamber view. (E)Two-dimensional and color Doppler ultrasonic images of case 14 showed left ventricular septal defect (VSD), and left-to-right shunt of defect part (color Doppler flow signal at the defect) in the left ventricular outflow tract view. LV, Left Ventricle. (F) Two-dimensional and color Doppler ultrasonic images of case 14 showed that the descending aortic arch extends to the left obviously in the long axis of the aortic arch view. AAO, Ascending Aorta; DAO, Descending Aorta.

respiratory distress, and was discharged after 27 days of symptomatic treatment. Regular check-ups were made. His height and weight were below 3 percentile at two years old. His cardiac evaluation showed RAA, but no other cardiac symptoms for the time being.

Discussion

Williams–Beuren syndrome (WBS) is a relatively rare microdeletion disorder, manifests as cardiovascular disease, intellectual disability, behavioral and cognitive abnormalities, developmental delay, renal anomalies, and characteristic facial features. Cardiovascular abnormalities, such as suvalvular aortic stenosis (SVAS) and stenosis of other large arteries, are the main cause of morbidity and mortality, and occur in 50%–80% of patients with WBS (15). Prenatal ultrasound diagnosis is relatively difficult for WBS. Various cardiovascular anomalies, ranging from ventricular septal defect to elastin arteriopathy (for example, SVAS), can theoretically be detected by prenatal ultrasound but in clinical practice it is quite difficult (9). Another common prenatal finding of WBS is IUGR, but IUGR is nonspecific and can result from a variety of maternal, fetal, and placental conditions. As a consequence, prenatal ultrasound features of WBS remain incomplete and atypical.

Since the first prenatal WBS case reported in 2009, a total of twenty-nine prenatal cases have been described previously. Here we report 14 cases of WBS diagnosed prenatally by SNP array. Prenatal ultrasound findings of WBS are diversified, ranging from almost no manifestations (Case 13 in our study, at 20 weeks of gestation) to multiple malformations (Case 11 and 12 in our study). Although it is difficult to make a clear diagnosis of WBS in prenatal ultrasound, we may be able to summarize some specific prenatal phenotypes from these 43 cases to provide some insights for the prenatal diagnosis of WBS. The fetuses with WBS manifest IUGR (55.8%, 24/43), abnormal fetal placental Doppler indices(16.3%, 7/43), cardiovascular abnormalities (53.5%, 23/43), which encompass SVAS (21.7%, 5/23), VSD (26.1%, 6/23), AC (17.4%, 4/23), vascular ring (21.7%, 5/23), PAS(8.7%, 2/23), PLSVC(8.7%, 2/23), and TOF (4.3%, 1/23). Some other rare ultrasound findings include thickened NT/ NF(9.3%, 4/43),, polyhydramnios (7.0%, 3/43) fetal hydrops (4.7%, 2/43), duodenal atresia (4.7%, 2/43), echogenic bowel (4.7%, 2/43), intracardiac echogenic focus (IEF) (4.7%, 2/43), renal cyst (4.7%, 2/43), absence of venous duct (2.3%, 1/43), omphalocele (2.3%, 1/43), nasal bone dysplasia (2.3%, 1/43), single umbilicalartery (SUA) (2.3%, 1/43), bilateral subependymal cysts (2.3%, 1/43). Most intrauterine features described in the present case series are consistent with the reports in literature.

TABLE 2 Intrauterine phenotype features of all reported fetuses with williams–beuren syndrome (WBS).

	NO.	Intrauterine abnomalities																	
		IUGR	Congenital cardiovascular defects	Abnormal fetal placental Doppler indices	Thickened NT /NF	Polyhydramnios	Bilateral subependymal cysts	fetal hydrops/ hydroderma/ pleural effusion	Absence of venous duct	DA	low-lying CM	Limb abnormalities	Echogenic bowel	IEF	SUA	Omphalocele	Nasal bone dysplasia	Fetal right nasolacrimal duct cyst	Renal cyst
Present cases	case 1	+	PLSVC, elevated blood flow rate of the aortic valve	–	–	–	–	–	–	–	–	–	–	–	–	–	–	–	–
	case 2	+	–	elevated S/D,absence of diastolic of MCA	–	–	–	–	–	–	–	–	–	–	–	–	–	–	–
	case 3	+	–	elevated S/D	Thickened NT	–	–	–	–	–	–	–	–	–	–	–	–	–	–
	case 4	+	–	–	–	–	–	–	–	–	–	–	–	–	–	–	–	–	–
	case 5	+	–	elevated S/D	–	–	–	–	–	–	–	–	–	–	–	–	–	–	–
	case 6	–	–	elevated S/D	–	+	+	fetal hydrops	–	–	–	–	–	–	–	–	–	–	–
	case 7	+	Vascular ring: RAA	–	–	–	–	–	–	–	–	–	–	–	–	–	–	–	–
	case 8	–	Vascular ring	–	Thickened NT	–	–	hydroderma	–	–	–	–	–	–	–	–	–	–	–
	case 9	+	enlarged right atrium	Absence of diastolic of UA	–	–	–	–	+	–	–	–	–	–	–	–	–	–	–
	case 10	–	–	–	–	+	–	Left pleural effusion	–	–	–	–	–	–	–	–	–	–	–
	case 11	+	Vascular ring: RAA;PRUV	elevated S/D	–	–	–	–	–	+	–	–	–	–	–	–	–	–	–
	case 12	–	–	–	Thickened NF	–	–	–	–	–	+	+	–	–	–	–	–	–	–
	case 13	–	–	–	–	–	–	–	–	–	–	–	–	–	–	–	–	–	–
	case 14	+	VSD	–	–	–	–	–	–	–	–	–	–	–	–	–	–	–	–
Dadelszen et al., 2000	case 15	–	Severe SVAS, PAS	Absence of diastolic of UA	–	+	–	fetal hydrops	–	–	–	–	–	–	–	–	–	–	–
Kontos et al., 2008	case 16	–	small VSD	–	–	–	–	–	–	–	–	–	–	–	–	–	–	–	–
Krzeminska et al., 2009	case 17	+	SVAS	–	–	–	–	–	–	–	–	–	+	–	–	–	–	–	–
Popowski, Vialard,	case 18	+	small SVAS	–	–	–	–	–	–	–	–	–	–	–	–	–	+	–	–

(*continued*)

10.3389/fped.2023.1141665

TABLE 2 Continued

	NO.	Intrauterine abnomalities																	
		IUGR	Congenital cardiovascular defects	Abnormal fetal placental Doppler indices	Thickened NT /NF	Polyhydramnios	Bilateral subependymal cysts	fetal hydrops/ hydroderma/ pleural effusion	Absence of venous duct	DA	low-lying CM	Limb abnormalities	Echogenic bowel	IEF	SUA	Omphalocele	Nasal bone dysplasia	Fetal right nasolacrimal duct cyst	Renal cyst
Leroy, Bault, & Molina, 2011																			
Marcato et al., 2014	case 19	+	−	−	−	−	−	−	−	−	−	−	+	−	−	−	−	−	−
	case 20	+	−	−	−	−	−	−	−	−	−	−	−	−	−	−	−	−	−
	case 21	+	−	−	−	−	−	−	−	−	−	−	−	−	−	+	−	−	−
Kobalka, Mrak, Gunning, 2017	case 22	−	AC, cardiomegaly	−	−	−	−	−	−	−	−	−	−	−	−	−	−	−	−
Srinivasan, Howley, Cuneo,& Chatfield, 2018	case 23	+	SVAS,bilateral PAS	−	−	−	−	−	−	−	−	−	−	−	−	−	−	−	−
MZ Yuan et al. 2019	case 24	+	VSD	−	−	−	−	−	−	−	−	−	−	−	−	−	−	−	−
	case 25	+	−	−	−	−	−	−	−	−	−	−	−	+	+	−	−	−	−
	case 26	+	−	−	−	−	−	−	−	−	−	−	−	−	−	−	−	−	−
	case 27	+	VSD	−	−	−	−	−	−	−	−	−	−	−	−	−	−	−	−
	case 28	+	AC,PLSVC	−	−	−	−	−	−	−	−	−	−	−	−	−	−	−	−
	case 29	+	−	−	−	−	−	−	−	−	−	−	−	−	−	−	−	−	−
	case 30	+	RAA	−	−	−	−	−	−	−	−	−	−	−	−	−	−	−	−
YH Dang et al. 2019	case 31	−	−	−	−	−	−	−	−	−	−	−	−	−	−	−	−	+	−
	case 32	−	−	−	Thickened NF	−	−	−	−	−	−	−	−	−	−	−	−	−	−
	case 33	−	Coronary veins widened, small amount of pericardial effusion	−	−	−	−	−	−	−	−	−	−	+	−	−	−	−	−

(*continued*)

10.3389/fped.2023.1141665

TABLE 2 Continued

	NO.	Intrauterine abnomalities																	
		IUGR	Congenital cardiovascular defects	Abnormal fetal placental Doppler indices	Thickened NT /NF	Polyhydramnios	Bilateral subependymal cysts	fetal hydrops/ hydroderma/ pleural effusion	Absence of venous duct	DA	low-lying CM	Limb abnormalities	Echogenic bowel	IEF	SUA	Omphalocele	Nasal bone dysplasia	Fetal right nasolacrimal duct cyst	Renal cyst
	case 34	–	Fetal right ventricle slant, tricuspid regurgitation	–	–	–	–	–	–	–	–	–	–	–	–	–	–	–	–
	case 35	–	–	–	–	–	–	–	–	–	–	–	–	–	–	–	–	–	+
Ruibin Huang et al. 2022	case 36	–	–	–	–	–	–	–	–	–	–	–	–	–	–	–	–	–	+
	case 37	–	AC	–	–	–	–	–	–	–	–	–	–	–	–	–	–	–	–
	case 38	–	–	–	–	–	–	–	–	+	–	–	–	–	–	–	–	–	–
	case 39	–	TOF, SVAS, RAA	–	–	–	–	–	–	–	–	–	–	–	–	–	–	–	–
	case 40	–	VSD, AC	–	–	–	–	–	–	–	–	–	–	–	–	–	–	–	–
	case 41	+	PAS	–	–	–	–	–	–	–	–	–	–	–	–	–	–	–	–
	case 42	+	–	–	–	–	–	–	–	–	–	–	–	–	–	–	–	–	–
	case 43	–	VSD	–	–	–	–	–	–	–	–	–	–	–	–	–	–	–	–

IUGR, intrauterine growth retardation; VSD, ventricular septal defect; AC, aortic coarctation; PLSVC, persistent left superior vena cava; RAA, right aortic arch; SVAS, supravalvular aortic stenosis; PAS, pulmonary artery stenosis; SUA, single umbilical artery; IEF, intracardiac echogenic focus; +, feature present; –, feature absent.

10.3389/fped.2023.1141665

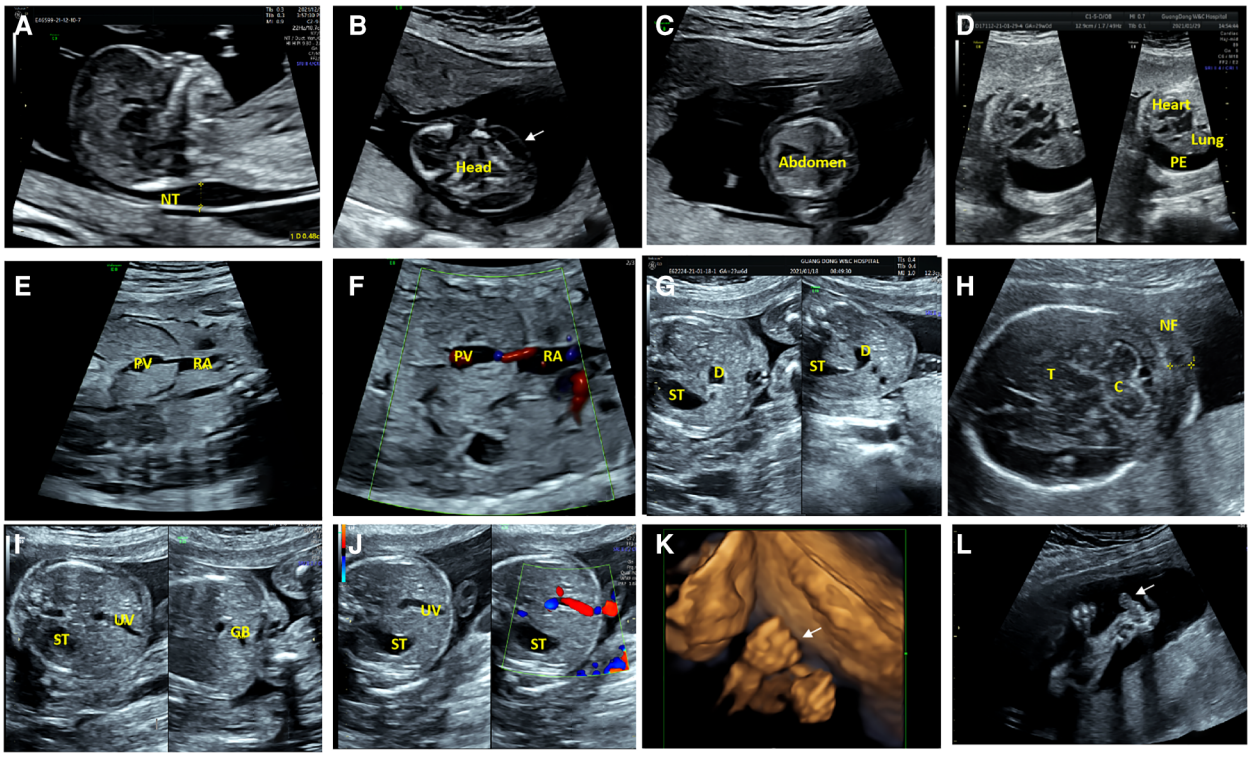

FIGURE 2
Less common ultrasound features in our study. (A) The ultrasonic examination of case 8 showed a thickened nuchal translucency (NT) in the midsagittal view. (B,C) The transverse view of the fetal brain and abdomen of case 8 showed hydroderma (the white arrow). (D) The ultrasound examination of case 10 showed a left pleural effusion (PE), and dextroposition of heart in the four-chamber view. (E,F) Two-dimensional and color Doppler ultrasonic images of case 9 showed the absence of venous duct and abnormal connection between the portal vein (PV) sinus and the right atrium (RA) in the oblique coronal view. (G)The transverse view of the upper abdomen of the fetus 11 presented a typical double bubble sign. The anechoic region on the left side of the abdomen is the stomach (ST) and the anechoic region on the right is the expanded duodenum (D). (H) The ultrasonic examination of the case 12 showed a thickened nuchal fold (NF) in the transverse view of cerebellar. C, Cerebellum; T, Thalamus. (I,J) Two-dimensional and color Doppler ultrasonic images of the fetus 11 showed that the umbilical vein(UV) runs towards to the stomach(ST), and the gallbladder(GB) is located to the left of the umbilical vein in the transverse view of the abdomen. (K) Three-dimensional ultrasonic images of the fingers showed the hands of case 12 presented in a continuous "Thumb-in-Fist Posture". (L) The ultrasonic examination of case 12 showed that thumbs were continuously adducted, and hypoechoic mass presented in the left radial volar.

Cardiovascular abnormalities, RAA combined with PRUV and elevated S/D, were first described in our study. IUGR and cardiovascular abnormalities are the most common prenatal features of WBS. SVAS and VSD are the most common cardiac defects, followed by vascular lesion of vascular ring. The vascular ring could be diagnosed as early as 13 weeks in our study. Moreover, we found seven WBS fetus with the intrauterine features of abnormal fetal placental doppler indices, including five with elevated S/D, one with absence of diastolic of MCA and one with absence of diastolic of umbilical UA. The S/D, RI and PI values of the UA and MCA could reflect the resistance of blood vessels during blood circulation (16). When the S/D, PI, RI values of the MCA blood flow decreased gradually, and the UA resistance index shows a gradual upward trend, especially when the end-diastolic blood flow loss waveform appeared, it could predict the occurrence of fetal distress (17). Elastin is the major component of the extracellular matrix in many tissues. In terms of vascular development, it plays a role in arterial wall development by regulating smooth muscle proliferation. Elastin deficiency induces excessive proliferation of these cells, leading to arterial wall remodeling and obstructive vascular disease (18). We speculate that the haplo-insufficiency of *ELN* may be relevant to the hemodynamic changes of fetuses with WBS. Summarizing the prenatal phenotypes of WBS would provide insights for ultrasound detection, and may lead to early diagnosis and active treatment for patients at risk.

Currently, the most widely used techniques to detect microdeletion include FISH, multiplex ligation-dependent probe amplification (MLPA) and chromosomal microarray analysis (CMA). FISH has the disadvantage of labor-intensive and time-consuming, the exact size of detected CNVs cannot be determined, and cannot be used in atypical CNVs cases. MLPA assay has been utilized to screen for unknown CNVs, but MLPA also has disadvantages: the relatively small number of probes cover only a few exons and regulatory regions in WBSCR, and since non-overlapping and widely scattered probes are used, breakpoints often cannot be defined precisely. Within the last 10 years, fetal genetics has advanced further with the widespread use of CMA. In addition to provide precise breakpoints for deletion boundaries and provide detection of atypical deletions,

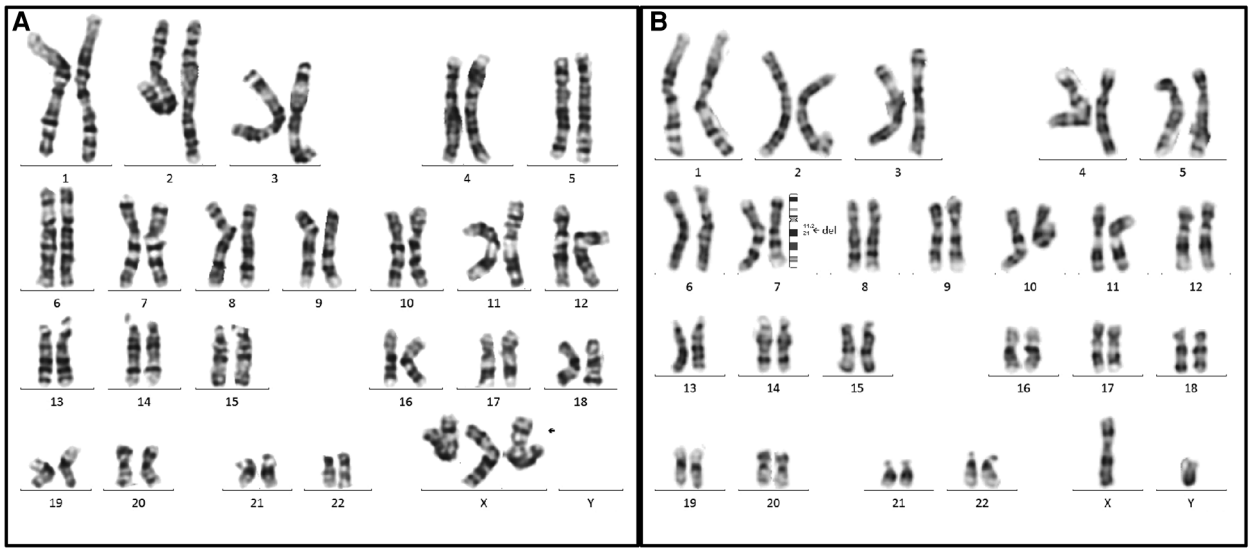

FIGURE 3
Two abnormal karyotypes in our case series. (A) The karyotype on the left is for the case 9 (47, XXX), the arrow indicated the extra X chromosome. (B) The karyotype on the right is for case 12. The arrow elicited that the breakpoints of the deletion were located between 7q11.2 and 7q21, and the karyotype was described as 46,XY, del(7)(q11.2q21).

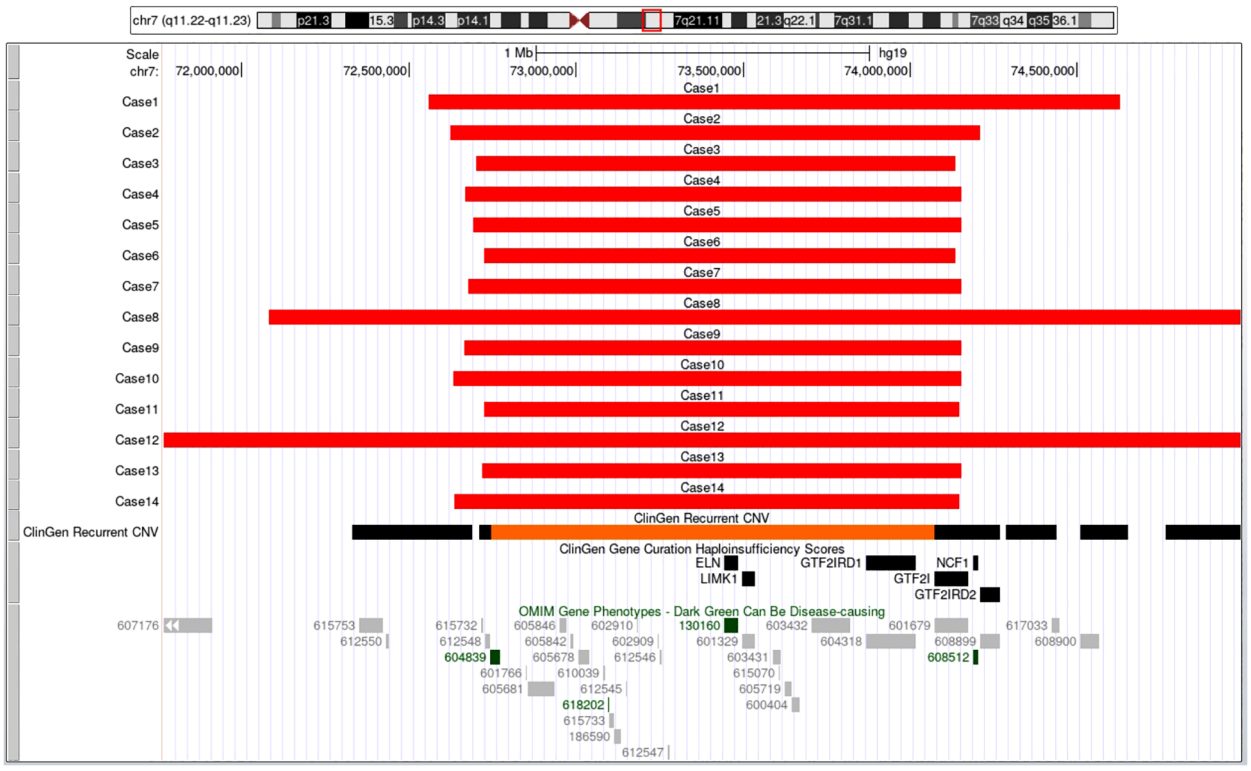

FIGURE 4
The breakpoints and covered genes of each microdeletion of the 14 fetuses, including the well-known OMIM disease-causing gene *ELN* (130,160) and NCF1 (608,512). Eleven cases had common deletion sizes ranged from 1.4 to 1.5 Mb. Case 1 had 2.1Mb deletions at 7q11.22-q21.11, involved 40 protein-coding genes including *ELN* (130,160). Case 8 had 5.5Mb deletions at 7q11.22-q21.11, involved 71 protein-coding genes including *ELN* (130,160). Case 12 had 21.4Mb deletions at 7q11.21-q21.11, involving 93 protein-coding genes, among which 82 genes including *AUTS2* (607,270) and *ELN* (130,160) were OMIM genes.

CMA can also determine additional CNV elsewhere in the genome. Furthermore, next-generation sequencing may eventually be utilized to perform combined single-nucleotide polymorphism, CNV and structural variant detection in fetal samples. Trio-MES also contains the parental detection, which may assist in determining parental inheritance. With the decrease of the cost, next-generation sequencing may become widely used in prenatal diagnosis.

Conclusions

In summary, prenatal ultrasound findings of WBS cases are diversified, with IUGR, cardiovascular abnormalities and abnormal fetal placental doppler indices being the most common intrauterine phenotypes. Our case series may help expand the prenatal phenotypes of WBS, including cardiovascular abnormalities RAA combined with PRUV and elevated S/D. These findings may provide insights for possible prenatal diagnosis of WBS by high-resolution ultrasound.In the meantime, with the decrease of the cost, next-generation sequencing may become widely used in prenatal diagnosis.

Data availability statement

The original contributions presented in the study are included in the article/Supplementary Materials, further inquiries can be directed to the corresponding author.

Ethics statement

This study has been approved by the Institutional Review Board/ Medical Ethics Committee of Guangdong Women and Children Hospital (IRB reference number: 201801073). Written informed consent was obtained from each participating family.

Author contributions

YW, CL and AY conceived and designed the study. YW, CL, RH, JG, JL, XZ, YX, JW and AY carried out the research. RH, JL, JG and JW analyzed and interpreted data. YW, CL and YX drafted the manuscript, and AY revised it. All authors contributed to the article and approved the submitted version.

Funding

This study was supported by the Guangzhou Basic and Applied Basic Research Funding Project (Grant No. 202102020847). The funding body did not play a role in the design of the study, collection, analysis, interpretation of data, or in writing the manuscript.

Acknowledgments

We are grateful to the family members who consented to participate in this study. We are grateful to Li Cui for assistance with the data analysis and manuscript preparation.

Conflict of interest

The authors declare that the research was conducted in the absence of any commercial or financial relationships that could be construed as a potential conflict of interest.

Publisher's note

References

1. Kozel BA, Barak B, Kim CA, Mervis CB, Osborne LR, Porter M, et al. Williams syndrome. *Nat Rev Dis Primers*. (2021) 7(1):42. doi: 10.1038/s41572-021-00276-z

2. von Dadelszen P, Chitayat D, Winsor EJ, Cohen H, MacDonald C, Taylor G, et al. De novo 46,XX,t(6;7)(q27;q11;23) associated with severe cardiovascular manifestations characteristic of supravalvular aortic stenosis and Williams syndrome. *Am J Med Genet*. (2000) 90(4):270–5. doi: 10.1002/(SICI)1096-8628(20000214)90:4<270::AID-AJMG2>3.0.CO;2-R

3. Kobalka AJ, Mrak RE, Gunning WT. A case report of in utero williams syndrome arterial malformation. *Fetal Pediatr Pathol*. (2017) 36(6):452–6. doi: 10.1080/15513815.2017.1379040

4. Kontos H, Manolakos E, Malligiannis P, Plachouras N, Ploumis N, Mihalatos M, et al. Prenatal diagnosis of a fetus with 7q11.23 deletion detected by multiplex ligation-dependent probe amplification (MLPA) screening. *Prenat Diagn*. (2008) 28(6):556–8. doi: 10.1002/pd.2020

5. Krzeminska D, Steinfeld C, Cloez JL, Vibert M, Chery M, Menzies D, et al. Prenatal diagnosis of Williams syndrome based on ultrasound signs. *Prenat Diagn*. (2009) 29(7):710–2. doi: 10.1002/pd.2263

6. Marcato L, Turolla L, Pompilii E, Dupont C, Gruchy N, De Toffol S, et al. Prenatal phenotype of Williams-Beuren syndrome and of the reciprocal duplication syndrome. *Clin Case Rep*. (2014) 2(2):25–32. doi: 10.1002/ccr3.48

7. Popowski T, Vialard F, Leroy B, Bault JP, Molina-Gomes D. Williams-Beuren syndrome: the prenatal phenotype. *Am J Obstet Gynecol*. (2011) 205(6):e6–8. doi: 10.1016/j.ajog.2011.09.017

8. Srinivasan S, Howley LW, Cuneo BF, Chatfield KC. In-utero idiopathic ductal constriction: a prenatal manifestation of Alagille and Williams syndrome arteriopathy. *J Perinatol*. (2018) 38(11):1453–6. doi: 10.1038/s41372-018-0221-9

9. Yuan M, Deng L, Yang Y, Sun L. Intrauterine phenotype features of fetuses with Williams-Beuren syndrome and literature review. *Ann Hum Genet*. (2020) 84 (2):169–76. doi: 10.1111/ahg.12360

10. Dang Y, Wan S, Zheng Y, Song T, Li C, Li Y, et al. The prenatal diagnosis of seven fetuses with 7q11.23 microdeletion or microduplication. *Fetal Pediatr Pathol*. (2020) 39(4):269–76. doi: 10.1080/15513815.2019.1651802

11. Huang R, Zhou H, Fu F, Li R, Lei T, Li Y, et al. Prenatal diagnosis of Williams-Beuren syndrome by ultrasound and chromosomal microarray analysis. *Mol Cytogenet*. (2022) 15(1):27. doi: 10.1186/s13039-022-00604-2

12. Stengel-Rutkowski S, Wirtz A, Hahn B, Hofmeister A, Murken JD. Routine G-banding in prenatal diagnosis of chromosomal disorders. *Hum Genet*. (1976) 31 (2):231–4. doi: 10.1007/BF00296151

13. Xiang J, Ding Y, Song X, Mao J, Liu M, Liu Y, et al. Clinical utility of SNP array analysis in prenatal diagnosis: a cohort study of 5000 pregnancies. *Front Genet*. (2020) 11:571219. doi: 10.3389/fgene.2020.571219

14. Vetro A, Pisano T, Chiaro S, Procopio E, Guerra A, Parrini E, et al. Early infantile epileptic-dyskinetic encephalopathy due to biallelic PIGP mutations. *Neurol Genet*. (2020) 6(1):e387. doi: 10.1212/NXG.0000000000000387

15. Li L, Huang L, Luo Y, Huang X, Lin S, Fang Q. Differing microdeletion sizes and breakpoints in chromosome 7q11.23 in williams-beuren syndrome detected by chromosomal microarray analysis. *Mol Syndromol*. (2016) 6(6):268–75. doi: 10.1159/000443942

16. Rizzo G, Mappa I, Rizzo G, D'Antonio F. International gestational age-specific centiles for umbilical artery Doppler indices: a longitudinal prospective cohort study of the INTERGROWTH-21st project. *Am J Obstet Gynecol*. (2021) 224(2):248–9. doi: 10.1016/j.ajog.2020.08.110

17. Yin Q, Zhang Y, Ma Q, Gao L, Li P, Chen X. The clinical value of blood flow parameters of the umbilical artery and middle cerebral artery for assessing fetal distress. *Am J Transl Res*. (2021) 13 (5):5280–6. PMID 34150119; PMC8205795

18. Dridi SM, Foucault BA, Igondjo TS, Senni K, Ejeil AL, Pellat B, et al. Vascular wall remodeling in patients with supravalvular aortic stenosis and Williams Beuren syndrome. *J Vasc Res*. (2005) 42(3):190–201. doi: 10.1159/000085141

frontiers | Frontiers in Genetics

TYPE Original Research
PUBLISHED 16 May 2023
DOI 10.3389/fgene.2023.1155211

OPEN ACCESS

EDITED BY
Jordi Pérez-Tur,
Spanish National Research Council (CSIC), Spain

REVIEWED BY
Enrique Medina-Acosta,
State University of Northern Rio de Janeiro, Brazil
Sonal Rajiv Bakshi,
Nirma University, India

*CORRESPONDENCE
Priyanka Srivastava,
srivastavapriy@gmail.com

RECEIVED 31 January 2023
ACCEPTED 02 May 2023
PUBLISHED 16 May 2023

CITATION
Srivastava P, Bamba C, Chopra S, Rohilla M, Chaudhry C, Kaur A, Panigrahi I and Mandal K (2023), Identification of genetic alterations in couples and their products of conceptions from recurrent pregnancy loss in North Indian population.
Front. Genet. 14:1155211.
doi: 10.3389/fgene.2023.1155211

Identification of genetic alterations in couples and their products of conceptions from recurrent pregnancy loss in North Indian population

Priyanka Srivastava[1]*, Chitra Bamba[1], Seema Chopra[2], Minakshi Rohilla[2], Chakshu Chaudhry[1], Anupriya Kaur[1], Inusha Panigrahi[1] and Kausik Mandal[3]

[1]Genetic Metabolic Unit, Department of Pediatrics, Advanced Pediatric Centre, Post Graduate Institute of Medical Education and Research, Chandigarh, India, [2]Department of Obstetrics and Gynaecology, Post Graduate Institute of Medical Education and Research, Chandigarh, India, [3]Department of Medical Genetics, Sanjay Gandhi Postgraduate Institute of Medical Sciences (SGPGIMS), Lucknow, India

Background: Recurrent pregnancy loss (RPL) is one of the most common pregnancy-related complications, which can be stressful and emotionally draining for a couple. Genetic alterations, which are responsible for RPL, can be present in either of the three genomes: mother, father, or their fetuses. In addition, environmental factors interacting with these three genomes can affect germline cells. With this aim, the present study was conducted to understand the underlying etiology of RPL using Next-generation sequencing (NGS; couple exome and TRIO exomes) in combination with cytogenetic tests [karyotyping and chromosomal microarray (CMA)].

Material & Methods: In present study we recruited 61 couples with RPL (history of ≥ 2 abortions) and 31 products of conceptions (POCs). For all couples karyotyping was done at the time of recruitment, followed by collection of POC samples and parental blood samples. Before processing POC samples for CMA, they were checked for maternal cell contamination (MCC) by QF-PCR. In POC samples with no pathogenic variant, TRIO exome sequencing was done. Further, in case of unavailability of POC sample, couple exome sequencing was done for RPL couples.

Results: In six individuals out of 61 couples (5%), abnormality in karyotypes was detected. Among 116 normal karyotypes, there were 11 heteromorphisms (9.5%), for which the couples had to be counselled and reassured. Out of the 31 POCs, 10 were excluded because of MCC (around 30%) and one had major aneuploidy. CMA in POCs identified pathogenic copy number variations (CNVs) in 25% of cases (5/20) and variant of unknown significance (VUS) in 20% of cases (4/20). Autosomal trisomy was the most frequent chromosomal abnormality diagnosed. NGS was performed to establish single-gene causes of RPL. Couple exome sequencing was performed in 20 couples, and 14 were found to be carriers for autosomal recessive conditions. A total of 50 potential disease-causing variants in 40 genes were identified in 33 of 40 individuals (82.5%). Putative causative variants were identified in 37.5% of the TRIO cases (3/8). Mutations in few important genes (*SRP54, ERBB4, NEB, ALMS, ALAD, MTHFR, F5,* and *APOE*), which are involved in vital pathways, early embryonic development, and fetal demise, were identified in the POCs.

Conclusion: It enhances our understanding of prenatal phenotypes of many Mendelian disorders. These mutated genes may play an auxiliary role in the development of treatment strategies for RPL. There was no correlation of the number of abortions with etiological yield of any technique to detect the cause of RPL. This study shows the utilization of combination of techniques in improving our understanding of the cause of early embryonic lethality in humans.

KEYWORDS

recurrent pregnancy loss, next-generation sequencing, chromosomal microarray, copy number variations, chromosomal aberrations, sequence variations, multiplex ligation-dependent probe amplification

1 Introduction

Recurrent pregnancy loss (RPL) is defined as two or more clinical pregnancy losses before 20 weeks of gestation (Practice committee, 2020). It affects 2–5% of couples trying to conceive (Ford and Schust, 2009). RPL can culminate into bad obstetric history (BOH), which implies previous unfavorable fetal outcome in terms of two or more consecutive spontaneous abortions, early neonatal deaths, still births, intrauterine fetal deaths, intrauterine growth retardation, and congenital anomalies (Singh and Sidhu, 2010). It is a major health concern and sometimes misconsidered as infertility. RPL is an emotionally challenging and a taxing condition for the couples, especially for maternal health issues. If a pregnancy is delayed or not successful because of any reason, the available reproductive years are shortened, resulting in a sense of urgency to conceive. Advanced maternal age is one of the highly associated factors with miscarriage (Gardner and Sutherland, 2004). It is very important to find out the reason behind miscarriage so that subsequent measures could to be taken to avoid the recurrence of such situation. Genetic factors such as chromosomal anomalies, particularly balanced translocations, are the major cause (approximately 5% prevalence in couples) for RPL (Ford and Schust, 2009). This prevalence is significantly higher than the normal population (~1 in 500) (Jacobs et al., 1974).

A major number of couples with RPL (41.4%) have chromosomal abnormality, which can be picked up by karyotyping (Sugiura-Ogasawara et al., 2012). Chromosomal imbalances in gametes, resulting from balanced translocation in one of the couples, give rise to systemic errors in mitotic process during the early developmental stage of the conceptus. In about 50% of the couples with RPL, the underlying cause remains unsolved (Christiansen et al., 1990), although there might be involvement of genetic factors. The challenging key question in investigating the inherited predisposition to RPL is to decide the study subject in RPL (Rull et al., 2012). People have used conventional karyotyping and array-based comparative genomic hybridization in couples with RPL. Little focus has been given on the use of whole-exome/-genome sequencing in lethal *in utero* fetal disorders. Recent studies showed there are few gene sequence variations in couples with the history of RPL with or without their abortus that might contribute to RPL or related lethal birth defects (Quintero-Ronderos et al., 2017; Najafi et al., 2021; Xiang et al., 2021).

The genetic studies designed to explore the genes and mechanism behind pathogenesis of RPL have several challenges and there have been no consistent results due to variations in the selection of study subjects (couples with a history of RPL or female patients, or product of conception (POC) and controls. Due to complexities in collecting and processing the clinical samples from couples with a history of RPL and pregnancy loss events, there are limited genetic studies on the RPL families. In this study, both the genome of the parents and POC were examined. POCs were analyzed using CMA, and the cases without abnormal CNVs were subjected to TRIO exome analysis. India being a densely populated and diverse country with varied ethnicity and marriages in blood relations, we assumed that we would get certain novel autosomal recessive conditions. In this study, we have targeted a less explored area of genetics, especially in the Indian scenario to find out the genetic etiology of RPL; some of them undescribed previously. Apart from this, we have found the contribution of chromosomal and single gene disorders give rise to pregnancy loss, many a times *de novo* and at times inherited. This approach can help identify more genes core to human development and causative of RPL. The information from RPL testing can be helpful for patients and physicians to understand the cause of miscarriage and subsequently to develop a plan to support a successful future pregnancy.

2 Methodology

2.1 Study design

A multicenter prospective study was carried out over a period of 2 years (2020–2022). Medical genetic centers from two different tertiary care hospitals in North India participated in the study. Ethical clearance was taken from the ethics committees of both Institutes. All experimental protocols were approved by the Institutional Ethical Committees.

2.2 Subjects and sample size

It was a descriptive pilot study, so the sample size was not calculated. This study included 61 consecutive couples (122 individuals) with the history of RPL who visited the OPD/IPD of any of the two medical genetics centers during the miscarriage (POC samples were obtained) or after the miscarriage (genetic counselling for future pregnancy). An informed consent for testing under research and publication of data was taken as per the protocol.

2.3 Clinical details

A detailed clinical history was obtained from each patient, which included their obstetric history at present gestation, gestational duration in previous miscarriages, and family history of RPL (if any). All couples were evaluated for systemic illnesses, and their previous medical history was taken.

2.4 Samples

2.4.1 Products of conception

POC samples sent from other centers and in-house in two centers were included. In-house, POCs were collected freshly in normal saline with aseptic precautions. All POC samples were checked for quality. Highly putrefied samples and samples collected in formalin were discarded. The remaining samples were checked under a microscope for chorionic villi or fetal tissue. Of the 61 samples, eight samples were putrefied, 14 came in formalin, and in eight samples, no chronic villi or fetal tissue could be obtained. Only 31 were processed further. In apparently 12 freshly obtained POC samples with good chorionic villi, culture was initiated for fetal karyotyping and obtaining fetal cells. For all 31 POC samples, which were selected for further processing, DNA was extracted from part of the sample using the QIAamp DNA Tissue extraction kit (QIAGEN, Hilden, Germany). Extracted DNA was quantified spectrophotometrically at 260 nm using Nanodrop (Thermo Nanodrop 2000), and the quality of DNA was assessed at 260/280 nm $\leq$ 1.8.

2.4.2 Peripheral blood samples

Blood samples of couples were collected into the heparin tube and EDTA tube (2 mL each) from the couples for diagnostic chromosome and molecular analysis, testing for maternal cell contamination (MCC) in POC and further testing. DNA from peripheral blood samples was extracted using QIAGEN kits as per the manufacturer's guidelines. Extracted DNA quality and quantity were checked using the Nanodrop instrument for further downstream processing.

2.5 QF-PCR in POC samples

QF-PCR was performed using the Devyser Compact v3 kit, and the markers specific to the chromosomes 13, 18, 21, X, and Y were amplified (Torres et al., 2021). The amplified markers were then subjected to capillary electrophoresis. The data were analyzed using GeneMapperTM (Thermofisher) and interpreted to determine the MCC and aneuploidy of fetus for specific chromosomes. QF-PCR in POC samples with markers corroborated with that of the mothers was carried out to check for MCC. Before proceeding with cytogenetic microarray and/or exome sequencing in POC, MCC and major chromosomal aneuploidies in 13, 18, 21, and sex chromosomes were ruled out.

2.6 Karyotyping in couples

From blood collected in heparin, karyotyping of couples has been carried out. G-banded karyotyping was carried out using trypsin–Giemsa banding preparations.

2.7 Other tests for RPL

All female partners were examined for thrombophilia (factor V Leiden, prothrombin G20210A gene mutation), antiphospholipid antibodies (APLA), lupus anticoagulant, anticardiolipin antibodies, anti-β_2-glycoprotein I antibodies, hormonal status (thyroid stimulating hormone (TSH), T3, T4, and prolactin), and ultrasonography for uterine anomalies.

2.8 Multiplex ligation-dependent probe amplification (MLPA) in POC samples

MLPA for subtelomeric region was performed using SALSA MLPA Probemix P036 Subtelomeres Mix 1(MRC Holland) as per the manufacturer's protocol.

2.9 Chromosomal microarray (CMA) in POC samples

CMA was performed using the Affymetrix 750K array Cytoscan kit in DNA samples extracted from POC samples as per the manufacturer's recommendations. The Affymetrix 750K array Cytoscan kit has more than 750,000 markers (including 200,000 SNPs and 550,000 non-polymorphic probes).

Data were analyzed using ChAS software (Thermofisher Scientific, MA, United States) using a UCSC genome browser based on the GRCh38 genome assembly. Analysis of copy number variations (CNVs) was carried out using various tools and software like DECIPHER (https://decipher.sanger.ac.uk), DGV (http://dgv.tcag.ca/dgv), OMIM (www.omim.org), and ClinVar (https://www.ncbi.nlm.nih.gov/clinvar/). The interpretation of CNVs was based on recommended ACMG guidelines (South et al., 2013).

2.10 Next-generation sequencing

NGS was carried out using the Illumina HiSeq X10 platform (Illumina, Inc., San Diego, CA, United States). Briefly, DNA was sheared to produce 150–250 bp fragments for library preparation. Hybridization was carried out using the whole-exome ~67 Mb Agilent Sure Select Clinical Research Exome V2 capture kit, following size selection, end-repair, phosphorylation, and adapter ligation to the DNA fragments according to the manufacturer's protocol. Exome Library QC was checked on a Bioanalyzer (Agilent, United States) and quantified using Qubit (Invitrogen, United States). The libraries were sequenced as paired-end reads (2 × 150) for ~80–100× coverage on HiSeq X (Illumina, CA). Couple exome or TRIO exome was carried out as per the availability of POC tissue and DNA quality.

2.10.1 Data analysis

Sequence reads were aligned to human genome assembly GRCH37 using the Burrows–Wheeler Aligner (BWA) with the MEM algorithm. Variant calling and data processing were carried out using the Genome Analysis Toolkit (GATK, version 4.0,4.0,

Broad Institute, https://software.broadinstitute.org/gatk/). Variant annotation was performed using ANNOVAR software (http://annovar.openbioinformatics.org/en/latest/). Filtering criteria used to narrow down the search of the causative variant: Synonymous, non-frameshift, or unknown variants, and low-quality reads were removed; frequency cut-off for population databases was set as <1% in dbSNP (http://www.ncbi.nlm.nih.gov/snp/), 1000 Genomes (http://browser.1000genomes. org/index.html), ESP6500 (http://evs.gs.washington.edu/EVS/), Exome Aggregation Consortium (ExAC; http://exac.broadinstitute.org/), and the Genome Aggregation Database (gnomAD; http://gnomad.broadinstitute.org/). Insilico analysis tools: PolyPhen2 (http://genetics.bwh.harvard.edu/pph2/), SIFT (http://sift.jcvi.org/), MutationTaster (http://mutationtaster.org/), and FATHMM-MKL (http://fathmm.biocompute.org.uk/fathmmMKL.htm) were used for variant effect prediction. ClinVar (ncbi.nlm.nih.gov/clinvar/), Human Genome Mutation Database: HGMD (https://www.hgmd.cf.ac.uk/ac/all.php), and DECIPHER database (https://decipher.sanger.ac.uk/) were used for identifying the reported or known SNVs and CNVs and the associated phenotypes.

2.10.2 Validation of variants

Few of the putative variants identified by exome sequencing were confirmed by targeted sequencing and mutation analysis by polymerase chain reaction (PCR), followed by Sanger sequencing of the amplicon using BIG Dye Terminator (Applied Biosystems 3130 Genetic Analyzer; Applied Biosystems, Foster City, CA, United States). The raw data obtained were subsequently analyzed for the nucleotide variants (Supplementary Figure S2B).

2.11 Statistical analysis

Pearson correlation coefficient was applied in couples with different positive results and their experience of number of miscarriages in an attempt to find out if there is any effect of certain causes on number of abortions, and significance of the result was tested using online tool Statistics Kingdom (https://www.statskingdom.com/).

3 Results

3.1 Demography

In this study, the mean age of women was 29.9 years (25–40) and the mean age of men was 33.5 years (27–44). In two out of 61 (3%) couples, systemic illnesses, i.e., myotonic dystrophy (RPL52) and systemic lupus erythematosus (RPL34), were the probable causes of RPL (Supplementary Table S1). However, their POC samples were collected but could not be processed further due to putrefied tissue and MCC, respectively. No other obvious genetic or non-genetic causes were identified as the etiology of RPL in the remaining couples during the initial evaluation for endocrine causes and conditions leading to thrombophilia. While evaluating the past history, in two women, where previous POCs were subjected to genetic analysis, some abnormalities were found. They were, however, unrelated to the causes of RPL, i.e., one had monosomy X (POC9) and the other had trisomy 13 (POC8) (both detected by subtelomeric MLPA) (Supplementary Table S1). In our cohort, the number of women with previous two miscarriages was 12, three miscarriages in 27 women, four miscarriages in 10 women, five miscarriages in seven women, and ≥ 6 miscarriages in five women. We have tried to find if there was any correlation with the number of abortions and positive yield of chromosomal aberrations in POC (detected either by karyotype/QFPCR/MLPA/CMA), karyotype of couple, variations in the same gene for autosomal recessive conditions detectable by couple exome sequencing, or a positive result in trio exome. There was no significant correlation found with chromosomal aberrations in the POC and also with abnormalities detected by couple karyotype (Table 1). Women did not have any uterine malformations.

3.2 QF PCR in POC samples

Among 61 POCs, 50% (31/61) POCs were suitable for further processing. However, for the downstream processing (CMA and NGS), only 20 POCs were processed. In one sample (POC6), chromosomal aneuploidy trisomy 21 was detected by QF-PCR. The finding was corroborated by MLPA (subtelomeres) and by karyotyping. Ten samples were positive for MCC (Supplementary Table S1).

3.3 Multiplex ligation-dependent probe amplification (MLPA) in POC samples

MLPA was performed in nine samples where QF PCR ruled out maternal contamination. It confirmed trisomy 21 in one sample (POC6), which corroborated with QFPCR results and later on confirmed by karyotyping (Supplementary Table S1). This sample was not processed for cytogenetic microarray (CMA). In another sample, there was doubtful trisomy 11 (probe ratio 1.36 and 1.38 for p and q arms, respectively). This sample (POC39) was further processed for CMA, which confirmed trisomy 11 (Table 2).

3.4 Karyotyping of couples

In six (5%) out of 122 individuals (61 couples), abnormality in karyotyping was detected (Table 3). Robertsonian translocation was present in two individuals and three were found to be balanced reciprocal translocation carriers. One individual was found to be mosaic for 46, XX and 46, XXX cell lines. The remaining 95% couples had normal karyotypes. Among 116 normal karyotypes, there were 11 heteromorphisms (9.5%), for which the couples were counselled and reassured (Figure 1). Out of the total, one rare type of heteromorphism pericentric inversion of chromosome Y was identified in an individual, which is reported to have no clinical significance (Verma et al., 1982).

TABLE 1 Correlation of the number of abortions with a positive yield of different techniques.

Parameter	Value	Value	Value	Value
	X: Number of abortions Y: Positive results in POC QF-PCR or CMA	X: Number of abortions Y: Positive results in the couple karyotype	X: Number of abortions Y: Positive results of sequence changes in the same gene for AR conditions by the couple exome	X: Number of abortions Y: Positive results in the trio exome
Pearson correlation coefficient (r)	0.2851	0.1123	−0.137	−0.207
p-value	0.2103	0.3888	0.5659	0.6233
Covariance	0.1524	0.0459	−0.105	−0.089
Sample size (n)	21	61	20	8
Statistic	1.2967	0.8682	−0.585	−0.518
Interpretation	Results of the Pearson correlation indicated that there is a non-significant small positive relationship between X and Y ($r(19) = .285$, $p = .210$).	Results of the Pearson correlation indicated that there is a non-significant small positive relationship between X and Y ($r(59) = .112$, $p = .389$).	Results of the Pearson correlation indicated that there is a non-significant very small negative relationship between X and Y ($r(18) = .137$, $p = .566$).	Results of the Pearson correlation indicated that there is a non-significant very small negative relationship between X and Y ($r(6) = .207$, $p = .623$).

TABLE 2 Details of CNVs detected in POCs.

ID	Type	Location	Size	No. of OMIM genes	Genomic co-ordinates	Interpretation	Comments
POC3	Loss	Chr17p11.2	775 Kb	4	arr[GRCh38] 17p11.2(21,660,410_2,243,5981)x1	VUS	
POC4	Loss	Chr14q13.2	246 Kb	3	arr[GRCh38] 14q13.2(34,823,799_35,070,625)x1	VUS	
POC5	Loss	Chr2q34	113 Kb	1	arr[GRCh38] 2q34(212,138,454_212,252,393)x1	VUS	
POC57	Gain	Chr7q36.3	1.7 Mb	5	arr[GRCh38] 7q36.3(157,546,042–159,327,017)x3	VUS	
POC18	Mosaic Loss	Chr19p13.3	47.9 Mb		arr[GRCh38] 19p13.3q13.33(260,912_8,250,320)x1 [0.26]	Likely pathogenic	Undetectable in the karyotype of the couple and likely to be *de novo*
	Loss	Chr17q24.2	1 Mb	9	arr[GRCh38] 17q24.2(67,202,603–68,276,036)x1		
POC23	Gain	Chr9p24.3	90.3 Mb	455	arr[GRCh38] 9p24.3q22.2(208,455_90,568,721)x3	Pathogenic	9:15 translocation detected in the male partner
	Loss	Chr15q11.2	21.3 Mb	339	arr[GRCh38] 15q11.2q15.3(22,582,283_43,964,261)X1	Pathogenic	
POC29	Loss	Chr11q24.3	6.8 Mb	50	arr[GRCh38] 11q24.3q25(128,253,364–135,067,522)x1	Pathogenic	
	Gain	Chr14	34.1 Mb	435	arr[GRCh38] 14q24.2q32.33(71,951,262–106,071,000)x3	Pathogenic	
POC33	Mosaic Gain	ChrX	155 Mb	-	arr[GRCh38] (X)x2 [0.30], (Y)x1	Pathogenic	
POC39	Gain	Trisomy Chr11	134 Mb	1671	arr[GRCh38] 11p15.5q25(230,615_134,938,470)x3	Pathogenic	

*VUS, variant of unknown significance.

TABLE 3 Karyotype data on couples with the history of recurrent pregnancy loss.

Chromosomal anomaly	Karyotype	Total no. of cases
Normal polymorphism		
Heteromorphism	46, XY, 9qh+	1
	46,XY, 9qh+,14ps+ & 21ps+	1
	46,XX,15ps, 21ps++	1
	46,XX,21ps+	1
	46,XY,21ps+	1
	46, XY,22ps+	1
	46,XY,13ps+,21ps+,22ps+	1
	46,XX,9qh+ & 22ps+	3
	46, X inv (Y) (p11.2q11.23)	1
Abnormal karyotype		
Balanced Robertsonian translocation	45, XX; rob (13,14) (q10:q10)	1
	45, XX, t (22:22) (q10; q10)	1
Balanced reciprocal translocation	46, XX, t (9; 15) (q22; q15)	1
	46, XX, t (5:15) (q23; q24)	1
	46, XY t (11:14) (q23; q31)	1
Mosaic	46, XX- 94% of cells and three cells showed karyotype of 47, XXX—6%	1

3.5 Karyotype from POC

Karyotype from POC was carried out for 12 samples, where good chorionic villi were obtained. These 12 samples were subjected to culture where eight showed good growth and in four, there was culture failure. Trisomy 21 was detected in one POC sample (POC6) (12%). In this pregnancy, cystic hygroma was detected in ultrasonography early in pregnancy (13 weeks).

3.6 Cytogenetic microarray

CMA in POCs identified pathogenic CNVs in 25% cases (5/20) and variant of unknown significance (VUS) CNVs in 20% cases (4/20) (Figure 1). In the remaining 55% cases, no significant CNVs were identified.

3.6.1 Pathogenic CNVs

1. POC18 showed a low-level mosaic loss (26%) involving chromosome 19 (47.9 Mb) within region p13.3q13.33, indicating monosomy for this region (Supplementary Figure S1A). Monosomy of chromosome 19 is associated with pre- and postnatal growth retardation, psychomotor and language delay, hyperactivity, brachydactyly, hearing loss, anteverted nares, synophrys, hypodontia, and short neck. These were not detected in karyotype in either of the couple, suggesting it to be *de novo*. In addition, 1 Mb loss was detected on chromosome 17q24.2, indicating monosomy of this region, which included nine OMIM genes. Heterozygous loss of function variations of the *BPTF* gene is associated with delayed psychomotor development and intellectual disability, poor growth, small head size, dysmorphic facial features, and mild abnormalities of hands and feet.
2. POC23 showed a 90.3 Mb duplication of chromosome 9 and a deletion of 21.3 Mb on 15q11.2 (Supplementary Figure S1B). The observed duplication is consistent with partial trisomy 9. Partial trisomy of the short arm including the long arm of chromosome 9 is among the most common autosomal structural chromosomal anomalies.

CMA analysis showed another deletion spanning ~21.3 Mb on chromosome 15q11.2-q15.3. This deletion overlaps with 15q deletion syndrome or distal 15q monosomy. Couple karyotyping showed 46,XX,t(9; 15) (q22; q15) in the female partner. CMA findings of duplication on chromosome 9 and deletion on chromosome 15 in POC corroborate with chromosomal translocation in couples at these loci.

3. In POC 29, CMA analysis showed a deletion spanning about ~6.8 Mb on chromosome 11q24.3q25, including 50 genes. Deletion on 11q24.3q25 overlaps with 11q deletion syndrome, also known as Jacobsen syndrome (JBS: OMIM 147791) critical region. *ETS1* and *FLN1* are critical genes that have been proposed for causing Jacobsen syndrome phenotypes. Furthermore, the *FLN1* gene was present in the deleted region of the current case.

CMA analysis also showed a duplication spanning about 34.1 Mb on chromosome 14q24.2q32.33, including 435 genes.

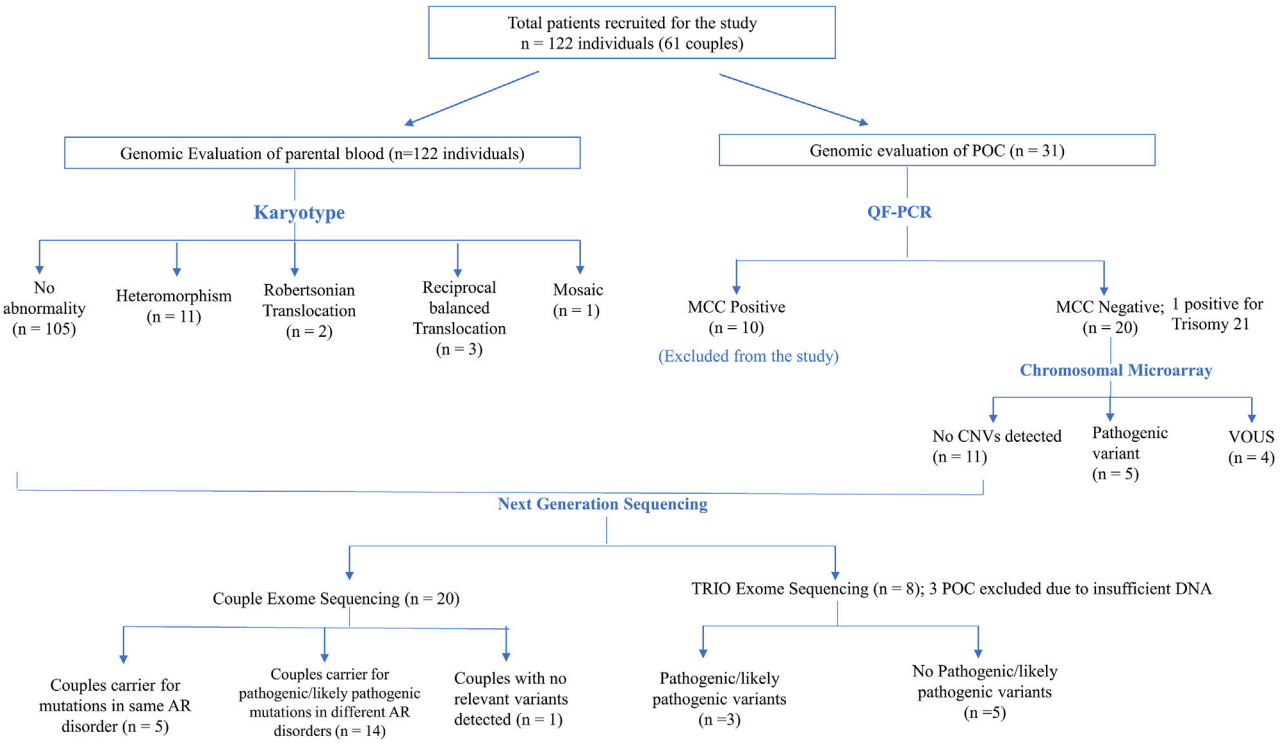

FIGURE 1
Flowchart depicting the details of samples analyzed in this study and summary of the CNVs and SNVs identified.

The observed duplication overlaps with a partial trisomy of 14q. In the submitted sample, the deletion on chromosome 11q and duplication on chromosome 14q suggest chromosomal rearrangement at these loci, such as translocation. The male partner was found to be a carrier of balanced translocation 46, XY,t(11:14) (q23; q31) (Supplementary Figure S1C).

4. POC33, CMA analysis showed a mosaic gain (~30%) involving all SNPs on chrX (155 Mb) from Xpter to qter along with a single copy of Y-chromosome, indicating a rare form of Klinefelter syndrome. This condition is known as mosaic Klinefelter syndrome and individuals with this condition can have milder signs and symptoms than others with the XXY condition. Karyotypes of couples were normal (Supplementary Figure S1D).
5. POC39, the CMA analysis showed complete duplication on chromosome 11 spanning the entire chromosome (Supplementary Figure S1E). This duplication is consistent with complete trisomy 11. Complete trisomy 11 is an extremely rare phenomenon, and very little is known regarding the possible phenotypic features, as most cases of complete trisomy 11 are usually lethal and spontaneously aborted in the first trimester. The couple had a previous baby with developmental delay, whose karyotype, subtelomeric MLPA, and CMA were normal. Karyotypes of couples were also normal. Trisomy 11 in this instance is likely to be a *de novo* event.

3.6.2 VUS CNVs

1. One couple (RPL3) was presented with a history of previous three abortions in the first trimester. Karyotypes of the couple were normal. POC3 CMA testing showed a loss at the cytoband region 17p11.2 spanning about 775 kbp (~0.8 MB) encompassing four genes. There were two OMIM genes, *KCNJ18* and *PRG4*, present on the deleted segment. Variants in the *KCNJ18* gene have been found to be associated with thyrotoxic periodic paralysis-2 (TTPP2), but its haploinsufficiency association with the clinical phenotypes is yet to be identified. p53-responsive gene 4 (*PRG4*) overexpression (upregulated) in the apoptotic cells is mainly in association with *p53*. Since this deleted region has not been well established with syndromes or recurrent abortions and there is no established evidence in the literature, the observed finding has been labeled as VUS.
2. CMA of POC4 revealed a 247 Kb deletion on the chromosome 14q13.2 region, which includes three OMIM genes; *BAZ1A* (605680), *SRP54* (604857), and *FAM177A1* (619181). Among them, *SRP54* is associated with the autosomal dominant form of neutropenia (MIM# 618752).
3. CMA of POC5 showed heterozygous deletion of 113 Kb on chromosome 2q34, which includes only a single OMIM gene *ERBB4*.
4. CMA of POC57 identified a gain of 1.7 Mb on chromosome 7q36.3, which includes five OMIM genes. Clinical significance of the genes in the context of this patient's phenotype is unknown.

TABLE 4 Couple exome (carrier status of genes which might explain the bad obstetric history: both partner carriers of mutations in the same gene for autosomal recessive disorders).

Couple ID	Gene	Wife	Husband	Disease
RPL2		W2	H2	
	PCNT	Status: CARRIER	Status: CARRIER	Microcephalicosteodysplastic primordial dwarfism type II (OMIM#210720)
		Variant: c.3710A>G (p.His1237Arg)	Variant: c.1334_1335del(p.Lys445ThrfsTer12)	Mode of inheritance: AR
		Zygosity: Heterozygous	Zygosity: Heterozygous	
		Classification: VUS (PM2 and BP4)	Classification: Likely pathogenic (PVS1 and PM2)	
		Accession: VCV000211856.7	Accession: SCV003804961	
RPL5		W5	H5	
	MTHFR	Status: CARRIER Variant: c.1286A>C(p.Glu429Ala)	Status: CARRIER	Homocystinuria due to methylene tetrahydrofolate reductase deficiency (OMIM#236250) Mode of inheritance: AR
		Zygosity: Heterozygous	Variant: c.1286A>C(p.Glu429Ala)	
		Classification: VUS (PP4 and BP6)	Zygosity: Heterozygous	
		Accession: VCV000003521.78	Classification: VUS (PP4 and BP6)	
			Accession: VCV000003521.78	
RPL16		W16	H16	
	ALMS1	Status: CARRIER	Status: CARRIER	Alstrom syndrome (OMIM#203800) Mode of inheritance: AR
		Variant: c.11734A>C(p.Ser3912Arg) Zygosity: Heterozygous	Variant: c.1420C>A(p.His474Asn) Zygosity: Heterozygous	
		Classification: VUS (PM2)	Classification: VUS (PM2 and BP4)	
		Accession: VCV000403949.6	Accession: VCV000459855.13	
RPL21		W21	H21	
	PKD1L1	Status: CARRIER	Status: CARRIER	Visceral heterotaxy-8 (OMIM#617205)
		Variant: c.8005C>T, (p.Arg2669Ter)	Variant: c.310G>A, (p.Ala104Thr)	Mode of inheritance: AR
		Zygosity: Heterozygous	Zygosity: Heterozygous	
		Classification: Pathogenic (PVS1, PM2, and PP5)	Classification: VUS (PM2) dbSNP: rs544795414	
		Accession: VCV001686969.1	Accession: SCV003806426	
RPL33		W33	H33	
	NEB	Status: CARRIER	Status: CARRIER	Arthrogryposis multiplex congenita 6 (OMIM#619334) Mode of inheritance: AR
		Variant: c.11706C>A (p.Asp3902Glu)	Variant: c.22454C>T (p.Thr7485Ile)	
		Zygosity: Heterozygous	Zygosity: Heterozygous	
		Classification: VUS (PM1+PM2+BP1)	Classification:	
			VUS (PM1+PM2+BP1)	
		Accession: SCV003804962	Accession: VCV000968876.7	
	INPPL1	Status: CARRIER	Status: CARRIER	Opsismodysplasia (258480)
		Variant: c.2839C>T(p.Pro947Ser) Zygosity: Heterozygous Classification: VUS (PM1+PM2+PP3)	Variant: c.3394G>A (p.Glu1132Lys)	Mode of inheritance: AR
		Accession: SCV003804963	Zygosity: Heterozygous	

(Continued on following page)

TABLE 4 (*Continued*) Couple exome (carrier status of genes which might explain the bad obstetric history: both partner carriers of mutations in the same gene for autosomal recessive disorders).

Couple ID	Gene	Wife	Husband	Disease
			Classification: VUS (PM1+PM2+PP3)	
			Accession: VCV001391913.2	

*VUS, variant of unknown significance; AR, autosomal recessive.

3.7 Next-generation sequencing-based approaches

3.7.1 Couple exomes

In the absence/inadequate POC DNA or in the case of MCC positive POC samples, couple exome sequencing was adopted in 20 couple samples. Out of the 20 couples, five couples (25%) were found to be a carrier of the mutation in the same genes (*PCNT, MTHFR, ALMS1, PKD1L1, NEB*, and *INPPL1*) causing autosomal recessive (AR) syndromes (Tables 4, 5). Fourteen couples (70%) were found to be carriers for pathogenic or likely pathogenic variants in other AR conditions (Table 6). No pathogenic or likely pathogenic variant was identified in one couple. According to the American College of Medical Genetics and Genomics guidelines (ACMG) (Richards et al., 2015), a total of 50 potential disease-causing variants in 40 genes were identified in 33 out of 40 individuals (82.5%), making them carriers of various AR disorders (Tables 4, 6).

3.7.2 Carrier for autosomal recessive Mendelian disorders

Five couples were identified with putative candidate gene variants in same gene qualifying them as carriers for autosomal recessive conditions (Table 5) which can be the putative causative variant in fetus (Table 4; Figure 1).

1. RPL2 couple: This RPL2 couple was found to be carriers of a likely pathogenic variant and a VUS in the *PCNT* gene (p.Lys445ThrfsTer12 and p.His1237Arg). The *PCNT* gene is causative of AR microcephalic osteodysplastic primordial dwarfism type II (OMIM#210720).
2. RPL5 couple: This RPL5 couple presented with a history of RPLs and hydrops. Both of them were found to be carriers for the same variant for methylenetetrahydrofolate reductase (*MTHFR*) deficiency. Sanger validation has been performed for this variant (Supplementary Figure S2Bi). This missense variant NM_005957.5 (*MTHFR*):c.1286A>C (p.Glu429Ala) has been reported in ClinVar as likely pathogenic (Accession: VCV000003521.78). The observed variant is a well-known polymorphism and has been observed with a high allele frequency in both 1000 Genomes and gnomAD databases. The reference base is conserved across the species, and *in silico* predictions by PolyPhen and SIFT are damaging. This variant has been reported to cause an increased risk of fetal abnormalities by Pezzetti et al. (2004). For these reasons, this variant has been classified as VUS likely to be pathogenic.
3. RPL16 couple: This non-consanguineously married couple, presented with history of three miscarriages and 4th pregnancy showed omphalocele on ultrasound at 14 weeks 4 days gestation age. On doing the couple exome, both of them were incidentally found to be carriers of sequence variations in the *ALMS1* gene, which is causative of Alstrom syndrome (ALMS). ALMS is caused by homozygous or compound heterozygous mutation in the *ALMS1* gene on chromosome 2p13. The missense variant NM_015120.4 (*ALMS1*):c.11734A>C (p.Ser3912Arg) was identified in the wife, which is reported as VUS in ClinVar (Accession: VCV000403949.6). The p.Ser3912Arg variant is observed in 6/30,604 (0.0196%) alleles from individuals of gnomAD South Asian background in gnomAD. Another missense variant c.1420C>A (p.His474Asn) in the same gene in the heterozygous state was detected in the spouse sample. This variant was reported as VUS in ClinVar (Accession: VCV000459855.13). The p.His474Asn variant is observed in 12/30,596 (0.0392%) alleles from individuals of gnomAD South Asian background in gnomAD. Both the missense variants were predicted to be damaging by both SIFT and PolyPhen2. For these reasons, these variants have been classified as VUS. Sanger validation has been performed for both the variants (Supplementary Figure S2Bii).
4. RPL21 couple: This couple was found to be carriers of VUS in the *PKD1L1* gene (p.Ala104Thr) and a pathogenic variant in the *PKD1L1* gene (p.Arg2669Ter), respectively. The homozygous variant in the *PKD1L1* gene is responsible for visceral heterotaxy-8 (OMIM#617205).
5. RPL33 couple: This non-consanguineously married couple presented with a history of five recurrent miscarriages. During 6th gestation, CMA of POC was indicative of mosaic Klinefelter syndrome. Couple karyotype was reported normal. Couple exome sequencing revealed the carrier status of the couple for two AR disorders.

The first disorder was arthrogryposis multiplex congenita-6 (AMC6)/Nemaline myopathy-2 (NEM2), which is caused by homozygous or compound heterozygous mutation in the *NEB* gene on chromosome 2q23. The wife was found to be a carrier of missense variant NM_001271208.2:c.22454C>T (p.Thr7485Ile) in the *NEB* gene. Another missense variant c.22454C>T (p.Thr7485Ile) in the same gene in the heterozygous state was detected in the spouse sample (Table 4). The missense variant c.22454C>T (p.Thr7485Ile) was found in ClinVar (Accession: VCV000968876.7) with a classification of VUS. This variant is observed in 11/30,602 (0.0359%) alleles from individuals of gnomAD South Asian background in gnomAD. The p.Asp3902Glu variant is novel (not in any individuals) in gnomAD. Both the variants were predicted to be damaging by both SIFT and PolyPhen2, and the mutant residues were

TABLE 5 OMIM phenotypes related to mutated genes.

Gene	Associated disease/OMIM	Phenotype
PCNT	Microcephalic osteodysplastic primordial dwarfism type II (OMIM#210720)	MOPD II is characterized by intrauterine growth retardation, severe proportionate short stature, and microcephaly. It is distinct from Seckel syndrome (see 210,600) by more severe growth retardation, radiologic abnormalities, and absent or mild mental retardation
	Mode of inheritance: AR	
MTHFR	Homocystinuria due to methylene tetrahydrofolate reductase	Homocystinuria due to methylenetetrahydrofolate reductase deficiency is caused by homozygous or compound heterozygous mutation in the *MTHFR* gene on chromosome 1p36. Methylenetetrahydrofolate reductase deficiency is a common inborn error of folate metabolism. The phenotypic spectrum ranges from severe neurologic deterioration and early death to asymptomatic adults. In the classic form, both thermostable and thermolabile enzyme variants have been identified
	Deficiency (OMIM#236250)	
	Mode of inheritance: AR	
ALMS1	Alstrom syndrome (OMIM#203800)	Alstrom syndrome (ALMS) is caused by homozygous or compound heterozygous mutation in the *ALMS1* gene on chromosome 2p13. This disorder is characterized by progressive cone–rod dystrophy leading to blindness, sensorineural hearing loss, childhood obesity associated with hyperinsulinemia, and type 2 diabetes mellitus. Dilated cardiomyopathy occurs in approximately 70% of patients during infancy or adolescence. Renal failure and pulmonary, hepatic, and urologic dysfunction are often observed, and systemic fibrosis develops with age
	Mode of inheritance: AR	
PKD1L1	Visceral heterotaxy-8 (OMIM#617205)	Autosomal visceral heterotaxy-8 (HTX8) is an autosomal recessive developmental disorder characterized by visceral situs inverses associated with complex congenital heart malformations caused by defects in the normal left–right asymmetric positioning of internal organs.
	Mode of inheritance: AR	
NEB	Arthrogryposis multiplex congenita-6 (OMIM#619334)	Arthrogryposis multiplex congenita-6 (AMC6) is characterized by polyhydramnios and reduced fetal movements. Affected individuals have congenital joint contractures, dysmorphic facial features, distal skeletal anomalies with clenched hands and clubfeet, and edema with fetal hydrops. Fetal demise or termination of pregnancy often occurs after the ultrasound detection of abnormalities. Those that survive birth have significant hypotonia with absent spontaneous movements, respiratory insufficiency, arthrogryposis, and multiple pterygia. Skeletal muscle is hypoplastic, immature, and underdeveloped with nemaline rods, poorly developed sarcomeres, and poor cross-striation. Death in infancy usually occurs
	Nemaline myopathy-2 (NEM2)	
	Mode of inheritance: AR	
INPPL1	Opsismodysplasia (OMIM#258480)	Opsismodysplasia (OPSMD) is caused by homozygous or compound heterozygous mutation in the *INPPL1* gene on chromosome 11q13. This disorder is characterized by short limbs, small hands and feet, relative macrocephaly with a large anterior fontanel, and characteristic craniofacial abnormalities including a prominent brow, depressed nasal bridge, a small anteverted nose, and a relatively long philtrum. Death *in utero* or secondary to respiratory failure during the first few years of life has been reported, but there can be long-term survival. Typical radiographic findings include shortened long bones with delayed epiphyseal ossification, severe platyspondyly, metaphyseal cupping, and characteristic abnormalities of the metacarpals and phalanges
	Mode of inheritance: AR	

conserved in all mammalian species. For these reasons, these variants have been classified as VUS.

Both were found to be carriers for another AR disorder: opsismodysplasia (OPSMD), which is caused by homozygous or compound heterozygous mutation in the *INPPL1* gene on chromosome 11q13. The husband was found to be a carrier for missense variant NM_001567.4 (*INPPL1*):c.3394G>A (p.Glu1132Lys), which is reported as VUS in ClinVar (Accession: VCV001391913.2). The p.Glu1132Lys variant is observed in 4/30,238 (0.0132%) alleles from individuals of gnomAD South Asian background in gnomAD.

Another missense novel variant in the same gene in the heterozygous state c.2839C>T (p.Pro947Ser) was detected in the spouse sample, which is not reported in any database. Both the missense variants were predicted to be damaging by both SIFT and PolyPhen2. The mutant residues were conserved in all mammalian species. For these reasons, this variant has been classified as VUS. Sanger validation has been performed for these variants (Supplementary Figure S2Biii).

3.7.3 Other findings (incidentally detected important variations)

Other pathogenic and likely pathogenic variants identified in autosomal recessive disorders are given in Table 6. These variants were grouped into a separate table as both of the couple were not found to be carriers for the same genes. These variants were found in either of the couple in genes *HBB, CFTR, ACADS, ALOXE, VPS13A, MKS1, MTHFR, F5, ACADM, GMPPB, GNRHR, AMN, CERKL, CEP63, ASPM, EPM2A, SH3TC2,*

TABLE 6 Couple exome sequencing (incidentally detected important variations).

Patient ID	Gene	Variant	Zygosity	OMIM genes	Inheritance	Classification
W2	*CHST3*	c.533dup, p.Ala179ArgfsTer141	Heterozygous	Spondyloepiphyseal dysplasia with congenital joint dislocations (OMIM#143095)	AR	Pathogenic
		Accession: VCV000432012.15				
	G6PD	c.1003G>A, p.Ala335Thr	Heterozygous	Nonspherocytichemolyticanemia due to G6PD deficiency (OMIM#300908)	XLD	Pathogenic
		Accession: VCV000010363.35				
H2	*KIAA0556*	c.274_275del, p.Phe92LeufsTer23	Heterozygous	Joubert syndrome 26 (OMIM#616784)	AR	Pathogenic
		Accession: SCV003804999 rs1254671898				
H11	*ACADM*	c.486 + 1G>A	Heterozygous	Medium chain acyl-CoA dehydrogenase deficiency (OMIM# 201450)	AR	Pathogenic
		Accession: VCV000371544.9				
W11	*GNRHR*	c.785G>A (p.Arg262Gln)	Heterozygous	Hypogonadotropic hypogonadism-7 with or without anosmia (HH7) (OMIM# 146110)	AR	Likely pathogenic
		Accession: VCV000016024.20				
H16	*AMN*	c.1006 + 34_1007- 31del	Heterozygous	Imerslund–Grasbeck syndrome (OMIM# 618882)	AR	Pathogenic
		Accession: VCV000056742.4				
H21	*CFTR*	c.3209G>A, p.Arg1070Gln	Heterozygous	Cystic fibrosis (OMIM#219700)	AR	Pathogenic
		Accession: VCV000634835.1				
	SLC24A5	c.494C>G, p.Ser165Ter	Heterozygous	Oculocutaneous albinism-6 (OMIM#113750)	AR	Pathogenic
		Accession: SCV003804979				
	RARS2	c.1026G>A, p.Met342Ile	Heterozygous	Pontocerebellar hypoplasia type 6 (OMIM#611523)	AR	Likely pathogenic
		Accession: VCV000215064.20				
W21	*DOCK7*	c.1511_1513del, p.Pro504_Ter505delinsArg	Heterozygous	Fetal akinesia deformation sequence −3 (OMIM#618389)/Congenital myasthenic syndrome-10 (OMIM#254300)	AR	Pathogenic
		Accession: SCV003804980				
W35	*CFTR*	c.1367T>C, (p.Val456Ala)	Heterozygous	Cystic fibrosis (OMIM#219700)	AR	Pathogenic
		Accession: VCV000035821.37				
H35	*HBB*	c.27dupG (p.Ser10Valfs*14)	Heterozygous	Beta-thalassemia (OMIM# 613985)	AR	Pathogenic
		Accession: VCV000036308.80				
W37	*HBB*	c.27dupG (p.Ser10Valfs*14)	Heterozygous	Beta-thalassemia (OMIM# 613985)	AR	Pathogenic
		Accession: VCV000036308.80				
H37	*CFTR*	c.1367T>C (p.Val456Ala)	Heterozygous	Cystic fibrosis (OMIM#219700)	AR	Pathogenic
		Accession: VCV000035821.37				
	ACADS	c.136C>T (p.Arg46Trp) Accession: VCV000003825.12	Heterozygous	Acyl-CoA dehydrogenase, short chain, deficiency of (OMIM#201470)	AR	Pathogenic
	ALOXE3	c.1630C>T, (p.Gln544Ter) VCV000449286.4	Heterozygous	Congenital ichthyosis, 3 (OMIM# 606545)	AR	Pathogenic
	VPS13A	c.3740_3741insAGAG (p.Ser1249ArgfsTer11)	Heterozygous	Choreoacanthocytosis (OMIM#200150)	AR	Pathogenic
		Accession:				
		SCV003804981				
	MKS1	c.1450_1453dupGGCA (p.Thr485Argfs)	Heterozygous	Bardet–Biedl syndrome 13, Meckel Syndrome 1 (OMIM#615990)/Joubert syndrome 28 (OMIM# 617121)	AR	Pathogenic
		Accession:				
		SCV003804983				

(Continued on following page)

TABLE 6 (*Continued*) Couple exome sequencing (incidentally detected important variations).

Patient ID	Gene	Variant	Zygosity	OMIM genes	Inheritance	Classification
W40	*IL11RA*	c.709C>T (p.Arg237Ter)	Heterozygous	Craniosynostosis and dental anomalies (OMIM#614188)	AR	Pathogenic
		Accession:				
		VCV001074686.3				
	LMBRD1	c.399delA (p.Lys133Asnfs*17)	Heterozygous	Methylmalonic aciduria and homocystinuria, cblF type (OMIM#277380)	AR	Likely pathogenic
		Accession:				
		SCV003804992				
	PAH	c.355C>T (p.Pro119Ser)	Heterozygous	Phenylketonuria (OMIM#261600)	AR	Likely pathogenic
		Accession:				
		VCV000092741.19				
W44	*CERKL*	c.316C>A, (p.Arg106Ser)	Heterozygous	Retinitis pigmentosa 26 (OMIM# 608380)	AR	Likely pathogenic
		Accession:				
		VCV000438054.10				
H44	*CEP63*	c.1833del, (p.Leu612Ter)	Heterozygous	Seckel syndrome 6 (OMIM# 614728)	AR	Pathogenic
		Accession:				
		SCV003804993				
W45	*ASPM*	c.2783del, (p.Ala928ValfsTer7)	Heterozygous	Primary microcephaly-5 (OMIM# 608716)	AR	Pathogenic
		Accession:				
		SCV003804994				
	EPM2A	c.179G>A, (p.Trp60Ter)	Heterozygous	Progressive myoclonic epilepsy-2 (OMIM#254780)	AR	Pathogenic
		Accession:				
		SCV003804995				
H45	*SH3TC2*	c.3511C>T, (p.Arg1171Cys)	Heterozygous	Charcot–Marie–Tooth disease type 4C (OMIM# 601596)	AR	Likely pathogenic
		Accession:				
		VCV000448370.30				
W48	*SLC6A19*	c.311G>A, (p.Trp104Ter)	Heterozygous	Hartnup disorder (OMIM#234500)	AR	Pathogenic
		Accession:				
		SCV003804998				
H48	*HADHA*	c.1195C>T, (p.Arg399Ter)	Heterozygous	Mitochondrial trifunctional protein deficiency (OMIM#609015)/LCHAD deficiency (OMIM#609016)	AR	Pathogenic
		Accession:				
		VCV000449455.12				
H53	*ABCA4*	c.5882G>A, p.Gly1961Glu	Heterozygous	Cone–rod dystrophy-3 (OMIM#604116)/ Retinitis pigmentosa-19 (OMIM#601718)/ Stargardt disease-1 (OMIM#248200)	AR	Pathogenic
		Accession:				
		VCV000007888.78				
W53	*PMPCB*	c.524G>A, p.Arg175His	Heterozygous	Multiple mitochondrial dysfunctions syndrome-6 (OMIM#617954)	AR	Likely pathogenic
		Accession:				
		VCV000523140.3				
	MYO7A	c.5345G>C, p.Gly1782Ala	Heterozygous	Deafness −2 (OMIM#600060)/Usher syndrome, type-1B (OMIM#276900)	AR	Likely pathogenic
		Accession:				

(Continued on following page)

TABLE 6 (*Continued*) Couple exome sequencing (incidentally detected important variations).

Patient ID	Gene	Variant	Zygosity	OMIM genes	Inheritance	Classification
		VCV000560898.6				
H55	*CPLANE1*	c.3056_3059dupTGTG (p.Trp1020Cysfs*6) SUB12936984	Heterozygous	Joubert syndrome 17 (OMIM# 614615)/ Orofaciodigital syndrome VI (OMIM#277170)	AR	Likely pathogenic
W55	*HYDIN*	c.12444-1G>A	Heterozygous	Ciliary dyskinesia, primary, 5 (OMIM# 608647)	AR	Pathogenic
		Accession:				
		SCV003836565				
H60	*G6PD*	c.563C>T (p.Ser188Phe)	Hemizygous	Glucose-6-phosphate dehydrogenase deficiency (OMIM#300908)	XLR	Likely pathogenic
		Accession:				
		VCV000100057.65				
H61	*GUCY2D*	c.849C>A, p.Tyr283Ter	Heterozygous	Choroidal dystrophy-1 (OMIM#215500)/ Leber congenital amaurosis 1 (OMIM#204000)/Congenital stationary night blindness type 1I (OMIM#618555)	AR	Pathogenic
		Accession:				
		VCV000521653.4				
	PTPRQ	c.3308_3309del, p.Leu1103ArgfsTer4	Heterozygous	Deafness 84A (OMIM#613391)	AR	Pathogenic
		Accession:				
		SCV003804996				
W61	*F5*	c.1601G>A, p.Arg534Gln	Heterozygous	Factor V deficiency (OMIM#227400)	AR	Likely pathogenic
		Accession:				
		VCV000000642.85				
	RTN4IP1	c.59G>A, p.Trp20Ter	Heterozygous	Optic atrophy 10 with or without ataxia, mental retardation, and seizures (OMIM#616732)	AR	Pathogenic
		Accession:				
		VCV001405046.2				
	GAS8	c.495 + 1G>T	Heterozygous	Primary ciliary dyskinesia, 33 (OMIM#616726)	AR	Pathogenic
		Accession:				
		SCV003806425				
	MARS1	c.1793G>A, p.Arg598His	Heterozygous	Nonphotosensitive trichothiodystrophy-9 (OMIM#619692)/Interstitial lung and liver disease (OMIM#615486)	AR	Pathogenic
		Accession:				
		VCV001172763.3				

*AR, autosomal recessive; AD, autosomal dominant; XLD, X-linked dominant; XLR, X-linked recessive.

SLC6A1, HADHA, CHST3, G6PD, KIAA0556, PKD1L1, SLC24A5, RARS2, DOCK7, PKD1L1, CPLANE1, HYDIN, GUCY2D, PTPRQ, SLX4, RTN4IP1, GAS8, MARS1, ABCA4, PMPCB, and *MYO7A* (Table 6).

3.7.4 Trio exomes

Trio exome analysis was performed in eight trios to identify the genomic reason of unexplained RPL. Putative causative variants were identified in three trios (Table 7; Figure 1).

1. **RPL28:** Trio exome analysis showed a frameshift *de novo* variant c.413dup (p.Met138fs) in the *F5* gene. Susceptibility to RPL-1 (RPRGL1) (MIM#614389) is conferred by variation in the coagulation factor V gene. This variant was not present in parents. As per ACMG guidelines, this variant is predicted to be likely pathogenic (PVS1 and PM2).
2. **RPL27:** NGS Trio revealed a homozygous missense variant c.388T>C (p.Cys130Arg) in the *APOE* gene in fetus and parents were found to be carriers for the same. This variant is reported as pathogenic in ClinVar (Accession: VCV000441268.4). *APOE* has been shown to be associated with an elevated risk of recurrent miscarriage.
3. **RPL50:** RPL50 showed a homozygous missense variant NM_000031.6(*ALAD*):c.446G>A (p.Arg149Gln) in fetus, which has not been reported previously in the database. The p.Arg149Gln missense variant is predicted to be damaging by both SIFT and PolyPhen2. The arginine residue at codon 149 of *ALAD* is conserved in all mammalian species. For these reasons, this variant has been classified as VUS. The

TABLE 7 Trio exome results.

ID	Gene	Variant	Zygosity (in POC)	OMIM disorder	Inheritance	Origin	Classification as per ACMG guidelines
RPL27	*APOE*	c.388T>C	Homozygous	Recurrent pregnancy loss susceptible gene	AR	Inherited	Likely pathogenic (PM2 and PP5)
		p.Cys130Arg					
		Accession: VCV000441268.4 (rs429358)					
RPL28	*F5*	c.413dup	Heterozygous	Thrombophilia OMIM# (188055)	AD	*De novo*	Likely pathogenic (PVS1 and PM2)
		p.Met138fs					
		Accession: SCV003804964					
RPL50	*ALAD*	c.446G>A (p.Arg149Gln)	Homozygous	Porphyria, acute hepatic (OMIM#612740)	AR	Inherited	VUS (PM2, PP2, and PP3)
		Accession: SCV003804978					

*AR, autosomal recessive; AD, autosomal dominant; VUS, variant of unknown significance.

same variant in the heterozygous state was detected in the father and the mother, and Sanger validation has been performed for the same (Supplementary Figure S2A). Porphyria, acute hepatic, is caused by mutation in the gene encoding delta-aminolevulinate dehydratase on chromosome 9q32. The disorder is characterized by the failure to thrive, respiratory analysis, vomiting, abdominal colic, hypotonia, muscle weakness, hemolytic anemia, and porphyria. A study has showed that porphyria disorder is closely associated with pregnancy risk (Tollånes et al., 2011).

4 Discussion

This present study represents an Indian series of complete cytogenetic and molecular analyses of the first-trimester pregnancy loss abortus (31 POCs) and further evaluation in couples (61 couples). The various laboratory techniques used were karyotyping, CMA, and couple/trio exome sequencing. Most miscarriages were in the first trimester, and we had little information on fetal anomalies or phenotypes except embryonic lethality. This made the analysis and interpretation more complex. From each family, we could get only one POC and could not get the samples from previous pregnancies to verify the variant and do the segregation analysis. Because of the dense Indian population and marriages within blood relations, we hypothesized that there would be detection of some autosomal recessive Mendelian disorders in fetuses. There can be early embryonic lethality in such conditions, and in view of the absence of detailed prenatal phenotypes and associated laboratory test reports, some of the causes are often missed (Jelin and Vora, 2018).

Cytogenetic analysis of POCs is important to get a clue of the cause of fetal lethality/loss. This information can be used to estimate the risks of recurrence in future pregnancies. From India, a study by Dutta et al. (2011) showed majority of the cases of RPL was having balanced reciprocal translocations (Dutta et al., 2011). In our study, the most frequent chromosome abnormalities diagnosed in fetuses were autosomal trisomy and double segment imbalances (DSIs). Recently, Gajjar et al., showed causative CNVs in 38% of the POC samples (Gajjar et al., 2023) while pathogenic CNVs were identified in 25% of the POCs in our study.

Among chromosomal aberrations in fetuses, trisomy 9 was detected in a fetus (POC23) along with monosomy of 15q11.2. Trisomy 9 is a rare and often fatal chromosomal abnormality which occurs in approximately 2.4% of pregnancy losses (Miryounesi et al., 2016). Clinical phenotypes are craniofacial dysmorphism including hypertelorism, prominent nose, deep-set eyes, and down-slanting palpebral fissures (Temtamy et al., 2007). The specific symptoms of partial trisomy 9 are varied depending on the size of duplication on chromosome 9p and 9q. 15q11.2 microdeletion syndrome is a relatively rare chromosomal abnormality, which is characterized by pre- and postnatal growth restriction, developmental delay, variable degrees of intellectual disability, hand and foot anomalies, and mild craniofacial dysmorphism (Rudaks et al., 2011). The reports of 15q11.2 microdeletion on prenatal ultrasonographic abnormalities are rare. Other features are neonatal lymphedema, heart malformations, aplasia cutis congenita, aortic root dilatation, and autistic spectrum disorder have also been reported (Pinson et al., 2005). POC29 revealed double segment imbalance deletion at chromosome 11q24.3 and duplication of 14q24.2q32.33. Both are terminal, and the underlying cause was balanced translocation in any one partner of the couple. Deletion at chromosome 11q24.3 is linked with the Jacobsen syndrome critical region. Reported patients had pancytopenia of variable degrees (including thrombocytopenia) and neonatal bleeding (Serra et al., 2021). Fetal growth retardation, low birth weight, and perinatal asphyxia are risk factors which have contributed to variable clinical severity (Ichimiya et al., 2018). Trisomy 11 was detected in one fetus (POC39). Full trisomy 11 has not been reported in live births and presumably leads to early pregnancy loss (Balasubramanian et al., 2011). Few cases with partial trisomy 14q were reported with carrying pericentric inversion in one of the parents and proband with recombinant chromosome 14 (Kurtulgan et al., 2015).

Among VUS CNVs, few important genes were identified. In POC5, a small deletion in 2q34 was identified, which encompasses a gene *ERBB4* that is an important receptor in the control of fetal lung type II cell maturation (Zscheppang et al., 2007). Downregulation of the *ERBB4* gene is responsible for insufficient fetal surfactant production which further leads to respiratory distress syndrome in preterm infants (Zscheppang et al., 2007).

Couples with a karyotype in one of the partners showing heteromorphisms were counselled that they were normal variations; counselling could alleviate their anxiety and guilt, somewhat helping them to cope with the mishap. Similarly, POCs showing non-recurrent causes like trisomy 21 in POC6 and trisomy 11 in POC39 helped in finding a definitive cause at least for that loss and help in making them understand that chromosomal and genetic defects might be acquired *de novo* and there remains a fair chance of normal natural pregnancy outcome in future pregnancies. During follow-up in RPL6, we observed that there was a successful natural pregnancy and the baby is about 8 months now. They had undergone prenatal testing at 16 weeks for Down syndrome in view of the previously detected trisomy 21 in POC6.

Doing NGS on couples with the history of RPL and POCs is an efficient approach to identify the lethal genes and genes essential for embryonic development. Additionally, it gives the advantage of identifying certain prenatal phenotypes of many Mendelian conditions. In our study, 98% of variants were autosomal recessive. In the absence of the POC sample, couple exome sequencing was carried out. Carrier couples (RPL33) were identified with the variants in the *NEB* gene, which is responsible for AR Arthrogryposis multiplex congenita-6 (AMC6). Clinical features of AMC6 include congenital joint contractures, facial dysmorphism, skeletal anomalies, and edema with fetal hydrops. Death in infancy or fetal demise usually occurs (Ahmed et al., 2015; Rocha et al., 2021). This couple was also found to be carriers for mutation in the *INPPL1* gene, which is responsible for AR opsismodysplasia (OPSMD). No anomalies could be detected in our case because of early miscarriage.

Other AR gene *ALMS* variants were identified in couples with the history of RPL (RP16). Dilated cardiomyopathy occurs in approximately 70% of patients during infancy or adolescence (Marshall et al., 1997; Collin et al., 2002). Severe form of this disorder can be the cause of RPL in this couple.

RPL5 couple was found to be carriers for mutation in the *MTHFR* gene. It is already known that women with a *MTHFR* variant have a higher risk for pregnancy-related issues such as miscarriages, preeclampsia, or a baby born with birth defects, such as spina bifida. The theory behind the connection between the *MTHFR* mutation and pregnancy loss is that tiny blood clots are formed because of homocysteinemia, which blocks the flow of nutrition to the placenta, essentially starving the fetus and triggering a spontaneous abortion (Dell'dera et al., 2018). Another gene in the list was *PCNT* causing MOPD II (Couple RPL2), which is characterized by intrauterine growth retardation, severe proportionate short stature, and microcephaly. This can be the cause of fetal demise in this case.

Interestingly, in trio exome (RPL50), fetus was found to harbor homozygous variant in the *ALAD* gene which is responsible for porphyria, acute hepatic. Both parents were found to be carriers for the same. Fujita et al., 1987 reported a case with severe infantile-onset of acute hepatic porphyria (612,740), where the couple also had four successive pregnancy losses (Fujita et al., 1987). We have found *de novo* likely pathogenic variant the *F5* gene in fetus (RPL28). This gene encodes a protein called coagulation factor V, which plays a critical role in the coagulation system. In response to injury, it leads to a series of chemical reactions that forms blood clots. Pregnancy failure is often known to be associated with mutations that promote thrombophilia (Hansda and Roychowdhury, 2012). There are many supporting evidence that women with thrombophilia have higher risk of pregnancy-related venous thromboembolism and possibly other pregnancy-related issues such as pregnancy loss (Calderwood and Greer, 2005). We have found a homozygous variant in fetus, which was inherited from parents (RPL27). Research studies have showed a relationship between RPL and apolipoprotein E (Apo E) gene polymorphisms (Li et al., 2014).

By doing the carrier screening for various AR disorders, especially for pathogenic/likely pathogenic variants, we got additional information about the carrier status of various common (thalassemia, cystic fibrosis, and G6PD deficiency) and rare disorders (Table 6). Based on the carrier status of the couple and knowledge of the lethal genes involved in embryo development, it is important to counsel the families regarding risks of recurrence and future pregnancy options (Soden et al., 2014; Alamillo et al., 2015).

Early embryonic lethality leads to the termination of pregnancy. The causes being many ranging from maternal illness, *de novo* or inherited chromosomal anomalies in the embryo to various single gene disorders, sometimes inherited in autosomal recessive or X-linked manner from healthy parents, and sometimes as new autosomal dominant lethal mutations during gametogenesis. Our study aimed to find a systemic approach with a combination of techniques which can be carried out to understand the underlying cause. With a very high chance of insufficient/poor quality tissue of POC and maternal contamination, it is probably a good practice to obtain tissue antenatally after consent: as the couple RPL6 who opted for the collection of antenatal tissue before MTP lest good quality sample could not be obtained after termination. We could obtain the result by karyotyping and QF-PCR only. In the case of POC29, once the POC was found suitable, with negative MCC report, CMA was performed, which revealed double segment imbalance involving chromosomes 11 and 14 and male partner in the couple was found to be carrier of balanced translocation involving the aforementioned chromosomes. The cases where no chromosomal aberrations were found were subjected to trio exome or couple exome and causative variants were identified in some as in couple RPL 33. However, good POC samples could not be obtained in a huge number of couples and we directly went ahead with couple exome. In case of uncertainties, a combination of tests had been definitely useful.

With the advent of robust tools for sequencing the genome, various researchers have been trying to find novel genes using exome sequencing of the couple or trio to explain the underlying causes of RPLs (Quintero-Ronderos et al., 2017; Xiang et al., 2021). Although there had been some genes which had been recurrently implicated, the etiology remains unexplained in a very big proportion of couples. In our study, we used exome sequencing in a very small number of couples/trio and that remains the major caveat of our study. Nevertheless, we were able to highlight the importance of genetic testing in the POC in spite of difficulties in obtaining good samples and a very high failure rate of testing. A systematic approach and redefining testing types would be helpful in finding the cause in the increasing number of couples and thereby would help in counselling for future pregnancies.

Data availability statement

The datasets presented in this study are available in the ClinVar, corresponding accession numbers are given in the tables. Novel

variants have been submitted and can be found here: https://www.ncbi.nlm.nih.gov/clinvar/submitters/507431/.

Ethics statement

The studies involving human participants were reviewed and approved by the Institutional Ethical Committee, PGIMER, Chandigarh. The patients/participants provided their written informed consent to participate in this study. Written informed consent was obtained from the individual(s) for the publication of any potentially identifiable images or data included in this article.

Author contributions

PS, CB, and KM: Study conception and design, and preparation of the manuscript. SC and MR: Patient enrollment and clinical procedures. IP, AK, and KM: Editing and critical review of the manuscript. All authors approved the final version of the manuscript. All authors listed have made a substantial, direct, and intellectual contribution to the work and approved it for publication.

Funding

This study was funded by the Science and Engineering Research Board (SERB), Department of Science and Technology (DST), New Delhi (CRG/2020/002787).

Acknowledgments

The authors sincerely thank the patient' families for their cooperation, Priya Kumari Keshri of Motherhood clinic, Lucknow, for referring patients and the Science and Engineering Research Board (SERB), Department of Science and Technology (DST), New Delhi, India, for funding.

Conflict of interest

The authors declare that the research was conducted in the absence of any commercial or financial relationships that could be construed as a potential conflict of interest.

Publisher's note

All claims expressed in this article are solely those of the authors and do not necessarily represent those of their affiliated organizations, or those of the publisher, the editors, and the reviewers. Any product that may be evaluated in this article, or claim that may be made by its manufacturer, is not guaranteed or endorsed by the publisher.

Supplementary material

The Supplementary Material for this article can be found online at: https://www.frontiersin.org/articles/10.3389/fgene.2023.1155211/full#supplementary-material

References

Ahmed, A. A., Skaria, P., Safina, N. P., Thiffault, I., Kats, A., Taboada, E., et al. (2015). Arthrogryposis and pterygia as lethal end manifestations of genetically defined congenital myopathies. *Am. J. Med. Genet.* 176A, 359–367. doi:10.1002/ajmg.a.38577

Alamillo, C. L., Powis, Z., Farwell, K., Shahmirzadi, L., Weltmer, E. C., Turocy, J., et al. (2015). Exome sequencing positively identified relevant alterations in more than half of cases with an indication of prenatal ultrasound anomalies. *Prenat. Diagn* 35 (11), 1073–1078. doi:10.1002/pd.4648

Balasubramanian, M., Peres, L. C., and Pelly, D. (2011). Mosaic trisomy 11 in a fetus with bilateral renal agenesis: co-incidence or new association?. *Clin. Dysmorphol.* 20 (1), 47–49. doi:10.1097/MCD.0b013e32833ff2e9

Calderwood, C. J., and Greer, I. A. (2005). The role of factor V Leiden in maternal health and the outcome of pregnancy. *Curr. Drug Targets* 6 (5), 567–576. doi:10.2174/1389450054546024

Christiansen, O. B., Mathiesen, O., Lauritsen, J. G., and Grunnet, N. (1990). Idiopathic recurrent spontaneous abortion. Evidence of a familial predisposition. *Acta Obstet. Gynecol. Scand.* 69, 597–601. doi:10.3109/00016349009028702

Collin, G. B., Marshall, J. D., Ikeda, A., So, W. V., Russell-Eggitt, I., Maffei, P., et al. (2002). Mutations in ALMS1 cause obesity, type 2 diabetes and neurosensory degeneration in Alström syndrome. *Nat. Genet.* 31, 74–78. doi:10.1038/ng867

Dell"dera, D., L"piscopia, A., Simone, F., Lupo, M. G., Epifania, A. A., and Allegretti, A. (2018). Methylenetetrahydrofolate reductase gene C677T and A1298C polymorphisms and susceptibility to recurrent pregnancy loss. *Biomed. Rep.* 8 (2), 172–175. doi:10.3892/br.2018.1039

Dutta, U. R., Rajitha, P., Pidugu, V. K., and Dalal, A. B. (2011). Cytogenetic abnormalities in 1162 couples with recurrent miscarriages in southern region of India: Report and review. *J. assisted reproduction Genet.* 28 (2), 145–149. doi:10.1007/s10815-010-9492-6

Ford, H. B., and Schust, D. J. (2009). Recurrent pregnancy loss: Etiology, diagnosis, and therapy. *Rev. Obstet. Gynecol.* 2, 76–83.

Fujita, H., Sassa, S., Lundgren, J., Holmberg, L., Thunell, S., and Kappas, A. (1987). Enzymatic defect in a child with hereditary hepatic porphyria due to homozygous delta-amino levulinic acid dehydratase deficiency: Immunochemical studies. *Pediatrics* 80 (6), 880–885.

Gajjar, K., Patel, A., Patel, B., Chettiar, S., and Jhala, D. (2023). Array comparative genomic hybridization analysis of products of conception in recurrent pregnancy loss for specific anomalies detected by USG. *Reprod. Fertil.* 4, 22–0092. doi:10.1530/RAF-22-0092

Gardner, M. R. J., and Sutherland, G. R. (2004). *Chromosome abnormalities and genetic counseling*. Oxford University press, 368.

Hansda, J., and Roychowdhury, J. (2012). Study of thrombophilia in recurrent pregnancy loss. *J. Obstet. Gynaecol. India* 62 (5), 536–540. doi:10.1007/s13224-012-0197-x

Ichimiya, Y., Wada, Y., Kunishima, S., Tsukamoto, K., Kosaki, R., Sago, H., et al. (2018). 11q23 deletion syndrome (jacobsen syndrome) with severe bleeding: A case report. *J. Med. Case Rep.* 12 (1), 3. doi:10.1186/s13256-017-1535-5

Jacobs, P. A., Melville, M., Ratcliffe, S., Keay, A. J., and Syme, J. (1974). A cytogenetic survey of 11,680 newborn infants. *Ann. Hum. Genet.* 37 (4), 359–376. doi:10.1111/j.1469-1809.1974.tb01843.x

Jelin, A. C., and Vora, N. (2018). Whole exome sequencing: Applications in prenatal genetics. *Obstet. Gynecol. Clin. N. Am45(1)* 45, 69–81. doi:10.1016/j.ogc.2017.10.003

Kurtulgan, H. K., Özer, L., Yıldırım, M. E., Ünsal, E., Aktuna, S., Baltacı, V., et al. (2015). Recombinant chromosome with partial 14 q trisomy due to maternal pericentric inversion. *Mol. Cytogenet* 8, 92. doi:10.1186/s13039-015-0195-7

Li, J., Chen, Y., Wu, H., and Li, L. (2014). Apolipoprotein E (Apo E) gene polymorphisms and recurrent pregnancy loss: a meta-analysis. *J. Assist. Reprod. Genet.* 31 (2), 139–148. doi:10.1007/s10815-013-0128-5

Marshall, J. D., Ludman, M. D., Shea, S. E., Salisbury, S. R., Willi, S. M., LaRoche, R. G., et al. (1997). Genealogy, natural history, and phenotype of Alström syndrome in a large Acadian kindred and three additional families. *Am. J. Med. Genet.* 73, 150–161. doi:10.1002/(sici)1096-8628(19971212)73:2<150:aid-ajmg9>3.0.co;2-y

Miryounesi, M., Dianatpour, M., Shadmani, Z., and Ghafouri-Fard, S. (2016). Report of a case with trisomy 9 mosaicism. *Iran. J. Med. Sci.* 41 (3), 249–252.

Najafi, K., Mehrjoo, Z., Ardalani, F., Ghaderi-Sohi, S., Kariminejad, A., Kariminejad, R., et al. (2021). Identifying the causes of recurrent pregnancy loss in consanguineous couples using whole exome sequencing on the products of miscarriage with no chromosomal abnormalities. *Sci. Rep11(1)* 11, 6952. doi:10.1038/s41598-021-86309-9

Pezzetti, F., Martinelli, M., Scapoli, L., Carinci, F., Palmieri, A., Marchesini, J., et al. (2004). Maternal MTHFR variant forms increase the risk in offspring of isolated nonsyndromic cleft lip with or without cleft palate. *Hum. Mutat.* 24 (1), 104–105. doi:10.1002/humu.9257

Pinson, L., Perrin, A., Plouzennec, C., Parent, P., Metz, C., Collet, M., et al. (2005). Detection of an unexpected subtelomeric 15q26.2 --> qter deletion in a little girl: Clinical and cytogenetic studies. *Am. J. Med. Genet. A* 138A (2), 160–165. doi:10.1002/ajmg.a.30939

Practice Committee of the American Society for Reproductive Medicine (2020). Definitions of infertility and recurrent pregnancy loss: A committee opinion. *FertilSteril* 113 (3), 533–535. doi:10.1016/j.fertnstert.2019.11.025

Quintero-Ronderos, P., Mercier, E., Fukuda, M., González, R., Suárez, C. F., Patarroyo, M. A., et al. (2017). Novel genes and mutations in patients affected by recurrent pregnancy loss. *PloS one* 12 (10), e0186149. doi:10.1371/journal.pone.0186149

Richards, S., Aziz, N., Bale, S., Bick, D., Das, S., Gastier-Foster, J., et al. (2015). Standards and guidelines for the interpretation of sequence variants: A joint consensus recommendation of the American College of medical genetics and genomics and the association for molecular pathology. *Med* 17 (5), 405–424. doi:10.1038/gim.2015.30

Rocha, M. L., Dittmayer, C., Uruha, A., Korinth, D., Chaoui, R., Schlembach, D., et al. (2021). A novel mutation in NEB causing foetal nemaline myopathy with arthrogryposis during early gestation. *Neuromusc. Disord.* 31, 239–245. doi:10.1016/j.nmd.2020.11.014

Rudaks, L. I., Nicholl, J. K., Bratkovic, D., and Barnett, C. P. (2011). Short stature due to 15q26 microdeletion involving IGF1R: Report of an additional case and review of the literature. *Am. J. Med. Genet. A* 155A (12), 3139–3143. doi:10.1002/ajmg.a.34310

Rull, K., Nagirnaja, L., and Laan, M. (2012). Genetics of recurrent miscarriage: challenges, current knowledge, future directions. *Front. Genet.* 3, 34. doi:10.3389/fgene.2012.00034

Serra, G., Memo, L., Antona, V., Corsello, G., Favero, V., Lago, P., et al. (2021). Jacobsen syndrome and neonatal bleeding: Report on two unrelated patients. *Ital. J. Pediatr.* 47 (1), 147. doi:10.1186/s13052-021-01108-2

Singh, G., and Sidhu, K. (2010). Bad obstetric history: A prospective study. *Med. J. Armed Forces India* 66 (2), 117–120. doi:10.1016/S0377-1237(10)80121-2

Soden, S. E., Saunders, C. J., Willig, L. K., Farrow, E. G., Smith, L. D., Petrikin, J. E., et al. (2014). Effectiveness of exome and genome sequencing guided by acuity of illness for diagnosis of neurodevelopmental disorders. *Sci. Transl. Med.* 6 (265), 265ra168. doi:10.1126/scitranslmed.3010076

South, S. T., Lee, C., Lamb, A. N., Higgins, A. W., and Kearney, H. M. (2013). ACMG standards and guidelines for constitutional cytogenomic microarray analysis, including postnatal and prenatal applications: Revision 2013. *Genet. Med.* 15 (11), 901–909. doi:10.1038/gim.2013.129

Sugiura-Ogasawara, M., Ozaki, Y., Katano, K., Suzumori, N., Kitaori, T., and Mizutani, E. (2012). Abnormal embryonic karyotype is the most frequent cause of recurrent miscarriage. *Hum. Reprod. Oxf. Engl.* 27 (8), 2297–2303. doi:10.1093/humrep/des179

Temtamy, S. A., Kamel, A. K., Ismail, S., Helmy, N. A., Aglan, M. S., El Gammal, M., et al. (2007). Phenotypic and cytogenetic spectrum of 9p trisomy. *Genet. Couns.* 18, 29–48.

Tollånes, M. C., Aarsand, A. K., and Sandberg, S. (2011). Excess risk of adverse pregnancy outcomes in women with porphyria: a population-based cohort study. *J. Inherit. Metab. Dis.* 34 (1), 217–223. doi:10.1007/s10545-010-9231-2

Torres, M. R., Carrasco, P., Santos, C., Bueno, G., Martínez-Bonet, E., Carreto, P., et al. (2021). Contingent prenatal screening for frequent aneuploidies with cell-free fetal DNA analysis. *Taiwan J. Obstet. Gynecol.* 60 (4), 745–751. doi:10.1016/j.tjog.2021.05.028

Verma, R. S., Rodriguez, J., and Dosik, H. (1982). The clinical significance of pericentric inversion of the human Y chromosome: A rare "third" type of heteromorphism. *J. Hered.* 73 (3), 236–238. doi:10.1093/oxfordjournals.jhered.a109627

Xiang, H., Wang, C., Pan, H., Hu, Q., Wang, R., Xu, Z., et al. (2021). Exome-sequencing identifies novel genes associated with recurrent pregnancy loss in a Chinese cohort. *Front. Genet12* 12, 746082. doi:10.3389/fgene.2021.746082

Zscheppang, K., Liu, W., Volpe, M. V., Nielsen, H. C., and Dammann, C. E. (2007). ErbB4 regulates fetal surfactant phospholipid synthesis in primary fetal rat type II cells. American journal of physiology. *Lung Cell. Mol. Physiol.* 293 (2), L429–L435. doi:10.1152/ajplung.00451.2006

frontiers | Frontiers in Pediatrics

TYPE Original Research
PUBLISHED 30 May 2023
DOI 10.3389/fped.2023.1202100

OPEN ACCESS

EDITED BY
Jordi Pérez-Tur,
Spanish National Research Council (CSIC), Spain

REVIEWED BY
Dorota Pastuszak-Lewandoska,
Medical University of Lodz, Poland
Sulev Kõks,
Murdoch University, Australia

*CORRESPONDENCE
Ran Tao
chrtao@zju.edu.cn

†These authors have contributed equally to this work and share first authorship

RECEIVED 07 April 2023
ACCEPTED 10 May 2023
PUBLISHED 30 May 2023

CITATION
Shi J, He L, Zheng H, Li W, Huang S, Li Y and Tao R (2023) Association of *IL-4* and *IL-18* genetic polymorphisms with atopic dermatitis in Chinese children.
Front. Pediatr. 11:1202100.
doi: 10.3389/fped.2023.1202100

Association of *IL-4* and *IL-18* genetic polymorphisms with atopic dermatitis in Chinese children

Jianrong Shi[1†], Lin He[1†], Huiwen Zheng[2], Wei Li[1], Shuangshuang Huang[1], Yunling Li[2] and Ran Tao[1*]

[1]Department of Clinical Laboratory, the Children' s Hospital, Zhejiang University School of Medicine, National Clinical Research Center for Child Health, Hangzhou, China, [2]Department of Dermatology, The Children' s Hospital, Zhejiang University School of Medicine, Hangzhou, China

Background: Atopic dermatitis (AD) is a common chronic inflammatory skin disease, adversely affecting nearly 20% of the pediatric population worldwide. Interleukin-4 (IL-4) and interleukin-18 (IL-18) are considered to be involved in the pathogenesis and development of AD. The aim of this study was to investigate the association of *IL-4* and *IL-18* gene polymorphisms with the susceptibility and severity of AD in Chinese children.
Methods: Six candidate single nucleotide polymorphisms (SNPs) in *IL-4* and *IL-18* genes were genotyped through multi-PCR combined with next-generation sequencing in 132 AD children and 100 healthy controls, and all the analyses were performed on blood genome DNA.
Results: The frequencies of G allele, CG genotype and CG + GG genotype of *IL-4* rs2243283, as well as the haplotype *IL-4*/GTT (rs2243283-rs2243250-rs2243248) were all significantly decreased in AD patients compared with the controls [G vs. C: $P = 0.033$, OR = 0.59; CG vs. CC: $P = 0.024$, OR = 0.47; CG + GG vs. CC: $P = 0.012$, OR = 0.49; GTT vs. CCT: $P = 0.011$, OR = 0.65]. Moreover, the frequencies of A allele, AA genotype and AG + AA genotype of *IL-18* rs7106524, along with the haplotype *IL-18*/CAA (rs187238-rs360718-rs7106524) were statistically increased in the severe AD patients (A vs. G: $P < 0.001$, OR = 2.79; AA vs. GG: $P = 0.003$, OR = 5.51; AG + AA vs. GG: $P = 0.036$, OR = 2.93; CAA vs. CAG: $P = 0.001$, OR = 2.86).
Conclusions: Our findings suggested that genetic variation in *IL-4* rs2243283 such as G allele, CG genotype and CG + GG genotype might confer the reduced susceptibility to AD in Chinese children. Furthermore, A allele, AA genotype and AG + AA genotype of *IL-18* rs7106524 explored the strong association with severity in Chinese AD children.

KEYWORDS
interleukin-4, interleukin-18, atopic dermatitis, polymorphisms, susceptibility, inflammation

1. Introduction

Atopic dermatitis (AD), also known as eczema, is a recurrent inflammatory skin disease that adversely affects a significant proportion of the pediatric population (10%–20%) (1). The quality of life in patients with AD seriously decreased due to the characteristics of intense pruritus, diffuse xerosis and sleep disturbance (2). Although the pathogenesis of AD has not been completely understood, immune imbalance and skin barrier dysfunction

led by the interaction of genetic predisposition, immune and microbiome are considered to be the critical causes of AD (1, 3).

It has been confirmed that the immune imbalance between T helper (Th) lymphocytes 1 and 2 can result in abnormal cytokine production, which plays a crucial role in the occurrence and development of immune-mediated and allergic disorders, such as AD, asthma, and allergic rhinitis (4, 5). Interleukin-4 (IL-4), mainly produced by mast cells and activated T cells including Th2 cells, is an important driver of type 2 immunity in these diseases. IL-4 is also considered central to the pathogenesis of AD and key drug target (6). It has been shown that IL-4 acts on both immune cells and histiocytoes, mediating multiple steps of the AD pathogenicity cascade. On the one hand, IL-4 could cause differentiation of naïve $CD4^+$ T cells to Th2 cells and induce T cytotoxic 2 (Tc2) cells and group-2 innate lymphoid cells (ILC2) development (6, 7). Through downregulating filaggrin (FLG) expression, IL-4 also amplifies the effects of histamine and stimulates immunoglobulin E (IgE) production by B cells, which could inhibit skin barrier function and induce pruritus or anaphylaxis in skin lesions of acute AD (8, 9). On the other hand, IL-4 regulates the activity of dendritic cells, decreasing their expression of IL-12 and major histocompatibility complex (MHC) class II and increasing IL-10 production, thereby amplifying type 2 inflammation (10). Moreover, mouse model studies have established the centrality of IL-4 in the pathogenesis of AD, highlighting its capability to induce all the histopathological features of AD (6). In summary, the role of IL-4 in the pathogenesis of AD and in mediating a variety of clinical features, including skin inflammation and pruritus, is well established.

Although type 2 inflammation is the dominant immune mechanism, there is growing evidence that AD involves multiple immune pathways. Interleukin-18 (IL-18), identified as an IFN-γ inducing factor, is a pro-inflammatory cytokine that plays a critical role in Th1 lymphocytes activation. Moreover, IL-18 synergistically stimulates the production of IgE and Th2 cytokines with IL-12 (11, 12). It has been presented that IL-18 is overexpressed in both AD patients and animal model, suggesting that IL-18 might play a certain role in the pathogenesis and development of dermatitis (13). Recent evidence also demonstrated that IL-18 deficiency alleviated AD-induced lesions by reducing corticotropin-releasing hormone receptor (CRHR) 2 expression in a mouse model (14). Furthermore, Zedan et al. reported that serum IL-18 levels were significantly increased in AD patients and strongly correlated with AD activity, suggesting that IL-18 may help to assess AD activity and therefore would be useful in predicting disease progression (12).

In addition, it has been proposed that the gene polymorphisms of several cytokines are related to immune imbalance in allergic diseases such as bronchial asthma (15). Previous surveys have also indicated that genetic predisposition profoundly affected the onset and severity of AD (16, 17). To our knowledge, several single nucleotide polymorphisms (SNPs) of *IL-4* and *IL-18* genes have been identified their relevance to AD in Macedonian children, Saudi Arabian population, and Egyptians (18–20). Nevertheless, there have been few studies to date on the linkage between these two cytokines polymorphisms and AD in Chinese population. Therefore, in this study, three SNPs of *IL-4* and three SNPs of *IL-18* associated with AD or other allergic diseases in previous researches (19–23) were selected to explore their correlation with the susceptibility and severity of AD in Chinese Han children, so as to assess the population-specific prediction of *IL-4* and *IL-18* genetic variation for AD. This will provide researchers and clinicians with more baseline information including the identifiable risk factors, which may help predict the occurrence and prevent the progression of allergic dermatitis.

2. Materials and methods

2.1. Subjects

From February 2021 to August 2021, the children with AD attending the dermatology clinic of the Children's Hospital of Zhejiang University School of Medicine were used as the study subjects. Inclusion criteria were determined as follows: newly diagnosed AD patients in accordance with the AD diagnostic criteria of Hanifin and Rajka (1); Age less than 18 years; all subjects and their parents consented to participate in the study. Children with any other systemic inflammatory and autoimmune diseases or a history of medication for skin dysfunctions were excluded. The severity of AD was assessed by the Severity Scoring of Atopic Dermatitis (SCORAD) index (1). In order to observe the association of *IL-4* and *IL-18* SNPs with the severity of AD, AD cases were separated into two subgroups, namely, mild-to-moderate (SCORAD: 0–50) and severe subgroup (SCORAideD: > 50) (1, 24). Meanwhile, one hundred unrelated healthy subjects without a history of atopic or autoimmune disorders were enrolled from the physical examination department in our hospital as controls. All AD cases and controls were of Chinese Han ethnicity. The present study was approved by the Ethics Committee of the Children's Hospital of Zhejiang University School of Medicine in accordance with the principles of the Declaration of Helsinki (2021-IRB-009).

2.2. Genotype assessment

One milliliter peripheral blood samples from each subjects were collected in ethylene diamine tetraacetic acid (EDTA) anticoagulant tubes and 200 μl of each specimen was taken for DNA extraction and genotyping. DNA was extracted by Biospin genomic DNA Extraction Kit (BIOER technology, #BSC06S1) and its purity and concentration were detected by Nanodrop1000c spectrophotometer of ThermoScience Company in the United States. The integrity of DNA was observed by 1% agarose gel electrophoresis. The qualified DNA samples were kept at −20 °C for the subsequent genetic analysis.

Three *IL-4* SNPs rs2243283, rs2243250, rs2243248 and three *IL-18* SNPs rs187238, rs360718, rs7106524 were genotyped by multiplex PCR combined with next-generation sequencing technique on X-10 Illumina, a high-throughput genotyping

platform of Shanghai BioWing Applied Biotechnology Company (http://www.biowing.com.cn/) (25). The first round PCR was carried out on Gene Amp PCR System 9600 (Norwalk, USA) in the following conditions: 95 °C for 15 min; 4 cycles of 94°C for 30 s, 60°C for 10 min and 72°C for 30 s; 20 cycles of 94°C for 30 s, 60°C for 1 min and 72°C for 30 s. 1 μl of the first round product could be used as a sample for the second round of PCR under these conditions: 95°C for 15 min; 5 cycles of 94°C for 30 s, 60°C for 4 min and 72°C for 30 s; 10 cycles of 94°C for 30 s, 65°C for 1 min and 72°C for 30 s. The detailed primers used for genotyping were shown in Table 1. Then the products of the second round PCR were purified and sequenced on the X-10 platform. All the sequencing data were analyzed by Illumabcl2fastq software.

2.3. Statistical analysis

Statistical analysis was performed by the software of Statistical Package for Social Science (SPSS) (version 22.0) (IBM, USA). Continuous variables were shown as mean ± standard deviation (SD), and comparisons between groups were made by *t*-test or Anova variance analysis. Categorical variables were expressed as percentages or ratios. Comparisons between groups were performed using Fisher's exact test or Pearson's chi-square test. Genotypic frequencies of all participants were examined for Hardy-Weinberg equilibrium (HWE) before analysis. HWE, linkage-disequilibrium and haplotypes were achieved via Haploview version 4.2 program ($D' > 0.5$ and $r^2 > 0.33$ indicate strong linkage disequilibrium). All *P* values were bidirectional, and $P < 0.05$ was considered statistically significant. Odds ratio (OR) and 95% confidence intervals (CIs) of different groups or subgroups were calculated using the unconditional logistic regression analysis.

3. Results

3.1. Demographics

The detailed demographics of 132 AD patients and 100 controls were provided in Table 2. There were 73 males and 59 females with an average age of 2.6 ± 2.1 years in the case group, including 99 (75.00%) mild-to-moderate AD and 33 (25.00%) severe AD. The healthy controls were composed of 66 boys and 34 girls with an average age of 4.9 ± 1.9 years. No significant differences were found in term of gender and age either between the cases and controls, or between the mild-to-moderate subgroup and the severe subgroup.

3.2. Association between genetic polymorphisms and AD susceptibility

The successful genotyping rates of six SNPs were 94.4%–100%. The genotype distributions of all six SNPs in different groups or subgroups were all in agreement with HWE.

As shown in Table 3, the frequency of the mutant G allele of *IL-4* rs2243283 was significantly lower in AD patients comparing to controls (G vs. C: $P = 0.033$, OR = 0.59, 95% CI = 0.38–0.94). Accordingly, we found that carriers with CG genotype of *IL-4* rs2243283 had a statistically decreased risk of AD than carriers with CC genotype ($P = 0.024$; OR = 0.47, 95% CI = 0.27–0.81). Furthermore, the risk of AD susceptibility also reduced when CG and GG genotypes were analyzed together (CG + GG vs. CC: $P = 0.012$, OR = 0.49, 95% CI = 0.28–0.83) (Table 4). No significant differences in allele or genotype frequencies of the other five SNPs were found between AD patients and controls.

In haplotype analysis, the three SNPs of *IL-4* were located in the same haplotype block with a state of linkage disequilibrium ($D' > 0.5$, $r^2 > 0.33$). Comparing to the haplotype CCT composed

TABLE 1 Primer sequences for genotyping.

Polymorphic site	Location (GRCh38)	Primer sequence (Forward)	Primer sequence (Reverse)
IL-4 rs2243283	Chr5:132680901	AGGTGAACAGATTTGGGATATGAC	AATTGAACTCTTGATCTTCTGCTG
IL-4 rs2243250	Chr5:132673462	TTATGGGTAAGGACCTTATGGAC	TATTTTAACCTGGCTTCTTCCAAG
IL-4 rs2243248	Chr5:132672952	ACCTTATTGTGTCCACATGAATTC	CTCCCAAAGCTCTGAGATTACAG
IL-18 rs187238	Chr11:112164265	GAAATAAAGTGGCAGAGGATACG	GGAAGTCTGAAAATGAAGAGAGAC
IL-18 rs360718	Chr11:112164016	ATGGCTGACTTTCCAAATAAAGAG	GACAGTCAGCAAGGAATTGTCTC
IL-18 rs7106524	Chr11:112162913	TTGAGAAAGTCTCGCTCTGTTTAG	CTTTCAGGCCAGGTGCACTAG

TABLE 2 Comparison of the demographics between AD patients and the controls.

characteristics	Number	Gender		*P* value	Age	*P* value
		Male [*n* (%)]	Female [*n* (%)]		Years mean ± SD	
Controls	100	66 (66.00)	34 (34.00)	0.131	4.9 ± 1.9	0.232
AD patients	132	73 (55.30)	59 (44.70)		2.6 ± 2.1	
Mild-to-Moderate	99	54 (54.55)	45 (45.45)	0.919	2.6 ± 2.2	0.723
Severe	33	19 (57.58)	14 (42.42)		2.5 ± 1.9	

AD, atopic dermatitis; SD, standard deviation.

TABLE 3 Allele frequencies of six SNPs of *IL-4* and *IL-18* in AD patients and the controls.

Gene	SNPs	Allele	Patients [*n* (%)]	Controls [*n* (%)]	χ^2	*P* value	OR (95% CI)
IL-4	rs2243283(C > G)	C	218 (82.58)	148 (74.00)	4.52	0.033*	1.00
		G	46 (17.42)	52 (26.00)			0.59 (0.38–0.94)
	rs2243250 (C > T)	C	46 (17.83)	39 (19.70)	0.15	0.699	1.00
		T	212 (82.17)	159 (80.50)			0.89 (0.55–1.42)
	rs2243248 (T > G)	T	247 (93.56)	187 (93.50)	<0.01	1.000	1.00
		G	17 (6.44)	13 (6.50)			1.01 (0.48–2.13)
IL-18	rs187238 (C > G)	C	235 (89.02)	166 (86.46)	0.47	0.495	1.00
		G	29 (10.98)	26 (13.54)			0.79 (0.45–1.39)
	rs360718 (A > C)	A	233 (88.26)	171 (86.36)	0.22	0.641	1.00
		C	31 (11.74)	27 (13.64)			0.84 (0.49–1.47)
	rs7106524 (G > A)	G	133 (50.38)	94 (47.96)	0.18	0.675	1.00
		A	131 (49.62)	102 (52.04)			0.91 (0.63–1.31)

SNP, single nucleotide polymorphism; OR, odds ratio; 95% CI, 95% confidence interval.
*Statistically significant ($P < 0.05$).

TABLE 4 Genotype analysis of *IL-4* rs2243283 in AD patients and the controls.

Genotypes	Patients [*n* (%)]	Controls [*n* (%)]	χ^2	*P* value	OR (95% CI)
CC	90 (68.18)	51 (51.00)	7.42	0.024*	1.00
CG	38 (28.79)	46 (46.00)			0.47 (0.27–0.81)
GG	4 (3.03)	3 (3.00)			0.76 (0.16–3.57)
CG + GG/CC	42 (31.82)	49 (49.00)	6.34	0.012*	0.49 (0.28–0.83)
CC + CG/GG	128 (96.97)	97 (97.00)	<0.01	1.000	1.01 (0.22–4.55)

SNP, single nucleotide polymorphism; OR, odds ratio; 95% CI, 95% confidence interval.
*Statistically significant ($P < 0.05$).

TABLE 5 Haplotype frequencies of *IL-4* gene for risk of AD.

Haplotypes (rs2243283, rs2243250, rs2243248)	Patients [*n* (%)]	Controls [*n* (%)]	χ^2	*P* value	OR (95% CI)
CCT	39 (14.77)	26 (13.00)	-	-	1.00
CTT	162 (61.36)	112 (56.00)	0.11	0.744	0.95 (0.72–1.25)
GTT	42 (15.91)	43 (21.50)	6.86	0.011*	0.65 (0.47–0.90)
CCG	9 (3.41)	7 (3.50)	0.02	0.896	0.92 (0.53–1.62)

OR, odds ratio; 95% CI, 95% confidence interval.
*Statistically significant ($P < 0.05$); Haplotypes with the frequencies under 0.05 were not included in haplotype analysis.

of *IL-4* rs2243283, rs2243250 and rs2243248, the frequency of haplotype GTT in AD patients was significantly lower than that in controls (GTT vs. CCT: $P = 0.011$, OR = 0.65, 95% CI = 0.47–0.90) (Table 5). The frequencies of the other two haplotypes CTT and CCG did not differ between AD cases and controls.

3.3. Association between genetic polymorphisms and AD severity

As shown in Table 6, the mutant A allele of *IL-18* rs7106524 was associated with a higher risk of severe AD compared with the wild G allele ($P < 0.001$; OR = 2.79, 95% CI = 1.55–5.03). Consistent with the results of allele analysis, the carriers with AA genotype of *IL-18* rs7106524 had an increased risk of severe AD as compared to those with GG genotype ($P = 0.003$; OR = 5.51, 95% CI = 1.77–17.14). Similar risk trends were observed when AA and AG genotypes were analyzed together (AG + AA vs. GG: $P = 0.036$, OR = 2.93, 95% CI = 1.04–8.27) (Table 7). Additionally, the frequency of rs7106524 GG + AG genotype was significantly lower than that in AA genotype ($P < 0.001$; OR = 0.25, 95% CI: 0.11–0.58). No correlation was found between the other five SNPs and the severity of AD.

Furthermore, the haplotypes consisting of *IL-18* rs187238, rs360718 and rs7106524 were analyzed for their association with AD severity. The three SNPs of *IL-18* were also located in the same haplotype block with a state of linkage disequilibrium ($D' > 0.5$, $r^2 > 0.33$). As shown in Table 8, the haplotype CAA was related to an increased risk of severe AD contrasted with the wild haplotype CAG ($P = 0.001$; OR = 2.86, 95% CI = 1.49–5.49). Another haplotype GCG did not present a correlation to AD severity.

4. Discussion

AD has always been a hot research topic owing to its high prevalence, recurrence, disability and cost of care (26). Over the past few decades, knowledge of AD has evolved tremendously with insights into pathogenesis, epidemiology, impact of disease, and new therapies (27). Genetic predisposition, epidermal dysfunction, and T-cell driven inflammation are thought to be involved in the complex pathophysiology of AD (1). Among these, genetic predisposition has been reported as the strongest identifiable risk factor and an important contributor influencing the disease incidences and development of AD (1). The current literature has provided evidence for the relationship between genetic polymorphisms of relevant mediators and AD, and thus far, more than 34 AD-related genic causes have been identified, including *FLG*, *IL-13*, *RAD50*, *LRRC32*, *IL2/IL21*, *PRR5l*, *CLEC16A/DEXI*, *ZNF652*, *RUNX3*, *ERBB3*, *IL6R*, *CD207*, *PPP2R3C*, *IL-7R*, *STAT3*, *ZBTB10* and *TLR4*, etc (1, 16, 17).

TABLE 6 Allele frequencies of six SNPs of *IL-4* and *IL-18* in patients with mild-to-moderate and severe AD.

Gene	SNPs	Allele	AD patients		χ^2	*P* value	OR (95% CI)
			Mild-to-Moderate [*n* (%)]	Severe [*n* (%)]			
IL-4	rs2243283 (C > G)	C	164 (82.83)	54 (81.82)	0.04	0.851	1.00
		G	34 (17.17)	12 (18.18)			1.07 (0.52–2.22)
	rs2243250 (C > T)	C	39 (19.70)	13 (19.70)	<0.01	1.000	1.00
		T	159 (80.30)	53 (80.30)			1.00 (0.50–2.02)
	rs2243248 (T > G)	T	187 (94.44)	60 (90.91)	0.52	0.469	1.00
		G	11 (5.56)	6 (9.09)			1.70 (0.60–4.79)
IL-18	rs187238 (C > G)	C	174 (87.88)	61 (92.42)	1.05	0.306	1.00
		G	24 (12.12)	5 (7.58)			0.59 (0.22–1.63)
	rs360718 (A > C)	A	172 (86.87)	61 (92.42)	1.47	0.225	1.00
		C	26 (13.13)	5 (7.58)			0.54 (0.20–1.48)
	rs7106524 (G > A)	G	112 (56.57)	21 (31.82)	12.13	<0.001*	1.00
		A	86 (43.43)	45 (68.18)			2.79 (1.55–5.03)

SNP, single nucleotide polymorphism; OR, odds ratio; 95% CI, 95% confidence interval.
*Statistically significant ($P < 0.05$).

TABLE 7 Genotype analysis of *IL-18* rs7106524 in patients with mild-to-moderate and severe AD.

Genotype	AD patients		χ^2	*P* value	OR (95%CI)
	Mild-to-Moderate [*n* (%)]	Severe [*n* (%)]			
GG	34 (34.34)	5 (15.15)	11.71	0.003*	1.00
AG	44 (44.44)	11 (33.33)			1.70 (0.54–5.36)
AA	21 (21.21)	17 (51.52)			5.51 (1.77–17.14)
AG + AA/GG	65 (65.66)	28 (84.84)	4.38	0.036*	2.93 (1.04–8.27)
GG + AG/AA	78 (78.79)	16 (48.48)	11.09	<0.001*	0.25 (0.11–0.58)

SNP, single nucleotide polymorphism; OR, odds ratio; 95% CI, 95% confidence interval.
*Statistically significant ($P < 0.05$).

TABLE 8 Haplotype frequencies of *IL-18* gene in patients with mild-to-moderate and severe AD.

Haplotypes (rs187238, rs360718, rs7106524)	AD patients [*n* (%)]		χ^2	*P* value	OR (95%CI)
	Mild-to-Moderate	Severe			
CAG	83 (41.92)	16 (24.24)	-	-	1.00
CAA	78 (39.39)	43 (65.15)	10.42	0.001*	2.86 (1.49–5.49)
GCG	10 (5.05)	2 (3.03)	<0.01	1.000	1.04 (0.21–5.19)

OR, odds ratio; 95% CI, 95% confidence interval.
*Statistically significant ($P < 0.05$); Haplotypes with the frequencies under 0.05 were not included in haplotype analysis.

In this case-control study, the results demonstrated the association of *IL-4* gene polymorphisms with the susceptibility to AD in Chinese Han children. The data showed that the mutant G allele, CG genotype and CG + GG genotype of *IL-4* rs2243283 were associated with a significantly reduced risk of AD. We also found a correlation between *IL-4*/GTT haplotype composed of rs2243283, rs2243250, rs2243248 and lower AD risk. As reported, rs2243283 gene variants have been confirmed to correlate to some chronic inflammatory and immune diseases, such as asthma, chronic periodontitis, and autoimmune hepatitis (22). However, as we know, rare studies focused on the linkage of this SNP with AD. Therefore, our data might provide a new risk predictor for estimating AD predisposition. Except for rs2243283, the other two SNPs of *IL-4* had no relationship with AD in the present study. *IL-4* rs2243250 (−590C/T) is a common locus in researches on the association of *IL-4* gene polymorphisms with AD. But the findings regarding the correlation between *IL-4* rs2243250 and AD susceptibility are controversial. Consistent with our results were the investigations conducted in the Saudi and Macedonian pediatric population (18, 19). Inconsistent with our data were the surveys carried out among Czech children and another subset of Chinese pediatric participants (28, 29). Chinese academic Shang H reported that the 590 T and 589 T alleles may be related to the increased risk of AD, based on a case-control study that enrolled 82 AD patients and 100 healthy controls (29). Whether the discrepancy between our data and the above result is due to different sample sizes remains to be clarified by further investigations with larger numbers of participants. The contradictions in these findings also might be attributed to different genetic backgrounds and environments (30). The larger studies in populations with the same ethnic background are needed to confirm or refute these results. Additionally, no link of *IL-4* genetic polymorphisms to AD severity was found in this study. With the exception of one report published in 2002 that indicated the *IL-4* 590 T allele was associated with the severity of AD (31), several researches in recent years showed no relevance between *IL-4* rs2243250 and AD severity (29, 30).

Besides the etiology diagnosis of AD, studies on prediction of the AD severity remains challenging. Several inflammation-related gene polymorphisms are attached with the severity of AD and could be used to predict potential severity (16, 32, 33). IL-18 is a glycoprotein encoded by the *IL-18* gene, which has been mapped to chromosome 11q22.2-q22.3 (34). And its length is approximately 21.61 kb (34). Although serum level of IL-18 was regarded as a possible biomarker for the severity of AD (35), there was few publications so far on the association between *IL-18* genetic variations and AD severity. The present study was

conducted for the first time in Chinese Han children and revealed the relation of *IL-18* polymorphisms to AD severity. Our data explored that A allele, AA genotype and AG + AA genotype of *IL-18* rs7106524, as well as *IL-18*/CAA haplotype consisting of rs187238, rs360718 and rs7106524 were associated with a high risk of severe AD, suggesting the genetic polymorphisms of *IL-18* rs7106524 might be used as potential predictors of AD severity. Consequently, the results may be useful in making appropriate therapy recommendations and preventing dermatitis development. Nevertheless, the functions of the investigated polymorphisms are still not well elucidated, so further studies are still needed to explore the potential molecular mechanisms underlying the association between *IL-18* rs7106524 polymorphism and AD severity.

In addition, no linkage between *IL-18* genetic polymorphisms and susceptibility to AD was found, inconsistent with several previous investigations. For example, the merged quantitative analysis in a recent meta-analysis study displayed that *IL-18* rs187238 polymorphisms might affect the risk of AD in overall population (36). This discrepancy between studies might still be due to the sample size and ethnicity. Future multicenter studies with a large sample size will be carried out to further explore the relationship between genetic variation in cytokines and AD. Besides, whether nucleotide polymorphisms in *IL-4* and *IL-18* genes affect alterations in amino acid sequences and protein secondary structure, and whether they subsequently influence expression levels and protein functions, deserve deeper consideration and require prospective work to elucidate. Perhaps, in-depth cell-specific transcriptomic investigation will guide better understanding of cellular impact and underlying mechanisms of the IL-4 and IL-18 signaling pathways, and then lead to better drug targets for AD treatment.

5. Conclusion

In summary, the results of the current study revealed that the CG genotype of *IL-4* rs2243283 and the *IL-4*/GTT haplotype confer the decreased susceptibility to AD in Chinese pediatric population. And *IL-18* rs7106524 AA genotype and the *IL-18*/CAA haplotype might serve as predictors of high risk for severe AD in Chinese children.

Data availability statement

The data presented in the study are deposited in the figshare repository, accession number https://doi.org/10.6084/m9.figshare.22776002.v1.

Ethics statement

The studies involving human participants were reviewed and approved by Institutional Ethics Committee of the Children's Hospital, Zhejiang University School of Medicine. Written informed consent to participate in this study was provided by the participants' legal guardian/next of kin.

Author contributions

JS and LH completed the experimental part of the study, performed data analysis and interpretation, drafted the manuscript. HZ, WL, and RT contributed to the study conception and design. HZ and YL collected patients' information. RT supervised the entire study and provided academic guidance throughout the study process. All authors contributed to the article and approved the submitted version.

Funding

This work was supported by Zhejiang Provincial Natural Science Foundation of China (LY21H040002) and Zhejiang Province Research Project of Public Welfare Technology Application (LGF22H110001).

Acknowledgments

We thank all the participants and staffs who help us in the process of this study.

Conflict of interest

The authors declare that the research was conducted in the absence of any commercial or financial relationships that could be construed as a potential conflict of interest.

Publisher's note

References

1. Langan SM, Irvine AD, Weidinger S. Atopic dermatitis. *Lancet*. (2020) 396 (10247):345–60. doi: 10.1016/S0140-6736(20)31286-1

2. Ramirez FD, Chen S, Langan SM, Prather AA, McCulloch CE, Kidd SA, et al. Assessment of sleep disturbances and exhaustion in mothers of children with atopic dermatitis. *JAMA Dermatol*. (2019) 155(5):556–63. doi: 10.1001/jamadermatol.2018.5641

3. Wang HN, Ji K, Zhang LN, Xie CC, Li WY, Zhao ZF, et al. Inhibition of c-fos expression attenuates IgE-mediated mast cell activation and allergic inflammation

by counteracting an inhibitory AP1/Egr1/IL-4 axis. *J Transl Med*. (2021) 19(1):261. doi: 10.1186/s12967-021-02932-0

4. Liang Y, Chang C, Lu Q. The genetics and epigenetics of atopic dermatitis-filaggrin and other polymorphisms. *Clin Rev Allergy Immunol*. (2016) 51(3):315–28. doi: 10.1007/s12016-015-8508-5

5. Piazza S, Fumagalli M, Martinelli G, Pozzoli C, Maranta N, Angarano M, et al. Hydrolyzable tannins in the management of Th1, Th2 and Th17 inflammatory-related diseases. *Molecules*. (2022) 27(21):7593. doi: 10.3390/molecules27217593

6. Chiricozzi A, Maurelli M, Peris K, Girolomoni G. Targeting IL-4 for the treatment of atopic dermatitis. *Immunotargets Ther*. (2020) 9:151–6. doi: 10.2147/ITT.S260370

7. Pelly VS, Kannan Y, Coomes SM, Entwistle LJ, Rückerl D, Seddon B, et al. IL-4-producing ILC2s are required for the differentiation of TH2 cells following heligmosomoides polygyrus infection. *Mucosal Immunol*. (2016) 9(6):1407–17. doi: 10.1038/mi.2016.4

8. Tsuji G, Hashimoto-Hachiya A, Kiyomatsu-Oda M, Takemura M, Ohno F, Ito T, et al. Aryl hydrocarbon receptor activation restores filaggrin expression via OVOL1 in atopic dermatitis. *Cell Death Dis*. (2017) 8(7):e2931. doi: 10.1038/cddis.2017.322

9. Oetjen LK, Mack MR, Feng J, Whelan TM, Niu H, Guo CJ, et al. Sensory neurons co-opt classical immune signaling pathways to mediate chronic itch. *Cell*. (2017) 171 (1):217–28. doi: 10.1016/j.cell.2017.08.006

10. Teraki Y, Hotta T, Shiohara T. Increased circulating skin-homing cutaneous lymphocyte-associated antigen (CLA)+ type 2 cytokine-producing cells, and decreased CLA+ type 1 cytokine-producing cells in atopic dermatitis. *Br J Dermatol*. (2000) 143(2):373–8. doi: 10.1046/j.1365-2133.2000.03665.x

11. Lee JH, Cho DH, Park HJ. IL-18 and cutaneous inflammatory diseases. *Int J Mol Sci*. (2015) 16(12):29357–69. doi: 10.3390/ijms161226172

12. Zedan K, Rasheed Z, Farouk Y, Alzolibani AA, Bin Saif G, Ismail HA, et al. Immunoglobulin e, interleukin-18 and interleukin-12 in patients with atopic dermatitis: correlation with disease activity. *J Clin Diagn Res*. (2015) 9(4):WC01-5. doi: 10.7860/JCDR/2015/12261.5742

13. Tanaka T, Tsutsui H, Yoshimoto T, Kotani M, Matsumoto M, Fujita A, et al. Interleukin-18 is elevated in the sera from patients with atopic dermatitis and from atopic dermatitis model mice, NC/Nga. *Int Arch Allergy Immunol*. (2001) 125 (3):236–40. doi: 10.1159/000053821

14. Chen JL, Niu XL, Gao YL, Ma L, Gao XH, Chen HD, et al. IL-18 knockout alleviates atopic dermatitis-like skin lesions induced by MC903 in a mouse model. *Int J Mol Med*. (2020) 46(2):880–8. doi: 10.3892/ijmm.2020.4630

15. Babusikova E, Jurecekova J, Jesenak M, Evinova A. Association of gene polymorphisms in interleukin 6 in infantile bronchial asthma. *Arch Bronconeumol*. (2017) 53(7):381–6. doi: 10.1016/j.arbres.2016.09.012

16. Shi J, He L, Tao R, Zheng H, Li W, Huang S, et al. TLR4 Polymorphisms as potential predictors of atopic dermatitis in Chinese Han children. *J Clin Lab Anal*. (2022) 36:e24385. doi: 10.1002/jcla.24385

17. Bin L, Leung DY. Genetic and epigenetic studies of atopic dermatitis. *Allergy Asthma Clin Immunol*. (2016) 12:52. doi: 10.1186/s13223-016-0158-5

18. Stavric K, Peova S, Trajkov D, Spiroski M. Gene polymorphisms of 22 cytokines in Macedonian children with atopic dermatitis. *Iran J Allergy Asthma Immunol*. (2012) 11(1):37–50.

19. Hussein YM, Alzahrani SS, Alharthi AA, Alhazmi AS, Ghonaim MM, Alghamdy AA, et al. Gene polymorphism of interleukin-4, interleukin-4 receptor and STAT6 in children with atopic dermatitis in taif, Saudi Arabia. *Immunol Invest*. (2016) 45 (3):223–34. doi: 10.3109/08820139.2015.1135943

20. Ibrahim GH, ElTabbakh MT, Gomaa AH, Mohamed EA. Interleukin-18 gene polymorphisms in Egyptian patients with allergic diseases. *Am J Rhinol Allergy*. (2012) 26(5):385–9. doi: 10.2500/ajra.2012.26.3806

21. Gao SJ, Zhang L, Lu W, Wang L, Chen L, Zhu Z, et al. Interleukin-18 genetic polymorphisms contribute differentially to the susceptibility to crohn's disease. *World J Gastroenterol*. (2015) 21(28):8711–22. doi: 10.3748/wjg.v21.i28.8711

22. Jin T, Zhang Y, Sun Y, Wu J, Xiong Z, Yang Z. IL-4 gene polymorphisms and their relation to steroid-induced osteonecrosis of the femoral head in Chinese population. *Mol Genet Genomic Med*. (2019) 7(3):e563. doi: 10.1002/mgg3.563

23. Al-Naseri MA, Salman ED, Ad'Hiah AH. Association between interleukin-4 and interleukin-10 single nucleotide polymorphisms and multiple sclerosis among Iraqi patients. *Neurol Sci*. (2019) 40(11):2383–9. doi: 10.1007/s10072-019-04000-4

24. Yao X, Song ZQ, Li W, Liang YS, Zhao Y, Cao H, et al. Guidelines for diagnosis and treatment of atopic dermatitis in China (2020). *Int J Dermatol Venereol*. (2021) 4 (1):1–9. doi: 10.1097/JD9.0000000000000143

25. Chen K, Zhou YX, Li K, Qi LX, Zhang QF, Wang MC, et al. A novel three-round multiplex PCR for SNP genotyping with next generation sequencing. *Anal Bioanal Chem*. (2016) 408(16):4371–7. doi: 10.1007/s00216-016-9536-6

26. Silverberg JI. Public health burden and epidemiology of atopic dermatitis. *Dermatol Clin*. (2017) 35(3):283–9. doi: 10.1016/j.det.2017.02.002

27. Tracy A, Bhatti S, Eichenfield LF. Update on pediatric atopic dermatitis. *Cutis*. (2020) 106(3):143–6. doi: 10.12788/cutis.0077

28. Kayserova J, Sismova K, Zentsova-Jaresova I, Katina S, Vernerova E, Polouckova A, et al. A prospective study in children with a severe form of atopic dermatitis: clinical outcome in relation to cytokine gene polymorphisms. *J Investig Allergol Clin Immunol*. (2012) 22(2):92–101.

29. Shang H, Cao XL, Wan YJ, Meng J, Guo LH. IL-4 Gene polymorphism may contribute to an increased risk of atopic dermatitis in children. *Dis Markers*. (2016) 2016:1021942. doi: 10.1155/2016/1021942

30. Liang J, Liu Y, Xue R, Chen L, Chen H, Shao L, et al. Interleukin 4 -590C/T (rs2243250) polymorphism is associated with increased risk of atopic dermatitis: meta-analysis of case-control studies. *Dermatitis*. (2017) 28(2):144–51. doi: 10.1097/DER.0000000000000265

31. Söderhäll C, Bradley M, Kockum I, Luthman H, Wahlgren CF, Nordenskjöld M. Analysis of association and linkage for the interleukin-4 and interleukin-4 receptor b; alpha; regions in Swedish atopic dermatitis families. *Clin Exp Allergy*. (2002) 32 (8):1199–202. doi: 10.1046/j.1365-2745.2002.01452.x

32. Gleń J, Trzeciak M, Sobjanek M, Bandurski T, Wilkowska A, Nedoszytko B, et al. Interleukin-13 promoter gene polymorphism -1112 C/T is associated with atopic dermatitis in Polish patients. *Acta Dermatovenerol Croat*. (2012) 20(4):231–8.

33. Wilkowska A, Gleń J, Zabłotna M, Trzeciak M, Ryduchowska M, Sobjanek M, et al. The association of GM-CSF -677A/C promoter gene polymorphism with the occurrence and severity of atopic dermatitis in a Polish population. *Int J Dermatol*. (2014) 53(3):e172–4. doi: 10.1111/ijd.12245

34. Al-Shobaili HA, Ahmed AA, Alnomair N, Alobead ZA, Rasheed Z. Molecular genetic of atopic dermatitis: an update. *Int J Health Sci (Qassim)*. (2016) 10(1):96–120.

35. Thijs J, Krastev T, Weidinger S, Buckens CF, de Bruin-Weller M, Bruijnzeel-Koomen C, et al. Biomarkers for atopic dermatitis: a systematic review and meta-analysis. *Curr Opin Allergy Clin Immunol*. (2015) 15(5):453–60. doi: 10.1097/ACI.0000000000000198

36. Han L, Lu S, Ning H. The risk of atopic dermatitis may be affected by IL-1B +3954 C/T and IL-18 -137G/C polymorphisms: evidence from a meta-analysis. *Postepy Dermatol Alergol*. (2021) 38(5):808–14. doi: 10.5114/ada.2020.95956

frontiers | Frontiers in Genetics

TYPE Original Research
PUBLISHED 08 June 2023
DOI 10.3389/fgene.2023.1204296

OPEN ACCESS

EDITED BY
Jordi Pérez-Tur,
Spanish National Research Council (CSIC), Spain

REVIEWED BY
Ewelina Bukowska-Olech,
Poznan University of Medical Sciences, Poland
Martin Lowe,
The University of Manchester, United Kingdom
Ayano Satoh,
Okayama University, Japan

*CORRESPONDENCE
Roy Morello,
rmorello@uams.edu

RECEIVED 12 April 2023
ACCEPTED 25 May 2023
PUBLISHED 08 June 2023

CITATION
Dimori M, Pokrovskaya ID, Liu S, Sherrill JT, Gomez-Acevedo H, Fu Q, Storrie B, Lupashin VV and Morello R (2023), A *Rab33b* missense mouse model for Smith-McCort dysplasia shows bone resorption defects and altered protein glycosylation.
Front. Genet. 14:1204296.
doi: 10.3389/fgene.2023.1204296

A *Rab33b* missense mouse model for Smith-McCort dysplasia shows bone resorption defects and altered protein glycosylation

Milena Dimori[1], Irina D. Pokrovskaya[1], Shijie Liu[1], John T. Sherrill[2], Horacio Gomez-Acevedo[3], Qiang Fu[4], Brian Storrie[1], Vladimir V. Lupashin[1] and Roy Morello[1,2,5]*

[1]Department of Physiology and Cell Biology, University of Arkansas for Medical Sciences, Little Rock, AR, United States, [2]Department of Orthopaedic Surgery, University of Arkansas for Medical Sciences, Little Rock, AR, United States, [3]Department of Biomedical Informatics, University of Arkansas for Medical Sciences, Little Rock, AR, United States, [4]Department of Internal Medicine, Division of Endocrinology, University of Arkansas for Medical Sciences, Little Rock, AR, United States, [5]Division of Genetics, University of Arkansas for Medical Sciences, Little Rock, AR, United States

Smith McCort (SMC) dysplasia is a rare, autosomal recessive, osteochondrodysplasia that can be caused by pathogenic variants in either *RAB33B* or *DYM* genes. These genes codes for proteins that are located at the Golgi apparatus and have a role in intracellular vesicle trafficking. We generated mice that carry a *Rab33b* disease-causing variant, c.136A>C (p.Lys46Gln), which is identical to that of members from a consanguineous family diagnosed with SMC. In male mice at 4 months of age, the *Rab33b* variant caused a mild increase in trabecular bone thickness in the spine and femur and in femoral mid-shaft cortical thickness with a concomitant reduction of the femoral medullary area, suggesting a bone resorption defect. In spite of the increase in trabecular and cortical thickness, bone histomorphometry showed a 4-fold increase in osteoclast parameters in homozygous *Rab33b* mice suggesting a putative impairment in osteoclast function, while dynamic parameters of bone formation were similar in mutant *versus* control mice. Femur biomechanical tests showed an increased in yield load and a progressive elevation, from WT to heterozygote to homozygous mutants, of bone intrinsic properties. These findings suggest an overall impact on bone material properties which may be caused by disturbed protein glycosylation in cells contributing to skeletal formation, supported by the altered and variable pattern of lectin staining in murine and human tissue cultured cells and in liver and bone murine tissues. The mouse model only reproduced some of the features of the human disease and was sex-specific, manifesting in male but not female mice. Our data reveal a potential novel role of RAB33B in osteoclast function and protein glycosylation and their dysregulation in SMC and lay the foundation for future studies.

KEYWORDS

Smith-McCort dysplasia, RAB33B, GTPases, bone, Golgi, glycosylation

Introduction

Smith-McCort (SMC) dysplasia and Dyggve-Melchior-Clausen (DMC) dysplasia are similar, rare, autosomal recessive, osteochondrodysplasias that share identical radiologic features and cartilage histology (Kaufman et al., 1971; Beighton, 1990; Nakamura et al., 1997; Neumann et al., 2006). Skeletal defects present after birth, usually between 18 and 48 months of age, and are progressive resulting in significant deformities (Tuysuz et al., 2021). Typical features of the disease are short trunk dwarfism with barrel-shaped chest, short neck, double-humped vertebral bodies, platyspondyly, and lacy iliac crests, which can be accompanied by additional defects such as genu valgum, brachydactyly, joint contractures and others (Tuysuz et al., 2021). DMC patients can be distinguished from SMC patients by the presence of intellectual disability and coarse facies (Nakamura et al., 1997; Burns et al., 2003; Dupuis et al., 2015). The first genetic locus for Smith-McCort dysplasia (SMC1) was identified on chromosome 18q21 and associated with homozygous or compound heterozygous pathogenic variants in the *DYM* gene (encoding Dymeclin) (Cohn et al., 2003). Pathogenic variants in the same gene also cause Dyggve-Melchior-Clausen disease, making SMC and DMC allelic disorders (Ehtesham et al., 2002; El Ghouzzi et al., 2003). Dymeclin is a poorly characterized intracellular protein involved in Golgi organization, intracellular vesicle trafficking, and the accumulation of extracellular cell surface collagens (Osipovich et al., 2008; Denais et al., 2011; Dupuis et al., 2015). A second locus for Smith-McCort dysplasia (SMC2) was identified on chromosome 4q31 (Alshammari et al., 2012; Dupuis et al., 2013). SMC2 is caused by homozygous or compound heterozygous pathogenic variants in the *RAB33B* gene, which encodes a small GTP-binding protein within the large superfamily of small GTPases. These enzymes function as molecular switches and regulate a variety of cellular processes by transducing intracellular information and alternating between an active GTP-bound and an inactive GDP-bound state (Cherfils and Zeghouf, 2013). RAB proteins perform their regulatory function by recruiting a variety of effectors to mediate different functions in membrane transport, including vesicle trafficking, docking and fusion (Hutagalung and Novick, 2011; Morgan et al., 2019; Roy and Roux, 2020). RAB33B localizes to the medial Golgi apparatus (Zheng et al., 1998; Starr et al., 2010; Pusapati et al., 2012; Morgan et al., 2019), and its depletion using siRNA resulted in a significantly increased number of Golgi-associated vesicles per stack, suggesting a functional role of the protein in vesicle trafficking at the Golgi apparatus level (Starr et al., 2010). RAB33B is also involved in membrane fusion events, e.g., between autophagosomes and lysosomes (Itoh et al., 2008) and in post-Golgi vesicular trafficking to the plasma membrane, and in particular in delivering β1 integrin cargo for the formation of focal cell contacts with the extracellular matrix (Bjornestad et al., 2022). A close paralog of *RAB33B* is *RAB33A*; while these two genes appear to co-regulate aspects of CNS development, *RAB33A* expression seems to be primarily restricted to the CNS while *RAB33B* is expressed in several tissues (Cheng et al., 2006; Huang et al., 2019). Thus, disease-causing variants in either *RAB33B* or *DYM* appear to affect the Golgi apparatus, the central organelle that coordinates protein processing, glycosylation and secretion. Because of the importance of the extracellular matrix (ECM) and of secreted growth/signaling factors during skeletal formation, development and homeostasis, we hypothesized that the underlying disease mechanism in SMC may be associated with defective Golgi-dependent protein processing/glycosylation leading to skeletal defects. However, the molecular connection between *RAB33B* genetic alterations and defects in skeletal development is unknown. We generated mice that carry a *Rab33b* missense disease-causing variant identical to that described in a consanguineous family where multiple members were diagnosed with SMC (Alshammari et al., 2012). To characterize the phenotype of this new mouse model, we performed a variety of *ex-vivo* and *in vitro* assays, including dual X-ray absorptiometry (DEXA) and micro-computed tomography (μCT) at 6 weeks (young) and 4 months (mature) of age in male and female mice, in addition to bone histology/histomorphometry, X-ray imaging, biomechanical tests, and lectin staining of cell and tissue sections. Our results indicate a mild phenotype consistent with osteoclast defective bone resorption and altered protein glycosylation with an impact on bone material properties.

Methods

Mouse generation, genotyping and ethic statement

The University of Arkansas for Medical Sciences (UAMS) IACUC committee approved all animal procedures performed in this study, which were conducted in accordance with local, State and US Federal regulations. Mice were housed in ventilated cages in a pathogen free facility at 22°C, in a 12-h light/dark cycle, and supplied with water and standard chow at libitum. The Rab33b p.Lys46Gln (NM_031296:c.136A>C) missense pathogenic variant was knocked into the mouse genome using a CRISPR/Cas9 approach by the local UAMS Transgenic Core facility; a few silent nucleotide changes upstream of the mutation were also introduced to facilitate mouse genotyping (see Figure 1). Four founder mice were obtained and bred with a C57B6 mate purchased from the JAX labs. Offspring were genotyped by PCR and the region of interest was sequenced (Sanger). Two males and two females (F1) were confirmed to be heterozygous for the desired mutation and were bred to generate heterozygous, homozygous mutant (*Rab33b*$^{A136C/A136C}$) and wild-type mice for the study. PCR genotyping was performed with the GoTaq G2 Hot Start Polymerase reagent (cat# M7423 Promega) using a Master Cycler thermocycler (Eppendorf). An example gel image of the genotyping results is shown in Figure 1B. For primer sequences and PCR conditions, please see Supplementary Material S1. The skeletal phenotype of male and female mice was analyzed at 6 weeks and at 4 months of age. Mouse body weights were obtained at each time points before tissue harvest.

Cell culture and RNA interference

Primary calvarial osteoblasts were obtained from 3–5 days old pups as previously described (Morello et al., 2006) and were grown in Alpha-MEM, supplemented with 10% Fetal Bovine Serum (FBS), L-Glutamine (2 mM), 100 unit/ml penicillin, and 100 mg/ml streptomycin. Briefly, calvariae were dissected, washed in sterile

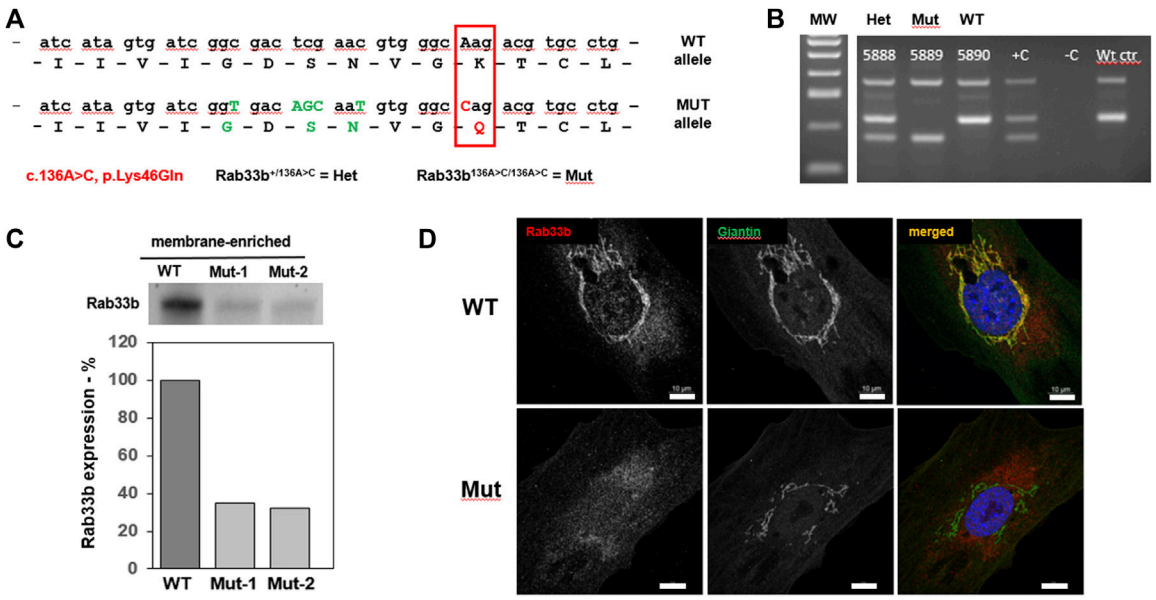

FIGURE 1
Generation of a new mouse model for SMC. **(A)**. Diagram of the partial nucleotide and amino acidic sequence of RAB33B indicating the c.136A>C (p.Lys46Gln) disease-causing variant (red box) introduced in the mutant allele as well as the upstream silent nucleotide changes shown in green fonts. Henceforth, mice carrying one mutant allele will be referred to as Het while homozygous mice will be referred to Mut. **(B)**. Example of a genotyping gel, including positive and negative control samples. **(C)**. Western Blot using a RAB33B antibody on membrane-enriched lysates of freshly dissected adult liver from 1 wild-type (WT) and 2 *Rab33b* mutant mice, separated by SDS-PAGE. Relative quantification of the bands is shown below the stained membrane. **(D)**. Immunofluorescence staining of RAB33B (red) and the Golgi marker Giantin (green) on primary calvarial osteoblasts. Scale bars = 10 µm.

PBS 3 times and digested with Collagenase P (1 mg/ml) in a 6-well plate for 20 min at 37°C with vigorous shaking every 5 min. After 20 min the medium was removed, and the digestion step was repeated. Then 1 ml of digestion media with double amount of collagenase was added and each calvaria was finely minced with sterile scissors, incubated for 1 h at 37°C, with vigorous shaking every 5–10 min. Alpha-MEM with 15% FBS complete medium (3.75 ml) was then added until the next day. Cells were then re-suspended with a pipette and allowed to attach to the plate for 4–6 h. Finally, the wells were washed twice with sterile PBS, 2 ml of culture medium was added to each well and the cells were grown for 24–48 h. HeLa cells stably expressing Golgi enzyme GalNAcT2-GFP were cultured in DMEM supplemented with 10% fetal bovine serum (FBS) and 0.45 mg/ml of Geneticin in a humidified incubator at 37°C and 5% CO2. siRNA directed against Rab33b has been described previously (Starr et al., 2010). Control siRNA was siControl, non-targeting siRNA (UAGCGACUAAACACAUCA A). All siRNAs were manufactured by Dharmacon RNA Technologies. siRNA duplexes were transfected at a final concentration of 200 nM using Oligofectamine (Invitrogen) according to the manufacturer's protocol with minor modifications. In brief, ~70,000 HeLa cells stably expressing GalNAcT2-GFP were seeded per 35 mm tissue culture dish containing 12 mm diameter coverslips (Fisher Scientific). Cells were cultured overnight and then transfected with the corresponding siRNA in the absence of FBS. To achieve maximal knockdown, second cycle of siRNA transfection was performed 24 h after the initial transfection. 96 h after the first transfection cycle, cells were fixed with 1% paraformaldehyde for immunofluorescence staining (300 cells counted and mean pixel intensity averaged) or lysed for Western blotting to determine Rab33B protein knockdown level. For the osteoclastogenesis assay, please see Supplementary Material S1

Western blot, immunofluorescence, and lectin staining

HeLa cells were lysed in 2% SDS, followed by standard SDS–PAGE (~12% acrylamide) and Western blotting. Antibodies used for Western blotting (WB) were anti-Rab33B (Frontier Institute, Clone D5) and anti-α-tubulin (Sigma-Aldrich). The blots were scanned and analyzed with an Odyssey Infrared Imaging System (LICOR Biosciences). HeLa cells stably expressing GalNAcT2-GFP were transfected with corresponding siRNA as described above, and then fixed with 1% paraformaldehyde and blocked with 0.1% BSA in PBS. Cells were incubated for 30 min with Alexa Fluor 555 conjugated WGA lectin or Alexa Fluor 488 conjugated GSII lectin diluted in PBS. Confocal image stacks were taken for the analysis of Rab33B and GalNAcT2-GFP distribution, while wide-field images were captured for surface lectin distribution. Both wide-field images and confocal image stacks were collected with a 63x/1.40 numerical aperture objective and a Zeiss 200M inverted microscope. Confocal image stacks were produced with a BD CARV II spinning disk confocal accessory mounted on the microscope. Images were processed with iVision-MAC software.

Preparation of mouse tissue and cell lysates and WB analysis was done as described earlier (Sumya et al., 2021). Please also see

Supplementary Material S1. For WB analysis 10–20 µg of protein was loaded into Genescript (8%–16%) gradient gel. Proteins were transferred onto nitrocellulose membrane using the Thermo Scientific Pierce G2 Fast Blotter. Membranes were washed in PBS, blocked in Odyssey blocking buffer (LI-COR) for 20 min, and incubated with primary antibodies rRab33 (Santa Cruz, 1:500) or lectin Helix Pomatia Agglutinin (HPA)-Alexa 647 (Thermo Fisher, 1:1000) for 1 h at room temperature or overnight at 4°C. Membranes were washed with PBS and incubated with secondary fluorescently-tagged antibodies (Alexa Fluor 647 Donkey anti-mouse, Jackson Immuno Research/705605–151, 1:8000) diluted in Odyssey blocking buffer for 1 h. Blots were then washed with PBS and imaged using the Odyssey Imaging System. Images were processed using the LI-COR Image Studio software.

Super-resolution AiryScan fluorescent microscopy

Immunofluorescence microscopy was done using the previous protocol (Willett et al., 2013) with some additional modifications. Briefly, primary mouse osteoblasts grown on 12-mm round coverslips to 80%–90% confluence were fixed with paraformaldehyde (PFA, freshly made from 16% stock solution) diluted in phosphate-buffered saline (PBS) for 15 min at room temperature. For the lectin staining, 1% PFA was used for fixation, followed by incubations with 50 mM ammonium chloride for 5 min and two incubations in the blocking buffer (0.1% BSA in PBS). After that, cells were incubated with HPA-647 diluted in blocking buffer for 30 min. For the antibody staining cells were fixed with 4% PFA, treated with 50 mM ammonium chloride (5 min), and permeabilized with 0.1% Triton X-100 (1 min) followed by two incubations with the blocking buffer. After 45 min incubation with primary antibodies: Giantin (Covance PRB-114C rabbit 1:100 and rRab33b (Frontier Institute Clone D5, mouse 1:30, diluted in the antibody buffer (1% cold fish gelatin, 0.1% saponin in PBS), cells were washed three times in PBS and incubated with fluorescently conjugated secondary antibodies diluted in antibody buffer for 30 min. Cells were washed four times with PBS, then coverslips were dipped in PBS and water 10 times each and mounted on glass microscope slides using Prolong® Gold antifade reagent (Life Technologies). Cells were imaged with a 63 × oil 1.4 numerical aperture (NA) objective of an LSM880 Zeiss Laser inverted microscope with Airyscan using ZEN software. Labeling of unmasked paraffin sections with fluorescently labeled lectins (HPA-647, 1:500, Wheat Germ Agglutinin-Rhodamine Red, 1: 500, GNL-Alexa 647 1:500) was performed as above.

Dual-energy X-ray absorptiometry and digital X-ray imaging

A DEXA scanner (PIXIMUS2, Lunar, Madison, WI) was used after sacrifice to determine the femur, lumbar spine, and whole body bone mineral content (BMC) and bone mineral density (BMD) in 6 weeks and 4 months old mice, according to standard procedures. One full scan per mouse was performed and analyzed with PIXImus software 2.1 (GE/Lunar). The head and the neck were excluded from whole body calculations by drawing a ROI. The PIXImus was calibrated with a phantom (corresponding to bone mineral density = 0.0622 g/cm2 and 11.3% fat) on each day of testing according to the manufacturer's instructions.

The skeleton of a select group of mice, including both male and females mice at different age, was also digitally X-ray imaged using an UltraFocus Faxitron instrument (Hologic).

Micro-computed tomography

Femurs and lumbar spines were dissected from male and female mice at 6 weeks and 4 months of age and fixed in 95% ethanol (excluding the 4 months old femurs that were frozen instead for biomechanical assessment). Femur lengths were measured using a digital caliper. Micro-CT analysis was performed on a MicroCT 40 (Scanco Medical AG, Bassersdorf, Switzerland) using a 12 µm isotropic voxel size. For details, please see Supplementary Material S1 Bone trabecular and cortical parameters were determined as described (Suva et al., 2008). Standard nomenclature guidelines were followed to report all micro-CT measurements (Bouxsein et al., 2010).

Biomechanics

Femurs from 4 months old male mice were harvested, wrapped in saline-soaked gauze and frozen at −20. Bones were allowed to thaw for at least 2 h at room temperature before micro-CT scanning. After micro-CT scanning, these same femurs were tested in a 3-point bending test using an ElectroForce 5500 Test Instrument (TA Instruments, Delaware, United Stataes) with a ramp rate of 0.05 mm/s and support span of 8 mm, and running WinTest software version 8.2. Moment of Inertia (MOI) values were derived from micro-CT scans of the same femur. Load-displacement curves were generated for each sample and representative curves are shown in Figure 7B. Structural properties of stiffness, yield and maximum load, post-yield displacement and work-to-fracture were calculated for each sample. Material properties of Young's Modulus, yield and maximum stress, were also calculated for each sample.

Histology and histomorphometry

For the assessment of the epiphyseal growth plate and measurement of the bone formation rate, mice were injected by i.p. with 30 mg/kg Alizarin red (alizarin-3-methyliminodiacetic acid, Sigma cat: A3882) and calcein (Sigma cat: C0875) dyes at 6 and 2 days before sacrifice, for the 6 weeks old mice, and at 7 and 2 days before sacrifice for the 4 months old mice. Right legs and lumbar spines were collected, fixed in Millonig's solution overnight, and dehydrated in graded series of increasingly concentrated ethanol before embedding in methyl-methacrylate according to standard procedure (Gruenwald et al., 2014). Serial, coronal, 5 µm thick sections through the center of the vertebral body of L3 and L4 were generated and the entire cancellous bone area of L4 was analyzed. Sections were stained with Tartrate-resistant acid

phosphatase (TRAP) and counterstained with Fast Green for counting osteoclast parameters. Unstained sections were used for fluorescent double label analysis and calculation of dynamic parameters of bone formation using a Nikon Eclipse E400 microscope equipped with fluorescent light, an Olympus DP73 camera and OsteoMeasure7 software (OsteoMetrics, Inc.). The abbreviations recommended by the American Society for Bone and Mineral Research Histomorphometric Nomenclature Committee (Dempster et al., 2013).

Statistical analysis

Among the genotype groups, statistical comparisons for DEXA, micro-computed tomography and biomechanics were performed with one-way ANOVA when normality (Shapiro's test) and homogeneity of variance (Levene's test) were below 0.05 level of statistical significance. Otherwise, non-parametric test (Krustal-Wallis) were used. Post-hoc analysis was performed (Dunn's test) for comparisons below 0.05 level of statistical significance, and *p*-values were adjusted for multiple comparisons.

Results

Generation of a mouse model to study SMC

To study the role of RAB33B in the skeleton we generated mice that carry a *Rab33b* missense pathogenic variant, c.136A>C (p.Lys46Gln), which was identified in members of a consanguineous family diagnosed with SMC (Alshammari et al., 2012). This variant replaces a highly conserved lysine within the GxxxxGK [S/T] guanine nucleotide-binding GTPase domain of RAB33B with a glutamine residue and in humans causes substantial protein loss in affected individuals (Alshammari et al., 2012). Using a CRISPR/Cas9 approach, we introduced the mutation into the mouse genome together with a few silent nucleotide changes just upstream of the Lysine 46 coding triplet, which were introduced to facilitate mouse genotyping (Figure 1). Four founder mice were generated and each of them was bred with a C57B6 mate. Offspring from each mating pair was genotyped by PCR and then the region of interest was sequenced (Sanger). Two males and two females (F1) were confirmed to be heterozygous for the desired mutation and were crossed to generate homozygous mice (Figure 1B). Homozygous $Rab33b^{A136C/A136C}$ mice were born at the expected Mendelian ratio and did not show macroscopic differences compared to their WT or heterozygous littermates.

Effects of the *Rab33b* p.Lys46Gln disease variant at the cellular level

To study the effects of the p.Lys46Gln pathogenic variant on the level of expression of RAB33B protein, we collected livers from homozygous mutant and WT adult mice and performed Western blot analysis. The liver provides a ready source for a membrane-enriched preparation that makes it easier to detect membrane-associated proteins that are not expressed at high levels such as RAB33B. Western blot showed 40%–60% reduction of the RAB33B protein in homozygous mutant livers compared to a WT control, suggesting that the p.Lys46Gln variant has a hypomorphic effect and does not result in complete loss of protein expression in the mouse model (Figure 1C). See also Supplementary Figure S1 for a total liver lysate. This observation was confirmed using immunofluorescence on primary calvarial osteoblasts. In these cells we observed co-localization of the RAB33B protein with the Golgi marker Giantin in WT control cells but levels of RAB33B protein were significantly reduced in cells from homozygous mutant mice (Figure 1D). We then separated on a polyacrylamide gel the same membrane-enriched liver fractions used for the detection of the RAB33B protein, transferred proteins to the membrane, and stained with the fluorescently labelled *Helix pomatia* agglutinin (HPA), a lectin that selectively binds to α-N-acetylgalactosamine residues (Tn antigen), an intermediate glycan transiently accumulated during O-glycosylation of proteins in the Golgi. With some degree of variability, a few distinct bands showed significantly increased HPA staining in the homozygous mutant compared to the WT control lysates, indicating altered proteins glycosylation in liver tissue (Figure 2A). To confirm this finding in bone cells, we performed immunofluorescence on primary calvarial osteoblasts and, in some cells more than others, observed a modest increase in HPA staining in the homozygous mutant compared to WT osteoblasts (Figure 2B). To evaluate potential glycosylation defects in human cells, we used a short interference RNA approach to downregulate the expression of RAB33B in HeLa cells (Figure 2C). We then used these HeLa cells and stained them with multiple fluorescently labelled lectins, including *Wheat Germ Agglutinin* (WGA) and *Griffonia simplicifolia* (GSII). These lectins recognize terminal α-N-acetylglucosamine and sialic acid (WGA) or α-N-acetylglucosamine residues (GSII), common for protein N-glycosylation in the Golgi. While the GSII staining was not significantly different from control cells, HeLa cells that expressed less RAB33B showed a prominent increase in WGA staining compared to controls and quantified by normalized mean pixel intensity (Figure 2D), supporting the notion that RAB33B-deficient cells display altered protein glycosylation.

Effects of the *Rab33b* p.Lys46Gln variant on the skeleton

Because the effects of the p.Lys46Gln variant in the mouse were unknown and difficult to predict across species, we decided to study the skeleton of both heterozygous and homozygous mutant mice. We did this in actively growing 6 weeks old mice and in fully grown, young adult mice at 4 months (16 weeks) of age, which have a fully mature skeleton. Other than a small (decreased) but significant difference in body weight in homozygous mutant compared to WT males at 6 weeks of age, body weight and femur lengths were not different among male or female mice at either age (Figure 3A and data not shown). Dual energy absorptiometry (DEXA) to determine their bone mineral density (BMD) and bone mineral content (BMC) showed a mild increase in BMD in the lumbar spine of heterozygous male mice at 4 months (p = 0.047 vs. WT) (Figure 3B). No differences were noted in young males or in female mice of either age (Figure 3B and Supplementary Figure S2). Micro-

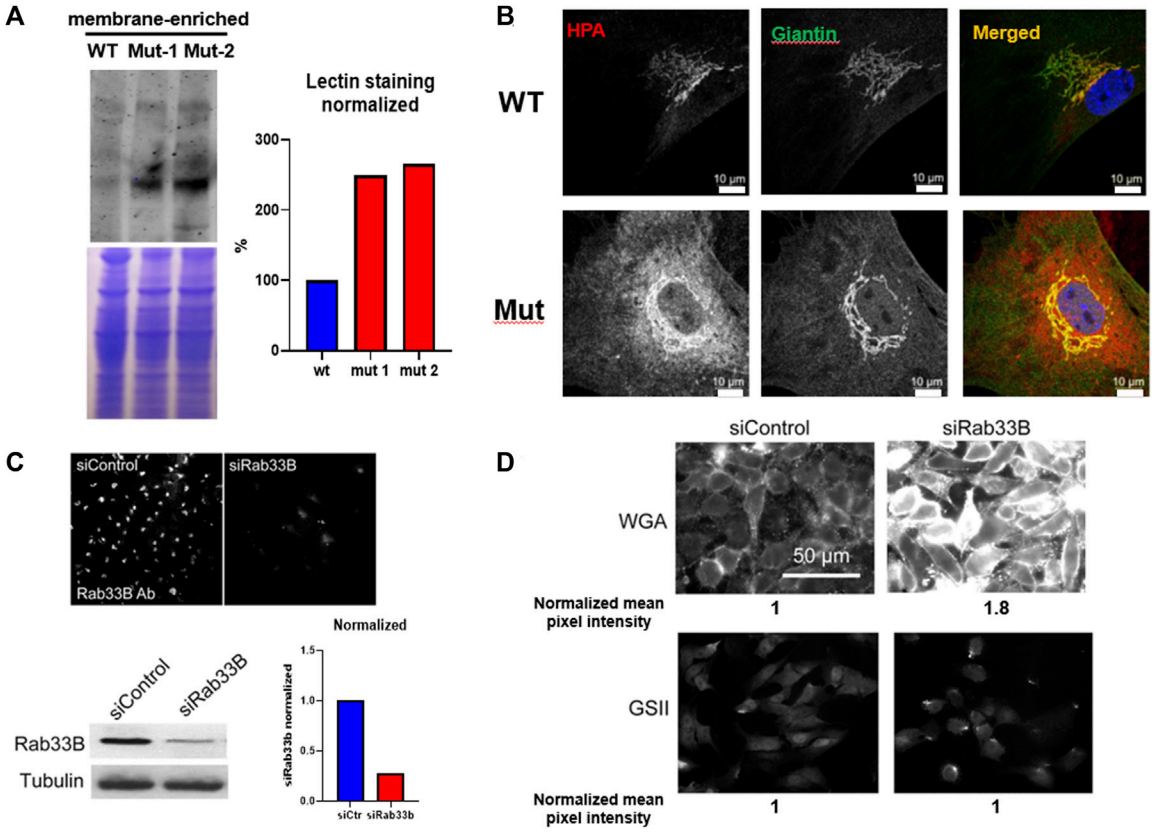

FIGURE 2
The *Rab33b* c.136A>C variant causes altered protein glycosylation. **(A)**. Western Blot using the same membrane-enriched lysates of freshly dissected adult liver shown in Figure 1, separated by SDS-PAGE and stained with the *Helix pomatia* agglutinin (HPA) lectin which selectively binds to α-N-acetylgalactosamine residues. The normalized lectin staining quantification is also shown. **(B)**. Immunofluorescence staining using HPA and the Golgi marker Giantin on primary calvarial osteoblasts and showing increased HPA staining inside the mutant osteoblasts. Scale bars = 10 µm **(C)**. Immunofluorescence and western blot on HeLa cells transfected with either control or siRNA against Rab33b (siRab33b), showing significantly reduced RAB33B protein levels as quantified in the graph. **(D)**. The same HeLa cells stained with WGA and GSII lectins. WGA staining was increased in cells transfected with siRab33b as quantified by normalized mean pixel intensity (average of 300 cells).

computed tomography (microCT) showed no differences in bone volume/tissue volume (BV/TV) or trabecular bone number (Tb.N) in the lumbar spine, but the bone trabecular thickness (Tb.Th) was significantly higher in heterozygous 4 month-old males compared to WT (p = 0.024 vs. WT) (Supplementary Figure S3). Other parameters measured in the spine were not different. No differences were noted in the spine of 6-week-old females (Supplementary Figure S4) and no additional microCT analyses were performed in females. The analysis of distal femurs in male mice confirmed the increased trabecular thickness observed in the spine, but again only in 4 months old heterozygous mice (p = 0.046 vs. WT) (Figure 4). Femoral volumetric bone mineral density (vBMD) was elevated at both 6 weeks and 4 months of age in heterozygous males vs. WT (p = 0.002 and p = 0.062, respectively) (Figure 4A). Additional mid-shaft femoral cortical parameters showed a significant increase in cortical thickness in both heterozygous and homozygous male mice at 4 months (p = 0.024 each vs. WT) (Figure 4B). While the periosteal circumference and total mid-shaft area (cross sectional area) were not different compared to control mice, indicating bones of similar size and diameter, both the inner medullary radius and endosteal circumference were significantly smaller in homozygous male mice at 4 months of age which resulted in a decreased medullary area (Figures 4B,C). Overall, the increased trabecular and cortical thickness and reduced medullary area at 4 months in Rab33b mutant mice suggested a potential reduction in bone resorption. To evaluate for changes at the bone cellular level that could explain these observations, we performed bone histomorphometry on L4 vertebral bodies (lumbar spine) in 4-month-old male mice. Dynamic parameters of bone formation, including mineralizing surfaces over bone surfaces (MS/BS), mineral apposition rate (MAR) and bone formation rate (BFR/BS) trended, on average, to be mildly elevated but without reaching the significance level (Figure 5A). Conversely and surprisingly, osteoclast numbers (N.Oc./B.Pm and N.Oc./T.Ar) and surfaces (Ocs/BS) were about 4 folds higher in the homozygous mutant compared to WT spines, with heterozygous mice showing a similar, though less pronounced, elevation of the osteoclast parameters compared to WT mice (Figures 5B,C). An *in vitro* osteoclast differentiation assay using bone marrow macrophages

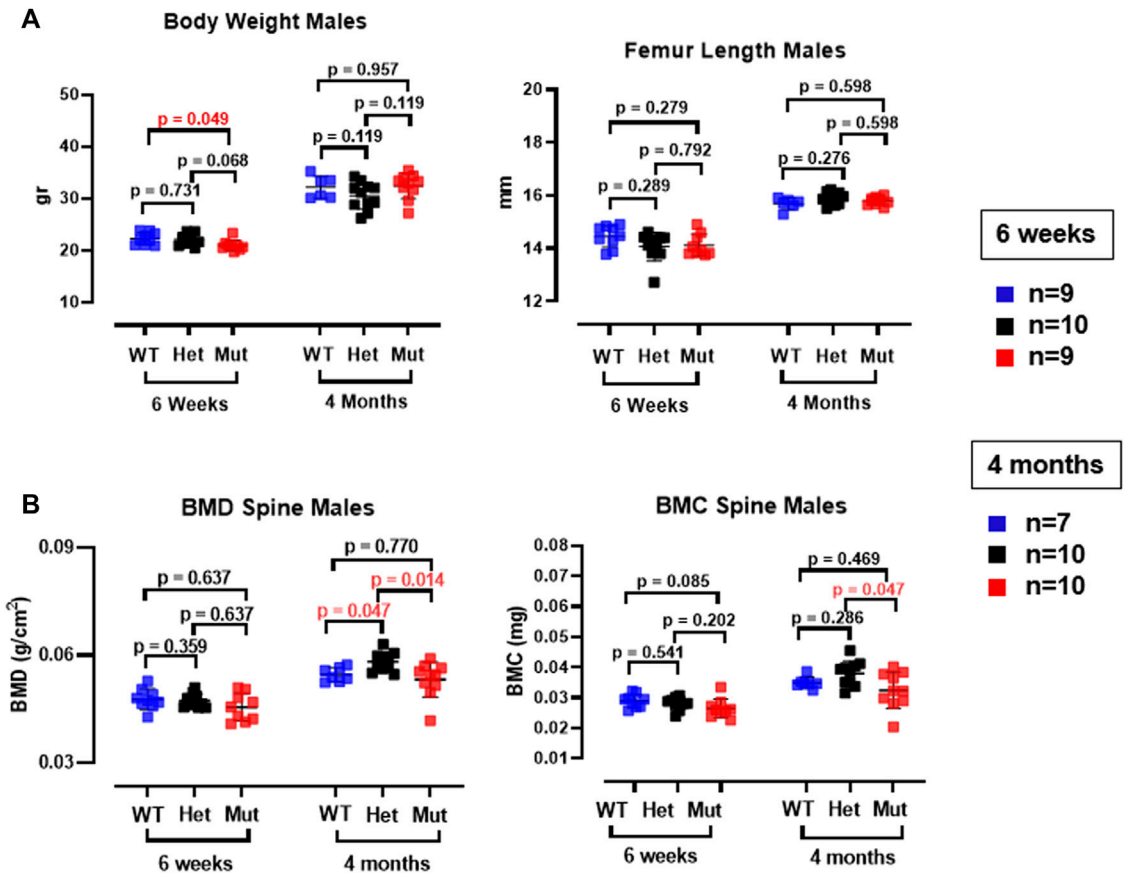

FIGURE 3
Body weight, femur length and DEXA measurements in *Rab33b* mutant male mice. **(A)**. Body weight and femur length were not different between heterozygous or homozygous and WT male mice at 6 weeks or 4 months of age. **(B)**. Lumbar spine bone mineral density (BMD) and bone mineral content (BMC) in male mice at 6 weeks and 4 months of age. Note the small but significant increase in the BMD in the spine in het mice.

from WT and *Rab33b* mutant mice showed increased osteoclastogenesis, consistent with what we observed *in vivo* (Supplementary Figure S5). The finding of elevated osteoclasts parameters in spite of increased trabecular and cortical thickness suggested that these cells are not able to properly resorb bone and pointed to a putative functional important role for RAB33B in this cell lineage.

Biomechanical assessment of Rab33b mutant femurs

The higher femoral volumetric bone mineral density and cortical thickness suggested that *Rab33b* mutant mice may have altered biomechanical bone properties compared to controls. To assess this, we next performed a femoral three-point bending structural mechanical test in 4 month-old male mice. Standard mechanical properties derived from this test identified a significantly elevated yield load (yield force) in both heterozygous and homozygous mice compared to controls (p = 0.001 and p = 0.013, respectively). Stiffness was also significantly elevated but only in heterozygous males (p = 0.01 vs. WT) (Figure 6A). Interestingly, the calculation of the corresponding estimated material properties such as Young's modulus (Elastic Modulus), yield stress and ultimate stress showed a progressive elevation of these parameters from WT to heterozygous to homozygous mutant mice, although only the yield stress was significantly different in homozygous and heterozygous compared to WT mice (p = 0.0002 and p = 0.049, respectively) (Figure 6B). A representative load-displacement curve comparing WT vs. homozygous male mice is shown in Figure 6C.

Histology and lectin staining on bone tissue sections

Mild alterations in growth plate and cartilage histology were reported earlier due to mutations in Dymeclin (Osipovich et al., 2008). To determine if the growth plate morphology was affected in *Rab33b* mutant mice, we performed histology of distal femurs and proximal tibias in 6-day-old and 6-week-old mice and stained

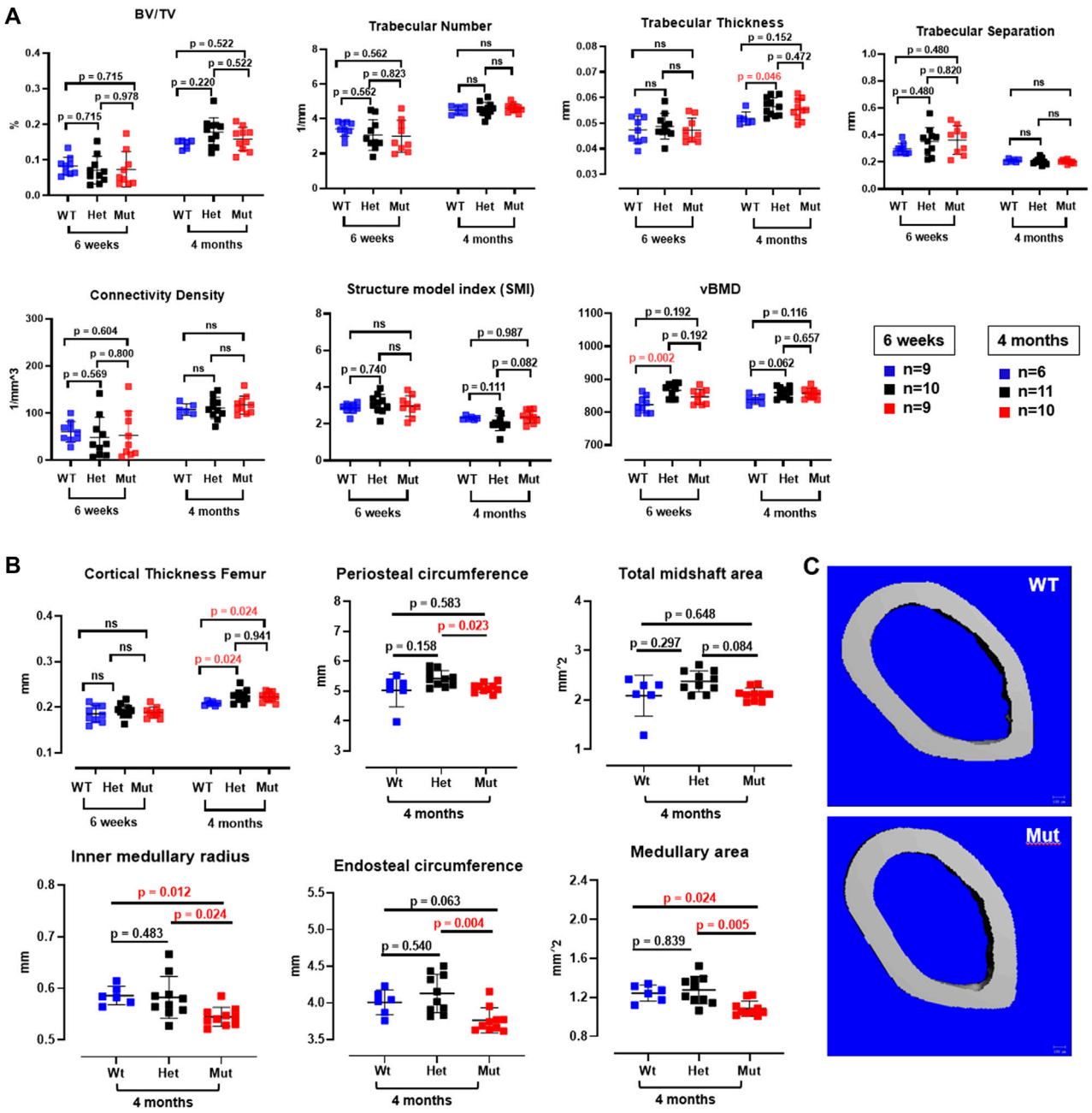

FIGURE 4
MicroCT analysis of male femurs. **(A)**. Trabecular bone parameters in the femur were measured at both 6 weeks and 4 months of age in all mouse genotypes. Trabecular thickness was elevated at 4 months of age in heterozygous *Rab33b* mice. vBMD was also higher in het mice at 6 weeks of age. **(B)**. Cortical bone parameters at the femur midshaft showed increased cortical thickness at 4 months in both heterozygous and homozygous *Rab33b* mutant mice. While total midshaft area and periosteal circumference were not different from control mice, homozygous Rab33b mutant mice had decreased medullary area, endosteal circumference and inner medullary radius compared to heterozygous and WT mice. **(C)**. Representative microCT 3D-rendering of the femur midshaft from a control and homozygous mutant mouse.

sections with Safranin-o and Alcian Blue for a qualitative assessment of proteoglycan expression. Neither the morphology of the growth plate nor the staining with Safranin-o and/or Alcian Blue revealed any striking differences between homozygous and WT mutant mice (Figure 7A). Next, to assess the potential difference in the expression of specific cellular sugar residues on these tissue sections, we proceeded to stain 6-day-old sections (derived from n = 2 WT and n = 3 homozygous mutants) with 2 fluorescently labeled lectins, Wheat Germ Agglutinin (WGA) and *Galanthus Nivalis Lectin* (GNL) and acquired immunofluorescence light images at the confocal microscope. GNL recognizes terminal mannose residues in immature N-glycosylated proteins. We observed differences

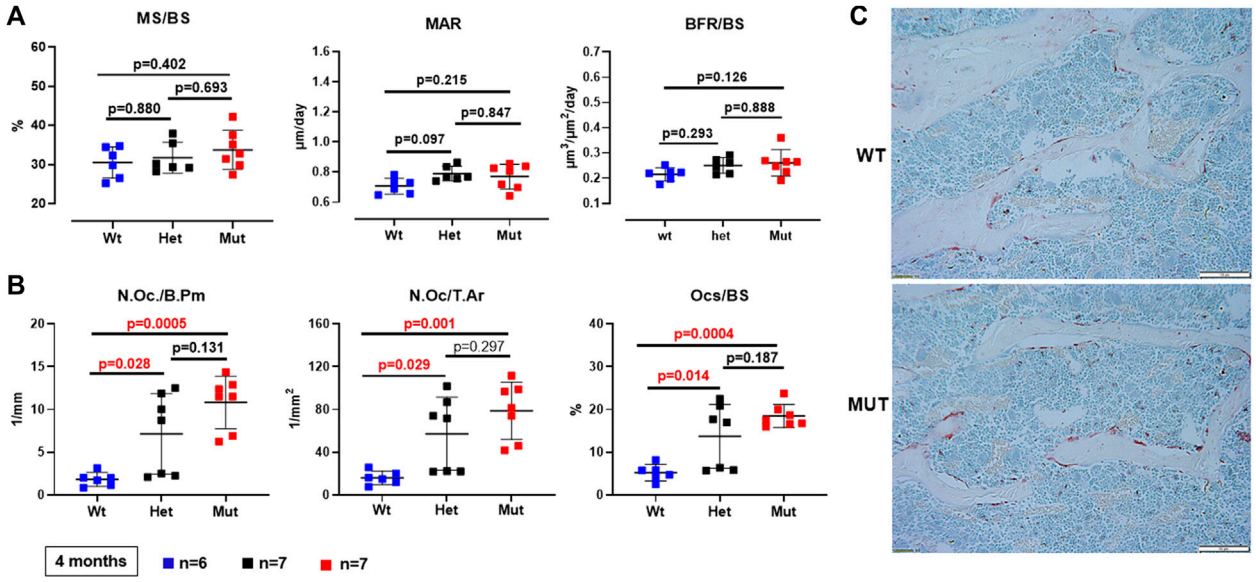

FIGURE 5
Bone histomorphometry of the lumbar spine (L4). **(A)**. Dynamic parameters of bone formation (MS/BS = mineralizing surfaces/bone surfaces; MAR = mineral apposition rate; BFR/BS = bone formation rate/bone surfaces) were not significantly different among genotypes. **(B)**. Osteoclast parameters (N.Oc/B.Pm = number of osteoclasts/bone perimeter; N.Oc/T.Ar = number of osteoclasts/tissue area; OcS/BS = osteoclast surface/bone surface) were increasingly elevated in heterozygous and homozygous compared to WT mice. **(C)**. Representative images showing trabecular bone within a vertebral section and TRAP-positive (Tartrate-resistant acid phosphatase) osteoclasts from a WT and a homozygous mutant *Rab33b* mouse.

between WT and Rab33b homozygous mutant samples but with significant variability among samples of different genotypes and also within the same genotype using identical acquisition parameters (Figure 7B).

X-ray images of the skeleton

Finally, because SMC patients show a pathognomonic malformation of vertebrae, characterized by double-humped vertebral bodies and platyspondyly, causing short neck and trunk with barrel-shaped chest, we carefully analyzed the skeleton of *Rab33b* mutant mice to determine if this mouse model reproduced similar vertebral morphological defects. Digital X-ray images acquired either at 6 weeks of age or between 4 and 6 months of age did not show any atypical skeletal malformation in either heterozygous or homozygous mice compared to WT controls (Figure 8).

Discussion

The disease mechanisms causing Smith-McCort skeletal dysplasia, due to *RAB33B* pathogenic variants, are not well understood. In this study we generated mice that carry a *Rab33b* disease-causing variant, c.136A>C (p.Lys46Gln), which is identical to that of members from a consanguineous family diagnosed with SMC2, and studied their skeleton. The *Rab33b* variant caused a mild increase in trabecular bone thickness in the spine and femur and in femoral mid-shaft cortical thickness with a concomitant reduction of the femoral medullary area at 4 months of age. Since we found no differences in dynamic parameters of bone formation in mutant *versus* control mice, we sought to investigate a potential reduction in trabecular and endosteal bone resorption activity. However, bone histomorphometry unexpectedly showed a 4-fold increase in osteoclast parameters in homozygous *Rab33b* mice. Because the increased number of osteoclast cells did not translate in reduced bone mass, it suggested a putative impairment of bone resorption and a potential novel role of RAB33B in osteoclast function which needs to be further explored. Femur three-point bending biomechanical tests showed an increased in yield load and a progressive elevation, from WT to heterozygote to homozygous mutants, of all bone intrinsic properties. These findings indicate an overall impact on bone material properties which may be caused by disturbed protein glycosylation in cells contributing to skeletal formation, as suggested by the altered and variable pattern of lectin staining. Overall, the phenotype of either heterozygous or homozygous mice was subtle, did not reproduce some of the typical features of the human disease and was also sex-specific, manifesting in males but not females.

From our work, two aspects are emerging on the role of RAB33B in the skeleton. The first is the novel potential role of RAB33B in osteoclast function; the second is its role at the Golgi apparatus to allow correct protein processing and glycosylation. Our findings add more evidence to the important role that several RAB proteins play in osteoclast biology and bone resorption (for a review, see (Roy and Roux, 2018; Roy and Roux, 2020)). For instance, the downregulation of RAB7 was shown to impair the formation of the osteoclast F-actin

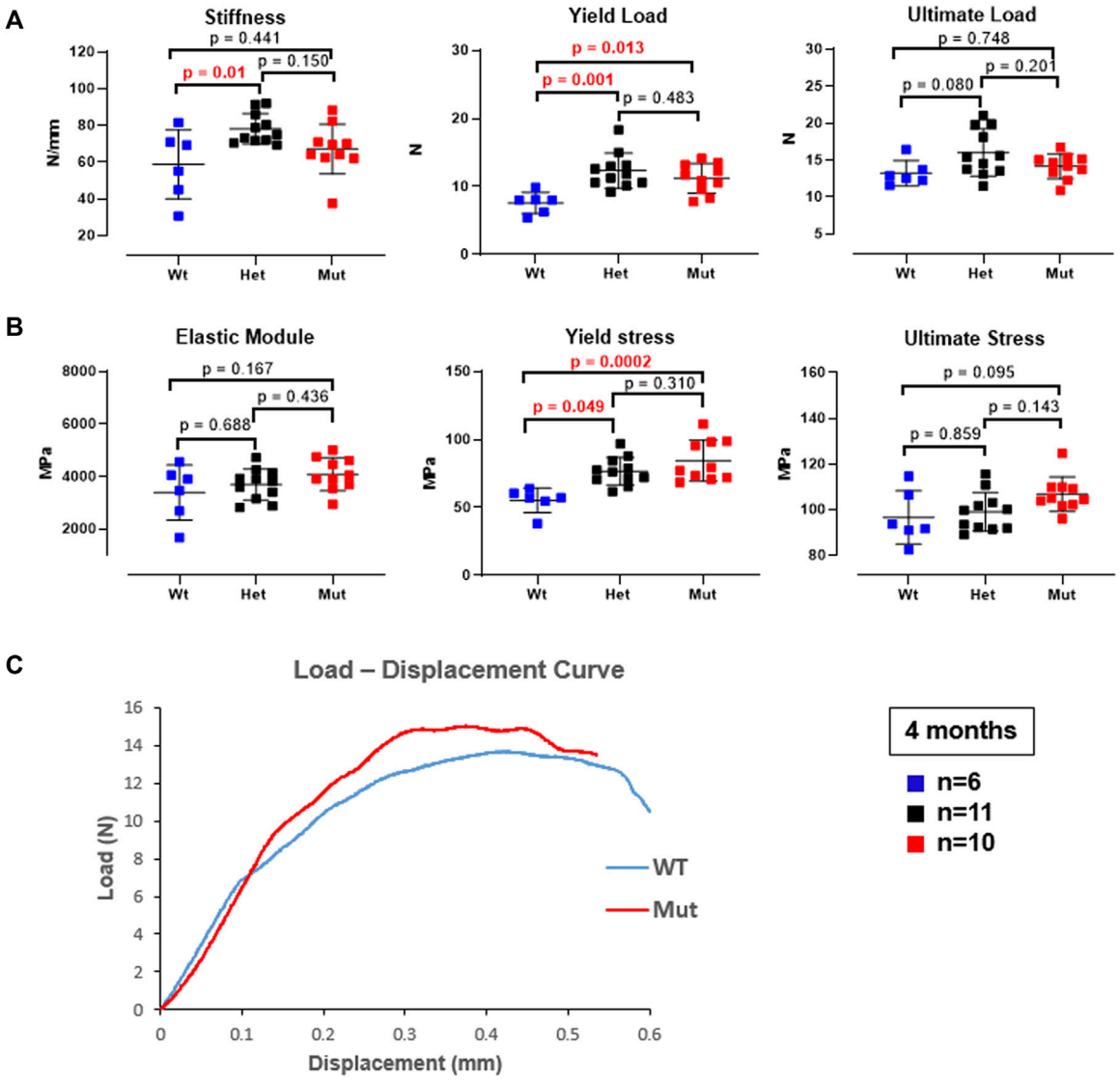

FIGURE 6
Three-point bending biomechanical test on femurs from 4-month-old male mice. **(A)**. Bone mechanical properties, including stiffness and yield load were elevated in het mice and the yield load was also elevated in mut mice compared to controls. **(B)**. The corresponding estimated material properties, including Elastic modulus, yield stress, and ultimate stress trended progressively higher and reached significance for the yield stress in both het and mutant compared to WT control mice. **(C)**. Representative load-displacement curve from a homozygous mutant and a WT control mouse.

ring and the process of osteoclast polarization, causing a severe reduction in bone resorption (Zhao et al., 2001). Importantly, mutations in an effector of RAB7, PLEKHM1, cause a form of osteopetrosis in humans (Van Wesenbeeck et al., 2007; Bo et al., 2016). Several other Rab-GTPases, their regulators, GEFs and GAPs, and effectors are expressed in osteoclasts and although their role is not fully understood, they are believed to take part in endosomal trafficking processes that are important for the formation of the osteoclast ruffle border, a key structure for bone resorption, but are also involved in the process of autophagy (Zhao et al., 2002; Roy and Roux, 2018; Roy and Roux, 2020). Autophagy in osteoclasts can promote podosome disassembly and thus facilitate cell motility (Zhang et al., 2020). *RAB33B* is expressed in human osteoclasts (Roy and Roux, 2020) and in non-osteoclastic cells, it is also involved in autophagosome formation and maturation (Itoh et al., 2008; Itoh et al., 2011; Morgan et al., 2019). In addition, a recent siRNA screen to identify RAB proteins involved in cell migration, identified RAB33B as a strong candidate in the regulation of focal adhesion dynamics by modulating the delivery of integrins to focal adhesions (Bjornestad et al., 2022). Therefore, RAB33B could be important in numerous aspects of osteoclast biology. These range from the establishment of the actin ring, a specialized adhesion structure that osteoclasts coordinate to seal onto the bone surface, to the genesis of the ruffled border, to the autophagosome formation and potentially, osteoclast motility. These processes warrant future investigations, preferably in the context of a complete loss of function of RAB33B in primary osteoclast cells.

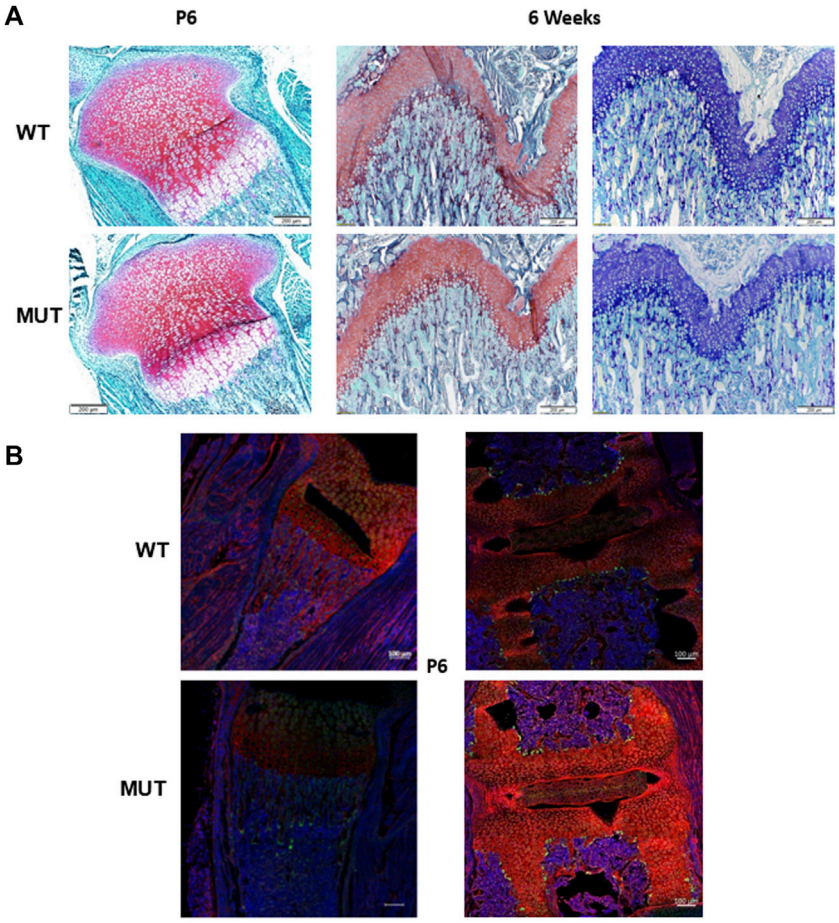

FIGURE 7
Histology and immunofluorescence staining. **(A)**. Safranin-O and Alcian blue staining of tibia growth plates from 6 days old and 6 weeks old showed no macroscopic differences between homozygous mutant and WT control mice. **(B)**. Qualitative WGA (red) and GNL (green) lectin immunofluorescence staining in proximal tibia (left) and spine (right) at P6 showed variable and often inconsistent results between sections from homozygous mutant and WT control mice.

Our findings in the Golgi apparatus suggested that disruption of RAB33B function results in altered protein glycosylation, likely due to its role in normal vesicular trafficking at this organelle. Although we encountered significant variability in the lectin staining assays that we performed on murine primary cells and tissues, primary RAB33B mutant osteoblasts as well as liver lysates appeared to have increased staining with Helix pomatia agglutinin (HPA) which binds to N-acetylgalactosamine residues. This indicates alterations in protein O-glycosylation compared to WT controls. Furthermore, data from HeLa cells in which RAB33B expression was significantly reduced by siRNA, showed a clear increase in WGA staining compared to control cells, supporting the link between RAB33B function and Golgi glycosylation. A disturbed protein glycosylation process was also indicated by the altered and contrasting staining with WGA in RAB33B mutant 6-day old embryo sections of long bones and spines compared to WT. WGA binds N-acetylglucosamine and sialic acid residues which are sugar structures common to many membrane proteins. Conversely, staining with GNL which binds to mannose residues was mostly unchanged in mutant compared to WT mice. Changes in protein glycosylation can affect many proteins, both intracellular as well as those that are membrane-bound or secreted. Osteoblasts, in addition to type I collagen, secrete several other proteins that are either components of the extracellular matrix (ECM) or bind to the ECM, e.g., osteocalcin, and some of them are known to regulate the matrix mineralization process. The changes that we observed in 3-pt bending tests of the femurs showed altered bone material properties which are indeed consistent with a likely effect of altered protein glycosylation onto bone accrual and mineralization. Such changes resulted in an increased yield load and yield stress and indicate that the mutant bones required more force before beginning to irreversibly bend. These data, together with the slight increase in ultimate load and ultimate stress, suggest that intrinsically, *Rab33b* mutant bones may be stronger compared to WT bones. Interestingly, among all the typical features that SMC2 patients may present (Alshammari et al., 2012; Dupuis et al., 2013; Tuysuz et al., 2021), skeletal fractures are not one of them which supports our finding. Finally, changes in protein glycosylation have also been

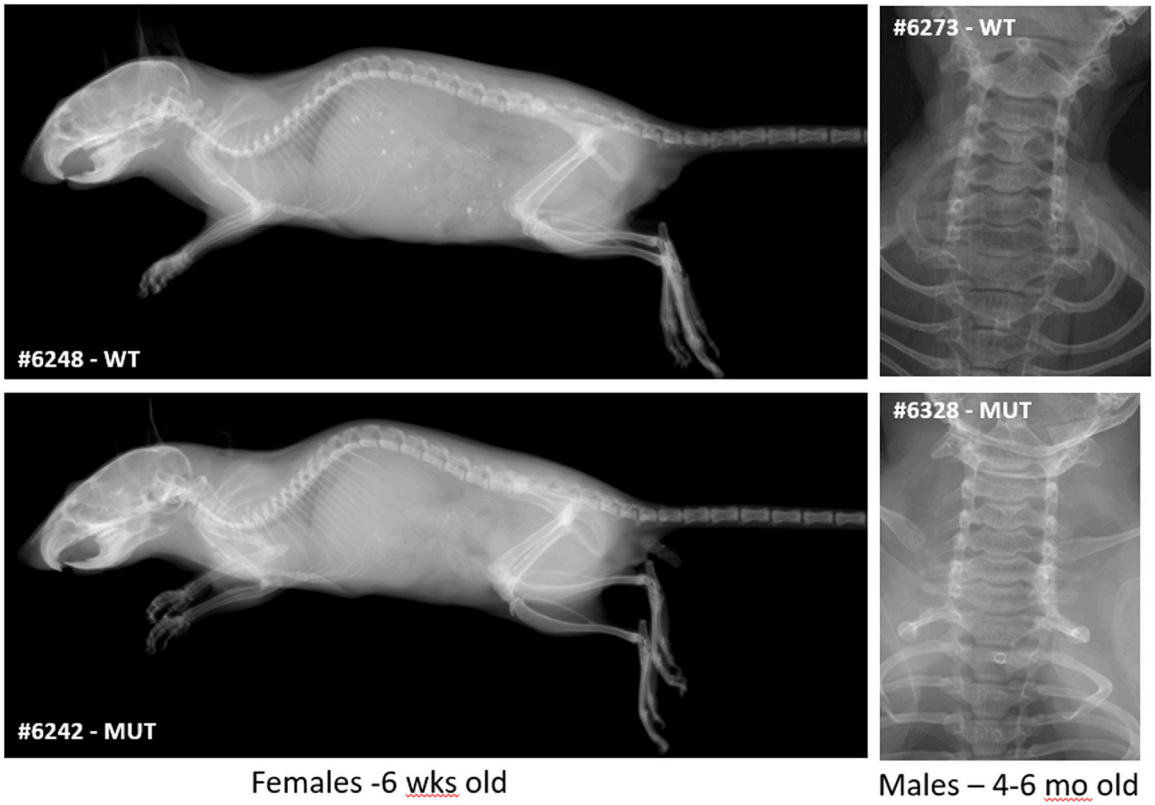

FIGURE 8
Skeletal survey. X-ray images at either 6 weeks (full skeleton) or 4–6 months of age (upper thoracic and neck area) did not show significant macroscopic differences or cervical vertebral malformations typical of SMC2.

showed to impact mesenchymal stem cell differentiation and ultimately, the function of osteoblasts (Wilson et al., 2018). Therefore, future studies will also need to assess such potential outcomes in a *Rab33b* loss of function model.

Our work has some limitations. A study in primary cells derived from SMC2 patients indicated that, while the p.Lys46Gln variant is expected to impair the GTPase activity, it also severely reduced RAB33B protein levels (Alshammari et al., 2012), suggesting that the disease phenotype may result from a combination of the two effects. Conversely, the same amino acid change in the murine model only caused about 40%–60% reduction of RAB33B protein levels in homozygous mice and yielded a mild phenotype with a poor representation of the clinical features of the human disease. This perhaps indicates that RAB33B protein levels are also important since a residual enzymatic activity may, in part, compensate for the effects of the mutation. The most common clinical findings in SMC patients, including short neck and trunk, platyspondyly, hyperlordosis, various joint abnormalities, and short bones allude to a potential defect in endochondral ossification during growth, perhaps also mediated by a chondrocyte defect, which is not reproduced by our mouse model. The indication that protein glycosylation is affected in the mouse is an important finding and justifies future follow-up studies using a comprehensive mass-spectrometry glycomic approach in a complete loss of function model of *Rab33b* to better comprehend the underlying disease mechanism. The hypomorphic nature of the p.Lys46Gln variant in the mouse could also have contributed to the phenotype variability that we observed both *in vitro* and *ex vivo* with the lectin staining. The murine model may also be less sensitive to the effects of the p.Lys46Gln variant compared to humans. This is not an uncommon observation in mouse models of human disease (e.g. (Chen et al., 1998)). The outcomes of a complete *Rab33b* knockout remain to be tested. Furthermore, potential compensatory effects of the closely related paralog gene, *Rab33a*, could not be excluded and may be more prominent in the mouse compared to humans (see (Homma et al., 2021) for a phylogenetic tree of RABS). It is also interesting to note that, while the effects of the *Rab33b* variant were subtle, they were only detected in male (both heterozygous and homozygous) and not female mice. While we don't have a current explanation for this sex difference, a total of fifteen SMC2 patients (9 females) have currently been described in the literature and we found no reference that the disease presents earlier and/or with more severity in males *versus* females (Alshammari et al., 2012; Dupuis et al., 2013; Salian et al., 2017; Tuysuz et al., 2021). This aspect may require further attention by clinicians.

In conclusion, as the Golgi apparatus is central to both secretory cargo transport and protein and lipid glycosylation,

future studies of the effects of *Rab33b* pathogenic variants on the skeleton will provide additional opportunities to determine whether these are caused by a failure in cargo transport, a failure in glycosylation or a combination of both. Distinct bands in gel suggest strong effects on a limited set of proteins. The identification of specific cargos and/or glycosylation protein targets in both osteoclasts and osteoblasts will be important to further improve our understanding of RAB33B and Smith-McCort dysplasia.

Data availability statement

The original contributions presented in the study are included in the article/Supplementary Material S1, further inquiries can be directed to the corresponding author.

Ethics statement

The animal study was reviewed and approved by the Institutional Care and Animal Use Committee (IACUC) of the University of Arkansas for Medical Sciences.

Author contributions

MD performed the majority of the experimental work; IP and VL contributed to protein liver extractions, Western blot and immunofluorescence staining; SL performed lectin staining on Hela cells transfected with siRNA; JS calculated parameters derived from the biomechanical assays; HG-A performed most statistical analyses; QF designed the guide RNAs and generated the knock-in mice using Crispr/Cas9 technology; BS, VL, and RM conceived the project, designed experiments and interpreted the experimental data. RM wrote the initial manuscript draft and all other authors contributed to its final form. All authors contributed to the article and approved the submitted version.

Funding

This work was initially partially supported by a Barton Pilot project to BS from the University of Arkansas for Medical Science (UAMS). Subsequent support also came from a Pilot Project of the Center for Musculoskeletal Disease Research (COBRE Grant)—P20 GM125503 from NIGMS (RM), R01 GM083144 (VVL), R01 GM092960 and U54 GM105814 (BS), UAMS Institutional Funds, and U54 TR001629 from NCATS. RM would also like to acknowledge the guidance provided during preparation of this manuscript made possible by the center for Childhood Obesity Prevention funded by the NIGMS under Award Number P20GM109096. The content is solely the responsibility of the authors and does not necessarily represent the official views of the National Institutes of Health.

Conflict of interest

The authors declare that the research was conducted in the absence of any commercial or financial relationships that could be construed as a potential conflict of interest.

Publisher's note

Supplementary material

The Supplementary Material for this article can be found online at: https://www.frontiersin.org/articles/10.3389/fgene.2023.1204296/full#supplementary-material

SUPPLEMENTARY FIGURE S1
Western Blot using a RAB33B antibody on membrane-enriched and total lysates of freshly dissected adult liver from 1 wild-type (WT) and 2 *Rab33b* mutant mice, separated by SDS-PAGE. Relative quantification of the bands is shown below the stained membrane.

SUPPLEMENTARY FIGURE S2
DEXA measurements in Rab33b mutant female mice at 6 weeks and 4 months of age. No significant differences were detected other than a small increase in BMC in the spine of mutant compared to het but not to WT controls.

SUPPLEMENTARY FIGURE S3
MicroCT analysis of male lumbar spines. Trabecular bone parameters in the spine were measured at both 6 weeks and 4 months of age in all mouse genotypes. Trabecular thickness was elevated at 4 months of age in both heterozygous and homozygous *Rab33b* mutant mice. BV/TV = bone volume/tissue volume; Tb-N = trabecular number; Tb-Th = trabecular thickness; Tb-Sp = trabecular separation; Conn density = connectivity density; SMI = structure model index; vBMD = volumetric bone mineral density.

SUPPLEMENTARY FIGURE S4
MicroCT analysis of female lumbar spines at 6 weeks of age. No significant differences were detected.

SUPPLEMENTARY FIGURE S5
Osteoclastogenesis assay. Trap-positive osteoclasts derived from bone marrow macrophages extracted from long bones of WT and homozygous mutant mice (n=1 – in 5 technical replicates) and treated with M-CSF and RANKL. The lower panels show higher magnification of yellow boxed areas.

References

Alshammari, M. J., Al-Otaibi, L., and Alkuraya, F. S. (2012). Mutation in RAB33B, which encodes a regulator of retrograde Golgi transport, defines a second Dyggve--Melchior--Clausen locus. *J. Med. Genet.* 49 (7), 455–461. doi:10.1136/jmedgenet-2011-100666

Beighton, P. (1990). Dyggve-Melchior-Clausen syndrome. *J. Med. Genet.* 27 (8), 512–515. doi:10.1136/jmg.27.8.512

Bjornestad, S. A., Guadagno, N. A., Kjos, I., and Progida, C. (2022). Rab33b-exocyst interaction mediates localized secretion for focal adhesion turnover and cell migration. *iScience* 25 (5), 104250. doi:10.1016/j.isci.2022.104250

Bo, T., Yan, F., Guo, J., Lin, X., Zhang, H., Guan, Q., et al. (2016). Characterization of a relatively malignant form of osteopetrosis caused by a novel mutation in the PLEKHM1 gene. *J. Bone Min. Res.* 31 (11), 1979–1987. doi:10.1002/jbmr.2885

Burns, C., Powell, B. R., Hsia, Y. E., and Reinker, K. (2003). Dyggve-melchior-clausen syndrome: Report of seven patients with the Smith-McCort variant and review of the literature. *J. Pediatr. Orthop.* 23 (1), 88–93. doi:10.1097/01241398-200301000-00018

Chen, H., Lun, Y., Ovchinnikov, D., Kokubo, H., Oberg, K. C., Pepicelli, C. V., et al. (1998). Limb and kidney defects in Lmx1b mutant mice suggest an involvement of LMX1B in human nail patella syndrome. *Nat. Genet.* 19 (1), 51–55. doi:10.1038/ng0598-51

Cheng, E., Trombetta, S. E., Kovacs, D., Beech, R. D., Ariyan, S., Reyes-Mugica, M., et al. (2006). Rab33A: Characterization, expression, and suppression by epigenetic modification. *J. Invest. Dermatol* 126 (10), 2257–2271. doi:10.1038/sj.jid.5700386

Cherfils, J., and Zeghouf, M. (2013). Regulation of small GTPases by GEFs, GAPs, and GDIs. *Physiol. Rev.* 93 (1), 269–309. doi:10.1152/physrev.00003.2012

Cohn, D. H., Ehtesham, N., Krakow, D., Unger, S., Shanske, A., Reinker, K., et al. (2003). Mental retardation and abnormal skeletal development (Dyggve-Melchior-Clausen dysplasia) due to mutations in a novel, evolutionarily conserved gene. *Am. J. Hum. Genet.* 72 (2), 419–428. doi:10.1086/346176

Dempster, D. W., Compston, J. E., Drezner, M. K., Glorieux, F. H., Kanis, J. A., Malluche, H., et al. (2013). Standardized nomenclature, symbols, and units for bone histomorphometry: A 2012 update of the report of the ASBMR histomorphometry nomenclature committee. *J. Bone Min. Res.* 28 (1), 2–17. doi:10.1002/jbmr.1805

Denais, C., Dent, C. L., Southgate, L., Hoyle, J., Dafou, D., Trembath, R. C., et al. (2011). Dymeclin, the gene underlying Dyggve-Melchior-Clausen syndrome, encodes a protein integral to extracellular matrix and golgi organization and is associated with protein secretion pathways critical in bone development. *Hum. Mutat.* 32 (2), 231–239. doi:10.1002/humu.21413

Dupuis, N., Fafouri, A., Bayot, A., Kumar, M., Lecharpentier, T., Ball, G., et al. (2015). Dymeclin deficiency causes postnatal microcephaly, hypomyelination and reticulum-to-Golgi trafficking defects in mice and humans. *Hum. Mol. Genet.* 24 (10), 2771–2783. doi:10.1093/hmg/ddv038

Dupuis, N., Lebon, S., Kumar, M., Drunat, S., Graul-Neumann, L. M., Gressens, P., et al. (2013). A novel RAB33B mutation in Smith-McCort dysplasia. *Hum. Mutat.* 34 (2), 283–286. doi:10.1002/humu.22235

Ehtesham, N., Cantor, R. M., King, L. M., Reinker, K., Powell, B. R., Shanske, A., et al. (2002). Evidence that Smith-McCort dysplasia and Dyggve-Melchior-Clausen dysplasia are allelic disorders that result from mutations in a gene on chromosome 18q12. *Am. J. Hum. Genet.* 71 (4), 947–951. doi:10.1086/342669

El Ghouzzi, V., Dagoneau, N., Kinning, E., Thauvin-Robinet, C., Chemaitilly, W., Prost-Squarcioni, C., et al. (2003). Mutations in a novel gene Dymeclin (FLJ20071) are responsible for Dyggve-Melchior-Clausen syndrome. *Hum. Mol. Genet.* 12 (3), 357–364. doi:10.1093/hmg/ddg029

Gruenwald, K., Castagnola, P., Besio, R., Dimori, M., Chen, Y., Akel, N. S., et al. (2014). Sc65 is a novel endoplasmic reticulum protein that regulates bone mass homeostasis. *J. Bone Min. Res.* 29 (3), 666–675. doi:10.1002/jbmr.2075

Homma, Y., Hiragi, S., and Fukuda, M. (2021). Rab family of small GTPases: An updated view on their regulation and functions. *Febs J.* 288 (1), 36–55. doi:10.1111/febs.15453

Huang, L., Urasaki, A., and Inagaki, N. (2019). Rab33a and Rab33ba mediate the outgrowth of forebrain commissural axons in the zebrafish brain. *Sci. Rep.* 9 (1), 1799. doi:10.1038/s41598-018-38468-5

Hutagalung, A. H., and Novick, P. J. (2011). Role of Rab GTPases in membrane traffic and cell physiology. *Physiol. Rev.* 91 (1), 119–149. doi:10.1152/physrev.00059.2009

Itoh, T., Fujita, N., Kanno, E., Yamamoto, A., Yoshimori, T., and Fukuda, M. (2008). Golgi-resident small GTPase Rab33B interacts with Atg16L and modulates autophagosome formation. *Mol. Biol. Cell* 19 (7), 2916–2925. doi:10.1091/mbc.e07-12-1231

Itoh, T., Kanno, E., Uemura, T., Waguri, S., and Fukuda, M. (2011). OATL1, a novel autophagosome-resident Rab33B-GAP, regulates autophagosomal maturation. *J. Cell Biol.* 192 (5), 839–853. doi:10.1083/jcb.201008107

Kaufman, R. L., Rimoin, D. L., and McAlister, W. H. (1971). The Dyggve-Melchior-Clausen syndrome. *Birth Defects Orig. Artic. Ser.* 7 (1), 144–149.

Morello, R., Bertin, T. K., Chen, Y., Hicks, J., Tonachini, L., Monticone, M., et al. (2006). CRTAP is required for prolyl 3- hydroxylation and mutations cause recessive osteogenesis imperfecta. *Cell* 127 (2), 291–304. doi:10.1016/j.cell.2006.08.039

Morgan, N. E., Cutrona, M. B., and Simpson, J. C. (2019). Multitasking rab proteins in autophagy and membrane trafficking: A focus on Rab33b. *Int. J. Mol. Sci.* 20 (16), 3916. doi:10.3390/ijms20163916

Nakamura, K., Kurokawa, T., Nagano, A., Nakamura, S., Taniguchi, K., and Hamazaki, M. (1997). Dyggve-melchior-clausen syndrome without mental retardation (Smith-McCort dysplasia): Morphological findings in the growth plate of the iliac crest. *Am. J. Med. Genet.* 72 (1), 11–17. doi:10.1002/(sici)1096-8628(19971003)72:1<11::aid-ajmg3>3.0.co;2-y

Neumann, L. M., El Ghouzzi, V., Paupe, V., Weber, H. P., Fastnacht, E., Leenen, A., et al. (2006). Dyggve-melchior-clausen syndrome and Smith-McCort dysplasia: Clinical and molecular findings in three families supporting genetic heterogeneity in Smith-McCort dysplasia. *Am. J. Med. Genet. A* 140 (5), 421–426. doi:10.1002/ajmg.a.31090

Osipovich, A. B., Jennings, J. L., Lin, Q., Link, A. J., and Ruley, H. E. (2008). Dyggve-melchior-clausen syndrome: Chondrodysplasia resulting from defects in intracellular vesicle traffic. *Proc. Natl. Acad. Sci. U. S. A.* 105 (42), 16171–16176. doi:10.1073/pnas.0804259105

Pusapati, G. V., Luchetti, G., and Pfeffer, S. R. (2012). Ric1-Rgp1 complex is a guanine nucleotide exchange factor for the late Golgi Rab6A GTPase and an effector of the medial Golgi Rab33B GTPase. *J. Biol. Chem.* 287 (50), 42129–42137. doi:10.1074/jbc.M112.414565

Roy, M., and Roux, S. (2020). Rab GTPases in osteoclastic bone resorption and autophagy. *Int. J. Mol. Sci.* 21 (20), 7655. doi:10.3390/ijms21207655

Roy, M., and Roux, S. (2018). Rab GTPases in osteoclastic endomembrane systems. *Biomed. Res. Int.* 2018, 4541538. doi:10.1155/2018/4541538

Salian, S., Cho, T. J., Phadke, S. R., Gowrishankar, K., Bhavani, G. S., Shukla, A., et al. (2017). Additional three patients with Smith-McCort dysplasia due to novel RAB33B mutations. *Am. J. Med. Genet. A* 173 (3), 588–595. doi:10.1002/ajmg.a.38064

Starr, T., Sun, Y., Wilkins, N., and Storrie, B. (2010). Rab33b and Rab6 are functionally overlapping regulators of Golgi homeostasis and trafficking. *Traffic* 11 (5), 626–636. doi:10.1111/j.1600-0854.2010.01051.x

Sumya, F. T., Pokrovskaya, I. D., and Lupashin, V. (2021). Development and initial characterization of cellular models for COG complex-related CDG-II diseases. *Front. Genet.* 12, 733048. doi:10.3389/fgene.2021.733048

Tuysuz, B., Geyik, F., Yildirim, T., Alkaya, D. U., Sharifova, S., and Kafadar, A. (2021). Seven patients with Smith-McCort dysplasia 2: Four novel nonsense variants in RAB33B and follow-up findings. *Eur. J. Med. Genet.* 64 (7), 104248. doi:10.1016/j.ejmg.2021.104248

Van Wesenbeeck, L., Odgren, P. R., Coxon, F. P., Frattini, A., Moens, P., Perdu, B., et al. (2007). Involvement of PLEKHM1 in osteoclastic vesicular transport and osteopetrosis in incisors absent rats and humans. *J. Clin. Invest.* 117 (4), 919–930. doi:10.1172/JCI30328

Willett, R., Kudlyk, T., Pokrovskaya, I., Schonherr, R., Ungar, D., Duden, R., et al. (2013). COG complexes form spatial landmarks for distinct SNARE complexes. *Nat. Commun.* 4, 1553. doi:10.1038/ncomms2535

Wilson, K. M., Jagger, A. M., Walker, M., Seinkmane, E., Fox, J. M., Kroger, R., et al. (2018). Glycans modify mesenchymal stem cell differentiation to impact on the function of resulting osteoblasts. *J. Cell Sci.* 131 (4), jcs209452. doi:10.1242/jcs.209452

Zhang, Y., Cui, Y., Wang, L., and Han, J. (2020). Autophagy promotes osteoclast podosome disassembly and cell motility athrough the interaction of kindlin3 with LC3. *Cell Signal* 67, 109505. doi:10.1016/j.cellsig.2019.109505

Zhao, H., Ettala, O., and Vaananen, H. K. (2002). Intracellular membrane trafficking pathways in bone-resorbing osteoclasts revealed by cloning and subcellular localization studies of small GTP-binding rab proteins. *Biochem. Biophys. Res. Commun.* 293 (3), 1060–1065. doi:10.1016/S0006-291X(02)00326-1

Zhao, H., Laitala-Leinonen, T., Parikka, V., and Vaananen, H. K. (2001). Downregulation of small GTPase Rab7 impairs osteoclast polarization and bone resorption. *J. Biol. Chem.* 276 (42), 39295–39302. doi:10.1074/jbc.M010999200

Zheng, J. Y., Koda, T., Fujiwara, T., Kishi, M., Ikehara, Y., and Kakinuma, M. (1998). A novel Rab GTPase, Rab33B, is ubiquitously expressed and localized to the medial Golgi cisternae. *J. Cell Sci.* 111 (8), 1061–1069. doi:10.1242/jcs.111.8.1061

frontiers | Frontiers in Pediatrics

TYPE Original Research
PUBLISHED 13 June 2023
DOI 10.3389/fped.2023.1184529

OPEN ACCESS

EDITED BY
Jordi Pérez-Tur,
Spanish National Research Council (CSIC), Spain

REVIEWED BY
Aldesia Provenzano,
University of Florence, Italy
Francisco Cammarata-Scalisi,
Regional Hospital of Antofagasta, Chile

*CORRESPONDENCE
Antonio Federico Martínez-Monseny
✉ antoniofederico.martinez@sjd.es

RECEIVED 11 March 2023
ACCEPTED 15 May 2023
PUBLISHED 13 June 2023

CITATION
Lourdes V-H, Mario S-C, Didac C-A, Mercè B, Loreto M, Leticia P, Lucia FA, Martínez-Monseny AF and Mercedes S (2023) Beyond the known phenotype of sotos syndrome: a 31-individuals cohort study.
Front. Pediatr. 11:1184529.
doi: 10.3389/fped.2023.1184529

Beyond the known phenotype of sotos syndrome: a 31-individuals cohort study

Vega-Hanna Lourdes[1], Sanz-Cuesta Mario[2], Casas-Alba Didac[3,4], Bolasell Mercè[3], Martorell Loreto[3], Pías Leticia[3,4], Feller Ana Lucia[5], Antonio Federico Martínez-Monseny[3]* and Serrano Mercedes[4,6]

[1]Department of Pediatrics, Hospital Sant Joan de Déu Barcelona, Barcelona, Spain, [2]Department of Pediatrics, Hospital de Sant Boi, Parc Sanitari Sant Joan de Déu, Barcelona, Spain, [3]Department of Genetic and Molecular Medicine/IPER, Institut de Recerca, Hospital Sant Joan de Déu Barcelona, Barcelona, Spain, [4]Pediatric Neurology Department, Institut de Recerca, Hospital Sant Joan de Déu, Barcelona, Spain, [5]Departamen of Pediatrics, Hospital J P Garrahan, Buenos Aires, Argentine, [6]Centro de Investigación Biomédica en Red de Enfermedades Raras (CIBERER), Instituto de Salud Carlos III, Barcelona, Spain

Introduction: Sotos Syndrome (SS, OMIM#117550) is a heterogeneous genetic condition, recognized by three main clinical features present in most cases: overgrowth with macrocephaly, typical facial appearance and different degrees of intellectual disability. Three different types are described caused by variants or deletions/duplications in *NSD1, NFIX* and *APC2* genes. We aimed to describe a cohort of pediatric patients reporting the typical and unexpected findings in order to expand the phenotype of this syndrome and trying to find genotype-phenotype correlations.
Methods: In our referral center, we collected and analyzed clinical and genetic data of 31-patients cohort diagnosed with SS.
Results: All of them presented with overgrowth, typical dysmorphic features and different degree of developmental delay. Although structural cardiac defects have been reported in SS, non-structural diseases such as pericarditis were outstanding in our cohort. Moreover, we described here novel oncological malignancies not previously linked to SS such as splenic hamartoma, retinal melanocytoma and acute lymphocytic leukemia. Finally, five patients suffered from recurrent onychocryptosis that required surgical procedures, as an unreported prevalent medical condition.
Discussion: This is the first study focusing on multiple atypical symptoms in SS at the time that revisits the spectrum of clinical and molecular basis of this heterogeneous entity trying to unravel a genotype-phenotype correlation.

KEYWORDS

sotos syndrome, phenotype, overgrowth, *NSD1*, *NFIX*, *APC2*

1. Introduction

Sotos Syndrome (SS, OMIM#117550) is a heterogeneous genetic condition, recognized by three main clinical features present in most cases: overgrowth, defined as height and/or head circumference at least two standard deviations above the mean; typical facial appearance and different degrees of intellectual disability. Indeed, SS is the most frequent genetic cause of overgrowth, with an estimated incidence of 1/14.000 live births (1–3).

More than 90% of the patients present an autosomal dominant deletion or variant in the Nuclear Receptor SET Domain–containing protein 1 (*NSD1*) gene, located at chromosome 5q35, encodes a histone methyltransferase that catalyzes the transfer of methyl groups to lysine residues of histone tails: more specifically lysine residue 36 of histone H3 (H3K36)

and less frequently lysine residue 20 of histone H4 (H4K20) (4). These methylation marks are most frequently associated with transcriptional activation but can be associated with repression depending on the cellular context (5). Loss of function experiments in animal models revealed that *NSD1* is essential for normal development and has been confirmed to also play an important role in human developmental syndromes, such as SS, as well as in different types of malignancies (6–10).

Other causes may correspond to variants in the recently described *NFIX* or *APC2* genes (located on chromosome 19p13) that explain SS type two (also called Malan syndrome) and SS type three (11–13). There are also other syndromes characterized by overgrowth, mainly Tatton-Brown-Rahman Syndrome, Weaver Syndrome, or Sotos-like Syndrome, caused by variants in *DNMT3A*, *EZH2,* and *SETD2* genes, respectively (14, 15).

The typical overgrowth pattern of SS starts prenatally, where patients may have higher mean birth length, weight, and head circumference, but contrarily, many reach adulthood with a height within the upper normal range. Hypotonia, feeding difficulties, hypoglycemia, and neonatal jaundice are also commonly found during the perinatal period (16–18).

SS dysmorphic features include macrocephaly and dolichocephaly, frontal bossing, high anterior hairline, down-slanted palpebral fissures, high arched palate, pointed and triangular chin, and large hands and feet. Clinically, SS patients may present neurodevelopmental delays associated with learning and behavior problems, attention deficit with hyperactivity, and socialization disturbances with autistic traits (19–23). Other complications include epilepsy, impaired vision and hearing, cardiac, urinary, and orthopedic defects, recurrent infections, and increased oncological risk (5, 24).

In this work, we aimed to describe a cohort of pediatric patients diagnosed with SS, focusing on the unreported medical complications, and expanding the clinical and genetic profile of the syndrome. We reevaluate the possibility of un-described phenotype-genotype correlations.

2. Materials and methods

2.1. Patient cohort

We conducted a descriptive, observational, and ambispective study. We included patients according to the following criteria: pediatric patients (between 2 and 18 years at the time of diagnosis) with a confirmed molecular diagnosis of SS attended at a tertiary hospital [Hospital Sant Joan de Déu (HSJD), Barcelona Spain] between January 2012 and July 2020.

We analyzed the medical records of a total of 31 pediatric patients. Information on clinical characteristics and complementary exams was analyzed. Adolescence was considered between 10 and 19 years of age, according to the World Health Organization definition.

Parents or legal representatives gave their written informed consent, and children/adolescents gave their assent. Blood samples were obtained in accordance with the Declaration of Helsinki revised in 2013.

2.2. Genetic analyses

In most patients (particularly the older individuals who underwent previous study protocols), genetic screening was performed using either Multiple Ligation Probe Assay (MLPA) or Array-CGH to search Deletions/Duplications of *NSD1* and *NFIX* genes. In many patients (with negative MLPA/Array-CGH or those more recently enrolled) Sanger studies or clinical exome sequencing and subsequent confirmation and segregation of variants with Sanger sequencing was performed. All variants resulted *de novo*.

SALSA MLPA Probemix P026-E2 Sotos (MRC-Holland) has one probe for each one of the 23 exons from *NSD1* and the 10 exons of *NFIX* genes and allowed us to detect any alteration at the exon level.

Array-CGH analysis was performed using a comparative genomic hybridization oligonucleotide microarray (qChipCM, 8×60 K; qGenomics). The submitted sample was hybridized against a commercial reference DNA of the same sex (Agilent Technologies). The quality of the data obtained was evaluated following the manufacturer's recommendations.

Primers used for sanger sequencing were designed with Primer3 program (httP://bioinfo.ut.ee/primer3/ analysis was performed by comparison with the reference sequence for *NSD1* (NM_0022455.5).

Exome sequencing of the coding regions (exons, and 25 bp intronic regions flanking the exon) of 6,710 genes associated with pathology according to the Human Gene Mutation Database (HGMD), GeneTest.org, and the Online Mendelian Inheritance in Man catalog (OMIM) was performed. Next-generation sequencing (NGS) techniques were employed using enrichment by hybridization in solution with an Illumina design kit (TruSight One Sequencing Panel) and subsequent sequencing on an Illumina NextSeq500 sequencer. The bioinformatic analysis for the exome data was carried out using a pipeline developed in the bioinformatics unit within our hospital.

2.3. Clinical follow up

Once the SS diagnosis is established, the follow up of these patients consists of a once per year visit in a multidisciplinary visit including genetics and neuropediatrics. During these follow-ups, a detailed physical examination is performed, which includes anthropometric measurements, dysmorphologic descriptions, and back examinations for scoliosis. Additionally, endocrinology visits are appointed biannually, and oncological assessments are performed by specialists when the genetic diagnostic is confirmed. All the families have the contact of a patient manager, in case any health complication or necessity appears.

Since other comorbidities need to be ruled out at the time of diagnosis and during the follow up, an echocardiogram and renal ultrasound tests are routinely performed. Individuals are also systematically, referred for an audiology assessment.

10.3389/fped.2023.1184529

TABLE 1 Common features and other features not found in literature.

Common and previously reported features	Number (% of total)	Other features not found formerly in literature	Number (% of total)
Perinatal			
Hypotonia	11 (36)	Ovarian cysts (oophorectomy)	1 (3)
Neonatal Jaundice	11 (36)		
High weight or height (>4 kg or >52 cm)	9 (41)		
Prematurity (moderate)	7 (26)		
Respiratory distress syndrome	2 (7)		
Neurological			
Neurodevelopmental delay	24 (77)	Chronic mixed headache	3 (10)
Epilepsy	14 (45)		
ADHD	8 (26)		
Autism Spectrum Disorders	4 (13)		
Febrile seizures	4 (13)		
Neuroimaging[a]			
Ventricular dilation	13 (54)	Chiari malformation type 1	1 (4)
Hypoplasia or agenesis of corpus callosum	8 (33)	Septum pellucidum cyst	1 (4)
Subcortical WM lesions	4 (17)	Epidural Hematoma	1 (4)
Germinolitic cysts	3 (13)		
Cortical dysplasia	2 (8)		
Heart disease			
Atrial septal defect	4 (13)	Recurrent pericarditis	2 (7)
Aortic valve regurgitation	2 (7)	Ventricular preexcitation	1 (3)
Mitral valve prolapse	2 (7)	Cor triatriatum Dexter	1 (3)
Persistent ductus arteriosus	1 (3)	Left ventricular hypertrophy	1 (3)
		Aortopulmonary fistula	1 (3)
Ophthalmological			
Strabismus	8 (26)	Cataract (bilateral)	3 (10)
Hyperopia	6 (19)	Retinal melanocytoma	1 (3)
Congenital nystagmus	4 (13)	Pseudopapiledema	1 (3)
Astigmatism	3 (10)	Optic nerve	1 (3)
Retinal atrophy	3 (10)	Hypoplasia	
Skeletal			
Scoliosis	11 (36)	Onychocryptosis	5 (16)
Pes valgus	7 (23)	Craniosynostosis	2 (7)
Otolaryngological			
Adenoid and tonsilar hypertrophy	6 (19)	Turbinate hypertrophy	1 (3)
Chronic otitis media	6 (19)	Orbitary cellulitis	1 (3)
Hearing loss (conductive)	5 (16)		
Obstructive sleep apnea	4 (13)		
Dental			
Multiple caries disease	9 (29)		
Early dental eruption	3 (10)		
Dental agenesia	2 (7)		
Gastroenterological			
	4 (13)	Gastric volvulus	1 (3)
Gastroesophageal reflux (severe)			
Constipation (severe)	2 (7)	Cholelithiasis (asymptomatic)	1 (3)
		Celiac disease	1 (3)
Genitourinary			
Vesicoureteral reflux	3 (10)	Renal lithiasis	2 (7)
Duplicated collecting system	3 (10)		
Recurrent urinary infections	2 (7)		
Urinary tract dilation (high risk)	1 (3)		
Pneumological and immunological			
Asthma (persistent or (intermittent)	7 (23)	Cilia immotile syndrome	1 (3)
Pneumoallergen sensitivity	3 (10)	Splenic hamartoma	1 (3)
Food allergies	1 (3)	Impaired B cell maturation	1 (3)
Recurrent pneumonia	1 (3)		

[a]Neuroimaging was performed in 24 patients.

2.4. Statistical analyses

Descriptive analyses were performed using univariate (Chi squared tests corrected by Pearson and Fisher's exact tests). Two-sided tests yielding a $p < 0.05$ was considered statistically significant. SPSS statistics for Windows, version 23.0 (IBM Corp., Armonk, NY, USA) was used to perform all statistical analysis.

2.5. Ethical approval

The study protocol was reviewed and approved by the Research & Ethics Committee of the Hospital Sant Joan de Déu, Barcelona, Spain (Project Internal Code PIC-08-19). The study was conducted in accordance with the Declaration of Helsinki, Good Clinical Practices, and applicable regulatory requirements. All parents and adult patients provided written informed consent, and adolescent patients able to understand the procedure gave their assent prior to patient enrollment.

3. Results

We analyzed 31 patients (16 males and 15 females) between 2 and 25 years of age (12.9 ± 5.9) in the last evaluation. The mean age at diagnosis was 8.0 (±5.9) years with a mean follow up time of 8.8 (±5.3) years. The clinical data of our cohort is described in **Table 1** and **Supplementary Table S1**.

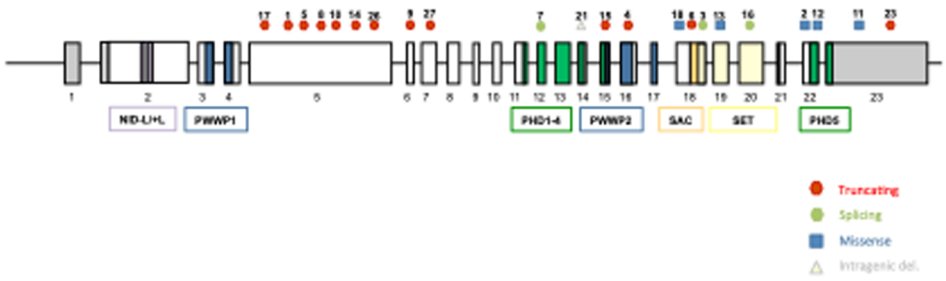

FIGURE 1
Schematic representation of *NSD1* gene, showing the localization of the variants described in our cohort. All 23 exons of *NSD1* are presented by boxes and introns are represented by lines. The domains of *NSD1* are represented with different colored boxes. *NSD1* contain two nuclear receptor interacting domains (NID), two proline-tryptophan-tryptophan-proline (PWWP), five plant homeodomain zinc fingers (PHD), the catalytic Su(var)3–9, enhancer-of-zeste, Trithorax (SET) and the C-terminal C5HCH (Cys-His) domain (SAC). Missense variants are represented with blue squares, truncating variants with red circles, intragenic deletions with yellow triangles and splicing variants with green circles.

TABLE 2 Description of the genetic variants identified in each patient.

Patient	Variants
1	*NSD1 (NM_022455.5):c.1810C > T (p.Arg604Ter)*
2	*NSD1 (NM_022455.5):c.6364T > C (p.Phe2122Leu)*
3	*NSD1 (NM_022455.5):c.5892 + 1G > C*
4	*NSD1 (NM_022455.5):c.5332C > T (p.Arg1778Ter)*
5	*NSD1 (NM_022455.5):c.1973_1974insATCA (p.Asp659SerfsTer2)*
6	*NSD1 (NM_022455.5):c.5730dup (p.Cys1911MetfsTer9)*
7	*NSD1 (NM_022455.5) c.4765 + 2T > G*
8	*NSD1 (NM_022455.5):c.2362C > T (p.Arg788Ter)*
9	*NSD1 (NM_022455.5):c.3811A > T (p.Lys1271Ter)*
10	*NSD1 (NM_022455.5)*:c.1870InsT (p.Ile623Ter)
11	*NSD1 (NM_022455.5):c.6558T > G (p.His2186Gln)*
12	*NSD1 (NM_022455.5):c.6377A > T (p.Asp2126Val)*
13	*NSD1 (NM_022455.5):c.5920G > A (p.Glu1974Lys)*
14	*NSD1* (NM_022455.5):c.2276C > G (p.Ser759Ter)
15	*NSD1* (NM_022455.5):c.5229G > A (p.Trp1743Ter)
16	*NSD1* (NM_022455.5):c.6010-1G > A
17	*NSD1 (NM_022455.5)*:c.1243C > T (p.Gln415Ter)
18	*NSD1* (NM_022455.5):c.5892G > T (p.Lys1964Asn)
19	*NSD1* deletion[a]
20	*NSD1* deletion[a]
21	*NSD1* (NM_022455.5):c.5079delTTACCCT (p.Phe1693Ter)
22	*NSD1* deletion[a]
23	*NSD1* (NM_022455.5):c.7485delA (p.Gly2496ValfsTer82)
24	*NSD1* deletion[a]
25	*NSD1* deletion[a]
26	*NSD1 (NM_022455.5)*:c.2859dupT (p.Lys954Ter)
27	*NSD1* (NM_022455.5):c.4035dupT (p.Glu1346Ter)
28	*NFIX (NM_001271043.2):c.554T > C (p.Leu185Pro)*
29	*NFIX* (NM_001271043.2):c.276delG (p.Glu94ter)
30	*NFIX (NM_001271043.2)*: c.367C > T (p.Arg123Trp)
31	NFIX (ENST00000676441.1):c.67_73dup (p.Glu25ValfsTer31)

[a]By SALSA MLPA Probemix P026-E2 Sotos (MRC-Holland).

3.1. Molecular findings

Out of all patients, 27 (87%) corresponded to variants of the *NSD1* gene, with 18 point variants (5 missense and 13 truncating), 7 deletions, and 2 duplications (Figure 1). There were 4 patients who presented variants of the *NFX1* gene, with 2 missense variants, 1 deletion, and 1 duplication. The description of the genetic variants identified in each patient are stated in Table 2.

3.2. Perinatal characteristics

Hypotonia and neonatal jaundice were observed in a third of the individuals, showing a significant difference in those premature patients ($p = 0.049$ and $p = 0.003$ respectively). Only 12.9% presented feeding difficulties, being more prevalent in females ($p = 0.043$) and in patients with *NFIX* variants ($p = 0.003$). Seven subjects were born moderately preterm (Table 1).

3.3. Growth and characteristic facial appearance

High birth length (>52 cm) and weight (>4 Kg) was observed in 40.9% of the patients. A pronounced subsequent postnatal growth (at least 2 SD above the mean) was maintained in almost half of the patients. Macrocephaly (at least 2 SD above the mean) was present in 50% of the patients.

A characteristic facial appearance consisting of a high and broad forehead, sparse frontotemporal hair, downslanted palpebral fissures, malar flushing, and a pointed chin was present in all patients. Three patients presented microretrognathia and one patient presented facial asymmetry.

3.4. Developmental and neurological disorders

Psychomotor delay and a varying range of intellectual disability were observed in most patients (77.4%). As neurological comorbidities, epileptic seizures were found in almost half of the sample (45.2%), of which nine patients required medical treatment: valproic acid (VPA) in three patients; levetiracetam (LEV) and topiramate (TPM) both in one patient each; and

associations of VPA plus LEV and VPA plus vigabatrin (VGB), both in two patients, respectively. Two patients suffered from simple febrile seizures, not followed by epilepsy.

In terms of behavioral disorders, attention-deficit hyperactivity disorder (ADHD) was diagnosed in eight patients (25.8%) and socialization difficulties were evident in seven patients (22.6%), including four with severe autism spectrum disorder (ASD) (12.9%). This last diagnosis was more prevalent in male patients ($p = 0.05$).

Meanwhile, other comorbidities such as impulsive behavior and anxiety disorder were diagnosed in 11 patients (35.5%), being the latter more prevalent in teenagers and young adults ($p = 0.01$).

No genetic correlations were identified between variants, affected genes, and the presence of epilepsy or behavioral disorders.

3.5. Heart disease

Regarding heart disease, 13 patients (41.9%) were diagnosed with some form of it. Cardiac structural defects were the most frequent (38.7%) (**Table 1**), and patients with hypotonia at birth were at increased risk of developing them ($p = 0.042$). These included atrial septal defects and persistent ductus arteriosus, observed in four patients, one of which was a preterm baby. Other findings included the diagnosis of mitral valve prolapse, *cor triatriatum dexter,* and left ventricle hypertrophy.

Two patients presented recurrent pericarditis with pericardial effusion (**Figure 2**). Clinical presentation started with a viral infection as a trigger leading to pericarditis without positive evidence of infectious or rheumatic etiology. These patients underwent multiple relapses and ended up depending on chronic immunosuppressant therapy (corticosteroid therapy). Both cases of pericarditis were detected in patients with *NSD1* affectations. One of them presented an *NSD1* deletion, and the other one a nonsense variant in the same gene *NSD1*:c.3811A > T (p.Lys1271Ter).

Arrhythmia was detected in one patient, which was further diagnosed with ventricular preexcitation without paroxysmal tachycardia. There was no statistically significant correlation between the presence of heart disease (structural or not) and molecular findings.

3.6. Ophthalmological disorders

Twenty-two patients (71%) presented ophthalmological disorders, including strabismus (eight patients) and refractive defects (hyperopia in six patients and astigmatism in three patients) as the most prevalent. Congenital nystagmus affected four patients. Moreover, three patients showed bilateral cataracts that needed surgery during the first months of life, and three developed retinal atrophy. One subject presented a retinal melanocytoma, explained in the oncological findings section.

3.7. Otolaryngological disease

Chronic otitis media leading to conductive hearing loss and adenoid and tonsil hypertrophy were the most prevalent diseases, both in six patients. Four of the subjects suffered from apnea-hypopnea syndrome, due to adenoid and tonsil hypertrophy or microretrognathia, plus the hypotonic muscle tone. Two patients presented cholesteatoma, one of them associated with hypoacusis. Both patients required surgical intervention.

3.8. Traumatological and orthopedic disorders

The most frequent skeletal finding in our cohort was scoliosis, present in 11 patients (35.5%), two of them required surgical intervention. Pes valgus was observed in seven patients (22.6%). Five patients (16.1%) suffered from recurrent onychocryptosis needing surgical procedures due to the lack of improvement with conservative treatment.

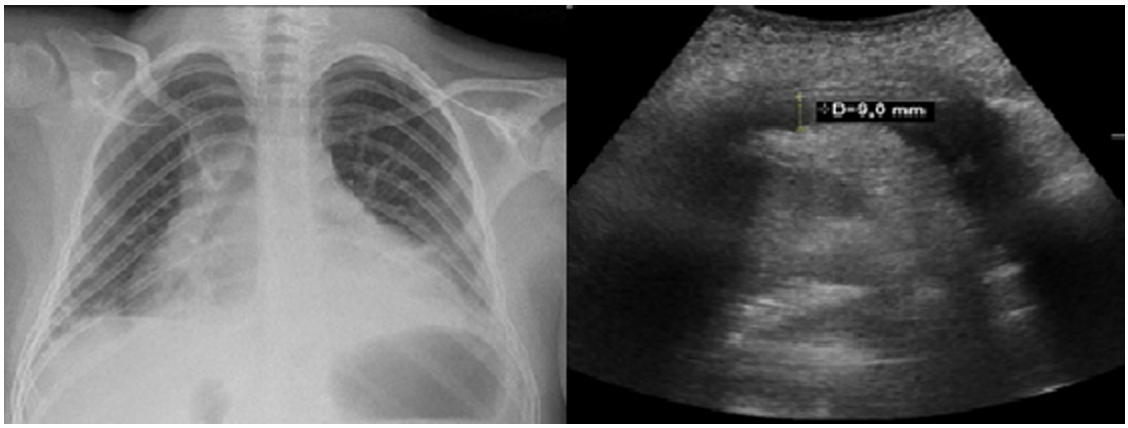

FIGURE 2
Pericardial effusion. **Left**: Thorax radiography showing cardiomegaly. **Right**: echocardiogram of patient with pericardial effusion of 9 mm.

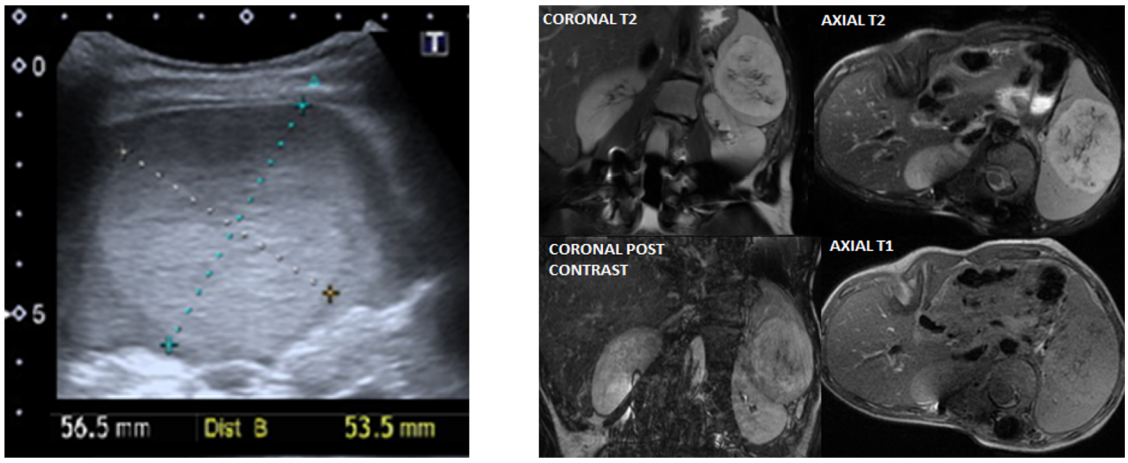

FIGURE 3
Splenic hamartoma clinical imaging. **Left** panel: Ultrasound of a patient with well-defined splenic solid mass, 5.7 × 5.4 centimeters, isoechoic, with calcifications dotted inside. **Right** panel: MRI imaging of the same patient that shows stable mass of 7.2 × 5.9 × 6.9 cm, hyperintense in T2, isointense in T1, without fat, with enhancement in small hemorrhagic areas.

3.9. Genitourinary and endocrinological findings

Eight patients (25.8%) suffered from genitourinary pathology including urinary tract dilation, duplicated collecting system, renal dysplasia/hypoplasia, or renal agenesis. Unilateral cryptorchidism was reported in two patients. One child suffered from hydrocele testicle and needed surgical treatment. One boy presented idiopathic precocious puberty without abnormalities at the sellar and suprasellar regions in neuroimaging.

3.10. Oncological findings

Within our cohort, we identified three different oncological presentations. One case of splenic hamartoma (**Figure 3**), diagnosed at seven years of age, in a routine study that remained stable in subsequent controls; one case of retinal melanocytoma, diagnosed at one year of age, showing spontaneous involution; and one case of acute lymphocytic leukemia diagnosed at 14 years of age, to whom chemotherapy treatment is currently ongoing. Missense variants in the *NSD1* gene were drivers of increased oncological malignancies compared to *NFIX* alterations ($p = 0.049$) in our cohort.

4. Discussion

SS is a rare genetic disorder characterized by a range of features, which have mainly been described in adult populations and small pediatric cohorts with overgrowth syndromes. In this study, we aim to provide a comprehensive description of the typical and atypical findings in a large cohort of pediatric patients with SS, all followed in the same center.

Regarding the conventional and extensively documented observations, the prevailing feature observed in all patients was the distinct facial appearance. While macrocephaly is commonly regarded as a hallmark symptom of SS, it was only detected in half of our patient cohort. Nonetheless, the particular skull shape was also observed in the non-macrocephalic subjects, pointing towards SS as a potential diagnosis.

There were no specific remarkable perinatal findings. Mild prematurity, neonatal jaundice, and perinatal global hypotonia are frequently found in SS individuals and may rise the suspicion of a genetic condition. Contrarily, hypoglycemia was not as frequent as expected.

As for neurological assessment, neurodevelopment delay was present in 77.4% of the sample. Classically, SS patients reported in the literature always presented with intellectual disability. For example, some studies found that 5q35 microdeletions are linked with lower scores in cognitive, adaptive functioning, and behavioral domains (25). However, other studies are starting to show a varying range of cognitive ability and some patients can be found within a normal cognitive range (18, 21).

In our sample, the range of intellectual difficulties is also wide, with many patients attending normal schooling with some subject adaptations. ADHD has been reported as a very prevalent neurodevelopmental disorder in this population (19) and probably is underdiagnosed in our cohort since the coexistence of intellectual disability and ADHD traits may complicate the diagnosis.

The present study reveals a notable prevalence of ASD traits in our sample, despite not meeting all of the classical criteria for ASD. This finding is consistent with previous reports in the literature (19–22). Again, the coexistence of a typical behavioral phenotype with traits of other neurodevelopmental conditions (perhaps not fulfilling the classical criteria), complicates the diagnosis. However, particular recognition and correct management of

ADHD and ASD may have a relevant impact on the patient's development, including academic achievements, social inclusion, but also the quality of their home life.

Regarding behavioral issues, tantrums and anxiety were found to be the most prevalent. The behavioral disturbances observed may be attributed, in part, to the characteristics of ADHD and ASD, such as impulsiveness, rigidity, and social difficulties. In view of our results and the impact on patients' and families' wellbeing, guidelines need to include mental health experts (both psychologists and psychiatrists) implied in the assessment and follow-up of this group of patients. Regarding epilepsy, in concordance with the literature (5, 26), presented in half of our patients and was well controlled with antiepileptic drugs, mostly in monotherapy. None of the patients presented neurological regression due to uncontrolled epilepsy. The presence of febrile seizures was not related to subsequent epilepsy.

In our study, we wanted to take a holistic view of SS by considering a wide array of comorbidities and make an exhaustive analysis to expand the clinical phenotype. Subsequently, we have identified a series of characteristics linked to SS in our cohort, rarely described in the literature. One such characteristic is the presence of recurrent pericarditis or arrhythmias.

According to established studies, between 20% and 50% of SS patients may present with cardiac defects (27), but these usually include septal or valvular defects.

In our cohort, two patients exhibited recurring pericarditis, which manifested at comparable ages (nine and ten years old) and with similar clinical presentations (associated with viral infection triggers, multiple relapses, and dependence on corticosteroid treatment). Despite the patients' similar presentations, infectious and rheumatologic etiologies were ruled out. Recently, one study reported pericarditis in a patient with SS, which was observed in the context of SARS-CoV-2 infection, highlighting SS as a potential risk factor for this condition during viral infections (28). Therefore, the possibility of recurrent idiopathic pericarditis and the benefit of corticosteroid treatment should be considered in SS patients.

In addition, there have been infrequent reports of arrhythmogenic mechanisms. In a study by Segreti et al., a Brugada syndrome was identified in a patient with SS (29). Similarly, Sharma et al. reported a case of overgrowth and dysmorphic features in a patient with Wolff Parkinson White Syndrome (WPWS) in 2003, even though no genetic findings were reported, and SS was not formally diagnosed (30). In our own cohort, we have also observed a comparable form of arrhythmia, suggesting a potential underlying mechanism that warrants further investigation in future studies.

The increased oncological risks afflicting SS patients are of great concern to geneticists, pediatricians, oncologists, and families. Somatic variants affecting *NSD1* have been identified in various types of tumors, suggesting a potential tumor suppressing role (31). Tauchmann et al. recently reviewed the role and molecular functions of *NSD1*, in which it is shown to be widely expressed in different tissues, playing an important role in human developmental syndromes, such as SS, as well as in different types of malignancies (32, 33).

Indeed, the genetic profile of SS has great repercussions on the clinical presentation of these patients. In our study, we found a correlation between oncological risk and missense *NSD1*. Future studies to understand the functional involvement of these variants and the role of *NSD1* would be of great interest. Most of the reported malignancies in SS have been solid tumors, such as Wilms tumor, hepatocarcinoma, neuroectodermal tumor, small cell lung carcinoma, teratomas, and neuroblastoma. However, other malignancies, including lymphoproliferative disorders such as acute lymphoblastic leukemia, B-cell lymphoblastic lymphoma, and other non-Hodgkin lymphomas, have also been reported (34, 35).

In our cohort, two patients presented solid tumors: one of them corresponds to a stable splenic hamartoma, and another one presented a retinal melanocytoma as a finding on ocular examination, asymptomatic at the time of diagnosis. None of these tumors had been previously described in SS.

Interestingly, although with less involvement in the severity of the disease but potentially very afflictive, five patients presented onychocryptosis, not previously associated with this pathological entity. Particular nail care may be useful to prevent this outstanding complication in our cohort, probably explained by distal phalanx or nail malformations or connective tissue anomalies.

Since it is difficult to determine if these atypical findings are sporadic or clearly secondary to SS, we recommend increasing awareness among physicians, annotating and reporting them. Associating these new phenotypes with the wider SS clinical spectrum should be considered.

Future descriptions are needed on this issue in order to expand the specific follow-up protocols. What does seem mandatory is the need for a multidisciplinary approach to patients with SS.

5. Conclusions

This study deepens in the already known phenotype but also considers multiple atypical findings that may have been not described but are probably frequent and relevant in SS. Remarkably recurrent pericarditis, onychocryptosis, and unusual malignancies were found in our large pediatric sample indicating that multidisciplinary and comprehensive follow-up recommendations are needed. The clinical and molecular spectrum of SS in this sample is described in detail, highlighting the importance of continuously revisiting and expanding the phenotype and genotype of rare diseases, as well as, exploring the possible correlations among them. Unfortunately, we were not able to establish a clear correlation between phenotype and genotype. However, we found that ASD is more frequently diagnosed in males than in females; contrarily feeding disorders are more prevalent in females. *NFIX* patients had more prevalent feeding disorders but fewer malignancies than *NSD1* patients. The findings of this study can aid in directing follow-up, screening for associated comorbidities, and assessing newly described health complications. Overall, this study emphasizes the need for continued research into rare diseases to better

understand their clinical and molecular characteristics, revisit and redesign follow-up guidelines, and, as a final goal, improve patients' and families' outcomes and wellbeing.

Data availability statement

The raw data supporting the conclusions of this article will be made available by the authors, without undue reservation.

Ethics statement

The studies involving human participants were reviewed and approved by Research & Ethics Committee of the Hospital Sant Joan de Déu, Barcelona, Spain (the internat evaluation code PIC-08-19). Written informed consent to participate in this study was provided by the participants' legal guardian/next of kin.

Author contributions

V-HL visited patients, coordinated and contributed to the data extraction, wrote mostly the manuscript and provided feedback on the report. S-CM contributed to data extraction, helped write the manuscript and provided feedback on the report. C-AD, BM, PL, and FL visited patients, helped write the manuscript and provided feedback on the report. ML contributed to molecular studies. AM and SM visited patients, designed the study, coordinated the data extraction, helped write the manuscript and coordinated the manuscript revisions. All authors contributed to the article and approved the submitted version.

Acknowledgments

We thank the patients and families for their active participation in this study and the clinicians that recruited them.

Conflict of interest

The authors declare that the research was conducted in the absence of any commercial or financial relationships that could be construed as a potential conflict of interest.

Publisher's note

Supplementary material

The Supplementary Material for this article can be found online at: https://www.frontiersin.org/articles/10.3389/fped.2023.1184529/full#supplementary-material

References

1. Lapunzina P. Síndrome de Sotos. *Protoc Diagn ter Pediatr*. (2010) 1:71–9.

2. Cole TR, Hughes HE. Sotos syndrome: a study of the diagnostic criteria and natural history. *J Med Genet*. (1994) 31(1):20–32. doi: 10.1136/jmg.31.1.20

3. Ko JM. Genetic syndromes associated with overgrowth in childhood. *Ann Pediatr Endocrinol Metab*. (2013) 18(3):101–5. doi: 10.6065/apem.2013.18.3.101

4. Rayasam GV, Wendling O, Angrand PO, Mark M, Niederreither K, Song L, et al. NSD1 Is essential for early post-implantation development and has a catalytically active SET domain. *EMBO J*. (2003) 22(12):3153–63. doi: 10.1093/emboj/cdg288

5. Foster A, Zachariou A, Loveday C, Ashraf T, Blair E, Clayton-Smith J, et al. The phenotype of sotos syndrome in adulthood: a review of 44 individuals. *Am J Med Genet C Semin Med Genet*. (2019) 181(4):502–8. doi: 10.1002/ajmg.c.31738

6. Rio M, Clech L, Amiel J, Faivre L, Lyonnet S, Le Merrer M, et al. Spectrum of NSD1 mutations in sotos and weaver syndromes. *J Med Genet*. (2003) 40 (6):436–40. doi: 10.1136/jmg.40.6.436

7. Waggoner DJ, Raca G, Welch K, Dempsey M, Anderes E, Ostrovnaya I, et al. NSD1 Analysis for sotos syndrome: insights and perspectives from the clinical laboratory. *Genet Med*. (2005) 7(8):524–33. doi: 10.1097/01.GIM.0000178503.15559.d3

8. Ha K, Anand P, Lee JA, Jones JR, Kim CA, Bertola DR, et al. Steric clash in the SET domain of histone methyltransferase NSD1 as a cause of sotos syndrome and its genetic heterogeneity in a Brazilian cohort. *Genes (Basel)*. (2016) 7(11):96. doi: 10.3390/genes7110096

9. Berdasco M, Esteller M. Genetic syndromes caused by mutations in epigenetic genes. *Hum Genet*. (2013) 132(4):359–83. doi: 10.1007/s00439-013-1271-x

10. Choufani S, Cytrynbaum C, Chung BH, Turinsky AL, Grafodatskaya D, Chen YA, et al. NSD1 Mutations generate a genome-wide DNA methylation signature. *Nat Commun*. (2015) 6:10207. doi: 10.1038/ncomms10207

11. Türkmen S, Gillessen-Kaesbach G, Meinecke P, Albrecht B, Neumann LM, Hesse V, et al. Mutations in NSD1 are responsible for sotos syndrome, but are not a frequent finding in other overgrowth phenotypes. *Eur J Hum Genet*. (2003) 11 (11):858–65. doi: 10.1038/sj.ejhg.5201050

12. Cecconi M, Forzano F, Milani D, Cavani S, Baldo C, Selicorni A, et al. Mutation analysis of the NSD1 gene in a group of 59 patients with congenital overgrowth. *Am J Med Genet A*. (2005) 134(3):247–53. doi: 10.1002/ajmg.a.30492

13. Tatton-Brown K, Douglas J, Coleman K, Baujat G, Chandler K, Clarke A, et al. Multiple mechanisms are implicated in the generation of 5q35 microdeletions in sotos syndrome. *J Med Genet*. (2005) 42(4):307–13. doi: 10.1136/jmg.2004.027755

14. Tatton-Brown K, Seal S, Ruark E, Harmer J, Ramsay E, Del Vecchio Duarte S, et al. Mutations in the DNA methyltransferase gene DNMT3A cause an overgrowth syndrome with intellectual disability. *Nat Genet*. (2014) 46(4):385–8. doi: 10.1038/ng.2917

15. Marzin P, Rondeau S, Aldinger KA, Alessandri JL, Isidor B, Heron D, et al. SETD2 Related overgrowth syndrome: presentation of four new patients and review of the literature. *Am J Med Genet C Semin Med Genet*. (2019) 181(4):509–18. doi: 10.1002/ajmg.c.31746

16. Douglas J, Tatton-Brown K, Coleman K, Guerrero S, Berg J, Cole TR, et al. Partial NSD1 deletions cause 5% of sotos syndrome and are readily identifiable by multiplex ligation dependent probe amplification. *J Med Genet*. (2005) 42(9):e56. doi: 10.1136/jmg.2005.031930

17. Priolo M, Schanze D, Tatton-Brown K, Mulder PA, Tenorio J, Kooblall K, et al. Further delineation of malan syndrome. *Hum Mutat*. (2018) 39(9):1226–37. doi: 10.1002/humu.23563

18. Tatton-Brown K, Rahman N. Clinical features of NSD1-positive sotos syndrome. *Clin Dysmorphol*. (2004) 13(4):199–204. doi: 10.1097/00019605-200410000-00001

19. Lane C, Milne E, Freeth M. Cognition and behaviour in sotos syndrome: a systematic review. *PLoS One*. (2016) 11(2):e0149189. doi: 10.1371/journal.pone.0149189

20. Harris JR, Fahrner JA. Disrupted epigenetics in the sotos syndrome neurobehavioral phenotype. *Curr Opin Psychiatry*. (2019) 32(2):55–9. doi: 10.1097/YCO.0000000000000481

21. Lane C, Milne E, Freeth M. The cognitive profile of sotos syndrome. *J Neuropsychol*. (2019) 13(2):240–52. doi: 10.1111/jnp.12146

22. Lane C, Milne E, Freeth M. Characteristics of autism spectrum disorder in sotos syndrome. *J Autism Dev Disord*. (2017) 47(1):135–43. doi: 10.1007/s10803-016-2941-z

23. Ball LJ, Sullivan MD, Dulany S, Stading K, Schaefer GB. Speech-language characteristics of children with sotos syndrome. *Am J Med Genet A*. (2005) 136A (4):363–7. doi: 10.1002/ajmg.a.30799

24. van Haelst MM, Hoogeboom JJ, Baujat G, Brüggenwirth HT, Van de Laar I, Coleman K, et al. Familial gigantism caused by an NSD1 mutation. *Am J Med Genet A*. (2005) 139(1):40–4. doi: 10.1002/ajmg.a.30973

25. Siracusano M, Riccioni A, Frattale I, Arturi L, Dante C, Galasso C, et al. Cognitive, adaptive and behavioral profile in sotos syndrome children with 5q35 microdeletion or intragenic variants. *Am J Med Genet A*. (2023). doi: 10.1002/ajmg.a.63211

26. Nicita F, Ruggieri M, Polizzi A, Mauceri L, Salpietro V, Briuglia S, et al. Seizures and epilepsy in sotos syndrome: analysis of 19 Caucasian patients with long-term follow-up. *Epilepsia*. (2012) 53(6):e102–5. doi: 10.1111/j.1528-1167.2012.03418.x

27. Letter to the Editor Congenital Heart Defects in Sotos Syndrome To the Editor. (1999) 172(November 1998):9670810.

28. Citoni B, Digilio MC, Capolino R, Gagliardi MG, Campana A, Drago F, et al. SARS-CoV-2 and pre-tamponade pericardial effusion. Could sotos syndrome be a major risk factor? *Genes (Basel)*. (2021) 12(11):1782. doi: 10.3390/genes12111782

29. Segreti A, Piccirillo F, Crispino SP, Cocchia F, Martucciello A, Calabrese V, et al. Simultaneous presence of Brugada and overgrowth syndromes. *Monaldi Arch Chest Dis*. (2023). doi: 10.4081/monaldi.2023.2521

30. Sharma PP, Vidaillet H, Dietz J. Patient with sotos syndrome, Wolff-Parkinson-White pattern on electrocardiogram, and two right-sided accessory bypass tracts. *Am J Med Genet A*. (2003) 116A(4):372–5. doi: 10.1002/ajmg.a.10022

31. Villani A, Greer MC, Kalish JM, Nakagawara A, Nathanson KL, Pajtler KW, et al. Recommendations for cancer surveillance in individuals with RASopathies and other rare genetic conditions with increased cancer risk. *Clin Cancer Res*. (2017) 23(12):e83–e90. doi: 10.1158/1078-0432.CCR-17-0631

32. Brioude F, Toutain A, Giabicani E, Cottereau E, Cormier-Daire V, Netchine I. Overgrowth syndromes—clinical and molecular aspects and tumour risk. *Nat Rev Endocrinol*. (2019) 15(5):299–311. doi: 10.1038/s41574-019-0180-z

33. Tauchmann S, Schwaller J. NSD1: a lysine methyltransferase between developmental disorders and cancer. *Life (Basel)*. (2021) 11(9):877. doi: 10.3390/life11090877

34. Al-Mulla N, Belgaumi AF, Teebi A. Cancer in sotos syndrome: report of a patient with acute myelocytic leukemia and review of the literature. *J Pediatr Hematol Oncol*. (2004) 26(3):204–8. doi: 10.1097/00043426-200403000-00013

35. Kaya Z, Keser E, Atalay E, Kayhan G, Karamercan S, Topuz B, et al. Two distinct syndromic children with T-acute lymphoblastic leukemia: noonan syndrome and sotos syndrome. *Leuk Res*. (2022) 123:106981. doi: 10.1016/j.leukres.2022.106981

frontiers | Frontiers in Genetics

TYPE Original Research
PUBLISHED 29 June 2023
DOI 10.3389/fgene.2023.1203891

OPEN ACCESS

EDITED BY
Jordi Pérez-Tur,
Spanish National Research Council (CSIC), Spain

REVIEWED BY
Nadja Kokalj Vokač,
UKC MB, Slovenia
Thomas Liehr,
Friedrich Schiller University Jena, Germany

*CORRESPONDENCE
Ting Hu,
huting4123@163.com

RECEIVED 11 April 2023
ACCEPTED 20 June 2023
PUBLISHED 29 June 2023

CITATION
Liao N, Zhang Z, Liu X, Wang J, Hu R, Xiao L, Yang Y, Lai Y, Zhu H, Li L, Liu S, Wang H and Hu T (2023), A chromosomal microarray analysis-based laboratory algorithm for the detection of genetic etiology of early pregnancy loss. *Front. Genet.* 14:1203891. doi: 10.3389/fgene.2023.1203891

A chromosomal microarray analysis-based laboratory algorithm for the detection of genetic etiology of early pregnancy loss

Na Liao[1,2,3], Zhu Zhang[1,2,3], Xijing Liu[1,2,3], Jiamin Wang[1,2,3], Rui Hu[1,2,3], Like Xiao[1,2,3], Yunyuan Yang[1,2,3], Yi Lai[1,2,3], Hongmei Zhu[1,2,3], Lingping Li[1,2,3], Shanling Liu[1,2,3], He Wang[1,2,3] and Ting Hu[1,2,3]*

[1]Department of Medical Genetics, West China Second University Hospital, Sichuan University, Chengdu, Sichuan, China, [2]Department of Obstetrics and Gynecology, West China Second University Hospital, Sichuan University, Chengdu, Sichuan, China, [3]Key Laboratory of Birth Defects and Related Diseases of Women and Children (Sichuan University), Ministry of Education, Chengdu, China

Background: Chromosomal abnormalities are a major cause of early pregnancy loss. However, models synthesizing existing genetic technologies to improve pregnancy outcomes are lacking. We aim to provide an integrated laboratory algorithm for the genetic etiology of couples who experienced pregnancy loss.

Methods: Over a 6-year period, 3,634 products of conception (POCs) following early pregnancy loss were collected. The clinical outcomes from a laboratory algorithm based on single nucleotide polymorphism (SNP) array, fluorescence *in situ* hybridization (FISH), and parental chromosomal karyotyping assays were comprehensively evaluated.

Results: In total, 3,445 of 3,634 (94.8%) POCs had no maternal-cell contamination. Of those POCs, the detection rate of abnormal results was 65.2% (2,247/3,445), of which 91.2% (2,050/2,247) had numerical chromosomal abnormalities, 2.7% (60/2,247) had copy-number variations (CNVs) ≥10 Mb, 2.7% (61/2,247) had CNVs of terminal deletion and duplication, 2.8% (62/2,247) had CNVs <10 Mb, and 0.6% (14/2,247) had uniparental disomy. Furthermore, FISH confirmed 7 of the 60 POCs with mosaic aneuploids below 30% based on the SNP array results as tetraploid. Of the 52 POCs with CNVs of terminal deletion and duplication, 29 couples had balanced rearrangements based on chromosomal karyotyping.

Conclusion: The integrated SNP array-based algorithm combined with optional FISH and parental chromosomal karyotyping is an effective laboratory testing strategy, providing a comprehensive and reliable genetic investigation for the etiology of miscarriage, regardless of the number of miscarriages and the method of conception.

KEYWORDS

chromosomal abnormality, chromosomal microarray analysis, copy-number variation, uniparental disomy, miscarriage, pregnancy loss, products of conception, first trimester

Introduction

Pregnancy loss is the most common pregnancy-related complication and the risk of miscarriage is approximately 10%–15% in all clinically recognized pregnancies, most of which occur during the first trimester (Rai and Regan, 2006; Dhillon et al., 2014; Colley et al., 2019). Of these early pregnancy losses, 50%–70% are caused by chromosomal abnormalities, including numerical and structural abnormalities (Hassold et al., 1980; Menasha et al., 2005). Specifically, balanced structural chromosomal abnormalities, mostly balanced reciprocal or Robertsonian translocations, are observed in approximately 2%–5% of couples who experienced pregnancy loss (Practice Committee of the American Society for Reproductive Medicine, 2012). Antiphospholipid syndrome, prothrombotic states, uterine anomalies, maternal endocrine disorders, psychological factors, and lifestyle are also associated with pregnancy loss (Practice Committee of the American Society for Reproductive Medicine, 2012).

Genome-wide, high-resolution molecular technologies, including chromosomal microarray analysis (CMA) and next-generation sequencing (NGS), have become broadly implemented. Consequently, pathogenic/likely pathogenic (P/LP) copy-number variations (CNVs) have been identified in approximately 15%–30% of patients with neurodevelopmental disorders and 6% of fetuses with structural anomalies observed by ultrasound (Manning et al., 2010; Miller et al., 2010; Wapner et al., 2012). Thus, a CNV assessment is the first-tier recommendation for these conditions (Miller et al., 2010; American College of Obstetricians and Gynecologists Committee on Genetics, 2013). Although several studies have explored the clinical utility of CMA or NGS in products of conception (POCs) (Zhang et al., 2009; Li et al., 2013; Kooper et al., 2014; Shen et al., 2016), until 2016, the Society for Maternal-Fetal Medicine recommended against using CMA as a first-line test to evaluate first-trimester pregnancy loss due to limited data (Society for Maternal-Fetal Medicine Dugoff et al., 2016).

Several large cohort studies have recently evaluated the diagnostic yield of different chromosomal testing techniques (Shearer et al., 2011; Levy et al., 2014; Rosenfeld et al., 2015; Fan et al., 2020; Wang et al., 2020). However, models synthesizing existing genetic technologies to improve pregnancy outcomes are lacking. Therefore, we performed a large-scale retrospective study to build an integrated CMA-based laboratory algorithm for the genetic etiology of early pregnancy loss, regardless of the number of miscarriages and the method of conception. We also aimed to provide practical genetic counseling recommendations for couples who have experienced pregnancy loss.

Materials and methods

Specimen collection

From January 2016 to October 2021, POCs of early pregnancy loss prior to 13 gestational weeks were collected for this 6-year retrospective study at a tertiary-level referral center (West China Second University Hospital, Sichuan University). Trained clinical geneticists performed pretest counseling for parents who intended to seek a possible genetic etiology. Before testing, written informed consent was obtained from all couples agreeing to undergo a single nucleotide polymorphism (SNP) array analysis, and consecutive parental consent was obtained in instances of positive POC results. Those with a pregnancy history were recruited regardless of the conception method (natural conception or assisted reproductive technology [ART]). The Medical Ethics Committee of West China Second University Hospital approved the study design.

POCs obtained by suction curettage or spontaneous passage were collected in 15 mL conical tubes with saline solution and stored at 4°C. A saline solution rinse was performed three or more times; then, chorionic villi were dissected from the maternal decidua using forceps and scissors and divided into two samples, if necessary: one for CMA and one for consecutive fluorescence *in situ* hybridization analysis (FISH).

DNA isolation

Whole-genome DNA was extracted from POC samples using a QIAamp DNA Mini Kit (Qiagen, Valencia, CA, United States). A NanoDrop One microvolume UV-Vis spectrophotometer (Thermo Fisher Scientific, Madison, GA, United States) was used to determine the DNA's quantity and quality. DNA denaturation was confirmed via electrophoresis on a 1% agarose gel. Poor-quality DNA samples were excluded.

CMA

Whole-genome DNA was subjected to SNP array analysis using the CytoScan 750 K Array (Thermo Fisher Scientific, Santa Clara, CA, United States). The GRCh38 (hg18) genome was used for annotation. CNVs >100 kb or those that affected >50 contiguous probes were considered. Terminal regions of homozygosity (ROHs) > 5 Mb or interstitial ROHs >10 Mb were analyzed using the uniparental disomy (UPD) tool_0.2 software to separate the results into UPD or consanguinity based on comparisons with the parental results as described in our previous study (Hu et al., 2021).

The chromosomal abnormalities detected by the SNP array were classified into five groups: 1) numerical chromosomal abnormalities, including single aneuploidy, multiple aneuploidy, mosaic aneuploidy, and polyploidy; 2) CNVs ≥10 Mb (large CNVs), those with gains or losses of chromosome regions >10 Mb; 3) CNVs of terminal deletion and duplication, those with one deletion and one duplication at the ends of different chromosomes or the same chromosome; 4) CNVs <10 Mb (submicroscopic CNVs), those with gains or losses of chromosome regions <10 Mb; and 5) UPD, those with both homologous chromosomes inherited from one parent based on a comparison with the parental SNP array results.

Significant maternal cell contamination (MCC) was defined as levels of maternal cells exceeding 30%, tested directly by an SNP array (Zahir and Marra, 2015); patients with significant MCC were excluded.

Quantitative fluorescent polymerase chain reaction (QF-PCR)

The SNP array limit of detection for low-level mosaicism is 10%–20% (Cross et al., 2007). Therefore, if the MCC below 30% was suspected by the SNP array, QF-PCR of the chorionic villi and

maternal peripheral blood was subsequently performed to validate the proportion of maternal DNA in female embryos.

QF-PCR was performed using 20 highly polymorphic short tandem repeat markers, including four for chromosome 21 (D13S628, D13S742, D13S634, and D13S305), four for chromosome 18 (D18S1002, D18S391, D18S535, and D18S386), six for chromosome 21 (D21S1433, 21q11.2, D21S1411, D21S1414, D21S1412, and D21S1445), and six for sex chromosomes (AMXY, DXS1187, DXS8377, DXS6809, DXS981, and SRY).

FISH analysis

Mosaicism for CNVs ≥5 Mb was tested directly by SNP array when the proportion exceeded the 30% detection threshold. If the SNP array mosaicism result was below 30%, FISH was simultaneously performed for confirmation, which could also detect potential tetraploids as incidental findings.

AneuVysion probe sets (Vysis/Abbott, Downers Grove, IL, United States) that probed for chromosomes 2, 4, 5, 7, 9, 12, 13, 15, 16, 17, 18, 21, 22, X, and Y were used for hybridization to the chorionic interphase cells of POCs according to the manufacturer's instructions.

Chromosomal karyotyping

When CNVs of terminal deletion and duplication or trisomy associated with acrocentric chromosomes (13, 14, 15, 21, and 22) were detected in the POCs, peripheral blood samples from the couple were karyotyped by traditional cytogenetic G-band analysis with a resolution of 450–550 bands to confirm whether one parent had reciprocal translocations, inversions, or Robertsonian translocations.

Statistical analyses

Statistical analyses were performed using SPSS software v24.0 (IBM Corp., Armonk, NY, United States). Continuous variables were compared using Student's t-test, and categorical variables were compared using chi-square or Fisher's exact analyses, as appropriate. Data are presented as means ± standard deviations. A logistic regression analysis was also conducted with adjustments for potential confounding effects. A p-value of <0.05 was considered statistically significant.

Results

Specimen characteristics and general findings

Initially, 3,634 POCs were recruited for this study; 189 (5.20%) samples were excluded for significant MCC (38 samples) or poor DNA quality (151 samples); thus, 3,445 samples were included in the analyses. In total, 57 samples had a suspected MCC below 30% by SNP array and underwent QF-PCR analysis. In addition, 46 samples were confirmed to have 10%–29% MCC, which did not influence the results; thus, they were not excluded. The testing turnaround time ranged from 3 to 7 days (4.36 ± 1.79 days). The maternal ages ranged from 19 to 46 years (31.04 ± 4.30 years), and the number of pregnancies lost ranged from 1 to 6 (1.73 ± 0.92 times), including 2,711 (78.7%) cases with recurrent miscarriage (RM). Additionally, 1,746 pregnancies developed via ART (50.7%).

Overall, 1,198 (34.8%) cases had normal results, 2,247 (65.2%) had abnormal results, of which 2,050 (91.2%) had numerical chromosomal abnormalities, 60 (2.7%) had CNVs ≥10 Mb (excluding four combined with numerical abnormalities), 61 (2.7%) had CNVs of terminal deletion and duplication (excluding five combined with numerical abnormalities), 62 (2.8%) had CNVs <10 Mb (excluding 28 combined with numerical abnormalities), and 14 (0.6%) had UPD (excluding four combined with numerical abnormalities) (Table 1).

The maternal age was significantly higher for those with abnormal results than for those with normal results (31.32 ± 4.49 vs. 30.52 ± 3.86, $p < 0.001$), and participants with numerical chromosomal abnormalities were significantly older than those with other abnormalities (31.43 ± 4.53 years vs. 30.07 ± 3.68 years, $p < 0.001$). In contrast, participants with abnormal results had fewer lost pregnancies than those with normal results (1.69 ± 0.88 vs. 1.81 ± 0.99, $p = 0.025$). However, the number of lost pregnancies did not differ between participants with numerical abnormalities and those with other abnormalities (1.68 ± 0.87 vs. 1.79 ± 0.88, $p = 0.241$). In addition, the RM proportion did not differ between participants with abnormal and normal results (48.2% [1,084/2,247] vs. 50.8% [609/1,198], $p = 0.147$) or between participants with numerical and other abnormalities (52.4% [1,074/2,050] vs. 45.7% [90/197], $p = 0.072$). The proportion of those conceived via ART did not differ between participants with abnormal and normal results (51.5% [1,157/2,247] vs. 49.2% [589/1,198], $p = 0.194$), but significantly more for participants with numerical abnormalities than those with other abnormalities (52.3% [1,072/2,050] vs. 43.1% [85/197], $p = 0.014$). However, when maternal age was considered, the difference was statistically significant ($p = 0.417$).

Numerical chromosomal abnormalities

Most of the numerical chromosomal abnormalities (2,050/2,247 [91.2%]) were single aneuploids (1,530/2,247 [68.1%]). Trisomy was the most common abnormality, occurring in 1,279 of 1,530 cases (83.6%), followed by monosomy (249/1,530 [16.3%]) and tetrasomy (2/1,530 [0.1%]). Aneuploidy was identified in every chromosome except chromosome 1; the most common was trisomy 16 (412/1,530 [26.9%]), followed by monosomy X (236/1,530 [15.4%]) and trisomy 22 (197/1,530 [12.9%]) (Table 1).

Of those with abnormal results, 4.9% (111/2,247) had multiple aneuploids, of which 92.8% (103/111) had double aneuploids. Furthermore, 5.6% (125/2,247) had mosaic aneuploids, of which 48.0% (60/125) were below 30%, including seven cases combined with the following: CNVs ≥10 Mb (n = 3), CNVs of terminal deletion and duplication (n = 1), CNVs <10 Mb (n = 2), or UPD (n = 1) (Table 1).

TABLE 1 Summary and characterization of chromosomal abnormalities identified by CMA in 3445 POC samples.

	n (%)			Maternal age (mean ± SD)	Miscarriages (mean ± SD)	ART (n (%))	RM (n (%))
Single aneuploidy	1,530 (44.4)			31.60 ± 4.60	1.67 ± 0.90	824 (53.9)	1,231 (80.5)
trisomy		1,279 (83.6)					
chr 2			40 (3.1)				
chr 3			27 (2.1)				
chr 4			49 (3.8)				
chr 5			16 (1.3)				
chr 6			22 (1.7)				
chr 7			30 (2.3)				
chr 8			42 (3.3)				
chr 9			26 (2.0)				
chr 10			29 (2.3)				
chr 11			20 (1.6)				
chr 12			16 (1.3)				
chr 13			75 (5.9)				
chr 14			44 (3.4)				
chr 15			93 (7.3)				
chr 16			412 (32.2)				
chr 17			11 (0.9)				
chr 18			21 (1.6)				
chr 19			1 (0.1)				
chr 20			28 (2.2)				
chr 21			80 (6.3)				
chr 22			197 (15.4)				
tetrasomy		2 (0.1)					
chr 13			1 (50.0)				
chr 15			1 (50.0)				
monosomy		249 (16.3)					
chr 21			13 (5.2)				
chr X			236 (94.8)				
Multiple aneuploidy	111 (3.2)			31.96 ± 5.36	1.75 ± 0.96	59 (53.2)	89 (80.2)
Mosaic anueploidy	125 (3.6)			31.35 ± 3.89	1.45 ± 0.58	74 (59.2)	93 (74.4)
Polyploidy	284 (8.2)			30.35 ± 3.89		115 (40.5)	258 (90.8)
triploidy		277 (97.5)					
tetraploidy		7 (2.5)					
CNVs> 10 Mb	60 (1.7) [4]*			30.84 ± 3.41	1.75 ± 0.83	30 (47.6)	53 (84.1)
P CNVs		38 (63.3)					
LP CNVs		20 (33.3) [3]*					
VUS		2 (3.3) [1]*					
CNVs of terminal deletion and duplication	61 (1.8) [5]*			29.42 ± 3.37	1.72 ± 0.72	26 (44.1)	50 (84.7))

(Continued on following page)

TABLE 1 (*Continued*) Summary and characterization of chromosomal abnormalities identified by CMA in 3445 POC samples.

	n (%)			Maternal age (mean ± SD)	Miscarriages (mean ± SD)	ART (n (%))	RM (n (%))
≥10 Mb		40 (65.6) [2]*					
<10 Mb		21 (34.4) [3]*					
CNVs<10 Mb	62 (1.8) [28]*			30.07 ± 4.40	1.97 ± 0.96	19 (30.6)	55 (88.7)
P CNVs		21 (33.9) [11]*					
LP CNVs		-					
VUS		41 (66.1) [17]*					
UPD	14 (0.4) [4]*			29.31 ± 3.00	1.60 ± 1.02	10 (71.4)	8 (57.2)
Normal	1,198 (34.8)			30.52 ± 3.86	1.81 ± 0.99	589 (49.2)	874 (73.0)
Total	3,445 (100.00)			31.08 ± 4.31	1.60 ± 0.92	1746 (50.7)	2,711 (78.7)

CMA: chromosomal microarray analysis; POC: products of conception; SD: standard deviation; ART: assisted reproductive technology; RM: recurrent miscarriage; P CNVs: pathogenic copy number variations; LP CNVs: likely pathogenic copy number variations; VUS: variations of uncertain significance; UPD: uniparental disomy.
[]*: cases combained with numerical abnormalities.

Of the 284 polyploid samples, 277 (97.5%) were triploid, and 7 (2.5%) were tetraploid. All tetraploid cases (11.7%, 7/60) were initially misdiagnosed as mosaic aneuploids below 30% involving one or more chromosomes by SNP array but confirmed as tetraploid by FISH.

Of the 504 trisomy cases associated with acrocentric chromosomes, 423 (83.9%) couples underwent chromosomal karyotyping of peripheral blood samples. Robertsonian translocations in one partner were detected in 27 couples (6.4%), 70.4% of which involved chromosomes 13 and 14 (der (13; 14) (q10; q10)).

Large CNVs

CNVs ≥10 Mb were observed in 64 cases, including four combined with numerical abnormalities. Of the 23 cases (35.9%) with more than one CNV, 8 (34.8%) involved submicroscopic CNVs, including 3 cases with *de novo* pathogenic CNVs (No. 14 and No. 25 with haploinsufficiency regions [1p36 terminal region and 22q11.2 recurrent (DGS/VCFS) region] and No.38 with a haploinsufficiency gene [FOXC1]) (Supplementary Table S1).

CNVs of terminal deletion and duplication

CNVs of terminal deletion and duplication were identified in 66 cases, including 5 combined with numerical chromosomal abnormalities; 61 cases (92.4%) and 5 cases (7.6%) had terminal deletion/duplication coupled with terminal duplication/deletion from different chromosomes and the same chromosome, respectively. In total, 23 cases (34.8%) had one of the terminal deletions/duplications below the traditional cytogenetic G-band analysis resolution (<10 Mb), and 1 case (No. 112; 1.5%) had both a terminal deletion and duplication below 10 Mb (Supplementary Table S2).

Overall, 14 couples declined chromosomal karyotyping of peripheral blood samples. Of the consenting couples, 29 (55.8%) had confirmed balanced chromosome rearrangements, of which 27 couples (93.1%) had reciprocal translocations and 2 (6.9%) had inversions (Supplementary Table S2).

Submicroscopic CNVs

CNVs <10 Mb were identified in 90 cases, including 28 combined with numerical chromosomal abnormalities. In total, 97 CNVs (51 microdeletions and 46 microduplications) were detected by the SNP array, including 6 cases with multiple CNVs. Of these, 33 (34.0%) pathogenic P) CNVs and 64 (66.0%) variants of uncertain significance (VUS) were identified (Supplementary Table S3).

Furthermore, seven recurrent (n ≥ 2) CNVs were identified, including six P CNVs in 14 cases: four had a microdeletion associated with the 17p12 recurrent (HNPP/CMT1A) region, two had a microdeletion and two had a microduplication associated with the 16p11.2 recurrent region, two had a microdeletion and two had a microduplication associated with the 22q11.2 recurrent (DGS/VCFS) region, and two had a microdeletion associated with steroid sulphatase deficiency. Additionally, one VUS was identified in four cases, which was a microduplication associated with the 16p13.11 recurrent region (Supplementary Table S3).

Parental confirmation by SNP array was performed in 72.2% (65/90) of cases. The proportions of P CNVs parentally inherited or *de novo* were 47.8% (11/23) and 52.2% (12/23), respectively; for VUS, it was 74.5% (35/47) and 25.5% (12/47), respectively. Significantly more *de novo* P CNVs than *de novo* VUS CNVs were identified ($p = 0.027$) (Supplementary Table S3).

UPD

UPD was detected in 18 cases, including four combined with numerical chromosomal abnormalities; none were from consanguineous couples. Whole-genome uniparental isodisomy (isoUPD) was observed in seven cases; all were confirmed as

complete hydatidiform moles by pathological examinations. In addition, single-chromosome isoUPD (involving chromosomes 1, 4, 6, 7, 8, and 17) was identified in seven cases. Interestingly, one case of isoUPD 6 was associated with mosaic trisomy 6 (arr (6)x3 [0.46]). Finally, single-chromosome uniparental iso-heterodisomy (iso-heteroUPD; involving chromosomes 4, 11, and 17) was identified in four cases; all were maternal UPDs based on parental confirmations.

Discussion

Miscarriage is a multifactorial condition, and advanced maternal age is the only etiological risk factor for aneuploidy (Nagaoka et al., 2012). Consistent with previous studies, more numerical chromosomal abnormalities occurred with increasing maternal age (Zhu et al., 2018). Furthermore, the frequency of normal embryonic results increased as the number of lost pregnancies increased, consistent with the findings of Ogasawara *et al.* (Ogasawara et al., 2000). Moreover, aneuploidy is more likely to cause spontaneous miscarriage than RM (Bianco et al., 2006; Campos-Galindo et al., 2015); however, we found that the proportion of RM did not differ between those with normal and abnormal results. This result likely is because most couples did not seek genetic etiology after the first spontaneous miscarriage. Several studies (Martínez et al., 2010; Qin et al., 2013) found no increased risk of chromosomal abnormalities resulting from ART (Martínez et al., 2010; Qin et al., 2013). In contrast, we observed a considerably higher rate of numerical chromosomal abnormalities after ART, but a logistic regression analysis confirmed that advanced maternal age contributed to the statistical significance.

Tetraploidy (4n) is a severe chromosomal abnormality characterized by two extra haploid sets of chromosomes, with a reported frequency of 1.4%–9.2% among first-trimester miscarriages (Gug et al., 2020). Gug *et al.* (Gug et al., 2020) reported that approximately 30% of first-trimester polyploidies detected by standard karyotype testing were tetraploids. The empirical limitation of the SNP array is that tetraploidy comprising two diploid cell lines cannot be detected (South et al., 2013; Gug et al., 2020). Notably, in our study, all seven tetraploid cases were initially misdiagnosed as mosaic aneuploids but were later confirmed to have two diploid cell lines by FISH. Additionally, we found that the incidence of tetraploidy with a 2:2 parental contribution was significantly higher than that of a 1:3 parental contribution. However, we did not perform FISH for those with negative SNP array results; thus, some tetraploids with a 2:2 parental contribution could have been missed. Therefore, we recommend FISH as a complementary technique to detect tetraploids when a negative result is detected by the SNP array, especially for mosaic aneuploids.

POC as a proband could be used to uncover the potential existence of a balanced translocation in either partner (Zhu et al., 2018). We detected 27 couples (0.8%) with Robertsonian translocations and 27 couples (0.8%) with reciprocal translocations, which is much higher than the incidence in the general population (0.1%–0.2%) (Morin et al., 2017). Couples in which one partner has a balanced translocation or inversion have an overall miscarriage risk as high as 49% due to unbalanced gametes (De Braekeleer and Dao, 1990). However, *in vitro* fertilization and preimplantation genetic testing (PGT) for structural rearrangement have significantly reduced the incidence of miscarriage for carrier couples. Moreover, parents with submicroscopic balanced translocations have a high possibility of birth with untoward outcomes rather than a first-trimester miscarriage (Morin et al., 2017). According to our results, 24 cases (36.4%) had at least one of the terminal deletions/duplications below traditional cytogenetic G-band analysis resolution. For these couples, the POC findings by CMA may help increase the positive detection rate of parental balanced translocations and the precision of the breakpoints by sub-bands. Thus, we recommend parental karyotyping after detecting CNVs of terminal deletion and duplication or aneuploids associated with acrocentric chromosomes in POCs.

Submicroscopic CNVs are considered coincidental findings in first-trimester miscarriages (Levy et al., 2014). Recently, Wang *et al.* (Wang et al., 2020) identified three recurrent submicroscopic CNVs (microdeletions in 22q11.21, 2q37.3, and 9p24.3p24.2) presumably associated with miscarriage. However, in our large-scale cohort, only two cases (0.6‰) with 22q11.21 deletion were detected, significantly lower than the previously reported prevalence (3.2%) in fetuses with congenital heart disease (Wang et al., 2018). Moreover, the small proportion (1.8%) of cases with independent submicroscopic CNVs also indicates it has a limited role in miscarriage. In addition, the frequency of P/LP CNVs in our study (0.6% [21/3,445]) was dramatically lower than that in fetuses with a normal ultrasound examination and a normal karyotype (1.7%) (Practice Bulletin No, 2016). Our findings support that large chromosomal abnormalities are more likely to be lethal, leading to miscarriage, whereas submicroscopic CNVs could result in a viable pregnancy (Wang et al., 2020). The role of P/LP CNVs in first-trimester miscarriages is controversial. However, the role of P/LP CNVs has been well-studied in patients with structural anomalies and neurodevelopmental disorders (Manning et al., 2010; Miller et al., 2010; Wapner et al., 2012). Therefore, detecting submicroscopic CNVs in POCs has crucial clinical implications because couples themselves may be carriers, with a 50% recurrent risk in all future pregnancies. Particularly, for recurrent pathogenic CNVs with incomplete penetrance and variable expressions, such as 1q21.1 distal deletions and duplications, 16p11.2 proximal and distal deletions and duplications, and 22q11.21 duplications, these CNVs can be inherited from parents with a mild or even normal phenotype (Rosenfeld et al., 2013). Thus, we recommend performing parental confirmation when P/LP CNVs are detected in POCs. PGT should be performed to improve pregnancy outcomes for these carrier couples.

In this study, we identified 18 UPD cases, which is an advantage of using the SNP array for the genetic etiology of miscarriage. The common mechanisms resulting in UPD involve trisomy rescue, monosomy rescue, and somatic mitotic crossing over (Del Gaudio et al., 2020). One limitation of the SNP array is its inability to detect hetero-UPD. However, four cases of iso-heteroUPD were detected after comparisons with the parental results. In addition, isoUPD may contain homozygosity of some lethal autosomal-recessive mutations that contribute to miscarriage, and this should be implemented in future studies. For the seven cases with whole-genome isoUPD, complete hydatidiform moles (CHMs) were simultaneously confirmed by pathological examinations. CHMs are purely androgenetic conceptions (only paternal genetic material is present) and are usually diploid (two paternal chromosome complements without a maternal chromosome complement) (Ronnett, 2018). However, most couples preferred to confirm the CHM diagnosis

only by pathological examinations. Thus, we recommend SNP array and pathological examinations if CHMs are suspected.

Conclusion

Herein, we provide an integrated laboratory algorithm for the genetic etiology of early pregnancy loss. Furthermore, we recommend an SNP array of POCs as a first-tier technique regardless of the number of miscarriages and the method of conception. However, SNP arrays have a limited range and, thus, difficulties detecting low-level mosaicism. Thus, we recommend FISH as a complementary technique to detect tetraploids if a negative SNP assay result is obtained, especially for mosaic aneuploids. Finally, we recommend parental karyotyping in cases with large CNVs, especially for those with CNVs of terminal deletion and duplication or aneuploids associated with acrocentric chromosomes. In addition, a parental SNP array should be administered if pathogenic CNVs are detected.

Data availability statement

All datasets generated for this study are included in the article/Supplementary Material. Further inquiries can be directed to the corresponding author.

Ethics statement

The study was approved by the Medical Ethics Committee of West China Second University Hospital (IRB no. 2013-26, approval date 28 December 2013), and all patients signed informed consent forms to participate.

Author contributions

NL collected the data and wrote the manuscript. ZZ, XL, and JW analyzed the data. RH, LX, and YY collected the samples and performed the experiments. YL, HZ, and LL analyzed the experimental results. SL and HW designed the experiments. TH designed the experiments and revised the manuscript. All authors contributed to the article and approved the submitted version.

Funding

This work was supported by the National Key Research and Development Program of China (2022YFC2703302), Sichuan Science and Technology Program, China (2021YFS0078 and 2022YFS0078), and Fundamental Research Funds for the Central Universities (SCU 2022F4080).

Acknowledgments

We would like to thank all doctors who helped with patient recruitment. We are grateful to all the team members for their contributions to data collection and integrity.

Conflict of interest

The authors declare that the research was conducted in the absence of any commercial or financial relationships that could be construed as a potential conflict of interest.

Publisher's note

Supplementary material

The Supplementary Material for this article can be found online at: https://www.frontiersin.org/articles/10.3389/fgene.2023.1203891/full#supplementary-material

References

American College of Obstetricians and Gynecologists Committee on Genetics (2013). Committee opinion no. 581: The use of chromosomal microarray analysis in prenatal diagnosis. *Obstet. Gynecol.* 122 (6), 1374–1377. doi:10.1097/01.AOG.0000438962.16108.d1

Bianco, K., Caughey, A. B., Shaffer, B. L., Davis, R., and Norton, M. E. (2006). History of miscarriage and increased incidence of fetal aneuploidy in subsequent pregnancy. *Obstet. Gynecol.* 107 (5), 1098–1102. doi:10.1097/01.AOG.0000215560.86673.22

Campos-Galindo, I., García-Herrero, S., Martínez-Conejero, J. A., Ferro, J., Simón, C., and Rubio, C. (2015). Molecular analysis of products of conception obtained by hysteroembryoscopy from infertile couples. *J. Assist. Reprod. Genet.* 32 (5), 839–848. doi:10.1007/s10815-015-0460-z

Colley, E., Hamilton, S., Smith, P., Morgan, N. V., Coomarasamy, A., Allen, S., et al. (2019). Potential genetic causes of miscarriage in euploid pregnancies: A systematic review. *Hum. Reprod. Update* 25 (4), 452–472. doi:10.1093/humupd/dmz015

Cross, J., Peters, G., Wu, Z., Brohede, J., and Hannan, G. N. (2007). Resolution of trisomic mosaicism in prenatal diagnosis: Estimated performance of a 50K SNP microarray. *Prenat. Diagn* 27 (13), 1197–1204. doi:10.1002/pd.1884

De Braekeleer, M., and Dao, T. N. (1990). Cytogenetic studies in couples experiencing repeated pregnancy losses. *Hum. Reprod.* 5 (5), 519–528. doi:10.1093/oxfordjournals.humrep.a137135

Del Gaudio, D., Shinawi, M., Astbury, C., Tayeh, M. K., Deak, K. L., and Raca, G.ACMG Laboratory Quality Assurance Committee (2020). Diagnostic testing for uniparental disomy: A points to consider statement from the American College of medical genetics and genomics (ACMG). *Genet. Med.* 22 (7), 1133–1141. doi:10.1038/s41436-020-0782-9

Dhillon, R. K., Hillman, S. C., Morris, R. K., McMullan, D., Williams, D., Coomarasamy, A., et al. (2014). Additional information from chromosomal microarray analysis (CMA) over conventional karyotyping when diagnosing chromosomal abnormalities in miscarriage: A systematic review and meta-analysis. *BJOG* 121 (1), 11–21. doi:10.1111/1471-0528.12382

Fan, L., Wu, J., Wu, Y., Shi, X., Xin, X., Li, S., et al. (2020). Analysis of chromosomal copy number in first-trimester pregnancy loss using next-generation sequencing. *Front. Genet.* 11, 545856. doi:10.3389/fgene.2020.545856

Gug, C., Burada, F., Ioana, M., Riza, A. L., Moldovan, M., Mozos, I., et al. (2020). Polyploidy in first and second trimester pregnancies in Romania - a retrospective study. *Clin. Lab.* 66 (4). doi:10.7754/Clin.Lab.2019.190649

Hassold, T., Chen, N., Funkhouser, J., Jooss, T., Manuel, B., Matsuura, J., et al. (1980). A cytogenetic study of 1000 spontaneous abortions. *Ann. Hum. Genet.* 44 (2), 151–178. doi:10.1111/j.1469-1809.1980.tb00955.x

Hu, T., Tian, T., Zhang, Z., Wang, J., Hu, R., Xiao, L., et al. (2021). Prenatal chromosomal microarray analysis in 2466 fetuses with ultrasonographic soft markers: A prospective cohort study. *Am. J. Obstet. Gynecol.* 224 (5), 516.e1–516.e16. doi:10.1016/j.ajog.2020.10.039

Kooper, A. J., Faas, B. H., Feenstra, I., de Leeuw, N., and Smeets, D. F. (2014). Best diagnostic approach for the genetic evaluation of fetuses after intrauterine death in first, second or third trimester: QF-PCR, karyotyping and/or genome wide SNP array analysis. *Mol. Cytogenet* 7 (1), 6. doi:10.1186/1755-8166-7-6

Levy, B., Sigurjonsson, S., Pettersen, B., Maisenbacher, M. K., Hall, M. P., Demko, Z., et al. (2014). Genomic imbalance in products of conception: Single-nucleotide polymorphism chromosomal microarray analysis. *Obstet. Gynecol.* 124 (2), 202–209. doi:10.1097/AOG.0000000000000325

Li, G., Liu, Y., He, N. N., Hu, L. L., Zhang, Y. L., Wang, Y., et al. (2013). Molecular karyotype single nucleotide polymorphism analysis of early fetal demise. *Syst. Biol. Reprod. Med.* 59 (4), 227–231. doi:10.3109/19396368.2012.750696

Manning, M., and Hudgins, L.Professional Practice and Gu and idelines Committee (2010). Array-based technology and recommendations for utilization in medical genetics practice for detection of chromosomal abnormalities. *Genet. Med.* 12 (11), 742–745. doi:10.1097/GIM.0b013e3181f8baad

Martínez, M. C., Méndez, C., Ferro, J., Nicolás, M., Serra, V., and Landeras, J. (2010). Cytogenetic analysis of early nonviable pregnancies after assisted reproduction treatment. *Fertil. Steril.* 93 (1), 289–292. doi:10.1016/j.fertnstert.2009.07.989

Menasha, J., Levy, B., Hirschhorn, K., and Kardon, N. B. (2005). Incidence and spectrum of chromosome abnormalities in spontaneous abortions: New insights from a 12-year study. *Genet. Med.* 7, 251–263. doi:10.1097/01.gim.0000160075.96707.04

Miller, D. T., Adam, M. P., Aradhya, S., Biesecker, L. G., Brothman, A. R., Carter, N. P., et al. (2010). Consensus statement: Chromosomal microarray is a first-tier clinical diagnostic test for individuals with developmental disabilities or congenital anomalies. *Am. J. Hum. Genet.* 86 (5), 749–764. doi:10.1016/j.ajhg.2010.04.006

Morin, S. J., Eccles, J., Iturriaga, A., and Zimmerman, R. S. (2017). Translocations, inversions and other chromosome rearrangements. *Fertil. Steril.* 107 (1), 19–26. doi:10.1016/j.fertnstert.2016.10.013

Nagaoka, S. I., Hassold, T. J., and Hunt, P. A. (2012). Human aneuploidy: Mechanisms and new insights into an age-old problem. *Nat. Rev. Genet.* 13 (7), 493–504. doi:10.1038/nrg3245

Ogasawara, M., Aoki, K., Okada, S., and Suzumori, K. (2000). Embryonic karyotype of abortus in relation to the number of previous miscarriages. *Fertil. Steril.* 73 (2), 300–304. doi:10.1016/s0015-0282(99)00495-1

Practice Bulletin No (2016). Practice Bulletin No:162: Prenatal diagnostic testing for genetic disorders. *Obstet. Gynecol.* 127 (5), e108–e122. doi:10.1097/AOG.0000000000001405

Practice Committee of the American Society for Reproductive Medicine (2012). Evaluation and treatment of recurrent pregnancy loss: A committee opinion. *Fertil. Steril.* 98 (5), 1103–1111. doi:10.1016/j.fertnstert.2012.06.048

Qin, J. Z., Pang, L. H., Li, M. Q., Xu, J., and Zhou, X. (2013). Risk of chromosomal abnormalities in early spontaneous abortion after assisted reproductive technology: A meta-analysis. *PLoS One* 8, e75953. doi:10.1371/journal.pone.0075953

Rai, R., and Regan, L. (2006). Recurrent miscarriage. *Lancet* 368, 601–611. doi:10.1016/S0140-6736(06)69204-0

Ronnett, B. M. (2018). Hydatidiform moles: Ancillary techniques to refine diagnosis. *Arch. Pathol. Lab. Med.* 142 (12), 1485–1502. doi:10.5858/arpa.2018-0226-RA

Rosenfeld, J. A., Coe, B. P., Eichler, E. E., Cuckle, H., and Shaffer, L. G. (2013). Estimates of penetrance for recurrent pathogenic copy-number variations. *Genet. Med.* 15 (6), 478–481. doi:10.1038/gim.2012.164

Rosenfeld, J. A., Tucker, M. E., Escobar, L. F., Neill, N. J., Torchia, B. S., McDaniel, L. D., et al. (2015). Diagnostic utility of microarray testing in pregnancy loss. *Ultrasound Obstet. Gynecol.* 46 (4), 478–486. doi:10.1002/uog.14866

Shearer, B. M., Thorland, E. C., Carlson, A. W., Jalal, S. M., and Ketterling, R. P. (2011). Reflex fluorescent *in situ* hybridization testing for unsuccessful product of conception cultures: A retrospective analysis of 5555 samples attempted by conventional cytogenetics and fluorescent *in situ* hybridization. *Genet. Med.* 13 (6), 545–552. doi:10.1097/GIM.0b013e31820c685b

Shen, J., Wu, W., Gao, C., Ochin, H., Qu, D., Xie, J., et al. (2016). Chromosomal copy number analysis on chorionic villus samples from early spontaneous miscarriages by high throughput genetic technology. *Mol. Cytogenet* 9, 7. doi:10.1186/s13039-015-0210-z

Society for Maternal-Fetal MedicineDugoff, L., Norton, M. E., and Kuller, J. A. (2016). The use of chromosomal microarray for prenatal diagnosis. *Am. J. Obstet. Gynecol.* 215 (4), B2–B9. Electronic address: pubs@smfm.org. doi:10.1016/j.ajog.2016.07.016

South, S. T., Lee, C., Lamb, A. N., Higgins, A. W., and Kearney, H. M.Working Group for the American College of Medical Genetics and Genomics Laboratory Quality Assurance Committee (2013). ACMG standards and guidelines for constitutional cytogenomic microarray analysis, including postnatal and prenatal applications: Revision 2013. *Genet. Med.* 15 (11), 901–909. doi:10.1038/gim.2013.129

Wang, Y., Cao, L., Liang, D., Meng, L., Wu, Y., Qiao, F., et al. (2018). Prenatal chromosomal microarray analysis in fetuses with congenital heart disease: A prospective cohort study. *Am. J. Obstet. Gynecol.* 218 (2), 244.e1–244.e17. doi:10.1016/j.ajog.2017.10.225

Wang, Y., Li, Y., Chen, Y., Zhou, R., Sang, Z., Meng, L., et al. (2020). Systematic analysis of copy-number variations associated with early pregnancy loss. *Ultrasound Obstet. Gynecol.* 55 (1), 96–104. doi:10.1002/uog.20412

Wapner, R. J., Martin, C. L., Levy, B., Ballif, B. C., Eng, C. M., Zachary, J. M., et al. (2012). Chromosomal microarray versus karyotyping for prenatal diagnosis. *N. Engl. J. Med.* 367 (23), 2175–2184. doi:10.1056/NEJMoa1203382

Zahir, F. R., and Marra, M. A. (2015). Use of affymetrix arrays in the diagnosis of gene copy-number variation. *Curr. Protoc. Hum. Genet.* 85, 8.13.1–8.13.13. doi:10.1002/0471142905.hg0813s85

Zhang, Y. X., Zhang, Y. P., Gu, Y., Guan, F. J., Li, S. L., Xie, J. S., et al. (2009). Genetic analysis of first-trimester miscarriages with a combination of cytogenetic karyotyping, microsatellite genotyping and arrayCGH. *Clin. Genet.* 75 (2), 133–140. doi:10.1111/j.1399-0004.2008.01131.x

Zhu, X., Li, J., Zhu, Y., Wang, W., Wu, X., Yang, Y., et al. (2018). Application of chromosomal microarray analysis in products of miscarriage. *Mol. Cytogenet* 11, 44. doi:10.1186/s13039-018-0396-y

frontiers | Frontiers in Genetics

TYPE Original Research
PUBLISHED 13 July 2023
DOI 10.3389/fgene.2023.1188361

OPEN ACCESS

EDITED BY
Jordi Pérez-Tur,
Spanish National Research Council (CSIC), Spain

REVIEWED BY
Hiroshi Takashima,
Kagoshima University, Japan
Fiore Manganelli,
University of Naples Federico II, Italy

*CORRESPONDENCE
Xiaoxuan Liu,
lucyan_liu@bjmu.edu.cn
Dongsheng Fan,
dsfan@sina.com

†These authors have contributed equally to this work and share first authorship

RECEIVED 17 March 2023
ACCEPTED 03 July 2023
PUBLISHED 13 July 2023

CITATION
Ma Y, Duan X, Liu X and Fan D (2023), Clinical and mutational spectrum of paediatric Charcot-Marie-Tooth disease in a large cohort of Chinese patients. *Front. Genet.* 14:1188361. doi: 10.3389/fgene.2023.1188361

Clinical and mutational spectrum of paediatric Charcot-Marie-Tooth disease in a large cohort of Chinese patients

Yan Ma[1,2,3†], Xiaohui Duan[4†], Xiaoxuan Liu[1,2,3*] and Dongsheng Fan[1,2,3*]

[1]Department of Neurology, Peking University Third Hospital, Beijing, China, [2]Beijing Key Laboratory of Biomarker and Translational Research in Neurodegenerative Diseases, Beijing, China, [3]Key Laboratory for Neuroscience, National Health Commission/Ministry of Education, Peking University, Beijing, China, [4]China-Japan Friendship Hospital, Beijng, China

Background: Charcot-Marie-Tooth disease (CMT) is the most common inherited neurological disorder suffered in childhood. To date, the disease features have not been extensively characterized in the Chinese paediatric population. In this study, we aimed to analyse the clinical profiles and genetic distributions of a paediatric CMT cohort in China.

Methods: A total of 181 paediatric CMT patients were enrolled. After preexcluding *PMP22* duplication/deletion by multiplex ligation-dependent probe amplification (MLPA), Sanger sequencing, targeted next-generation sequencing (NGS) or whole-exome sequencing (WES) was performed to obtain a genetic diagnosis. Detailed information was collected to explore the spectrum of subtypes and genotype-phenotype correlations.

Results: Pathogenic mutations were identified in 68% of patients in this study; with *PMP22* duplication, MFN2 and *GJB1* were the most frequent disease-causing genes. Of note, respect to the higher prevalence worldwide, CMT1A (18.2%) was relatively lower in our cohort. Besides, the mean age at onset (8.3 ± 5.7 years) was significantly older in our series. In genotype-phenotype analyse, *PMP22* point mutations were considered the most severe genotypes and were mostly *de novo*. In addition, the *de novo* mutations were identified in up to 12.7% of all patients, which was higher than that in other studies.

Conclusion: We identified a relatively lower detection rate of *PMP22* duplication and a higher frequency of *de novo* variants among paediatric patients in China. We also identified the genetic and phenotypic heterogeneity of this cohort, which may provide clues for clinicians in directing genetic testing strategies for Chinese patients with early-onset CMT.

KEYWORDS

paediatric Charcot-Marie-Tooth disease, inherited peripheral neuropathy, genetic distribution, genotype-phenotype correlations, *de novo* variants

Introduction

Charcot-Marie-Tooth disease (CMT) is one of the most common inherited peripheral neuropathies with a prevalence of 1 in 2,500 individuals (Skre, 1974). As a collection of clinically and genetically heterogeneous disorders, CMT varies strikingly in terms of phenotypes and severity, especially in paediatric populations. In clinical practice, whereas CMT patients share common characteristics of progressive distal muscle weakness, sensory loss and deformity (Klein, 2020), they also have a clinically heterogeneous set of disorders, spanning a spectrum from mildly symptomatic forms to those resulting in severe disability. Based on median motor nerve conduction velocity (MNCV), CMT can be categorized as demyelinating type (median MNCV<38 m/s), axonal type (median MNCV>38 m/s) and intermediated type (median MNCV 25–45 m/s) (Pareyson and Marchesi, 2009). In each category, inheritance patterns may be autosomal dominant, autosomal recessive, or X-linked.

Recently, next-generation sequencing (NGS) and whole-exome sequencing (WES) have resulted in a rapid expansion of the genetic diagnosis of CMT, with over 100 genes identified and many more still to be discovered (Padilha et al., 2020). In comparison to CMT of all age groups, childhood-onset patients may present more phenotypic variability and mutation-specific manifestations (Cornett et al., 2016). In addition, it is worth noting that *de novo* cases are not rare for CMT, especially in the earlier-onset group (Landrieu and Baets, 2013; Ma et al., 2021). Therefore, owing to the clinical complexity and genetic diversity, the diagnosis of paediatric CMT is always difficult. Furthermore, previous published studies also illustrated that the distribution of subtypes varied in different geographical regions (Fridman et al., 2015). Thus, a comprehensive knowledge of the distribution of mutations within earlier-onset subgroup in different areas is important and challenging.

Paediatric CMT, with disease onset in the first 2 decades, is a group that deserves further attentions. First, the presentation of paediatric patients is quite different from that of adult patients in terms of disease severity and clinical features, as symptoms can be insidious and severely disabling. Besides, there are obvious delays in achieving motor milestones in earlier-onset patients, which may lead to a considerable socioeconomic burden (Baets et al., 2011). In addition, improved genetic diagnosis rate in paediatric patients may help facilitate clinical trials of the upcoming disease-modifying treatment. To date, studies on paediatric CMT have mainly been based on patients of European origins, with a reported diagnosis rate of 75.6%–92% (Cornett et al., 2016; Hoebeke et al., 2018; Argente-Escrig et al., 2021). However, the disease characteristics of paediatric CMT have not been extensively characterized in the Chinese population thus far, either in mutation spectrum or phenotypic analysis. Therefore, the clinical heterogeneity in patients of different origins, coupled with the expanding genetic diversity in earlier-onset CMT leads to a great need for in-depth studies on the mutational spectrum and detailed genotype-phenotype correlations in Chinese patients.

Thus, we conducted a study in a large paediatric CMT population in China, analysing the mutational distribution and clinical characteristics. In addition, we further explored the subtype frequencies and the genotype-phenotype correlations in this series, to provide some clues for clinicians in directing genetic testing strategies and selecting disease modifying therapies for early-onset CMT patients of Chinese origin.

Materials and methods

Participants

A cohort of early-onset (age 0–20 years) CMT patients was enrolled consecutively in this study at Peking University Third Hospital and China-Japan Friendship Hospital from 2007 to 2021. The clinical criteria used for the diagnosis of CMT are well established in the literature (Bird, 1998). For all patients, clinical features, family history and the electrophysiological data were carefully collected and recorded. Experienced neurologists who specialized in inherited neuropathies evaluated the clinical data of all patients. Disease burden were assessed by Charcot-Marie-Tooth Paediatric Scale (CMTPedS) (Burns et al., 2012). On the basis of the disease burden scores, patients were classified as having mild, moderate, or severe disease (CMTPedS of ≤14, 15–29, or ≥30, respectively). Follow-up was carried out every 6 months through telephone calls or in-person interviews. The institutional ethics committee of Peking University Third Hospital approved this study. Patients or their legal guardians provided written, informed consents to participate in this study (2019-005-02).

Gene screening strategy and genetic analysis

Genomic DNA was collected and extracted from peripheral blood leukocytes by standard procedures according to the manufacturer's instructions. From 2007 to 2013, the duplication/deletion mutation of *PMP22* gene was pre-excluded in all clinically suspected demyelinating CMT patients by multiplex ligation-dependent probe amplification (MLPA) according to the guidelines. Then Sanger sequencing was used to detect missense mutation of *PMP22* (NM_153321), *GJB1* (NM_0001097642) and *MPZ* (NM_000530). In patients with axonal CMT, we investigated *MFN2* (NM_014874), *GJB1, MPZ, HSPB1* (NM_001540) and *HSPB8* (NM_014365) by direct Sanger sequencing. From 2014 to 2018, a targeted NGS panel covering 165 genes associated with inherited neuropathies was introduced for all suspected cases after excluding *PMP22* duplication/deletion mutation. Since 2019, an upgraded WES (Agilent Human All Exon V6) was performed on the index patients. The samples were sequenced on the HiSeq2500 and NEXTSEQ 500 (Illumina, San Diego, CA, United States) to discover causal genes. Identified variants by NGS or WES were further validated by Sanger sequencing. All previously reported pathogenic mutations were confirmed with reference to the Human Gene Mutation Database (HGMD) (http://www.hgmd.cf.ac.uk/ac/index.php). Moreover, novel variants were interpreted and classified according to the American College of Medical Genetics and Genomics/Association for Molecular Pathology (ACMG/AMP) standards and guidelines (Richards et al., 2015). A flow chart for gene screening strategy (Supplementary Figure S1) and a list of gene panel of NGS

(Supplementary Table S1) are summarized in the Supplementary Materials.

Statistical analysis

All statistical analyses were performed using GraphPad Prism 7.0 (GraphPad Software, Inc., CA, United States) and SPSS V.23.0 software (IBM Corp., Armonk, United States). Descriptive statistics such as age at onset (AAO); electrophysiological parameters were expressed as mean ± SD (range).

Results

Characteristics of study participants

A total of 181 patients of Chinese descent from two clinical centres were recruited in this study. Of those patients, 41.4% (75/181) were classified as having demyelinating CMT, 47% (85/181) as having axonal CMT and 8.3% (15/181) as having intermediated CMT. In addition, six patients met the diagnostic criteria for hereditary neuropathy with liability to pressure palsies (HNPP). According to the inheritance patterns, 61 (33.7%) patients were categorized having autosomal dominant CMT, 30 (16.6%) as having autosomal recessive CMT and 12 (6.6%) as having X-linked CMT (CMTX). Furthermore, among 78 sporadic patients, 23 (12.7%) cases were identified to be of *de novo* origins. For all modes of inheritance, the median AAO was 8.3 ± 5.7 (0–19) years, with a mean diagnostic age of 14.3 ± 6.0 (0.5–19.5) years. In general, most patients first noticed symptoms such as weakness, falls and pes cavus at disease onset. Additionally, according to disease severity, *PMP22* point mutation and *MPZ* were prone to cause the most severe phenotypes. The detailed CMTPedS based on different genotypes were summarized in the Supplementary Table S2.

Distribution of CMT subtypes

Among the different CMT subtypes, patients with demyelinating CMT presented with an earlier onset age (5.9 ± 5.5 years). Although most were associated with classic demyelinating phenotypes (55/75, 73.3%), there was considerable phenotypic heterogeneity such as prominent deep sensory disturbances (*SH3TC2, PRX*) and scoliosis (*SH3TC2, MPZ,* and *PMP22*). On electrophysiological examination, motor conduction velocity (MCV) values were uniformly decreased, with some even below 10 m/s. For the patients with axonal CMT, the AAO was higher (7.8 ± 5.6 years) than that in patients with demyelinating forms. Clinical presentation showed an absence of upper limb involvement in approximately half of the patients. Mutation-specific manifestations were also obvious, with *GARS* mutation manifesting as predominant upper limbs involvement. Moreover, 12 patients reported clinically pure motor involvement with only slight sensory impairment on electrophysiological examination. Furthermore, the disease severity also varied in axonal CMT according to different pathological mutations. In contrast, patients of intermediate CMT mainly had the classic phenotype, with a relatively benign disease course of late-onset (10.2 ± 4.5 years) and mild peripheral neuropathy (Table 1).

Genotypes distribution characteristics

Among all 181 index patients, pathogenic mutations were identified in 123 patients, with a diagnostic rate of 68% (123/181). In all CMT subtypes, the leading causes were CMT1A/*PMP22* duplication (18.2%; 33/181), CMT2A/*MFN2* mutation (7.7%; 14/181) and CMTX1/*GJB1* mutation (6.6%; 12/181). In addition, casual mutation were identified in the following genes: *GDAP1* (5%; 9/181), *PMP22* point mutation (4.4%; 8/181), *IGHMBP2* (3.3%; 6/181), *MORC2* (3.3%; 6/181), *MPZ* (2.2%; 4/181), *SORD* (1.7%; 3/181) and *SH3TC2*(1.7%; 3/181). Furthermore, mutations in the remaining CMT-related genes (i.e., *HSPB1, PRX, BSCL2, DYNC1H1, HINT1, GARS, AARS, MARS, HK1, TRPV4, KIF5A, EGR2, FGD4, MTMR2, SPG11, NEFL, DHTKD1*) were each responsible for <1% of all CMT cases. According to the clinical subtypes, *PMP22* duplication, *MFN2* and *GJB1* were the most common causative genes in demyelinating CMT, axonal CMT and CMTX respectively.

Of the patients with demyelinating CMT, 76% (57/75) carried a genetic mutation, with the most frequent genetic causes being *PMP22* duplication (44%, 33/75), *PMP22* point mutation (10.7%, 8/75) and *GDAP1* mutation (5.3%, 4/75), accounting for 60% of all demyelinating CMT patients with an identified mutation. For patients with axonal CMT, 60% had a genetically confirmed diagnosis (51/85), which was lower than that for patients with the demyelinating subtype. Moreover, mutational screening showed marked genetic heterogeneity, with mutations in *MFN2* (16.5%; 14/85), *IGHMBP* (7.1%; 6/85) and *MORC2* (7.1%; 6/85) being the three most frequent causes. For intermediated CMT, specific genetic mutations were identified in 80% (12/15) of patients. Of note, up to 12.7% (23/181) of patients were found to have *de novo* mutations with the following distribution (11 mutations in *PMP22*, three in *MFN2*, three in *MPZ*, and three in *MORC2*), which was not rare. Genotype distribution details are summarized in Figure 1.

Genotype-phenotype correlations

In terms of AAO, CMT can be further categorized into infantile-onset (<3 years), childhood-onset (3–10 years) and adolescent-onset (11–20 years) subtypes. In general, childhood-onset (38.1%; 69/181) was the most common subtype, with a successful genetic diagnosis rate of 66.7% (46/69). In this group, mutations in *PMP22, MFN2, GJB1*, and *GDAP1* were the most common causal mutations. Significantly, patients with infantile-onset CMT had the highest mutation detection rate of 79.6% (39/49), among whom mutations in *PMP22, MFN2*, and *IGHMBP2* were the top three common causes of pathologies. In the adolescent-onset group, the diagnosis rate was 60.3% (38/63), with mutations in PMP22 duplication, *GJB1, MFN2,* and *SORD* being the major aetiologies. The detailed genetic distribution according to AAO is shown in Figure 2.

There were some mutation-specific manifestations among the CMT subtypes. *PMP22* point mutations were found in patients with the most severe demyelinating CMT subtypes (CMTPedS = 32.2 ± 6.5). Among these patients, 87.5% (7/8) developed the disease before

TABLE 1 Comparisons of clinical and electrophysiological data in pediatric CMT.

	CMT (*n* = 181)	Demyelinating CMT (*n* = 75)	Axonal CMT (*n* = 85)	Intermediated CMT (*n* = 15)
AAO (year)	8.3 ± 5.7	5.9 ± 5.5	7.8 ± 5.6	10.2 ± 4.5
Diagnostic age (year)	14.3 ± 6.0	12.4 ± 7.1	13.8 ± 6.3	15.6 ± 3.9
Disease duration (year)	5.9 ± 4.1	6.6 ± 4.9	6.1 ± 4.0	6.5 ± 3.7
Gender (M/F)	101/80	43/32	43/42	12/3
Clinical features				
Pes cavus (%)	66.9	73.3	65.9	66.7
Weakness in lower limbs (%)	94.5	97.3	94.1	100
Weakness in upper limbs (%)	44.2	40	43.5	60
Hypoaesthesia (%)	38.7	37.3	37.6	46.7
Deep sensory disturbance (%)	23.2	29.3	21.2	20
Scoliosis (%)	9.9	16	7.1	0
Classic phenotype (%)	61.3	73.3	48.2	66.7
Electrophysiological parameters				
Median Nerve MCV (m/s)	35.1 ± 11.8	14.6 ± 9.7	56.5 ± 3.3	29.9 ± 10.2
Median Nerve CMAP (mv)	3.9 ± 2.6	3.2 ± 2.4	5.1 ± 1.3	2.6 ± 1.8
Ulnar Nerve MCV (m/s)	36.3 ± 8.7	17.9 ± 6.8	53.3 ± 4.5	33.3 ± 6.9
Ulnar CMAP (mv)	3.6 ± 2.3	2.1 ± 1.6	4.4 ± 1.8	3.5 ± 2.1
Median Nerve SCV (m/s)	35.2 ± 14.4	21.5 ± 8.8	53.3 ± 4.5	27.2 ± 13.4
Median Nerve SNAP (μV)	2.6 ± 1.9	0.4 ± 1.1	4.6 ± 0.7	3.4 ± 2.9
Ulnar Nerve SCV (m/s)	32.9 ± 17.5	21.4 ± 8.3	22.9 ± 17.9	26.9 ± 15.9
Ulnar Nerve SNAP (μV)	2.2 ± 1.8	0.1 ± 0.4	4.7.±1.2	1.6 ± 1.4

AAO, age at onset; CMT, Charcot-Marie-Tooth disease; MCV, motor conduction velocity; CMAP, compound muscle action potential; SNAP, sensory nerve action potential; SCV, sensory nerve conduction velocity.

the age of 3 years and 62.5% (5/8) were severely affected. Moreover, *de novo* variants at specific amino acid positions, e.g., p. S72W, p. S79P, and p. G150V caused the severe phenotypes of Dejerine-Sottas disease (DSS), which manifests as earlier onset, delayed motor development, hypotonia and profoundly slowed MCV (<15 m/s) (Agrahari et al., 2015). The second most severe paediatric CMT subtype in the cohort was caused by *MPZ* mutation. Certain *de novo* variants, such as p. R98C, p. S233Rfs*18 and the novel p. L174Rfs*66 were associated with clinical features of weakness, atrophy, deformity and motor retardation. Furthermore, patients with SH3TC2 variants also presented with a moderate to severe phenotype, which usually manifested as severe weakness, sensory ataxia and scoliosis. In particular, for patients who developed symptoms before 10 years of age, the disease seemed to be more severe than that of the other subgroups. In addition, disease progression gradually stabilized with increasing age.

With regard to disease severity, *PMP22* duplication and *MFN2* mutations were the most frequent causes of moderate phenotypes. In addition, mutations in *GJB1* and *GDAP1* were prone to cause mild phenotypes. The phenotypes of *PMP22* point mutations were confirmed to be severe clinical features, accounting for 29.4% (5/17) of the severe cases in total, followed by *MPZ* and *SH3TC2* mutations.

Discussion

In this study, we identified genotype and phenotype distributions of paediatric CMT patients in a large Chinese cohort. We also performed an in-depth genotype-phenotype correlation study, which was the largest study focused on paediatric CMT patients in China thus far. In our findings, the mean age when parents first noticed symptoms was 8.3 ± 5.7 years, which was significantly older than that in the French study (4.1 years) (Hoebeke et al., 2018). Similarly, the diagnostic age was also significantly different between these two studies (14.3 years in the Chinese patients vs. 8.3 years in the French cohort). It should be noted that the demyelinating CMT (AAO = 5.9 ± 5.5 years) in our series only accounted for 41.4% (75/181) of all CMT compared to that of 61.3% in the French cohort, which may partly explain the differences in onset age. Besides, the longer diagnostic delay in our study may largely due to the feasibility to access to our specialized clinics rather than disease severity.

Based on clinical subtypes, demyelinating CMT manifests with earlier disease onset than other CMT subtypes. Clinically, the majority (73.3%) of demyelinating CMT patients presented with typical phenotypes, whereas axonal CMT patients varied strikingly in terms of clinical features due to specific genotypes. In addition to the classic features of progressive distal muscle weakness, CMT2A patients may present with complex phenotypes, including tremor, optic atrophy and pyramidal signs. Additionally, 14.1% of axonal CMT patients are characterized as having motor-predominant neuropathy, which is difficult to distinguish from distal hereditary motor neuropathies (dHMN) (Liu et al., 2020). For CMT1X, males were more affected than females, with a mild to moderate phenotype of adolescent-onset and intermediate slowing in electrophysiological examination, which was in consistent with previous reports (Panosyan et al., 2017).

Overall, a confirmed genetic diagnosis was achieved in 123 of 181 patients (68%), with a higher detection rate in patients with the demyelinating forms (57/75; 76%) than in those with the axonal

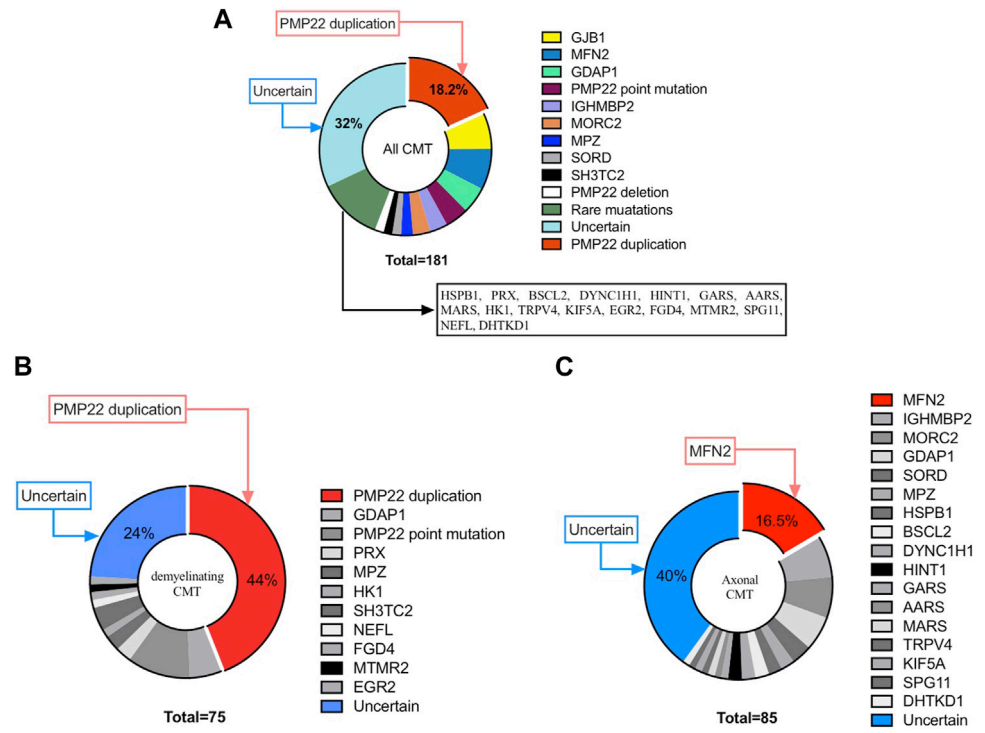

FIGURE 1
Distribution of Chinese paediatric CMT patients in our cohort. **(A)** Distribution of CMT. **(B)** Distribution of demyelinating CMT. **(C)** Distribution of axonal CMT.

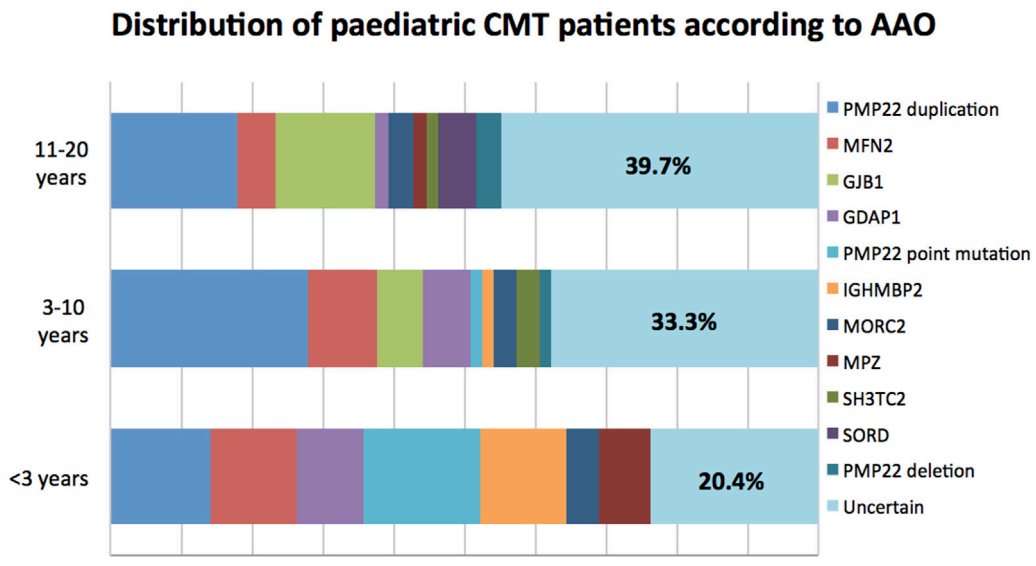

FIGURE 2
Distribution of paediatric CMT patients according to AAO.

forms (51/85; 60%). Compared among patients of all ages, the genetic confirmation rate in our paediatric cohort was similar to that reported in South China (70%) (Xie et al., 2021) and Taiwan (73.1%) (Hsu et al., 2019). However, this rate was higher than that worldwide (60.4%) (Fridman et al., 2015), suggesting that paediatric patients has a higher genetic diagnosis rate than those of all age groups. Nevertheless, this result is somewhat lower than that in other series when comparing within the paediatric groups (Cornett et al., 2016; Hoebeke et al., 2018; Argente-Escrig et al., 2021) (Table 2). To date, the largest paediatric series based on eight

TABLE 2 Gene distributions compared with previous studies.

Gene	This study (*n* = 181)	Cornett et al. (*n* = 520)	Hoebeke et al. (*n* = 75)	Argente-Escrig H. et al. (*n* = 99)
AAO (years)	0–20	3–20	0–18	0–20
PMP22 duplication	33 (18.2)	252 (48.5)	46 (61.3)	37 (37.4)
PMP22 point mutation	8 (4.4)	9 (1.7)	-	-
PMP22 deletion	3 (1.7)	5 (1.0)	-	-
GJB1	12 (6.6)	10 (1.9)	2 (2.6)	8 (8.1)
MFN2	14 (7.7)	31 (6.0)	11 (14.7)	3 (3.0)
GDAP1	9 (5)	3 (0.6)	1 (1.3)	10 (10.1)
IGHMBP2	6 (3.3)	-	-	-
MORC2	6 (3.3)	-	-	-
MPZ	4 (2.2)	15 (2.9)	1 (1.3)	3 (3.0)
SH3TC2	3 (1.7)	13 (2.5)		2 (2.0)
SORD	3 (1.7)			
HSPB1	2 (1.1)			
PRX	2 (1.1)	1 (0.2)	1 (1.3)	
BSCL2	2 (1.1)			
DYNC1H1	2 (1.1)			1 (1.0)
HINT1	2 (1.1)			
GARS	1 (0.6)	4 (0.8)		
AARS	1 (0.6)			
MARS	1 (0.6)			
TRPV4	1 (0.6)	1 (0.2)		
HK1	1 (0.6)		1 (1.3)	3 (3.0)
KIF5A	1 (0.6)			
EGR2	1 (0.6)			2 (2.0)
FGD4	1 (0.6)	1 (0.2)		2 (2.0)
MTMR2	1 (0.6)	2 (0.4)		
SPG11	1 (0.6)			
NEFL	1 (0.6)	3 (0.6)		
DHTKD1	1 (0.6)			
Uncertain	58 (32)	127 (24.4)	6 (8.0)	20 (20.2)

AAO, age at onset.

sites reported a diagnosis rate of 75.6% (Cornett et al., 2016). In another study from France, up to 92% of patients received a genetic diagnosis (Hoebeke et al., 2018). Compared with these studies, the reasons for our low mutation detection rate may be partly due to the small proportion of patients carrying *PMP22* duplication (18.2% of patients in our study versus 37.4%–61.3% in the aforementioned studies). It is worth noting that in other studies based on Chinese populations, CMT1A also only accounted for 19.5%–29.5% of CMT cases (Liu et al., 2020; Xie et al., 2021), with a similar rate in Japan and Korea (15%–26.3%) (Choi et al., 2004; Abe et al., 2011). The difference in the prevalence of *PMP22* duplication might be attributed to the heterogeneity among patients of different origins as well as the underestimation of mild patients in our country who did not receive detailed examination at hospitals. Therefore, this result indicates that although some asymptomatic or mild CMT1A cases may be missed in diagnosis, there is indeed distributional heterogeneity among patients of different origins.

In our current series, the most frequent disease-causing genes were *PMP22* duplication, followed by *MFN2* and *GJB1*. This distribution of genetic subtypes in our patients was similar to those reported previously in Chinese patients. A study focused on South Chinese CMT patients identified *PMP22* (19.1%–29%),

GJB1 (13.5%–13.8%) and *MFN2* (6.5%–10.1%) as the most frequent causative genes (Chen et al., 2019; Xie et al., 2021). In another study, *PMP22* (48.7%), *GJB1* (9.4%) and *MFN2* (3.3%) also ranked as the top three disease-causing genes in a Taiwanese CMT population (Hsu et al., 2019). Likewise, compared with Caucasian paediatric populations, the genetic spectrum was partly different in our cohort. Except for the remarkably lower detection rate of *PMP22* duplication in our study, mutations in *IGHMBP2, MORC2,* and *SORD*, manifesting as predominantly motor involvement, were also first discussed in pediatric CMT. In contrast, the proportions of the other frequent causative genes in our study, such as *GJB1, MFN2* and *MPZ* were similar to those reported in studies of European ancestry (Cornett et al., 2016; Hoebeke et al., 2018; Pipis et al., 2020; Argente-Escrig et al., 2021). Among rare genes, *GDAP1* was also reported in most paediatric CMT series, with a distribution of 0.6%–10.1% in Caucasian patients and 5% in our cohort.

There was marked genetic heterogeneity according to AAO in our findings. In the infantile-onset group, the diagnosis rate ranked the highest at 79.6%, with mutations in the *PMP22, MFN2,* and *IGHMBP2* genes being the three most frequent causes. As age increased, the diagnosis rate was gradually decreased, with 66.6% in the childhood-onset group and 60.3% in the adolescent-onset group. Following the three most frequent genes, the remaining common causative genes of childhood-onset CMT were *GDAP1, SH3TC2,* and *MORC2*, while *HSPB1* and *SORD* were mostly implicated in adolescent-onset CMT. In addition, disease severity was correlated with particular genotypes. Generally, earlier onset was the most predictive marker of significant disease severity for most CMT subtypes, while for CMT1A, the disease worsened consistently throughout childhood and adolescence, which was in line with previous studies (Cornett et al., 2016). For all subtypes, symptoms related to disease severity including decreased hand dexterity and weakness in ankle dorsiflexion. In comparison to patients with other genotypes, patients with *PMP22* point mutation developed a severe phenotype with significant disability, accounting for 29.4% of the severe cases in total. In the CMT2A subgroup, patients with an AAO before 10 years tended to have more severe disease than those in the late-onset subgroup.

The most common phenotypes for infantile-onset patients were DSS in our findings. Genetically, most cases are caused by a dominant or *de novo* mutation in the *PMP22, MPZ* or *EGR2* genes (Gargaun et al., 2016; Grosz et al., 2019; Yoshimura et al., 2019). In addition to *PMP22* mutations, variants in rare genes, e.g., *EGR2, PRX*, and *FGD4* were found more frequently due to the introduction of NGS and WES, which was consistent with previous studies (Yoshimura et al., 2019).

Interestingly, the presence of *de novo* variants was identified in 12.7% of all patients and thus was not rare. Certain *PMP22* variants, such as p. S72W, p. S79P and p. G150V, were mainly observed to occur *de novo*. In addition, patients carrying *de novo* variants of *MPZ* (p. R98C, p. S233Rfs*18 and p. L174Rfs*66) were also uncommon, with a severe DSS phenotype of motor retardation, weakness and foot deformity. In previous studies, *de novo* variants for *MFN2* were not rare. In some series of CMT2A patients, a frequency of *de novo MFN2* variants has been reported of 14.4%–35.0% (Ma et al., 2021; Verhoeven et al., 2006; Kijima et al., 2005). In pediatric group, the frequency may be higher, with up to 45.5% (5/11) being reported of *de novo* in a French CMT2A cohort (Hoebeke et al., 2018). In literature, *de novo* variants are common disease mechanism in some childhood onset inherited diseases; it is associated with a reduced life expectancy and reduced reproductive fitness. As *de novo* variants are usually too deleterious to be passed on in evolution, it is more common in pediatric patients rather than other age groups (Mohiuddin et al., 2022). Compared with European paediatric CMT patients, in whom *de novo* variants were identified in only 6%–6.5% (Yoshimura et al., 2019; Argente-Escrig et al., 2021), the frequency in our cohort was to some extent higher. Except for the possible geographic differences, the reason that less awareness of disease might deceive mild non-*de novo* individuals to access to our specialized clinics may also contribute to the lower frequency in our cohort. Considering that the prevalence of *de novo* variants was highest in early-onset and severe cases, genetic screening should be performed in patients with early-onset and severe peripheral neuropathy regardless of family history.

In our cohort, variants in *IGHMBP2, MORC2,* and *SORD* accounted for a certain proportion of paediatric CMT patients, which was not reported in previous studies from Western countries. Recently, the *SORD* gene has been considered one of the most frequent causative genes for autosomal recessive axonal CMT or dHMN (Cortese et al., 2020), which share a phenotype of motor-predominant peripheral neuropathy. In this study, we identified three patients carrying either a homozygous or a compound heterozygous c.757delG (p. Ala253GlnfsTer27) variant, which was consistent with the literature (Liu et al., 2021). However, *MORC2* variants are clinically heterogeneous with phenotypes that can be characterized by congenital or early-onset spinal muscular atrophy like or pure motor axonal neuropathy (Sevilla et al., 2016). Therefore, genetic screening according to the clinical phenotype should be conducted in paediatric patients in whom CMT is suspected especially for autosomal recessive inheritance or newly discovered genes.

In summary, this study represented a major effort to investigate paediatric CMT characteristics in a Chinese population. In-depth analysis highlighted the relatively lower detection rate of *PMP22* duplication and higher frequency of *de novo* variants among paediatric patients in this specific geographic region. In addition, we illustrated genetic heterogeneity according to AAO, disease severity and clinical features. Indeed, since patients were recruited from two clinic centres, the results of the study could not represent the whole Chinese pediatric population. In the future, longitudinal studies and multi-centre studies would yield more information and analytical results.

Data availability statement

The raw data supporting the conclusion of this article will be made available by the authors, without undue reservation.

Ethics statement

The studies involving human participants were reviewed and approved by the Institutional Ethics Committee of Peking University Third Hospital (2019-005-02). Written informed consent to participate in this study was provided by the participants' legal guardian/next of kin.

Author contributions

XL and DF conceptualized and designed the study. YM, XD, and XL performed data analysis. YM wrote the manuscript. XD, XL, and DF revised the manuscript. All authors contributed to the article and approved the submitted version.

Funding

This study was supported by the National Natural Science Foundation of China under Grant (No. 81873784, No. 82071426), Clinical Cohort Construction Program of Peking University Third Hospital (No. BYSYDL2019002, No. BYSYDL2021007) and Clinical Medicine Plus X-Youth Scholars Project, Peking University, the Fundamental Research Funds for the Central Universities (PKU2021LCXQ019).

Acknowledgments

We thank the patients for their consent and participation in this study.

Conflict of interest

The authors declare that the research was conducted in the absence of any commercial or financial relationships that could be construed as a potential conflict of interest.

Publisher's note

All claims expressed in this article are solely those of the authors and do not necessarily represent those of their affiliated organizations, or those of the publisher, the editors and the reviewers. Any product that may be evaluated in this article, or claim that may be made by its manufacturer, is not guaranteed or endorsed by the publisher.

Supplementary material

The Supplementary Material for this article can be found online at: https://www.frontiersin.org/articles/10.3389/fgene.2023.1188361/full#supplementary-material

References

Abe, A., Numakura, C., Kijima, K., Hayashi, M., Hashimoto, T., and Hayasaka, K. (2011). Molecular diagnosis and clinical onset of Charcot-Marie-Tooth disease in Japan. *J. Hum. Genet.* 56, 364–368. doi:10.1038/jhg.2011.20

Agrahari, A., and George Priya Doss, C. (2015). Impact of I30T and I30M substitution in MPZ gene associated with dejerine-sottas syndrome type B (dssb): A molecular modeling and dynamics. *J. Theor. Biol.* 382, 23–33. doi:10.1016/j.jtbi.2015.06.019

Argente-Escrig, H., Frasquet, M., Vázquez-Costa, J. F., Millet-Sancho, E., Pitarch, I., Tomás-Vila, M., et al. (2021). Pediatric inherited peripheral neuropathy: A prospective study at a Spanish referral center. *Ann. Clin. Transl. Neurol.* 8 (9), 1809–1816. doi:10.1002/acn3.51432

Baets, J., Deconinck, T., De Vriendt, E., Zimoń, M., Yperzeele, L., Van Hoorenbeeck, K., et al. (2011). Genetic spectrum of hereditary neuropathies with onset in the first year of life. *Brain.* 134(Pt 9): 2664–2676. doi:10.1093/brain/awr184

Bird, T. D. (1998). "Charcot-marie-tooth hereditary neuropathy overview," in *GeneReviews®*. M. P. Adam, G. M. Mirzaa, R. A. Pagon, S. E. Wallace, L. J. Bean, K. W. Gripp, et al. (Seattle (WA): University of Washington, Seattle).

Burns, J., Ouvrier, R., Estilow, T., Shy, R., Laurá, M., Pallant, J. F., et al. (2012). Validation of the Charcot-Marie-Tooth disease pediatric scale as an outcome measure of disability. *Ann. Neurol.* 71 (5), 642–652. doi:10.1002/ana.23572

Chen, C. X., Dong, H. L., Wei, Q., Li, L. X., Yu, H., Li, J. Q., et al. (2019). Genetic spectrum and clinical profiles in a southeast Chinese cohort of Charcot-Marie-Tooth disease. *Clin. Genet.* 96 (5), 439–448. doi:10.1111/cge.13616

Choi, B. O., Lee, M. S., Shin, S. H., Hwang, J. H., Choi, K. G., Kim, W. K., et al. (2004). Mutational analysis of PMP22, MPZ, GJB1, EGR2 and NEFL in Korean Charcot-Marie-Tooth neuropathy patients. *Hum. Mutat.* 24 (2), 185–186. doi:10.1002/humu.9261

Cornett, K. M., Menezes, M. P., Bray, P., Halaki, M., Shy, R. R., Yum, S. W., et al. (2016). Phenotypic variability of childhood charcot-marie-tooth disease. *JAMA Neurol.* 73 (6), 645–651. doi:10.1001/jamaneurol.2016.0171

Cortese, A., Zhu, Y., Rebelo, A. P., Negri, S., Courel, S., Abreu, L., et al. (2020). Biallelic mutations in SORD cause a common and potentially treatable hereditary neuropathy with implications for diabetes. *Nat. Genet.* 52 (5), 473–481. doi:10.1038/s41588-020-0615-4

Fridman, V., Bundy, B., Reilly, M. M., Pareyson, D., Bacon, C., Burns, J., et al. (2015). CMT subtypes and disease burden in patients enrolled in the inherited neuropathies consortium natural history study: A cross-sectional analysis. *J. Neurol. Neurosurg. Psychiatry* 86 (8), 873–878. doi:10.1136/jnnp-2014-308826

Gargaun, E., Seferian, A. M., Cardas, R., Le Moing, A. G., Delanoe, C., Nectoux, J., et al. (2016). EGR2 mutation enhances phenotype spectrum of Dejerine-Sottas syndrome. *J. Neurol.* 263 (7), 1456–1458. doi:10.1007/s00415-016-8153-9

Grosz, B. R., Golovchenko, N. B., Ellis, M., Kumar, K., Nicholson, G. A., Antonellis, A., et al. (2019). A *de novo* EGR2 variant, c.1232A > G p. Asp411Gly, causes severe early-onset Charcot-Marie-Tooth Neuropathy Type 3 (Dejerine-Sottas Neuropathy). *Sci. Rep.* 9 (1), 19336. doi:10.1038/s41598-019-55875-4

Hoebeke, C., Bonello-Palot, N., Audic, F., Boulay, C., Tufod, D., Attarian, S., et al. (2018). Retrospective study of 75 children with peripheral inherited neuropathy: Genotype-phenotype correlations. *Arch. Pediatr.* 25 (8), 452–458. doi:10.1016/j.arcped.2018.09.006

Hsu, Y. H., Lin, K. P., Guo, Y. C., Tsai, Y. S., Liao, Y. C., and Lee, Y. C. (2019). Mutation spectrum of charcot-marie-tooth disease among the han Chinese in taiwan. *Ann. Clin. Transl. Neurol.* 6 (6), 1090–1101. doi:10.1002/acn3.50797

Kijima, K., Numakura, C., Izumino, H., Umetsu, K., Nezu, A., Shiiki, T., et al. (2005). Mitochondrial GTPase mitofusin 2 mutation in Charcot-Marie-Tooth neuropathy type 2A. *Hum. Genet.* 116 (1-2), 23–27. doi:10.1007/s00439-004-1199-2

Klein, C. J. (2020). Charcot-Marie-Tooth disease and other hereditary neuropathies. *Contin. (Minneap Minn)* 26 (5), 1224–1256. doi:10.1212/CON.0000000000000927

Landrieu, P., and Baets, J. (2013). Early onset (childhood) monogenic neuropathies. *Handb. Clin. Neurol.* 115, 863–891. doi:10.1016/B978-0-444-52902-2.00049-7

Liu, X., Duan, X., Zhang, Y., and Fan, D. (2020a). Clinical and genetic diversity of *PMP22* mutations in a large cohort of Chinese patients with charcot-marie-tooth disease. *Front. Neurol.* 11, 630. doi:10.3389/fneur.2020.00630

Liu, X., Duan, X., Zhang, Y., Sun, A., and Fan, D. (2020b). Molecular analysis and clinical diversity of distal hereditary motor neuropathy. *Eur. J. Neurol.* 27 (7), 1319–1326. doi:10.1111/ene.14260

Liu, X., He, J., Yilihamu, M., Duan, X., and Fan, D. (2021). Clinical and genetic features of biallelic mutations in SORD in a series of Chinese patients with charcot-marie-tooth and distal hereditary motor neuropathy. *Front. Neurol.* 12, 733926. doi:10.3389/fneur.2021.733926

Ma, Y., Sun, A., Zhang, Y., Fan, D., and Liu, X. (2021). The genotype and phenotype features in a large Chinese MFN2 mutation cohort. *Front. Neurol.* 12, 757518. doi:10.3389/fneur.2021.757518

Mohiuddin, M., Kooy, R. F., and Pearson, C. E. (2022). *De novo* mutations, genetic mosaicism and human disease. *Front. Genet.* 13, 983668. doi:10.3389/fgene.2022.983668

Padilha, J. P. D., Brasil, C. S., Hoefel, A. M. L., Winckler, P. B., Donis, K. C., Brusius-Facchin, A. C., et al. (2020). Diagnostic yield of targeted sequential and massive panel approaches for inherited neuropathies. *Clin. Genet.* 98 (2), 185–190. Epub 2020 Jun 29. doi:10.1111/cge.13793

Panosyan, F. B., Laura, M., Rossor, A. M., Pisciotta, C., Piscosquito, G., Burns, J., et al. (2017). Cross-sectional analysis of a large cohort with X-linked Charcot-Marie-Tooth disease (CMTX1). *Neurology* 89 (9), 927–935. doi:10.1212/WNL.0000000000004296

Pareyson, D., and Marchesi, C. (2009). Diagnosis, natural history and management of Charcot-Marie-Tooth disease. *Lancet. Neurology* 8 (7), 654–667. doi:10.1016/S1474-4422(09)70110-3

Pipis, M., Feely, S. M. E., Polke, J. M., Skorupinska, M., Perez, L., Shy, R. R., et al. (2020). Natural history of charcot-marie-tooth disease type 2A: A large international multicentre study. *Brain* 143 (12), 3589–3602. doi:10.1093/brain/awaa323

Richards, S., Aziz, N., Bale, S., Bick, D., Das, S., Gastier-Foster, J., et al. (2015). Standards and guidelines for the interpretation of sequence variants: A joint consensus recommendation of the American College of medical genetics and Genomics and the association for molecular Pathology. *Genet. Med.* 17, 405–424. doi:10.1038/gim.2015.30

Sevilla, T., Lupo, V., Martínez-Rubio, D., Sancho, P., Sivera, R., Chumillas, M. J., et al. (2016). Mutations in the MORC2 gene cause axonal Charcot-Marie-Tooth disease. *Brain* 139, 62–72. doi:10.1093/brain/awv311

Skre, H. (1974). Genetic and clinical aspects of Charcot-Marie-Tooth's disease. *Clin. Genet.* 6 (2), 98–118. doi:10.1111/j.1399-0004.1974.tb00638.x

Verhoeven, K., Claeys, K. G., Züchner, S., Schröder, J. M., Weis, J., Ceuterick, C., et al. (2006). MFN2 mutation distribution and genotype/phenotype correlation in Charcot-Marie-Tooth type 2. *Brain*. 129(Pt 8), 2093–2102. doi:10.1093/brain/awl126

Xie, Y., Lin, Z., Liu, L., Li, X., Huang, S., Zhao, H., et al. (2021). Genotype and phenotype distribution of 435 patients with Charcot-Marie-Tooth disease from central south China. *Eur. J. Neurol.* 28 (11), 3774–3783. doi:10.1111/ene.15024

Yoshimura, A., Yuan, J. H., Hashiguchi, A., Ando, M., Higuchi, Y., Nakamura, T., et al. (2019). Genetic profile and onset features of 1005 patients with Charcot-Marie-Tooth disease in Japan. *J. Neurol. Neurosurg. Psychiatry* 90 (2), 195–202. doi:10.1136/jnnp-2018-318839

frontiers | Frontiers in Genetics

TYPE Original Research
PUBLISHED 17 August 2023
DOI 10.3389/fgene.2023.1237912

OPEN ACCESS

EDITED BY
Jordi Pérez-Tur,
Spanish National Research Council (CSIC), Spain

REVIEWED BY
Miguel Angel Alcántara-Ortigoza, National Institute of Pediatrics, Mexico
Tiantian Xiao,
Chengdu Women and Children's Central Hospital, China

*CORRESPONDENCE
Meimei Liu,
mm7723@163.com

RECEIVED 10 June 2023
ACCEPTED 04 August 2023
PUBLISHED 17 August 2023

CITATION
Yang W, Zu S, Jin Q, Liu Y, Wang C, Shen H, Wang R, Zhang H and Liu M (2023), Fetal hyperechoic kidney cohort study and a meta-analysis.
Front. Genet. 14:1237912.
doi: 10.3389/fgene.2023.1237912

Fetal hyperechoic kidney cohort study and a meta-analysis

Wei Yang[1,2], Shujing Zu[2], Qiu Jin[1], Yu Liu[1], Chao Wang[1], Huimin Shen[1], Ruijing Wang[1], Hui Zhang[2] and Meimei Liu[1]*

[1]Department of Obstetrics and Gynecology, The Second Affliliated Hospital of Harbin Medical University, Harbin, China, [2]Department of Prenatal Diagnosis, Harbin Red Cross Central Hospital, Harbin, China

Objective: To investigate the positive rate of chromosomal and monogenic etiologies and pregnancy outcomes in fetuses with hyperechoic kidney, and to provide more information for genetic counseling and prognosis evaluation.

Methods: We performed a retrospective analysis of 25 cases of hyperechoic kidney diagnosed prenatal in the Second Affiliated Hospital of Harbin Medical University and Harbin Red Cross Central Hospital (January 2017–December 2022). Furthermore, we conducted a meta-analysis of a series of hyperechoic kidneys (HEK) in the literature to assess the incidence of chromosomal and monogenic etiologies, mortality, and pooled odds ratio (OR) estimates of the association between the incidence of these outcomes and other associated ultrasound abnormalities.

Results: 25 fetuses of HEK were enrolled in the cohort study, including 14 with isolated hyperechoic kidney (IHK) and 11 with non-isolated hyperechoic kidney (NIHK). Chromosomal aneuploidies were detected in 4 of 20 patients (20%). The detection rate of pathogenic or suspected pathogenic copy number variations (CNVs) was 29% (4/14) for IHK and 37% (4/11) for NIHK. Whole exome sequencing (WES) was performed in 5 fetuses, and pathogenic genes were detected in all of them. The rate of termination of pregnancy was 56% in HEK. 21 studies including 1,178 fetuses were included in the meta-analysis. No case of abnormal chromosome karyotype or (intrauterine death)IUD was reported in fetuses with IHK. In contrast, the positive rate of karyotype in NIHK was 22% and that in HEK was 20%, with the ORs of 0.28 (95% CI 0.16–0.51) and 0.25, (95% CI 0.14–0.44), respectively. The positive rate of (chromosome microarray analysis) CMA in IHK was 59% and that in NIHK was 32%, with the ORs of 1.46 (95% CI 1.33–1.62) and 0.48 (95% CI, 0.28–0.85), respectively. The positive rate of monogenic etiologies in IHK was 31%, with the OR of 0.80 (95% CI 0.25–2.63). In IHK, the termination rate was 21% and neonatal mortality was 13%, with the ORs of 0.26 (95% CI, 0.17–0.40), 1.72 (95% CI, 1.59–1.86), and that in NIHK was 63%, 0.15 (95% CI, 0.10–0.24); 11%, 0.12 (95% CI, 0.06–0.26), respectively. The intrauterine mortality in NIHK group was 2%, with the OR of 0.02 (95% CI, 0.01–0.05). *HNF1B* variant has the highest incidence (26%) in IHK.

Conclusion: The positive rate of karyotype was 20% in HEK and 22% in NIHK. The positive rate of CMA was 32% in NIHK and 59% in IHK. The positive rate of IHK monogenic etiologies was 31%. *HNF1B* gene variation is the most common cause of IHK. The overall fetal mortality rate of NIHK is significantly higher than that of IHK. The amount of amniotic fluid, kidney size and the degree of corticomedullary differentiation have a great impact on the prognosis, these indicators should be taken into consideration to guide clinical consultation and decision-making.

KEYWORDS
fetus, hyperechoic kidney, prenatal diagnosis, ultrasound, metaanalysis, CMA, CNV-seq

Introduction

Congenital abnormalities of the kidneys and urinary tracts (CAKUT) are one of the most common fetal structural abnormalities, occurring in about 30%–50% of prenatally diagnosed malformations (Hutson et al., 1985; Deng et al., 2022). CAKUT often result in a series of defects in the kidneys and outflow tracts, including the ureters, the bladder, and urethra. The prevalence is estimated at 4–60 per 10,000 births, depending on the registry, with variation due to differences in sample size, method of diagnosis, and ethnic differences between studies (Tain et al., 2016). A subset of CAKUT patients may show only a hyperechoic kidney on fetal ultrasound during pregnancy, showing clear structural abnormalities only in the third trimester or after birth. Fetal hyperechoic kidney (HEK) may be transient in pregnancy, or may be an ultrasound manifestation of CAKUT or some syndromes, HEK are associated with a wide range of etiologies and prognoses. Prenatal counselling and management can be extremely challenging, especially for isolated HEK (Deng et al., 2022).

Hyperechoic kidneys (HEK) are occasionally seen on routine renal ultrasound scan, or with other clinical indications detected on late pregnancy scans, caused by renal abnormalities (Reisman et al., 1991), such as renal dysplasia, fibrosis, interstitial infiltration, tubular/glomerular dilatation, or microcysts (Dias et al., 2014). HEK can be a first indicator of underlying kidney disease and are detected in approximately 1.6 out of 1,000 scans (AM et al., 1983; Yulia et al., 2021), while HEK are almost exclusively pathogenic in childhood the implications of this finding are less clear in the prenatal period (Digby et al., 2021), because of this uncertainty, it may be difficult for families facing such prenatal findings to make informed decisions during pregnancy.

The differential diagnosis of fetal isolated hyperechoic kidney includes autosomal dominant and autosomal recessive polycystic kidney disease (ADPKD and ARPKD) respectively, congenital nephrotic syndrome, renal vein thrombosis and obstructive uropathy (Shuster et al., 2019). In non-isolated fetal hyperechoic kidney, differential diagnoses include aneuploidy, mainly trisomy 13 syndrome, fetal infections such as cytomegalovirus, Meckel-Gruber syndrome and other renal ciliopathies, and other monogenic disorders associated with CAKUT, including overgrowth syndrome, Examples include Beckwith-Wiedemann, Perlman, and Simpson-Golabi-Behmel syndrome (Avni et al., 2012; Shuster et al., 2019).

Traditional karyotyping, such as G-banding, has been the standard method for detecting various chromosomal abnormalities for decades. With the improvement of prenatal diagnosis technology, more and more prenatal fetal abnormalities are diagnosed not only by ultrasound and chromosome karyotype detection, but also by the maturity of CMA and CNV-seq technology, which has greatly improved the detection rate of chromosomal abnormalities. Different genetic diagnosis strategies have also found more gene abnormalities related to HEK. The study (Deng et al., 2022) showed that about 64.29% of fetal HEK were related to genetic factors, and the detection rate of single gene variation was higher than that of chromosome abnormality and copy number variation. And in IHK cases, the positive rate of single gene variants was 50% (4/8). The characteristics of oligohydramnios and fetal kidney size ≥2SD from the mean are associated with poorer outcomes, such as neonatal death (Mashiach et al., 2005), but are often not specific to a single underlying cause. Their absence does not guarantee favorable outcomes (i.e., live birth and child survival without renal impairment) (Digby et al., 2021).

The purpose of this cohort study and meta-analysis was to determine the positive rate of chromosomal and monogenic etiologies, perinatal mortality and related factors in IHK and NIHK fetuses, so that clinicians can determine the prognosis of the fetus and provide accurate counseling for parents better.

Materials and methods

Cohort study

We reviewed all 3,995 cases of prenatal diagnosis in the Second Affiliated Hospital of Harbin Medical University and Harbin Red Cross Central Hospital (January 2017 to December 2022), of which 251 cases were fetal kidney related abnormalities. Including ultrasound soft indicators, hydronephrosis and renal structural abnormalities. Ultrasound showed that there were 25 cases of fetal hyperechoic kidney, including 14 cases of IHK (Table 1) and 11 cases of NIHK (Table 2). All patients underwent at least two genetic tests and were followed up by telephone within 6 months to 1 year after the expected date of delivery, including newborn survival and urinary status. We recorded the condition of patients, and statistically analyzed the results of patient detection and prognosis. SPSS27.0 statistical software, Chi-square test was used to compare the differences between groups. Due to the small sample size, Fisher exact probability method was used, and $p < 0.05$ was considered statistically significant.

Meta-analysis

Literature search

In February 2023, were searched by two researchers using combinations of the following keywords: “fetus,” “antenatal,” “prenatal,” fetus*,” “fetal,” “kidney,” “kidney*,” “hyperechoic” and “hyperechoic*.” For all data-bases, the last search was run on 28 February 2023.

The Chinese language databases Wanfang Data, China National Knowledge Infrastructure (CNKI), and China Biomedical Literature Database (CBM) (from 1 January 1990 to 28 February 2023) were searched by two researchers using the Chinese terms for “fetal,” “kidneys,” and “hyperechoic.” Additionally, English language databases PubMed, Embase,

TABLE 1 Etiological and prognostic follow-up of IHK in our cohort.

	NO.	Age (y)	GW	Ultrasound results	Karyotype	CNV-seq	WES(Trio)	Outcomes
1	190034	26	25	Bilateral kidney echogenic, oligohydramnios	—	(−)	—	(−)
2	200244	31	28	Bilateral kidney echogenic	—	**1.del(17) (q12)** chr17: g34800000_36260000del,1.46 Mb,**p**; **2.dup(8) (q11.1)** chr8: g.46880000_47500000dup,0.62 Mb, **lb**	—	TOP
3	210040	38	19	Bilateral kidney echogenic	(−)	(−)	**1.*PKHD1*** chr6: 51921499 NM_138694.3:c.1690C>T, (p.Arg564*), EX18/CDS17, (**het,p**)PKD type 4 with or without polycystic liver disease (OMIM:263200)/AR, Father het	TOP
							2.*PKHD1* chr6: 51918033 NM_138694.3:c.1981A>C, (p.Thr661Pro), EX21/CDS20, (**het, vous**)AR, Mother het	
							3.*NUP85* chr17:73231283	
							NM_024844.3:c.1856C>T, (p.Thr619Ile), EX18/CDS18, (het, vous) Nephrotic syndrome type17, (OMIM: 618176)/AR, Father het	
							4.*NUP85* chr17: 73228963 NM_024844.3:c.1414A>G, (p.Ile472Val), EX15/CDS15, (het, vous) AR, Mother het	
4	210086	33	24	Bilateral kidney echogenic, oligohydramnios, consider infantile polycystic kidney disease	(−)	(−)	**1.*PKHD1*** chr6: 51513947 NM_138694.3:c.11246C>T, (p.Pro3749Leu) EX62/CDS61 (het,vous) PKD type 4 with or without polycystic liver disease (OMIM:2632 00)/AR, Mother het	TOP
							2.*PKHD1* chr6:5152425 NM_138694.3: c.10679C>G, (p.Ser3560Cy s), EX61/ CDS60 (het,vous)/AR, Father (het)	
5	210323	26	29	Bilateral kidney echogenic	—	(−)	**1.*PKD1*** chr16: 2158269 NM_001009944.2:c.6899delG, (p.Cys2300Leufs*14) EX15/CDS15, (**het**/Father het/Mother wt,**p**) PKD type1, (OMIM:173900)/AD; **2.*PKD1*** chr16:2162862 NM_001009944.2: c.3088G>A, (p.Val1030Met) EX13/ CDS13, (het/Father wt/Mother het vous) AD; **3.*COL4A3*** chr2: 228131184–228131186 NM_000091.4: c.1367_1369del, ATC (p.Tyr456del) EX22/CDS22, (**het**/Father wt/Mother het, **lp**) Autosomal dominant Alport syndrome (OMIM:104200)/AD, Benign familial hematuria (OMIM:141200)/AD, Autosomal recessive Alport syndrome type 2 (OMIM:203780)/AR	ADPKD
6	220253	34	22	Bilateral kidney echogenic	(−)	**dup (X) (p22.31p22.31)*1** 1.77 Mb, **p**, X-linked ichthyosis	**1.*PKHD1*** chr6: 51798938 NM_138694.3:c.6091del G, (p.Ala2031Leufs *2) EX37/CDS36, (het/ Father het/Mother wt, p)PKD type 4 with or without more Cystic liver (OMIM:263200)/AR; **2.*PKHD1*** chr6: 51927371 NM_138694.3:c.1064T>G (p.Val355Gly) EX14/CDS13, (het/Father wt/Mother het,vous) **supplement 1: *STS*** chrX:6968338–7268302 NM_000351.4:	TOP

(Continued on following page)

TABLE 1 (*Continued*) Etiological and prognostic follow-up of IHK in our cohort.

	NO.	Age (y)	GW	Ultrasound results	Karyotype	CNV-seq	WES(Trio)	Outcomes
							EX1-EX10E Del, (het/Father hem/ Mother wt,p),X-linked ichthyosis (OMIM:308100)/XL	
7	220302	30	18	Bilateral kidney echogenic	(−)	(−)	—	(−)
8	Y18002	30	20	Bilateral kidney echogenic	(−)	**del(4q13.3)**,130.91 kb, vous; **del(15q13.2)**, 200.68 kb, vous; **dup(15q13.3)** 489.55 kb, vous	—	(−)
9	Y19113	30	22	Bilateral kidney echogenic	T21	T21	—	TOP
10	Y19158	28	24	Bilateral kidney echogenic	(−)	(−)	—	(−)
11	Y19255	40	24	Bilateral kidney echogenic	T21	T21	—	TOP
12	Y20138	36	25	Bilateral kidney echogenic, Bilateral kidneys are full in shape	(−)	**dup(7p21.3)**,102.32 kb, vous **dup(17p12)**, 110.08 kb, vous	—	(−)
13	Y21263	34	27	Bilateral kidney echogenic	(−)	(−)	—	(−)
14	Y21447	31	19	Bilateral kidney echogenic, enlarged	(−)	**del(8p22p22)**, 205.37 kb vous	—	(−)

(−), nothing abnormal detected; TOP, termination of pregnancy; /, undetected; het, heterozygous; wt, wild type; hem, hemizygous; p, pathogenicity; lp, likely pathogenicity; b, benign; lb, likely benign; GW, gestational weeks; T, Trisomy; vous, variants of uncertain clinical significance.

Cochrane Library and Web of Science (from 1 January 1945 to 28 February 2023) were searched by two researchers using combinations of the following keywords: "fetus," "antenatal," "prenatal," fetus*," "fetal," "kidney," "kidney*," "hyperechoic" and "hyperechoic*." The amount of amniotic fluid was assessed by a semiquantitative method. Diagnostic criteria were based on ultrasonographic assessment of AFV (amniotic fluid volume) or AFI (amniotic fluid index): AFV ≥ 8 cm or AFI ≥ 25 cm for polyhydramnios, and AFV ≤ 2 cm or AFI ≤ 5 cm for oligohydramnios (Phelan et al., 1987; Moore and Cayle, 1990). Kidneys were considered as hyperechogenic when the renal parenchyma was of greater echogenicity than adjacent liver tissue. The size of the kidneys was selected as standard deviations above or below the mean derived from the growth charts of Cohen et al. (1991) Renal enlargement was defined as kidney size ≥ 2 SD or a renal volume above the 90th percentile for gestational age (Chitty and Altman, 2003), kidney reduction was defined as kidney size ≤ 2 SD or a renal volume below the 10th percentile for gestational age, and between the two cutoff values was defined as normal kidney. Isolated hyperechogenic kidneys was defined by the absence of structural abnormalities. Review Manager 5.4.1 software was used for the meta-analysis to determine the incidence of chromosomal abnormalities and gene abnormalities in hyperechogenic kidneys, and the OR of the different outcomes and 95% confidence interval (CI) were calculated. Follow PRISMA (http://www.prisma-statement.org/) and MOOSE (Stroup et al., 2000) guidelines. We manually searched the reference lists of relevant articles and reviews for additional reports. The study has been registered in the PROSPERO database (registration No. CRD42023424469).

Inclusion criteria

Inclusion criteria were studies reporting fetal, neonatal, and infant outcomes. Renal hyperechogenicity was diagnosed on prenatal ultrasound. The primary outcomes were termination of pregnancy (TOP), intrauterine death (IUD) and neonatal death (NND).

Study selection

Screening was performed independently by two investigators based on inclusion and exclusion criteria. Any disagreements were resolved by discussion with a third researcher. The inclusion criteria is that patients with fetal renal hyperechogenicity confirmed by fetal ultrasound in the second or third trimester, including singleton and twin pregnancies.

Exclusion criteria were as follows: 1) Reviews and case reports; 2) animal research; 3) There was no further testing or follow-up outcome.

Data extraction

Two researchers independently screened the literature, extracted and cross-checked the data. Differences, if any, are resolved through discussion or negotiation with a third party. During literature screening, the title of the paper was read first, and after

TABLE 2 Etiological and prognostic follow-up of NIHK in our cohort.

N	NO.	Age (y)	GW	Ultrasound results	Karyotype	CNV-seq	WES (Trio)	Outcomes
1	170015	21	24	Fetal meningocele, hyperechoic bilateral kidneys, hexadactyly, Meckel-Gruber syndrome considered	—	umbilical cord **dup(1) (q21.1)** (145380001–145840000) 0.46 Mb, vous	umbilical cord: **1.** ***CC2D2A*** (het) chr4: 15565018 AR Meckel -Gruber Syndrome, **lp**; **2.** ***NUTM2B/IL17RD*****, lp**; **3.** ***DBT/NOS3*****, lp**	TOP
2	Q170004	28	21	High value of left ventricle, bilateral renal pelvis separation, bilateral renal parenchyma echo enhancement, excessive amniotic fluid	failed	(–)	—	TOP
3	180151	25	22	NT 5.6 mm, Cerebellar vermiform dysplasia, left cleft lip and palate, single atrium, endocardial pad defect, right ventricular double outlet, persistent left upper cavity, pulmonary artery stenosis, six fingers, toes, partial syndactyly possible, small omphalocele, umbilical cord cyst? The echo of both kidneys was enhanced	T13	T13	—	TOP
4	Q210001	22	25	Brain abnormalities: Dandy-Walker syndrome, arachnoid cysts; Cervical hygroma; Both kidneys increased echogenicity; Oligohydramnios	(–)	(–)	—	TOP
5	Y18243	34	22	The fetal right kidney is echogenic with multiple anechoic masses (considering the possibility of polycystic dysplasia); the left renal pelvis is separated, and the fetal heart rate is slightly faster	(–)	**dup(16p11.2p11.2)** 621.32 kb, vous	—	(–)
6	Y18280	27	22	Left kidney pelvic ectopic, slightly higher echo, mild hydrops; Fetal gallbladder morphology is slightly full	(–)	**del(14q31.3q31.1)** 303.82 kb, vous	—	(–)
7	Y18300	29	23	Fetal right lateral ventricle high value; Bilateral renal structural abnormalities: left renal corticomedul-medullary boundary blurred, parenchymal echo obviously enhanced; Multiple cysts (not excepting left renal polycystic dysplasia), renal pelvis separation; The cortical echo of the right kidney was increased, and the renal pelvis was separated	(–)	(–)	—	(–)
8	Y19125	31	19	NF thickening, neck and facial subcutaneous soft tissue thickening; Left nasal bone is short, right nasal bone is not explored (consider right nasal bone missing); Strong spot of left and right ventricle and mild regurgitation of tricuspid valve; The kidneys were highly echogenic and the liver was coarsely echogenic	T21	T21	—	TOP
9	Y19182	26	18	Blake cyst may be between the fourth ventricle and posterior fossa cisterna, and fetal septum pellucidum is small. Kidneys slightly larger; Fetal left ventricular hyperechoic spot	(–)	**del(9p23p23)** 338.97 kb, **lb**	—	TOP
10	Y21182	27	24	Uneven fetal development; Narrow septum pellucidum; Strong spot in right ventricle; Both kidneys are echogenic	(–)	**del(16p11.2p11.2)** 358.22 kb,**p**; **dup(5p15.2p15.2)** 178.09 kb, vous	—	TOP

(Continued on following page)

TABLE 2 (*Continued*) Etiological and prognostic follow-up of NIHK in our cohort.

N	NO.	Age (y)	GW	Ultrasound results	Karyotype	CNV-seq	WES (Trio)	Outcomes
11	Y21275	25	24	High posterior Angle of left ventricle, enhanced echo in both kidneys, separation of renal pelvis, small anechoic mass in right kidney, cyst considered	(−)	**del(17q12q12)** 1.83 Mb, **p**	—	TOP

(−), nothing abnormal detected; TOP, termination of pregnancy; /, undetected; het, heterozygous; wt, wild type; hem, hemizygous; p, pathogenicity; lp, likely pathogenicity; b, benign; lb, likely benign; GW, gestational weeks; T, Trisomy; vous, variants of uncertain clinical significance.
The bold value indicates the presence of microdeletions/microrepeats on the chromosome, or it may not be bold, just to be more eye-catching.

excluding obviously irrelevant literature, the abstract and full text were further read to determine inclusion. Contact original study authors when necessary for information not identified but important to this study.

Data extraction included: 1) Basic information of the included studies: Research title, first author, published journals, etc. 2) the baseline characteristics of the research object and further detection methods; 3) Key elements of risk of bias assessment; 4) Outcome indicators of interest and follow-up prognosis data.

Quality assessment of the selected articles

The Newcastle-Ottawa scale was used to evaluate the quality of the included literature, according to NOS, each study is judged on three broad perspectives: selection, comparability and results, i.e., the selection of the study groups; the comparability of the groups and the ascertainment of outcome of interest. Assessment of the selection of a study includes the evaluation of the representativeness of the exposed cohort, selection of the non-exposed cohort, ascertainment of exposure and the demonstration that the outcome of interest was not present at the start of study. Assessment of the comparability of the study includes the evaluation of the comparability of cohorts based on the design or analysis. Finally, the ascertainment of the outcome of interest includes the evaluation of the type of the assessment of the outcome of interest, its length and the adequacy of follow up. According to NOS, a study can be awarded a maximum of one star for each numbered item within the Selection and Outcome categories. A maximum of two stars can be given for Comparability (Wells et al., 2011). There are 8 items with a total score of 9 stars, studies with at least 6 stars rated as high quality.

Statistical analysis

Review manager 5.4.1 software was used for statistical analysis. The single group rate was used as the effect analysis statistic, and its 95% confidence interval (CI) was given. The I2 was used to quantitatively determine the size of heterogeneity. The fixed effect and random effect models were used for meta-analysis. When $p > 0.10$ and I2< 50%, there was no statistical heterogeneity among the results of each study, then the fixed effect model was used for meta-analysis. Otherwise, there was statistical heterogeneity among the results of each study, and the sources of heterogeneity were further analyzed. After excluding the influence of obvious clinical heterogeneity, a random effect model was used for meta-analysis. The test level for the meta-analysis was set at $\alpha = 0.05$. Methods such as subgroup analysis or sensitivity analysis were used to deal with significant clinical heterogeneity, or only descriptive analyses were performed.

Results

Cohort study

There were 25 HEK cases in our cohort, including 14 IHK cases and 11 NIHK cases. Among all the cases, 4 cases were unable to perform amniotic fluid karyotype analysis due to gestational age over 25 weeks. Karyotyping failed in 1 case (NO. Q170004), the fetus was terminated because of multiple malformations, as shown in Figure 1A for the ultrasound images. 4 cases (20%) of aneuploidy were detected in 20 cases, of which 18% (2/11) were IHK and 22% (2/9) were NIHK. Copy number variation sequencing (CNV-seq) based on next-generation sequencing (NGS) was used to detect copy number variations (CNVs) in all 25 HEK cases, and 8 cases were pathogenic and suspected pathogenic, among which the detection rate of IHK was 29% (4/14), including 1 fetus (NO. 200244) of 17q12 deletion syndrome, the ultrasound image is shown in Figure 1B, which shows enhanced echo in both kidneys. A pathogenic CNV associated with X-linked ichthyosis was also found in case 6 (NO. 220253). The results of the other 2 cases (NO. Y19113 and NO. Y19255) were consistent with the karyotype test, and both were trisomy 21 syndrome. The abnormal detection rate of CNV in NIHK group was 37% (4/11), including 1case (NO. Y21275) of 17q12 deletion syndrome. The overall detection rate of variants of unknown clinical significance was 24%, only 1 case of benign or suspected benign variants was detected, and the detection rate was 4% in the NIHK group. There were 10 cases with no definite abnormality, accounting for 40%. A total of 5 cases underwent whole exome sequencing (WES), and no kidney-related pathogenic variants were detected in their karyotypes and CNV-seq. The results of WES in 4 cases of IHK group showed that 3 cases had compound heterozygosity of *PKHD1* gene. The case No. 5 of IHK has a compound heterozygous *PKD1*

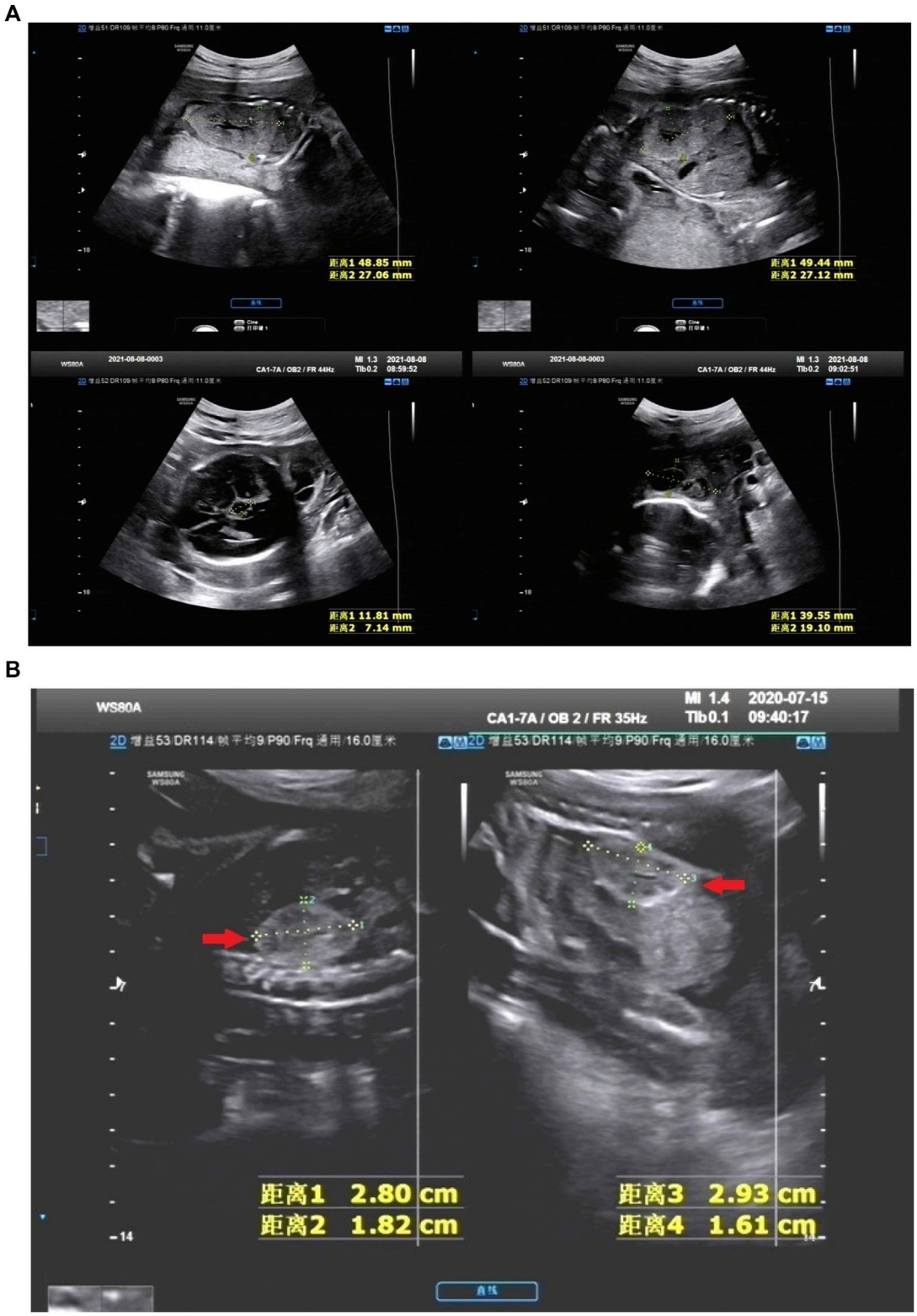

FIGURE 1
(A) NO. Q210001 in NIHK group, the ultrasound images of 28 weeks showed the size of the left kidney was 48.85 mm*27.06 mm and that of the right kidney was 49.44 mm*27.12 mm, the echo of the renal parenchyma was thickened and enhanced; An 11.81 mm*7.14 mm anechoic area was found in the midline below the third ventricle, Dandy-Walker syndrome with arachnoid cyst was considered; There was a 39.55 mm*19.10 mm anechoic area in the left posterior part of the neck, which was separated by a light band, It was considered as a cystic hygroma of the neck. This case was accompanied by oligohydramnios. **(B)** NO. 200244 in IHK group, the ultrasound images of 25 weeks showed bilateral hyperechoic kidneys, the size of the right kidney was 28 mm*18 mm and that of the left kidney was 29 mm*16 mm, within normal limits.

TABLE 3 Etiology and outcome statistics of IHK and NIHK in our cohort.

Testing and follow-up		IHK (14)		NIHK (11)		Total (25)		χ^2	p
		Number	p1	Number	p2	Number	p3		
karyotype	abnormal	2	0.18 (2/11)	2	0.22 (2/9)	4	0.2	0.318	>0.05
	normal	9	0.82 (9/11)	7	0.78 (7/9)	16	0.8		
	undetected	3	—	2 (1failed)	—	5	—		
CNV-seq	p/lp	4	0.29	4	0.37	8	0.32	3.53	>0.05
	vous	3	0.21	3	0.27	6	0.24		
	b/lb	0	0	1	0.09	1	0.04		
	normal	7	0.50	3	0.27	10	0.40		
WES	abnormal	4	1	1	1	5	1	—	—
	undetected	10	—	10	—	20	—		
follow-up	TOP	6	0.43	8	0.73	14	0.56	—	>0.05
	Survived well	8 (1ADPKD)	0.57	3	0.27	11	0.44		

p, pathogenicity; lp, likely pathogenicity; b, benign; lb, likely benign; TOP, termination of pregnancy; ADPKD, autosomal dominant polycystic kidney disease.

genotype, involving a pathogenic and an uncertain significance variant, while the fetus is also heterozygous for a *COL4A3* gene variant responsible of the autosomal dominant form of Alport syndrome. Only 1 case of WES in NIHK group, the results showed that the suspected pathogenic gene *CC2D2A* was detected, which was related to Meckel-Gruber Syndrome. The follow-up results showed that 14 cases (56%) had termination of pregnancy (TOP), the TOP rate was 43% (6/14) in the IHK group and 73% in the NIHK group. 11 patients survived well, including 1 case with ADPKD, and no neonatal deaths occurred. In the IHK group, Case 1, and Case 4 had less amniotic fluid, Case 4 was diagnosed with *PKHD1* and the pregnancy was terminated, and case 1 was born normally. Case 14 had slightly enlarged kidneys and was born normally. In the NIHK group, the pregnancy was terminated in case 4 with oligohydramnios and case 9 with renal enlargement. However, there was no significant difference in the detection rate of abnormal karyotypes and CNV-seq between IHK and NIHK groups (Table 3).

Results of literature screening and characteristics of included studies

Retrieving articles according to predefined search terms, among the 311 Chinese and English articles identified, we eliminated 39 duplicate articles, 118 reviews, consensus and case reports, and 115 articles with irrelevant abstract and title, and finally selected the remaining 39 articles. After further research, a total of 21 articles (Decramer et al., 2007; Su et al., 2022; Li et al., 2007; Morr et al., 2022, Chaumoitre et al., 2006; Digby et al., 2021; Mashiach et al., 2005; Estroff et al., 1991; Yulia et al., 2021; Shuster et al., 2019; Deng et al., 2022; Gilboa et al., 2016; Tsatsaris et al., 2002; Emmanuelli et al., 2010; Carr et al., 1995; Heidet et al., 2010; Li et al., 2020; Zhang et al., 2017; Huang, 2014; Xie et al., 2022; Chen et al., 2022) were included in the final analysis (Figure 2; Table 4). Overall 1,178 cases arising from these studies were considered in the present meta-analysis. Table 4 records the basic information of the included studies, including author, year, nationality, study design, gestational age at prenatal ultrasound diagnosis, outcome observation indicators, and follow-up time limit. The NOS was used to the quality assessment of the included studies (Table 5). The studies showed good overall scores for the selection and comparability of study groups, and for the identification of outcomes of interest; Studies were of high overall quality with a minimum score of 6 stars. Most of these studies had retrospective designs and some had small sample sizes, which may have contributed to the heterogeneity of the observed results. The total number of IHK and NIHK fetuses and the number of abnormal karyotypes, CMA and monogenic etiologies detected in each group are shown in Table 6.

Positive rate of karyotype in NIHK

In 6 articles (Li et al., 2007; Huang, 2014; Digby et al., 2021; Deng et al., 2022; Morr et al., 2022; Xie et al., 2022), a total of 91 NIHK fetus were included, of which 16 abnormal karyotypes were detected. The heterogeneity test for all studies yielded I2 = 23%. We choose the results of the fixed effects model. Meta-analysis showed that positive rate of karyotype in NIHK with the OR of 0.28, (95% CI 0.16–0.51) (Figure 3A), the *p*-value was 0.22 (95% CI 0.14–0.34).

Positive rate of karyotype in HEK

In 10 articles (Mashiach et al., 2005; Li et al., 2007; Emmanuelli et al., 2010; Huang, 2014; Zhang et al., 2017; Shuster et al., 2019; Digby et al., 2021; Deng et al., 2022; Morr et al., 2022; Xie et al.,

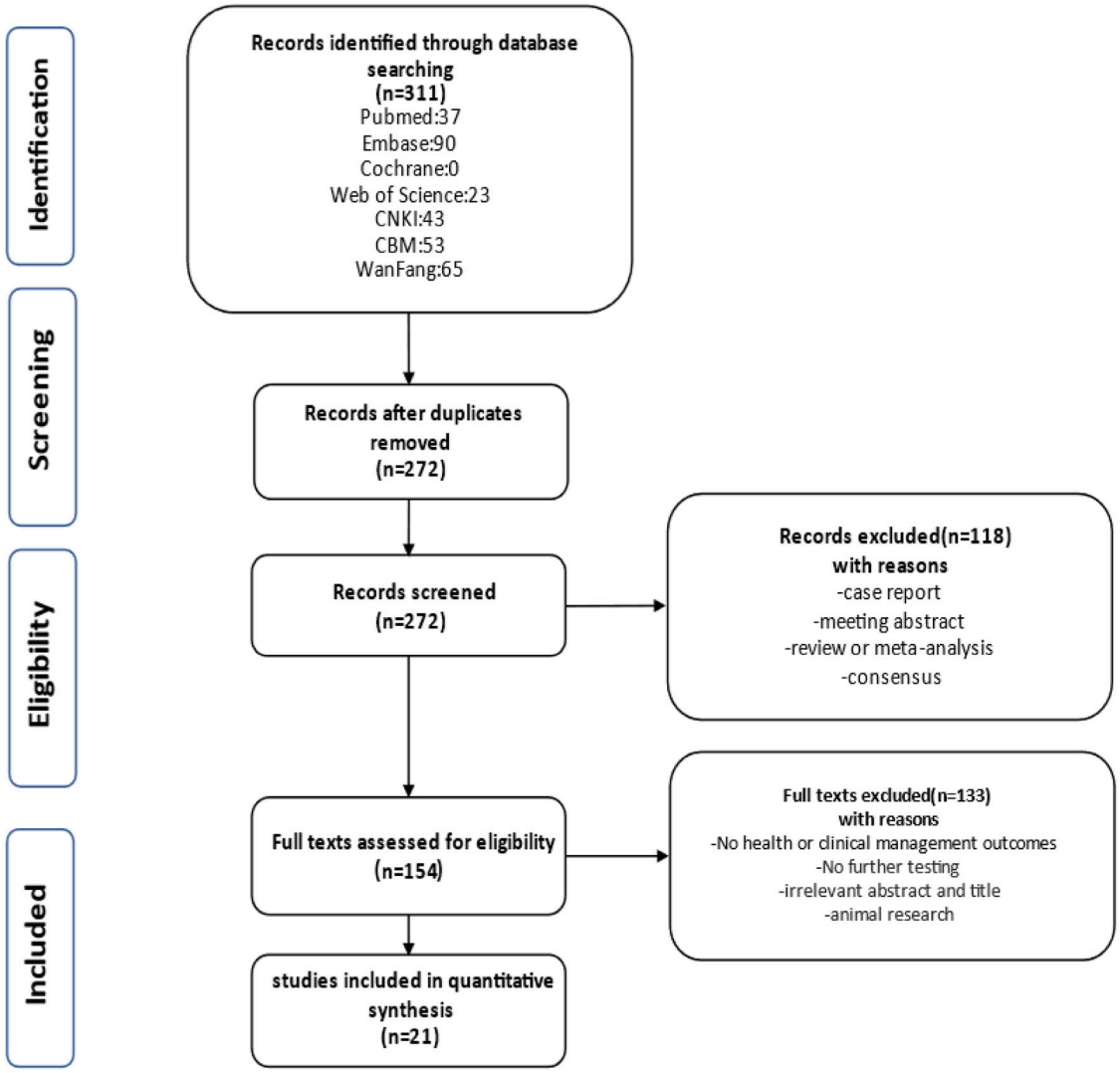

FIGURE 2
Flowchart of study selection.

2022), a total of 137 HEK fetus were included, of which 16 abnormal karyotypes were detected. The heterogeneity test for all studies yielded I2 = 22%. We choose the results of the fixed effects model. Meta-analysis showed that positive rate of karyotype in HEK was 32%, with the OR of 0.25, (95% CI 0.14–0.44) (Figure 3B), the *p*-value was 0.20 (95% CI 0.12–0.31).

Positive rate of CMA in NIHK

In 5 articles (Su et al., 2022; Digby et al., 2021; Deng et al., 2022; Zhang et al., 2017; Chen et al., 2022), a total of 61 NIHK fetus were included, of which 19 CMA abnormalities were detected. The heterogeneity test for all studies yielded I2 = 0%. We choose the results of the fixed effects model. Meta-analysis showed that the positive rate of CMA in NIHK patients with the OR of 0.48, (95% CI 0.28–0.85) (Figure 4A) the *p*-value was 0.32 (95% CI 0.22–0.46).

Positive rate of CMA in IHK

A total of 120 patients with IHK were included in the 6 articles (Huang, 2014; Gilboa et al., 2016; Li et al., 2020; Digby et al., 2021; Deng et al., 2022; Su et al., 2022), among which 33 cases of CMA abnormalities were detected. The heterogeneity test for all studies was I2 = 41%. We choose the results of the fixed effects model. Meta-analysis showed that the positive rate of CMA in IHK patients with the OR of 1.46 (95% CI 1.33–1.62) (Figure 4B). The *p*-value was 0.59 (95% CI 0.57–0.62).

Positive rate of monogenic etiologies in IHK

A total of 147 cases of HEK fetuses were included in the 6 articles (Decramer et al., 2007; Digby et al., 2021; Shuster et al., 2019; Deng et al., 2022; Heidet et al., 2010; Zhang et al., 2017), of which 77 cases were found to have monogenic etiologies by prenatal diagnosis or

TABLE 4 List of the included studies.

Author	Year	Country	Study design	Study period	GW	Outcomes observed	Duration of follow-up	n
Yulia, A	2021	United Kingdom	Retrospective	2002–2017	21 (13–37)	US, creatinine, hypertension requiring medication or major kidney surgery, dialysis or kidney transplant	up to 1 year of age	316
DigbyADDIN	2021	Canada	Retrospective	2013–2019	21 (12–39)	US, blood pressure, creatinine/eGFR or urinalysis, kidney surgery, dialysis or kidney transplant	2–71 months	31
Emmanuelli, V	2010	France	Retrospective	1997–2008	25 (21–37)	US, Blood pressure and renal function	12–132 months	17
Decramer, S	2007	France	Retrospective	1987–2005	26.0 ± 5.68 (18–35)	US, serum creatinine, AST, ALT, GGT, GFR, pancreatic enzymes, blood glucose, insulin, and glycosylated hemoglobin	69.16 (6–180) months	62
Tsatsaris, V	2002	France	Prospective	1985–1996	18–37	US, postnatal US, blood pressure, serum creatinine, proteinuria, renal biopsy when available	84 (34–132) months	43
Estroff, J. A	1991	United States	Retrospective	1987–1990	16–40	postnatal US, serum creatinine	—	19
Su, J	2022	China	Retrospective	2013–2019	14–36	US	—	48
Shuster, S	2019	Canada	Retrospective	2000–2015	17	US	—	52
Heidet, L	2010	France	Retrospective	before 2019	12–32	US, serum creatinine	1–17 years	55
Carr, M. C	1995	United States	Retrospective	1990–1993	—	US, serum creatinine, electrolytes, A voiding cystourethrogram or radionuclide cystogram	3 years	8
Mashiach, R	2005	Israel	Retrospective	1996–2002	16–40	US, serum creatinine, electrolytes	3 years	7
Deng, L	2022	China	Retrospective	2016–2020	28–42	postnatal neonatal renal ultrasound examination, blood pressure, renal function, urine routine, growth and development	1 month-3 years 7 months	28
Gilboa, Y	2016	Israel	Prospective	2006–2015	22–33	US, renal function	4 years	7
Morr, A	2022	Germany	Retrospective	2000–2018	26 (12–34)	US, renal function	2–16 years	23
K. CHAUMOITRE	2006	France	Retrospective	1990–2002	13–36	US	0–7 years	30
Dongqing Xie	2022	China	Retrospective	2015–2018	17–38	US	11 month-3 years 10 months	26
Fei Chen	2022	China	Retrospective	2014–2020	27 (13–33)	US	—	74
Chunling Li	2020	China	Retrospective	2015–2019	15–37	US	—	210

(Continued on following page)

10.3389/fgene.2023.1237912

TABLE 4 (*Continued*) List of the included studies.

Author	Year	Country	Study design	Study period	GW	Outcomes observed	Duration of follow-up	n
Junhua Huang	2014	China	Retrospective	2011–2013	27–39	US, fetal autopsy	—	26
Xiaoxiao Zhang	2017	China	Retrospective	2009–2015	20–38	US	0–6 years	65
Hui Li	2007	China	Retrospective	2000–2004	25–39	prenatal US features, the neonatal renal ultrasound, blood pressure, renal function, urine routine, growth and development status, renal biopsy if necessary	2–6 years	31

US, ultrasound. GW, gestational weeks.

autopsy. The heterogeneity test was I2 = 86% for all studies. We choose the results of the random effects model. The positive rate of monogenic etiologies in HEK patients was 44%, with OR of 0.80 (95% CI 0.25–2.63) (Figure 4C).

Subgroup analysis

Subgroup analysis of mortality by different amniotic fluid volume in IHK showed the total heterogeneity I^2 = 74% and subgroup heterogeneity I^2 = 48.4%, pooled OR 0.31 (95% CI 0.15–0.62); However, in NIHK, the total heterogeneity I2 = 68%, and the heterogeneity of subgroups I2 = 81.8%, pooled OR 0.54 (95% CI 0.34–0.88) (Supplementary Figures S1, S2). In subgroup analyses based on kidney size differential mortality showed the total heterogeneity and subgroup heterogeneity were high, as follows: IHK total I2 = 77%, subgroup I2 = 94.5%; NIHK total I2 = 87%, subgroup I2 = 76.3% (Supplementary Figures S3, S4). The total number of fetuses and deaths in each group, the OR, 95% CI, and *p* values are recorded in Table 7.

Pooled proportions of the adverse outcomes

The mortality of IHK and NIHK mainly includes termination of pregnancy (TOP), intrauterine death (IUD), neonatal death (ND), and even child death during long-term follow-up. 15 studies (Estroff et al., 1991; Tsatsaris et al., 2002; Mashiach et al., 2005; Decramer et al., 2007; Li et al., 2007; Emmanuelli et al., 2010; Heidet et al., 2010; Gilboa et al., 2016; Zhang et al., 2017; Shuster et al., 2019; Li et al., 2020; Digby et al., 2021; Yulia et al., 2021; Deng et al., 2022; Su et al., 2022) recorded the TOP 111 cases of 528 IHK fetuses, with the pooled OR of 0.26 (95% CI 0.17–0.40); Among 579 NIHK fetuses in 11 studies (Su et al., 2022; Morr et al., 2022, Chaumoitre et al., 2006; Digby et al., 2021; Yulia et al., 2021; Deng et al., 2022; Li et al., 2020; Zhang et al., 2017; Huang, 2014; Xie et al., 2022; Chen et al., 2022), 318 fetuses were terminated (TOP), with the pooled OR of 1.72 (95% CI 1.59–1.86); There was no intrauterine death in IHK fetus during pregnancy. Of 273 NIHK fetuses in the 2 studies (Yulia et al., 2021; Chen et al., 2022), 6 cases had intrauterine death, with the OR of 0.02 (95% CI 0.01–0.05), heterogeneity I2 = 0; There were 39 neonatal deaths in 328 IHK fetuses in 9 studies (Estroff et al., 1991; Tsatsaris et al., 2002; Mashiach et al., 2005; Decramer et al., 2007; Li et al., 2007; Emmanuelli et al., 2010; Zhang et al., 2017; Shuster et al., 2019; Yulia et al., 2021), with the OR of 0.15 (95% CI 0.10–0.24), I2 = 30%; There were 413 NIHK fetuses in 6 studies (Morr et al., 2022, CHAUMOITRE et al., 2006; Digby et al., 2021; Yulia et al., 2021; Li et al., 2020; Huang, 2014), 43 of them had neonatal death, with the OR of 0.12 (95% CI 0.06–0.26), I2 = 65%; 3 of 31 IHK fetuses in 1 study (Li et al., 2007) and 1 of 30 NIHK fetuses in 1 study (CHAUMOITRE et al., 2006) had childhood death, with the OR of 0.11 (95% CI 0.03–0.35) and 0.03 (95% CI 0.00–0.25), respectively. For the survival of *postpartum* neonates and children, such as the need for transplantation surgery, dialysis treatment, hypertension and diabetes drug treatment, there were 30 cases of 147 IHK fetuses in 6 studies (Estroff et al., 1991; Tsatsaris et al., 2002; Emmanuelli et al., 2010; Shuster et al., 2019; Yulia et al., 2021; Su et al., 2022), with

TABLE 5 Quality assessment of the included studies according to NOS.

Study	Selection	Comparability	Outcome
Yulia et al. (2021)	★★★	★	★★★
Digby et al. (2021)	★★★	★★	★★★
Emmanuelli et al. (2010)	★★	★★	★★★
Decramer et al. (2007)	★★★	★★	★★
Tsatsaris et al. (2002)	★★	★★	★★★
Estroff et al. (1991)	★★★	★★	★★
Su et al. (2022)	★★★	★	★★
Shuster et al. (2019)	★★	★★	★★
Heidet et al. (2010)	★★★	★	★★
Carr et al. (1995)	★★	★	★★★
Mashiach et al. (2005)	★★★	★★	★★★
Deng et al. (2022)	★★★	★★	★★★
Gilboa et al. (2016)	★★★	★	★★★
Morr et al. (2022)	★★	★★	★★★
Chaumoitre et al. (2006)	★★	★★	★★★
Xie et al. (2022)	★★★	★★	★★★
Chen et al. (2022)	★★★	★	★★
Li et al. (2020)	★★★	★★	★★
Huang (2014)	★★	★	★★
Zhang et al. (2017)	★★★	★	★★★
Li et al. (2007)	★★★	★★	★★★

The Newcastle-Ottawa scale (NOS). Selection: 1. Representative for the population; 2. Ascertainment of exposure; 3. Consecutive patients; 4. Outcome not present at the start of the study. Outcomes:1. Assessment of outcome well performed; 2. select an adequate follow up period; 3. Adequacy of follow up.

the OR of 0.28 (95% CI 0.17–0.46), I2 = 20%. Among 93 NIHK fetuses in 6 articles (Su et al., 2022; Morr et al., 2022, CHAUMOITRE et al., 2006; Digby et al., 2021; Yulia et al., 2021; Deng et al., 2022), 20 cases had *postpartum* abnormalities, the OR 1.28 (95% CI 1.12–1.47), I2 = 30% (Table 8).

Pooled proportions for the etiology in IHK

Due to the uncertainty of intrarenal and extrarenal abnormalities, the diagnosis of NIHK is also diverse, involving various systems of the whole body, including various chromosomal abnormalities and even monogenic etiologies, while in IHK, the causes of diagnosis are relatively limited. Among 232 fetuses in 7 articles (Tsatsaris et al., 2002; Mashiach et al., 2005; Emmanuelli et al., 2010; Shuster et al., 2019; Li et al., 2020; Digby et al., 2021; Deng et al., 2022), 37 fetuses were diagnosed as ADPKD. There were 51/243 cases of ARPKD in 7 studies (Estroff et al., 1991; Tsatsaris et al., 2002; Mashiach et al., 2005; Emmanuelli et al., 2010; Shuster et al., 2019; Li et al., 2020; Digby et al., 2021). Three out of 93 cases of MCKD were reported in 2 studies (Mashiach et al., 2005; Li et al., 2020). The number of *HNF1B* variants diagnosed in 5 articles (Heidet et al., 2010; Gilboa et al., 2016; Li et al., 2020; Digby et al., 2021; Deng et al., 2022) was 47/175. One article (Li et al., 2020) reported that 4 aneuploidy cases were detected in 86 IHK fetuses. Two BBS were detected in 36 fetuses in the 2 articles (Emmanuelli et al., 2010; Digby et al., 2021). There were also 3 articles (Estroff et al., 1991; Tsatsaris et al., 2002; Deng et al., 2022) in which 27 other abnormalities were detected in 70 fetuses, It mainly includes *WTX* mutation, renal tubular disease, Familial nephroblastoma, AD CAKUT, Type II Ivemark Syndrome, renal agenesis, Beckwith-Wiedemann syndrome; In 7 studies (Estroff et al., 1991; Tsatsaris et al., 2002; Mashiach et al., 2005; Emmanuelli et al., 2010; Gilboa et al., 2016; Li et al., 2020; Deng et al., 2022), 42 out of 187 fetuses eventually returned to normal, hyperechogenicity disappeared; The OR (95% CI) and *p*-values are shown in Table 9, the diagnosis was made by ultrasound or pathology or gene diagnosis.

Mortality for poor or absent corticomedultural differentiation (CMD)

Only a few studies (Decramer et al., 2007, CHAUMOITRE et al., 2006; Deng et al., 2022) reported renal CMD and the mortality of

TABLE 6 The detection of chromosomal and monogenic etiologies in IHK and NIHK.

Study	Total sample	N of IHK	N of NIHK	N of karyotypes abnormalities		N of CMA abnormalities		N of monogenic etiologies	
				IHK	NIHK	IHK	NIHK	IHK	NIHK
Yulia et al., 2021	316	—	—	—	—	—	—	—	—
Digby et al. (2021)	31	19	11	0/2	3/6	1/2	6/11	1/1	1/1
Emmanuelli et al. (2010)	17	17	—	0/9	—	—	—	—	—
Decramer et al. (2007)	62	62	—	—	—	—	—	16/62	—
Tsatsaris et al. (2002)	43	43	—	—	—	—	—	—	—
Estroff et al. (1991)	19	19	—	—	—	—	—	—	—
Su et al. (2022)	48	36	12	—	—	16/36	3/12	—	—
Shuster et al. (2019)	52	52	—	0/18	—	1/34	—	22/22	—
Heidet et al. (2010)	55	55	—	—	—	—	—	34/55	—
Carr et al. (1995)	8	8	—	—	—	—	—	—	—
Mashiachet al. (2005)	7	7	—	0/3	—	—	—	—	—
Deng et al. (2022)	28	8	20	0/8	3/20	2/8	5/19	3/6	10/10
Gilboa et al. (2016)	7	7	—	—	—	5/7	—	—	—
Morr et al. (2022)	23	—	23	—	2/14	—	—	—	6/6
Chaumoitre et al. (2006)	30	—	30	—	—	—	—	—	—
Xie et al. (2022)	26	15	11	—	1/5	—	—	—	11/11
Chen et al. (2022)	74	—	74	—	—	—	5/17	—	—
Li et al. (2020)	210	86	124	—	—	9/32	—	—	—
Huang (2014)	26	—	26	—	4/26	0/1	—	—	—
Zhang et al. (2017)	65	31	34	0/6	0/14	—	0/2	1/1	—
Li et al. (2007)	31	25	6	—	3/6	—	—	—	—
total	1,178	490	371	0/46	16/91	34/120	19/61	77/147	28/28

fetuses with poor or absent renal corticomedultural differentiation was calculated, with an OR of 1.87 (95% CI 1.66–2.11), heterogeneity I^2 = 7% (Figure 5), Thus, the mortality rate of fetuses with poor or absent renal CMD is 65%.

Sensitivity analysis

Sensitivity analyses were performed by individually excluding each included study to determine whether the combined results of the other studies were stable, and look for sources of heterogeneity. Sensitivity analysis was performed for data with >50% heterogeneity, as shown in Supplementary Figures S5–S7. The positive rate of monogenic etiologies in IHK with the OR of 0.45 (95% CI 0.19–1.08), *p*-value was 31%. In IHK fetuses, the mortality rate of oligohydramnios with an OR of 0.52 (95% CI 0.30–0.90), I2 = 49%, *p*-value was 34%; the mortality rate of normal amniotic fluid volume with an OR of 0.08 (95% CI 0.03–0.22), I2 = 24%, *p*-value was 7%. There was a statistically significant difference in mortality between the two groups. In NIHK fetuses, the neonatal mortality with an OR of 0.17 (95% CI 0.12–0.25), I^2 = 2%, *p*-value was 15%.

Discussion

Fetal hyperechoic kidney (HEK) is a heterogeneous disorder in etiology (Huang et al., 2023). As we know, more than half of HEK are related to genetic factors. Fetal structural abnormality is the main indication for invasive prenatal genetic testing, which is traditionally performed by karyotyping and chromosomal microarray analysis (CMA). In recent years, next-generation sequencing technology, especially exome sequencing (ES), as a powerful tool for the diagnosis of Mendelian diseases, has been widely used in clinical practice, and can provide an additional diagnostic rate of 8.5%–11.6% for fetuses with abnormal ultrasound, normal karyotype and CMA results (Lord et al., 2019; Fu et al., 2022).

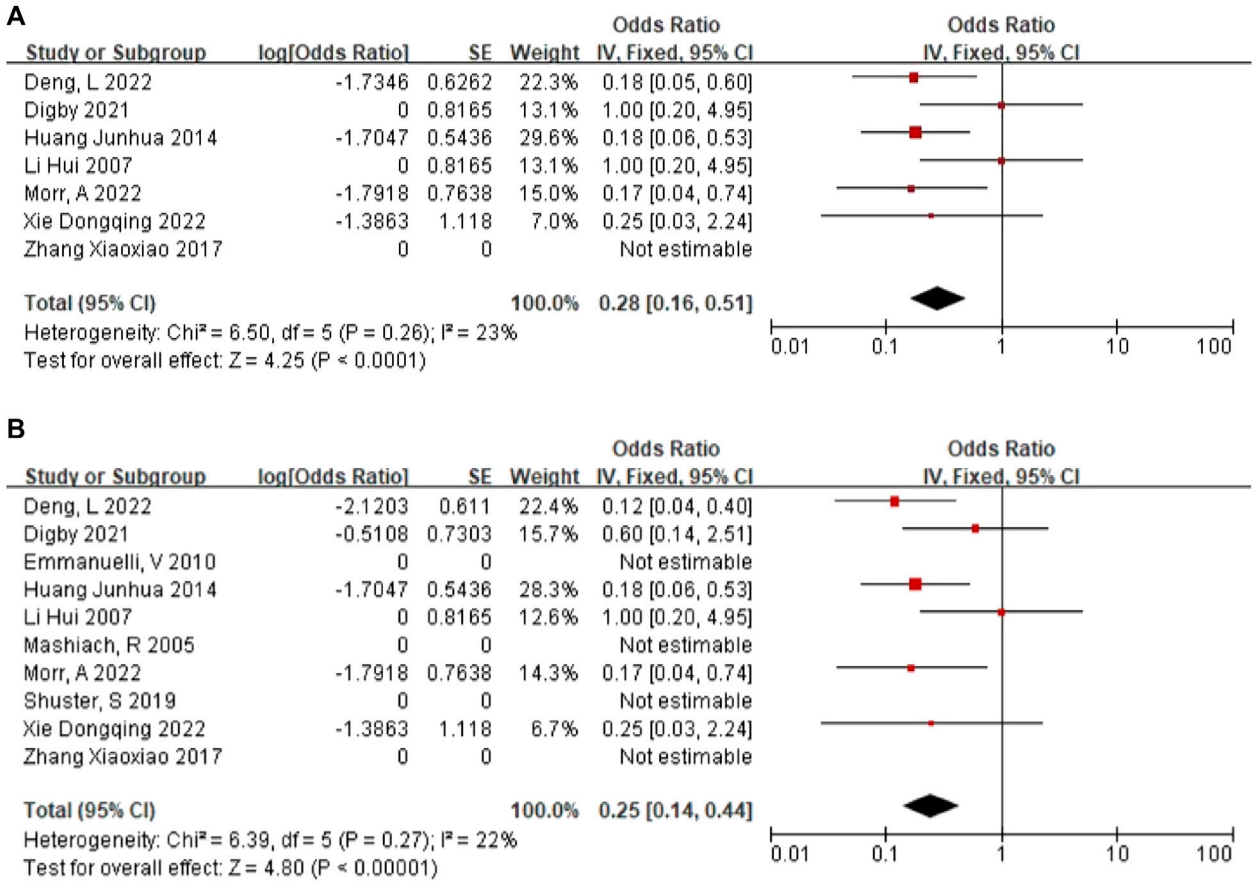

FIGURE 3
(A) The positive rate of karyotype in NIHK. **(B)** The positive rate of karyotype in HEK.

Based on the cohort study of hyperechoic kidney cases in recent years, we hope to find out the common etiologies and prognosis of hyperechoic kidney cases, evaluate the incidence and mortality of different causes, the efficacy of different detection methods for hyperechoic kidney cases, and explore the ultrasonic indicators that affect the prognosis of hyperechoic kidney cases. However, in recent years, the sample size in our cohort study was small, and the observable ultrasound findings were limited. Therefore, we included a retrospective cohort based on previous studies to increase the sample size and reduce the bias caused by insufficient samples. In addition, various ultrasound indicators affecting hyperechoic kidney cases, such as amniotic fluid volume, kidney size and CMD, were collected as far as possible. Another reason is that we wanted to verify the consistency with the results of the meta-analysis through a cohort study.

In our study, HEK included was classified as isolated and non-isolated and counted separately. In the cohort study, we found 25 cases of renal hyperechoic in recent years, accounting for about 10% of the cases of prenatal diagnosis of renal abnormalities and 0.6% of all cases of prenatal diagnosis of various indications. In IHK group, two fetuses were diagnosed with trisomy 21, which may seem unexpected, but they had different prenatal diagnostic indicators than ultrasound findings alone. Indications for non-invasive prenatal testing (NIPT) in NO. 19113 suggest a high risk of trisomy 21. Ultrasound images showed only bilateral hyperechoic kidneys. The prenatal diagnosis of NO. 19255 was indicative of advanced maternal age, the actual age was 40 years old, and ultrasound indicated bilateral hyperechoic kidneys of the fetus. Based on the indications, only karyotype and CNV-seq were tested in these two cases. However, hyperechoic kidney was found on ultrasound, we included these two cases in the IHK group. As we know, trisomy 21 syndrome may involve various systemic abnormalities, including some soft indicators, and of course may not be detected by ultrasound in the first and second trimester of pregnancy, perhaps as the pregnancy progresses, their ultrasound will show NIHK.

It is easy to find that the positive rate of CNV-seq in the NIHK group was higher than that in the IHK group. The positive rate of overall HEK fetal karyotype was 20%, and the abnormal detection rate of pathogenic CNVs was 32%, which was significantly higher than the detection rate of karyotype. The NIHK group also had a significantly higher TOP rate than the IHK group, with an overall TOP rate of 56%. However, due to the small sample size in our cohort, Fisher's exact probability chi-square test showed that there was no significant difference in the positive rate and TOP rate of genetic testing between the IHK group and the NIHK group. Due to the combination of multiple structural abnormalities, the increased possibility of poor fetal prognosis judged by doctors, and the

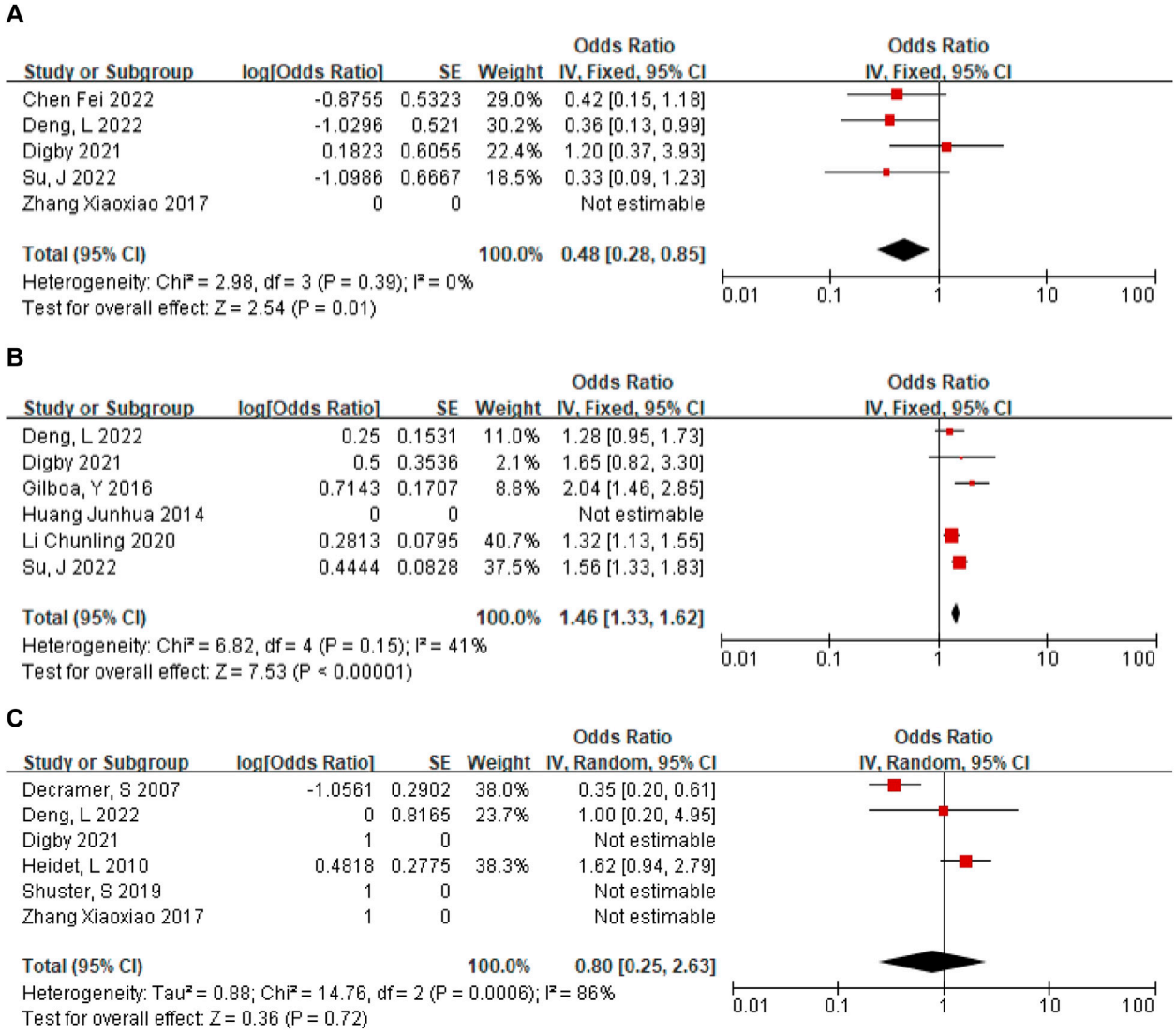

FIGURE 4
(A) The positive rate of CMA in NIHK. **(B)** The positive rate of CMA in IHK. **(C)** Positive rate of monogenic etiologies in IHK.

TABLE 7 Mortality analysis of different amniotic fluid volume and kidney size in IHK and NIHK.

	IHK mortality					NIHK mortality				
	Studies	Fetuses	OR	I^2 (%)	p	Studies	Fetuses	OR	I^2 (%)	p
Value of amniotic fluid										
AFV ≤ 2 cm or AFI ≤ 5 cm	5	52/150	0.60 [0.42, 0.85]	49	0.38	4	128/278	0.85 [0.67, 1.08]	34	0.46
Normal	4	10/109	0.15 [0.03, 0.79]	76	0.13	3	17/79	0.36 [0.21, 0.64]	41	0.26
AFV ≥ 8 cm or AFI ≥ 25 cm	0	0	0	—	0	1	3/23	0.15 [0.04, 0.50]	—	0.13
Kidney size										
Enlarged	6	57/157	0.56 [0.33, 0.98]	51	0.36	3	43/79	1.71 [1.56, 1.89]	91	0.63
Normal	4	7/119	0.07 [0.03, 0.15]	0	0.07	2	15/56	0.29 [0.02, 3.80]	90	0.22
Reduction	0	0	0	—	0	1	1/30	0.03 [0.00, 0.25]	—	0.03

TABLE 8 Pooled proportions of the different adverse outcomes in fetuses.

	IHK					NIHK				
	Studies	Fetuses	Or (95% CI)	I^2 (%)	p	Studies	Fetuses	Or (95% CI)	I^2 (%)	p
Mortality										
TOP	15	111/528	0.26 [0.17, 0.40]	68	0.21	11	318/579	1.72 [1.59, 1.86]	69	0.63
IUD	0	0	0	—		2	6/273	0.02 [0.01, 0.05]	0	0.02
ND	9	39/328	0.15 [0.10, 0.24]	30	0.13	6	43/413	0.12 [0.06, 0.25]	65	0.11
Death in Childhood	1	3/31	0.11 [0.03, 0.35]	—	0.1	1	1/30	0.03 [0.00, 0.25]	—	0.03
Postnatal outcome										
Intervention	6	30/147	0.28 [0.17, 0.46]	20	0.22	6	20/93	0.40 [0.18, 0.92]	40	0.29

TOP, Termination of pregnancy; IUD, Intrauterine death; ND, neonatal death; Intervention, Need for surgery or medical treatment (hypertension, diabetes, dialysis or transplantation in renal failure, etc.).

TABLE 9 Pooled proportions for the etiology in IHK.

Outcome	Studies	Proportion of deaths	Or (95% CI)	I^2 (%)	p
ADPKD	7	37/232	0.21 [0.14, 0.32]	20	0.17
ARPKD	7	51/243	0.28 [0.12, 0.66]	78	0.22
MCDK	2	3/93	0.09 [0.03, 0.33]	86	0.08
HNF1B mutation	5	47/175	0.35 [0.06, 1.98]	91	0.26
Aneuploidy	1	4/86	0.05 [0.02, 0.13]	—	0.05
BBS	2	3/36	0.10 [0.03, 0.32]	0	0.09
Others[a]	3	27/70	0.43 [0.11, 1.65]	78	0.30
normal	7	42/187	0.30 [0.21, 0.43]	0	0.23

[a]Others contained *WTX*, mutation, renal tubular disease, Familial nephroblastoma; AD, CAKUT, Type II, ivemark syndrome, renal agenesis, Beckwith-Wiedemann syndrome. BBS: Bardet-Biedl syndrome.

reasons of family members themselves, it is common for NIHK cases to refuse further WES and choose to terminate pregnancy, especially for families who have offspring and do not have the requirement of childbearing again. In the CNV-seq test results, we found that 6 fetuses carried variants of uncertain clinical significance (vous). At present, the correlation of these variants with ultrasonic manifestations and future pathogenicity is unknown. The risk of birth defects in fetuses without CNVs is currently 0.4% (Evans et al., 2016), so the risk of birth defects in fetuses with CNVs can be inferred to be no less than 0.4%. We recommend that the parents of the fetuses be tested for CNV-seq, indeed some of these variants are paternal or maternal, and there is no description of parental disease; However, some of the variants are still *de novo*. Although the current research shows that *de novo* variants are more likely to be pathogenic than hereditary variants, there is still no

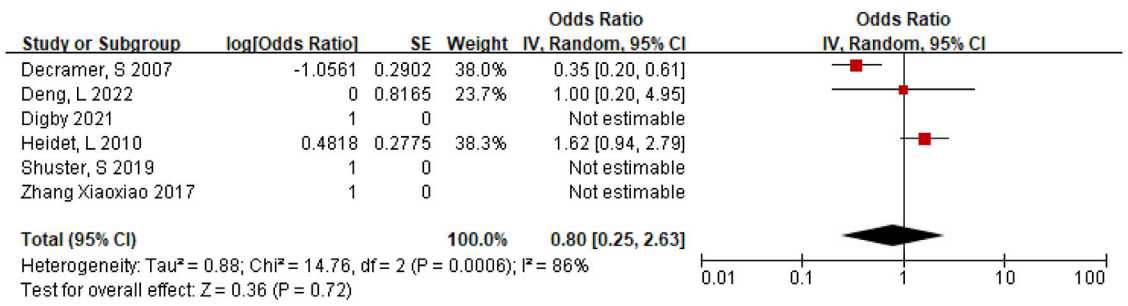

FIGURE 5
Mortality for poor or absent CMD.

evidence to judge the prognosis of the fetus, and only regular ultrasound examination can be relied on to assess the survival status and prognosis of the fetus. Therefore, most families still choose to continue pregnancy. Because of the uncertainty about fetal outcomes has led a small number of families to refuse parental CNV-seq testing.

Trio-WES tests were performed for 5 cases in which a search for monogenic etiologies was deemed necessary by the physician. Case NO. 210040 prenatal diagnosis was indicated by advanced age of the pregnant woman (>35 years old), adverse pregnancy history (the last pregnancy was terminated due to pathogenic mutation of *PKHD1* gene in the fetus), and the fetal ultrasound of this pregnancy indicated bilateral hyperechoic kidneys of the fetus. Considering the possibility of monogenic etiologies of the fetus, Trio-WES testing was performed. The prenatal diagnosis indication of NO. 210086 was bilateral hyperechoic kidneys and oligohydramnios indicated by fetal ultrasound. Infantile polycystic kidney was considered, and WES examination was conducted to verify the ultrasound diagnosis. The fetal ultrasound of NO. 210323 indicated bilateral hyperechoic kidneys. Due to the gestational week exceeding 25 weeks, and the pregnant woman and her family members refused cordocentesis, considering the possibility of fetal monogenic cause, amniocentesis was performed and amniotic fluid CNV-seq and trio-WES were examined. The indication of NO. 220253 was bilateral hyperechoic kidneys indicated by fetal ultrasound. After communication with the pregnant woman, 10 mL of amniotic fluid was extracted during amniocentesis for preservation, and the chromosome karyotype and CNV-seq detection of amniotic fluid were performed first. However, CNV-seq results showed that no kidney related copy number variation was found except for X-linked ichthyosis pathogenic variation. Therefore, WES testing was performed on the preserved amniotic fluid. The fetal ultrasound of case NO. 170015 indicated multiple malformations, which was considered Meckel-Gruber syndrome. The family requested termination of the pregnancy and WES testing of the fetal cord of the induced labor was performed to verify the ultrasound diagnosis. In all 5 cases of WES, monogenic etiologies that could not be found by karyotypes and CNV-seq were found, especially *PKHD1* was more common in renal hyperechogenicity, followed by *PKD1* gene. However, WES results of case 4 (NO. 210086) in IHK group showed complex heterozygous variation of *PKHD1* gene, both vous, which were maternal and paternal, respectively. This can lead to PKD type 4 with or without polycystic liver disease (OMIM: 263200), although there seems to be some difficulty in making a definitive diagnosis. Therefore, in this case, the fetal ultrasound examination at 29 weeks gestation showed oligohydramnios (less than that at 24 weeks gestation), bilateral hyperechoic kidneys with enlarged volume, and small bladder, which considered infantile polycystic kidney. Although the ultrasound diagnosis was not completely consistent with the genetic diagnosis, the risk of poor prognosis of the fetus was comprehensively assessed, so we agreed with the parents' decision to terminate the pregnancy based on the ultrasound diagnosis. For the 2 patients with 17q12 deletion syndrome whose CNVs were found, we did not perform WES testing again, but we speculated that *HNF1B* gene might be involved. These are common causes of hyperechoic kidney found in studies. Although some of our cases survived well within half a year to 1 year after delivery, some of them did not undergo genetic testing, and renal structural deterioration and even renal function decline may occur several years later, so these cases may need longer time follow-up and more frequent renal examination.

Unfortunately, we did not perform autopsy on fetuses obtained from termination of pregnancy, mainly because some pregnant women chose other hospitals for induced labor. The quantity of fetuses we obtained for induced labor was small, and ultrasound diagnosis of most fetuses was basically consistent with genetic diagnosis, so no autopsy was performed. Another reason is that the family cannot undergo an autopsy, although the individual ultrasound diagnosis is inconsistent with the genetic diagnosis, but before the termination of the pregnancy has shown ultrasonic manifestations such as oligohydramnios, and the ultrasound diagnosis predicts adverse fetal outcomes, the family has abandoned the autopsy, especially for those who have at least one child and no longer have the intention to have children.

The meta-analysis results showed that fetuses with hyperechoic kidney indicated by prenatal ultrasound had a risk of chromosomal and monogenic etiologies, especially in non-isolated cases. In cases of IHK, no positive results were found in 46 fetuses tested for karyotype. The positive rate of karyotype in NIHK was 22%, and that in HEK was 20%. This is consistent with the results in our cohort study. The positive rate of CMA was 32% in NIHK cases, previous studies (Nicolaides et al., 1992; Wapner et al., 2013) have shown that the incidence of chromosomal abnormalities is approximately 30% when multiple fetal abnormalities are detected, and is close to that in NIHK, however, this is lower than the 37% positive rate of the pathogenic variation of CNV-seq in our cohort study. The positive rate of CMA in IHK was 59%, which is similar to the results of a large Chinese cohort study (Su et al., 2022) but with a higher percentage, their finding was that hyperechoic kidney had the highest probability of diagnosis of pathogenic or probable pathogenic among all renal abnormalities detected by CMA (39.58%), IHK accounted for 44.44%, and NIHK was 25%. The rate of detection in the meta-analysis was higher than the 29% positive rate of CNV-seq testing in IHK cases in our series of studies. The reason for the large difference in results may be that the studies included in the meta-analysis, due to the limitations of the years and detection methods, not all cases were tested for CMA or CNV-seq; moreover, due to the small sample size tested, the positive ratio may eventually be high. Moreover, with the progress of pregnancy, some IHK cases may be transformed into NIHK by ultrasonography in the third trimester, but these cases were diagnosed as CMA positive in the second trimester, which may also be the reason for the high CMA positive rate in IHK cases.

Among the studies we retrieved and included, very few studies performed WES on HEK cases, and they mainly focused on NIHK cases, and some diagnoses were achieved by target gene sequencing. Since there are few studies on genetic testing of IHK cases and the detection method is not single, we analyzed the monogenic etiologies of IHK cases and found that the positive rate was 31%. Although a targeted gene sequencing article was excluded through sensitivity analysis, and the result was statistically significant, this single gene result may not fully explain the single gene etiology of IHK cases, targeted gene sequencing was performed in 3 of the 6 articles with single gene testing, and WES testing was performed in 8 cases in the remaining 3 articles, 5 of which were positive. As in our cohort study, all 5 WES tests were positive. Compared with WES, the diagnosis of IHK by targeted gene sequencing may be missed and the diagnosis rate may be reduced. In short, the quantity of IHK cases undergoing WES is too small, and more high-quality studies are needed to confirm it. Of course, it is not practical for all IHK cases undergo WES, but also according to the patient's indications, especially for bilateral hyperechoic renal fetuses with negative karyotype and CMA or CNV-

seq testing results. There may still be 31% of monogenic gene mutation. In all 28 cases of NIHK, the single gene results were positive, which seems easy to accept and expected.

Due to different years, detection methods are limited by testing technology, and some cases are diagnosed by clinical, ultrasound or autopsy cases. NIHK cases have large etiological heterogeneity due to the combination of abnormalities in each system, which we will not discuss. For the etiology of IHK cases, only 1 article (Li et al., 2020) reported aneuploidy, which could not truly reflect the proportion of aneuploidy in IHK. In addition, *HNF1B* variant is the most prevalent disease with 26%, which is contained in the 17q12 segment. In second place is ARPKD with a prevalence of 22%, ADPKD with 17%, Bardet-Biedl syndrome (BBS) and MCDK with 9% and 8%, respectively. There are other diseases that make up a large proportion of IHK, Such as *WTX* variant, renal tubular disease, nephroblastoma, autosomal dominant CAKUT (AD CAKUT), Type II Ivemark Syndrome, renal agenesis, Beckwith-Wiedemann syndrome (BWS). The good prognosis and disappearance of hyperechogenicity accounted for 23% of the cases.

In IHK cases, the subgroups with different amounts of amniotic fluid were subjected to sensitivity analysis, the mortality rate was 34% in oligohydramnios and 7% in the normal amniotic fluid group after sensitivity analysis, there was no deaths from IHK with polyhydramnios. Subgroup analysis showed that the mortality rate varied greatly with different amount of amniotic fluid and the results were statistically significant. Among NIHK cases, the mortality rate was 46% in the oligohydramnios group and 26% in the normal amniotic fluid group, and only one article reported the occurrence of fetal death in polyhydramnios, with a mortality rate of 13%. The large difference in mortality among the groups indicated that the amount of amniotic fluid was an important factor affecting fetal mortality.

The mortality rate in IHK was 36% in fetuses with enlarged kidneys and 7% in those with normal kidney size. No deaths were reported in fetuses with small kidney development. In the cases of NIHK, due to the limited number of relevant literature, the sensitivity analysis had little effect on the results of subgroup analysis, and the results were relatively stable. Therefore, the mortality rate of kidney enlargement was 55%, that of normal kidney was 22%, and that of relatively developed kidney was 3%. The mortality of NIHK was higher than that of IHK.

Termination (TOP) rates were 21% in IHK and 63% in NIHK. Although there was a large heterogeneity of TOP in both groups, the sensitivity analysis found that the results were relatively stable and meaningful, so the literature was not eliminated. In addition, the TOP probability is also affected by the results of prenatal diagnosis, which is partly related to the amniotic fluid volume and renal development changes suggested by ultrasound during pregnancy. Another part of the reason is that some pregnant women cannot accept further examination due to the limitation of previous diagnostic technology, family history of patients or some other subjective factors, and the attitude or legal requirements of hospitals in different countries on the behavior of pregnancy termination are not consistent, resulting in certain differences in the TOP rate in different regions. In addition, our assessment of the prognosis of HK is more focused on intrauterine death (IUD) and neonatal death (ND). In well-followed studies, the death of childhood kidney disease is also more significant for the long-term prognosis of IHK. No intrauterine deaths have been reported in IHK cases. Intrauterine mortality was 2% in NIHK cases. The neonatal mortality in IHK was 13%. NIHK has a large heterogeneity of neonatal mortality. After sensitivity analysis, 1study was excluded, in which 2 neonatal deaths were postoperative deaths of diaphragmatic hernia in the neonatal period. We were not sure whether the death was due to the disease itself or surgical complications, which led to unstable results, so it was no longer considered for inclusion, and the neonatal mortality was re-evaluated to be about 15%. 1study each reported childhood mortality in IHK and NIHK cases, with mortality rates of 10% and 3%, respectively. The childhood mortality rate of IHK is about three times higher than that of NIHK, which may not be the same as we expected. The main reason is that the number of literature is too small to conduct meta-analysis, and the number of childhood deaths reported by only one article is not enough to describe the real mortality rate. Secondly, we can also understand that NIHK patients with poor prognosis died before childhood due to their own combined abnormalities of other systems, both intrarenal and extrarenal. In addition, the follow-up of childhood deaths requires a long period of time, and different duration of follow-up also affects the long-term mortality results. Therefore, we may need more articles with long-term follow-up to understand the long-term survival and mortality of this disease. Not all survivors are healthy. 22% of IHK survivors are still likely to face hypertension, diabetes, renal failure, dialysis, kidney transplantation, etc., compared with 29% of NIHK survivors.

Fetuses with poor or absent CMD have a higher mortality rate of 65%. Cortico-medullary differentiation, a decrease in medullary and cortical thickness, is a hallmark of renal dysplasia (Devriendt et al., 2013), as a result, fetal mortality is higher, including family abandonment and death during pregnancy.

This meta-analysis comprehensively covered the etiology of IHK, the incidence of HEK monogenic etiologies, mortality, and prognostic healthy survival, disease survival, and prognostic survival factors. The main limitation of the current study is that most of the studies included were retrospective designs and some of the outcomes evaluated were reported only in a limited proportion of the included studies. In addition, as not all cases in the included studies were genetically tested, and not all were routinely measured kidney length, CMD, were only tested or measured when abnormalities were apparent, there may be selection bias. Nonetheless, the available data are sufficient to draw the conclusions.

Conclusion

The positive rate of karyotype was 20% in HEK and 22% in NIHK. The positive rate of CMA was 32% in NIHK and 59% in IHK. The positive rate of IHK monogenic etiologies was 31%. The most common etiology of IHK is the *HNF1B* variant. Oligohydramnios, renal enlargement and CMD with two or more items increase the possibility of poor prognosis. We currently recommend a detailed ultrasound scan of the HEK fetus, measuring kidney length, CMD in addition to the routine measurement of amniotic fluid, and periodically rechecking for changes. Interventional prenatal diagnosis is performed, including chromosome karyotype and CMA or CNV-seq, and WES testing is feasible when necessary, especially if the karyotype and CMA results are negative, do not ignore the possibility of monogenic etiologies Combined with various indicators, comprehensive evaluation of fetal

prognosis, avoid unnecessary termination of pregnancy, and also reduce the birth of defects to the greatest extent.

Data availability statement

The original contributions presented in the study are included in the article/Supplementary Material, further inquiries can be directed to the corresponding author.

Ethics statement

The studies involving humans were approved by the Ethics Committee of the Second Affiliated Hospital of Harbin Medical University. The studies were conducted in accordance with the local legislation and institutional requirements. The human samples used in this study were acquired from a by-product of routine care or industry. Written informed consent for participation was not required from the participants or the participants' legal guardians/next of kin in accordance with the national legislation and institutional requirements.

Author contributions

ML and WY contributed to the conception of the study; ML, WY, SZ, QJ, and HS contributed significantly to analysis and manuscript preparation and wrote the manuscript; WY, SZ, YL, CW, HZ, and RW performed the clinical detection and data analyses; ML, SZ, and HZ helped perform the analysis with constructive discussions. All authors contributed to the article and approved the submitted version.

Funding

Clinical research Special Fund of Wu Jie-Ping Medical Foundation [320.6750.18588 (10)]; Research project on the incidence of birth defects in Heilongjiang Province (2020-8).

Conflict of interest

The authors declare that the research was conducted in the absence of any commercial or financial relationships that could be construed as a potential conflict of interest.

Publisher's note

All claims expressed in this article are solely those of the authors and do not necessarily represent those of their affiliated organizations, or those of the publisher, the editors and the reviewers. Any product that may be evaluated in this article, or claim that may be made by its manufacturer, is not guaranteed or endorsed by the publisher.

Supplementary material

The Supplementary Material for this article can be found online at: https://www.frontiersin.org/articles/10.3389/fgene.2023.1237912/full#supplementary-material

SUPPLEMENTARY FIGURE S1
Subgroup analysis of different amniotic fluid mortality rates in IHK.

SUPPLEMENTARY FIGURE S2
Subgroup analysis of different amniotic fluid mortality rates in NIHK.

SUPPLEMENTARY FIGURE S3
Subgroup analysis of different kidney size mortality rates in IHK.

SUPPLEMENTARY FIGURE S4
Subgroup analysis of different kidney size mortality rates in NIHK.

SUPPLEMENTARY FIGURE S5
Sensitivity analysis of positive rate of IHK monogenic etiologies.

SUPPLEMENTARY FIGURE S6
Sensitivity analysis for subgroup analysis of IHK mortality by different amount of amniotic fluid.

SUPPLEMENTARY FIGURE S7
Sensitivity analysis of neonatal mortality heterogeneity in NIHK.

References

Am, K., Jm, R., and Rl, T. (1983). Causes of increased renal echogenicity in pediatric patients. *Pediatrics* 1983.

Avni, F. E., Garel, C., Cassart, M., D'haene, N., Hall, M., and Riccabona, M. (2012). Imaging and classification of congenital cystic renal diseases. *Ajr Am. J. Roentgenol.* 198 (5), 1004–1013. doi:10.2214/AJR.11.8083

Carr, M. C., Benacerraf, B. R., Estroff, J. A., and Mandell, J. (1995). Prenatally diagnosed bilateral hyperechoic kidneys with normal amniotic fluid: postnatal outcome. *J. Urol.* 153 (2), 442–444. doi:10.1097/00005392-199502000-00051

Chen, F., Yuan, T., Chen, M., Xie, Y., Li, N., Wei, J., et al. (2022). Genetic etiology and pregnancy outcome of fetal bilateral renal parenchymal hyperechogenicity. *Adv. Mod. Obstetrics And Gynecol.* 31 (4), 294–296. doi:10.13283/j.cnki.xdfckjz.2022.04.011

Chitty, L. S., and Altman, D. G. (2003). Charts of fetal size: kidney and renal pelvis measurements. *Prenat. Diagn* 23 (11), 891–897. doi:10.1002/pd.693

Cohen, H. L., Cooper, J., Eisenberg, P., Mandel, F. S., Gross, B. R., Goldman, M. A., et al. (1991). Normal length of fetal kidneys: sonographic study in 397 obstetric patients. *Ajr Am. J. Roentgenol.* 157 (3), 545–548. doi:10.2214/ajr.157.3.1872242

Decramer, S., Parant, O., Beaufils, S., Clauin, S., Guillou, C., Kessler, S., et al. (2007). Anomalies of the Tcf2 gene are the main cause of fetal bilateral hyperechogenic kidneys. *J. Of Am. Soc. Of Nephrol.* 18 (3), 923–933. doi:10.1681/ASN.2006091057

Deng, L., Liu, Y., Yuan, M., Meng, M., Yang, Y., and Sun, L. (2022). Prenatal diagnosis and outcome of fetal hyperechogenic kidneys in the era of antenatal next-generation sequencing. *Clin. Chim. Acta* 528, 52816–52828. doi:10.1016/j.cca.2022.01.012

Devriendt, A., Cassart, M., Massez, A., Donner, C., and Avni, F. E. (2013). Fetal kidneys: additional sonographic criteria of normal development. *Prenat. Diagn* 33 (13), 1248–1252. doi:10.1002/pd.4240

Dias, T., Sairam, S., and Kumarasiri, S. (2014). Ultrasound diagnosis of fetal renal abnormalities. *Best Pract. And Res. Clin. Obstetrics And Gynaecol.* 28 (3), 403–415. doi:10.1016/j.bpobgyn.2014.01.009

Digby, E. L., Liauw, J., Dionne, J., Langlois, S., and Nikkel, S. M. (2021). Etiologies and outcomes of prenatally diagnosed hyperechogenic kidneys. *Prenat. Diagn.* 41 (4), 465–477. doi:10.1002/pd.5883

Emmanuelli, V., Lahoche-Manucci, A., Holder-Espinasse, M., Devisme, L., Vaast, P., Dieux-Coeslier, A., et al. (2010). Prenatal diagnosis of hyperechogenic kidneys: a study of 17 cases. *J. De Gynecol. Obstetrique Biol. De La Reproduction* 39 (8), 637–646. doi:10.1016/j.jgyn.2010.07.012

Estroff, J. A., Mandell, J., and Benacerraf, B. R. (1991). Increased renal parenchymal echogenicity in the fetus: importance and clinical outcome. *Radiology* 181 (1), 135–139. doi:10.1148/radiology.181.1.1887022

Evans, M. I., Wapner, R. J., and Berkowitz, R. L. (2016). Noninvasive prenatal screening or advanced diagnostic testing: caveat emptor. *Am. J. Obstet. Gynecol.* 215 (3), 298–305. doi:10.1016/j.ajog.2016.04.029

Fu, F., Li, R., Yu, Q., Wang, D., Deng, Q., Li, L., et al. (2022). Application of exome sequencing for prenatal diagnosis of fetal structural anomalies: clinical experience and lessons learned from A cohort of 1618 fetuses. *Genome Med.* 14 (1), 123. doi:10.1186/s13073-022-01130-x

Gilboa, Y., Perlman, S., Pode-Shakked, N., Pode-Shakked, B., Shrim, A., Azaria-Lahav, E., et al. (2016). Prenatal diagnosis of 17q12 deletion syndrome: from fetal hyperechogenic kidneys to high risk for autism. *Prenat. Diagn.* 36 (11), 1027–1032. doi:10.1002/pd.4926

Heidet, L., Decramer, S., Pawtowski, A., Morinière, V., Bandin, F., Knebelmann, B., et al. (2010). Spectrum of Hnf1b mutations in A large cohort of patients who harbor renal diseases. *Clin. J. Am. Soc. Nephrol.* 5 (6), 1079–1090. doi:10.2215/CJN.06810909

Huang, J. (2014). Clinical analysis of fetal kidney enhanced echo. *Clin. Investig.* 22, 5.

Huang, R., Fu, F., Zhou, H., Zhang, L., Lei, T., Cheng, K., et al. (2023). Prenatal diagnosis in the fetal hyperechogenic kidneys: assessment using chromosomal microarray analysis and exome sequencing. *Hum. Genet.* 142 (6), 835–847. doi:10.1007/s00439-023-02545-1

Hutson, J., Ruth Mackenzie, J., Young, D., Mcnay, M., Whittle, M., and Raine, P. M. (1985). Antenatal diagnosis of surgical disorders by ultrasonography. *Lancet* 325 (8429), 621–623. doi:10.1016/s0140-6736(85)92154-3

Chaumoitre, K., Brun, M., Cassart, M., Maugey-Laulom, B., Eurin, D., Didier, F., and Avni, E. F. (2006) Differential diagnosis of fetal hyperechogenic cystic kidneys unrelated to renal tract anomalies: a multicenter study. *Ultrasound Obstet. Gynecol.*, 28, 911. doi:10.1002/uog.3856

Li, C., Liu, Y., Yang, P., Li, H., Wei, Y., Kersey, K., et al. (2020). Pharmacokinetics, safety, and tolerability of ledipasvir/sofosbuvir and sofosbuvir/velpatasvir in healthy Chinese subjects. *Chin. J. Of Ultrasound Med.* 36 (5), 448–457. doi:10.1016/j.clinthera.2020.01.013

Li, H., Liu, T., Liu, C., and Shang, T. (2007). Prenatal diagnosis and clinical prognosis of fetal hyperechogenic kidneys. *Chin. J. Of Obstetrics And Gynecol.* 42 (4), 236–238. doi:10.3760/j.issn:0529-567x.2007.04.006

Lord, J., Mcmullan, D. J., Eberhardt, R. Y., Rinck, G., Maher, E. R., Quinlan-Jones, E., et al. (2019). Prenatal exome sequencing analysis in fetal structural anomalies detected by ultrasonography (page): a cohort study. *Yearb. Of Paediatr. Endocrinol.* 393, 747–757. doi:10.1016/S0140-6736(18)31940-8

Mashiach, R., Davidovits, M., Eisenstein, B., Kidron, D., Kovo, M., Shalev, J., et al. (2005). Fetal hyperechogenic kidney with normal amniotic fluid volume: a diagnostic dilemma. *Prenat. Diagn* 25 (7), 553–558. doi:10.1002/pd.1185

Moore, T. R., and Cayle, J. E. (1990). The amniotic fluid index in normal human pregnancy. *Am. J. Obstet. Gynecol.* 162 (5), 1168–1173. doi:10.1016/0002-9378(90)90009-v

Morr, A., Mosimann, B., Tschumi, S., Surbek, D., and Raio, L. (2022). Differential diagnosis and prognosis of fetuses with bilateral enlarged, hyperechogenic kidneys: renal volume and amniotic fluid volume with advancing gestation. *Z. Fur Geburtshilfe Und Neonatol.* 226 (02), 98–103. doi:10.1055/a-1586-5493

Nicolaides, K. H., Snijders, R. J., Gosden, C. M., Berry, C., and Campbell, S. (1992). Ultrasonographically detectable markers of fetal chromosomal abnormalities. *Lancet* 340 (8821), 704–707. doi:10.1016/0140-6736(92)92240-g

Phelan, J. P., Smith, C. V., Broussard, P., and Small, M. (1987). Amniotic fluid volume assessment with the four-quadrant technique at 36-42 Weeks' gestation. *J. Reprod. Med.* 32 (7), 540–542.

Reisman, E. M., Kennedy, T. J., Roehrborn, C. G., and Mcconnell, J. D. (1991). A prospective study of urologist-performed sonographic evaluation of the urinary tract in patients with prostatism. *J. Of Urology* 145 (6), 1186–1189. doi:10.1016/s0022-5347(17)38570-1

Shuster, S., Keunen, J., Shannon, P., Watkins, N., Chong, K., and Chitayat, D. (2019). Prenatal detection of isolated bilateral hyperechogenic kidneys: etiologies and outcomes. *Prenat. Diagn* 39 (9), 693–700. doi:10.1002/pd.5418

Stroup, D. F., Berlin, J. A., Morton, S. C., Olkin, I., Williamson, G. D., Rennie, D., et al. (2000). Meta-analysis of observational studies in epidemiology: a proposal for reporting meta-analysis of observational studies in epidemiology (moose) group. *Jama* 283 (15), 2008–2012. doi:10.1001/jama.283.15.2008

Su, J., Qin, Z., Fu, H., Luo, J., Huang, Y., Huang, P., et al. (2022). Association of prenatal renal ultrasound abnormalities with pathogenic copy number variants in A large Chinese cohort. *Ultrasound Obstet. Gynecol.* 59 (2), 226–233. doi:10.1002/uog.23702

Tain, Y. L., Luh, H., Lin, C. Y., and Hsu, C. N. (2016). Incidence and risks of congenital anomalies of kidney and urinary tract in newborns: a population-based case-control study in taiwan. *Med. Baltim.* 95 (5), E2659. doi:10.1097/MD.0000000000002659

Tsatsaris, V., Gagnadoux, M. F., Aubry, M. C., Gubler, M. C., Dumez, Y., and Dommergues, M. (2002). Prenatal diagnosis of bilateral isolated fetal hyperechogenic kidneys. Is it possible to predict long term outcome? *Bjog Int. J. Of Obstetrics And Gynaecol.* 109 (12), 1388–1393. doi:10.1046/j.1471-0528.2002.02055.x

Wapner, R., Martin, C., Levy, B., Jackson, L., Eng, C. M., Zachary, J. M., et al. (2013). Chromosomal microarray versus karyotyping for prenatal diagnosis. *N. Engl. J. Med.* 367, 2175–2184. doi:10.1056/NEJMoa1203382

Wells, G., Shea, B., O'connell, D., Peterson, J., and Welch, V. (2011). The newcastle-ottawa scale (nos) for assessing the quality of case-control studies in meta-analyses. *Eur. J. Of Epidemiol.* 2011, 25603–25605.

Xie, D., Zhou, H., Lu, Y., Xu, H., Li, Q., Li, X., et al. (2022). Relationship between prenatal ultrasonographic characteristics of fetal bilateral hyperechogenic kidneys and pregnancy outcomes. *Chin. J. Of Med. Ultrasound (Electronic Ed.* 19 (5), 422–427. doi:10.3877/cma.j.issn.1672-6448.2022.05.006

Yulia, A., Napolitano, R., Aiman, A., Desai, D., Johal, N., Whitten, M., et al. (2021). Perinatal and infant outcome of fetuses with prenatally diagnosed hyperechogenic kidneys ultrasound in obstetrics and gynecology: the official journal of the international society of ultrasound in obstetrics and gynecology. *Ultrasound Obstet. Gynecol.* 57 (6), 953–958. doi:10.1002/uog.22121

Zhang, X., Wang, F., Chen, J., Fan, L., Shi, C., and Yang, H. (2017). Prenatal diagnosis and prognosis of fetal hyperechogenic kidney:A study of 65 cases. *Chin. J. Of Perinat. Med.* 20 (2), 85–90. doi:10.3760/cma.j.issn.1007-9408.2017.02.002

frontiers | Frontiers in Genetics

TYPE Original Research
PUBLISHED 22 August 2023
DOI 10.3389/fgene.2023.1235589

OPEN ACCESS

EDITED BY
Jordi Pérez-Tur,
Spanish National Research Council (CSIC), Spain

REVIEWED BY
Frederique Magdinier,
Institut National de la Santé et de la Recherche Médicale (INSERM), France
Edoardo Malfatti,
Hôpitaux Universitaires Henri Mondor, France

*CORRESPONDENCE
Emiliano Giardina,
emiliano.giardina@uniroma2.it

RECEIVED 06 June 2023
ACCEPTED 09 August 2023
PUBLISHED 22 August 2023

CITATION
Strafella C, Caputo V, Bortolani S, Torchia E, Megalizzi D, Trastulli G, Monforte M, Colantoni L, Caltagirone C, Ricci E, Tasca G, Cascella R and Giardina E (2023), Whole exome sequencing highlights rare variants in *CTCF*, *DNMT1*, *DNMT3A*, *EZH2* and *SUV39H1* as associated with FSHD.
Front. Genet. 14:1235589.
doi: 10.3389/fgene.2023.1235589

Whole exome sequencing highlights rare variants in *CTCF*, *DNMT1*, *DNMT3A*, *EZH2* and *SUV39H1* as associated with FSHD

Claudia Strafella[1], Valerio Caputo[1], Sara Bortolani[2], Eleonora Torchia[2], Domenica Megalizzi[1], Giulia Trastulli[1], Mauro Monforte[2], Luca Colantoni[1], Carlo Caltagirone[3], Enzo Ricci[2,4], Giorgio Tasca[2,5], Raffaella Cascella[1,6] and Emiliano Giardina[1,7]*

[1]Genomic Medicine Laboratory UILDM, IRCCS Santa Lucia Foundation, Rome, Italy, [2]Unità Operativa Complessa di Neurologia, Fondazione Policlinico Universitario A. Gemelli IRCCS, Rome, Italy, [3]Department of Clinical and Behavioral Neurology, IRCCS Fondazione Santa Lucia, Rome, Italy, [4]Istituto di Neurologia, Università Cattolica del Sacro Cuore, Rome, Italy, [5]John Walton Muscular Dystrophy Research Centre, Newcastle University and Newcastle Hospitals NHS Foundation Trusts, Newcastle UponTyne, United Kingdom, [6]Department of Biomedical Sciences, Catholic University Our Lady of Good Counsel, Tirana, Albania, [7]Medical Genetics Laboratory, Department of Biomedicine and Prevention, Tor Vergata University, Rome, Italy

Introduction: Despite the progress made in the study of Facioscapulohumeral Dystrophy (FSHD), the wide heterogeneity of disease complicates its diagnosis and the genotype-phenotype correlation among patients and within families. In this context, the present work employed Whole Exome Sequencing (WES) to investigate known and unknown genetic contributors that may be involved in FSHD and may represent potential disease modifiers, even in presence of a *D4Z4* Reduced Allele (DRA).

Methods: A cohort of 126 patients with clinical signs of FSHD were included in the study, which were characterized by *D4Z4* sizing, methylation analysis and WES. Specific protocols were employed for *D4Z4* sizing and methylation analysis, whereas the Illumina® Next-Seq 550 system was utilized for WES. The study included both patients with a DRA compatible with FSHD diagnosis and patients with longer *D4Z4* alleles. In case of patients harboring relevant variants from WES, the molecular analysis was extended to the family members.

Results: The WES data analysis highlighted 20 relevant variants, among which 14 were located in known genetic modifiers (*SMCHD1*, *DNMT3B* and *LRIF1*) and 6 in candidate genes (*CTCF*, *DNMT1*, *DNMT3A*, *EZH2* and *SUV39H1*). Most of them were found together with a permissive short (4–7 RU) or borderline/long DRA (8–20 RU), supporting the possibility that different genes can contribute to disease heterogeneity in presence of a FSHD permissive background. The segregation and methylation analysis among family members, together with clinical findings, provided a more comprehensive picture of patients.

Discussion: Our results support FSHD pathomechanism being complex with a multigenic contribution by several known (*SMCHD1*, *DNMT3B*, *LRIF1*) and possibly other candidate genes (*CTCF*, *DNMT1*, *DNMT3A*, *EZH2*, *SUV39H1*) to disease penetrance and expressivity. Our results further emphasize the importance of extending the analysis of molecular findings within the proband's family, with the

purpose of providing a broader framework for understanding single cases and allowing finer genotype-phenotype correlations in FSHD-affected families.

KEYWORDS

FSHD, exome, D4Z4, genetics, muscular dystrophy

1 Introduction

The introduction of Next-Generation Sequencing (NGS) into the clinical practice has revolutionized the genetic diagnosis and counseling approach of many Neuromuscular Diseases (NMDs).

In particular, NGS allows detecting a wide range of known genetic alterations associated with NMDs as well as identifying novel genetic variations that can expand the genetic heterogeneity of NMDs (Barp et al., 2021). However, reduced penetrance, variable onset, and expressivity as well as the presence of extra-muscular symptoms in many patients still make the genotype-phenotype correlation of NMDs challenging. Among them, FacioScapuloHumeral Dystrophy (FSHD) represents an excellent example of such level of complexity (Caputo et al., 2022a). FSHD (OMIM #158900, #158901, #619477, #619478) is a skeletal muscle disorder with an estimated prevalence of 1:8000–20.000 (Mostacciuolo et al., 2009; Deenen et al., 2014). A progressive and often asymmetric weakness of facial, shoulder and upper arm muscles are typical features of disease, although abdominal, hip girdle and lower leg muscles are also frequently involved (Preston et al., 2020). Typically, FSHD is inherited as an autosomal dominant disorder, although reduced penetrance and variable expressivity can occur among patients and within families (De Simone et al., 2017; Ricci et al., 2020). FSHD can be distinguished in two forms, namely, FSHD1 and FSHD2, although it can also occur as a compound form of disease (FSHD1+FSHD2). From a genetic perspective, FSHD is associated with the contraction of a macrosatellite repeat array on chromosome 4q35 that is referred to as *D4Z4*. This region normally consists of 11 to >100 Repeated Units (RU) of *D4Z4* elements, whereas it is reduced to 1–10 RU in FSHD1 subjects (Wijmenga et al., 1992). In addition to the *D4Z4* contraction, FSHD has been associated with the presence of pathogenic variants within the *SMCHD1* (18p11.32), *DNMT3B* (20q11.21) and *LRIF1* (1p13.3) genes. These genes have been described as disease modifiers in FSHD1 cases (i.e., with *D4Z4* size of 8–10 RU) or as causative genes in FSHD2 (with a *D4Z4* of 11–20 RU) (Sacconi et al., 2009; Lemmers et al., 2012; van der Boogard et al., 2016; Cascella et al., 2018; Strafella et al., 2019; Hamanaka et al., 2020). In addition, two subtelomeric variants have been identified at chromosome 4, namely, the 4qA and 4qB alleles. Although both are present in the general population, only the 4qA allele is associated with FSHD and it is thereby referred to as "permissive" allele (Lemmers et al., 2010). Moreover, the DNA methylation status of the *D4Z4* locus has been shown to significantly contribute to FSHD severity and penetrance (Lemmers et al., 2015; Himeda et al., 2019). Altogether, these events lead to the relaxation of chromatin conformation, which, in turn, results in the derepression of *DUX4* gene, which is stably transcribed in the presence of the 4qA haplotype containing a polyadenylation signal. In muscle cells, the aberrant expression of DUX4 has been associated with the induction of cell death, oxidative stress and inflammatory pathways, which are thought to be responsible for the progression of muscle damage also *in vivo* (Greco et al., 2020; Cohen et al., 2021).

Despite the progress made in the field, the wide range of mild to severe phenotypes, the occurrence of extra-muscular features, the variable age of onset and progression of disease advocate for FSHD being a complex disorder (Sacconi et al., 2019; Greco et al., 2020). In our practice, approximately 60% of patients with a clinical suspicion of disease are found to be carriers of a reduced *D4Z4* allele compatible with an FSHD1 diagnosis (Zampatti et al., 2019), a percentage that is highly variable and dependent on the experience of the different neurological centers referring the patients. In addition, a reduced *D4Z4* allele in combination with a permissive haplotype has been observed in approximately 3% of the healthy population (Scionti et al., 2012; Ricci et al., 2020). Furthermore, the disease severity has been shown to account for approximately 40% by familial factors and 10% by the *D4Z4* repeat array size (Mul et al., 2018). Given these premises, it is plausible that other (epi)genetic factors contribute to the clinical variability and heterogeneity of FSHD, and the knowledge of these could be important for increasing the accuracy of diagnosis and therefore genetic counseling of patients and families. To this purpose, the present work employed Whole Exome Sequencing (WES) to investigate known and unknown genetic contributors that may be involved in FSHD and may represent potential disease modifiers, even in presence of a *D4Z4* Reduced Allele (DRA). The study included both patients with a *D4Z4* Reduced Allele (DRA) compatible with FSHD diagnosis (≤10RU) and patients with longer *D4Z4* sizes. The study was performed on a large cohort of patients characterized by *D4Z4* sizing, methylation analysis and WES. In case of patients reporting variants of interest from WES analysis, the study was extended to the family members in order to provide a more comprehensive picture of the cases.

2 Methods

2.1 Study cohort

The study involved 126 Italian patients with clinical signs of FSHD, which accessed to the Genomic Medicine Laboratory-UILDM at the Santa Lucia Foundation IRCCS for the standard molecular diagnosis. The presence of *D4Z4* Reduced Allele (DRA) was evaluated during the diagnostic routine and was utilized to select the study cohort with the purpose of including patients with variable *D4Z4* size. In particular, the molecular assessment of DRA was performed using PFGE and Southern blotting followed by hybridization with specific probes P13-E11 as previously described (Zampatti et al., 2019). The patient's cohort displayed a variable number of RUs including 15 patients with 1–3 RUs,

80 patients with 4–7 RUs, 7 patients with 8–10 RUs, 2 patients with 11–20 RUs, 6 patients with RUs>20 RUs). Moreover, 16 patients carried two permissive (i.e., both 4qA) DRAs, in the size range between 3 and 20 RU (Supplementary Table S1). The patient's cohort presented a Female:Male (F:M) ratio of 45:55 and an average age of 52.5 ± 17.7 years. In addition, a cohort of 100 Italian subjects matched for age and sex were included in the study as reference group (Supplementary Table S1).

The clinical evaluation of patients was performed by expert neurologists from Fondazione Policlinico Gemelli IRCCS, using the Clinical Severity Scale (CSS) (Ricci et al., 1999) and the FSHD Clinical Score scale (Lamperti et al., 2010), scores specifically designed and validated to assess disease severity in FSHD patients. Muscle MRI was performed on a 1.5 T scanner (Siemens Magnetom Espree), according to published protocols (Tasca et al., 2014; Tasca et al., 2016; Giacomucci et al., 2020). Upper girdle and lower limb muscle MRI scans were evaluated for the presence of imaging patterns supporting the diagnosis of FSHD (Monforte et al., 2022).

Informed consent was obtained from all the subjects included in the present study.

2.2 DNA extraction and methylation analysis

The genomic DNA of patients was extracted from 400 µL of peripheral blood using MagPurix Blood DNA Extraction Kit and MagPurix Automatic Extraction System (Zinexts) according to the manufacturer's instructions.

Concerning the analysis of methylation, two regions of the *D4Z4* locus were evaluated, namely, the *DR1* (located 1 Kb upstream of the *DUX4* ORF and harboring 29 CpG sites) and the *DUX4*-PAS (containing 10 CpG sites located within the most distal part of the array and including the Polyadenylation Signal, PAS). In particular, the *DUX4*-PAS is specific for the 4q distal region; it is ampliefied only in presence of a 4qA allele and it provides information concerning the presence of a DRA (i.e., FSHD1). The DR1 region is located within each *D4Z4* RU on both chromosomes 4 and 10 and it is highly useful to identify FSHD2 subjects. The DNA from each patient underwent methylation analysis using a protocol based on Bisulfite Sequencing (BSS), Amplified Fragment Length Polymorphism (AFLP) and Machine Learning (ML) described in our previous work (Caputo et al., 2022b). The ML model employs the methylation levels of four CpG sites (*DUX4*-PAS_CpG6, *DUX4*-PAS_CpG3, DR1_CpG1 and DR1_Cpg22) to classify FSHD subjects from non-FSHD ones. Following a specific decision tree (available in Caputo et al., 2022b), the model classify subjects on the basis of specific thresholds of methylation of each CpG site and following a specific order of relevance, that is *DUX4*-PAS_CpG6; *DUX4*-PAS_CpG3; DR1_CpG1; DR1_CpG22.

The characterization of 4q subtelomeric variant was assessed for each converted DNA by means of traditional PCR and electrophoresis. In particular, this PCR employs specific primers for *DUX4*-PAS region, whose amplification is indicative of the presence of at least 4qA allele. The 4qB allele is detected by means of specific primers as well (Caputo et al., 2022b). Three possible 4q configurations were thus distinguished, namely, 4qA/4qA, 4qA/4qB and 4qB/4qB.

2.3 Whole Exome sequencing (WES)

Concerning WES analysis, the Illumina® Next-Seq 550 system was utilized. In particular, 30–50 ng/µL of DNA was employed for library preparation by means of Illumina® DNA Prep with Enrichment and Tagmentation kit according to manufacturer's instructions. The obtained libraries were sequenced at 2 × 100 bp and the sequencing quality of the resulting data was expected to reach a Quality score >30 (Q30) for ~80% of total called bases. The analysis of variants was performed, focusing on the variants located in genes (*SMCHD1*, *DNMT3B* and *LRIF1*) known to be associated with FSHD as well as genes that may represent candidate novel genes for the disease. The selection of these genes was performed considering their function as epigenetic regulators of *D4Z4*, their location near the *D4Z4* array or genes being targeted by *DUX4*. The list of selected genes was reported in Supplementary Table S2.

The resulting variants were visualized by Integrated Genome Viewer (v.2.7.2) and functionally annotated by means of BaseSpace Variant Interpreter (Illumina, v. 2.15.0.110), using GRCh37 as genome build. Only the variants reporting a minimum coverage of 20X were considered for subsequent analysis. Annotated variants were prioritized considering the type of variants (nonsense, frameshift, missense, splicing); the Minor Allele Frequency (MAF<0.001) in publicly available database (gnomAD) and in the internal reference group; their localization in regulatory regions or protein domains (by consultation of Uniprot and Decipher databases); their pathogenicity scores retrieved by interrogation of bioinformatics prediction tools. In particular, REVEL (Rare Exome Variant Ensemble Learner) is a meta-predictor tool for missense variants that integrates different scores (MutPred, FATHMM v2.3, VEST 3.0, PolyPhen-2, SIFT, PROVEAN, MutationAssessor, MutationTaster, LRT, GERP++, SiPhy, phyloP, phastCons) (Ioannidis et al., 2016). Moreover, Varsite (Laskowski et al., 2020) and Missense3D (Ittisoponpisan et al., 2019) were used to predict the potential effect of missense variants on protein structure and function, whereas variants within the splicing region were analyzed by Human Splicing Finder (v.3.1, https://www.genomnis.com/access-hsf).

The variants with a clinical significance were also confirmed by direct sequencing. To this purpose, the DNA was amplified by PCR, using the AmpliTaq Gold DNA Polymerase (Applied Biosystems) reagents in a total volume of 25 µL, following the manufacturer's instructions. Successively, direct sequencing of the amplified samples was performed by BigDye Terminator v3.1 Cycle Sequencing Kit (Thermo Fisher Scientific) and run on ABI3130xl (Applied Biosystems). The results were finally analyzed with Sequencing Analysis Software v.6 (Applied Biosystems). In addition, the variants of interest were also subjected to segregation analysis among family members, if available.

Finally, the variants were classified according to the ACMG Standards and Guidelines, which provide a clinical interpretation of variants, discriminating among benign, likely benign, with uncertain significance (VUS), likely pathogenic and pathogenic variants (Richards et al., 2015; Ellard et al., 2020). Bioinformatic online

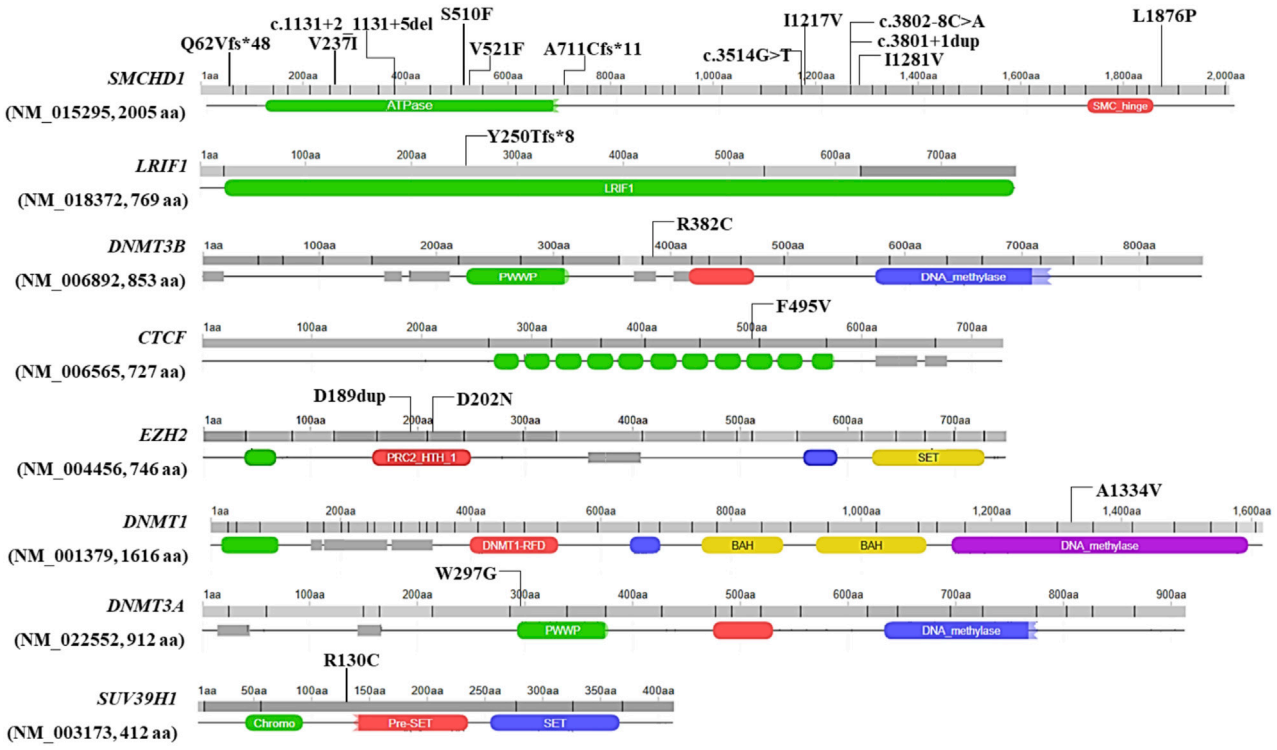

FIGURE 1
Illustration of the localization of the identified variants at level of the protein sequence. Missense variants are reported with their protein coding nomenclature whereas variants in the splicing regions are indicated with their nucleotide coding. The figure was built by retrieving the domain localization and visualization from Uniprot and Decipher, respectively.

platform (Varsome) and public database collecting data concerning DNA genetic variations (Clinvar, LOVD, Decipher) were also employed as supporting tools for the clinical interpretation of variants. In particular, the PP3 rule was applied following the ClinGen recommendations (Evidence-based calibration of computational tools for missense variant pathogenicity classification and ClinGen recommendations for clinical use of PP3/BP4 criteria) (Pejaver et al., 2022). Concerning the application of PM1 and PP2 rules, Decipher was utilized as supporting tool since it provides helpful and user-friendly tools for assigning such criteria. In particular, Decipher was consulted to visualize the gene and regional constraint (for PP2 application) to missense and loss-of-function variants and the localization of functional domains and regulatory regions (for PM1 rule) of the protein corresponding to the genes of interest. In addition, a "benign cut-off frequency" derived by Varsome was also utilized to compare the frequency of the identified variants in the specific genes and assess the BS1 rule in case of variants with a frequency exceeding the cut-off fixed for each gene.

3 Results

The patient's cohort displayed a variable number of RUs including 15 patients with 1–3 RUs, 80 patients with 4–7 RUs, 7 patients with 8–10 RUs, 2 patients with 11–20 RUs and six patients with RUs>20 RUs). Moreover, 16 patients carried two permissive (i.e., both 4qA) DRAs, in the size range between 3 and 20 RU. All of the patients carried at least a 4qA allele (Supplementary Table S1). The analysis of WES focused the attention on a set of genes selected by their function as epigenetic regulators of *D4Z4*, their location near the *D4Z4* array or genes being targeted by *DUX4* (Supplementary Table S2). Successively, the variants were prioritized according to their frequency, localization into regulatory or protein domains, and bioinformatics prediction.

Twenty variants, which were detected in 19 patients with clinical signs of FSHD, emerged from the analysis of WES data. In particular, 14 variants were located in known genes (*SMCHD1*, *DNMT3B* and *LRIF1*), whereas six variants were found in other genes of interest (namely, *CTCF*, *DNMT1*, *DNMT3A*, *EZH2*, *SUV39H1*). None of the variants was observed in the reference group. Interestingly, most of the variants were localized within a specific domain or region of interaction with other factors, thereby suggesting a potential functional effect (Figure 1).

Among the identified variants, 14 were detected in known FSHD2 causing genes (Table 1), namely, *SMCHD1* (n = 12), *DNMT3B* (n = 1) and *LRIF1* (n = 1). These variants were further investigated considering the type (3 frameshift, 4 spicing and 7 missense), frequency in gnomAD and bioinformatics prediction (Table 1). As a result, 12 out of 14 identified variants in known genes were found to be absent or extremely rare in gnomAD database, whereas two variants (*SMCHD1*:c.3841A>G and

TABLE 1 Description of the variants identified in known FSHD genes.

Gene name and constraints	Genomic position	Variant type	Variants nomenclature	GnomAD freq	In silico pathogenicity scores	In silico protein prediction	HSF
***SMCHD1* Z (Missense): 3.63 Z (LoF): 8.55 Freq cut-off: 0.00012**	18: 2688462	missense	c.709G>A (p.Val237Ile)	—	moderate pathogenic	The Val residue is very highly conserved Val237 interacts with ligand (ATP)	—
	18: 2739518	missense in splicing region	c.3514G>T (p.Val1172Phe)	—	strong pathogenic	A Val > Phe change is unfavoured in terms of conserved amino acid properties and it has a high "disease propensity" value of 1.20	Broken WT Donor Site. Alteration of the WT Donor site. Most probably affecting splicing
	18: 2743927	splicing	c.3801+1dup	—	na	na	—
	18: 2700830	missense	c.1561G>T (p. Val521Phe)	—	moderate pathogenic	A Val > Phe change is unfavoured in terms of conserved amino acid properties and it has a high 'disease propensity' value of 1.20 The Val residue at position 521 is well conserved	—
	18: 2700798	missense	c.1529C>T (p.Ser510Phe)	—	moderate pathogenic	A Ser > Phe change is a very large one and might result in a change to the protein's function A Ser > Phe change is highly unfavoured in terms of conserved amino acid properties The Ser residue at position 510 is highly conserved	—
	18: 2707627	frameshift	c.2129dup (p.A711Cfs*11)	—	na	na	—
	18: 2656258	frameshift	c.182_183dup (p.Q62Vfs*48)	—	na	na	—
	18: 2697122	splicing	c.1131 + 2_1131 + 5 del	—	na	na	—
	18: 2747559	missense	c.3841A>G (p.Ile1281Val)	0.000278	supporting benign	not significant impact	—
	18: 2743774	missense	c.3649A>G (p.Ile1217Val)	—	supporting benign	not significant impact	—
	18: 2747512	splicing	c.3802–8C>A	0.000004	na	na	not significant impact
	18: 2784527	missense	c. 5627T>C (p.Leu1876Pro)	—	uncertain	A Leu > Pro change is very highly unfavoured in terms of conserved amino acid properties and it has a very high 'disease propensity' value of 3.02	—
***LRIF1* Z (missense): 0.24 Z (LoF): 2.77 Freq: 0.0001**	1: 111494758	frameshift	c.748del (p.Tyr250ThrfsTer8)	—	na	na	—

(Continued on following page)

TABLE 1 (*Continued*) Description of the variants identified in known FSHD genes.

Gene name and constraints	Genomic position	Variant type	Variants nomenclature	GnomAD freq	In silico pathogenicity scores	In silico protein prediction	HSF
***DNMT3B* Z (Missense):1.5 Z LoF: 5.26 Freq: 0.00012**	20: 31383232	missense	c.1144C>T (p.Arg382Cys)	0.00053	uncertain	An Arg > Cys change is a very large one and might result in a change to the protein's function An Arg > Cys change is very highly unfavoured in terms of conserved amino acid properties and it has a high "disease propensity" value of 1.71 The Arg residue at position 382 is poorly conserved	

LoF: Loss of Function. na: not available. HSF: Human Splicing Finder. WT: Wild-Type. Freq: Frequency. Z: z score.

DNMT3B:c.1144C>T) reported a frequency higher than the fixed "benign cut-off frequency." The use of bioinformatic prediction tools predicted a deleterious or uncertain effect for most variants except for three, which were not reported to have a significant impact on protein function/structure or splicing. Moreover, patients harboring variants in known FSHD genes displayed variable *D4Z4* sizes, including six individuals displaying 4–7 RU, two subjects carrying 9–10 RU, one patient with a *D4Z4*>20RU and four patients with two permissive DRAs (namely, 8 + 6 RU, 5 + 10RU, 8 + 20RU, 13 + 20 RU). Segregation analysis was possible for six cases and showed two patients (FSHD13A and FSHD15A) with *de novo* variants, whereas the remaining ones were inherited or undetermined. Supporting these findings, methylation analysis revealed hypomethylation status consistent with FSHD phenotype in patients harboring such variants, especially in the DR1 region (Table 3). Interestingly, one patient (FSHD1A) harbored a variant in *SMCHD1*, a variant in *LRIF1* and a short DRA (4 RU). Segregation analysis showed that the *SMCHD1* variant was inherited from the unaffected father (FSHD1D), whereas the variant in *LRIF1* was inherited from the affected mother (FSHD1B), together with the short DRA. Methylation analysis in the patient and the family members revealed the lowest methylation levels in the FSHD1A patient with the three events compared to the other family members (Table 3).

Furthermore, the analysis of WES highlighted the presence of six variants in five genes, namely, *CTCF*, *DNMT3A*, *DNMT1*, *EZH2* and *SUV39H1* (Table 2). The variants were absent or very rare in gnomAD database. All of them were missense, except for one in-frame insertion located in *EZH2*. All of the genes harboring such variations presented a significant constraint (Z score ≥ 3.12) to missense variants, at level of the gene and regions including the identified variants. The application of prediction tools allowed assessing a potential effect of such variants on protein function, structure or splicing (Table 2). Moreover, all of the 6 variants were found in combination with a DRA ranging from 4 to 8 RU and, in two cases (FSHD2A and FSHD5A), with an additional permissive (i.e., 4qA) DRA < 20 RU. Segregation analysis among the available family members showed that the identified variants were found in affected individuals together with a DRA. Moreover, the assessment of methylation levels in families harboring such variants revealed hypomethylated profiles mostly consistent with the clinical status of family members (Table 3).

All molecular and clinical data concerning the families harboring variants in known and candidate genes for FSHD have been reported in Tables 3, 4, respectively.

Finally, all the variants identified in known and candidate genes were subjected to ACMG classification, which allowed identifying five Pathogenic variants, 7 Likely pathogenic, 7 VUS and one Likely Benign variant (Supplementary Table S3).

Altogether, these results showed variants in *SMCHD1* as one of the most frequent genetic alterations in this study together with *D4Z4* contraction, whereas variants in *LRIF1* and *DNMT3B* appeared as rarer events, although they may co-occur together with short *D4Z4* contraction and potentially contribute to phenotype variability. Importantly, the WES analysis identified variants in *CTCF*, *DNMT3A*, *DNMT1*, *EZH2* and *SUV39H1*, which have not been described in patients and families with FSHD before and, thus, they may represent novel candidate genetic modifiers for the disease. These variants were found in combination with a DRA, supporting the possibility that different genes can contribute to disease heterogeneity in presence of a FSHD permissive background.

4 Discussion

The comprehension of the mechanisms underlying the complex molecular background of FSHD is an area of active research. On this subject, recent studies described transcriptomic and proteomic markers associated with FSHD clinical severity and progression in muscle and blood (Banerji et al., 2019; Corasolla Carregari et al., 2020; Wong et al., 2020; Banerji et al., 2022). In addition, several studies highlighted DNA hypomethylation as a hallmark of disease (Hartwerk et al., 2013; Gaillard et al., 2014; Huichalaf et al., 2014; Calandra et al., 2016; Haynes et al., 2018; Lemmers et al., 2019; Roche et al., 2019; Gould et al., 2021; Banerji et al., 2022; Caputo et al., 2022b; Erdmann et al., 2022; Hiramuki et al., 2022). In this scenario, the identification of *SMCHD1*, *DNMT3B* and *LRIF1* as causative or modifier genes in FSHD1 and FSHD2 laid the foundations for considering FSHD as a complex disease, in which multiple genes are likely to contribute to the disease heterogeneity and variability (Caputo et al., 2022a) To this regard, NGS approaches are the ideal tool to allow the

TABLE 2 Description of the variants identified in candidate genes.

Gene name and constraints	Genomic position	Variant type	Variants nomenclature	GnomAD frequency	In silico pathogenicity scores	In silico protein prediction	HSF
***CTCF* Z (Missense): 4.44 Z (LoF): 5.079 Freq: 0.0001**	16: 67660583	missense	c.1483T>G (p.Phe495Val)	not found	moderate pathogenic	A Phe > Val change is unfavoured in terms of conserved amino acid properties and it has a high 'disease propensity' value of 1.29. The Phe residue at position 495 is very highly conserved	—
***EZH2* Z (Missense): 4.68 Z (LoF): 5.808 Freq: 0.0001**	7: 148525892	inframe insertion	c.566_568dup (p.Asp189 dup)	0.000004	moderate pathogenic	na	Alteration of auxiliary sequences: significant alteration of ESE/ESS motifs ratio. New Acceptor splice site: activation of a cryptic Acceptor site and potential alteration of splicing
	7: 148525853	missense	c.604G>A (p.Asp202Asn)	0.000004	supporting benign	not-significant impact	—
***DNMT1* Z (Missense): 4.99 Z (LoF): 8.20 Freq: 0.0001**	19: 10249229	missense	c.4001C>T (p.Ala1334Val)	0.00005	uncertain	The Ala residue at position 1334 is very highly conserved. This substitution disrupts all side-chain/side-chain H-bond(s) and/or side-chain/main-chain bond(s) H-bonds formed by a buried ALA residue	—
***DNMT3A* Z (Missense): 3.45 Z (LoF): 1.521 Freq: 0.00062**	2: 25470585	missense	c.889T>G (p. Trp297Gly)	0.000014	moderate pathogenic	A Trp > Gly chain is a very large one and might well result in a change to the protein's function A Trp > Gly change is highly unfavoured in terms of conserved amino acid properties and it has a very high 'disease propensity' value of 2.80 The Trp residue at position 297 is highly conserved. This substitution disrupts all side-chain/side-chain H-bond(s) and/or side-chain/main-chain bond(s) H-bonds formed by a buried Trp residue. This substitution results in a change between buried and exposed state of the target variant residue. TRP is buried and Gly is exposed	—
***SUV39H1* Z (Missense): 3.49 Z (LoF): 4.333 Freq: 0.0001**	X: 48558704	missense	c.421C>T (Arg141Cys)	not found	uncertain	A change from an Arg > Cys side chain is a very large one and might well result in a change to the protein's function. An Arg > Cys change is very highly unfavoured in terms of conserved amino acid properties	

(Continued on following page)

TABLE 2 (*Continued*) Description of the variants identified in candidate genes.

Gene name and constraints	Genomic position	Variant type	Variants nomenclature	GnomAD frequency	In silico pathogenicity scores	In silico protein prediction	HSF
						and it has a high "disease propensity" value of 1.71. The Arg residue at position 130 is fairly well conserved	

LoF, Loss of Function; na, not available; HSF, Human Splicing Finder; WT, Wild-Type; Freq, Frequency; H, Hydrogen; ESE/ESS (Exonic Splicing Enhancer/Exonic Splicing Silencer) Z, z score.

simultaneous investigation of known FSHD causing (*SMCHD1*, *DNMT3B* and *LRIF1*) and other potential candidate gene modifiers. Given these premises, the present study employed WES to investigate known and unknown genetic contributors that may be involved in FSHD, even in presence of a DRA. As a result, the analysis of WES data highlighted 20 variants in 19 patients with clinical signs of FSHD (15% of the total patients' cohort), including five Pathogenic variants, 7 Likely pathogenic, 7 VUS and one Likely Benign variant (Supplementary Table S3). Among them, 14 variants were detected in known FSHD genes (namely, *SMCHD1*, *LRIF1* and *DNMT3B*). In this case, *SMCHD1* appeared as the most frequently altered gene harbouring 12 variants. As expected, the variants were located throughout the entire gene (Figure 1) and were found to impact protein structure/functioning (in the case of missense variants mostly located in the ATPase domain of *SMCHD1*) or alter splicing and create Premature Termination Codon and truncated proteins (in the case of frameshift, stop-gained or splicing variants) (Table 1). These findings were in line with previous studies (Lemmers et al., 2019; Strafella et al., 2019) highlighting the ATPase domain as one of the most frequently affected domain by FSHD variants, especially by missense ones. Concerning Loss of function (LoF) variants identified in this study (namely, frameshift and intronic variants located in ±1-2 of splice site), they were scattered throughout the gene (Figure 1), consistently with other studies (Lemmers et al., 2019; Sacconi et al., 2019; Strafella et al., 2019; Giacomucci et al., 2020).

Segregation analysis was possible only for six patients carrying *SMCHD1* variants, among which two cases displayed *de novo* variants, whereas the remaining ones were inherited or undetermined (Table 3). Concerning the association with *D4Z4* size, 6 individuals carrying *SMCHD1* variants displayed 4–7 RU (that is clearly in the FSHD1 range); Two subjects showed a 9–10 RU DRA (borderline/short FSHD1 fragments); 1 patients had a *D4Z4*>20 RU (that is in the normal range) and 4 patients revealed two permissive (i.e., 4qA/4qA) DRAs (namely, 5 + 10 RU, 8 + 6 RU, 8 + 20 RU and 13 + 20RU). This result is consistent with the fact that *SMCHD1* can act as causative or modifier gene for FSHD (Lemmers et al., 2012; Sacconi et al., 2019; Strafella et al., 2019). In addition to previous studies, the present work highlighted six cases harbouring both short DRA (4–7 RU) and genetic variants in known FSHD genes (*SMCHD1* and *LRIF1*) and 1 case carrying detrimental variants in *SMCHD1* and *D4Z4* size>20RU, suggesting that these events may contribute to the disease variability among patients and families. In this regard, the FSHD1 family represented a very peculiar case, with the segregation of a short DRA (4 RU), a likely pathogenic variant in *LRIF1* and a VUS in *SMCHD1*. In this family, methylation analysis showed that the patient (FSHD1A) harbouring the three events displayed the lowest methylation levels compared to the affected mother (FSHD1B) and unaffected relatives (Table 3). Moreover, the clinical evaluation revealed a different degree of severity degree between the proband FSHD1A and the affected mother (FSHD1B), supporting a potential combined effect of the *LRIF1* and *SMCHD1* variants in worsening the phenotype (Table 4). Importantly, the *LRIF1* variant was detected at heterozygous state in FSHD1 family, which is in contrast with the other family described in literature (Hamanaka et al., 2020), in which biallelic *LRIF1* variants have been reported together with a permissive (4qA) and a *D4Z4* array of 13 RUs in a patient born from a consanguineous marriage.

The methylation analysis in patients carrying *SMCHD1* variants revealed a marked hypomethylation consistent with FSHD, especially at the level of the DR1 region (Table 3). This finding is consistent with previous studies (Hartwerk et al., 2013; Huichalaf et al., 2014; Caputo et al., 2022b; Hiramuki et al., 2022; Zheng et al., 2023). The striking DR1 hypomethylation supported a functional effect for the identified *SMCHD1* variants, even for those detected in patients carrying a short DRA (in the FSHD1 range). In fact, these patients displayed lower methylation levels compared to their family members carrying the short DRA only. Patient FSHD19A provided a valuable example of such condition, displaying a short DRA (6RU) combined with the *SMCHD1*:c.3802-8C>A variant, for which pathogenicity scores and prediction analysis supported a benign effect. In this case, the methylation analysis in FSHD19A patient revealed a marked reduction of methylation levels in DR1 compared to the other family member (FSHD19B), who displayed the same DRA and 4q subtype but was negative for the *SMCHD1* variant (Table 3). Moreover, other two *SMCHD1* variants were predicted as benign. However, the *SMCHD1*:c.3841A>G displayed a higher frequency than expected (Table 1) and the low methylation levels detected in the patient (FSHD17A) may be due to the presence of two permissive DRAs (8+6 RU). For the *SMCHD1*:c.3649A>G variant (detected in the FSHD18A patient), the methylation analysis did not reveal a marked reduction of DR1 methylation levels. Therefore, the prediction analysis was consistent with additional findings, such as frequency and/or methylation analysis, which equally supported a non-significant effect for both variants in these cases. Overall, the observation of differential methylation profiles in patients harbouring *SMCHD1* variants supports the hypothesis that the methylation analysis is more accurate for assessing the pathogenicity of *SMCHD1* variants compared to bioinformatics prediction tools. In addition, methylation analysis emerges as a useful tool to prioritize subjects in whom the research of variants in FSHD genes should be performed in parallel with *D4Z4* sizing.

TABLE 3 Molecular characterization of FSHD families harboring the variants identified by WES. The column reporting the *D4Z4* size shows the shortest permissive (4qA) allele compatible with the disease for patients 4qA/4qB considering that it is the only one permissive for FSHD. Concerning patients with 4qA/4qA, it has been reported the shortest allele compatible with FSHD, although those ones carrying both *D4Z4* alleles with a size <20 RU have been reported since they both could contribute to disease in these cases. The family link has been reported taking the proband as reference subject. The methylation data refer to the method described in Caputo et al. (2022b) that combines the methylation levels of four CpG sites (*DUX4*-PAS_CpG6, *DUX4*-PAS_CpG3, DR1_CpG1 and DR1_Cpg22) with machine-learning pipeline to classify FSHD subjects from non-FSHD ones (herein referred as to CTRL). Following a specific decision tree (available in Caputo et al., 2022b), the model classify subjects on the basis of specific thresholds of methylation of each CpG site and following a specific order of relevance, that is *DUX4*-PAS_CpG6; *DUX4*-PAS_CpG3; DR1_CpG1; DR1_CpG22. For more details concerning the method employed for methylation analysis, please refer to the article (Caputo et al., 2022b).The utilized thresholds are reported in brackets in each CpG site column. The decision nodes indicate the step of the decision tree utilized by the ML model. RU: Repeated Unit. ML: Machine Learning. CTRL: non-FSHD.

Family ID	ID patient (family link)	Status	*D4Z4* size (RU)	4q	Segregation analysis	*DUX4*-PAS (CpG 6) (≤78%)	*DUX4*-PAS (CpG 3) (≤0.34)	DR1 (CpG 1) (≤0.53)	DR1 (CpG 22) (≤0.99)	Decision Node	ML prediction
FSHD 1	A (proband)	affected	4	A/A	*SMCHD1*: c.5627T>C *LRIF1*: c.748del	57%	27%	48%	80%	3	FSHD
	B (mother)	affected	4	A/A	*LRIF1*:c.748delT	70%	31%	70%	95%	3	FSHD
	C (brother)	unaffected	>20	A/A	*SMCHD1*: c.5627T>C *LRIF1*: c.748del	94%	34%	51%	92%	7	FSHD
	D (father)	unaffected	>20	A/A	*SMCHD1*: c.5627T>C	91%	39%	71%	96%	10	CTRL
FSHD 2	A (proband)	affected	5 + 12	A/A	*CTCF*:c.1483T>G	67%	24%	47%	85%	3	FSHD
	B (son)	unaffected	12	A/B	*CTCF*:c.1483T>G	70%	21%	50%	80%	3	FSHD
	C (son)	unaffected	12	A/B	*CTCF*:c.1483T>G	82%	28%	58%	90%	8	CTRL
	D (son)	affected	5	A/B	Negative	34%	18%	54%	78%	3	FSHD
	E (husband)	unaffected	>20	B/B	Negative	—	—	—	—	10	—
FSHD 3	A (proband)	affected	5	A/A	*EZH2*: c.566_568dup	78%	38%	75%	100%	3	FSHD
	B (daughter)	unaffected	>20	A/A	*EZH2*: c.566_568dup	100%	41%	57%	91%	10	CTRL
	C (daughter)	affected	5	A/A	*EZH2*: c.566_568dup	82%	45%	75%	100%	11	CTRL
	D (husband)	unaffected	>20	A/A	Negative	93%	41%	60%	89%	10	CTRL
FSHD 4	A (proband)	affected	8	A/B	*EZH2*:c.604G>A	48%	15%	64%	64%	3	FSHD
	B (son)	na	8	A/A	Negative	92%	37%	72%	93%	10	CTRL
	C (daughter)	unaffected	14	A/A	*EZH2*:c.604G>A	86%	18%	28%	47%	7	FSHD
FSHD 5	A (proband)	affected	5 + 16	A/A	*DNMT3A*: c.889T>G	59%	12%	62%	100%	3	FSHD
	B (daughter)	unaffected	11 + 16	A/A	Negative	94%	32%	65%	94%	8	CTRL
FSHD 6	A (proband)	affected	6	A/B	*SUV39H1*: c.421C>T	68%	10%	72%	98%	3	FSHD
	B (son)	affected	6	A/B	Negative	78%	21%	67%	96%	3	FSHD
	C (daughter)	unaffected	6	A/B	*SUV39H1*: c.421C>T	39%	17%	42%	85%	3	FSHD
	D (husband)	unaffected	>20	A/B	Negative	95%	63%	69%	97%	10	CTRL

(Continued on following page)

TABLE 3 (*Continued*) Molecular characterization of FSHD families harboring the variants identified by WES. The column reporting the *D4Z4* size shows the shortest permissive (4qA) allele compatible with the disease for patients 4qA/4qB considering that it is the only one permissive for FSHD. Concerning patients with 4qA/4qA, it has been reported the shortest allele compatible with FSHD, although those ones carrying both *D4Z4* alleles with a size <20 RU have been reported since they both could contribute to disease in these cases. The family link has been reported taking the proband as reference subject. The methylation data refer to the method described in Caputo et al. (2022b) that combines the methylation levels of four CpG sites (*DUX4*-PAS_CpG6, *DUX4*-PAS_CpG3, DR1_CpG1 and DR1_Cpg22) with machine-learning pipeline to classify FSHD subjects from non-FSHD ones (herein referred as to CTRL). Following a specific decision tree (available in Caputo et al., 2022b), the model classify subjects on the basis of specific thresholds of methylation of each CpG site and following a specific order of relevance, that is *DUX4*-PAS_CpG6; *DUX4*-PAS_CpG3; DR1_CpG1; DR1_CpG22. For more details concerning the method employed for methylation analysis, please refer to the article (Caputo et al., 2022b).The utilized thresholds are reported in brackets in each CpG site column. The decision nodes indicate the step of the decision tree utilized by the ML model. RU: Repeated Unit. ML: Machine Learning. CTRL: non-FSHD.

Family ID	ID patient (family link)	Status	*D4Z4* size (RU)	4q	Segregation analysis	*DUX4*-PAS (CpG 6) (≤78%)	*DUX4*-PAS (CpG 3) (≤0.34)	DR1 (CpG 1) (≤0.53)	DR1 (CpG 22) (≤0.99)	Decision Node	ML prediction
FSHD 7	A (proband)	affected	4	A/B	*DNMT1*: c.4001C>T	56%	16%	45%	85%	3	FSHD
	B (daughter)	unaffected	17 + 17	B/B	Negative	—	—	—	—	10	—
FSHD 8	A (proband)	affected	5	A/B	*DNMT3B*: c.1144C>T	47%	16%	63%	93%	3	FSHD
FSHD 9	A (proband)	affected	7	A/A	*SMCHD1*: c.709G>A	62%	22%	47%	85%	3	FSHD
FSHD 10	A (proband)	affected	5 + 10	A/A	*SMCHD1*: c.3514G>T	32%	8%	31%	22%	3	FSHD
	B (father)	na	5	A/B	negative	85%	28%	57%	93%	8	CTRL
	C (mother)	na	10	A/B	*SMCHD1*: c.3514G>T	48%	9%	35%	64%	3	FSHD
FSHD 11	A (proband)	affected	13 + 20	A/A	*SMCHD1*: c.3801+1dup	49%	29%	41%	84%	3	FSHD
FSHD 12	A (proband)	affected	6	A/A	*SMCHD1*: c.1561G>T	43%	16%	19%	60%	3	FSHD
FSHD 13	A (proband)	affected	8 + 20	A/A	*SMCHD1*: c.1529C>T (*de novo*)	63%	31%	37%	57%	3	FSHD
	B (father)	na	8	A/B	negative	88%	38%	81%	97%	10	CTRL
	C (mother)	unaffected	20	A/B	negative	94%	67%	76%	97%	10	CTRL
FSHD 14	A (proband)	affected	9	A/A	*SMCHD1*: c.2129 dup	68%	48%	47%	86%	3	FSHD
	B (father)	affected		A/A	*SMCHD1*: c.2129 dup	84%	34%	46%	89%	7	FSHD
FSHD 15	A (proband)	affected	10	A/A	*SMCHD1*: c.182_183dup (*de novo*)	51%	10%	24%	58%	3	FSHD
	B (mother)	unaffected	10	A/A	negative	93%	32%	75%	98%	8	CTRL
	C (father)	unaffected	>20	A/A	negative	100%	39%	73%	100%	11	CTRL
FSHD 16	A (proband)	affected	>20	A/A	*SMCHD1*: c.1131 + 2_1131+5del	45%	15%	35%	66%	3	FSHD
FSHD 17	A (proband)	affected	8 + 6	A/A	*SMCHD1*: c.3841A>G	59%	16%	35%	77%	3	FSHD
FSHD 18	A (proband)	affected	7	A/B	*SMCHD1*: c.3649A>G	44%	11%	54%	90%	3	FSHD

(Continued on following page)

TABLE 3 (*Continued*) Molecular characterization of FSHD families harboring the variants identified by WES. The column reporting the *D4Z4* size shows the shortest permissive (4qA) allele compatible with the disease for patients 4qA/4qB considering that it is the only one permissive for FSHD. Concerning patients with 4qA/4qA, it has been reported the shortest allele compatible with FSHD, although those ones carrying both *D4Z4* alleles with a size <20 RU have been reported since they both could contribute to disease in these cases. The family link has been reported taking the proband as reference subject. The methylation data refer to the method described in Caputo et al. (2022b) that combines the methylation levels of four CpG sites (*DUX4*-PAS_CpG6, *DUX4*-PAS_CpG3, DR1_CpG1 and DR1_Cpg22) with machine-learning pipeline to classify FSHD subjects from non-FSHD ones (herein referred as to CTRL). Following a specific decision tree (available in Caputo et al., 2022b), the model classify subjects on the basis of specific thresholds of methylation of each CpG site and following a specific order of relevance, that is *DUX4*-PAS_CpG6; *DUX4*-PAS_CpG3; DR1_CpG1; DR1_CpG22. For more details concerning the method employed for methylation analysis, please refer to the article (Caputo et al., 2022b).The utilized thresholds are reported in brackets in each CpG site column. The decision nodes indicate the step of the decision tree utilized by the ML model. RU: Repeated Unit. ML: Machine Learning. CTRL: non-FSHD.

Family ID	ID patient (family link)	Status	*D4Z4* size (RU)	4q	Segregation analysis	*DUX4*-PAS (CpG 6) (≤78%)	*DUX4*-PAS (CpG 3) (≤0.34)	DR1 (CpG 1) (≤0.53)	DR1 (CpG 22) (≤0.99)	Decision Node	ML prediction
FSHD 19	A (proband)	affected	6	A/B	*SMCHD1*: c.3802–8C>A	54%	19%	39%	75%	3	FSHD
	B (son)	affected	6	A/B	negative	59%	14%	73%	96%	3	FSHD

Concerning the *DNMT3B* variant, the reported frequency did not support a deleterious effect, and the methylation analysis was lower in the *DUX4*-PAS region, consistently with the presence of a short DRA in the patient (FSHD8A).

In addition to the variants detected in known FSHD-causing genes, the present work highlighted the presence of six variants in five genes (*CTCF*, *DNMT1*, *DNMT3A*, *EZH2* and *SUV39H1*), which have been involved in the context of FSHD pathogenesis, although no variant has been described in any of them in FSHD patients. Interestingly, all of these genes have been described as epigenetic regulators of the *D4Z4* locus in the context of FSHD (Zeng et al., 2009; Neguembor et al., 2010; Huichalaf et al., 2014; Himeda et al., 2015). All of them have been found to participate in the maintenance of *DUX4*-repressive machinery, by regulating chromatin modifications (namely, the H3K27me3 and H3K9me3 repressive markers) or DNA methylation (Figure 2). The former are mainly mediated by the activity of EZH2 (which is a member of the Polycomb Repressor Complex 2, PRC2) and SUV39H1, whereas the latter are exerted by DNA Methyltransferases (DNMTs), including DNMT1, DNMT3A and DNMT3B, which are enriched to the FSHD locus and display a redundant role (Huichalaf et al., 2014; Haynes et al., 2018). Moreover, CTCF acts as a multifunctional protein that can mediate transcriptional silencing or activation by creating accessible or inaccessible loops of chromatin at specific sites (Ottaviani et al., 2009; Caputo et al., 2022a). Interestingly, the consultation of Uniprot database revealed that the variants identified in *EZH2* gene were located in the PRC2 complex domain, which interacts with DNMT1, DNMT3A and DNMT3B; the DNMT1 variant was located in the catalytic domain interacting with PRC2; the variant of *DNMT3A* is located in PWWP domain interacting with DNMT1 and DNMT3B. Moreover, the variant identified in *CTCF* has been found to be located in the Zinc Finger 9 (ZF9, C2H2-type 9), which has been involved in the formation and directionality of base-specific interactions between CTCF and its binding sites. Interestingly, the function of ZF9 (together with ZF10 and ZF11) enables CTCF to recognize different DNA sequences across the genome and to promote transcriptional insulation that has been previously described in the pathophysiology of FSHD (Ottaviani et al., 2009; Yin et al., 2017; Xu et al., 2018; Huang et al., 2021). Furthermore, the variant identified in *SUV39H1* was found upstream the pre-SET domain, which plays a structural function in stabilizing the SET domain of the protein. SUV39H1 has been previously proposed as a candidate gene for FSHD, because of its role in mediating the methylation of H3K9, which is critical for HP1γ/cohesion binding (both involved in DUX4 suppression), and for SMCHD1 recruitment, which in turn mediates DNA methylation at *D4Z4* (Zeng et al., 2009; Zeng et al., 2014; Sacconi et al., 2019). The consultation of public databases (Clinvar and LOVD) reported the *EZH2*:c.604G>A and *DNMT1*: c.4001C>T variants as VUS (Clinvar), whereas the other were not described either in Clinvar or in LOVD. In particular, the *EZH2*: c.604G>A was described as VUS for Weaver Smith Syndrome (OMIM #277590), an overgrowth syndrome characterized by accelerated skeletal maturation, characteristic facial appearance and camptodactyly. The *DNMT1*:c.4001C>T was reported as VUS for Hereditary Sensory Neuropathy-Deafness-Dementia Syndrome (OMIM #614116), a degenerative disorder of the central and peripheral nervous systems characterized by sensorineural hearing loss, cerebellar ataxia, narcolepsy and dementia.

Further evidence including functional studies will be needed to finally confirm the modulatory effect of the newly identified variants in FSHD. However, the above-discussed findings and the role of the genes in maintaining the repressive pressure on the *D4Z4* locus suggest that *CTCF*, *DNMT1*, *DNMT3A*, *EZH2* and *SUV39H1* might be further investigated as genes whose alteration contributes to the permissive (epi)genetic environment required to develop FSHD. Interestingly, the patients carrying a variant in one of the candidate genes showed variable *D4Z4* sizes, including permissive DRAs clearly falling in the FSHD1 range (n = 3), borderline/short fragments (n = 1) and 2 cases with two permissive (i.e., 4qA/4qA) alleles (namely, 5 + 12 RU and 5 + 16 RU) in the FSHD2 range. The integration of these findings with segregation analysis, methylation status, and clinical findings, provided a more comprehensive picture of the probands' and family phenotype (Table 4).

Methylation analysis in patients and family members harbouring variants in known and candidate genes was mostly consistent with affected/unaffected subjects, although family studies highlighted

10.3389/fgene.2023.1235589

TABLE 4 Clinical characterization of FSHD families harboring the variants identified by WES.

Family ID	ID patient	Sex	Age	Status	CSS	FCS	MRI pattern 1	MRI pattern 2	—
FSHD 1	A (proband)	M	39	affected	3.5	9	yes	yes	—
	B (mother)	F	74	affected	3	na	yes	yes	—
	C (brother)	M	43	unaffected	na	na	—	—	MRI na
	D (father)	M	78	unaffected	na	na	—	—	MRI na
FSHD 2	A (proband)	F	59	affected	3	4	yes	yes	—
	B (son)	M	29	unaffected	na	na	—	—	MRI na
	C (son)	M	32	unaffected	na	na	—	—	MRI na
	D (son)	M	36	affected	1	2	—	—	MRI na
	E (husband)	M	62	unaffected	0	0	—	—	MRI na
FSHD 3	A (proband)	F	58	affected	3.5	8	yes	yes	—
	B (daughter)	F	31	unaffected	0	0	no	no	Normal MRI
	C (daughter)	F	23	affected	1	2	no	no	—
	D (husband)	M	59	unaffected	0	0	—	—	MRI na
FSHD 4	A (proband)	M	58	affected	3	6	yes	Yes	
	B (son)	M	28	na	na	na	—	—	MRI na
	C (daughter)	F	27	unaffected	0	0	—	—	MRI na
FSHD 5	A (proband)	M	80	affected	4	4	yes	Yes	—
	B (daughter)	F	57	unaffected	—	—	—	—	MRI na
FSHD 6	A (proband)	F	79	affected	4	7	yes	Yes	—
	B (son)	M	51	affected	1	2	no	No	—
	C (daughter)	F	48	unaffected	0	0	—	—	MRI na
	D (husband)	M	76	unaffected	na	na	—	—	MRI na
FSHD 7	A (proband)	M	64	affected	3.5	7	—	—	UG MRI na
	B (daughter)	F	37	unaffected	na	na	—	—	MRI na
FSHD 8	A (proband)	F	27	affected	1	1	yes	no	—
FSHD 9	A (proband)	F	62	affected	4	8	yes	yes	—
FSHD 10	A (proband)	M	20	affected	1.5	3	yes	yes	—
	B (father)	M	56	na	na	na	—	—	MRI na
	C (mother)	F	49	na	na	na	—	—	MRI na
FSHD 11	A (proband)	F	75	affected	na	na	—	—	MRI na
FSHD 12	A (proband)	M	35	affected	2.5	6	yes	yes	—
FSHD 13	A (proband)	F	47	affected	3.5	na	yes	yes	—
	B (father)	M	71	na	na	na	—	—	MRI na
	C (mother)	F	68	unaffected	na	na	—	—	MRI na
FSHD 14	A (proband)	M	na	affected	3	8	yes	yes	—
	B (father)	M	50	affected	0.5	1	no	no	Normal MRI
FSHD 15	A (proband)	M	34	affected	1	2	yes	yes	—
	B (mother)	F	66	unaffected	na	na	—	—	MRI na
	C (father)	M	66	unaffected	na	na	—	—	MRI na

(Continued on following page)

TABLE 4 (*Continued*) Clinical characterization of FSHD families harboring the variants identified by WES.

Family ID	ID patient	Sex	Age	Status	CSS	FCS	MRI pattern 1	MRI pattern 2	—
FSHD 16	A (proband)	F		affected	3	na	yes	yes	—
FSHD 17	A (proband)	M		affected	na	na	—	—	MRI na
FSHD 18	A (proband)	M	56	affected	4	na	—	—	UG MRI na
FSHD 19	A (proband)	F	54	affected	4	7	—	—	UG MRI na
	B (son)	M	23	affected	1.5	na	yes	yes	—

CSS, Clinical Severity Score; FCS, FSHD Clinical Score; na, not available; UG, upper girdle; MRI pattern 1: trapezius involvement and bilateral subscapularis muscle sparing; MRI pattern 2: trapezius involvement, bilateral subscapularis and iliopsoas sparing and asymmetric involvement of upper and lower-limb muscles.

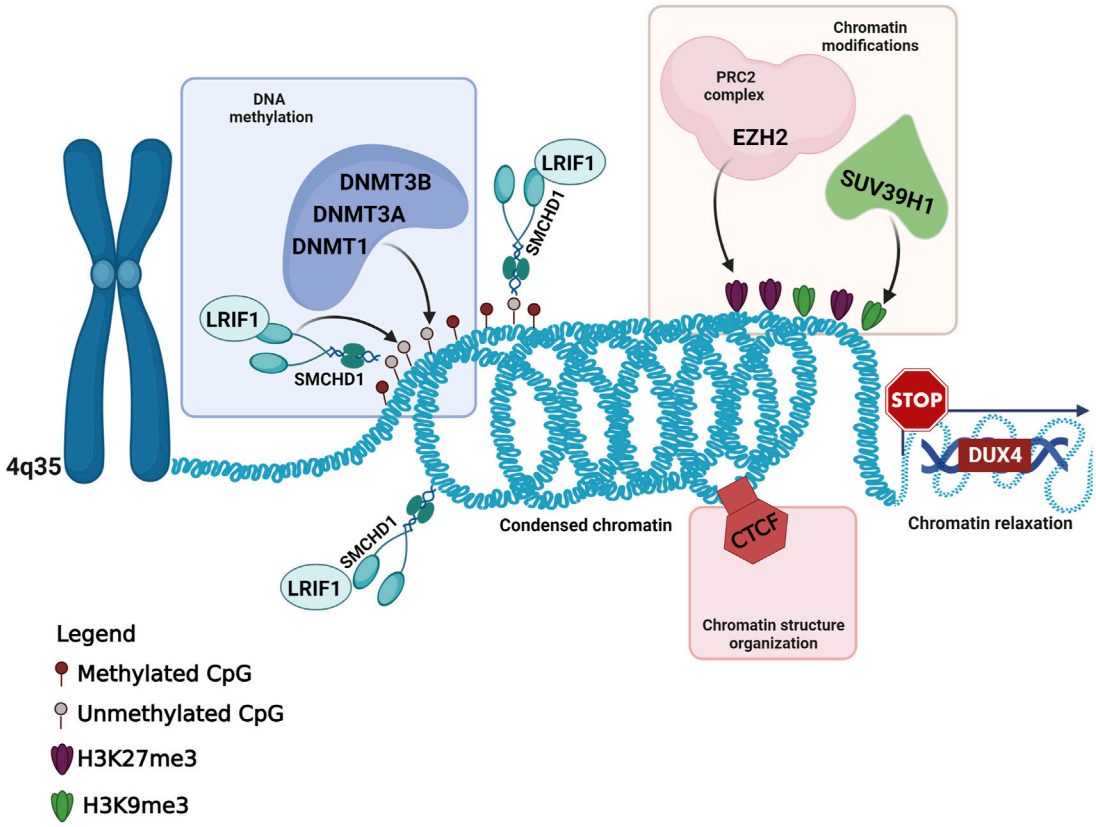

FIGURE 2
Overview of the known and candidate genes harboring the variants identified in FSHD patients and their role in the maintenance of the *DUX4*-repressive machinery. This figure has been created with Biorender.com.

reduced methylation profiles in five unaffected subjects (FSHD1C, FSHD2B, FSHD4C, FSHD6C and FSHD10C). Of note, all of them were positive to the variants segregating in the families and displayed variable *D4Z4* size, which may affect the penetrance of disease together with unknown mechanisms.

Moreover, we observed higher clinical scores together with lower methylation in *DUX4*-PAS and/or DR1 regions only in FSHD1, FSHD14 and FSHD19 families, whereas the other cases were *de novo* or we did not have enough clinical information or family member to test such a correlation. In general, methylation data appeared to be mostly associated with affected/unaffected status in this study, rather than with FSHD severity as proposed in other studies (Lemmers et al., 2015; Erdmann et al., 2022).

Overall, the variability in methylation profiles and disease severity observed in the families described in this study, could depend on several factors and patients' characteristics, including 4q configuration (*D4Z4* size, 4q genotype); the variable penetrance of DRA; age; other epigenetic modifications (such as X chromosome inactivation for the FSHD6 family harboring the variant in *SUV39H1*) and still unknown factors that altogether could contribute to the disease severity and clinical variability.

Nevertheless, the assessment of methylation status within the families proved to be a valuable tool not only for discriminating

affected subjects, but also for highlighting possible preclinical/asymptomatic conditions among members of the same family who may benefit from a clinical monitoring over time. Although the variants in candidate genes did not show a clear correlation with *D4Z4* size, methylation levels and clinical signs in the investigated patients (FSHD1C, FSHD2C, FSHD3B, FSHD3C, FSHD4C, FSHD6C), this study adds knowledge concerning the possible role of genetic features in the modulation of disease phenotype.

In conclusion, our results further support that FSHD is a complex disease, in which the presence of variations in several known (*SMCHD1*, *DNMT3B*, *LRIF1*) and possibly other genes (*CTCF*, *DNMT1*, *DNMT3A*, *EZH2*, *SUV39H1*) could influence the phenotype, penetrance and severity of disease among patients as well as within the same family. Our results further emphasize the importance of extending the analysis of molecular findings within the proband's family, with the purpose of providing a broader framework for understanding single cases and allow more accurate genotype-phenotype correlations in FSHD-affected families.

Data availability statement

The datasets presented in this article are not readily available because data obtained from whole exome sequencing are sensitive and. our ethics committee does not authorize the sharing of these data. Requests to access the datasets should be directed to the corresponding author.

Ethics statement

The studies involving humans were approved by Ethics Committee of Santa Lucia Foundation IRCCS, via Ardeatina 306, 00179, Rome. The studies were conducted in accordance with the local legislation and institutional requirements. Written informed consent for participation in this study was provided by the participants' legal guardians/next of kin. No potentially identifiable images or data are presented in this study.

Author contributions

Conceptualization: CS, VC, RC, EG, Methodology: CS, VC Formal analysis: CS, VC, DM, GT., LC Investigation: CS, VC, SB, ET, DM, GT, MM, LC Resources: CS, SB, ET, CC, ER, GT, EG, Writing-Original Draft: CS Writing-Review and Editing: CS, VC, MM, ER, GT, RC, EG, Supervision: CS, EG, Project administration: CS, EG, Funding acquisition. CS, CC, EG, All authors contributed to the article and approved the submitted version.

Funding

This research was supported by FSHD Society Research Grant #Winter 2021-0992658837 (COD:FSHD) to CS and by Ministry of Health (Ricerca Corrente) to CC.

Conflict of interest

The authors declare that the research was conducted in the absence of any commercial or financial relationships that could be construed as a potential conflict of interest.

Publisher's note

Supplementary material

The Supplementary Material for this article can be found online at: https://www.frontiersin.org/articles/10.3389/fgene.2023.1235589/full#supplementary-material

SUPPLEMENTARY TABLE S1
List of subjects included in the study. In the First Sheet ("Patient's cohort"), demographic (sex, anagraphic age), *D4Z4* size and methylation data of patients with clinical signs of FSHD have been reported. The column reporting the *D4Z4* size shows the shortest allele compatible with the disease, although patients carrying an additional permissive (i.e., 4qA) allele <20RU has also been reported. The Second sheet ("reference group") displays demographic data for the individuals employed as reference population.

SUPPLEMENTARY TABLE S2
List of genes investigated by analysis of WES data.

SUPPLEMENTARY TABLE S3
ACMG classification of identified variants in known and candidate genes for FSHD.

References

Banerji, C. R. S., Greco, A., Joosten, L. A. B., van Engelen, B., and Zammit, P. S. (2022). A circulating biomarker of facioscapulohumeral muscular dystrophy clinical severity, valid in skeletal muscle and blood. *bioRxiv*.

Banerji, C. R. S., and Zammit, P. S. (2019). PAX7 target gene repression is a superior FSHD biomarker than DUX4 target gene activation, associating with pathological severity and identifying FSHD at the single-cell level. *Hum. Mol. Genet.* 28, 2224–2236. doi:10.1093/hmg/ddz043

Barp, A., Mosca, L., and Sansone, V. A. (2021). Facilitations and hurdles of genetic testing in neuromuscular disorders. *Diagn. (Basel)* 11, 701. doi:10.3390/diagnostics11040701

Calandra, P., Cascino, I., Lemmers, R. J., Galluzzi, G., Teveroni, E., Monforte, M., et al. (2016). Allele-specific DNA hypomethylation characterises FSHD1 and FSHD2. *J. Med. Genet.* 53, 348–355. doi:10.1136/jmedgenet-2015-103436

Caputo, V., Megalizzi, D., Fabrizio, C., Termine, A., Colantoni, L., Bax, C., et al. (2022b). D4Z4 methylation levels combined with a machine learning pipeline highlight single CpG sites as discriminating biomarkers for FSHD patients. *Cells* 11, 4114. doi:10.3390/cells11244114

Caputo, V., Megalizzi, D., Fabrizio, C., Termine, A., Colantoni, L., Caltagirone, C., et al. (2022a). Update on the molecular aspects and methods underlying the complex architecture of FSHD. *Cells* 11, 2687. doi:10.3390/cells11172687

Cascella, R., Strafella, C., Caputo, V., Galota, R. M., Errichiello, V., Scutifero, M., et al. (2018). Digenic inheritance of shortened repeat units of the D4Z4 region and a loss-of-function variant in SMCHD1 in a family with FSHD. *Front. Neurol.* 9, 1027. doi:10.3389/fneur.2018.01027

Cohen, J., DeSimone, A., Lek, M., and Lek, A. (2021). Therapeutic approaches in facioscapulohumeral muscular dystrophy. *Trends Mol. Med.* 27, 123–137. doi:10.1016/j.molmed.2020.09.008

Corasolla Carregari, V., Monforte, M., Di Maio, G., Pieroni, L., Urbani, A., Ricci, E., et al. (2020). Proteomics of muscle microdialysates identifies potential circulating biomarkers in facioscapulohumeral muscular dystrophy. *Int. J. Mol. Sci.* 22, 290. doi:10.3390/ijms22010290

Deenen, J. C., Arnts, H., van der Maarel, S. M., Padberg, G. W., Verschuuren, J. J., Bakker, E., et al. (2014). Population-based incidence and prevalence of facioscapulohumeral dystrophy. *Neurology* 83, 1056–1059. doi:10.1212/WNL.0000000000000797

DeSimone, A. M., Pakula, A., Lek, A., and Emerson, C. P., Jr (2017). Facioscapulohumeral muscular dystrophy. *Compr. Physiol.* 7, 1229–1279. doi:10.1002/cphy.c160039

Ellard, S., Baple, E. L., Callaway, A., Berry, I., Forrester, N., Turnbull, C., et al. (2020). ACGS best practice guidelines for variant classification in rare disease 2020. Avaialble at: https://www.acgs.uk.com/media/11631/uk-practice-guidelines-for-variant-classification-v4-01-2020.pdf.

Erdmann, H., Scharf, F., Gehling, S., Benet-Pagès, A., Jakubiczka, S., Becker, K., et al. (2022). Methylation of the 4q35 D4Z4 repeat defines disease status in facioscapulohumeral muscular dystrophy. *Brain awac336* 146, 1388–1402. doi:10.1093/brain/awac336

Gaillard, M. C., Roche, S., Dion, C., Tasmadjian, A., Bouget, G., Salort-Campana, E., et al. (2014). Differential DNA methylation of the D4Z4 repeat in patients with FSHD and asymptomatic carriers. *Neurology* 83, 733–742. doi:10.1212/WNL.0000000000000708

Giacomucci, G., Monforte, M., Diaz-Manera, J., Mul, K., Fernandez Torrón, R., Maggi, L., et al. (2020). Deep phenotyping of facioscapulohumeral muscular dystrophy type 2 by magnetic resonance imaging. *Eur. J. Neurol.* 27, 2604–2615. doi:10.1111/ene.14446

Gould, T., Jones, T. I., and Jones, P. L. (2021). Precise epigenetic analysis using targeted bisulfite genomic sequencing distinguishes FSHD1, FSHD2, and healthy subjects. *Diagn. (Basel)* 11, 1469. doi:10.3390/diagnostics11081469

Greco, A., Goossens, R., van Engelen, B., and van der Maarel, S. M. (2020). Consequences of epigenetic derepression in facioscapulohumeral muscular dystrophy. *Clin. Genet.* 97, 799–814. doi:10.1111/cge.13726

Hamanaka, K., Šikrová, D., Mitsuhashi, S., Masuda, H., Sekiguchi, Y., Sugiyama, A., et al. (2020). Homozygous nonsense variant in LRIF1 associated with facioscapulohumeral muscular dystrophy. *Neurology* 94, e2441–e2447. doi:10.1212/WNL.0000000000009617

Hartweck, L. M., Anderson, L. J., Lemmers, R. J., Dandapat, A., Toso, E. A., Dalton, J. C., et al. (2013). A focal domain of extreme demethylation within D4Z4 in FSHD2. *Neurology* 80, 392–399. doi:10.1212/WNL.0b013e31827f075c

Haynes, P., Bomsztyk, K., and Miller, D. G. (2018). Sporadic DUX4 expression in FSHD myocytes is associated with incomplete repression by the PRC2 complex and gain of H3K9 acetylation on the contracted D4Z4 allele. *Epigenetics Chromatin* 11, 47. doi:10.1186/s13072-018-0215-z

Himeda, C. L., and Jones, P. L. (2019). The genetics and epigenetics of facioscapulohumeral muscular dystrophy. *Annu. Rev. Genomics Hum. Genet.* 20, 265–291. doi:10.1146/annurev-genom-083118-014933

Himeda, C. L., Jones, T. I., and Jones, P. L. (2015). Facioscapulohumeral muscular dystrophy as a model for epigenetic regulation and disease. *Antioxid. Redox Signal* 22, 1463–1482. doi:10.1089/ars.2014.6090

Hiramuki, Y., Kure, Y., Saito, Y., Ogawa, M., Ishikawa, K., Mori-Yoshimura, M., et al. (2022). Simultaneous measurement of the size and methylation of chromosome 4qA-D4Z4 repeats in facioscapulohumeral muscular dystrophy by long-read sequencing. *J. Transl. Med.* 20, 517. doi:10.1186/s12967-022-03743-7

Huang, H., Zhu, Q., Jussila, A., Han, Y., Bintu, B., Kern, C., et al. (2021). CTCF mediates dosage- and sequence-context-dependent transcriptional insulation by forming local chromatin domains. *Nat. Genet.* 53, 1064–1074. doi:10.1038/s41588-021-00863-6

Huichalaf, C., Micheloni, S., Ferri, G., Caccia, R., and Gabellini, D. (2014). DNA methylation analysis of the macrosatellite repeat associated with FSHD muscular dystrophy at single nucleotide level. *PLoS One* 9, e115278. doi:10.1371/journal.pone.0115278

Ioannidis, N. M., Rothstein, J. H., Pejaver, V., Middha, S., McDonnell, S. K., Baheti, S., et al. (2016). Revel: an Ensemble method for predicting the pathogenicity of rare missense variants. *Am. J. Hum. Genet.* 99, 877–885. doi:10.1016/j.ajhg.2016.08.016

Ittisoponpisan, S., Islam, S. A., Khanna, T., Alhuzimi, E., David, A., and Sternberg, M. J. E. (2019). Can predicted protein 3D structures provide reliable insights into whether missense variants are disease associated? *J. Mol. Biol.* 431, 2197–2212. doi:10.1016/j.jmb.2019.04.009

Lamperti, C., Fabbri, G., Vercelli, L., D'Amico, R., Frusciante, R., Bonifazi, E., et al. (2010). A standardized clinical evaluation of patients affected by facioscapulohumeral muscular dystrophy: the FSHD clinical score. *Muscle Nerve* 42, 213–217. doi:10.1002/mus.21671

Laskowski, R. A., Stephenson, J. D., Sillitoe, I., Orengo, C. A., and Thornton, J. M. (2020). VarSite: disease variants and protein structure. *Protein Sci.* 29, 111–119. doi:10.1002/pro.3746

Lemmers, R. J., Goeman, J. J., van der Vliet, P. J., van Nieuwenhuizen, M. P., Balog, J., Vos-Versteeg, M., et al. (2015). Inter-individual differences in CpG methylation at D4Z4 correlate with clinical variability in FSHD1 and FSHD2. *Hum. Mol. Genet.* 24, 659–669. doi:10.1093/hmg/ddu486

Lemmers, R. J., Tawil, R., Petek, L. M., Balog, J., Block, G. J., Santen, G. W., et al. (2012). Digenic inheritance of an SMCHD1 mutation and an FSHD-permissive D4Z4 allele causes facioscapulohumeral muscular dystrophy type 2. *Nat. Genet.* 44 (12), 1370–1374. doi:10.1038/ng.2454

Lemmers, R. J., van der Vliet, P. J., van der Gaag, K. J., Zuniga, S., Frants, R. R., de Knijff, P., et al. (2010). Worldwide population analysis of the 4q and 10q subtelomeres identifies only four discrete interchromosomal sequence transfers in human evolution. *Am. J. Hum. Genet.* 86, 364–377. doi:10.1016/j.ajhg.2010.01.035

Lemmers, R. J. L. F., van der Stoep, N., Vliet, P. J. V., Moore, S. A., San Leon Granado, D., Johnson, K., et al. (2019). SMCHD1 mutation spectrum for facioscapulohumeral muscular dystrophy type 2 (FSHD2) and Bosma arhinia microphthalmia syndrome (BAMS) reveals disease-specific localisation of variants in the ATPase domain. *J. Med. Genet.* 56, 693–700. doi:10.1136/jmedgenet-2019-106168

Monforte, M., Bortolani, S., Torchia, E., Cristiano, L., Laschena, F., Tartaglione, T., et al. (2022). Diagnostic magnetic resonance imaging biomarkers for facioscapulohumeral muscular dystrophy identified by machine learning. *J. Neurol.* 269, 2055–2063. doi:10.1007/s00415-021-10786-1

Mostacciuolo, M. L., Pastorello, E., Vazza, G., Miorin, M., Angelini, C., Tomelleri, G., et al. (2009). Facioscapulohumeral muscular dystrophy: epidemiological and molecular study in a north-east Italian population sample. *Clin. Genet.* 75, 550–555. doi:10.1111/j.1399-0004.2009.01158.x

Mul, K., Voermans, N. C., Lemmers, R. J. L. F., Jonker, M. A., van der Vliet, P. J., Padberg, G. W., et al. (2018). Phenotype-genotype relations in facioscapulohumeral muscular dystrophy type 1. *Clin. Genet.* 94, 521–527. doi:10.1111/cge.13446

Neguembor, M. V., and Gabellini, D. (2010). In junk we trust: repetitive DNA, epigenetics and facioscapulohumeral muscular dystrophy. *Epigenomics* 2, 271–287. doi:10.2217/epi.10.8

Ottaviani, A., Rival-Gervier, S., Boussouar, A., Foerster, A. M., Rondier, D., Sacconi, S., et al. (2009). The D4Z4 macrosatellite repeat acts as a CTCF and A-type lamins-dependent insulator in facio-scapulo-humeral dystrophy. *PLoS Genet.* 5, e1000394. doi:10.1371/journal.pgen.1000394

Pejaver, V., Byrne, A. B., Feng, B. J., Pagel, K. A., Mooney, S. D., Karchin, R., et al. (2022). Calibration of computational tools for missense variant pathogenicity classification and ClinGen recommendations for PP3/BP4 criteria. *Am. J. Hum. Genet.* 109, 2163–2177. doi:10.1016/j.ajhg.2022.10.013

Preston, M. K., Tawil, R., and Wang, L. H. (2020). "Facioscapulohumeral muscular dystrophy," in *GeneReviews® [internet]*. Editors M. P. Adam, D. B. Everman, G. M. Mirzaa, R. A. Pagon, S. E. Wallace, L. J. H. Bean, et al. (Seattle (WA): University of Washington, Seattle), 1993–2022.

Ricci, E., Galluzzi, G., Deidda, G., Cacurri, S., Colantoni, L., Merico, B., et al. (1999). Progress in the molecular diagnosis of facioscapulohumeral muscular dystrophy and correlation between the number of KpnI repeats at the 4q35 locus and clinical phenotype. *Ann. Neurol.* 45, 751–757. doi:10.1002/1531-8249(199906)45:6<751::aid-ana9>3.0.co;2-m

Ricci, G., Mele, F., Govi, M., Ruggiero, L., Sera, F., Vercelli, L., et al. (2020). Large genotype-phenotype study in carriers of D4Z4 borderline alleles provides guidance for facioscapulohumeral muscular dystrophy diagnosis. *Sci. Rep.* 10, 21648. doi:10.1038/s41598-020-78578-7

Richards, S., Aziz, N., Bale, S., Bick, D., Das, S., Gastier-Foster, J., et al. (2015). Standards and guidelines for the interpretation of sequence variants: A joint consensus recommendation of the American college of medical genetics and genomics and the association for molecular pathology. *Genet. Med.* 17, 405–424. doi:10.1038/gim.2015.30

Roche, S., Dion, C., Broucqsault, N., Laberthonnière, C., Gaillard, M. C., Robin, J. D., et al. (2019). Methylation hotspots evidenced by deep sequencing in patients with facioscapulohumeral dystrophy and mosaicism. *Neurol. Genet.* 5, e372. doi:10.1212/NXG.0000000000000372

Sacconi, S., Briand-Suleau, A., Gros, M., Baudoin, C., Lemmers, R. J. L. F., Rondeau, S., et al. (2019). FSHD1 and FSHD2 form a disease continuum. *Neurology* 92, e2273–e2285. doi:10.1212/WNL.0000000000007456

Scionti, I., Greco, F., Ricci, G., Govi, M., Arashiro, P., Vercelli, L., et al. (2012). Large-scale population analysis challenges the current criteria for the molecular diagnosis of fascioscapulohumeral muscular dystrophy. *Am. J. Hum. Genet.* 90, 628–635. doi:10.1016/j.ajhg.2012.02.019

Strafella, C., Caputo, V., Galota, R. M., Campoli, G., Bax, C., Colantoni, L., et al. (2019). The variability of SMCHD1 gene in FSHD patients: evidence of new mutations. *Hum. Mol. Genet.* 28, 3912–3920. doi:10.1093/hmg/ddz239

Tasca, G., Monforte, M., Iannaccone, E., Laschena, F., Ottaviani, P., Leoncini, E., et al. (2014). Upper girdle imaging in facioscapulohumeral muscular dystrophy. *PLoS One* 9, e100292. doi:10.1371/journal.pone.0100292

Tasca, G., Monforte, M., Ottaviani, P., Pelliccioni, M., Frusciante, R., Laschena, F., et al. (2016). Magnetic resonance imaging in a large cohort of facioscapulohumeral

muscular dystrophy patients: pattern refinement and implications for clinical trials. *Ann. Neurol.* 79, 854–864. doi:10.1002/ana.24640

van den Boogaard, M. L., Lemmers, R. J. L. F., Balog, J., Wohlgemuth, M., Auranen, M., Mitsuhashi, S., et al. (2016). Mutations in DNMT3B modify epigenetic repression of the D4Z4 repeat and the penetrance of facioscapulohumeral dystrophy. *Am. J. Hum. Genet.* 98, 1020–1029. doi:10.1016/j.ajhg.2016.03.013

Wijmenga, C., Hewitt, J. E., Sandkuijl, L. A., Clark, L. N., Wright, T. J., Dauwerse, H. G., et al. (1992). Chromosome 4q DNA rearrangements associated with facioscapulohumeral muscular dystrophy. *Nat. Genet.* 2, 26–30. doi:10.1038/ng0992-26

Wong, C. J., Wang, L. H., Friedman, S. D., Shaw, D., Campbell, A. E., Budech, C. B., et al. (2020). Longitudinal measures of RNA expression and disease activity in FSHD muscle biopsies. *Hum. Mol. Genet.* 29, 1030–1043. doi:10.1093/hmg/ddaa031

Xu, D., Ma, R., Zhang, J., Liu, Z., Wu, B., Peng, J., et al. (2018). Dynamic nature of CTCF tandem 11 Zinc fingers in multivalent recognition of DNA as revealed by NMR spectroscopy. *J. Phys. Chem. Lett.* 9, 4020–4028. doi:10.1021/acs.jpclett.8b01440

Yin, M., Wang, J., Wang, M., Li, X., Zhang, M., Wu, Q., et al. (2017). Molecular mechanism of directional CTCF recognition of a diverse range of genomic sites. *Cell. Res.* 27, 1365–1377. doi:10.1038/cr.2017.131

Zampatti, S., Colantoni, L., Strafella, C., Galota, R. M., Caputo, V., Campoli, G., et al. (2019). Facioscapulohumeral muscular dystrophy (FSHD) molecular diagnosis: from traditional technology to the NGS era. *Neurogenetics* 20, 57–64. doi:10.1007/s10048-019-00575-4

Zeng, W., Chen, Y. Y., Newkirk, D. A., Wu, B., Balog, J., Kong, X., et al. (2014). Genetic and epigenetic characteristics of FSHD-associated 4q and 10q D4Z4 that are distinct from non-4q/10q D4Z4 homologs. *Hum. Mutat.* 35, 998–1010. doi:10.1002/humu.22593

Zeng, W., de Greef, J. C., Chen, Y. Y., Chien, R., Kong, X., Gregson, H. C., et al. (2009). Specific loss of histone H3 lysine 9 trimethylation and HP1gamma/cohesin binding at D4Z4 repeats is associated with facioscapulohumeral dystrophy (FSHD). *PLoS Genet.* 5, e1000559. doi:10.1371/journal.pgen.1000559

Zheng, F., Qiu, L., Chen, L., Zheng, Y., Lin, X., He, J., et al. (2023). Association of 4qA-specific distal D4Z4 hypomethylation with disease severity and progression in facioscapulohumeral muscular dystrophy. *Neurology* 24, e225–e237. doi:10.1212/WNL.0000000000207418

frontiers | Frontiers in Genetics

TYPE Original Research
PUBLISHED 06 February 2024
DOI 10.3389/fgene.2024.1197151

OPEN ACCESS

EDITED BY
Jordi Pérez-Tur,
Spanish National Research Council (CSIC), Spain

REVIEWED BY
Xiaoping Luo,
Huazhong University of Science and Technology, China
Fazli Rabbi Awan,
National Institute for Biotechnology and Genetic Engineering, Pakistan

*CORRESPONDENCE
Hunjin Luo,
490824805@qq.com

RECEIVED 30 March 2023
ACCEPTED 19 January 2024
PUBLISHED 06 February 2024

CITATION
Luo H, Wang J, Chen J, Yi H, Yang X, Peng Y, Ni L, Yang Y-Q, Zhang X-M and Huang H (2024), Prevalence of inherited metabolic disorders among newborns in Zhuzhou, a southern city in China.
Front. Genet. 15:1197151.
doi: 10.3389/fgene.2024.1197151

Prevalence of inherited metabolic disorders among newborns in Zhuzhou, a southern city in China

Hunjin Luo*, Jiqing Wang, Junfeng Chen, Huijian Yi, Xiaodong Yang, Yao Peng, Liu Ni, Yi-Qiong Yang, Xiao-Min Zhang and Hongping Huang

Women and Children Healthcare Hospital of Zhuzhou, Zhuzhou, Hunan, China

Background and aims: Defective enzymes, cofactors, or transporters of metabolic pathways cause inherited metabolic disorders (IMDs), a group of genetic disorders. Several IMDs have serious consequences for the affected neonates. Newborn screening for IMDs is conducted by measuring specific metabolites between 3 and 7 days of life. Herein, we analyzed the incidence, spectrum, and genetic characteristics of IMDs in newborns in the Zhuzhou area.

Methods: Tandem mass spectrometry was conducted on 90,829 newborns who were admitted to the Women and Children Healthcare Hospital of Zhuzhou and requested for screening for IMDs. These newborns were subsequently subjected to next-generation sequencing and further validated using Sanger sequencing.

Results: 30 IMDs cases were found in 90,829 cases of newborns screened for IMDs, and the overall incidence was 1/3,027. The incidence of amino acid, organic acid, fatty acid oxidation and urea cycle disorders were 1/8,257, 1/18,165, 1/7,569, and 1/45,414, respectively. Additionally, 9 cases of maternal IMDs were found in our study, and unreported gene mutations of 3 cases IMDs were identified.

Conclusion: Our data indicated that IMDs are never uncommon in zhuzhou, meanwhile, we also found that primary carnitine deficiency was the only disorder of fatty acid oxidation in Zhuzhou, and the incidence (1/7,569) was higher than the national level, organic acid metabolic diseases are mostly inherited. Therefore, our study has clarified the disease spectrum and genetic backgrounds, contributing to the treatment and prenatal genetic counseling of these disorders in this region.

KEYWORDS

inherited metabolic disorders, neonates, metabolites, tandem mass spectrometry, sanger sequencing, next-generation sequencing

1 Introduction

Defects in enzymes, cofactors, or transporters of metabolic pathways cause inherited metabolic disorders (IMDs), a group of genetic disorders (Scala et al., 2012; Scaturro et al., 2013). Several IMDs have serious consequences in affected neonates, including drowsiness, irreversible intellectual disability, physical disability, coma, and even death (Saudubray et al., 2002; Wasant et al., 2002). The genealogy and incidence of genetic metabolic diseases vary greatly among different regions and ethnic groups (Chace et al., 2003). Mass spectrometry is characterized by high throughput, efficiency, and sensitivity, and can

simultaneously detect several metabolites (Millington et al., 1990; Rinaldo et al., 2006; Fernandez-Lainez et al., 2012). It is widely used in screening neonatal genetic metabolic diseases and is crucial in the early diagnosis of amino acid metabolic (Wilcken et al., 2003; Shi et al., 2012), organic acid metabolic, and fatty acid oxidation diseases. Tandem mass spectrometry (MS/MS)-based NBS was launched in 2004 in China, and the average incidence of IMDs in a preliminary study was 1/3,795 (Shi et al., 2012). In recent years, proteomics has been applied to the study of IMDs, and tandem mass spectrometry (MS/MS) technology has made key advances achieved in this field. This technology enables the analysis of large numbers of proteins in different body fluids (serum, plasma, urine, saliva, tears) with a single analysis of each sample, and can even be applied to dried samples (Chantada-Vazquez et al., 2022). Meanwhile, with the introduction of next-generation sequencing (NGS) for newborn screening (NBS), more inherited metabolic disorders (IMDs) can technically be included (Veldman et al., 2023). In this study, we retrospectively analyzed the screening results of various genetic metabolic diseases of 90,829 neonates born in Women and Children Healthcare Hospital of Zhuzhou from 2019 to 2022 based on 4 years of experience in MS/MS to understand the disease spectrum, incidence, and clinical phenotype characteristics of amino acid metabolic, organic acid metabolic, and fatty acid oxidation diseases.

2 Materials and methods

2.1 Newborns

From 2019 to 2022, 90,829 newborns born in the Women and Children Healthcare Hospital of Zhuzhou were screened for various genetic metabolic diseases using MS/MS. Written informed consent was obtained from all the guardians of the infants. This study was approved by the Women and Children Healthcare Hospital of Zhuzhou (ZZFY2022IRB06).

2.2 Reagents and instruments

The NeoBase™ nonderivatized MS/MS kit is a product of the PerkinElmer Company, and the series mass spectrometry analysis system (ACQUITY TQD) is a product of the Waters Company. The cutoff values were initially set with reference to the worldwide collaborative project and other screening centers (Niu et al., 2010), and as the number of samples increased, they were adjusted over time.

2.3 Sample collection, receiving, and MS/MS

Blood samples were collected using a heelstick and spotted on Whatman 903 filter paper. Blood collection for NBS is recommended between 3 and 7 days of life. Dried blood spot (DBS) samples were delivered using cold-chain transportation to the Women and Children Healthcare Hospital of Zhuzhou within 5 days. The DBSs with a diameter of 3.2 mm were collected using an automatic drilling instrument, and the amino acids, free carnitines, and 30 acylcarnitines in the DBSs were analyzed using the NeoBase™ nonderivative kit and MS/MS system (Waters-ACQUITY TQD). The internal standards of 12 amino acids and 8 acylcarnitines were used. The cut-off values were initially set with reference to the worldwide collaborative project and other screening centers. Meanwhile, the screening indicators and their positive cut-off values were set according to the disease characteristics and were adjusted over time as the number of samples increased. Furthermore, retrospective revisions were annually made. Newborns with the results of clear aberrant initial screening were immediately referred for confirmatory tests, including biochemical and genetic analyses, and newborns with the results of mild initial screening were recalled for repeated tests. If the second test was still positive, the patient was referred for confirmatory tests.

2.4 Genetic analysis

Genetic analysis was performed in the Genuine Diagnostics Company (Guangzhou, Guangdong, China). Briefly, the Sanger–Cusson method was used to sequence the exons and adjacent introns for positive cases of a certain disease. DBSs were used for whole-exome high-throughput sequencing for cases of multiple diseases corresponding to the same screening indicators, and the Sanger–Cusson method was used to verify the positive sites. The PubMed database, Human Gene Mutation Database (HGMD), ClinVar, OMIM database, and the 2020 edition of ACMG guidelines were searched to identify the pathogenic mutations.

2.5 Diagnosis

Metabolic disease specialists made the definitive diagnoses based on the patients' biochemical performance, genetic mutations, and clinical symptoms. Only patients diagnosed using genetic analysis were included in this study.

2.6 Statistical analysis

For cost calculation, the disease incidence rates were obtained from the NBS Management Information System, which covered all medical procedures for each NBS participant. Eleven diseases were diagnosed in 90,829 newborns who underwent MS/MS screening.

3 Results

3.1 Screening results of IMDs in 90,829 newborns

In total, 90,829 newborns were included in this study. A total of 1,089 suspected positive cases were screened using MS/MS, and the initial screening positivity rate was 1.199%. A total of 1,067 cases (97.9%) were successfully recalled, and the biochemical and gene

TABLE 1 Positive cases detected by MS/MS newborn screening.

Disorders	Positive cases	Frequency
Amino acid disorders	11(36.6%)	1/8,257
Phenylalanine hydroxylase deficiency (PAHD)	5	
Citrin deficiency (CD)	4	
Homocysteinemia (HCY)	1	
Hypermethioninemia (MET)	1	
Organic acid disorders	5(16.6%)	1/18,165
Short/branched chain acyl-CoA dehydrogenase deficiency (SCADD)	1	
Methylmalonic academia (MMA)	1	
Middle/branched chain acyl-CoA dehydrogenase deficiency (MCADD)	1	
Holocarboxylase synthetase deficiency (HCSD)	1	
Glutaric acidemia type I (GA-I)	1	
Fatty acid oxidation disorders	12(40%)	1/7,569
Primary carnitine deficiency (PCD)	12	
Urea cycle disorders	2(6.6%)	1/45,414
Ornithine transcarbamylase deficiency (OTCD)	2	
Total numbers	30	1/3,027

TABLE 2 Biochemical and genetic characteristics of nine patients with maternal disorders.

No.	Disorders	Abnormal parameter and concentration (μmol/L)	Affected gene	Genotype	
1	Primary carnitine deficiency (PCD)	C0: 3.56	SLC22A5	c.1400C>G (p.S467C)	c.1400C>G (p.S467C)
2	Primary carnitine deficiency (PCD)	C0: 4.37	SLC22A5	c.760C>T (p.R254*)	c.1400C>G (p.S467C)
3	Phenylalanine hydroxylase deficiency (PAHD)	Phe: 767.32 Phe/Tyr: 12.23	PTS	c.259C>T (p.P87S)	c.259C>T (p.P87S)
4	Phenylalanine hydroxylase deficiency (PAHD)	Phe: 428.95; Phe/Tyr:8.03	PAH	c.728G>A (p.R243Q)	c.728G>A (p.R243Q)
5	Phenylalanine hydroxylase deficiency (PAHD)	Phe: 311.25; Phe/Tyr: 6.23	PAH	c.728G>A (p.R243Q)	c.1174T>A (p.F392I)
6	Homocysteinemia (HCY)	Met:269.39	CBS	c.377T>C (p.M126T)	c.526G>A (p.E176K)
7	Hypermethioninemia (MET)	Met:217	MAT1A	c.433G>A (p.E145K)	c.529C>T (p.R177W)
8	Glutaric acidemia type I (GA-I)	C5DC + C6OH: 5.58	GCDH	c.416C>T (p.S139L)	c.892G>A (p.A298T)
9	Holocarboxylase synthetase deficiency (HCSD)	C5OH + C4DC: 1.56	HLCS	c.1522C>T (p.R508W)	c.1544G>A(p.S515)

sequencing results were combined to finally diagnose 30 IMD cases (Table 1), with a positive predictive value of 2.7%. Eleven IMD types were detected in 30 confirmed cases, with 1/3,027 as the overall IMD detection rate. Eleven, five, and twelve patients with amino acid (36.6%), organic acid (16.6%), and fatty acid oxidation (40%) disorders, respectively, were found. The incidences of amino acid metabolism, organic acid metabolism, and fatty acid oxidation metabolism disorders were 1/8,257, 1/18,165, and 1/7,569, respectively. Additionally, nine patients with maternal diseases were identified using our MS/MS NBS system (Table 2).

TABLE 3 Levels of abnormal parameters for different disorders of amino acid metabolism.

Amino acidemias (n = 11)	n (%)	Abnormal parameter	Concentration mean (μmol/L)	References range (μmol/L)
Phenylalanine hydroxylase deficiency (PAHD)	5 (45.4)	Phe	311.25/323.45/328.23/348.65/767.32	23–95
		Phe/Tyr	6.23/6.78/6.98/8.03/12.23	0.2–1.4
Citrin deficiency (CD)	4 (36.3)	Cit	41.19/56.53/57.32/93.53/	5.5–28
		Cit/Arg	3.23/4.44/4.45/9.56	0.35–15
Homocysteinemia (HCY)	1 (9)	Met	269.39	6.5–38
		Met/Phe	8.72	0.1–0.7
hypermethioninemia (MET)	1 (9)	Met	217	6.5–38
		Met/Phe	3.48	0.1–0.7

TABLE 4 Levels of abnormal parameters for different organic acid disorders.

Organic acidemias (n = 5)	n (%)	Abnormal parameter	Concentration mean (μmol/L)	References range (μmol/L)
Short/branched chain acyl-CoA dehydrogenase deficiency (SCADD)	1 (20)	C4	1.34	0.03–0.48
		C4/C2	0.06	0.004–0.04
		C4/C3	0.77	0.04–0.4
Methylmalonic academia (MMA)	1 (20)	C3	7.44	0.35–3.8
		C3/C0	0.41	0.01–0.2
		C3/C2	0.62	0.03–0.2
Middle/branched chain acyl-CoA dehydrogenase deficiency (MCADD)	1 (20)	C6	0.47	0.03–0.35
		C8	10.88	0.02–0.15
		C6DC	0.95	0.03–0.25
Holocarboxylase synthetase deficiency (HCSD)	1 (20)	C5OH + C4DC	1.56	0.07–0.37
Glutaric acidemia type I (GA-I)	1 (20)	C5DC + C6OH	5.58	0.03–0.24

3.2 Results of amino acid disorders

Four types of amino acid metabolic disorders (Phenylalanine hydroxylase deficiency (PAHD), citrin deficiency (CD), Hypermethioninemia (MET), and homocysteinemia (HCY) were detected, and PAHD deficiency was the most common (45.4%), followed by citrin deficiency (36.3%). Only one MET case (9%) and one HCY case (9%) were found. Among these cases, the phenylalanine concentration and phenylalanine/tyrosine ratio in patients with BH4D were significantly higher than those in patients with PAHD. Methionine concentrations in patients with MET and HCY were 217 and 269.39 μmol/L, respectively, which were higher than the reference range (reference range: 6.5–38 μmol/L) (Table3). The main mutations in the *PAH* gene of PAHD were c.728G>A (p.R243Q), c. 1,174> (p.F392I), c.259C>T (p.P87S), c.728G > A (p.R243Q), and c.433G > A c. C (p.S2R), and the mutations in the *CBS* gene of HCY were c.377T>C (p.M126T) and c.526G>A; (E176k). The mutations in the *MAT1A* gene of MET were c.433G>A (p.E145K) and c.529C>T; R177W). Four patients with CD had four different mutations in the *SLC25A13* gene.

3.3 Organic acid disorders and no reported gene mutations

Five types of organic acid disorders were detected in Zhuzhou: short-chain acyl-CoA dehydrogenase deficiency (SCADD), methylmalonic cademia (MMA), middle/branched chain acyl-CoA dehydrogenase deficiency (MCADD), holocarboxylase synthetase deficiency (HCSD), and type I glutaric cademia (GA-I) (Table 4). The incidence rate was 1/18,165, which was relatively low. Preliminary NBS results showed that C4 concentration with SCADD was slightly increased; the C4/C2 and C4/C3 ratios were higher than the normal range; C6, C8, and C6DC concentrations with MCADD was increased; the C5 concentration of MMA was high; and the C3/C0 and C3/C2 ratios were beyond the normal range

TABLE 5 Identification three novels mutation in disorders of amino acid metabolism and organic acid disorders.

Disorders	Affected gene	Genotype	Reported
Short/branched chain acyl-CoA dehydrogenasedeficiency (SCADD)	ACADM	c.893G>A(p.R298K)	No reported
		c.1097G>A (p.G366E)	reported
Middle/branched chain acyl-CoA dehydrogenase deficiency (MCADD)	ACADS	c.482G>A(p.S161N)	No reported
		c.1031A>G (p.E344G)	reported
Holocarboxylase synthetase deficiency (HCSD)	HLCS	c.1544G>A(p.S515)	No reported
		c.1522C>T (p.R508W)	reported

TABLE 6 Levels of abnormal parameters for different disorders of fatty acid oxidation disorders and Urea cycle disorders.

Fatty acid oxidation disorders and urea cycle disorders (n = 14)	n (%)	Abnormal parameter	Concentration mean (range) (μmol/L)	References range (μmol/L)
Primary carnitine deficiency (PCD)	12 (85.7)	C0	4.72 (3.56–7.94)	9–50
Ornithine transcarbamylase deficiency (OTCD)	2 (14.3)	Cit	1.4/1.6	5.5–28
		Orn/Cit	43.94/50.21	2.5–20

(Table 4). Ten different mutations in five genes (*GCDH*, *ACADM*, *ACADS*, *HLCS*, and *MMACHC*) were identified in the five patients with organic acid disorders. Notably, the three mutations (c.893G>A (p.R298K), c.482G>A (p.S161N), and c.1544G>A (p.S515)) of three of the genes (*ACADM*, *ACADS*, and *HLCS*) were not reported (Table 5). Additionally, mutations in two (*ACADM* and *ACADS*) of the five organic acid disorders were paternally inherited, whereas mutations in the other two diseases (HLCS and GA-I) were maternally inherited.

3.4 Fatty acid oxidation disorders (FAODs) and urea cycle disorder

Only one type of fatty acid metabolic disease–primary carnitine deficiency (PCD)–was diagnosed in Zhuzhou. Twelve patients were diagnosed with a 1/7,569 incidence rate. All infants diagnosed with PCD had low free carnitine levels, with an average C0 of approximately 4.72 (Table 6). Mutations in the *SLC22A5* gene were identified in 12 cases of neonatal PCD. The most common mutation was c.1400C>T (p.S467C), followed by c.760C>T (p.R254X), c.51C>G (p.F17L), and c.797C>T (p.P266L). Additionally, two cases of urea cycle disorders (ornithine transcarbamylase deficiency) were detected. Both patients had low citrulline levels and their Orn/Cit ratios were higher than the normal range (Table 6).

4 Discussion

MS/MS has become the main means to expand the screening of newborn IMDs. It can screen 40 to 50 disease types, including amino acid metabolism, organic acid metabolism, and fatty acid oxidation disorders (Schulze et al., 1999; Lindner et al., 2011; Ombrone et al., 2016). Newborn screening is an effective disease prevention measure, which can prevent children's intellectual disability and improve the quality of the birth population (Chace et al., 1999; American College of Medical Genetics Newborn Screening Expert, 2006). The data used in this study were obtained from the counties and districts of the city, covering the city's urban and suburban towns. From 2019 to 2022, 90,829 newborns were screened for 48 IMDs using MS/MS, and 11 diseases of four types (amino acid metabolic, organic acid, fatty acid oxidation, and urea cycle disorders) were detected. The total incidence rate was approximately 1/3,027. The incidence rates of neonatal amino acid metabolic, organic acid metabolic, and fatty acid oxidation diseases were approximately 1/11,831, 1/16,007, and 1/6,977, respectively. China is a large population, and according to the overall incidence of neonatal IMDs published by the state, about 3,000 patients accumulate every year. If these children are diagnosed and treated promptly, intellectual disability can be avoided. This has significant social and economic benefits.

The incidence rate of amino acid disorders in our study was lower (1/8,257) than that in Germany (26.3/100,000), the United Kingdom (26.7/100,000), and China (17.1/100,000) (Sanderson et al., 2006; Huang et al., 2022) and was even lower than that in neighboring Guangzhou (1/11,831) (Tang et al., 2021). Four amino acid disorders types were detected in our study, and PAHD accounted for the highest proportion of amino acid metabolic diseases. Some were mild cases, indicating that the incidence rate of amino acid metabolic diseases in this region is relatively low. In the future, primary prevention is expected to reduce such diseases to a lower level to improve the quality of the birth population.

Five types of organic acid metabolic diseases (short/branched chain acyl-CoA dehydrogenase deficiency (SCADD), methylmalonic cademia (MMA), middle/branched chain acyl-CoA dehydrogenase deficiency (MCADD), holocarboxylase synthetase (HCSD), and glutaric cademia type I (GA-I) were detected. The incidence of organic acid metabolic diseases in our

study was 1/18,165, which was lower than the national average (1/8,071) (Deng et al., 2021). Notably, this study reported three unreported mutations in three genes (*ACADM*, *ACADS*, and *HLCS*) [c.893G>A (p.R298K), c.482G>A (p.S161N), and c.1544G>A (p.S515)] (Table 5) The three genes were derived from three diseases (SCADD, MCADD, and HCSD), and all of them were compound heterozygous mutations. These newly discovered mutations are convenient for providing further genetic counseling and enriching the database information of organic acid metabolism diseases. Most of the five diseases were inherited from parents. The results of this study suggest that although the incidence of organic acid metabolic diseases is low in this region, the proportion of people carrying the gene mutations for organic acid metabolic diseases is relatively high.

The combined FAOD incidence is 1/9,300 in reports from Australia, Germany, and the United States; however, it is rarely identified in Asian countries. In this study, the incidence of FAOD was 1/7,569. This was higher than that in Zhejiang Province (1/32,354) (Huang et al., 2011), Suzhou City (1/10,041) (Luo et al., 2018), Shanxi Province (1/9,015) (Dai et al., 2021) and the national average level of 1/10,917 (Lindner et al., 2010; Deng et al., 2021; Pereira et al., 2021). Furthermore, only one fatty acid metabolic disease was found in this region. The common gene mutations was *SLC22A5* c.1400C>G (p.S467C), with 90% of patients with PCD having this gene mutation, of which two patients maternally inherited PCD. Notably, the incidence of fatty acid metabolism in the Zhuzhou area was higher than that in other areas, and only one disease (PCD) was found, and its incidence is much higher than that of the Chinese population. This suggests a regionally high incidence of IMDs in this area.

Thus, by analyzing the screening and genetic diagnosis results of 90,829 newborns with IMDs in Zhuzhou, the disease spectrum, incidence, and clinical phenotype characteristics of amino acid metabolic, organic acid, and fatty acid oxidation disorders in newborns were determined. However, this study provides a different perspective. The incidence of fatty acid oxidation disorders in the Zhuzhou was relatively high, and the incidence of PCD was higher than that of other IMDs, suggesting a high regional incidence of fatty acid oxidation disorders in this area. The prevalence of organic acid metabolic diseases is high, and most patients with organic acid metabolism are inherited from their parents. Scientifically screening and diagnosing IMD the cases using biochemical methods and second-generation sequencing are required to achieve early screening and diagnosis and to provide strong support for reducing neonatal birth defects.

5 Conclusion

We have provided the most comprehensive mutation spectrum for IMDs. Additionally, we provided intensive genetic counseling and methods for early diagnosis and treatment. Our study may provide a baseline for genetic counseling, public education, and a reference for improving the prevention of IMDs.

Data availability statement

The original contributions presented in the study are included in the article/Supplementary Material, further inquiries can be directed to the corresponding author.

Ethics statement

Written informed consents were obtained from all the infants' parents. This study was approved by Women and Children Healthcare Hospital of Zhuzhou (ZZFY2022IRB06).

Author contributions

HL and JW conceived and designed the study. HY and XY performed MS/MS for newborn screening and were responsible for recall; JC and LN conducted clinical genetic counseling and diagnosis; and Y-QY and YP conducted genetic detection. HH and X-MZ contributed to tracking the research objects. HL provided written guidance and corrections. All authors contributed to the article and approved the submitted version.

Acknowledgments

We are grateful to all the participants of this study and we thank X-MZ for his kind assistance with manuscript preparation. We would like to thank Editage (www.editage.com) for English language editing.

Conflict of interest

The authors declare that the research was conducted in the absence of any commercial or financial relationships that could be construed as a potential conflict of interest.

Publisher's note

Supplementary material

The Supplementary Material for this article can be found online at: https://www.frontiersin.org/articles/10.3389/fgene.2024.1197151/full#supplementary-material

References

American College of Medical Genetics Newborn Screening Expert, G. (2006). Newborn screening: toward a uniform screening panel and system--executive summary. *Pediatrics* 117, S296–S307. doi:10.1542/peds.2005-2633I

Chace, D. H., Diperna, J. C., and Naylor, E. W. (1999). Laboratory integration and utilization of tandem mass spectrometry in neonatal screening: a model for clinical mass spectrometry in the next millennium. *Acta Paediatr. Suppl.* 88, 45–47. doi:10.1111/j.1651-2227.1999.tb01156.x

Chace, D. H., Kalas, T. A., and Naylor, E. W. (2003). Use of tandem mass spectrometry for multianalyte screening of dried blood specimens from newborns. *Clin. Chem.* 49, 1797–1817. doi:10.1373/clinchem.2003.022178

Chantada-Vazquez, M. D. P., Bravo, S. B., Barbosa-Gouveia, S., Alvarez, J. V., and Couce, M. L. (2022). Proteomics in inherited metabolic disorders. *Int. J. Mol. Sci.* 23, 14744. doi:10.3390/ijms232314744

Dai, W., Yang, T., Wang, Y., Zhao, Q., Zhan, Y., Ye, J., et al. (2021). Rapid detection of twenty-nine common Chinese glucose-6-phosphate dehydrogenase variants using a matrix-assisted laser desorption/ionization-time of flight mass spectrometry assay on dried blood spots. *Clin. Biochem.* 94, 27–34. doi:10.1016/j.clinbiochem.2021.04.012

Deng, K., Zhu, J., Yu, E., Xiang, L., Yuan, X., Yao, Y., et al. (2021). Incidence of inborn errors of metabolism detected by tandem mass spectrometry in China: a census of over seven million newborns between 2016 and 2017. *J. Med. Screen* 28, 223–229. doi:10.1177/0969141320973690

Fernandez-Lainez, C., Aguilar-Lemus, J. J., Vela-Amieva, M., and Ibarra-Gonzalez, I. (2012). Tandem mass spectrometry newborn screening for inborn errors of intermediary metabolism: abnormal profile interpretation. *Curr. Med. Chem.* 19, 4511–4522. doi:10.2174/092986712803251539

Huang, X., Wu, D., Zhu, L., Wang, W., Yang, R., Yang, J., et al. (2022). Application of a next-generation sequencing (NGS) panel in newborn screening efficiently identifies inborn disorders of neonates. *Orphanet J. Rare Dis.* 17, 66. doi:10.1186/s13023-022-02231-x

Huang, X. W., Yang, J. B., Tong, F., Yang, R. L., Mao, H. Q., Zhou, X. L., et al. (2011). Screening for neonatal inborn errors of metabolism by electrospray ionization-tandem mass spectrometry and follow-up. *Zhonghua Er Ke Za Zhi* 49, 765–770.

Lindner, M., Gramer, G., Haege, G., Fang-Hoffmann, J., Schwab, K. O., Tacke, U., et al. (2011). Efficacy and outcome of expanded newborn screening for metabolic diseases--report of 10 years from South-West Germany. *Orphanet J. Rare Dis.* 6, 44. doi:10.1186/1750-1172-6-44

Lindner, M., Hoffmann, G. F., and Matern, D. (2010). Newborn screening for disorders of fatty-acid oxidation: experience and recommendations from an expert meeting. *J. Inherit. Metab. Dis.* 33, 521–526. doi:10.1007/s10545-010-9076-8

Luo, X., Wang, R., Fan, Y., Gu, X., and Yu, Y. (2018). Next-generation sequencing as a second-tier diagnostic test for newborn screening. *J. Pediatr. Endocrinol. Metab.* 31, 927–931. doi:10.1515/jpem-2018-0088

Millington, D. S., Kodo, N., Norwood, D. L., and Roe, C. R. (1990). Tandem mass spectrometry: a new method for acylcarnitine profiling with potential for neonatal screening for inborn errors of metabolism. *J. Inherit. Metab. Dis.* 13, 321–324. doi:10.1007/BF01799385

Niu, D. M., Chien, Y. H., Chiang, C. C., Ho, H. C., Hwu, W. L., Kao, S. M., et al. (2010). Nationwide survey of extended newborn screening by tandem mass spectrometry in Taiwan. *J. Inherit. Metab. Dis.* 33, S295–S305. doi:10.1007/s10545-010-9129-z

Ombrone, D., Giocaliere, E., Forni, G., Malvagia, S., and La Marca, G. (2016). Expanded newborn screening by mass spectrometry: new tests, future perspectives. *Mass Spectrom. Rev.* 35, 71–84. doi:10.1002/mas.21463

Pereira, S., Smith, H. S., Frankel, L. A., Christensen, K. D., Islam, R., Robinson, J. O., et al. (2021). Psychosocial effect of newborn genomic sequencing on families in the BabySeq project: a randomized clinical trial. *JAMA Pediatr.* 175, 1132–1141. doi:10.1001/jamapediatrics.2021.2829

Rinaldo, P., Zafari, S., Tortorelli, S., and Matern, D. (2006). Making the case for objective performance metrics in newborn screening by tandem mass spectrometry. *Ment. Retard. Dev. Disabil. Res. Rev.* 12, 255–261. doi:10.1002/mrdd.20130

Sanderson, S., Green, A., Preece, M. A., and Burton, H. (2006). The incidence of inherited metabolic disorders in the West Midlands, UK. *Arch. Dis. Child.* 91, 896–899. doi:10.1136/adc.2005.091637

Saudubray, J. M., Nassogne, M. C., De Lonlay, P., and Touati, G. (2002). Clinical approach to inherited metabolic disorders in neonates: an overview. *Semin. Neonatol.* 7, 3–15. doi:10.1053/siny.2001.0083

Scala, I., Parenti, G., and Andria, G. (2012). Universal screening for inherited metabolic diseases in the neonate (and the fetus). *J. Matern. Fetal Neonatal Med.* 25, 4–6. doi:10.3109/14767058.2012.716983

Scaturro, G., Sanfilippo, C., Piccione, M., Piro, E., Giuffre, M., and Corsello, G. (2013). Newborn screening of inherited metabolic disorders by tandem mass spectrometry: past, present and future. *Pediatr. Med. Chir.* 35, 105–109. doi:10.4081/pmc.2013.42

Schulze, A., Kohlmueller, D., and Mayatepek, E. (1999). Sensitivity of electrospray-tandem mass spectrometry using the phenylalanine/tyrosine-ratio for differential diagnosis of hyperphenylalaninemia in neonates. *Clin. Chim. Acta* 283, 15–20. doi:10.1016/s0009-8981(99)00016-9

Shi, X. T., Cai, J., Wang, Y. Y., Tu, W. J., Wang, W. P., Gong, L. M., et al. (2012). Newborn screening for inborn errors of metabolism in mainland China: 30 years of experience. *JIMD Rep.* 6, 79–83. doi:10.1007/8904_2011_119

Tang, C., Tan, M., Xie, T., Tang, F., Liu, S., Wei, Q., et al. (2021). Screening for neonatal inherited metabolic disorders by tandem mass spectrometry in Guangzhou. *Zhejiang Da Xue Xue Bao Yi Xue Ban.* 50, 463–471. doi:10.3724/zdxbyxb-2021-0260

Veldman, A., Kiewiet, M. B. G., Westra, D., Bosch, A. M., Brands, M. M. G., De Coo, R., et al. (2023). A delphi survey study to formulate statements on the treatability of inherited metabolic disorders to decide on eligibility for newborn screening. *Int. J. Neonatal Screen* 9, 56. doi:10.3390/ijns9040056

Wasant, P., Svasti, J., Srisomsap, C., and Liammongkolkul, S. (2002). Inherited metabolic disorders in Thailand. *J. Med. Assoc. Thai* 85 (2), S700–S709.

Wilcken, B., Wiley, V., Hammond, J., and Carpenter, K. (2003). Screening newborns for inborn errors of metabolism by tandem mass spectrometry. *N. Engl. J. Med.* 348, 2304–2312. doi:10.1056/NEJMoa025225

Frontiers in Genetics

Highlights genetic and genomic inquiry relating to all domains of life

The most cited genetics and heredity journal, which advances our understanding of genes from humans to plants and other model organisms. It highlights developments in the function and variability of the genome, and the use of genomic tools.

Discover the latest Research Topics

See more →

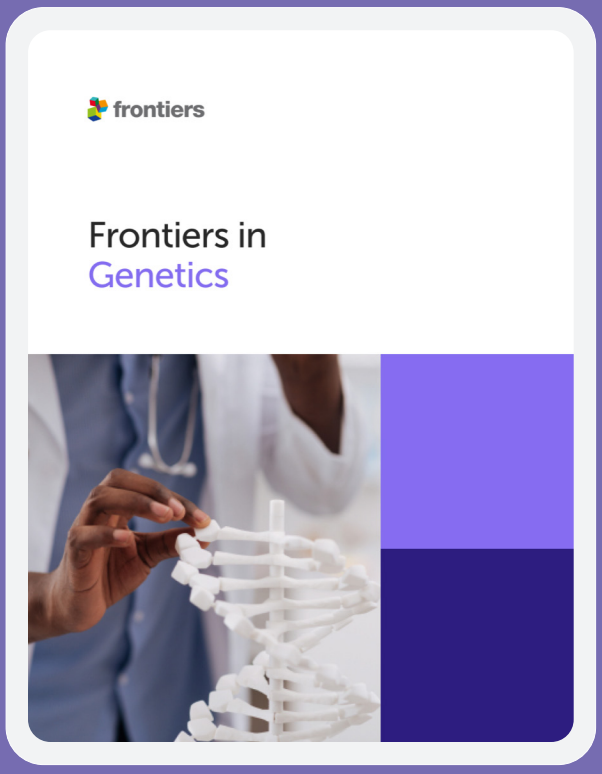

Frontiers

Avenue du Tribunal-Fédéral 34
1005 Lausanne, Switzerland
frontiersin.org

Contact us

+41 (0)21 510 17 00
frontiersin.org/about/contact